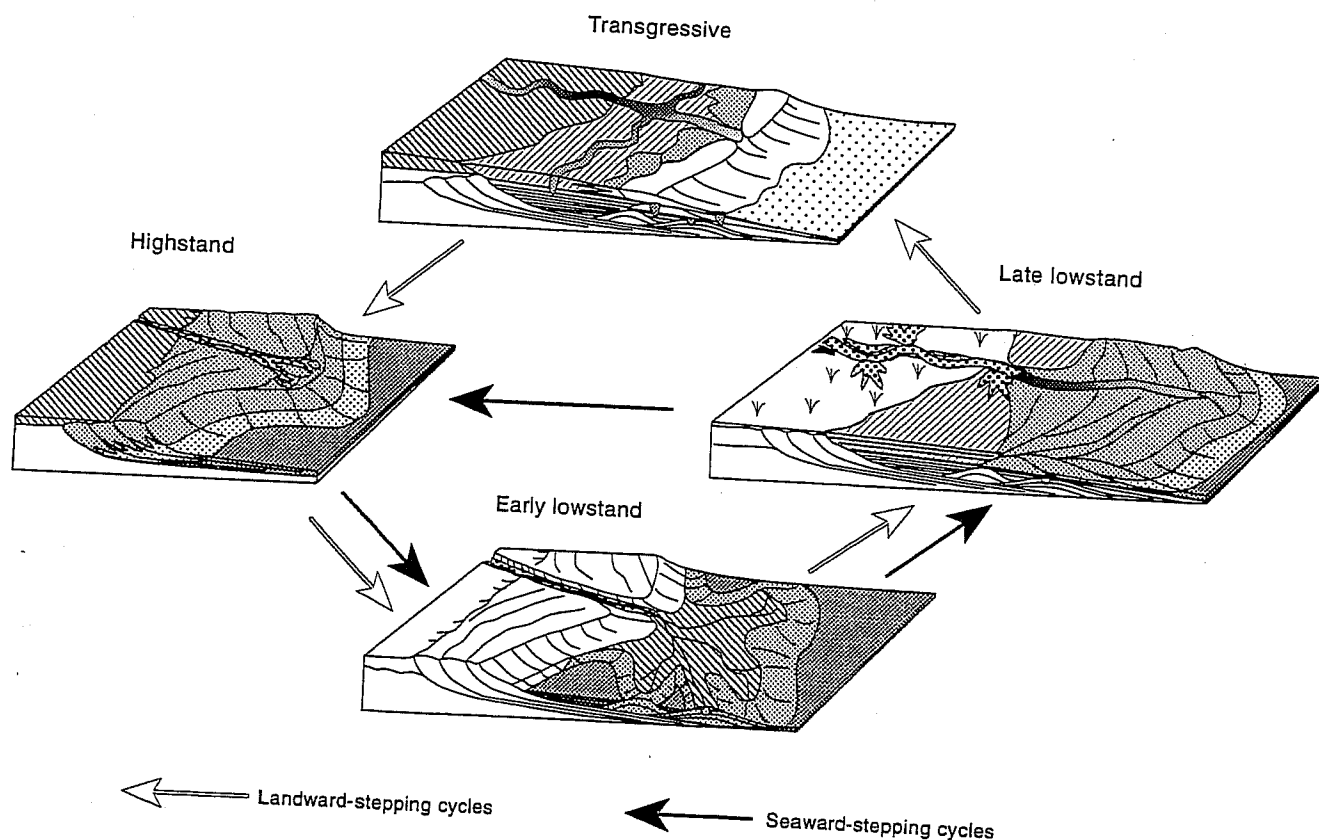




# Fourth International Reservoir Characterization Technical Conference *Proceedings*

Sponsored by  
Department of Energy,  
BDM-Oklahoma, Inc.,  
and  
American Association of Petroleum Geologists



Wyndham Greenspoint Hotel  
Houston, Texas • March 2 - 4, 1997

# RESERVOIR CHARACTERIZATION BASED ON TRACER RESPONSE AND RANK ANALYSIS OF PRODUCTION AND INJECTION RATES

Belkis T. Refunjol  
Lagoven, S.A., PDVSA, Venezuela

Larry W. Lake  
Center for Petroleum and Geosystems Engineering  
The University of Texas at Austin  
Austin, TX 78712

## ABSTRACT

Quantification of the spatial distribution of properties is important for many reservoir-engineering applications. But, before applying any reservoir-characterization technique, the type of problem to be tackled and the information available should be analyzed. This is important because difficulties arise in reservoirs where production records are the only information for analysis.

This paper presents the results of a practical technique to determine preferential flow trends in a reservoir. The technique is a combination of reservoir geology, tracer data, and Spearman rank correlation coefficient analysis. The Spearman analysis, in particular, will prove to be important because it appears to be insightful and uses injection/production data that are prevalent in circumstances where other data are nonexistent. The technique is applied to the North Buck Draw field, Campbell County, Wyoming.

This work provides guidelines to assess information about reservoir continuity in interwell regions from widely available measurements of production and injection rates at existing wells. The information gained from the application of this technique can contribute to both the daily reservoir management and the future design, control, and interpretation of subsequent projects in the reservoir, without the need for additional data.

## INTRODUCTION

Appropriate representation of reservoir heterogeneity is important to successful modeling of past and future production performance. Because of this, description and quantification of reservoir heterogeneity have achieved significant progress in recent years. Among the new developments are depositional and stochastic models of reservoir heterogeneities.

Generating good stochastic or geological models requires a lot of data. Thus, these technologies are difficult, if not impossible, in reservoirs where production records are the only data to be analyzed. Moreover, many models do not acknowledge the fluid processes taking place in the reservoir. The technique proposed here relies entirely on fluid data and uses only production records. We also use tracer data and results of a geologic study to validate the model.

The following sections contain the results from the tracer-response analysis and from the nonparametric statistical analysis of the production and injection rate ranks. The analysis is extended to investigate the effect of lag time on well-to-well correlations. The use of lag time analysis is, as far as we can tell, new to the application of Spearman rank analysis to production data. We conclude with a reservoir description based on rank correlation coefficient and gas tracer analysis.

## RESERVOIR OVERVIEW

The study area is the North Buck Draw field, located in Campbell County, Wyoming, approximately 60 miles northeast of Casper (Fig. 1). The field produces from the Lower Cretaceous Fall River Formation in the west-central portion of the Powder River Basin. The limits of the Buck Draw field and the delineation of the Fall River channel are shown on a structural map in Fig. 2.

**General Geology** - Several studies have been made of the Buck Draw field stratigraphy and depositional patterns (Hawkins and Formhals, 1985; Rasmussen *et al.*, 1985; Sellars and Hawkins, 1992). A recent interpretation (Gardner *et al.*, 1994) based on outcrop studies

revealed a complex valley-fill architecture and reservoir compartmentalization. The valley-fill system is interpreted to be composed of multilateral and vertical channel facies that change in character with geographic and stratigraphic position within a valley.

The main hydrocarbon-trapping mechanism at Buck Draw is the meandering of the channel. The reservoir is more shaley in the northwest portion of the field, with thin, low-permeability sands. This change in lithology is interpreted to form a barrier to hydrocarbon migration in the northwesterly direction. Other barriers are the shaley facies of the Fall River that form the bottom seal and the overlying shale of the lower Skull Creek (Sellars and Hawkins, 1992).

**Reservoir Development** - North Buck Draw field porosity and permeability are areally and vertically heterogeneous. Both properties appear to be greater along the middle-stream axis of the channel, with expected preferred fluid-flow direction along this axis. Generally, reservoir sand quality declines in a direction normal to the channel axis.

The reservoir fluid is a near-volatile oil; fluid properties fall between those of black and volatile oils. The fluid meets the majority of volatile-oil criteria, including large oil formation volume factors and solution gas-oil ratios (Hawkins, 1987). The bubblepoint pressure is 4,680 psia, and the reservoir fluid is a single-phase, low-viscosity (0.12 cp) fluid above this pressure. There is no free water in the reservoir.

North Buck Draw commercial production began in June 1983. In 1988 a pressure maintenance project was initiated by injecting gas. Radioactive tracers were injected into the reservoir and their occurrence was monitored at the producing wells from February 1989 until March 1993. These tracer data are used in this work as helpful information for the reservoir description.

## **TRACER BEHAVIOR AND RESERVOIR DESCRIPTION**

A total of seven injectors were tagged with one of six gas tracers in a three-stage program. The gas tracers used to distinguish breakthrough from the different injectors at each producer



were tritium (HT), krypton-85 (Kr-85), tritiated methane (CH<sub>3</sub>T), tritiated ethane (C<sub>2</sub>H<sub>5</sub>T), tritiated propane (C<sub>3</sub>H<sub>7</sub>T), and sulfur hexafluoride (SF<sub>6</sub>). The tracer program was carried out over a four-year period, long enough to use the tracer response data to define fluid movement for investigation of reservoir heterogeneity.

During the tracer project, samples to determine tracer concentration were taken from all of the producers in the field. Figure 3 shows the areal distribution of the tracer response in each producer, by displacing the inferred breakthrough times. Injector-producer communication is good for wells on the west side of the channel (injectors 11-18, 12-7, and 14-18). There was apparently no communication in wells to the east, injectors 22-17, 22-20, 23-31, and 23-8.

The arrival at the producers of the tagged gas injected in the west, some at early breakthrough times and some at late breakthrough times, indicated no sealing geological barriers are present. Conversely, the lack of response to tracers injected in wells on the east side of the reservoir indicates no communication or, at least, less communication between these wells and the rest of the reservoir.

The fluid characteristics are ideal for the use of tracer-response curves for calculating gas distribution and swept volumes based on the procedures commonly used in water tracing. The assumptions made were that partitioning into oil would be minimal at reservoir conditions and that, since the majority of tracers used in this project were light components, they would partition exclusively into the gas phase in the field test separators where samples were gathered for analysis.

Calculations were performed for each pair of wells with measured tracer response. The tracer recovery values obtained were extremely small, only 6 to 9% recovery after four years of injection.

Tracer	Injected into Well	Recovery, %
CH <sub>3</sub> T	11-18	9.0
C <sub>2</sub> H <sub>5</sub> T	12-7	8.6
C <sub>2</sub> H <sub>5</sub> T	14-18	6.2
Kr-85	23-8	9.2

However, there is a good chance that at least 50% of the wells showing tracer production were sampled after breakthrough had occurred. A large volume of tracer could have been produced before measurement started. The qualitative results of the tracing program were helpful in identifying directional flow trends when analyzed together with the Spearman rank correlation results as follows.

We made no further attempt to identify the causes for the low tracer recovery obtained.

## NONPARAMETRIC STATISTICS IN RESERVOIR DESCRIPTION

Parametric statistics involve the calculation of a statistic from a sample and the comparison of this statistic with a population parameter. If the statistic corresponds to a highly unlikely value of the parameter, the sample is assumed not to have come from the population described by the parameter (Volk, 1969). Parametric statistical tests often use the mean and variance of a distribution, which require operations on the original numerical values. Tests not employing these directly are called nonparametric methods; they generally depend on ranking, that is a set of observations arranged in order of size, rather than using their actual numerical values.

Nonparametric statistics do not require conditions on the parameters of the population from which the samples are drawn. They do not involve any assumptions about the distribution of the population; they are parameter-free. Certain assumptions are associated with most nonparametric statistical tests, such as that the observations are independent and that the variable under study has underlying continuity. These assumptions are fewer and less restrictive than those associated with parametric tests (Siegel, 1956). The price for using nonparametric statistics is a loss of strength in statistical tests; nevertheless, some nonparametric tests are highly efficient. For measuring the degree of correlation, correlation coefficients such as the Spearman or the Kendall coefficients are appropriate for ordinal scales.

The Spearman rank correlation coefficient ( $r_s$ ) is a function of the sum of the squares of the difference of the two rankings for each observation and the number of observations.

$$r_s = 1 - \frac{6}{n(n^2 - 1)} \sum_{i=1}^n d_i^2$$

where  $r_s$  = Spearman rank correlation coefficient

$d_i$  = difference between the rankings of the  $i$  th observations

$n$  = number of observations

Since  $r_s$  is a correlation coefficient, it has the property that  $-1 \leq r_s \leq 1$ . If there is perfect positive correlation, all the differences will be zero and  $r_s = 1$ . If there is perfect negative correlation, in which the low-ranking observation in one classification corresponds to the high-ranking observation in the other, the term  $6 \sum d_i^2$  will be equal to  $2n(n^2 - 1)$ , and the correlation coefficient will be equal to -1 (Volk, 1969). If the two ranking sets are independent,  $r_s$  will be zero.

If all the assumptions of the parametric statistical model are met in the data, the nonparametric statistical tests are wasteful of data. The degree of wastefulness is expressed by the power-efficiency of the nonparametric test (Siegel, 1956). The efficiency of the Spearman rank correlation when compared with the parametric correlation, the Pearson  $r$ , is about 91 percent (Hotelling and Pabst, 1936).

**Method Used** - Rank correlations are more suitable when data are not normally distributed. Production and injection rates are not likely to be normally distributed, so the significance of parametric statistics cannot be tested. All rates from production and injection histories in the North Buck Draw field show fluctuations about some average value, and it is the relationship between these fluctuations that should reflect reservoir heterogeneities and preferential flow trends. None of the rates at Buck Draw were normally distributed.

The Spearman rank correlation coefficient is a quick, simple, and powerful test of the existence of the association between variables, regardless of the population distribution from which the samples are drawn, that provides a tool for investigating the correlation between production and injection rates in the reservoir. The data used for the analysis were the monthly production and injection rates from wells in the North Buck Draw field. The Spearman rank

correlation coefficient was calculated between flow rates of injector/producer pairs of wells to establish dominant communication trends in the reservoir.

The calculations were based on the total (oil and gas) monthly fluid production and injection rates. The rates were converted to ranks, and the Spearman rank correlation coefficient was calculated for pairs composed of each injection well and all its adjacent production wells. The upper plot in Fig. 4 shows the well rate ranks for two typical wells, injector 11-10 and producer 33-7, in the Buck Draw field as a function of time.

In the Heffer *et al.* (1995) application, all of the correlations were sought at zero time lag, a reasonable assumption since that work was investigating pressure fluctuations carried primarily through the rock. Since we are dealing with fluctuations in fluid rates, the assumption of instantaneous response is inappropriate here, since fluids are more compressible. Consequently, we investigated the effect of nonzero time lags between injector-producer pairs.

We considered the effect of a possible lag time between the response of a producer and an injector in the application of the technique. The argument for doing this is that any response at a producer would occur at some time after the stimulus in the injector. The procedure employed for each pair of wells was first to convert production and injection rates to ranks and then to calculate the rank correlation coefficient at zero lag time. From this, a series of correlation coefficients were calculated by shifting the time for the producers starting at one month up to a shifted time no greater than half the total number of months in the period analyzed. The two lower plots in Fig. 4 show how the well rank histories change with lag time. In the case shown, the maximum  $r_s$  occurs at a time lag of 13 months. Note how shifting the lag time causes data to be discarded for both the injector and producer.

A extreme coefficient value occurs at the lag time of maximum correlation between producer and injector. This extreme correlation coefficient ( $r_{smax}$ ) was tested to determine whether it indicated a significant correlation between the production and injection rates for that specific pair of wells. Since the values of  $r_{smax}$  could be positive or negative, that is, there is no predicted direction of the coefficient, the test becomes a two-tailed test. The significant limit was established at 0.02, so that for an extreme value to be taken as significant, it had to be

outside the significant limits imposed by the 2%-level statistical tables. From this, a value of maximum rank correlation coefficient (extremal value) at a lag time of maximum correlation was obtained for each possible injection-production pair.

The observed correlation coefficient at each lag time was plotted for every possible adjoining pair of wells in the field. Plots in Fig. 5 present the correlation of the rates from injectors to the rates of surrounding producer wells. The results exhibit some negative  $r_{smax}$  values, which were interpreted as negative correlations. These negative correlations, which physically represent a decrease in injection rate with a subsequent increase in the production rate of the nearby well, could be explained by the influence of a third well. More analysis should be done to understand these negative correlations. See Refunjol (1996) for a possible way to account for them.

At first we paired every injector with every producer in the reservoir (96 pairs). This method gave a few well pairs that showed significant  $r_{smax}$  at multiple pattern spacing. Like the negative correlations mentioned above, this must be because of multiple well effects; consequently, we limited subsequent study to adjacent well pairs (40 pairs). Heffer *et al.* (1995) also mention such large correlation at a distance.

**Preferential Flow Direction Based on  $r_{smax}$** - One of the main objectives of this work was to infer preferential flow directions by the information provided from the rank correlation coefficient technique. To do this, the  $r_{smax}$  value was analyzed against information about the producer-injector distance in each pair, grouping the pairs based on the spatial orientation of the wells. This is, graphs were constructed for pairs of wells in four different groups: wells oriented N to N30E, N15E to N45E, N30E to N60E, and N45E to N75E. We constructed a histogram based on the orientation of the well pairs with maximum correlation ( $r_{smax}$ ). Using 30-degree-angle classes, Fig. 6 shows a higher frequency of correlation in pairs with an orientation between N31E and N60E. This is in accordance with the southwest-northeast permeability trend observed from the geologic studies.

Along a given direction, the value of  $r_{smax}$  decreases with increasing distance in all the data analyzed, especially in the N30E to N60E direction group (Fig. 7). This figure is actually an autocorrelogram that could be interpreted with conventional models such as the exponential or spherical (Jensen *et al.*, 1996); we show a least-square straight-line fit in Fig. 7. Whatever the model being used, there is clearly very long-range autocorrelation in the N30E to N60E direction, well in excess of 10,000 ft.

Another way to illustrate directional trends is to map  $r_{smax}$ . We did this by linearly interpolating along a line from an injector to a producer between the calculated value of  $r_{smax}$  and  $r_{smax}=1$ . This assumes that perfect correlation,  $r_{smax}=1$ , occurs when the injector and producer are coincident. After this interpolation, we contoured the interpolated values around each injector. Figures 8 to 11 display these maps for injectors 11-18, 12-7, 13-18, and 14-18. All four maps exhibit a clear pattern of southwest-northeast preferential flow trend as expected. These wells are located on the west flank of the channel. The four injectors to the east of the channel showed no preferential flow trends (22-20) or even no correlation at all (22-17, 23-8, and 23-31).

Injector 22-20 presented significant rank correlation coefficients when related to the four surrounding wells, but with no clear preferential direction of correlation. In the analysis of each of these four pairs of wells, we observed that the producers were closer to and more influenced by other injectors than to well 22-20, suggesting no reliable information.

## SUMMARY OF RESERVOIR DESCRIPTION AND CONCLUSIONS

With this research project, a practical and theoretically based technique was developed to determine preferential flow trends in a reservoir by integrating tracer response, Spearman rank correlation coefficient results, and reservoir geology. Most importantly, the work's basic information is tracer data and the widely available measurements of production and injection rates. This makes the technique suitable for implementation in all types of reservoirs, including ones with scarce information.

The Spearman rank correlation coefficient method appears to be successful, as measured by consistency with tracer breakthrough and geologic inference. The integrated reservoir description is summarized as follows:

- A southwest-northeast preferential flow trend is indicated.
- The middle-stream axis of the channel contains high-quality reservoir sand, with preferential flow direction along this axis.
- Communication is good between injectors on the west flank of the channel with the rest of the reservoir, especially in the southwest-northeast direction. Injectors located to the east flank of the channel are not effectively connected to the rest of the reservoir.

The information gained from the application of this technique can contribute to the daily reservoir management and the future design, control, and interpretation of subsequent projects in the reservoir. No additional data besides the available measurements of production and injection rates are required.

Although we have had some success in the description, significant questions must be answered before we can claim that the Spearman technique, by itself, is a useful characterization technique. These include the role of fluid compressibilities in the correlations, accounting for multiple-well correlation, and explanations for correlations at a distance. However, the Spearman technique uses data that are available in virtually all mature fields, and data that can be acquired with little additional expense. These advantages, plus the encouragement from this work, give ample justification for more research.

## ACKNOWLEDGMENTS

The authors acknowledge the data provided by Kerr-McGee, through the Deltas Industrial Affiliate Project at the Bureau of Economic Geology, and the permission to publish this paper. Thanks go to Christopher White for his valuable suggestions and to Drs. Mike King and Kes Heffer for their discussions on applications of the Spearman rank correlation technique. Thanks are also due to Lagoven, S.A. for permission for preparation and publication of this

paper. Larry W. Lake holds the W.A. (Tex) Moncrief Centennial Chair at The University of Texas.

## REFERENCES

- Gardner, M.H., W. Dharmasamadhi, B.J. Willis, S.P. Dutton, Q. Fang, S. Kattah, J. Yeh, and F. Wang, October 1994, "Reservoir characterization of Buck Draw field," Bureau of Economic Geology Deltas Industrial Associates field trip manual.
- Hawkins, C.M., and S. Formhals, 1985, "Geology and engineering aspects of Buck Draw field, Campbell and Converse counties, Wyoming," Wyoming Geological Association 36th Annual Field Conference guidebook, p. 33-45.
- Heffer, K.J., R.J. Fox, and C.A. McGill, October 1995, "Novel techniques show links between reservoir flow directionality, earth stress, fault structure and geomechanical changes in mature waterfloods," paper SPE 30711 presented at the Annual Technical Conference and Exhibition of the Society of Petroleum Engineers held in Dallas, TX.
- Hotelling, H. and M.R. Pabst, 1936, "Rank correlation and test of significance involving no assumptions of normality," Annual Math. Statist., p. 29-43.
- Jensen, J.L., L.W. Lake, P.W.M. Corbett, and D.J. Goggin, 1996, *Statistics for Petroleum Engineers and Geoscientists*, Prentice Hall PTR, Upper Saddle River, New Jersey 07458.
- Lake, L.W., 1989, *Enhanced Oil Recovery*, Prentice Hall, Englewood Cliffs, New Jersey.
- Mirzadjanzade, A.Kh., I.M. Ametov, A.A. Bokserman, and V.P. Filippov, October 1993, "New perspective trends of research in oil and gas recovery," paper presented at the 7th European IOR Symposium held in Moscow, Russia.
- Rasmussen, D.L., C.L. Jump, and K.A. Wallace, 1985, "Deltaic system in the early cretaceous Fall River formation, Southern Powder River basin, Wyoming," Wyoming Geological Association 36th Annual Field Conference guidebook, p. 91-111.
- Refunjol, B.T., 1996, "Reservoir characterization of North Buck Draw field based on tracer response and production/injection analysis," M.S. Thesis, The University of Texas at Austin.
- Sellars, R., and C.M. Hawkins, 1992, "Geology and stratigraphic aspects of Buck Draw field, Powder River basin, Wyoming," Wyoming Geological Association 43rd Annual Field Conference guidebook, p. 97-110.
- Siegel, S., 1956, *Nonparametric Statistics for the Behavioral Sciences*, McGraw-Hill Book Company, New York.
- Volk, W., 1969, *Applied Statistics for Engineers*, McGraw-Hill Book Company, New York.
- Zemel, B., 1995, *Tracers in the Oil Field*, Elsevier Science B. V., Amsterdam.



## LIST OF FIGURES

- Figure 1. Location map.
- Figure 2. Limits of North Buck Draw field.
- Figure 3. Tracer response pattern map.
- Figure 4. Spearman ranks between producer 33-7 and injector 11-16 vs. time for three time lags.
- Figure 5. Rank correlation coefficient vs. time lag.
- Figure 6. Histogram for preferential direction from maximum rank correlation in all wells.
- Figure 7. Rank correlation coefficient vs. distance for pairs on the N30E to N60E orientation.
- Figure 8. Iso- $r_{smax}$  map for injector 11-18.
- Figure 9. Iso- $r_{smax}$  map for injector 12-7.
- Figure 10. Iso- $r_{smax}$  map for injector 13-18.
- Figure 11. Iso- $r_{smax}$  map for injector 14-18.

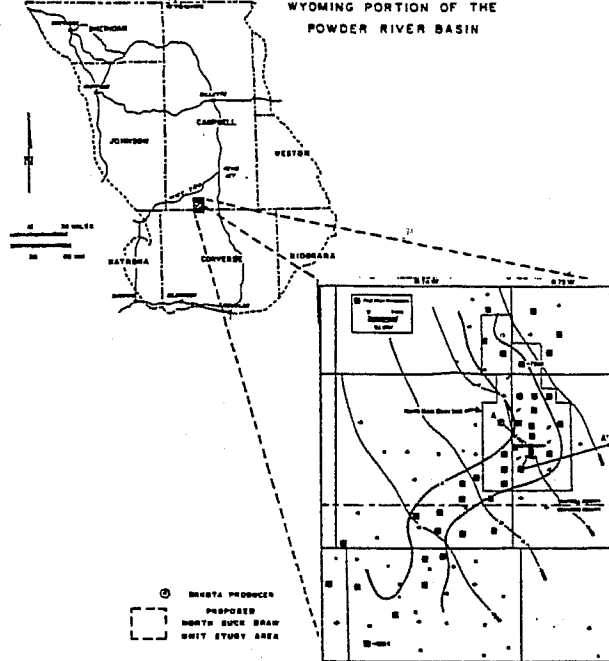


Figure 1. Location map.

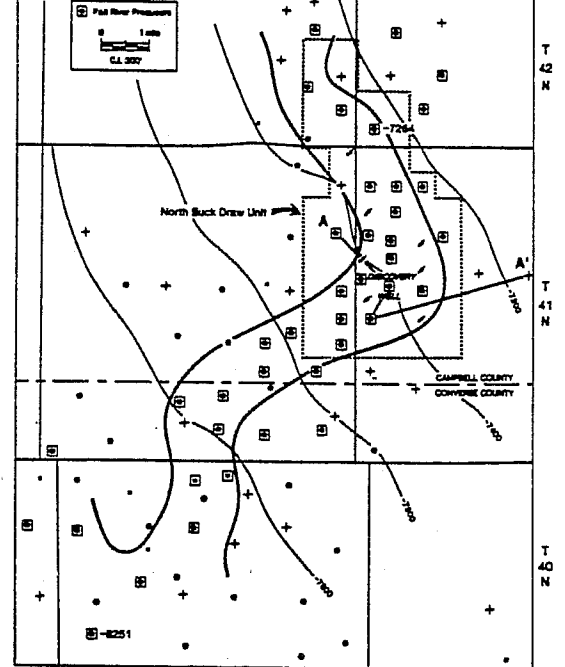


Figure 2. Limits of North Buck Draw field.

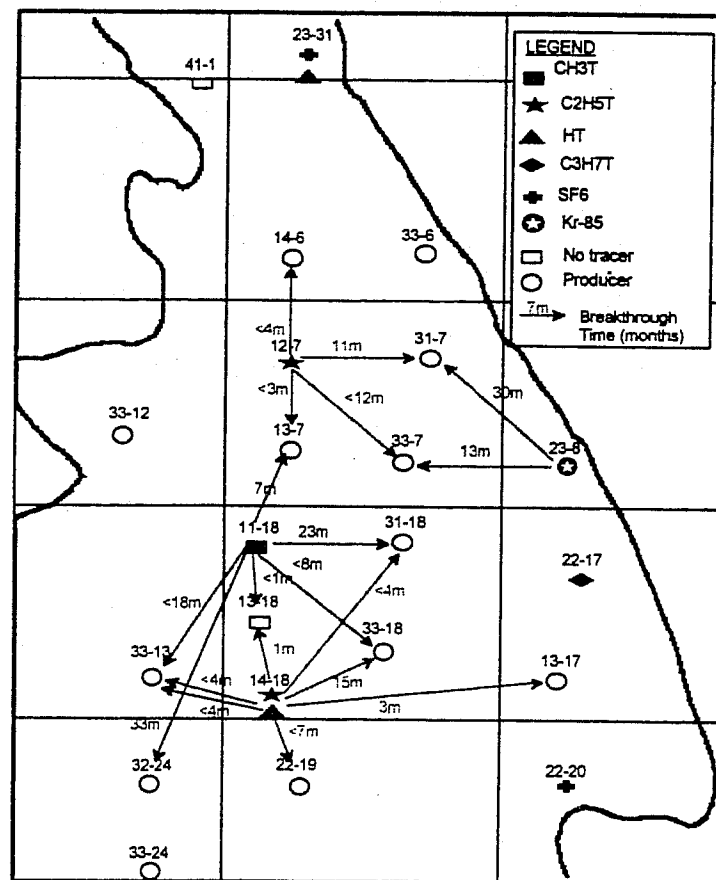


Figure 3. Tracer response pattern map.

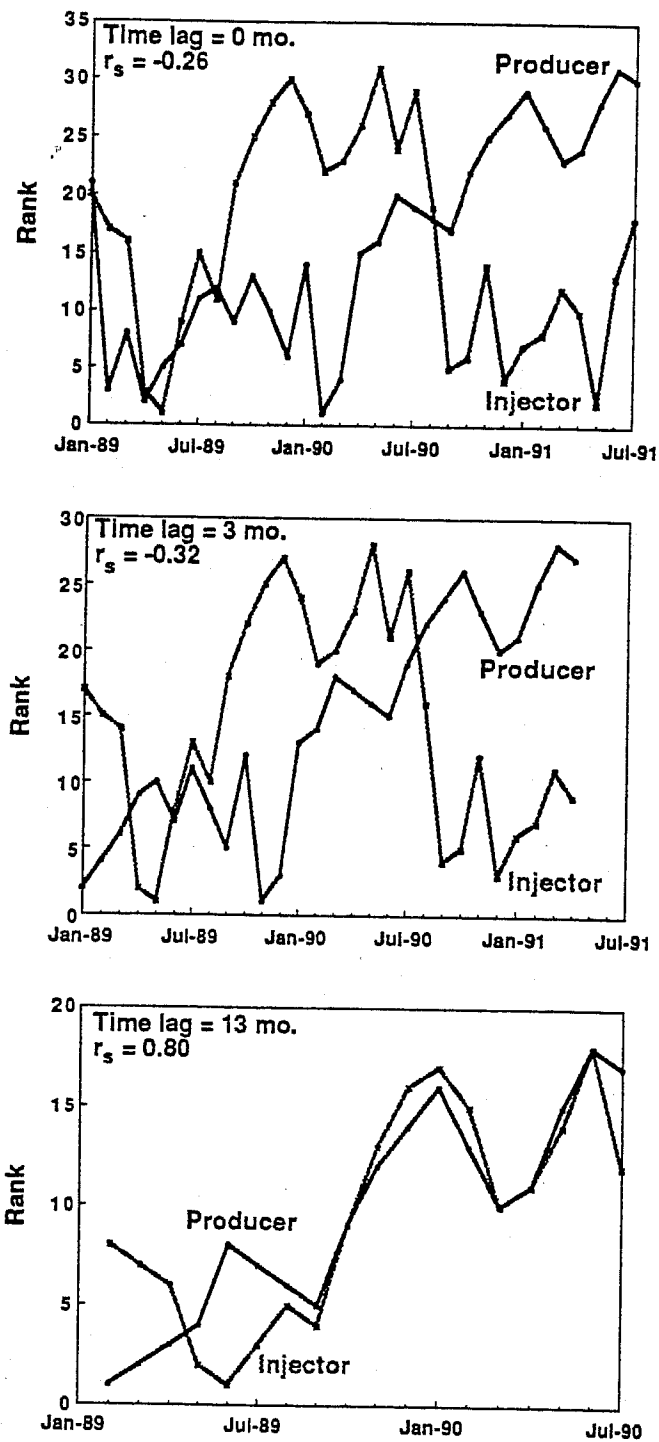


Figure 4. Spearman ranks between producer 33-7 and injector 11-16 vs. time for three time lags.

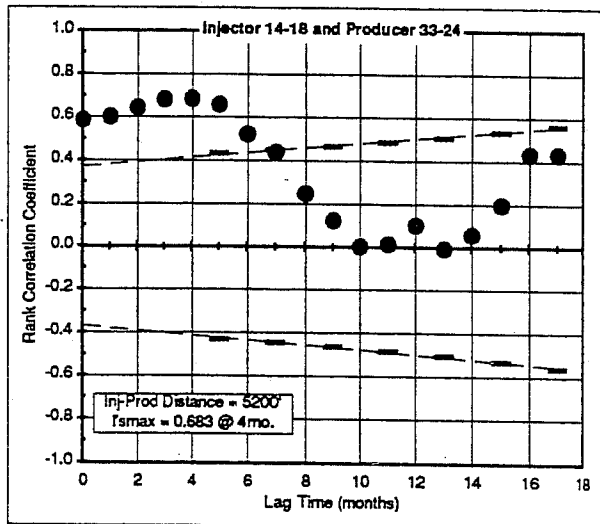
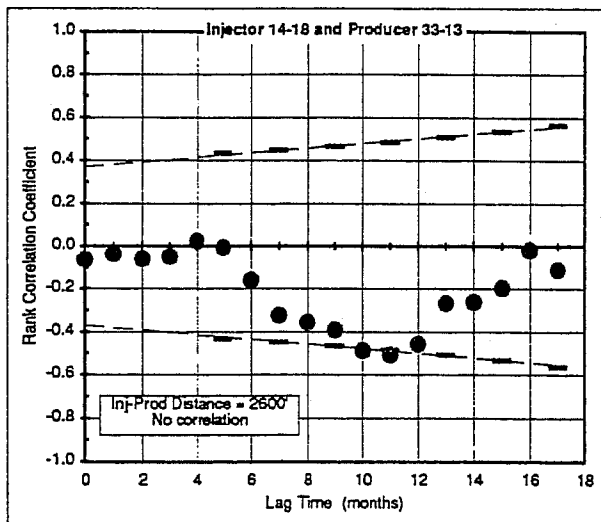
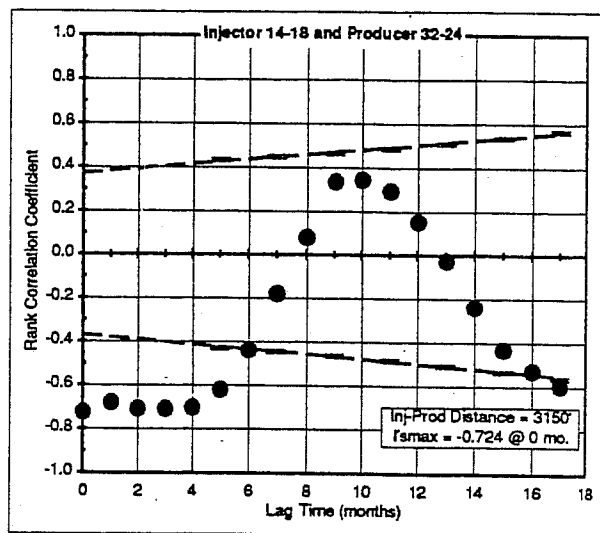
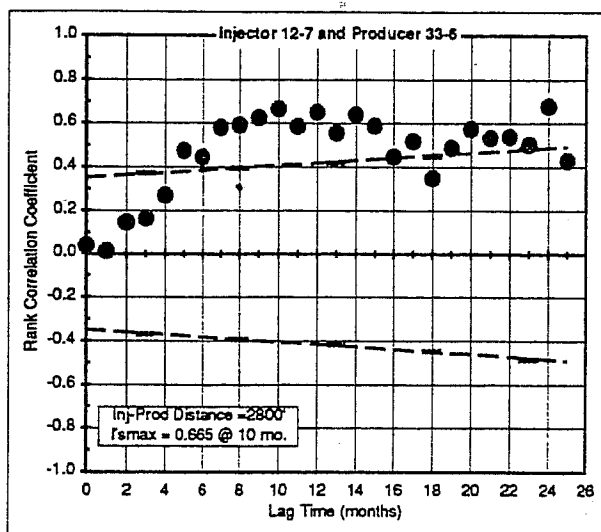


Figure 5. Rank correlation coefficient vs. lag time.

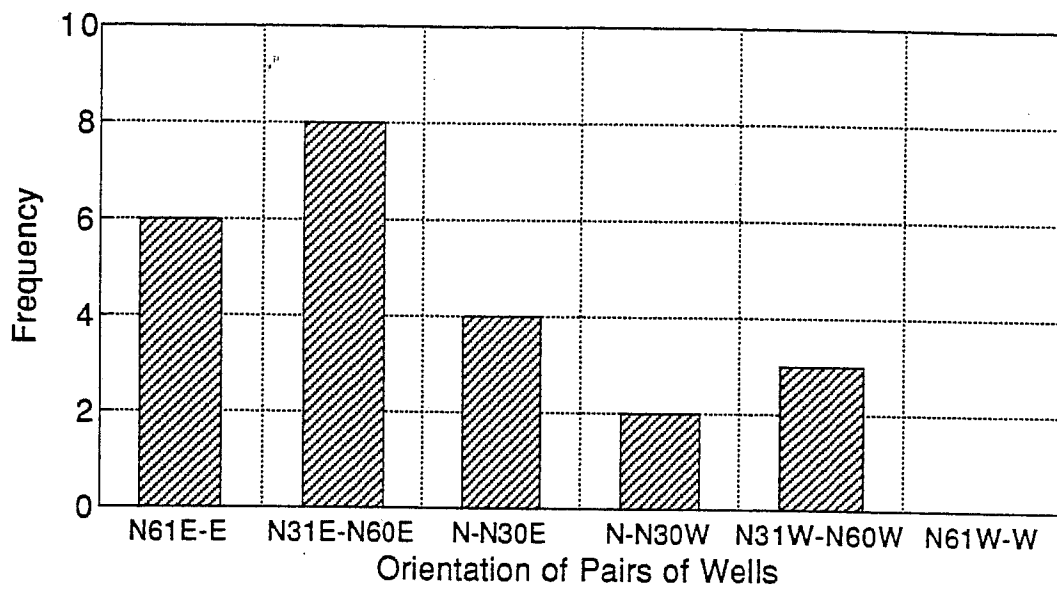


Figure 6. Histogram for preferential direction from maximum rank correlation in all wells.

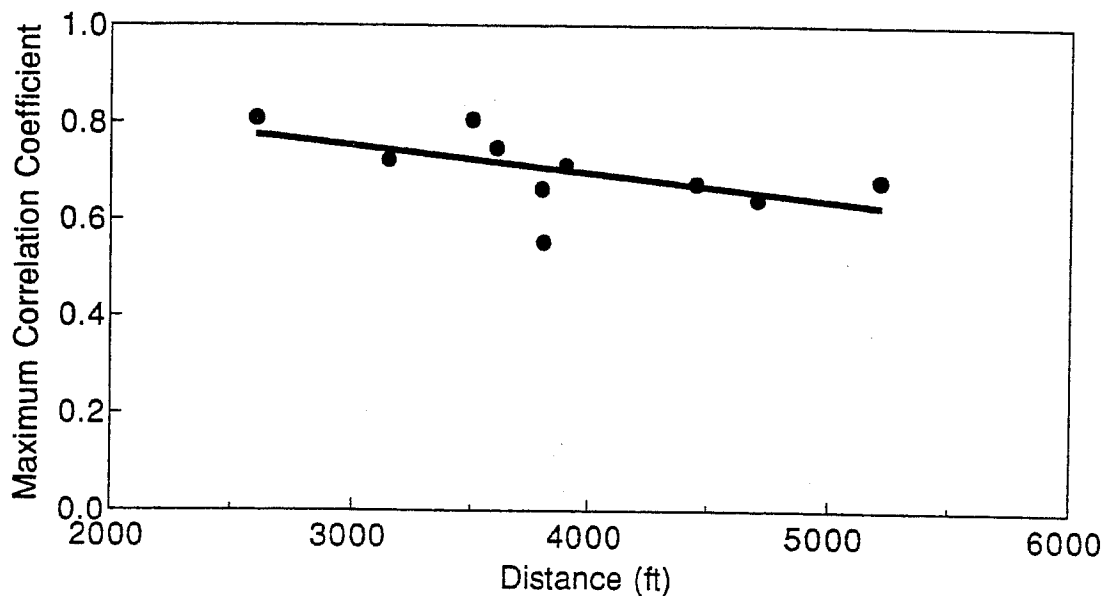


Figure 7. Rank correlation coefficient vs. distance for pairs on the N30E to N60E orientation.

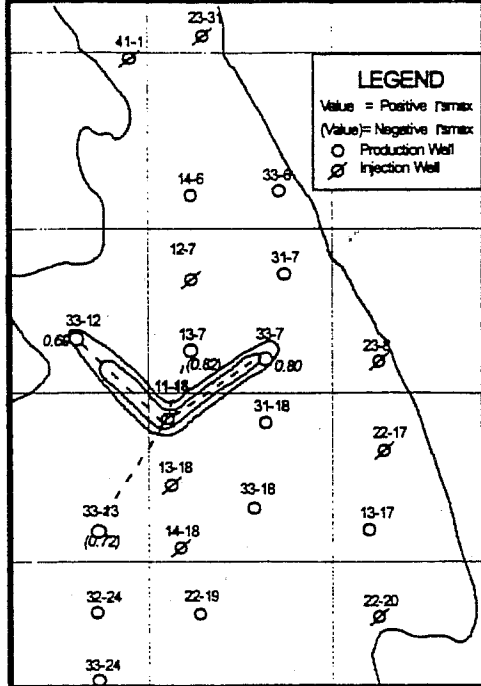


Figure 8. Iso-  $r_{smax}$  map for injector 11-18.

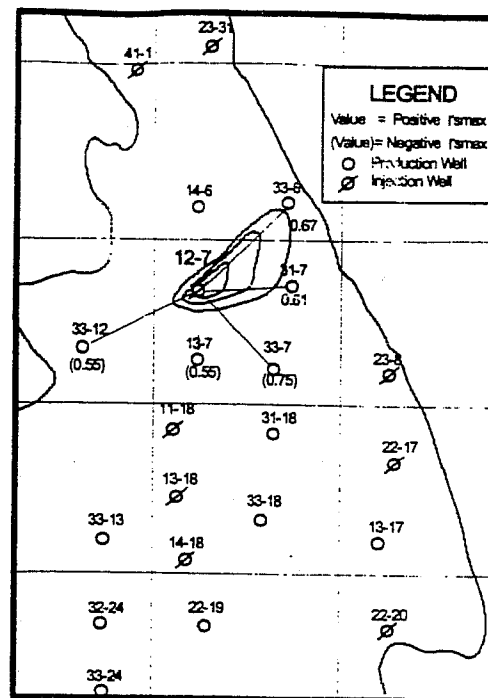


Figure 9. Iso-  $r_{smax}$  map for injector 12-7.

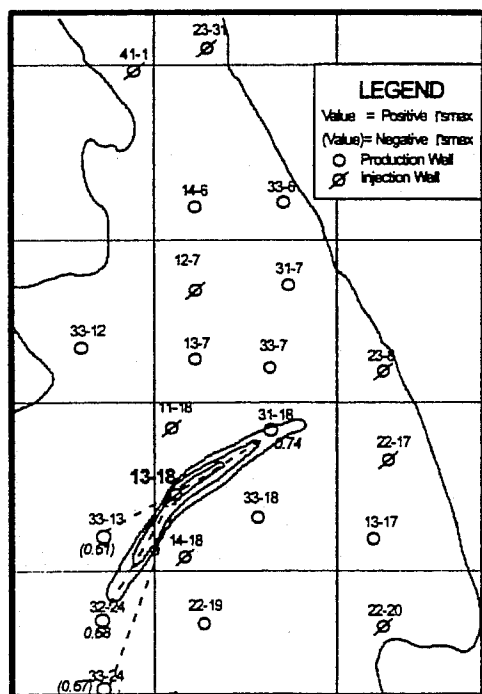


Figure 10. Iso-  $r_{smax}$  map for injector 13-18.

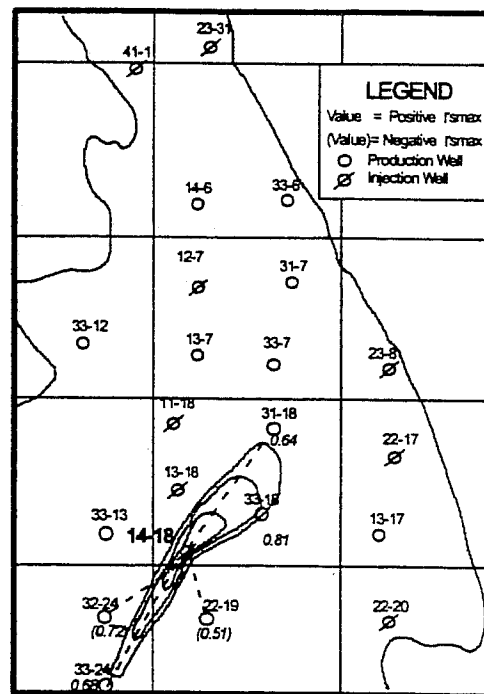


Figure 11. Iso-  $r_{smax}$  map for injector 14-18.



# Non-parametric Transformations for Data Correlation and Integration: From Theory to Practice

Akhil Datta-Gupta, Guoping Xue, and Sang Heon Lee

Department of Petroleum Engineering

Texas A&M University

College Station, Texas

## ABSTRACT

The purpose of this paper is two-fold. First, we introduce the use of non-parametric transformations for correlating petrophysical data during reservoir characterization. Such transformations are completely data driven and do not require *a priori* functional relationship between response and predictor variables which is the case with traditional multiple regression. The transformations are very general, computationally efficient and can easily handle mixed data types for example, continuous variables such as porosity, permeability and categorical variables such as rock type, lithofacies. The power of the non-parametric transformation techniques for data correlation has been illustrated through synthetic and field examples. Second, we utilize these transformations to propose a two-stage approach for data integration during heterogeneity characterization. The principal advantages of our approach over traditional cokriging or cosimulation methods are: (1) it does not require a linear relationship between primary and secondary data, (2) it exploits the secondary information to its fullest potential by maximizing the correlation between the primary and secondary data, (3) it can be easily applied to cases where several types of secondary or soft data are involved, and (4) it significantly reduces variance function calculations and thus, greatly facilitates non-Gaussian cosimulation. We demonstrate the data integration procedure using synthetic and field examples. The field example involves estimation of pore-footage distribution using well data and multiple seismic attributes.

## INTRODUCTION

During initial stages of data correlation, often we are interested in pursuing exploratory analysis. Rather than imposing our preconceived notions or models, we want to gain insight into the nature of the data set and if possible, the underlying phenomenon that might have produced the data set. Unfortunately traditional multiple regression techniques for data correlation are limited in this respect since they require *a priori* assumptions of functional forms relating the response (dependent) and predictor (independent) variables. This is a significant drawback for correlating rock or petrophysical properties because of the inexact nature of the underlying relationship. When used as a predictive tool for petrophysical data, conventional multiple regression suffers from several other limitations as discussed by Jensen and Lake, 1985, Wendt et al., 1986, and Xue et al., 1996(a).

Parametric transformations have been suggested for optimization of regression-based permeability-porosity predictions. Notable amongst these are the power transformations proposed by Jensen and Lake (1985). The underlying theory is that if the joint probability distribution function of two variables is binormal, their relationship will be linear (Hald, 1952). Several methods exist to estimate the exponents for power transformation. One method, described by Emerson and Stoto (1982 and adopted by Jensen and Lake (1985), is based on symmetrizing the probability distribution



function (p.d.f.). Another method is a trial-and-error approach based on a normal probability plot of the data. By power transforming permeability and porosity separately, the authors are able to improve permeability-porosity correlation. However, using a trial-and-error method for selecting exponents for power transformation is time consuming, and symmetrizing the p.d.f. does not necessarily guarantee a binormal distribution of transformed variables. Most importantly, there are no indications as to whether power transformations will work for multivariate cases. This is a severe limitation since we are often interested in correlating permeability with multiple well log responses.

We propose here a more adaptive approach offered by non-parametric transformation and regression methods for correlating petrophysical data (Hastie and Tibshirani, 1990; Xue et al, 1996(a)). Our approach is quite general and can be applied to other types of data such as Pressure-Volume-Temperature (PVT) data. The non-parametric transformation techniques generate regression relations in a flexible data-defined manner through the use of *conditional expectations* or *scatterplot smoothers* and in doing so, let the data itself suggest functional forms or detect inherent non-linearities. Optimal non-parametric transformations can be shown to produce maximum correlation in the transformed space (Breiman and Friedman, 1985). The power of these methods lie in their ability to directly incorporate multiple and mixed variables, both continuous and categorical, into correlation. Moreover, the transformations are computationally efficient, easy to use and can provide significant insight during exploratory data analysis.

Next, we utilize these non-parametric transformations to propose a two-stage approach to integrate seismic or other secondary data into reservoir characterization. First, we calibrate seismic and well data using optimal non-parametric transformations. Stochastic cosimulation is then carried out in the transformed space to generate conditional realizations of reservoir properties. The principal advantage of this approach over traditional cosimulation methods are: (1) it does not require a linear relationship between seismic and well data, (2) it exploits the secondary information to its fullest potential by maximizing the correlation between the primary and secondary data, and (3) it can be easily extended to cases where several types of soft data are involved. Moreover, the use of non-parametric transformations results in a significant reduction in variance function calculations and thus, greatly facilitates non-Gaussian cosimulation through the use of indicator approaches.

The organization of this paper is as follows. First, we briefly review the theory and motivation behind non-parametric transformations and regression. Next, we discuss application of such transformations for data correlation and integration. Finally, we present synthetic and field examples which demonstrate the power and utility of such transformations for correlating petrophysical properties using multiple regression. A field example involving integration of 3-D seismic data is also discussed to illustrate the data integration procedure.

## NON-PARAMETRIC TRANSFORMATION AND REGRESSION: THEORY

In general, the regression problem involves a set of predictors, for example, a  $p$ -dimensional random vector  $X$  and a random variable  $Y$  which is called the response variable. The aim of regression analysis is to estimate the conditional expectation,  $E(Y | X_1, X_2, \dots, X_p)$ . Conventional multiple regression requires a functional form to be presumed *a priori* for the regression surface, thus reducing the problem to that of estimating a set of parameters. Such parametric approach can be successful provided the model assumed is appropriate. When the relationship between the response and predictor variables is unknown or inexact, as is frequently the case for reservoir rock or petrophysical properties, parametric regression can yield erroneous and even misleading results. This is the primary motivation behind non-parametric regression techniques which make only few general assumptions about the regression surface (Friedman and Stuetzle, 1981).

The non-parametric transformations techniques generate regression relations in a flexible data-defined manner through the use of *scatterplot smoothers* and in doing so let the data suggest the functionalities. The most extensively studied non-parametric regression techniques (kernel, nearest neighbor or spline smoothing) are based on some sort of local averaging which take the form:

$$E(Y|x) = \sum_{i=1}^N H(x, x_i) y_i \quad (1)$$

where  $H(x, x')$  (the kernel function) usually has its maximum at  $x' = x$  with its absolute value decreasing as  $|x' - x|$  increases. A critical parameter in local averaging is the span  $s(x)$  which is the interval, centered at  $x'$ , over which most of the averaging takes place and thus, controls the bias-variance trade-off. Optimal span selection based on local cross-validation has been discussed by Friedman and Silverman (1989).

More recently, however, non-parametric regression techniques that are based on successive refinements have gained wide popularity in a variety of disciplines ranging from medical sciences to air pollution control (Hastie and Tibshirani, 1990). We will focus here on these non-parametric regression techniques that attempt to define the regression surface in an iterative fashion while remaining 'data-driven' as opposed to 'model-driven'. We can broadly classify them into those which do not transform the response variable (Generalized Additive Models) and those which do (Alternating Conditional Expectations and its variations). A brief discussion of these techniques follows. For further details, the reader is referred to Hastie and Tibshirani (1990), Buja *et al.* (1989) and Xue *et al.* (1996(a)).

### Generalized Additive Models (GAM)

An additive regression model has the general form:

$$E(Y|X_1, X_2, \dots, X_p) = \alpha + \sum_{l=1}^p \phi_l(X_l) + \varepsilon \quad (2)$$

where  $X_l$  are the predictors and  $\phi_l$  are functions of predictors. Thus additive models replace the problem of estimating a function of a  $p$ -dimensional variable  $X$  by one of estimating  $p$  separate one-dimensional functions,  $\phi_l$ . Such models are attractive if they fit the data since they are far easier to interpret than a  $p$ -dimensional multivariate surface.

The technique for estimating  $\phi_l$ 's is called the *local scoring* algorithm and uses scatterplot smoothers for example, a running mean, running median, running least squares line, kernel estimates or a spline (see Buja *et al.*, 1989 for a discussion of smoothing techniques). In order to motivate the algorithm, let us consider the following simple model:

$$E(Y|X_1, X_2) = \phi_1(X_1) + \phi_2(X_2) \quad (3)$$

Given an initial estimate  $\phi_1(X_1)$ , one way to estimate  $\phi_2(X_2)$  is to smooth the residual  $R_1 = Y - \phi_1(X_1)$  on  $X_2$ . With this estimate of  $\phi_2(X_2)$ , we can get an improved estimate  $\phi_1(X_1)$  by smoothing  $R_1 = Y - \phi_2(X_2)$  on  $X_1$ . The resulting iterative smoothing procedure is called *backfitting* (Hastie and Tibshirani, 1990) and forms the core of additive models.

In general, an algorithm for fitting a generalized additive model consists of a hierarchy of three modules: (i) *scatterplot smoothers* which can be thought of as a general regression tool for fitting functional relationship between response and predictor variables, (ii) a *backfitting* algorithm that cycles through the individual terms in the additive model and iteratively updates each using the Gauss-Siedel method by smoothing suitably defined partial residuals, and (iii) a *local scoring* algorithm that utilizes an iteratively reweighted least squares procedure (Hastie and Tibshirani, 1990) to generate a new additive predictor. A step by step procedure for the Generalized Additive Model can be found in Hastie and Tibshirani (1990).

## Response Transformation Models: ACE Algorithm and its Variations

The response transformation models generalize the additive model by allowing for a transformation of the response variable  $Y$ . The models have the following general form:

$$\theta(Y) = \alpha + \sum_{l=1}^p \phi_l(X_l) + \varepsilon \quad (4)$$

The main motivation behind response transformation is that often a simple additive model may not be appropriate for  $E(Y | X_1, X_2, \dots, X_p)$ , but may be quite appropriate for  $E\{\theta(Y) | X_1, X_2, \dots, X_p\}$ . An example of such model is the Alternating Conditional Expectation (ACE) algorithm and its modifications.

The ACE algorithm, originally proposed by Breiman and Friedman (1985), provides a method for estimating optimal transformations for multiple regression that result in a maximum correlation between a dependent (response) random variable and multiple independent (predictor) random variables. Such optimal transformations can be derived by minimizing the variance of a linear relationship between the transformed response variable and the sum of transformed predictor variables. For a given set of response variable  $Y$  and predictor variables  $X_1, \dots, X_p$ , the ACE algorithm starts out by defining arbitrary measurable mean-zero transformations  $\theta(Y)$ ,  $\phi_1(X_1), \dots, \phi_p(X_p)$ . The error ( $e^2$ ) not explained by a regression of the transformed dependent variable on the sum of transformed independent variables is (under the constraint,  $E[\theta^2(Y)] = 1$ )

$$e^2(\theta, \phi_1, \dots, \phi_p) = E\left\{\left[\theta(Y) - \sum_{l=1}^p \phi_l(X_l)\right]^2\right\} \quad (5)$$

The minimization of  $e^2$  with respect to  $\phi_1(X_1), \dots, \phi_p(X_p)$  and  $\theta(Y)$  is carried out through a series of single-function minimizations, resulting in the following equations

$$\begin{aligned} \phi_l(X_l) &= E[\theta(Y) - \sum_{j \neq l} \phi_j(X_j) | X_l] \\ \theta(Y) &= E\left[\sum_{l=1}^p \phi_l(X_l) | Y\right] / E\left[\sum_{l=1}^p \phi_l(X_l) | Y\right] \end{aligned} \quad (6)$$

Two basic mathematical operations involved in here are conditional expectations and iterative minimization and hence, the name *alternating conditional expectations*. The final  $\phi_l(X_l)$ ,  $l=1, \dots, p$  and  $\theta(Y)$  after the minimization are estimates of optimal transformation  $\phi_l^*(X_l)$ ,  $l=1, \dots, p$  and  $\theta^*(Y)$ . In transformed space, the response and predictor variables will be related as follows

$$\theta^*(Y) = \sum_{l=1}^p \phi_l^*(X_l) + \xi \quad (7)$$

where  $\xi$  is the misfit.

The optimal transformations are derived solely based on the data sets and can be shown to result in a maximum correlation in the transformed space (Breiman and Friedman, 1985). The transformations

do not require *a priori* assumptions of any functional form for the response or predictor variables and thus, provide a powerful tool for exploratory data analysis and correlation.

Although ACE is a potent and versatile approach for building correlations, it suffers from some anomalies when one views it as a regression tool. Such anomalies become particularly prominent in low-correlation settings. A modification of ACE designed primarily for regression problems was proposed by Tibshirani (1988) and differs from ACE in that it chooses  $\theta(Y)$  to achieve a special asymptotic variance stabilizing feature. The goal here is to estimate transformations  $\theta$  and  $\phi_l$  which have the following properties:

$$\begin{aligned} E\{\theta(Y)|X_1, X_2, \dots, X_p\} &= \sum_{l=1}^p \phi_l(X_l) \\ \text{Var}\{\theta(Y)|\sum_{l=1}^p \phi_l(X_l)\} &= \text{constant} \end{aligned} \quad (8)$$

The transformation  $\theta$  is assumed to be strictly monotone (and thus, invertible) and the conditional expectations are approximated using the scatterplot smoothing algorithm *supersmoother* (Friedman and Stuetzle, 1982). In the examples that follow, we use this modification of the ACE algorithm. A step by step procedure for the ACE model and its modification can be found in Hastie and Tibshirani (1990).

## NON-PARAMETRIC TRANSFORMATION: APPLICATION

In this section we discuss how the non-parametric transformation techniques discussed above can be applied for data correlation and integrating diverse data types. We will focus on the response transformation models since they are more general in nature and thus, encompass other non-parametric techniques.

### Data Correlations and Estimation

Non-parametric transformations techniques offer a flexible and data-driven approach to building correlation without *a priori* assumptions regarding functional relationship between response and predictor variables. The following equation is used to estimate or predict dependent variable,  $y_i^{\text{pre}}$  for any given data point  $\{x_{1i}, \dots, x_{pi}\}$  involving  $p$ - independent variables

$$y_i^{\text{pre}} = \theta^{*-1}\left[\sum_{l=1}^p \phi_l^*(x_{li})\right] \quad (9)$$

The calculation involves  $p$  forward transformations of  $\{x_{1i}, \dots, x_{pi}\}$  to  $\{\phi_1^*(x_{1i}), \dots, \phi_p^*(x_{pi})\}$ , and a backward transformation, Eq. 9. By restricting the transformation of the response variable to be monotone, we can ensure that  $\theta^*$  is invertible.

The power of non-parametric transformations as a tool for correlation lies in their ability to handle variables of mixed type. For example, we can easily incorporate categorical variables such as rock types and lithofacies into the correlation and also, handle missing data values without additional complications (Breiman and Friedman, 1985).

Our experience has shown that for most of the applications considered by us (petrophysical and PVT data), the non-parametric transformations  $\phi_l(X)$  and  $\theta(Y)$  can be fitted by simple functions such as polynomials, power functions or cubic splines (Xue *et al.*, 1996(a) Crogh, 1996). This allows for a rapid and powerful alternative to traditional multiple regression for building correlation for a variety of applications particularly in the presence of several predictor variables.

## Data Integration

One critical aspect of integrating different data types during reservoir characterization is the calibration between primary and secondary data, for example, correlating well and seismic data. Cokriging or cosimulation has traditionally been used for data integration in which such calibration is accomplished by modeling cross covariance functions. Given a primary variable (hard data)  $y(u_\alpha)$ , sampled at  $n$  locations, and secondary variables (soft data)  $x_1(u_\beta), \dots, x_p(u_\beta)$ , all assumed sampled at the same  $m$  locations, the full cokriging estimator of  $y(u)$  is

$$y(u) = \sum_{\alpha=1}^n \lambda_\alpha y(u_\alpha) + \sum_{\beta=1}^m \mu_{1\beta} x_1(u_\beta) + \dots + \sum_{\beta=1}^m \mu_{p\beta} x_p(u_\beta) \quad (10)$$

where,  $\lambda_\alpha$ 's are the weights for the primary variable  $y$ , and  $\mu_{l\beta}$ 's are the weights associated with the secondary variables,  $x_l$  ( $l=1, \dots, p$ ). However, in practice, several limitations restrict the application of full cokriging for data integration. First, the implementation of Eq.10 requires modeling of  $(p+1)^2$  variance functions which include  $(p+1)$  covariance functions and  $p(p+1)$  cross covariance functions. Modeling of variance functions becomes extremely tedious when several secondary variables are involved, for example multiple seismic attributes. Second, cokriging matrix may become unstable (close to singular) because of the sparse primary and dense secondary data samples (Alameida, 1993). Third, because the cross covariance functions can only capture the linearity between the primary and secondary data samples, the influence of secondary data samples on the cokriging estimator can be reduced significantly in the presence of non-linearity. This is particularly critical for integration of seismic data since in general the link between reservoir and seismic properties can be expected to be non-unique, multivariate and non-linear (Xue and Datta-Gupta, 1996(b)).

We propose here a two-stage approach to integrating seismic or other secondary data into reservoir characterization. First, we use the non-parametric transformational approach to calibrate the seismic and well data to maximize correlation between the two data sets. This leads to a set of transformations  $\theta^*, \phi_l^*, l=1, p$ . Cokriging or stochastic cosimulation is then carried out in the transformed space to generate conditional realizations of reservoir properties. The cokriging equations now take the following form

$$\theta^*(y(u)) = \sum_{\alpha=1}^n \lambda'_\alpha \theta^*(y(u_\alpha)) + \sum_{\beta=1}^m \mu'_\beta \phi_s^*(x(u_\beta)) \quad (11)$$

where  $\phi_s^*$  is the sum of transformed secondary data samples (for example, seismic attributes) as follows

$$\phi_s^*(x(u_\beta)) = \phi_1^*(x_1(u_\beta)) + \dots + \phi_p^*(x_p(u_\beta)) \quad (12)$$

Notice that the new formulation for cokriging estimator with optimal transformations (Eq.11) now contains only two terms compared to  $(p+1)$  terms in Eq.10. As a result, it reduces the number of variance functions required by cokriging from  $(p+1)^2$  to 4 regardless of the number of secondary variables involved. A further simplification can be made by introducing collocated cokriging

algorithm with Markov hypothesis (Alameida, 1993) into Eq.11 resulting in the following collocated cokriging estimator

$$\theta^*(y(u)) = \sum_{\alpha=1}^n \lambda_{\alpha}' \theta^*(y(u_{\alpha})) + \mu' \phi_s^*(x(u)) \quad (13)$$

The underlying assumption in Eq.13, in addition to Markov screening hypothesis, is that the secondary data samples must be available at every location where primary variable is to be estimated. This is always satisfied for seismic data.

Stochastic cosimulation algorithm provides another important tool for data integration. Such cosimulation generates multiple realizations of random field conditioned to prior information, allowing assessment of model uncertainty. Indicator cosimulation has the capability of integrating soft and hard data without the assumption of a multiGaussian distribution. The limitations of multiGaussian assumptions are well established in the literature (Journel and Alabert, 1990). The use of Markov-Bayes (Zhu and Journel, 1992) algorithm in conjunction with optimal transformation can significantly simplify the modeling of indicator variance function, especially when several type of soft data are involved.

In transformed space, we define hard indicator as

$$I(u_{\alpha}, \theta_j^*) = \begin{cases} 1, & \text{if } \theta^*[y(u_{\alpha})] \leq \theta_j^* \\ 0, & \text{otherwise} \end{cases} \quad (14)$$

where  $\theta_j^*$   $j=1, \dots, k$  are cutoffs for transformed hard data. Similarly, we define local soft indicator data, originating from the calibration between transformed hard data and the sum of transformed soft data

$$z(u_{\beta}, \theta_j^*) = \text{Prob}\{\theta^*[y(u_{\beta})] \leq \theta_j^* | \phi_s^*(u_{\beta})\} \in [0,1] \quad (15)$$

Having indicator coded the transformed data, we follow the procedure outlined by Zhu and Journel (1992). After simulation, we back transform to the original data space.

## RESULTS: SYNTHETIC AND FIELD EXAMPLES

In this section we describe application of the concepts discussed above to synthetic and field examples. The synthetic examples are designed to test the validity of our approach and to compare with the methods currently in practice. The field examples serve to illustrate the versatility to handle field scale applications.

### Data Correlation: A Synthetic Example

This synthetic example is designed to demonstrate the ability of non-parametric transformations to identify functional relationship during multiple regression and correlation. Our example involves 300 observations generated using the following model

$$y_i = x_{1i} + x_{2i}^2 + x_{3i}^3 + 0.1\varepsilon_i \quad (16)$$

where  $x_{1i}$ ,  $x_{2i}$ , and  $x_{3i}$  are independently drawn from a uniform distribution  $U(-0.5, 0.5)$ , and  $\varepsilon_i$  is drawn from a standard normal distribution  $N(0,1)$ . Fig. 1a through Fig. 1c show plots of  $y_i$  versus  $x_{1i}$ ,  $x_{2i}$ , and

$x_{3i}$ , respectively. Except for  $y_i$  versus  $x_{1i}$ , the functional relationships between the dependent variable  $y_i$  and independent variables  $x_{2i}$  and  $x_{3i}$  can not be identified from the scatterplots.

The optimal transformations for  $y_i$  and  $x_{1i}$ ,  $x_{2i}$ , and  $x_{3i}$  derived using ACE are plotted in Fig. 1d through Fig. 1g. The transformations for both  $y_i$  and  $x_{1i}$  yield essentially straight lines. The transformation for  $x_{2i}$  reveals a quadratic function and the transformation for  $x_{3i}$  reveals a cubic function. Thus ACE is able to identify the following optimal transformations

$$\begin{aligned}\theta^*(y_i) &\cong y_i \\ \phi_1^*(x_{1i}) &\cong x_{1i}, \quad \phi_2^*(x_{2i}) \cong x_{2i}^2, \quad \phi_3^*(x_{3i}) \cong x_{3i}^3\end{aligned}\quad (17)$$

This is, indeed, remarkable considering that the individual scatterplots hardly reveal any such relationships. A plot of transformed  $y_i$  versus the sum of transformed  $x_{1i}$ ,  $x_{2i}$  and  $x_{3i}$  is shown in Fig. 1h. The relationship can be fitted approximately by

$$\theta^*(y_i) \cong \phi_1^*(x_{1i}) + \phi_2^*(x_{2i}) + \phi_3^*(x_{3i}) \quad (18)$$

which is exactly optimal.

We also applied generalized additive model (GAM) to the same synthetic example. The results were almost identical to ACE and hence, are not shown here. This is indicated by the bootstrap prediction error obtained with the ACE and GAM models as summarized in Table 1. The bootstrap approach to estimating prediction error involves generating  $B$  bootstrap samples, for each sample drawing independently and with replacement from the original data. The correlation model is rebuilt using each sample and then applied to the original as well as bootstrap sample to obtain estimates of apparent error and bias (optimism). The details can be found in Efron and Tibshirani (1993). Because of the similar performance characteristics of ACE and GAM, we have restricted to application of ACE model only in the examples discussed below.

### Correlating Petrophysical Data: North Robertson Unit, West Texas

This field example serves to illustrate the versatility of non-parametric transformations to incorporate mixed data types, categorical and continuous, into correlation. The data belongs to the North Robertson Unit (NRU) located in Gaines County, West Texas. This is a mature, highly heterogeneous, shallow shelf carbonate reservoir. The reservoir interval is about 1400 ft in gross thickness with 90% of the interval being dolostone having a complex pore structure. Because of the diagenetic modification of the pore structure, no obvious relationship between porosity and permeability can be established at NRU even when the data are separated based on the depositional environment (Davies and Vessel, 1996). However, definition of rock types based on pore geometry analysis shows good relationship between permeability and porosity within each rock type. This is shown in Figs. 2a through 2c. Figure 2d shows the data for all three rock types combined and as expected, the correlation  $R^2$  is reduced significantly.

Next, we apply non-parametric transformations to the data. Instead of having three separate correlation for the rock types, we can now correlate permeability directly to porosity and rock type. The transformations are shown in Figs. 3a through 3c. The optimal correlation is shown in Fig. 3d with an  $R^2$  of 0.74 as compared to 0.45 as shown in Fig. 2d. On fitting the individual transformations with simple functions, we can derive an equation describing permeability as a function of porosity and rock type:

$$\theta^*(k) = 1.0258 [\phi_1^*(RT) + \phi_2^*(\phi)] \quad (19a)$$

where the functional form describing  $\theta^*(k)$ ,  $\phi_1^*(RT)$  and  $\phi_2^*(\phi)$  are shown in Figs. 3a through 3c. Given a porosity and rock type, we use Eq. 19 to compute  $\theta^*(k)$ . The corresponding permeability can then be obtained from Fig. 3c or using the fitted equation

$$k^{0.5} = 0.077 + 0.559\theta^*(k) + 0.752[\theta^*(k)]^2 \quad (19b)$$

Table 2 compares bootstrap prediction error associated with permeability estimates using different methods. Three choices have been compared – a single correlation using all rock types, separate correlation for each rock type and the correlation equation developed using the non-parametric approach. As expected, the correlation combining all rock types (Fig. 2d) performs the worst. The correlation based on optimal transformation (Fig. 3d) not only outperforms individual rock type correlation but also collapses them into a single convenient equation.

### Data Integration: A Synthetic Example

We simulated a 2-D synthetic case which includes one primary and two secondary variables having the following non-linear relationship

$$y(u) = x_1^{3.5}(u) + x_2(u) + \varepsilon \quad (20)$$

where  $u$  is the location in 2-D space and  $\varepsilon$  is random Gaussian noise. The simulation grid size is 60 by 40. The secondary variables  $x_1$  and  $x_2$  are generated using the following models

$$\begin{aligned} x_1(u) &= 0.4 [0.75 t_1(u) + 0.25 t_2(u)] + 1.2 \\ x_2(u) &= 2.0 [0.25 t_1(u) + 0.75 t_2(u)] + 6.0 \end{aligned} \quad (21)$$

In Eq.21,  $t_1$  and  $t_2$  are two mutually orthogonal realizations both with zero mean and unit variance. They are generated by unconditional sequential Gaussian simulations using a spherical semivariogram model. The constants in Eq.21 were selected such that the two secondary variables will have a balanced effect on the primary variable.

Fig. 4a through Fig. 4c show grayscale maps of the simulated  $x_1$ ,  $x_2$  and  $y$ . We use this simulated  $y$  as known exhaustive reference. Next, 120 data points (5% of total) are obtained by sampling the exhaustive  $y$  data at a regular spacing. These sampled  $y$  data, together with the exhaustive secondary data ( $x_1$  and  $x_2$  at 2400 locations) are then used to estimate  $y$  values at unsampled locations.

The first step in using our proposed approach for data integration is to derive optimal transformations using the ACE algorithm. In the transformed space, the non linearity between primary and secondary variables is virtually eliminated resulting in a maximal correlation  $R^2=0.912$  as shown in Fig. 5.

The second and third steps are application of optimal transformations to the sampled  $y$  data and to all secondary data. Fig. 6 shows a grayscale map of the sum of transformed  $x_1$  and  $x_2$ . Notice that because of the strong correlation established between the primary and secondary variables through the optimal transformations, many of the features of the exhaustive  $y$ -data is already apparent here.

Next, we perform cokriging using Eq. 13 to estimate the transformed primary values at all locations. The final step is back transformation to the original space. Fig. 7 shows the estimated primary values by cokriging using the optimal transformation approach. The correspondence with the original exhaustive reference (Fig. 4c) is, indeed, very good. For comparison purposes, we also conducted traditional ordinary kriging and cokriging estimation without using any transformations.

Fig. 8a and Fig. 8b show the scatterplots of true  $y$  (exhaustive reference) versus estimated  $y$  by traditional ordinary kriging and cokriging. Fig. 8c show the scatterplot of true  $y$  versus estimated  $y$  by cokriging using the optimal transformation approach. The power of the optimal transformation is quite evident from these results. By incorporating optimal transformations, we have improved the



correlation  $R^2$  to 0.86 compared to 0.72 obtained by using traditional cokriging. As expected ordinary kriging performs the worst since the secondary data sets are not used.

The cokriging estimation without transformations is affected by the non-linearity between  $y$  and  $x_1$ . This is reflected in the concave upward shape in Fig. 8b. Furthermore, in order to use the cokriging estimator (Eq.10), six variance functions are required for this case as opposed to three when optimal transformations are used, both assuming symmetry in cross covariance functions. Table 3 presents a quantitative comparison of the statistics of error distribution. The results clearly indicate the superiority of our proposed approach as evidenced by the small standard deviation of error distribution obtained using the optimal transformations.

We also performed indicator cosimulation using Markov-Bayes algorithm in conjunction with ACE transformations. Five cutoffs, corresponding to 10% 30%, 50% 70% and 90% of the c.d.f of the transformed dependent variable were used in these simulations. Figs. 9a and 9b shows two realizations of  $y$ . Both reproduce the features and statistics of the reference  $y$  very well. The use of ACE transformations greatly facilitates such indicator cosimulation process by reducing variance function calculations.

## Integration of Seismic Data: Stratton Field, South Texas

The Stratton field (Levey *et al.*, 1993) is located on the onshore South Texas Gulf Coast Basin. The Oligocene Frio formation is one of the largest gas productive interval. The middle Frio formation is characterized by a relatively gentle subsurface domal closure. It contains multiple stacked pay sandstones within a series of vertically stacked reservoir sequences referred to as the B-, C-, D-, E-, and F-series.

The available data for this study include 3-D seismic reflections and well log data from a two square-mile area of the Stratton field (Fig. 10). The seismic data consists of 100 inlines and 200 crosslines with a trace spacing of 55 ft in each direction. The well log data are from 21 wells. A zero offset vertical seismic profile (VSP) is available and used for establishing a correlation between the stratigraphic depth and seismic travel time (Fig. 11). The seismic and well log data are utilized to derive an integrated description of reservoir properties in the subject area using the proposed approach.

We selected F11 reservoir (Fig. 11) for our detailed study since it is thick and easy to be traced from seismic reflections in the study area. Our objective is to estimate pore footage ( $h \cdot \phi$ ) in the study area using the data from well logs as the primary data set and multiple seismic attributes from 3-D seismic reflections as the secondary data set.

The reservoir properties, mainly reservoir thickness and porosity, for various reservoir facies in the middle Frio formations in 21 wells are estimated using SP, neutron porosity, and density log following the approach reported in Levey *et al.* (1993). Time horizons corresponding to reservoir zones are picked from the 3-D seismic data. Three type of seismic attributes, viz. average seismic amplitude  $A_{AVG}$ , maximum amplitude  $A_{MAX}$ , and root mean square amplitude  $A_{RMS}$ , are extracted. Altogether 72 pairs of pore-footage data from middle Frio reservoirs (B to F series) in 21 wells with corresponding nearby seismic attributes are selected for the data calibration. Fig.12a through Fig.12c show the scatterplot of pore footage from wells versus seismic  $A_{AVG}$ ,  $A_{MAX}$ , and  $A_{RMS}$ . The highest linear correlation  $R^2=0.302$  is between pore footage and average amplitude. Such a low correlation between pore footage and seismic attributes is not unusual considering the thickness of the sandstone zone, variations in lithology and fluid content, and data noise.

Optimal transformations are derived based on this data set using the ACE algorithm. Fig. 12d is a scatterplot of the transformed pore footage versus the sum of transformed seismic attributes. The correlation  $R^2$  is improved to 0.465 ( $\rho=0.68$ ) after transformations. This is quite significant in view of the scatter in the original data.

Fig. 13 shows the grayscale map of one of the seismic attributes,  $A_{AVG}$  corresponding to reservoir F11. Three such seismic attributes  $A_{AVG}$ ,  $A_{MAX}$ , and  $A_{RMS}$ , comprise of our secondary data set whereas the pore footage at the wells are the primary data. We transformed all these seismic attributes and 21 pore-footage data using optimal transformations. Finally, we conducted a collocated

cokriging estimation for transformed  $h^*\phi$  at all grid locations. A grayscale map of the estimated  $h^*\phi$  by collocated cokriging after back transformation is shown in Fig. 14.

For comparison, we also conducted an ordinary kriging on  $h^*\phi$  data from the 21 wells and the results are shown in Fig. 15. Notice the severe smoothing effects of the ordinary kriging and the lack of detail between the wells because of the absence of secondary information.

## SUMMARY AND CONCLUSIONS

1. Non-parametric transformation techniques offer a powerful, versatile, and fully automated tool for building correlations for petrological variables. Such transformations, being totally data driven, provide a direct approach to identifying functional relationships between dependent and independent variables during multiple regression.

2. The power of non-parametric techniques lie in its ability to directly incorporate multiple and mixed variables, both continuous and categorical, into correlation. Moreover, the transformations are computationally efficient, easy to use and can provide significant insight during exploratory data analysis.

3. We have presented synthetic and field examples to demonstrate the application of non-parametric transformation techniques for data correlation. A comparison of bootstrap prediction error clearly reveals the superiority of such techniques compared to conventional methods.

4. Cokriging or cosimulation of multiple attributes is considerably simplified when carried out in conjunction with non-parametric transformations. The use of optimal transformations exploits the secondary data to its fullest potential and also allows for non-linearity between reservoir properties and seismic attributes.

5. The proposed data integration method greatly facilitates non-Gaussian cosimulation through the use of indicator approaches, particularly when multiple secondary variables are involved because of a significant reduction in variance function calculations.

6. Synthetic case study clearly shows that cokriging and collocated cokriging using optimal transformation is far superior to ordinary kriging and cokriging in reproducing exhaustive reference data. The field case study demonstrates its capability of integrating multiple seismic attributes with well data for reservoir characterization.

## ACKNOWLEDGMENT

We would like to thank Drs. Mohan Kelkar and Xuri Huang at the University of Tulsa for their help in acquiring some of the field data. This work has been partially funded by a grant from the Mathematical Sciences Division of the National Science Foundation.

## REFERENCES CITED

- Almeida, A., 1993, Joint simulation of multiple variable with a Markov-type coregionalization model: Ph.D Dissertation, Stanford University, Stanford, CA.
- Breiman, L. and J. H. Friedman, 1985, Estimating optimal transformations for multiple regression and correlation: *Journal of the American Statistical Association*, v. 80, No. 391, p.580.
- Buja, A., Trevor Hastie, and Robert Tibshirani, 1989, Linear smoothers and additive models: *The Annals of Statistics*, v. 17, p.453-510.
- Crogh, A., 1996, Improved correlations for retrograde gases, MS Thesis, Petroleum Engineering, Texas A&M.
- Davies, D. K. and R. K. Vessel, 1996, Flow unit characterization of a shallow shelf carbonate reservoir: North Robertson Unit, West Texas, SPE/DOE 35433 in proceedings of the SPE/DOE 10<sup>th</sup> Symposium on Improved Oil Recovery.

- Efron Bradley and Robert Tibshirani, 1993, An introduction to the Bootstrap: New York, Chapman and Hall, 436 p.
- Emerson, J. and M. Stoto, 1982, Exploratory methods for choosing power transformations: Journal of the American Statistical Association, v. 77, No. 377, p. 103-108.
- Friedman, J. H. and W. Stuetzle, 1981, Projection pursuit regression, Journal of the American Statistical Association, v. 76, No. 376, p.817.
- Friedman, J.H. and W. Stuetzle, 1982, Smoothing of scatterplots," Technical Report ORION006, Dept. of Statistics, Stanford University, California.
- Friedman, J. H. and B. W. Silverman, 1989, Flexible parsimonious smoothing and additive modeling, Technometrics, v. 31, No. 1, p. 3-20.
- Hald, A, 1952, Statistical theory with engineering applications, John Wiley and Sons, New York.
- Hastie, Trevor and R. Tibshirani, 1990, Generalized Additive Models: London, Chapman and Hall, 335 p.
- Jensen, J. L. and L.W. Lake, 1985, Optimization of regression-based porosity-permeability predictions: CWLS 10th Symposium, Calgary, Alberta, Canada, Sep. 29-Oct. 2, 1985.
- Journel, A.G. and F. G. Alabert, 1990, New method for reservoir mapping, Journal of Petroleum Technology (February), p. 212-218.
- Levey, R.A., et al., 1993, Secondary natural gas recovery: targeted technology applications for infield reserve growth in fluvial reservoirs, Stratton Field, South Texas: Topical Report, GRI Contract No. 5088-212-1718, Gas Research Institute, Chicago, Illinois, 244 p.
- Li, D, 1995, Scaling and upscaling of fluid flow through permeable media: Ph.D Dissertation, University of Texas, Austin, Texas, 302 p.
- Tibshirani, R., 1988, Estimating optimal transformations for regression via additivity and variance stabilization, Journal of American Statistical Association, V. 82, p. 559-568.
- Venables, W.N. and B. D. Ripley, 1994, Modern Applied Statistics with S-Plus: New York, Springer-Verlag, p. 247-261.
- Wendt, W.A., S. Sakurai., and P.H. Nelson, 1986, Permeability prediction from well logs using multiple regression: in Reservoir Characterization, Edited by Lake, L.W. and Carroll, H.B. Jr., Academic Press, Inc. Orlando, Florida, 659 p.
- Xue, G., A. Datta-Gupta, P. Valko, and T. Blasingame, 1996(a), Optimal transformations for multiple regression: application for permeability estimation from well logs, SPE/DOE 35412 in proceedings of the SPE/DOE 10<sup>th</sup> Symposium on Improved Oil Recovery.
- Xue, G., A. Datta-Gupta, 1996(b), A new approach for seismic data integration using optimal non-parametric transformations, SPE 36500 in proceedings of the 1996 SPE Annual Technical Meeting and Exhibition.
- Zhu, H. and A. Journel, 1992, :Formating and integrating soft data: stochastic imaging via the Markov-Bayes algoritm: in Geostatitics Troia'92, edited by A. Soares, Kluwer Academic Publishers, Dordrecht, The Netherlands, p. 1-12.

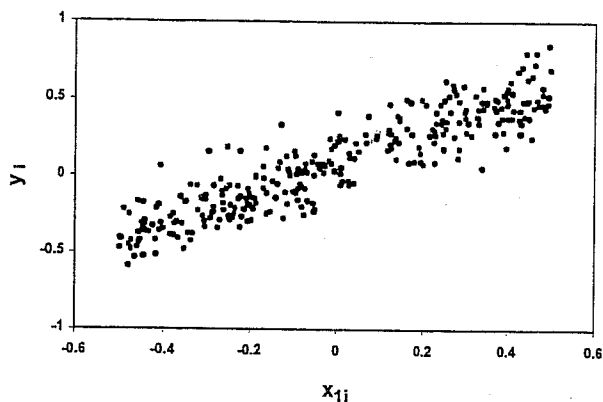


Fig. 1a-Scatterplot of  $y_i$  vs.  $x_{1i}$  simulated from multivariate model  $y_i = x_{1i} + x_{2i}^2 + x_{3i}^3 + 0.1\varepsilon_i$ , where  $x_{1i}$ ,  $x_{2i}$ , and  $x_{3i}$  are independently drawn from uniform distribution  $U(-0.5, 0.5)$ , and  $\varepsilon_i$  is independently drawn from standard normal distribution  $N(0, 1)$ .

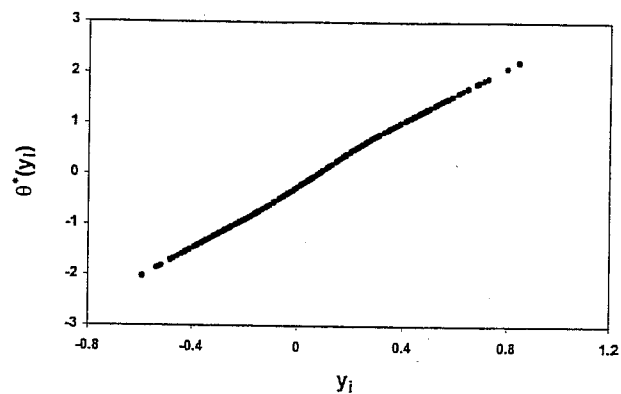


Fig. 1d-Optimal transformation of  $y_i$  by ACE.

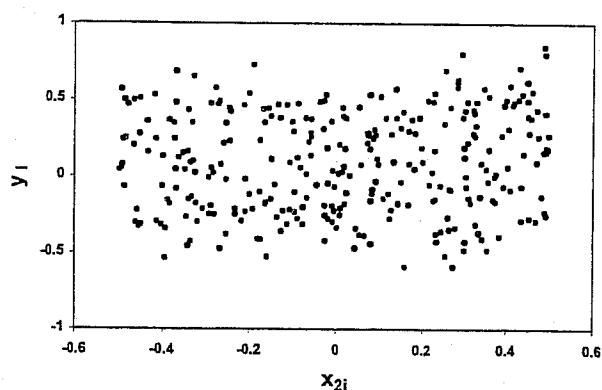


Fig. 1b-Scatterplot of  $y_i$  vs.  $x_{2i}$  simulated from multivariate model  $y_i = x_{1i} + x_{2i}^2 + x_{3i}^3 + 0.1\varepsilon_i$ .

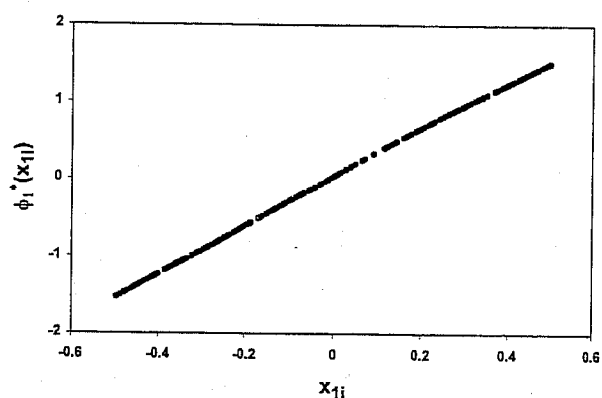


Fig. 1e-Optimal transformation of  $x_{1i}$  by ACE.

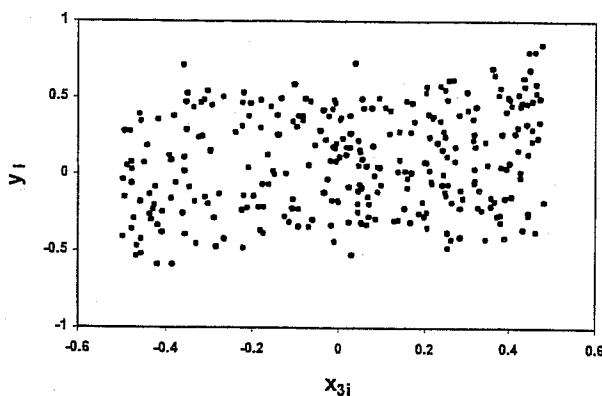


Fig. 1c-Scatterplot of  $y_i$  vs.  $x_{3i}$  simulated from multivariate model  $y_i = x_{1i} + x_{2i}^2 + x_{3i}^3 + 0.1\varepsilon_i$ .

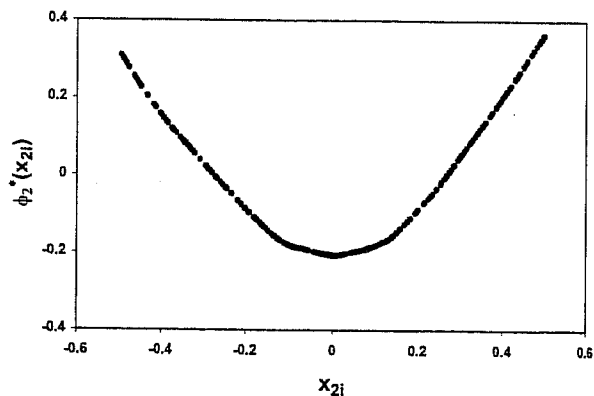


Fig. 1f-Optimal transformation of  $x_{2i}$  by ACE.

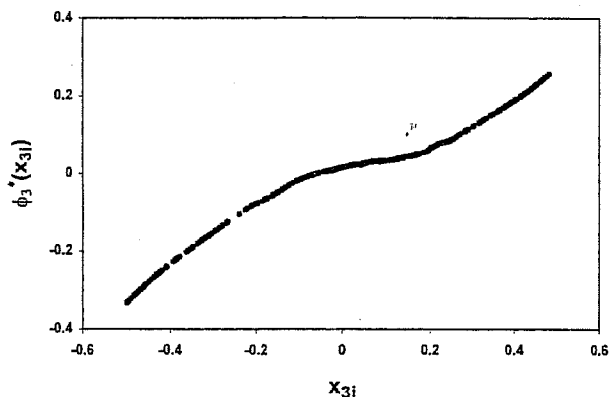


Fig. 1g-Optimal transformation of  $x_{3i}$  by ACE.

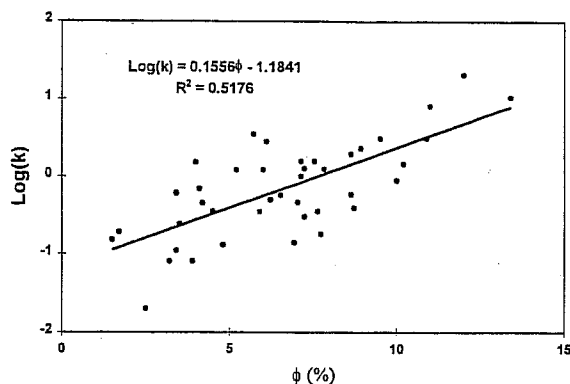


Fig. 2b-Logarithmically transformed permeability vs. core porosity of rock type 2. The solid straight line represents a linear regression of the data.

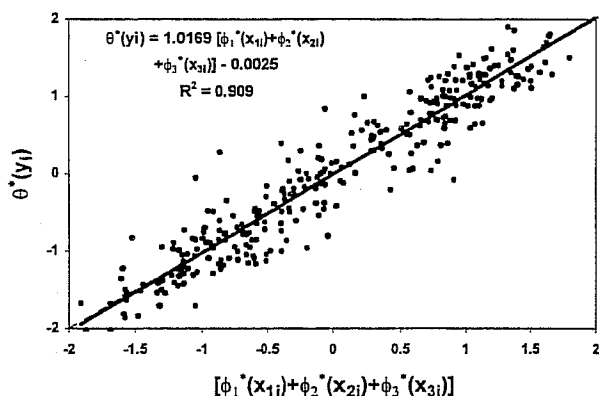


Fig. 1h-Optimal transformation of  $y_i$  vs. the sum of optimal transformations of  $x_{1i}$ ,  $x_{2i}$ , and  $x_{3i}$ . The solid straight line represents a linear regression of the data.

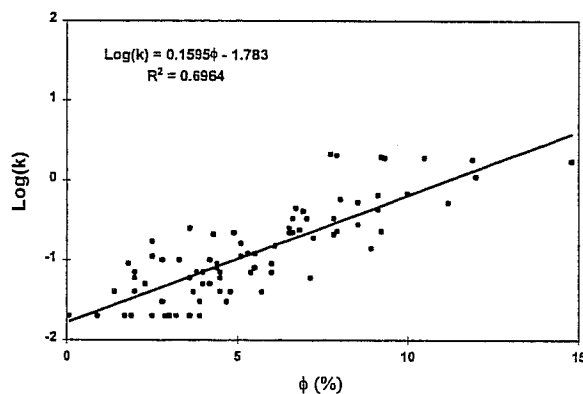


Fig. 2c-Logarithmically transformed permeability vs. core porosity of rock type 3. The solid straight line represents a linear regression of the data.

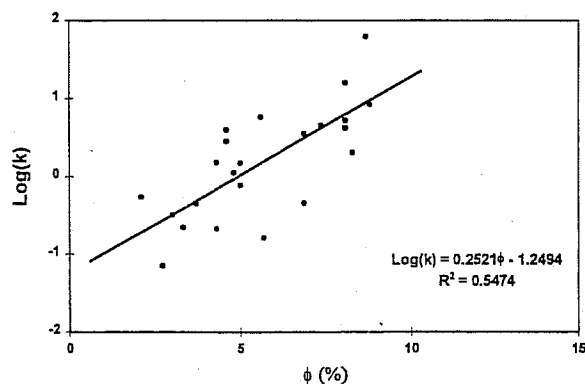


Fig. 2a-Logarithmically transformed permeability vs. core porosity of rock type 1. The solid straight line represents a linear regression of the data.

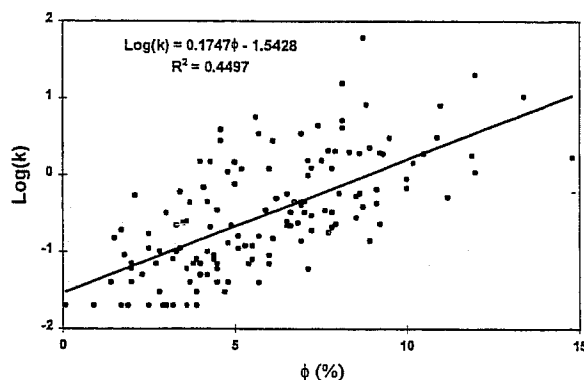


Fig. 2d-Logarithmically transformed permeability vs. core porosity of all rock types (rock type 1,2,&3). The solid straight line represents a linear regression of the data.

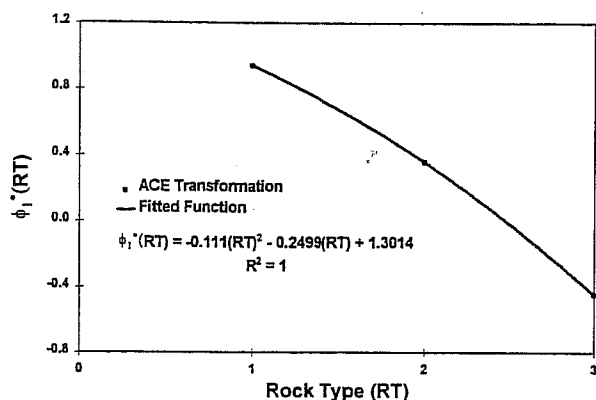


Fig. 3a-Optimal transformation of rock type by ACE . The solid line represents a fitted function.

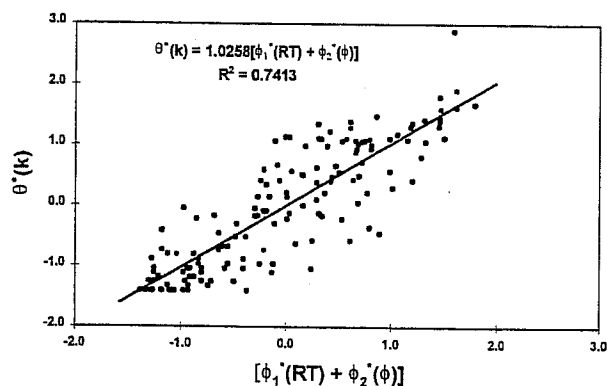


Fig. 3d-Optimal transformation of permeability vs. the sum of optimal transformations of rock type and porosity. The solid line represents a linear regression of the data.

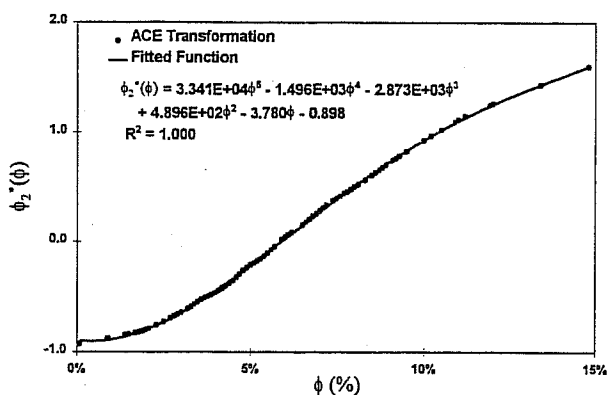


Fig. 3b-Optimal transformation of porosity type by ACE . The solid line represents a fitted function.

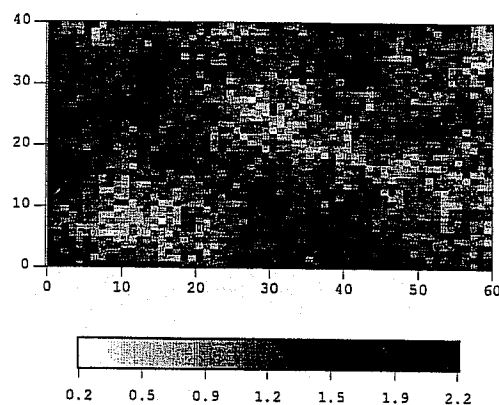


Fig. 4a-Grayscale map of simulated  $x_1$ . The simulation grid is 60 by 40.

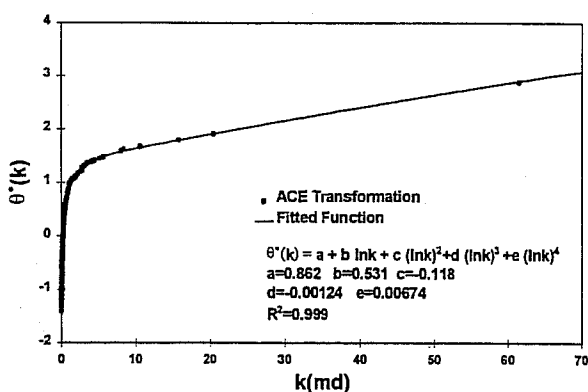


Fig. 3c-Optimal transformation of permeability by ACE . The solid line represents a fitted function.

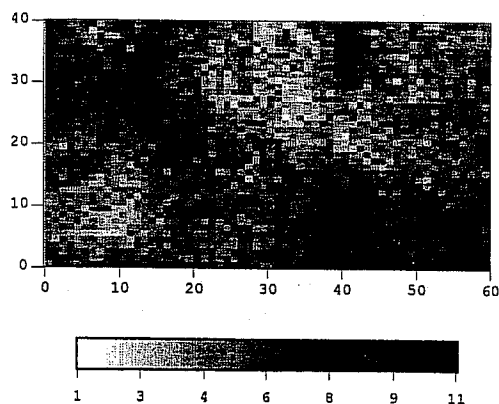


Fig. 4b-Grayscale map of simulated  $x_2$ .

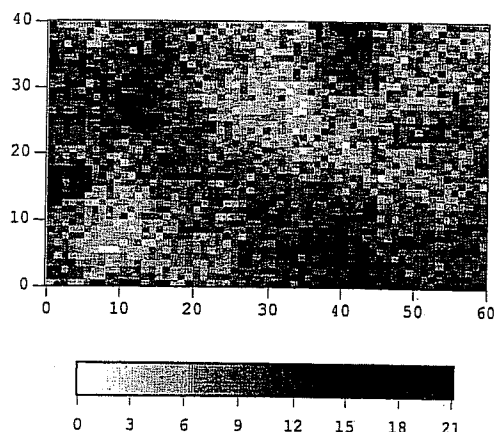


Fig. 4c-Grayscale map of simulated y.

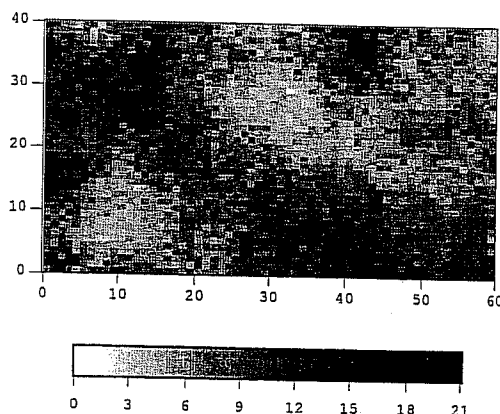


Fig. 7-Grayscale map of the estimated y by collocated cokriging using optimal transformations.

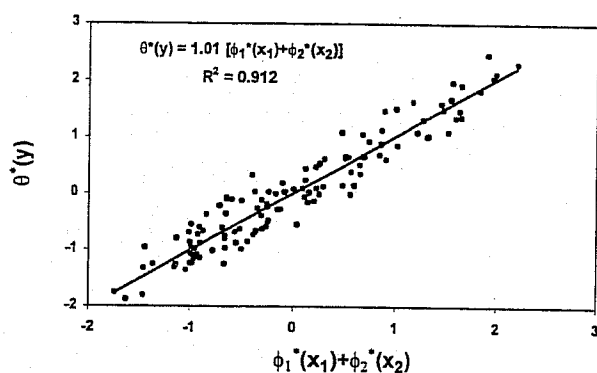


Fig. 5-Optimal correlation between primary (y) and secondary variables ( $x_1$  and  $x_2$ ) as derived by ACE. The solid line represents a linear regression of the transformed data.

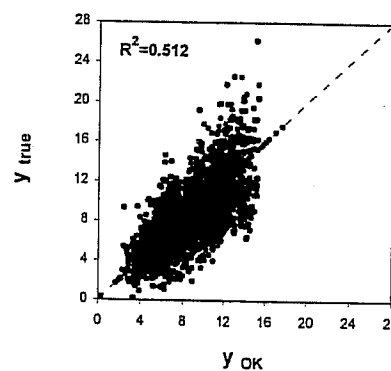


Fig. 8a-True y (reference) vs. the estimated y by ordinary kriging without using transformations. Secondary variables are not used.

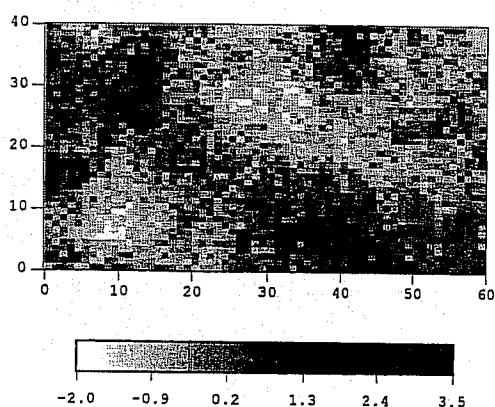


Fig. 6-Grayscale map of the sum of transformed  $x_1$  and  $x_2$ .

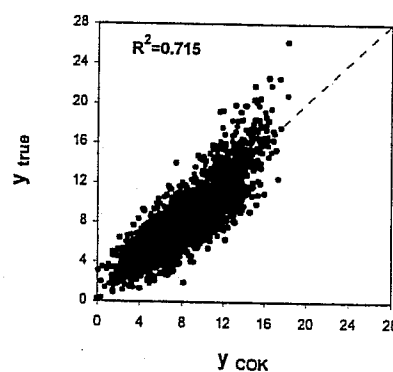


Fig. 8b-True y (reference) vs. the estimated y by cokriging without using transformations.

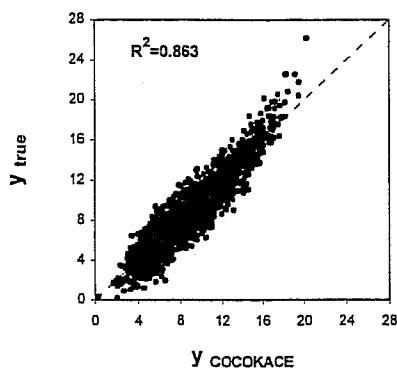


Fig. 8c-True y (reference) vs. the estimated y by collocated cokriging using optimal transformations by ACE.

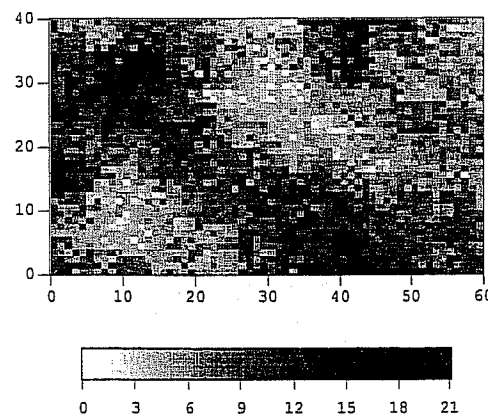


Fig. 9b-Grayscale map of y by indicator cosimulation using Markov-Bayes algorithm in conjunction with ACE. Realization 2.

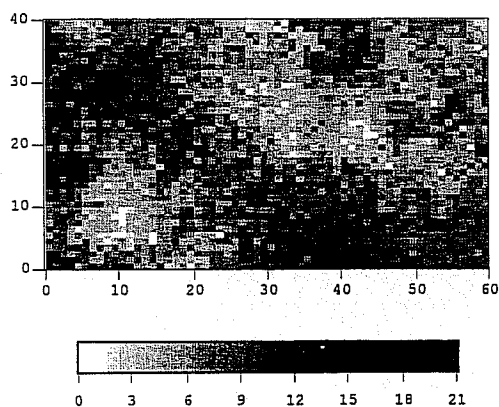


Fig. 9a-Grayscale map of y by indicator cosimulation using Markov-Bayes algorithm in conjunction with ACE. Realization 1

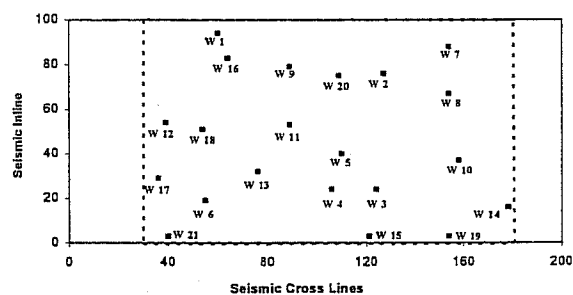


Fig. 10-3-D seismic survey and well location for the study area, Stratton field, South Texas. The dotted framed area is the mapping area.

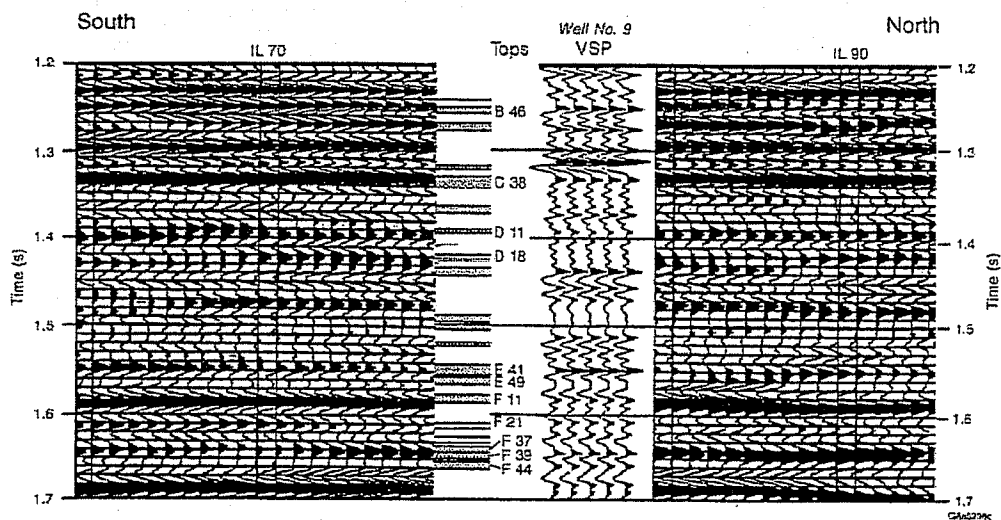


Fig. 11-Calibration of reservoirs using the vertical seismic profiles (VSP) in well 9. Notice the position of F11 reservoir used for the detailed study (Levey, et al., 1993).



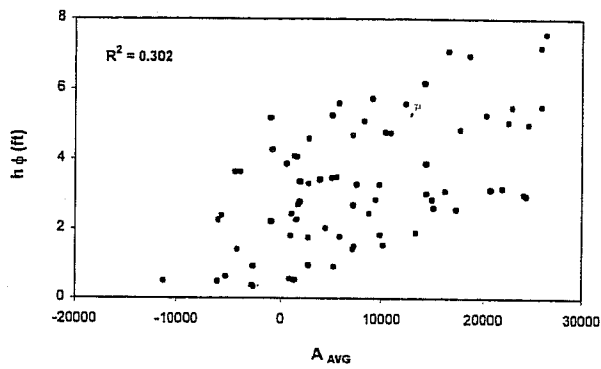


Fig. 12a-Pore footage vs. average seismic amplitude  $A_{AVG}$ .

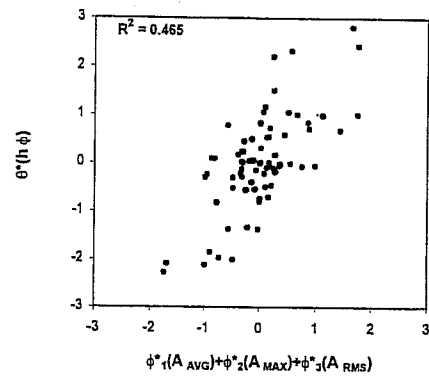


Fig. 12d-Optimal correlation of pore footage vs. seismic attributes as derived by ACE.

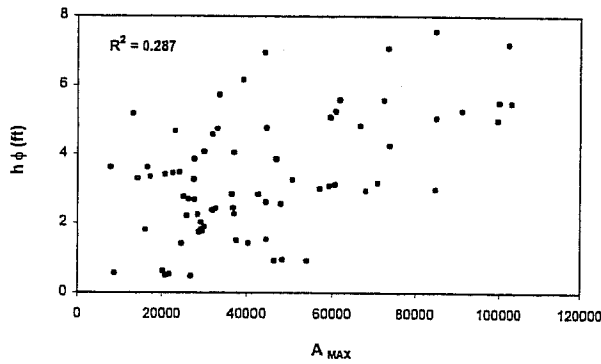


Fig. 12b-Pore footage vs. maximum seismic amplitude  $A_{MAX}$ .

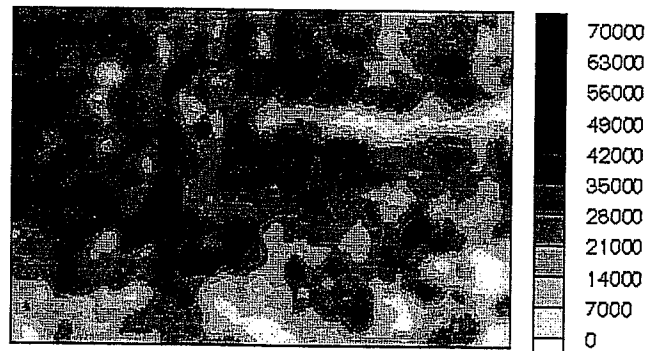


Fig. 13-Grayscale map of the average seismic amplitude  $A_{AVG}$  distribution corresponding to F11 reservoir.

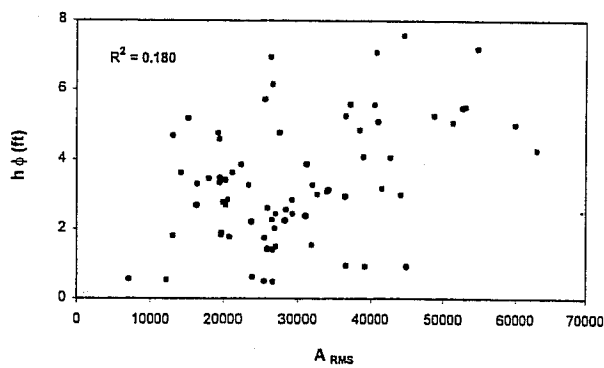


Fig. 12c-Pore footage vs. RMS seismic amplitude  $A_{RMS}$ .

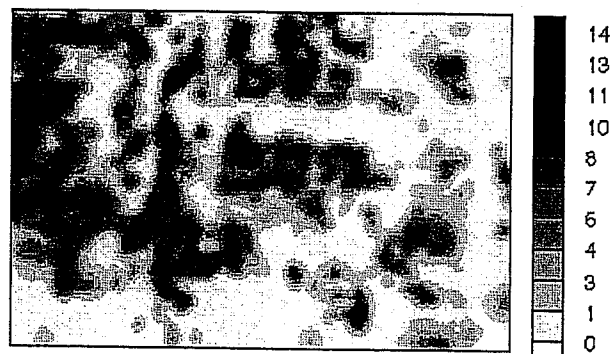


Fig. 14-Grayscale map of the estimated pore footage by collocated cokriging using optimal transformation by ACE.

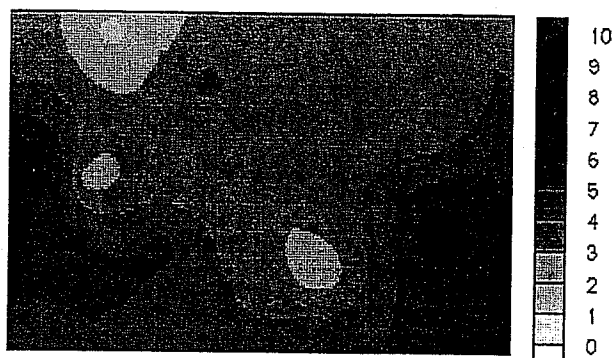


Fig. 15-Grayscale map of the estimated pore footage by ordinary kriging from well data alone.

Table 3. Summary Statistics for Error Distributions of  $y$  Estimated by Various Estimators

$ y_{\text{TRUE}} - y_{\text{EST}} $	Ordinary Kriging	Cokriging	Cokriging using ACE
Minimum	0.00	0.00	0.00
Maximum	11.07	7.95	5.91
Mean	1.86	1.44	1.00
Standard Dev.	1.58	1.20	0.80

Table 1. Bootstrap Estimates of Prediction Error (50 Bootstrap Replications)  
(Synthetic Example:  $y_i = x_{1i} + x_{2i} + x_{3i} + 0.1\epsilon_i$ )

Prediction error	ACE	GAM
Apparent error	0.009720	0.009308
Optimism	0.000379	0.000607
Total error	0.010099	0.009915

Table 2. Bootstrap Estimates of Prediction Error (100 Bootstrap Replications)  
(North Robertson Unit, West Texas)

Prediction error	Logarithmic Model with all Rock Types	Logarithmic Models for Individual Rock Types	ACE with all Rock Types
Apparent	28.9099	22.2025	23.5064
Optimism	0.5808	5.0077	2.3199
Total error	29.4907	27.2102	25.8263

,

# **A New Approach to Integrate Seismic and Production Data in Reservoir Models**

Ahmed Ouenes, Adwait Chawathé, William Weiss  
Petroleum Recovery Research Center, New Mexico Tech  
Socorro, New Mexico 87801 USA

Brian Cebull  
Nance Petroleum Corporation  
Billings, Montana, USA

## **ACKNOWLEDGMENTS**

This research was funded through the Advanced Reservoir Management project at Los Alamos National Laboratory. The authors greatly appreciate the financial support. The Petroleum Recovery Research Center authors would like to thank Nance Petroleum for providing the data and the continuous support for the project. The authors would like to thank James R. Ehrets and Beverly Blakeney DeJarnett for sharing their Nisku experience.

## **ABSTRACT**

A great deal of effort is devoted to reducing the uncertainties in reservoir modeling. For example, seismic properties are used to improve the characterization of interwell properties by providing porosity maps constrained to seismic impedance. Another means to reduce uncertainties is to constrain the reservoir model to production data. This paper describes a new approach where the production and seismic data are simultaneously used to reduce the uncertainties. In this new approach, the primary geologic parameter that controls reservoir properties is identified. Next, the geophysical parameter that is sensitive to the dominant geologic parameter is determined. Then the geology and geophysics are linked using analytic correlations. Unfortunately, the initial guess resulted in a reservoir model that did not match the production history. Since the time required for trial and error matching of production history is exorbitant, an automatic history matching method based on a fast optimization method was used to find the correlating parameters. This new approach was illustrated with an actual field in the Williston Basin. Upscaling problems do not arise since the scale is imposed by the size of the seismic bin (66m, 219 ft) which is the size of the simulator gridblocks.

## **INTRODUCTION**

The wide availability of 3D seismic and the fast development of 4D seismic brings new insights to the reservoir and creates new challenges in reservoir modeling. Since the interpretation of 3D/4D seismic data requires geologic input, and the use of 4D seismic in the modeling process must include a reservoir simulator; it appears that the full integration of geology, geophysics, and reservoir

engineering is becoming an urgent necessity. To respond to this need, there are few tools and methodologies that can be used, at this moment, to create integrated reservoir models that honor geology, geophysics and production history simultaneously. Historically, these three disciplines did not have many opportunities for mixing and cross-linking.

Three distinct stages can be identified from a reservoir modeling perspective. During the first stage (60s and 70s), reservoirs were considered as challenging mathematical inverse problems where the objective was to find a set of reservoir parameters (porosity, and permeability mainly) that matched past production performance. During this stage, the emphasis was on the mathematical optimization algorithms. Geologic and geophysical data was not a concern, and the scale considered was the reservoir simulator scale.

In the second stage (mid 80s to present), geostatistics was introduced in reservoir modeling. As a consequence, geologic constraints are honored in reservoir models and the scale considered becomes very small (log and core scale). This drastic reduction in scale led to reservoir models with a few million gridblocks which could not be simulated on a practical time scale. Hence, the issue of upscaling became crucial. The objective of upscaling algorithms is to derive a model that has a reasonable number of reservoir gridblocks and at the same time maintains the geologic and statistical properties of the original system. The important characteristic of this stage was the total absence of reservoir simulators during the modeling process. Reservoir simulation was used "downstream" where multiple geostatistical realizations were tested to bracket the uncertainties. Unfortunately, the range of production forecasted by the multiple geostatistical realizations could be very wide, therefore not very helpful when it came to identifying a new infill location or an optimal waterflood pattern. As a result, dynamic and seismic data became the primary constraints to be added to the reservoir model in order to reduce the range of the uncertainties.

During the third stage (early 90s to present), various researchers focused on different types of dynamic data to add as a constraint in reservoir modeling. Two approaches were proposed: the near wellbore (Deutsch, 1992, Chu et al., 1995) and the fieldwide approach (Sultan et al., 1993, Hird, 1993, Ouenes et al., 1994a). In the near wellbore approach, various methodologies were proposed to constrain geostatistical realizations with pressure transient data. Unfortunately, this approach improves the reservoir description only around the well providing the pressure data. In the second approach, production data from many wells were considered as a constraint. Both these approaches resuscitate the various optimization and computing problems encountered during the 1960-70s when reservoir modeling was mainly an inverse problem. But many aspects in solving inverse problems have changed in the last two decades. The major difference with the past is that; today, there are more efficient optimization algorithms running on faster computers. Furthermore, the availability of 3D and 4D seismic data brings additional information to solving the inverse problem. In the past, the increase of available data was "cursed" since it was viewed as an additional history matching or optimization constraint.

This paper describes a new approach that views seismic data as a "blessing" since it has been used to: 1) honor the geologic features, 2) reduce the number of optimization parameters considerably,

and 3) provide reservoir models that honor performance history.

## BACKGROUND

Until recently, the integration of seismic data in reservoir models was viewed from a geostatistical perspective (Doyen and Guidish 1992, Chambers et al., 1995). The large difference in scales between core (or log) and seismic data makes the integration of 3D seismic data in fine scale geostatistical models a challenging exercise. The question of how to upscale the geostatistical information to the scale of seismic data remains to be answered. Another direct approach to using 3D seismic data is identifying correlations between petrophysical and geophysical reservoir properties. Despite the problem of scale, this approach is commonly used and is available in commercial software. Although there is no doubt that the seismic response depends on reservoir properties, the problem is to find the underlying relationship at the considered scale. Recently, Chawathé et al. (1996) proposed a neural network approach to find the complex relationship that exists between seismic and log data. In contrast to previous work, the problem of scale does not exist since crosswell tomography was used as seismic information to map a reservoir property between two wells. This work indicates that even without the scale problem, the relationship between seismic and log data is very complex. The addition of scale problems worsen the task of relating log or core data to 3D seismic information. Based on these observations, another approach that circumvents the scale problems provides an alternative direction for reservoir modeling.

It is important to realize that the size of bins (few hundred feet) used in seismic surveys are similar to the size of gridblocks used in reservoir simulators. Hence, mathematical reservoir description may be viewed at the reservoir simulation scale which coincidentally is also the seismic scale. Furthermore, the availability of seismic data over the entire reservoir volume represents a distinct advantage over the geostatistical approach where the interwell properties are estimated. Based on these observations, it becomes clear that there is a perfect fit between production and seismic data. The problem is to find methodologies that can allow the integration of the two valuable pieces of information. Before describing the existing methodologies and a proposed new one, it is important to identify the main component of such an approach.

The main characteristic of these methodologies is the necessity to include a reservoir simulator and an iterative mechanism when searching for the optimal reservoir model. Although this is not new to reservoir modeling, it has been avoided due to lengthy computation times. However, in our experience using automatic history matching algorithms (Ouenes et al. 1994, Weiss et al. 1995) on actual reservoir studies leads to a considerable reduction in time delivering results and helping oil producers in their reservoir management strategies. The few minutes or hours required to generate a few geostatistical realizations is short compared to reservoir simulation times measured in days. However, when preferably comparing few days of simulation to six months for completing an entire reservoir study (which must include a history match of all the producing wells) simulation times are almost insignificant. Furthermore, by following some general guidelines described in the next sections, the total computation time can be considerably reduced.

Recently Huang and Kelkar (1996) proposed a technique to integrate seismic and production data. In their approach, the porosity map was constrained to seismic impedance. The permeability field, in turn, was derived from the porosity-permeability scatter plot. An iterative process that uses a heuristic optimization method was used to find the best permeability realization which led to the history match of bottom hole pressure at producing wells. As a result, the reservoir model honors seismic (impedance), geology (porosity-permeability correlation), and production data (bottom hole pressures).

## PROPOSED METHODOLOGY

The main characteristic of the proposed methodology is the emphasis given to geologic and geophysical interpretation of the data. The reservoir model becomes an integration tool where the geologists' and geophysicists' ideas are confronted by the reality of production history.

The methodology starts by a geologic study of the reservoir. The most plausible depositional environment must be identified. Furthermore the diagenetic factors that control reservoir quality must be isolated. In practice, the geologist proposes one or more primary geologic parameters that control the reservoir quality. This could be the volume of shale, the amount of anhydrite, the degree of dolomitization, or any other diagenetic factor. Since, the available information is often scarce, the initial geologic models may be approximate and incomplete. The proposed approach allows for re-evaluation of geologic interpretations.

After defining the geologic model and the primary geologic parameters, the geophysicist will try to identify the primary geophysical parameter. This is defined as the seismic measurement that is the most sensitive to the primary geologic parameter. Very often the acoustic impedance is used as an indicator of porosity and can be considered as a primary geophysical parameter. The Poissons ratio can be also a good indicator of changes in lithology. Hence, primary geologic parameters tightly related to lithology could benefit more from Poissons ratio if it is considered the primary geophysical parameter. In general, the choice of the primary geophysical parameter will depend on the availability of data and the type of reservoir considered.

The next step in this methodology is to define correlations between the primary geologic, geophysical parameters and the rock properties required in reservoir simulation (porosity, permeability, and initial fluid saturations). The analytical functions used to define the correlations depend on the type of parameters, and the amount of data available to build an initial estimate. The assumed correlations will include unknown coefficients to be estimated during the history matching process. The advantages of using correlations are two fold: first, the relationship between geologic, geophysical and reservoir properties is described quantitatively, and second is the considerable reduction of unknown coefficients in the history matching process. On the other hand, the disadvantage of the correlations is an oversimplification of the complex relationships that exist between primary geologic and geophysical parameters and reservoir properties. The proposed methodology is a trade-off between these advantages and disadvantages. This trade-off is illustrated with an application to a complex carbonate reservoir located in the Williston Basin (Montana).

## UNDERSTANDING RESERVOIR GEOLOGY

The considered oil reservoir is located in Northeast Montana and eight wells have been producing since 1979 from the Winniepegosis and Red River formations. Only a single well was completed in the Nisku formation which is about 2000 ft above the Red River. This well produced 125,000 bbl from the Nisku during its first 41 months. Since operating conditions inhibit dual completions and Nisku wells cost almost a million dollars, the need for a Nisku reservoir development plan is apparent. The size of the reservoir and optimum well density are the key unknowns. Recognizing the need for additional Nisku data, a 5000 acre 3-D seismic survey was conducted and processed. In addition to the seismic data, the open hole logs of the eight Red River wells provided reservoir thickness, porosity, and water saturation in the Nisku formation. Pressure data from drill stem tests and transient test were available at four wells at four different time periods. Due to sparse well coverage, and the lack of Nisku producing wells, there was a need to develop a methodology to integrate all the available data into a reservoir model.

The upper Devonian (late Frasnian) Nisku formation is found in Western Canada (Birdbear) and in the Williston Basin. The first fields producing from this formation date back to 1939 in Alberta (Canada). From the mid 1970s to mid 80s, new discoveries were made in the US, mainly in Montana. Although there are some general features common to the Nisku found in Western Canada and Montana, the formation exhibits some specific features in Montana. In eastern Montana, the Nisku produces from platformal buildups (Blakeney and Eby, 1988). The Nisku formation is described as a shallowing-upward carbonate/evaporate sequence with open marine dolomitic wackestones grading up into supratidal laminated dolomites and anhydrites. Nisku carbonates have been completely dolomitized. Ehrets and Kissling (1985) suggested that  $Mg^{++}$  enriched brines expelled from overlying evaporites during burial compaction provided the dolomitizing fluids. Therefore, reservoir quality is entirely dependent on the process of dolomitization. Ehrets and Kissling (1985) proposed a dolomitization model that explains reservoir development through paleostructural control (Fig. 1). Recently, Whittaker and Mountjoy (1996) have also suggested a similar model where migration pathways for the dolomitization fluids (dense brines) were influenced by depositional facies and subsurface structures. As a result, Nisku reservoir exhibits some clear characteristics directly related to this dolomitization process. One of these characteristics is the occurrence of the Nisku reservoir around structural noses. However, the thickness and quality of the reservoir varies significantly along the structure. The studied reservoir thins in the updip direction in a similar way to East Kevin field (Blakeney and Eby 1988). Ehrets and Kissling (1985) have indicated that the thick porous intervals are clearly associated with the flanks of the structure where bank deposits are best developed. On the other hand, the structure high, where intertidal conditions prevailed and where bank facies are poorly developed, porosity is less developed. This situation is also found in the studied field. Based on these observations and the model shown in Fig. 1, it appears that the thickness and porosity are the primary geologic parameters. Furthermore, the structural depth seems to be directly related to the thickness and porosity. Thin reservoir and low porosity is found updip, while downdip thickness and porosity improves significantly. Hence, building a reservoir model depends on the knowledge of structure.



## LINKING GEOLOGY TO GEOPHYSICS

The eight existing wells in the considered reservoir were all drilled on the structure high. Hence, if a mapping method is used to obtain the Nisku structure it would indicate a flat structure since there is no control data down-dip. Fortunately, a 3D seismic survey shows a Nisku structure (Fig. 2) that corroborates the platformal buildup theory. The two-way travel time recorded in the seismic data was converted to depth using the available well control. Unfortunately, the Nisku is thin and less than the 3D seismic vertical resolution. As a result, seismic amplitude or impedance data cannot be considered as primary geophysical parameters. Hence, the only available seismic information that can be considered as primary geophysical parameters is the two-way travel time converted to depth.

The link between geology and geophysics occurs through empirical correlations which include the geologic (porosity and thickness) and geophysical parameters (seismic depth).

Based on the data available at eight wells, we assumed the following correlations:

$$h = a_h \log[\log(d)] + b_h \quad (1)$$

$$\phi = a_\phi \log[\log(d)] + b_\phi \quad (2)$$

where,  $\phi$ , is the reservoir porosity,  $h$ , is the Nisku pay thickness and,  $d$ , is the subsea depth. The choice of the analytical function  $\log(\log)$  is arbitrary. The apparent relationship existing between the geologic and geophysical parameters seems highly non-linear which prompted us to use the log transform twice.

The choice of an analytical expression to describe the complex relationship that exists between geologic and geophysical parameters is a major problem. Unfortunately, there is no evident solution. However it is worth keeping in mind a few remarks when designing these analytical relationships. First, most of rock properties tend to have non-linear relationships with seismic properties. Second, when using very limited data to find these relationships, it is safer to use the functions in the known range of the input variables, and extrapolation may be misleading. For example, when choosing Eq. 2 to describe the relationship between porosity and depth, we verified that the lower depth available in the 3D survey does not lead to porosity higher than 30%, and the relationship is used only for the known range of depth. The limitations of using correlations are balanced by the reduction in the number of unknowns,  $a$  and  $b$ , in Eqs. 1 and 2. The available data at the existing wells provide an initial estimate of these coefficients and finding their optimal value will require the use of production data.

## HONORING PRODUCTION DATA

The correlations defined in Eqs. 1 and 2, combined with the existing data at the eight wells, provides

an estimate for porosity and thickness over the entire reservoir. For a complete and more accurate description of the reservoir, the porosity and thickness maps when used in a black oil reservoir simulator must lead to a production performance that matches the actual production and pressure data. Finding the optimal distribution of porosity and thickness consists of finding the coefficients  $a$  and  $b$  used in the correlations described in Eqs. 1 and 2 that lead to the match of past performance.

The complete description of the reservoir model used as input in a simulator requires the knowledge of permeability and initial water saturation. Based on the available data, we defined two more correlations that describe permeability and initial water saturation as a function of the primary geologic parameter,  $\phi$ .

$$S_{wi} = \alpha_s \log[\log(\phi)] + b_s \quad (3)$$

$$k = 10^{(a_k \phi - b_k)} \quad (4)$$

Establishing the complete reservoir model consists of determining the eight coefficients  $a$  and  $b$  used in the four equations depicted in equations (1 to 4) by matching reservoir performance.

## HISTORY MATCHING

The history matching process consists of finding the reservoir model that honors the past performance of all the wells, in our case the production history of one well. In the petroleum industry, this time consuming process is usually performed by engineers who change reservoir properties such as permeability manually in the simulator. Sometimes, the final reservoir model may not honor the existing production and pressure history. In this study, history matching is done automatically by a computer and the engineers devote most of their time to analyzing the results. In this case, the history matching problem solved by the computer is the following:

Find the eight unknown parameters used in the four correlations, and the reservoir relative permeability curves, that will match the available production and reservoir pressure.

The computer starts with a set of initial values for all the unknown parameters and creates a reservoir model. This initial reservoir model is fed to a black oil simulator to predict the production and pressure. As expected, the initial reservoir model does not fit the production history. The mismatch between the actual and simulated production and pressure is used to compute the error  $E$ :

$$E = \omega_i^{gas} \sum_{j=months} (GR_j^s - GR_j^f)^2 + \omega_i^{water} \sum_{j=months} (WR_j^s - WR_j^f)^2 + \omega_i^{pressure} \sum_{j=months} (P_j^s - P_j^f)^2 \quad (5)$$

where  $GR$  is the monthly gas rate,  $WR$ , is the monthly water rate,  $P$  is the pressure, and  $\omega$  are the weighting factors. The superscript  $s$  corresponds to simulated values and  $f$  corresponds to the field data. At this stage, the computer adjusts and changes the values of some of the unknown parameters. These new values will lead to new maps of porosity, thickness, permeability, and initial water saturation that can be tested with the black oil simulator. After running the simulator for 41 months of available production, a new error  $E_i$  that measures the mismatch between actual and simulated data can be computed for the new reservoir model. This new error  $E_i$  is compared to the previous error obtained with the previous reservoir model. If the new error  $E_i$  shows improvements over the previous error, then the current parameters tested will be considered as the best, and further adjustments are implemented on them. On the other hand, if the new error  $E_i$  is higher than the initial error, the current parameters will be discarded and a new set of parameters will be tested again. This iterative process continues until a good match of the field history is obtained.

The process of adjusting the unknown coefficients automatically depends on the optimization method used. The choice of an optimization algorithm is crucial since it controls the quality of the history match and the time required to reach a good match. The user has the choice between heuristic and deterministic optimization methods. In deterministic methods, the adjustments of the unknown parameters follows a strict rule very often involving the use of gradients. In heuristic method, the new values tested at each iteration involve the use of some random numbers. Both approaches have advantages and disadvantages. Briefly speaking, deterministic methods can be very fast if the search direction for the new values is oriented towards the optimal values. Unfortunately, this situation does not occur at each iteration and causes the algorithm to be trapped in local minima which do not lead to a good match of the production data. On the other hand, heuristic methods do not have privileged search directions and adjust the unknown parameters based on random rules. This approach has the advantage of escaping local minima at the expense of a large number of trials. Based on our experience using simulated annealing in automatic history matching and other reservoir description problems (Ouenes et al., 1994b), we have found that new deterministic optimization methods (Møller, 1993) allow faster convergence and have no local minima problems.

### History matching results

Using an automatic history matching algorithm and a black oil simulator, 41 months of production of the first Nisku well was matched. The reservoir model comprised 4060 gridblocks. The producing oil rate was used as a constraint in the simulator and monthly gas (Fig. 3) and water (Fig. 4) rates were matched. The mismatch of water production during the early months is due to the fact that the simulator does not account for completion fluids, but the simulated water rate comprises the actual reservoir water production. In addition to the production history, four pressure data were available and were matched as closely as possible. In addition to the correlations described in Eqs 1-4, the history matching procedure led to the estimation of field relative permeability and capillary pressure curves. These curves are given in the analytic form expressed as:

$$k_{r_w} = 0.145 \left( \frac{S_w - S_{wi}}{1 - S_{or} - S_{wi}} \right)^{1.8} \quad (6)$$

$$k_{r_o} = 0.94 \left( \frac{1 - S_{or} - S_w}{1 - S_{or} - S_{wi}} \right)^{2.4} \quad (7)$$

$$P_c = 28.0 \left( \frac{1 - S_{or} - S_w}{1 - S_{or} - S_{wi}} \right)^3 - 10.0 \quad (8)$$

where,  $S_{or} = 0.25$  and  $S_{wi} = 0.092$ . All the coefficients used in the analytical forms (Eqs. 6-8) were included as estimation parameters for the automatic history matching algorithm. Based on the available production and pressure data, the proposed methodology leads to a reservoir model that honors all the existing data. When new information becomes available (additional wells), this reservoir model could be refined by adding the new production constraints. However, this process will be faster since a reasonable initial guess (current reservoir model) is available. The same approach may be used in 4D seismic, where after each seismic survey a new reservoir model could be derived and used as initial guess for the next model. The resulting reservoir model was used to evaluate reservoir size and oil in place as well as a variety of reservoir management strategies to maximize the oil recovery.

## CONCLUSIONS

In this paper, a new approach to integrate seismic and production data in reservoir models was proposed and applied to an actual reservoir. Based on the results presented, the following conclusions can be drawn:

1. The understanding of the depositional environment and diagenetic changes is necessary for finding primary geologic parameters which will be used in reservoir modeling.
2. The identification of primary geophysical parameters, sensitive to changes in the primary geologic parameters, is crucial in finding the best correlations between geologic and

geophysical data.

3. Analytic functions can be used to describe the relationships between geologic and geophysical data.
4. Automatic history matching algorithms may be used to completely define the geology-geophysics relationships and constrain the reservoir model to existing production data.
5. The methodology was illustrated on an actual field and provided a unique opportunity to develop a complete reservoir model with very limited data.

## REFERENCES CITED

Blakeney, B., and Eby, D.E., 1988, Upper Devonian Nisku formation at East Kevin field, Sweet grass Arch, Montana: in S. M. Goolsby and M.W. Longman, Occurrence and petrophysical properties of carbonate reservoirs in the Rocky Mountain Region, Rocky Mountain Association of Geologists, Denver, p. 121-128.

Chambers, R.L., Zinger, M.A., and Kelly, M.C., 1995, Constraining geostatistical reservoir descriptions with 3-D seismic data to reduce uncertainty: in J.M. Yarus and R.L. Chambers, Stochastic Modeling and Geostatistics: Principles, Methods, and Case Studies: AAPG Computer Applications in Geology, p. 143-158.

Chawathé, A., Ouenes, A., Weiss, W.W., 1996, Estimation of reservoir properties using fuzzy logic, neural networks and crosswell tomography: PRRC report No. 96-37 and in final report for DOE contract No DE-AC22-93BC14893.

Chu, L., Reynolds, A. C., and Oliver, D. S., 1995, Computation of sensitivity coefficients for conditioning the permeability field to well test pressure data: IN-SITU, 19, May.

Deutsh, C., 1992, Annealing techniques applied to reservoir modeling and the integration of geological and engineering (well test) data, Ph.D. dissertation, Stanford university, CA.

Doyen, P.M., Guidish, T.M., 1992, Seismic discrimination of lithology and porosity, a Monte Carlo approach: in Investigations in Geophysics, London, Society of Explo. Geophy. p. 243-250.

Ehrets, J.R., and Kissling D.L., 1985, Deposition, diagenesis and paleostructural control of Duperow and Birdbear (Nisku) reservoirs, Williston basin: in M.W. Longman et al., Rocky Mountain carbonate reservoirs - A core workshop, SEPM core workshop No 7, Golden, p. 183-216.

Hird, K.B. 1993, A conditional simulation method for reservoir description using geological and well performance constraints: Ph.D. dissertation, University of Tulsa, OK.

Huang, A., Kelkar, M., 1996, Reservoir characterization by integration of seismic and dynamic data: paper SPE/DOE 35415 presented at the tenth symposium on improved oil recovery, Tulsa OK 21-24 April.

Møller, M.F., 1993, A scaled conjugate gradient algorithm for fast supervised learning, Neural Networks, v. 6, p. 525-533.

Ouenes, A., Weiss, W., Richardson, S., Sultan, J., Gum, T., and Brooks, L., 1994a, A new method to characterize fractured reservoirs: application to infill drilling: paper SPE/DOE 27799 presented at the symposium on improved oil recovery, Tulsa, April 17-20.

Ouenes, A., Bhagavan, S., Bunge, P., and Travis, B., 1994b, Application of simulated annealing and other global optimization methods to reservoir description: myths and realities: paper SPE 28415 presented at the SPE annual technical meeting, New Orleans, Sept. 25-28.

Weiss, W., Ouenes, A., and Sultan, J. 1995, Reservoir characterization of a slope/basin reservoir: paper SPE 29597 presented at the joint rocky mountain regional meeting and low permeability reservoirs symposium, Denver, March 20-22.

Sultan J., Ouenes, A., and Weiss, W. 1993, Reservoir description by inverse modeling: application to EVGSAU field: paper SPE 26478 presented at the 1993 SPE annual conference, Houston, Oct. 4-6.

Whittaker, S.G., and Mountjoy E. W., 1996, Diagenesis of an upper devonian carbonate-evaporite sequence: Birdbear formation, Southern interior plains, Canada, Journal of Sedimentary Research, v. 66, No 5, p. 965-975.

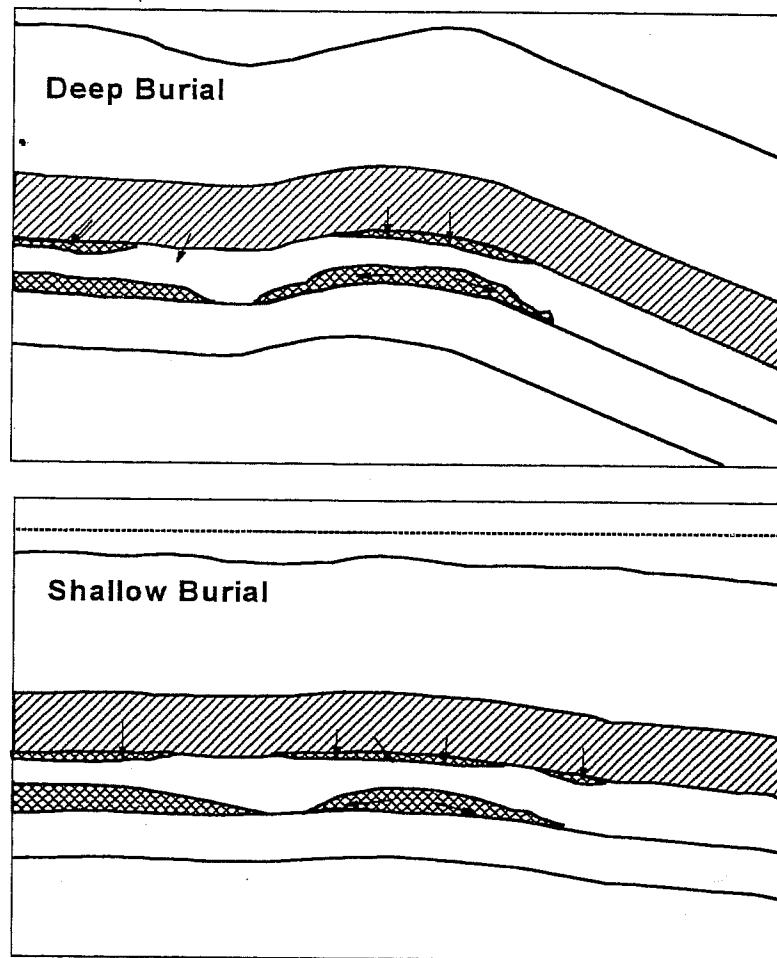


Figure 1: Diagenetic Model for the Nisku formation. The arrows indicate hypothesized flow directions for dolomitizing fluids through skeletal bank deposits during burial stages. (From Ehrets and Kissling, 1985)

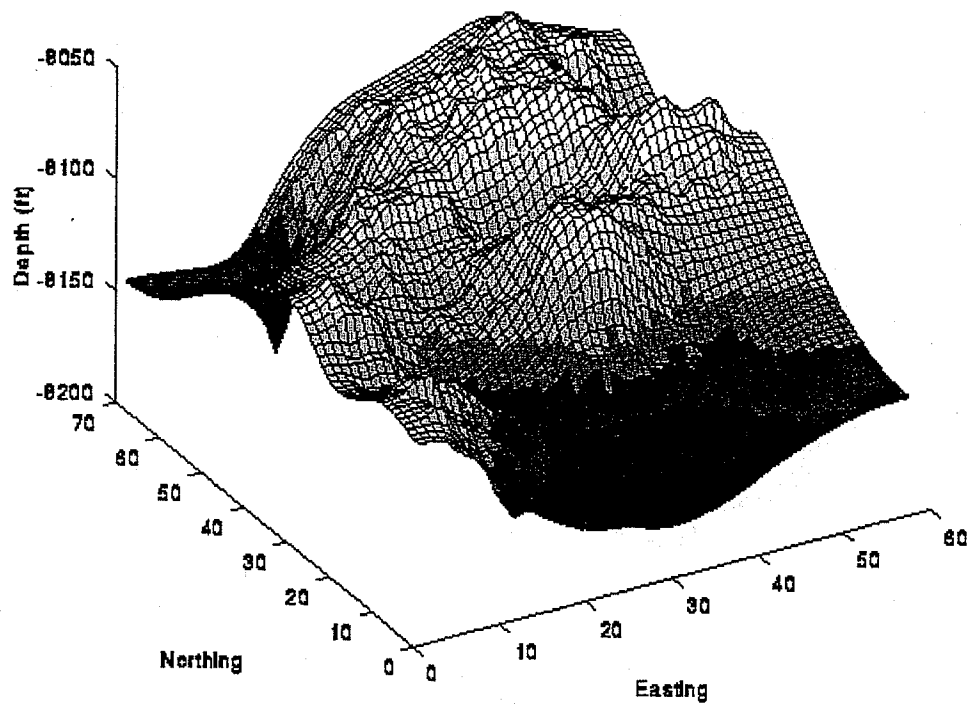


Figure 2: 3D seismic reservoir structure. The bin size is 66 m (219.4 ft) which also is the size of the grid block used in the black oil reservoir simulator.



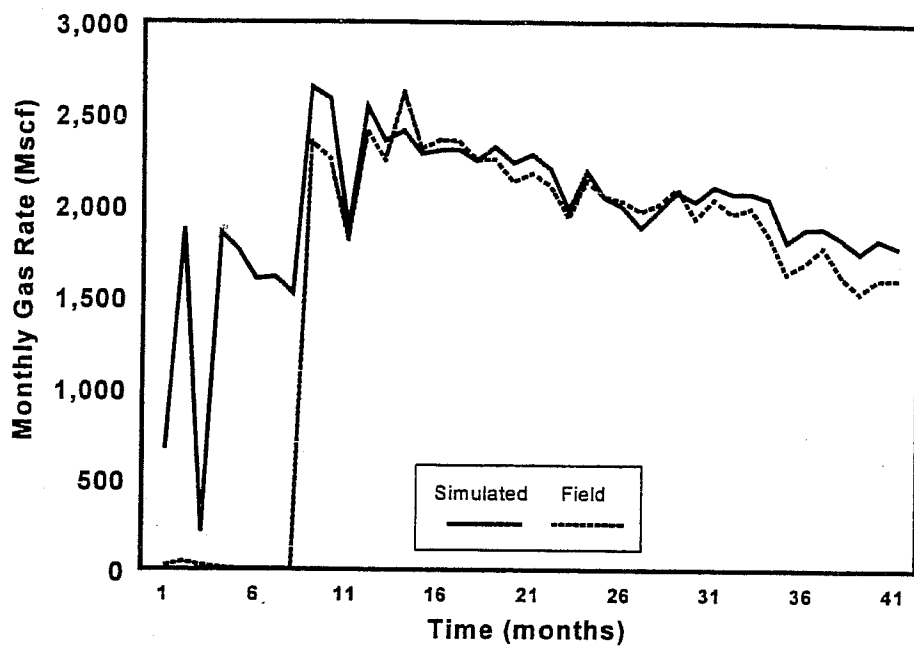


Figure 3: Monthly Gas Production Match.

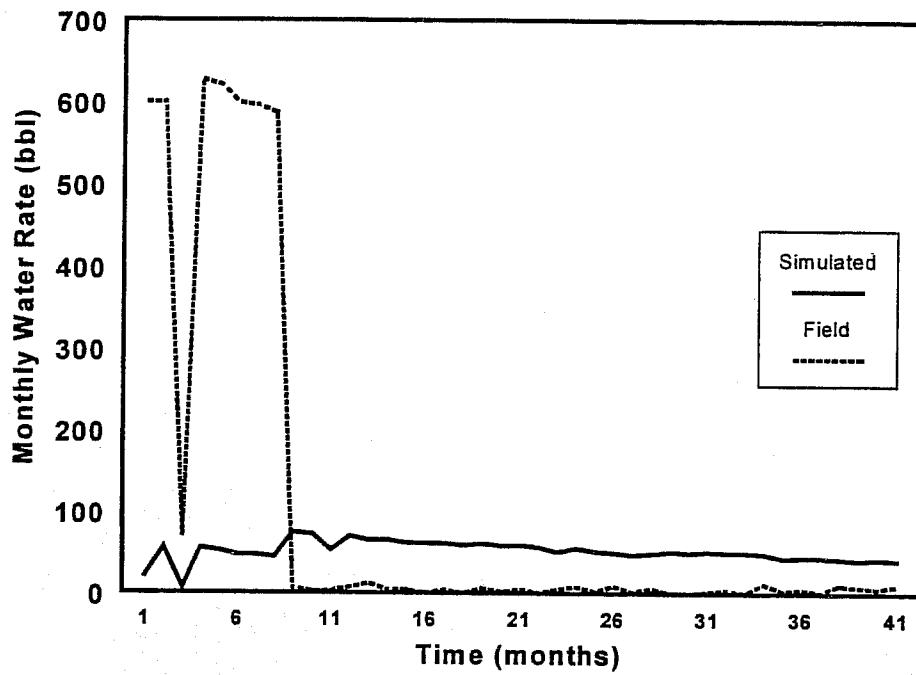


Figure 4: Monthly Water Production Match.

# **Predicting Interwell Heterogeneity In Fluvial-Deltaic Reservoirs: Outcrop Observations and Applications of Progressive Facies Variation Through a Depositional Cycle**

Paul R. Knox and Mark D. Barton

Bureau of Economic Geology, The University of Texas at Austin, Austin, Texas 78713

## **ACKNOWLEDGMENTS**

Studies contributing to this manuscript were partially funded by the U.S. Department of Energy under contract No. DE-FC22-93BC14959 and by the Gas Research Institute under contract No. 5089-260-1902. Mobil Exploration and Producing, U.S., provided subsurface data that made the reservoir characterization study possible. Project supervisors included William Fisher, Noel Tyler, Shirley Dutton, Raymond Levey, and Richard Major of The University of Texas at Austin, Richard Parker, Paul Wescott, and Anthony Garody of GRI, and Edith Allison and Chandra Nautiyal of the U.S. DOE. Assistance was provided by Ted Angle, Douglas Dawson, and Radu Boghici. Technical editing and comments of Steven Seni, Janok Bhattacharya, Brian Willis, Tucker Hentz, and Richard Major significantly improved the manuscript. Discussions with Lee McRae, Michael Gardner, and Tom Ryer also benefited the manuscript. Drafting was done by Randy Hitt, Kerza Prewitt, Joel Lardon, and Michelle Bailey under the direction of Richard Dillon and Joel Lardon. Publication authorized by the Director, Bureau of Economic Geology, The University of Texas at Austin.

## **ABSTRACT**

Nearly 11 billion barrels of mobile oil remain in known domestic fluvial-deltaic reservoirs despite their mature status. A large percentage of this strategic resource is in danger of permanent loss through premature abandonment. Detailed reservoir characterization studies that integrate advanced technologies in geology, geophysics, and engineering are needed to identify remaining resources that can be targeted by near-term recovery methods, resulting in increased production and the postponement of abandonment.

The first and most critical step of advanced characterization studies is the identification of reservoir architecture. However, existing subsurface information, primarily well logs, provides insufficient lateral resolution to identify low-permeability boundaries that exist between wells and compartmentalize the reservoir. Methods to predict lateral variability in fluvial-deltaic reservoirs have been developed on the basis of outcrop studies and incorporate identification of depositional setting and position within a depositional cycle.

The position of a reservoir within the framework of a depositional cycle is critical. Outcrop studies of the Cretaceous Ferron Sandstone of Utah have demonstrated that the architecture and internal heterogeneity of sandstones deposited within a given depositional setting (for example, delta front) vary greatly depending upon whether they were deposited in the early, progradational part of a cycle or the late, retrogradational part of a cycle. Specifically, incised valleys in progradational parts of cycles tend to be narrow, deep, and internally homogeneous, whereas those in retrogradational parts of a cycle tend to be wider, internally heterogeneous, and display lateral channel migration. Additionally, river-dominated deltaic systems are more common in progradational parts of cycles, and wave-dominated deltaic systems are more common in retrogradational parts. Varying accommodation appears to play a significant role in this process, but changes in sediment supply and physiography of the depositional surface also potentially contribute.

Detailed investigations of two fluvial upper delta plain reservoirs in the Oligocene Frio Formation of Tijerina-Canales-Blucher field, South Texas, have documented variability in reservoir architecture and internal heterogeneity that contribute to very different production behavior and different remaining potential. The Whitehill reservoir, deposited early in a depositional cycle, contains several laterally isolated channel belts that are internally homogeneous and can be efficiently drained by wells at a 40-acre spacing. In contrast, the Scott reservoir, deposited late in a depositional cycle, contains a single broad channel belt that is internally heterogeneous, with many depositional low-permeability barriers between 20-acre well locations that have prevented more than 90% of the mobile oil from being recovered. The Scott reservoir

contains significant infill potential, whereas the Whitehill reservoir may contain new pool potential in isolated stratigraphically trapped accumulations away from the structural crest.

The application of techniques similar to those used by this study in other fluvial-deltaic reservoirs will help to estimate the amount and style of remaining potential in mature reservoirs through a quicklook evaluation, allowing operators to focus characterization efforts on reservoirs that have the greatest potential to yield additional resources. These techniques can also be applied to more confidently predict stratigraphy and depositional heterogeneity between wells, allowing more accurate identification of reservoir architecture and compartmentalization. Application of these concepts to mature fluvial-deltaic reservoirs is the first step in locating untapped or incompletely drained compartments that can be targeted by near-term recovery methods to increase production and prevent premature field abandonments.

## INTRODUCTION

Unsuspected interwell-scale stratigraphic heterogeneity has contributed to a situation in which more than one-third of the mobile oil in domestic fluvial-deltaic reservoirs remains in place despite many decades of production. According to data from the U.S. Department of Energy TORIS database, 14.4 billion barrels (Bbbl) of oil have been produced from these reservoirs, but 10.8 Bbbl of mobile oil remain, with currently proved reserves equaling less than one-tenth of remaining volumes. The problem of stratigraphic heterogeneity is particularly pronounced in fluvial-deltaic reservoirs because fluvial and shallow marine sandstone bodies may appear laterally continuous but are commonly separated by impermeable abandoned-channel, marginal-marine, and marine mudstones. These long narrow isolated sandstone bodies are ineffectively contacted by conventionally patterned drilling grids and, in some cases, are internally compartmentalized by low-permeability layers that prevent efficient reservoir drainage.

The key to recovering the large volume of remaining mobile oil is to identify those reservoirs that have been poorly drained and apply integrated, advanced characterization methods to locate specific untapped or incompletely drained compartments. The critical first step in the characterization process is to determine the geometry of reservoir sandstones and bounding or

internal low-permeability layers. This process is complicated in fluvial-deltaic reservoirs because geometries may change laterally over distances less than the typical well spacing (Tyler and Finley, 1991), on which most subsurface data such as well logs are based.

Prediction of geometries and heterogeneity at the interwell scale is dependent upon a clear understanding of the depositional setting and the position of the reservoir within a depositional cycle. During the 1960s and 1970s, observations from modern depositional settings helped define major controls on deposition and preservation of sediments in various settings and were used to build facies models that lead to a basic understanding of field-scale reservoir architecture (for example, Coleman, 1982; Selley, 1978; Walker, 1979; Cant, 1982). During this time, models of delta evolution as a consequence of autocyclic lobe-switching were presented to explain cyclic deposition in deltaic settings (for example, Horne et al., 1978). It was recognized that delta style may change from fluvial-dominated to wave-dominated from early to late in a major depositional episode, perhaps as a result of decreased sediment supply (for example, Duncan, 1983). The concepts of sequence stratigraphy developed during the 1970s and 1980s improved the reliability of facies interpretation by more clearly defining the affects of changing relative sea level and sediment supply on depositional cyclicity, facies geometry, and stacking patterns (Vail et al., 1977; Jervey, 1988; Posamentier et al., 1988; Posamentier and Vail, 1988; Galloway, 1989a, b). The recent documentation of high-frequency depositional cycles and a hierarchy of cycle scales has increased the resolution of depositional models (Goldhammer et al., 1990; Mitchum and Van Wagoner, 1991) and underscored the potential of high-frequency eustatic changes to affect stratal geometries.

The advances provided by sequence stratigraphic concepts are being widely applied in order to predict lithology in exploration studies. Only recently, however, has the predictive framework of sequence and cyclic stratigraphy been thoroughly incorporated with facies models to go beyond the prediction of stratal geometries and document progressive changes in facies associations through a high-frequency depositional cycle. Workers in outcrops of carbonate sequences (Sonnenfeld, 1991; Kerans and Fitchen, 1995) and clastic successions (Cross et al., 1993; Gardner, 1993; and

Barton, 1994) recognized that the continually changing balance of depositional controls throughout a depositional cycle also resulted in changes in facies associations and their preservation potential within a depositional system. For example, facies associations in a delta deposited during a fall in relative sea level might correspond to models of river-dominated deltas because of increased fluvial input or decreased wave energy. Preservation of bedforms and facies in the updip area might be low because of pronounced sediment bypass caused by progressively decreasing accommodation. In contrast, deltaic deposits formed during rising relative sea level might correspond to wave- or tide-dominated depositional models because of decreased fluvial input. Preservation potential of these deposits would be increased because of greater accommodation.

This insight into facies associations in a high-frequency stratigraphic framework provides sufficiently detailed information to allow the prediction of reservoir architecture and heterogeneity at the between-well scale. Knox and McRae (1995) provided an early subsurface example demonstrating concomitant changes in reservoir production characteristics.

The primary objectives of this paper are (1) to summarize observations from Ferron Sandstone outcrops that demonstrate changes in facies associations through a depositional cycle and (2) to underscore the potential applications to oil and gas reservoir characterization using examples from mature Oligocene-age reservoirs in the Texas Gulf Coast. The remaining two sections of the Introduction will demonstrate the potential changes in reservoir heterogeneity resulting from differing position within a depositional cycle and summarize cyclic controls on interwell-scale heterogeneity.

## **A Tale of Two Reservoirs**

Characteristics of two vertically adjacent reservoirs in the Oligocene Frio Formation of South Texas illustrate the potential variability in heterogeneity and, consequently, production behavior, that can occur within a single depositional facies. Knox and McRae (1995) interpreted both the Scott and underlying Whitehill reservoirs from the Tijerina-Canales-Blucher field, Jim Wells

County, Texas, as having been deposited in a fluvial upper delta plain environment on the basis of regional setting and blocky to upward-fining log signature.

Although the fluvial upper delta plain depositional setting for these two reservoirs is similar, their production characteristics are very different. The Scott reservoir (dominantly oil-bearing) is nearing abandonment of its ten well completions (at a spacing of less than 40 acres) with more than 90% of the original oil still in place. In contrast, past production in the underdeveloped Whitehill reservoir (dominantly gas-bearing) has demonstrated that the reservoir can be effectively drained by completions at a 40 acre spacing. Knox and McRae (1995) stated that the vastly different drainage areas for completions in these reservoirs are greater than can be accounted for by the difference in mobility of the gas versus oil fluids, and point to differences in internal heterogeneity. Knox and McRae (1995) concluded that these differences in heterogeneity were the result of the different positions within a depositional cycle, with the Whitehill having been deposited during more pronounced progradation (low accommodation leading to scour and removal of fine-grained channel-fill facies, resulting in internal homogeneity) with the Scott being deposited during more pronounced aggradation (high accommodation leading to preservation of fine-grained channel-fill facies, resulting in greater internal heterogeneity).

### **Cyclic Controls on Interwell-Scale Heterogeneity**

The primary controls on clastic sediment deposition (and preservation) and resulting architecture and heterogeneity are accommodation, sediment flux, and antecedent physiography (Jervy, 1988; Posamentier et al., 1988; Van Wagoner et al., 1990, Goldhammer et al., 1990; Swift et al., 1991). Accommodation describes the potential space available for sediment to fill, sediment flux includes the rate and textural mix of sediment input, and antecedent physiography is the three-dimensional shape of the surface on which deposition takes place. These primary controls each have contributory factors that govern their net effects. Accommodation is the net result of subsidence (caused by tectonism, isostatic adjustments to sediment loading, etc., and sediment compaction) and eustasy (high-frequency climate-induced and longer-term geoidal and tectonic

forces). Sediment flux is the net result of tectonism in the source area, climate and changes in climate in the source area, and the changing hydraulic competency of the delivering medium (for example, water flow in a fluvial system or currents in a shelf system). Antecedent depositional topography affects accommodation in that, as relative sea level changes, deposition shifts landward or seaward and total accommodation is determined by both changing relative sea level and the slope of the surface to which deposition has shifted. Antecedent depositional topography affects sediment flux because topography governs wave, tide, and current energies.

Although the controls on sediment deposition are numerous and complex, an overwhelming number of workers have concluded that the sedimentary record (the end result of deposition and preservation) is inherently cyclic, and that this cyclicity occurs at many scales (see Goldhammer et al., 1990, and Mitchum and Van Wagoner, 1991 for more involved discussions). Many previous studies have subdivided depositional cycles into three parts (the highstand, lowstand, and transgressive systems tracts of Posamentier et al. (1988) and Posamentier and Vail (1988)). Various terminology has been applied to describe the hierarchy of scales of depositional cycles, such as parasequences, high-frequency sequences, sequences and composite sequences (Mitchum and Van Wagoner, 1991), and cycles, high-frequency sequences, and composite sequences (Kerans and Fitchen, 1995). Because we recognize marine flooding surfaces as the most useful surfaces in establishing a stratigraphic framework, we consider a generic depositional cycle (independent of scale) to begin at maximum flooding and progress from progradation through aggradation to retrogradation, culminating at a maximum flood. In this sense, the resulting depositional units are akin to genetic depositional sequences as defined by Galloway (1989a). The term 'order' has been used to describe the hierarchy, such as 3rd-, 4th-, and 5th-order (see Goldhammer et al., 1990, and Mitchum and Van Wagoner, 1991), and specific time spans have been assigned to various 'orders.' Unless a cycle is clearly constrained by age dating, we avoid the use of 'order' terminology. Instead, we have applied the generic terms of low-, intermediate-, and high-frequency to describe observed multifold cyclicity.



## INTERWELL-SCALE HETEROGENEITY IN OUTCROP

Stratigraphic complexities that result in between-well-scale reservoir heterogeneity are best described in outcrop where rapid lateral changes can be identified and described. The best outcrop sites occur where present landforms and original depositional trends combine to expose long, continuous portions parallel to depositional dip, with sufficient orthogonal exposures to provide information regarding strike-oriented variations. Additionally, stratigraphic units deposited under conditions of high sediment supply and high accommodation provide the best record of high-frequency depositional cyclicity because short-term changes in the balance of depositional controls that result in brief marine flooding events will be recorded by the abundant influx of sediment and preserved by rapid burial and limited ensuing incision.

The conjunction of these factors occurs in exposures of the Upper Cretaceous (Turonian) Ferron Sandstone Member of the Mancos Shale along the Molen Reef and Coal Cliffs fringing the San Rafael Swell of eastern Utah (Figure 1). Cliff faces of greater than 100 m height and 100 km in length expose the entire 250 m of the Ferron, which accumulated during an estimated 0.5 to 2 Ma. Early studies of the Ferron Sandstone Member of the Mancos Shale identified it as major sandstone body composed of two distinct clastic wedges, an early wedge derived from the northwest, typically referred to as the Clawson and Washboard sandstones, and a later wedge derived from the southwest (Hale, 1972), referred to as the Ferron sandstone. Ryer (1981) recognized the upper (Ferron) wedge as being composed of a series of sandstone tongues partially bounded by marine shales. Later studies (Ryer, 1993; Gardner, 1993; Barton, 1994) recognized that each of these tongues is further subdivided by marine shales associated with minor flooding events.

Stratal successions (high-frequency units) bounded by minor flooding surfaces are stacked in a systematic fashion to form five intermediate-frequency (IF) units bounded by major or more regionally extensive flooding surfaces (Figure 2). Within each IF unit, the stacking pattern of high-frequency (HF) units progresses from an initial aggradational-to-progradational set, to a downstepping set, then to an aggradational set, followed in some cases by a retrogradational set

(IF units 3, 4, and 5 in Figure 2). The downstepping set of HF units is interpreted to have been deposited during a fall in relative sea level whereas the aggradational to retrogradational sets are interpreted to have been deposited during a relative rise.

Within each HF unit, a surface characterized by deep fluvial incision and the development of paleosols separates the initial aggradational to progradational set of HF units from subsequent downstepping, aggradational, and retrogradational sets. This surface is interpreted as an unconformity developed during a fall in relative sea level. During a subsequent rise in sea level, incised valleys were filled with fluvial to estuarine deposits and interfluv areas, characterized by paleosols, were overlapped by marginal marine to coastal plain deposits.

Accompanying changes in stacking pattern of IF and HF units are progressive changes in facies associations. Variability of lithofacies geometry and heterogeneity were documented within delta front deposits of IF units by Gardner (1993). Subsequent studies by Barton recognized similar changes in delta-front deposits of HF units (Barton, 1995) as well as within incised valley deposits of IF units. The following discussion summarizes this observed variability and compares it to the position of the deposits within a depositional cycle.

### **Summary of Outcrop Observations**

Detailed observations of lithofacies types, geometry, and permeability were made in many cliff exposures within a 40-km section of Ferron sandstone outcrops (Figure 1) in which the high-frequency genetic stratigraphic framework had been established. These observations make possible a comparison of similar depositional settings at different times in a depositional cycle. Summarized below are comparisons of incised valley fill deposits from a seaward-stepping (low accommodation) IF unit and those from a landward-stepping (high-accommodation) IF unit and comparisons of delta front deposits from two vertically adjacent HF units occupying early and late portions of a lowstand within a seaward-stepping IF unit (see Figure 2).

Incised valley deposits identified by Barton (1995) in cycle 2 exposed along I-70 (Figure 1) are typical of incised valleys observed throughout cycles 2 and 3, which are IF units within the

seaward-stepping portion of the Ferron low-frequency depositional unit. Lithofacies, channelform boundaries, and permeability within this deposit are shown in Figure 3, along with the map view geometry of the valley system. These incised valley deposits tend to be internally relatively homogeneous in both lithology and permeability, with many vertically stacked channel-bar and -fill beds composed nearly exclusively of trough cross stratified sandstones lacking evidence of marine or tidal influence. Channel-on-channel boundaries exhibit thin intervals (0.1 to 1 m) of slightly reduced permeabilities consisting of basal channel lag deposits containing rounded mudclasts and dispersed clay. Valleys are narrow and deep, with width-depth ratios of approximately 7:1.

Valley fill deposits identified by Barton (1995) in cycle 5, a landward-stepping (high-accommodation) IF unit, are typified by outcrops at Muddy Creek (Figure 1). A cross-section of this valley fill, shown in Figure 3, illustrates that in contrast to valleys in cycles 2 and 3, these deposits consist of laterally stacked channelforms containing a heterolithic, upward-fining succession of trough cross strata through rippled strata typical of medium to high-sinuosity rivers. Permeability is somewhat more heterogeneous than in cycle 2 valley fills, with channel lag deposits draping lateral accretion surfaces and exhibiting pronounced reduced permeability arising from a greater volume of mudclasts and dispersed clay. A greater number of stratigraphically equivalent valleys are seen in map view (Figure 3), and each valley tends to have a higher width-depth ratio, approximately 40:1, than those in cycles 2 and 3. Gardner (1993) identified these features as distributary channels and suggested that the difference in morphology was a consequence of low versus high accommodation. Barton (1995) identified these features as incised valleys on the basis of fluvial incision that is several times as deep as a single barform is high. One possible explanation shared by both Gardner (1993) and Barton (1995) is that successive scour in a low accommodation setting removes the upper, fine-grained portion of the channel fill that is normally preserved during periods of higher accommodation, resulting in the marked differences in internal lithologic and petrophysical heterogeneity.

Delta front deposits in two HF units from both early and late lowstand periods in cycle 2 are seen at exposures in Dry Wash (Figure 1). These two units are vertically adjacent but exhibit vastly

different lithofacies and permeability distributions typical of opposing deltaic styles. Delta front deposits of the early lowstand HF unit show characteristics common in fluvial-dominated deltas such as prominent mouth bar facies and growth faulting, and permeability is consequently highly variable. In contrast, delta front deposits of late lowstand HF unit show characteristics common to wave-dominated deltas such as extensive strike-elongate shoreface facies and lagoon/washover facies, with limited lateral variations in permeability. Gardner (1993) documented this style of variability between successive IF units. Several depositional controls could account for the observed changes in depositional style in both IF and HF units. For instance, decreased sediment supply during the late lowstand time could provide more opportunity for mouth bar deposits to be reworked into strike-parallel shoreface facies. Alternatively, higher wave energy may be typical in late lowstand times because of progradation of the delta front into increasingly deeper waters (resulting from rising sea level) resulting in less dissipation of wave energy across the shelf.

Envisioned depositional models for Ferron IF depositional cycles are shown in Figure 4. Deposition progresses from (1) wave-dominated highstand deltas through (2) river-dominated deltas fed by incised valleys during early lowstand, to (3) wave-dominated deltas fed by sinuous fluvial systems in the late lowstand, and culminating with (4) barrier bars, lagoons, and estuaries during transgression. Lowstand deposits are better developed in seaward-stepping IF units and transgressive deposits are thin or absent in these units. The result of this pattern is progressive changes in volume and style of deposits in both the fluvial and deltaic depositional systems throughout intermediate- and low-frequency depositional cycles.

## **PREDICTING HETEROGENEITY IN THE SUBSURFACE**

The above outcrop observations from the Ferron Sandstone provide support to the concept that facies associations change progressively through a depositional cycle. These documented variability in permeability characteristics and facies geometries have significant potential impacts on subsurface reservoir behavior. Low-permeability bounding surfaces identified in outcrop are difficult to resolve in well logs and may have complex distributions between existing wellbores that

significantly impact the ability of the wellbore to communicate with fluids in the reservoir, decreasing per-completion production and leaving large areas of reservoir untapped or incompletely drained. Recognizing which reservoirs might contain such heterogeneities is important because it is those reservoirs that contain significant reserve-growth potential but which will require focused characterization efforts to locate and recover the large volumes of remaining mobile oil.

As outcrop studies of the Ferron indicate, an understanding of the depositional system and stratigraphic position of the reservoir within a larger depositional cycle framework can provide the basis for predicting between-well scale stratigraphic heterogeneity. This concept was applied to the Scott and Whitehill reservoirs mentioned above to evaluate the variability of production characteristics and investigate whether outcrop observations might supply insights into optimization of reservoir production. The Scott and Whitehill reservoirs were deposited in channelized upper delta plain settings and might be subject to the same trends in depositional controls as Ferron incised valleys. For instance, channels deposited during low accommodation might have poorer preservation of fine-grained channel-fill sediments and thus might be more internally homogeneous.

## **Methodology**

The first and most critical step in evaluating any reservoir from the standpoint of position within a depositional cycle is to establish a stratigraphic framework of low- and intermediate-frequency units from subregional information. This gross framework can then be subdivided into HF units within the field using a grid of stratigraphic sections on the basis of throughgoing surfaces that are assumed to correspond to minor flooding surfaces. Net sandstone maps are then prepared for each HF unit of interest and combined with maps of log pattern to interpret the lateral distribution of facies and identify reservoir architecture. Structure and net pay maps are created for each unit, and fluid contacts are determined and annotated. Petrophysical parameters such as porosity and water saturation are determined in order to calculate original hydrocarbons in place and area drained by each completion. Past completions are then mapped and tabulated by HF unit

to document past reservoir drainage and production behavior. This production behavior is a measure of heterogeneity within each architectural unit. Facies architecture and internal heterogeneity are then compared to the facies and position within an IF depositional unit to evaluate any correspondence with outcrop observations.

### **Subregional Stratigraphic Framework**

The Oligocene-age Frio reservoirs of T-C-B field lie within the Norias Deltaic system and Gueydan Fluvial system (Figure 5), as identified by Galloway (1982). The Frio has been divided into the upper, middle, and lower informal members by Galloway (1986). Each member spans 1 to 2 Ma and corresponds to a 3rd-order depositional unit (Mitchum and Van Wagoner, 1991). Further subdivision, down to the 4th-order level, was accomplished by correlating prominent maximum flooding surfaces. Based on their occurrence from 6 to 10 times within a 3rd-order unit, the units bounded by these surfaces are assumed to span approximately 0.1 to 0.6 Ma. These flooding surfaces are correlated from the downdip marine interval, where they can be more easily identified on well logs, into the updip, nonmarine area of T-C-B field. A 100-km-long dip-oriented stratigraphic cross section was constructed with wells spaced approximately every 3-5 km (Figure 6). The Scott and Whitehill reservoirs were found to lie within a single 4th-order unit, with its base being just below the Whitehill and its top being just above the Scott (Figure 6). The Whitehill, then, represents the earliest deposits of sandstone in the T-C-B area during this depositional cycle following maximum flooding, and the Scott represents the last deposits prior to the next maximum flooding.

### **Architecture of Reservoirs within the Scott/Whitehill Depositional Cycle**

The general stratigraphy and architecture of the Scott/Whitehill reservoir interval, a single 4th-order depositional cycle, have been deduced from careful well log correlation. The interval is subdivided into four fifth-order units by laterally continuous surfaces that may correspond to minor marine flooding (Figure 7). Each fifth-order unit ranges in thickness from 6 to 15 m, with each

successive unit generally thickening from the lower Whitehill at the base (6 m) through the upper Scott (15 m) at the top. Assuming equivalent time spans for each unit, this would suggest persistently increasing rates of accommodation.

Sandstones within the Scott/Whitehill interval display symmetrical, blocky, or upward-fining log patterns, range in thickness from 1 m to more than 15 m, and are separated by siltstones and mudstones of similar thickness. Thicker sandstones consist of amalgamated individual channel deposits, each of which reaches a maximum of 6 m in thickness. The dominance of blocky and upward-fining log patterns, the absence of microfauna, and the regional setting all indicate that these sandstones were deposited in an upper delta-plain fluvial setting. Depositional facies identified on the basis of log character include sandy point bar channel deposits, silty to muddy abandoned channel fill, rare sandy splay deposits, silty levee deposits, and fine-grained floodplain mudstones (Figure 7).

The lowermost fifth-order unit, referred to as the lower Whitehill unit, was deposited at the base of the depositional cycle (low accommodation). It is composed entirely of floodplain mudstone throughout the study area. Correlation in the T-C-B area shows no widespread sandstones at this stratigraphic level, but the existence of narrow localized channel deposits has not been ruled out because channel bodies may be narrower than the well spacing used for regional correlation (approximately 2 km apart).

The overlying fifth-order unit, the upper Whitehill unit, in the seaward-stepping to vertically stacked portion of the depositional cycle (low to intermediate accommodation), consists of three relatively narrow (1.5 km wide) but generally thin fluvial channel-belt deposits (Figure 8) separated by large areas of floodplain mudstone. These channel belts are generally dip-elongate and are typically less than 6 m in thickness. Greater thicknesses are the result of vertical stacking of broader channel belts (1.5 km wide) on top of very narrow channel belts (0.5 km wide) at the base of the interval. The comparatively broader channel belts in the middle and upper portion are interpreted to contain two to three incomplete, vertically amalgamated channel deposits, each

ranging from 1.5 to 3 m in thickness. Abandoned channel mudstones are more common in the uppermost channel deposits.

The next highest fifth-order unit, the lower Scott, in the vertically stacked to landward-stepping portion of the depositional cycle (intermediate to high accommodation), is similar to the upper Whitehill except that channel belts tend to be broader (2.5 km wide). Overall, the lower Scott contains a greater volume of sandstone than the underlying upper Whitehill interval.

The upper Scott fifth-order reservoir, at the top of the fourth-order unit and, thus, in the strongly landward-stepping portion of the depositional cycle (high accommodation), differs markedly from the underlying intervals. It is distinctly thicker and sandier, with a single broad channel belt (5.5 km wide) that covers the entire study area and consists of vertically amalgamated channel deposits (Figure 8). Dip-oriented bodies of sandstone having thicknesses in excess of 6 m are the result of two or three vertically amalgamated channel deposits. The geometry of individual channels within the channel belt is not resolvable with well logs, probably because the width of channels is less than the typical well spacing. The uppermost portion of the upper Scott unit is dominated by siltstones and mudstones of abandoned channel, levee, and floodplain deposits (Figure 7).

In summary, from the lower Whitehill fifth-order unit at the base of the fourth-order depositional cycle (lower accommodation) to the upper Scott unit at the top (highest accommodation), there is a progressive change in channel architecture. Individual fifth-order units become thicker upward, and net sandstone percentage increases. Channel belts become wider in each stratigraphically higher unit, and volumes of fine-grained channel-fill deposits, such as upper point bar and abandoned channel fill, increase upward. These features closely correspond to observed architecture in progradational and aggradational channel-fill facies in the outcropping Ferron incised valley channel deposits.



## Scott/Whitehill Internal Heterogeneity

Whereas the gross architecture of the reservoir compartments (channel belts) can be identified with reasonable accuracy from well log control, intracompartiment heterogeneity cannot. This is because boundaries between individual channel forms potentially occur between wells. In a subsurface setting, the most reliable measure of internal heterogeneity is production performance. The relative size of areas drained in a series of reservoirs is a measure of the internal complexity of the reservoirs, assuming similar drive mechanisms and fluid viscosities.

Reservoir compartment maps have been produced for the upper Whitehill and upper Scott intervals (Figure 8), documenting compartment boundaries and past completions. Structural closure in both cases occurs in areas of subtle highs on a gradually plunging anticlinal nose. The following discussion summarizes the production history of the two reservoirs and estimates drainage areas for successful completions.

The upper Whitehill has produced from two wells, one on the northern structural crest and another on the north flank (Figure 8c), in which perforations were structurally below the documented gas/water contact on the structural crest. Resistivity measurements indicate moderate gas saturations in the southern structure (Figure 8c), but no tests of this potential accumulation have been made. Mapping of channel belts and evidence of tightly carbonate cemented sandstone in one well (Figure 8c) suggest that the northernmost of the two completions is stratigraphically isolated from the structural crest. Volumetric calculations and evidence from wells postdating production indicate that the crestal completion drained approximately 40 acres. At present, insufficient data are available on the other well to document drainage area. Resistivities indicating oil or gas saturation occur in isolated channel belts away from the structural crest, indicating a component of stratigraphic trapping is possible in the upper Whitehill.

Eight wells have produced oil from the upper Scott on the main structural crest (Figure 8d). Cumulative production has ranged from less than 1,000 bbl to more than 54,000 bbl per well. Initial water cuts have varied widely and have been independent of structural position and offset production history, indicating a lack of communication between well locations. Volumetric

analyses suggest that completions have drained areas ranging from less than 1 acre to approximately 5 acres, significantly less than the completion in the Whitehill. Calculations indicate that despite completion at a 20- to 40-acre spacing, and the fact that all current completions are either abandoned, idle, or nearly watered out, less than 10 percent of the original oil in place has been recovered from the Scott.

Although some of the difference in recovery from the Whitehill and the Scott can be attributed to the different mobility ratios of oil and gas, a significant part is attributed to smaller compartment sizes in the Scott zone. This indicates that the upper Scott channel belt (upper portion of depositional cycle, higher accommodation) is much more internally heterogeneous than the upper Whitehill channel belts (lower portion of depositional cycle, lower accommodation).

### **Scott/Whitehill Summary**

As expected from outcrop observations of the Ferron Sandstone, a spectrum of reservoir styles exists within the upper delta-plain deposits of the Frio Formation in T-C-B field (Figure 9). This spectrum is, in part, the result of varying accommodation during deposition of the reservoir sandstones. Reservoirs within 5th-order units range from moderately narrow, internally homogeneous channel belts deposited under conditions of low accommodation in the seaward-stepping portion of a depositional cycle (4th-order unit) to broad internally heterogeneous channel belts laid down under conditions of high accommodation in the landward-stepping phase of a depositional cycle (4th-order unit). These reservoir styles contain varying reserve-growth potential and require very different strategies for optimum development. In general, upper delta-plain fluvial reservoirs in 5th-order units deposited during a landward-stepping period contain the greatest reserve-growth potential and may require the tightest well spacings for optimal reservoir drainage, whereas those deposited during a seaward-stepping period may contain narrow stratigraphically isolated accumulations that are internally homogeneous and present stepout opportunities in mature fields.

## **Application to Other Reservoir Successions**

Our studies of changing reservoir architecture and heterogeneity in an upper delta plain setting provide tremendous insight to production behavior in the T-C-B middle Frio reservoirs. However, other Frio reservoirs will undoubtedly display other vertical trends in characteristics. For example, time-equivalent deposits farther downdip will most likely preserve a greater volume of sandstones within the lower portion of the depositional unit because of greater accommodation, as suggested by Posamentier and Vail (1988). Deposits in the upper part of the downdip depositional unit will likely be mud-dominated as a consequence of decreased sand supply, as sand is preferentially stored in the proximal upper delta plain of the T-C-B area. Thus, specific characteristics of T-C-B reservoirs cannot be used as a model for all Frio fluvial deposits. Instead, studies in other settings must first identify the major flooding surfaces that bound cyclic patterns of deposition and then observe the general trends in sandstone percent and channel belt architecture before predicting between-well heterogeneity.

The above discussion of changing architecture and heterogeneity through a cycle focuses on accommodation trends. However, both the volume and grain size of sediment supplied, as well as physiography, can affect facies variability. The potential control that these factors can exert is recognized, but the relative importance of each has not been defined because of the limited scope of the subsurface study. Additional detailed studies are needed in a variety of settings to document the range of variability within low-frequency systems tracts. Ideally, those investigations will be able to quantify volumes and type of sediment within each high-frequency unit to clarify the changing role of sediment supply throughout a high-frequency depositional cycle. Outcrop investigations, such as those of the Ferron Sandstone, provide critical data that helps constrain reservoir interpretations.

## **Implications**

The model described for the Scott and Whitehill interval only addresses reservoirs deposited in an upper delta-plain fluvial setting. However, it represents a new generation of models for

reservoir characterization. Because rates of accommodation can be demonstrated to control sandstone body architecture and internal heterogeneity, and because these effects are different for each depositional setting but can be documented from outcrop work or implied from careful subsurface study, other models can be developed for reservoirs deposited in a spectrum of depositional settings. Any such models would ideally be based on outcrop observations because continuous lateral exposures are critical for identifying geometries and permeability characteristics of the surfaces that bound potential reservoir compartments. Further understanding of the cyclic nature of the stratigraphic record and the controls on that cyclicity will provide more accurate models and supply more specific guidelines for their application in various depositional settings.

The predictive nature of these new models will improve the accuracy of reservoir characterization studies and increase the use of reservoir characterization by operators of mature fields. The outcome will undoubtedly be increased recovery of oil and gas from reservoirs that otherwise might have been abandoned prematurely. This increased production will thus prevent permanent loss of vital hydrocarbon resources.

## CONCLUSIONS

Outcrop observations from the Cretaceous Ferron Sandstone of central Utah demonstrate that facies associations within a given depositional system vary progressively through both intermediate- and high-frequency depositional units. This is exemplified by changes from narrow, internally homogeneous incised valley fills characterized by vertical stacking of channelforms in IF units in the seaward-stepping part of a LF unit to broad, internally heterogeneous incised valley fills exhibiting lateral stacking of channelforms in IF units in the landward-stepping part of a LF unit. HF units vary within single IF units as delta front deposits progress from laterally heterogeneous fluvial-dominated successions in the early lowstand to more homogeneous, strike-oriented wave-dominated successions in the late lowstand.

These systematic changes are also observed in Oligocene Frio Formation reservoirs of the south Texas Gulf Coast. Changes in facies associations in subsurface reservoirs were accompanied

by dramatic changes in production behavior, requiring different reservoir management approaches and presenting varying opportunities for significant reserve growth potential. Upper delta plain fluvial channel belts deposited early in a depositional cycle are narrow, internally homogeneous, and may present reserve-growth opportunities in off-crest, stratigraphically isolated settings. In contrast, channel belts deposited late in the cycle are broad, internally heterogeneous, and are poorly contacted by typical completion spacings, resulting in significant remaining resources following conventional development.

Facies variability in these fluvial-deltaic successions corresponds with the position of a deposit within a depositional cycle that progresses from low accommodation to high accommodation. Although accommodation appears to be a strong controlling factor, changes in sediment supply and physiography may also exert controls on deposition and preservation. Further investigations are required to identify the possible effects of these controls and to document changes in a broader spectrum of depositional systems. A more complete understanding of facies variability within a depositional cycle will provide an important new technology that will allow the prediction of between-well architecture and heterogeneity in mature reservoirs, ultimately resulting in the improved identification and recovery of tremendous volumes of remaining resources.

## REFERENCES CITED

- Barton, M. D., 1994, Outcrop characterization of architecture and permeability structure in fluvial-deltaic sandstones, Cretaceous Ferron Sandstone, Utah: University of Texas at Austin, Ph.D. dissertation, 259 p.
- Barton, M. D., 1995, Sequence stratigraphy, facies architecture, and permeability structure of fluvial-deltaic reservoir analogs: Cretaceous Ferron Sandstone, Central Utah (Ferron GRI Fieldtrip Guidebook), Bureau of Economic Geology, The University of Texas at Austin, Austin, Texas, 139 p.
- Cant, D. J., 1982, Fluvial facies models and their application, *in* P. A. Scholle and D. Spearing, Sandstone depositional environments, The American Association of Petroleum Geologists, Tulsa, Oklahoma, p. 115–138.
- Coleman, J. M., 1982, Deltas: Processes of deposition and models for exploration, International Human Resources Development Corporation, Boston, 124 p.
- Cross, T. A., et al, 1993, Applications of high-resolution sequence stratigraphy to reservoir analysis, *in* R. Eschard, B. Doligez, eds., Subsurface reservoir characterization from outcrop observations, Editions Technip, Paris, p. 11–33.

- Duncan, E. A., 1983, Delineation of delta types: Norias delta system, Frio Formation, South Texas, Gulf Coast Association of Geological Societies Transactions, v. 33, p. 269-273.
- Galloway, W. E., 1982, Depositional architecture of Cenozoic Gulf Coastal Plain fluvial systems, in Ethridge, F. G., and Flores, R. M., eds., Recent and ancient nonmarine depositional environments: models for exploration: Society of Economic Paleontologists and Mineralogists, Special Publication 31, p. 127-155.
- \_\_\_\_\_. 1986, Depositional and structural framework of the distal Frio Formation, Texas coastal zone and shelf: The University of Texas at Austin, Bureau of Economic Geology Geological Circular 86-8, 16 p.
- \_\_\_\_\_. 1989a, Genetic stratigraphic sequences in basin analysis I: architecture and genesis of flooding-surface bounded depositional units: American Association of Petroleum Geologists Bulletin, v. 73, p. 125-142.
- \_\_\_\_\_. 1989b, Genetic stratigraphic sequences in basin analysis II: application to northwest Gulf of Mexico Cenozoic Basin: American Association of Petroleum Geologists Bulletin, v. 73, no. 2, p. 143-154.
- Gardner, M. N., 1993, Sequence stratigraphy and facies architecture of the Upper Cretaceous Ferron Sandstone Member of the Mancos Shale, East-Central Utah: Colorado School of Mines, Ph.D. dissertation, 528 p.
- Goldhammer, R. K., Dunn, P. A., and Hardie, L. A., 1990, Depositional cycles, composite sea-level changes, cycle stacking patterns, and the hierarchy of stratigraphic forcing: Examples from Alpine Triassic platform carbonates, Geological Society of America Bull., v. 102, p. 535-562.
- Hale, L. A., 1972, Depositional history of the Ferron Formation, central Utah, in plateau basin and range transition zone: Utah Geological Association, p. 115-138.
- Horne, J. C., et al., 1978, Depositional models in coal exploration and mine planning in Appalachian region, American Association of Petroleum Geologists Bulletin, v. 62, no. 12, p. 2379-2411.
- Jervey, M. T., 1988, Quantitative geological modeling of siliciclastic rock sequences and their seismic expression, in C. K. Wilgus, B. S. Hastings, C. G. St. C. Kendall, H. W. Posamentier, C. A. Ross, and J. C. Van Wagoner, eds., Sea-level changes: an integrated approach: Society of Petroleum Engineers Special Publication No. 42, p. 47-69.
- Kerans, C., and Fitchen, W. M., 1995, Sequence hierarchy and facies architecture of a carbonate-ramp system: San Andres Formation of Algerita Escarpment and Western Guadalupe Mountains, West Texas and New Mexico: The University of Texas at Austin, Bureau of Economic Geology Report of Investigations No. 235, 86 p.
- Knox, P. R., and McRae, L. E., 1995, Application of sequence stratigraphy to the prioritization of incremental growth opportunities in mature fields: an example from Frio fluvial-deltaic sandstones, TCB field, South Texas: Gulf Coast Association of Geological Societies Transactions, v. 45, p. 341-359.
- Mitchum, R. M., and Van Wagoner, J. C., 1991, High-frequency sequences and their stacking patterns: sequence-stratigraphic evidence of high-frequency eustatic cycles: Sedimentary Geology, v. 70, p. 131-160.

- Posamentier, H. W., Jervey, M. T., and Vail, P. R., 1988, Eustatic controls on clastic deposition I conceptual framework, *in* C. K. Wilgus, B. S. Hastings, C. G. St. C. Kendall, H. W. Posamentier, C. A. Ross, and J. C. Van Wagoner, eds., *Sea-level changes: an integrated approach*: Society of Economic Paleontologists and Mineralogists Special Publication No. 42, p. 109-124.
- Posamentier, H. W., and Vail, P. R., 1988, Eustatic controls on clastic deposition II sequence and systems tract models, *in* C. K. Wilgus, B. S. Hastings, C. G. St. C. Kendall, H. W. Posamentier, C. A. Ross, and J. C. Van Wagoner, eds., *Sea-level changes: an integrated approach*: Society of Economic Paleontologists and Mineralogists Special Publication No. 42, p. 125-154.
- Ryer, T. A., 1981, Deltaic coals of the Ferron Sandstone Member of the Mancos Shale: Predictive model for Cretaceous coal-bearing strata of the Western Interior: *American Association of Petroleum Geologists Bulletin*, v. 65, no. 11, p. 2323-2340.
- Ryer T. A., 1993, The autochthonous component of cyclicity in shoreline deposits of the Upper Cretaceous Ferron Sandstone, central Utah. *American Association of Petroleum Geologists Bulletin (Abstr.)*, v. 77, p. 175.
- Selley, R. C., 1978, *Ancient sedimentary environments*, Second Edition, Cornell University Press, Ithaca, New York, 287 p.
- Sonnenfeld, M. D., 1991, High-frequency cyclicity within shelf-margin and slope strata of the upper San Andres sequence, Last Chance Canyon, *in* S. Meader-Roberts, M. P. Candelaria, and G. E. Moore, eds., *Sequence stratigraphy, facies, and reservoir geometries of the San Andres, Grayburg, and Queen Formations, Guadalupe Mountains, New Mexico and Texas: Permian Basin Section*, Society of Economic Paleontologists and Mineralogists Publication 91-32, p. 11-51.
- Swift, D. J. P., Oertel, G. F., Tillman, R. W., and Thorne, J. A., 1991, Shelf sand and sandstone bodies: Geometries, facies, and sequence stratigraphy, *International Association of Sedimentologists Special Publication No. 14*, 532 p.
- Tyler, Noel, and Finley, R. J., 1991, Architectural controls on the recovery of hydrocarbons from sandstone reservoirs, *in* Miall, A. D., and Tyler, Noel, eds., *The three-dimensional facies architecture of terrigenous clastic sediments and its implications for hydrocarbon discovery and recovery*: Society of Economic Paleontologists and Mineralogists, *Concepts in Sedimentology and Paleontology*, v. 3, p. 1-5.
- Vail, P. R., Mitchum, R. M., Todd, R. G., Widmier, J. M., Thompson, S. III, Sangree, J. B., Bubb, J. N., and Hatlelid, W. G., 1977, Seismic stratigraphy and global changes of sea-level, *in* C. W. Payton, ed., *Seismic stratigraphic applications to hydrocarbon exploration*: AAPG Memoir No. 26, p. 49-212.
- Van Wagoner, J. C., Mitchum, R. C., Campion, K. M., and Rahmanian, V. D., 1990, Siliciclastic sequence stratigraphy: *American Association of Petroleum Geologists Methods in Exploration Series*, No. 7, p. 55.
- Walker, R. G., 1979, *Facies models*, First Edition, Geoscience Canada Reprint Series, 1, Toronto, Ontario, 317 p.

## FIGURE CAPTIONS

Figure 1. Location of Ferron Sandstone outcrops along the northwest flank of the San Rafael Swell in central Utah. Observations at indicated localities are discussed in the text.

Figure 2. Schematic cross-section depicting stratigraphic relationships within the five intermediate-frequency cycles of the Ferron sandstone.

Figure 3. Map view and cross-sections of incised valleys in the Ferron Sandstone from a low-accommodation (cycle 2) setting at the I-70 outcrop (a) and a high-accommodation (cycle 5) setting at the Muddy Creek outcrop (b).

Figure 4. Model showing evolution of Ferron depositional system during an intermediate-frequency relative sea level cycle in the Ferron sandstone. Wave-dominated shoreline systems develop during increases in relative sea level, whereas fluvial incision and river-dominated shoreline systems develop during falling relative sea level. Intermediate-frequency genetic units in seaward-stepping portions of the Ferron lack substantial transgressive deposits.

Figure 5. Location of the Tijerina-Canales-Blucher (T-C-B) field within the Frio Fluvial-Deltaic Sandstone (Vicksburg Fault Zone) Play in south Texas. Also shown are the major depositional systems active during Frio deposition, as defined by Galloway (1982). Cross section A-A' is shown in Figure 6.

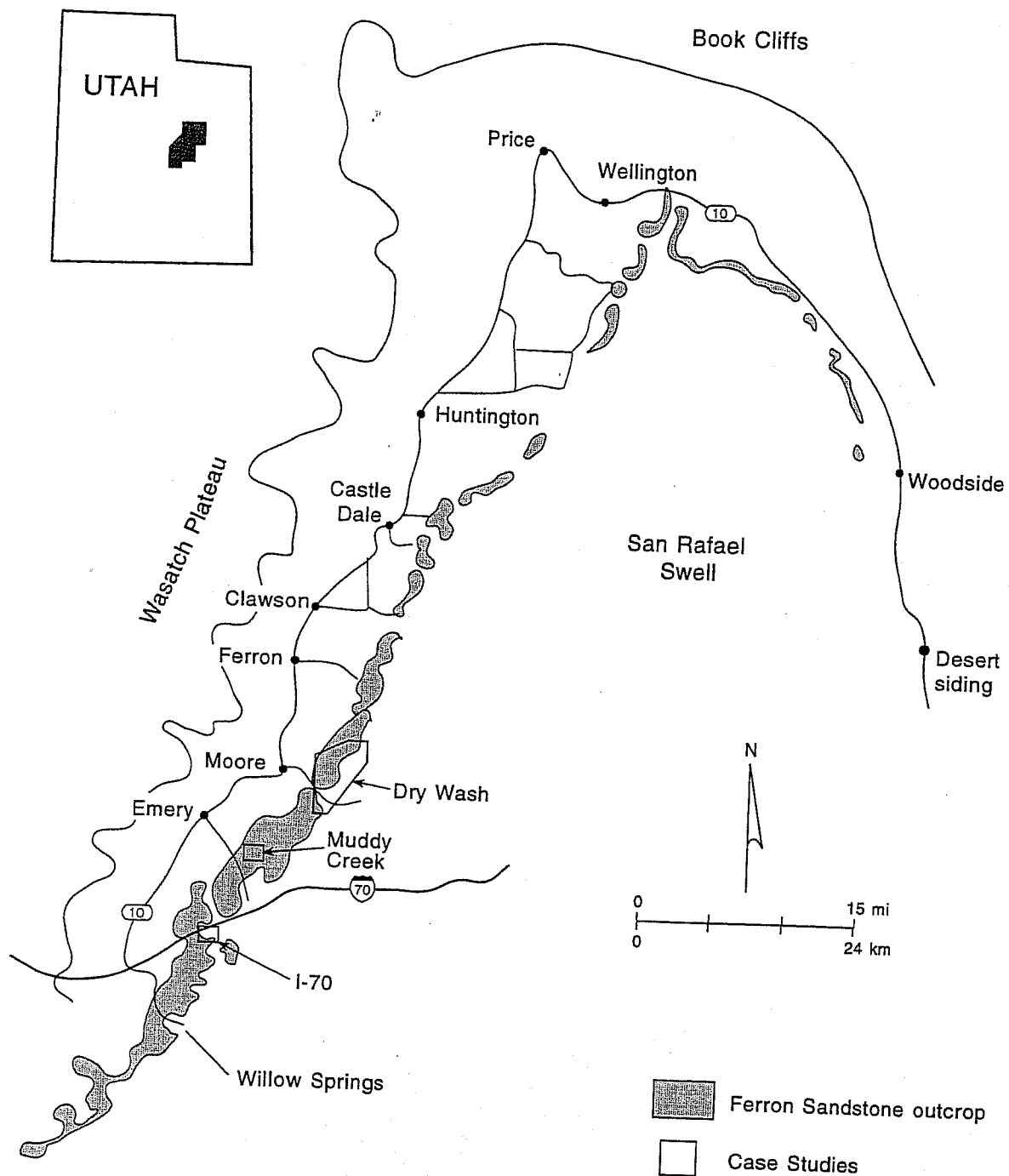
Figure 6. Dip-oriented stratigraphic cross section A-A' through the Frio Formation from updip of T-C-B field down to the present coastline. The Frio consists of three 3rd-order genetic units, each containing many 4th-order units (not all of which are shown). See Figure 5 for cross-section location.

Figure 7. Dip-oriented cross section B-B' showing the Scott/Whitehill 4th-order genetic unit, which contains at least four 5th-order genetic units. These are, from top down, the upper and lower Scott and the upper and lower Whitehill reservoir intervals. Cross-section location is given in Figure 8.

Figure 8. Net sandstone maps for the upper Whitehill (a) and upper Scott (b) reservoirs and compartment maps of the upper Whitehill (c) and upper Scott (d) reservoirs. Narrow, stratigraphically isolated channel belts of the upper Whitehill interval were deposited in the proximal upper delta plain during the early part of a depositional cycle, whereas the broad, internally complex channel belt of the upper Scott interval was deposited during the latest portion of a depositional cycle.

Figure 9. Spectrum of upper delta plain fluvial reservoir architecture, internal heterogeneity, production characteristics, and reserve-growth potential in the Scott/Whitehill interval.





**Figure 1**

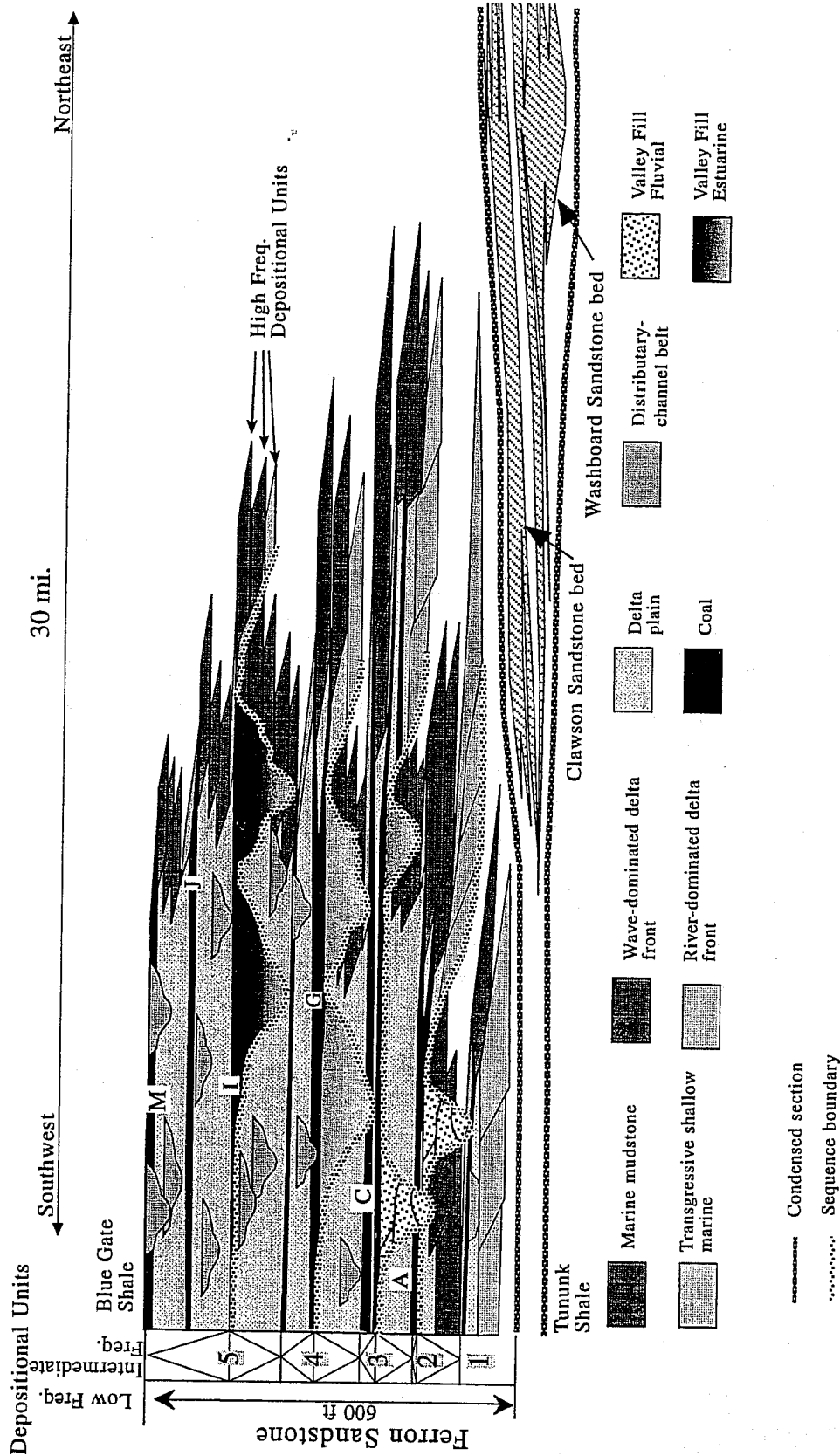


Figure 2. Schematic cross-section depicting stratigraphic relationships of Ferron Sandstone in central Utah.

Figure 2

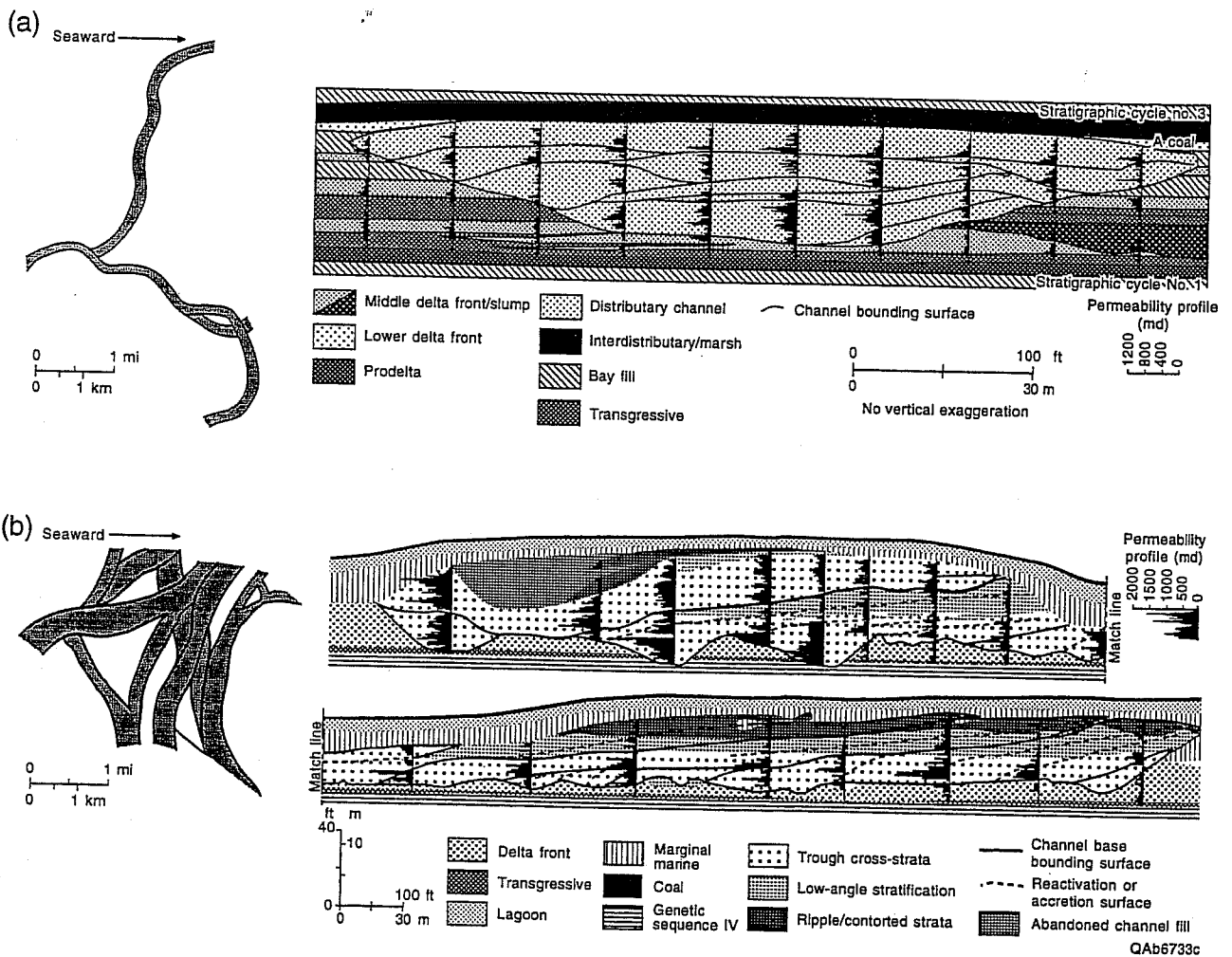


Figure 3

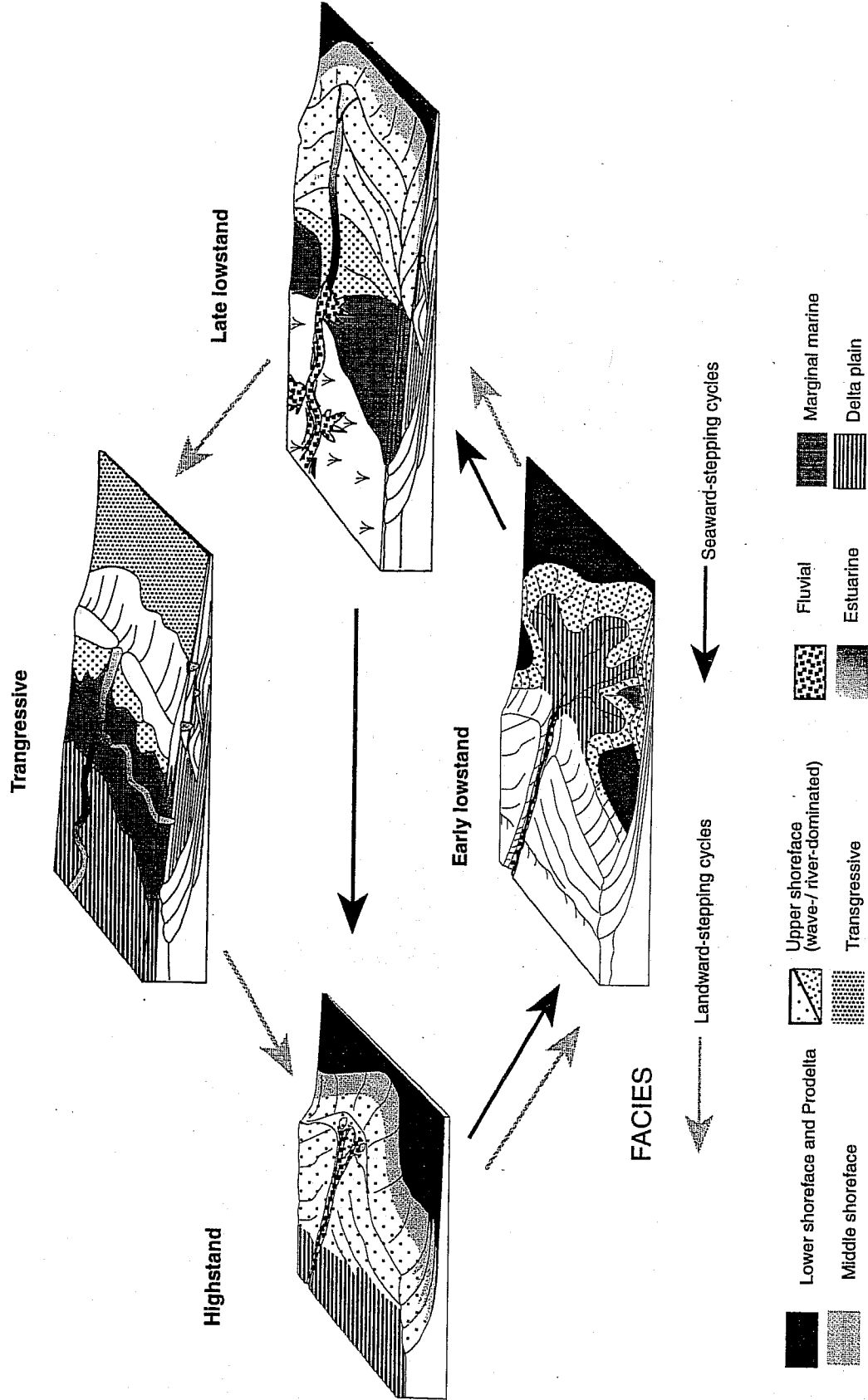
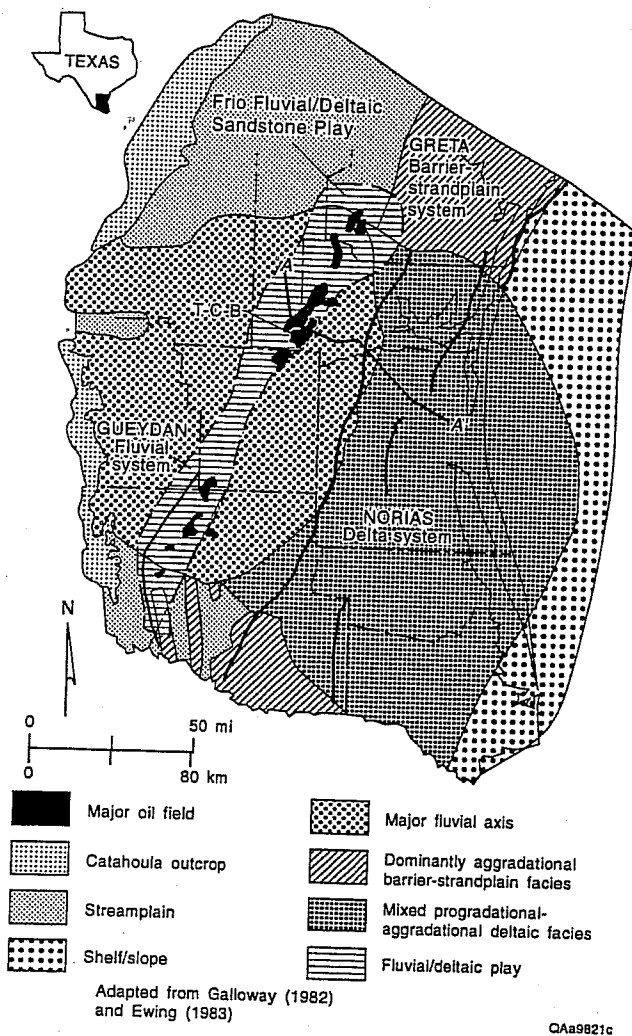
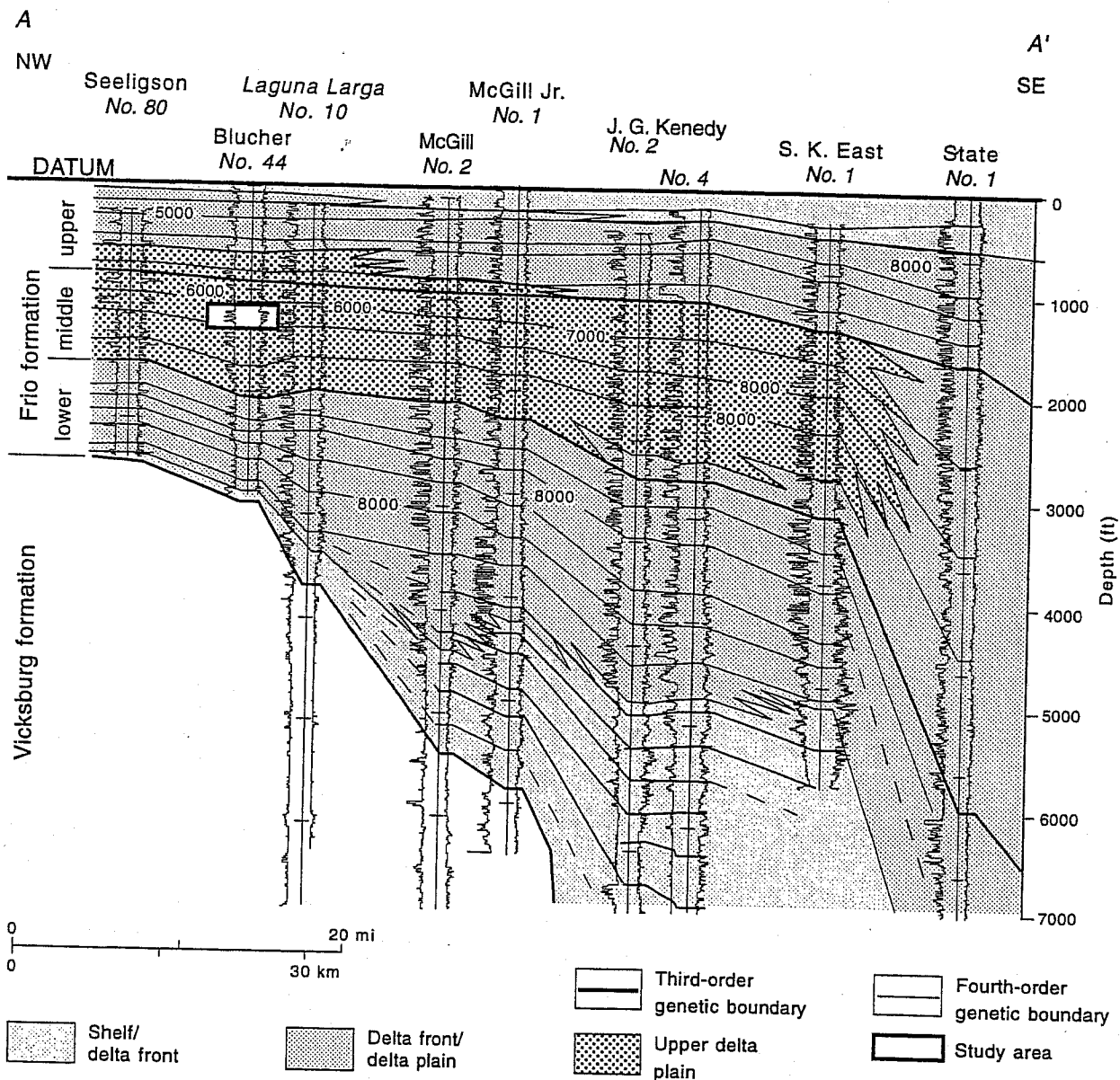


Figure 4



**Figure 5**



**Figure 6**

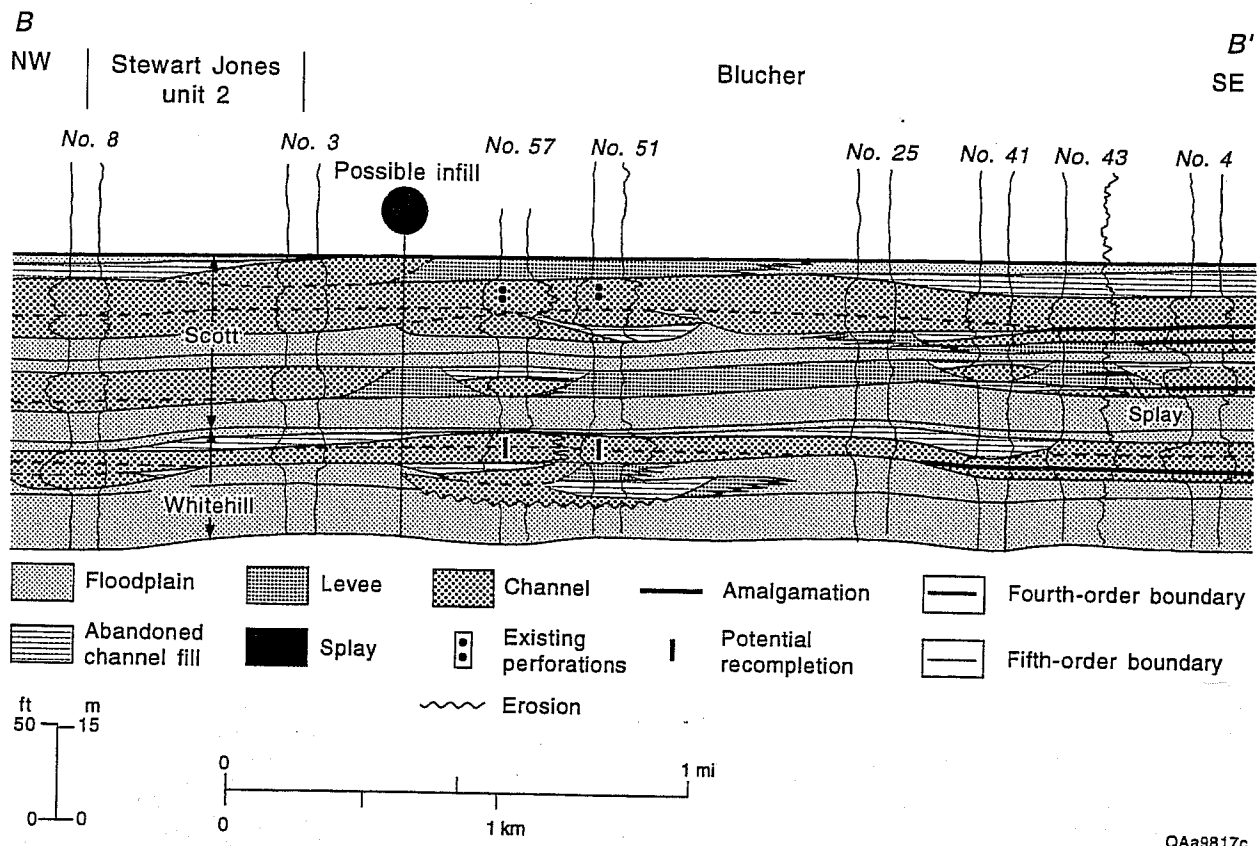


**Figure 7**

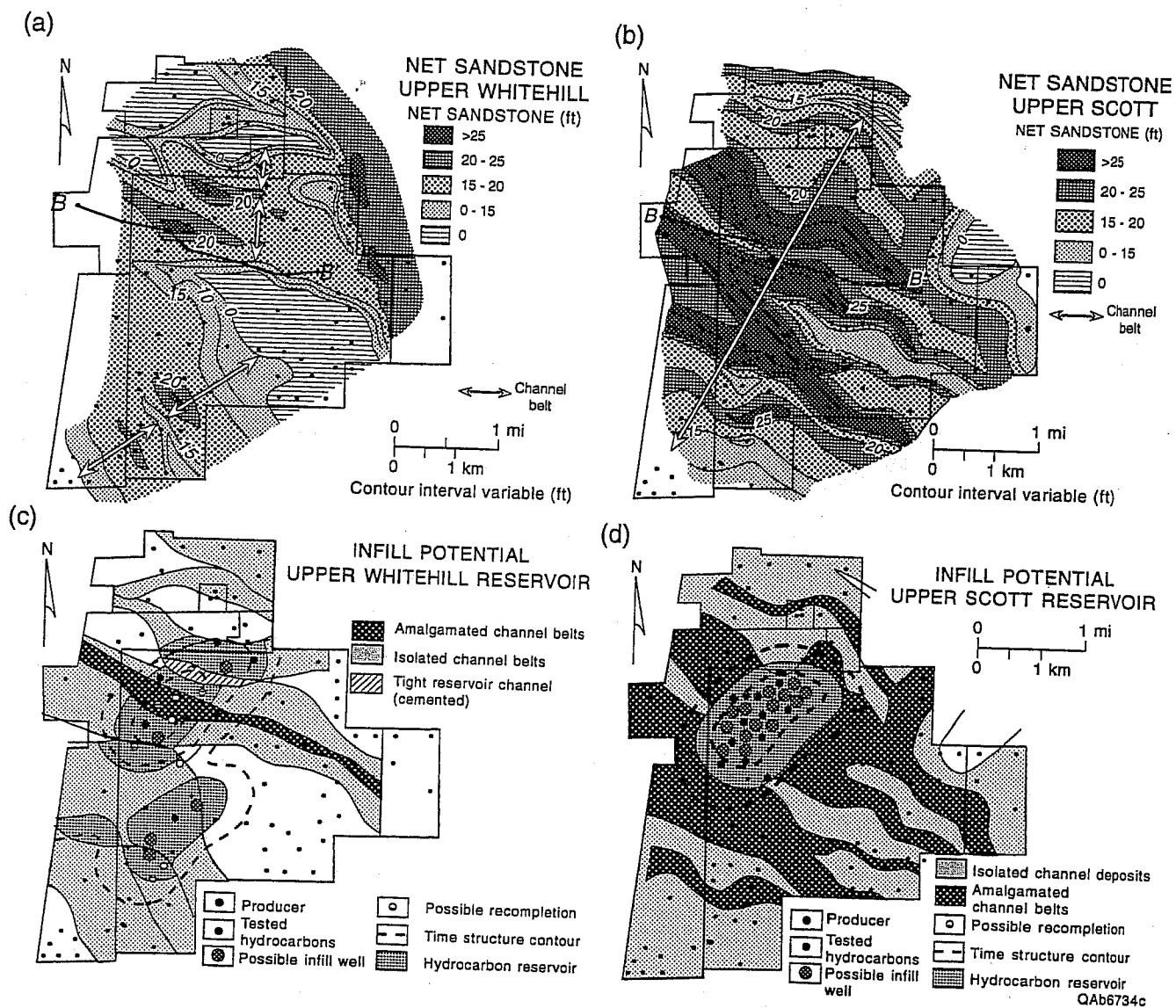
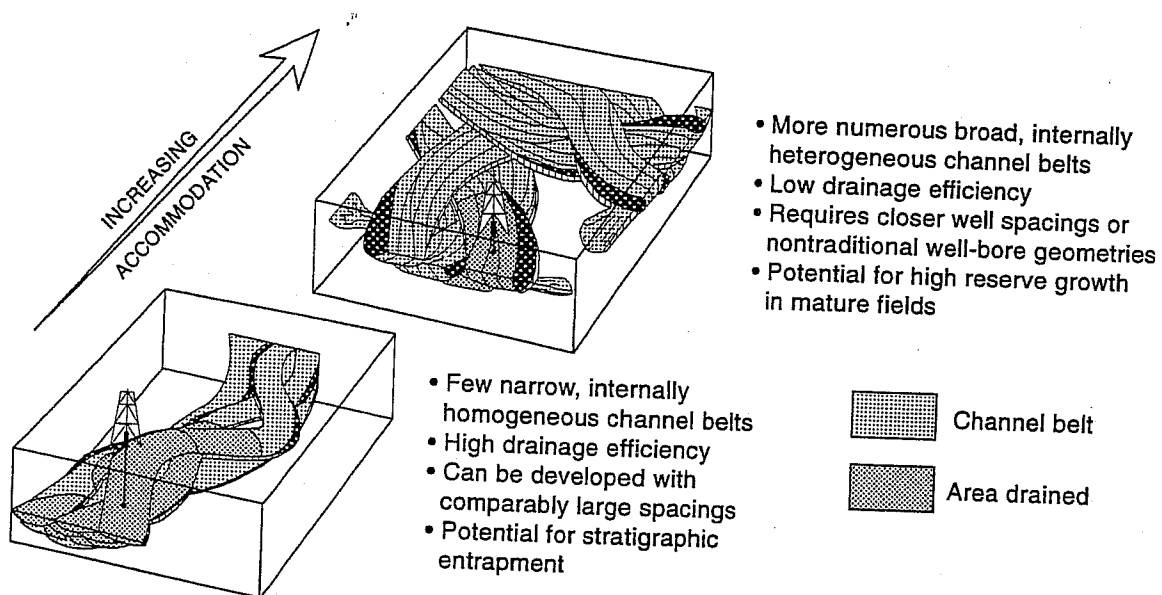


Figure 8





QA603c

**Figure 9**

# Reducing Uncertainty in Geostatistical Description With Well Testing Pressure Data

Albert C. Reynolds<sup>1</sup>, Nanqun He<sup>1</sup> and Dean S. Oliver<sup>2</sup>

<sup>1</sup> Department of Petroleum Engineering, University of Tulsa, Tulsa, OK 74104

<sup>2</sup> Chevron Petroleum Technology Company, P. O. Box 446, La Habra, CA 90633

## ABSTRACT

Geostatistics has proven to be an effective tool for generating realizations of reservoir properties conditioned to static data, e.g., core and log data and geologic knowledge. Due to the lack of closely spaced data in the lateral directions, there will be significant variability in reservoir descriptions generated by geostatistical simulation, i.e., significant uncertainty in the reservoir descriptions. In past work, we have presented procedures based on inverse problem theory for generating reservoir descriptions (rock property fields) conditioned to pressure data and geostatistical information represented as prior means for log-permeability and porosity and variograms. Although we have shown that the incorporation of pressure data reduces the uncertainty below the level contained in the geostatistical model based only on static information (the prior model), our previous results assumed did not explicitly account for uncertainties in the prior means and the parameters defining the variogram model.

In this work, we investigate how pressure data can help detect errors in the prior means. If errors in the prior means are large and are not taken into account, realizations conditioned to pressure data represent incorrect samples of the a posteriori probability density function for the rock property fields, whereas, if the uncertainty in the prior mean is incorporated properly into the model, one obtains realistic realizations of the rock property fields.

## ACKNOWLEDGEMENTS

This work was supported by a grant from the Strategic Research Department of Chevron Petroleum Technology Company and the member companies of Tulsa University Petroleum Reservoir Exploitation Projects (TUPREP). This support is gratefully acknowledged. Yafes Abacioglu, who also has implemented the techniques presented here, reviewed the manuscript and offered constructive comments.

## INTRODUCTION

Our objective is to generate realizations of three-dimensional rock property fields (simulator gridblock values of log-permeability and porosity) conditioned to a prior model and well-test pressure data. The prior model is based on a multivariate Gaussian distribution with known covariance matrix and uncertain prior means. As in previous related work (e.g., Oliver, 1994; Chu et al., 1995a; Reynolds et al., 1995; He et al., 1996), the prior covariance matrix can be derived from given variograms for the log-permeability and porosity fields and the associated cross-variograms.

Unlike the past work mentioned above, we specifically account for uncertainty in the prior means by introducing a partially doubly stochastic prior model using basic ideas described in Tjelmeland et al. (1994). Our basic procedure for generating realizations of the rock property fields relies on generating the joint probability density function (pdf) for the rock property fields and the errors in the prior means conditioned to pressure data, and then sampling this pdf to obtain realizations. Although we do not have permission to publish the actual data here, this work was actually motivated by a field study in which we found that the prior mean for permeability was significantly overestimated in the geostatistical model and resulted in unrealistic descriptions of the permeability field if the realizations of the permeability field were conditioned to pressure data without accounting for the uncertainty in the prior mean.

An efficient procedure for sampling the pdf is obtained by adapting ideas and techniques presented in Oliver (1996) and Oliver et al. (1996a) to the problem considered here. A procedure for generating the maximum a posteriori estimates of the rock property fields and prior means is also presented. Specific realizations and maximum a posteriori estimates are generated by minimizing an appropriate objective function using the Gauss-Newton method. Sensitivity coefficients are computed using the procedure presented by He et al. (1996).

It is important to note that our objective in generating realizations of rock property fields is to obtain a set of realizations which represent a correct sampling of the probability density function for the rock property fields. By making a performance prediction with each realization, one can then evaluate the uncertainty in the predicted parameters, e.g., break through time or cumulative oil production. If one simply generates a set of realizations that honor all the data, but the set does not provide a correct sampling of the probability density function, we know of no feasible procedure for evaluating the uncertainty in performance predictions.

## RESERVOIR MODEL

The reservoir is assumed to be a rectangular parallelepiped of uniform thickness  $h$ . Reservoir boundaries are assumed to be no-flow boundaries. Three-dimensional single-phase flow in a Cartesian coordinate system is considered. The reservoir can contain any number of complete-penetration or restricted-entry vertical wells. Each well is produced at a specified rate where the rate may vary with time; pressure buildup at a well is simulated by setting the rate to zero subsequent to a producing period. Interference or observation wells are simulated by setting the rate to zero at all times. Fluid properties are assumed to be known. We assume a slightly compressible fluid of constant compressibility and viscosity. In all results, the values of the following parameters are fixed:  $c_t = 10^{-5}$  psi<sup>-1</sup>,  $\mu = 0.8$  cp. and  $r_w = 0.3$  ft at all wells.

The permeability and porosity fields are assumed to be heterogeneous. Permeability may be either isotropic or anisotropic, but we assume that the principal axes of permeability coincide with the directions of the x-y-z coordinate system, i.e., the only permeabilities involved are  $k_x$ ,  $k_y$  and  $k_z$ . The variogram for each permeability field may be anisotropic. The variogram for porosity may also be anisotropic. Permeability attributes ( $k_x$ ,  $k_y$  and  $k_z$ ) are assumed to have

log-normal distributions with variances given by  $\sigma_{k_x}^2$ ,  $\sigma_{k_y}^2$ ,  $\sigma_{k_z}^2$ . Porosity is assumed to be normal with variance given by  $\sigma_\phi^2$ . Each rock property attribute is modeled as a stationary Gaussian random function so that the covariance functions are directly related to the variograms (Journal and Huijbregts, 1978). The correlation coefficients between the various attributes are assumed to be known, but may be zero. As discussed in more detail later, prior estimates of the means of the attributes are assumed to be uncertain.

As indicated in the preceding paragraph, our model is quite general, however, the specific examples presented here pertain to a case where  $k_x = k_y = k$  and  $k_z = 0.1k$  at all gridblocks. Thus, in generating realizations of the rock property fields, realizations of porosity and  $\ln(k)$  are generated and the corresponding realizations for the vertical permeability field is determined explicitly via the relation  $k_z = 0.1k$  which is applied at each gridblock. As in Chu et al. (1995), the cross variogram between porosity and log-permeability is generated using the screening hypothesis of Xu et al. (1992). This eliminates the necessity of specific modeling of the cross variogram.

For given rock property fields, pressure responses are obtained by a standard purely-implicit, seven-point finite-difference simulator, where wellbore pressure is related to the well's gridblock pressures by Peaceman's method (1983); see Chu et al. (1995a) and He et al. (1996). To test the procedures used to resolve rock property fields, a simulator is used to generate synthetic multiwell pressure data, which is then assumed to represent measured wellbore pressure data.

### Prior and A Posteriori Probability Density Functions

$N$  denotes the number of simulator gridblocks. For the specific problems considered here, the rock property model, or vector of rock property model parameters, is given by

$$m = \begin{bmatrix} m_\phi \\ m_k \end{bmatrix}, \quad (1)$$

where  $m_\phi$  is the  $N$ -dimensional column vector of gridblock porosities,  $m_k$  is the  $N$ -dimensional column vector of gridblock values of  $\ln(k)$ . Note the dimension of  $m$  is  $N_p = 2N$ . To use standard notation from probability theory, we let  $M$  denote the random vector of rock property model parameters, with specific realizations denoted by  $m$  given in Eq. 1. For a fully anisotropic permeability field, the model  $m$  must be modified so that it includes components for  $\ln(k_x)$ ,  $\ln(k_y)$ ,  $\ln(k_z)$  and porosity and the covariance matrix given by Eq. 2 below must also be modified; see He et al. (1996).

As in our past work (Oliver, 1994; He et al., 1996; Oliver et al., 1996a), the prior model is assumed to have a multivariate Gaussian probability density function with prior covariance matrix,  $C_M$ . For the specific examples given here,  $C_M$  is given by

$$C_M = \begin{bmatrix} C_\phi & C_{\phi k} \\ C_{\phi k} & C_k \end{bmatrix}, \quad (2)$$

where  $C_\phi$  is the covariance matrix for gridblock porosities derived from the porosity variogram,  $C_k$  is the covariance matrix for gridblock  $\ln(k)$ 's derived from the variogram for  $\ln(k)$ ,  $C_{\phi k}$  is the cross covariance matrix between porosity and  $\ln(k)$  at the set of gridblocks.

Throughout,  $m_{prior}$  is the vector containing the prior means of the model parameters, i.e.,

$$m_{prior} = \begin{bmatrix} m_{prior,\phi} \\ m_{prior,k} \end{bmatrix}. \quad (3)$$

Since  $\ln(k)$  and porosity are modeled as stationary random functions in the prior model,  $m_{prior,\phi}$  and  $m_{prior,k}$  are treated as constant vectors although the general formulation presented allows each entry of  $m_{prior}$  to be different. The random vector  $\Theta$  represents the error in or correction to  $m_{prior}$  with  $\theta$  denoting specific realizations of  $\Theta$ . Introduction of  $\Theta$  allows for the incorporation of uncertainty in the vector of prior means, whereas, in our past work, (Oliver, 1994; He et al., 1996; Oliver et al., 1996), we assumed no error in  $m_{prior}$ . The pdf for  $\Theta$  is assumed to be Gaussian and is given by

$$p_\Theta(\theta) = a \exp \left( -\frac{1}{2}(\theta - \theta_0)^T C_\Theta^{-1}(\theta - \theta_0) \right), \quad (4)$$

where  $\theta_0$  is the mean or expectation of the random vector  $\Theta$  and  $C_\Theta$  is the associated covariance matrix. In this work, we assume that errors in the prior means are independent so  $C_\Theta$  is a diagonal matrix. Although it is appropriate to choose  $\theta_0 = 0$ , the derivation is done for any value of  $\theta_0$ . The conditional distribution (pdf) of  $M$  given  $\Theta = \theta$  is given by

$$p_{M|\Theta}(m|\theta) = a \exp \left( -\frac{1}{2}(m - m_{prior} - \theta)^T C_M^{-1}(m - m_{prior} - \theta) \right). \quad (5)$$

so the joint pdf for  $M$  and  $\Theta$  is given by

$$p_{\hat{M}}(\hat{m}) = p_{\hat{M}}(m, \theta) = p_{M|\Theta}(m|\theta)p_\Theta(\theta) = a \exp \left( -\frac{1}{2}(m - m_{prior} - \theta)^T C_M^{-1}(m - m_{prior} - \theta) - \frac{1}{2}(\theta - \theta_0)^T C_\Theta^{-1}(\theta - \theta_0) \right), \quad (6)$$

where

$$\hat{M} = \begin{bmatrix} M \\ \Theta \end{bmatrix}. \quad (7)$$

For simplicity, a realization  $\hat{m}$  of  $\hat{M}$  is sometimes written as  $(m, \theta)$  instead of  $(m^T, \theta^T)^T$ . Throughout, the superscript  $T$  is used to denote the transpose of a matrix or vector. For convenience, we refer to  $m_{prior}$  as the prior mean, however, one should note that Eq. 5 indicates that the conditional expectation of  $M$  is given by  $E[M|\Theta = \theta] = m_{prior} + \theta$ .

All measured well-test pressure data that will be used as conditioning data is incorporated in the  $N_d$ -dimensional column vector  $d_{obs}$ . Note  $N_d$  is the total number of observed or measured pressure data used as conditioning data. As is standard,  $d$  represents the corresponding vector

of pressures that will be calculated for a given realization  $m$  of the rock property fields and the relationship between the data and  $m$  is represented by

$$d = g(m). \quad (8)$$

Given a specific  $m$ , Eq. 8 represents the operation of calculating wellbore pressures by running the reservoir simulator.

As in our earlier work (Oliver, 1994; He et al., 1996; Oliver et al., 1996a), we assume that the random vector  $\epsilon$  which represents measurement errors consists of independent identically distributed random variables with zero mean and variance  $\sigma_d^2$  so that the data covariance matrix  $C_D$  is a diagonal matrix with all diagonal entries equal to  $\sigma_d^2$ . Given  $m$ , the observed pressure data may be regarded as a realization of the random vector  $D = g(m) + \epsilon$ . Thus, the a posteriori pdf for  $\hat{M}$  conditional to the observed pressure data,  $d_{obs}$ , can be derived as in Tjelmeland et al. (1994) by a standard applications of Bayes theorem and is given by

$$\pi(m, \theta) = p_{\hat{M}|D}(\hat{m}|d_{obs}) = a \exp \left( -\frac{1}{2}(g(m) - d_{obs})^T C_D^{-1}(g(m) - d_{obs}) - \frac{1}{2}(m - m_{prior} - \theta)^T C_M^{-1}(m - m_{prior} - \theta) - \frac{1}{2}(\theta - \theta_0)^T C_\Theta^{-1}(\theta - \theta_0) \right), \quad (9)$$

where the first equality of Eq. 9 simply defines notation. Eq. 9 gives the pdf we wish to sample to generate realizations  $(m, \theta)$  of  $\hat{M}$ . To generate the most probable model (maximum a posteriori estimate) for  $\hat{M}$ , we need to minimize the objective function  $O(\hat{m})$  given by

$$O(\hat{m}) = \frac{1}{2}(g(m) - d_{obs})^T C_D^{-1}(g(m) - d_{obs}) + \frac{1}{2}(m - m_{prior} - \theta)^T C_M^{-1}(m - m_{prior} - \theta) + \frac{1}{2}(\theta - \theta_0)^T C_\Theta^{-1}(\theta - \theta_0) \quad (10)$$

At this point, the dimension of  $\theta$  is the same as the dimension of  $m$ , i.e.,  $N_p$ .

## NEWTON ITERATION

It is convenient to partition the gradient as

$$\nabla O(\hat{m}) = \begin{bmatrix} \nabla_m O(\hat{m}) \\ \nabla_\theta O(\hat{m}) \end{bmatrix} \quad (11)$$

where  $\nabla_m$  represents the gradient operator with respect to  $m$  and  $\nabla_\theta$  represents the gradient operator with respect to  $\theta$ . Using basic vector calculus, it follows that

$$\nabla_\theta O(\hat{m}) = -C_M^{-1}(m - m_{prior} - \theta) + C_\Theta^{-1}(\theta - \theta_0). \quad (12)$$

Similarly,

$$\nabla_m O(\hat{m}) = G^T C_D^{-1}(g(m) - d_{obs}) + C_M^{-1}(m - m_{prior} - \theta), \quad (13)$$

where  $G^T$  is the transpose of the  $N_d \times N_p$  sensitivity coefficient matrix  $G$  which is defined as

$$G = \nabla_m [g(m)^T]. \quad (14)$$

Using Eqs. 12 and 13 in Eq. 11 gives the total gradient of the objective function. Again using basic vector calculus, the Hessian matrix for the Gauss-Newton iteration is given by

$$H = \begin{bmatrix} G^T C_D^{-1} G + C_M^{-1} & -C_M^{-1} \\ -C_M^{-1} & C_M^{-1} + C_\Theta^{-1} \end{bmatrix}. \quad (15)$$

The Hessian is guaranteed to be positive semidefinite. It is well known (Fletcher, 1987) that if the Hessian is modified, the Gauss-Newton method will still converge to the same maximum a posteriori estimate provided the modified Hessian is positive definite. Thus, in order to obtain a simpler computational scheme, we replace the Hessian  $H$  by  $\hat{H}$  where

$$\hat{H} = \begin{bmatrix} G^T C_D^{-1} G + C_M^{-1} & O \\ O & C_M^{-1} + C_\Theta^{-1} \end{bmatrix}. \quad (16)$$

Since  $C_D$ ,  $C_M$  and  $C_\Theta$  are all positive definite matrices, it is clear that  $\hat{H}$  is positive definite.

When  $\hat{H}$  is used as the modified Hessian in the Newton iteration procedure, the overall iteration can be decomposed as follows:

$$(G_l^T C_D^{-1} G_l + C_M^{-1}) \delta m^{l+1} = -G_l^T C_D^{-1} (g(m^l) - d_{obs}) - C_M^{-1} (m^l - m_{prior} - \theta^l) \quad (17)$$

$$(C_M^{-1} + C_\Theta^{-1}) \delta \theta^{l+1} = C_M^{-1} (m^l - m_{prior} - \theta^l) - C_\Theta^{-1} (\theta^l - \theta_0), \quad (18)$$

$$m^{l+1} = m^l + \mu_l \delta m^{l+1}, \quad (19)$$

$$\theta^{l+1} = \theta^l + \mu_l \delta \theta^{l+1} \quad (20)$$

where  $l$  refers to the iteration index and  $\mu_l$  is the step size determined by the restricted step method (Fletcher, 1987). Note in the spirit of the restricted step, it is important to use the same value of  $\mu_l$  in both Eqs. 19 and 20, otherwise we effectively change the search direction. Note by replacing  $H$  by  $\hat{H}$ , we avoid inversion of  $H$ , i.e., we have “decoupled” the iteration on the model ( $m$ ) from the iteration on the correction ( $\theta$ ) to the prior mean.

The prior mean given by Eq. 2 can be written as

$$m_{prior} = \begin{bmatrix} m_{prior,\phi} & e \\ m_{prior,k} & e \end{bmatrix}, \quad (21)$$

where  $e$  is the  $N$ -dimensional column vector with all entries equal to unity. More generally, we let  $e$  represents a column vector of dimension  $N_e$  with all components equal to unity, i.e.,

$$e = [1, 1, \dots, 1]^T, \quad (22)$$

and assume that  $m_{prior}$  has the form

$$m_{prior} = \begin{bmatrix} m_{prior,1} e \\ m_{prior,2} e \\ \vdots \\ m_{prior,N_a} e \end{bmatrix}. \quad (23)$$

In this case, it is reasonable to require that the correction to the prior mean have the same structure as  $m_{prior}$ , i.e., we require that

$$\theta = \begin{bmatrix} \alpha_1 e \\ \alpha_2 e \\ \vdots \\ \alpha_{N_a} e \end{bmatrix} = \begin{bmatrix} \theta_1 e \\ \theta_2 e \\ \vdots \\ \theta_{N_a} e \end{bmatrix}, \quad (24)$$

for some constants,  $\alpha_j$ ,  $j = 1, 2, \dots, N_a$ . Since  $m_{prior}$  and  $\theta$  are both  $N_p$ -dimensional column vectors,  $N_a N_e = N_p$ . For the case where all attributes are modeled as stationary random functions,  $N_a$  is equal to the number of attributes, e.g.,  $N_a = 2$  if Eq. 3 applies. However, if the mean of each attribute varies from gridblock to gridblock, then  $N_a = N_p$  (the dimension of the model  $m$ ). In this case,  $e$  is one dimensional and Eq. 24 does not place any restrictions on the components of  $\theta$ . When Eq. 24 applies,  $C_\theta$  is defined as a block diagonal matrix with the  $j$ th diagonal block given by  $\sigma_{\theta,j}^2 I$  for  $j = 1, 2, \dots, N_a$  where  $I$  is the  $N_e \times N_e$  identity matrix.

The  $(N_a N_e) \times N_a = N_p \times N_a$  matrix  $E$  is defined by

$$E = \begin{bmatrix} e & O & \dots & O \\ O & e & \dots & O \\ \vdots & \vdots & \ddots & \vdots \\ O & O & \dots & e \end{bmatrix}, \quad (25)$$

so the transpose of  $E$  is given by

$$E^T = \begin{bmatrix} e^T & O & \dots & O \\ O & e^T & \dots & O \\ \vdots & \vdots & \ddots & \vdots \\ O & O & \dots & e^T \end{bmatrix}, \quad (26)$$

If  $N_a = N_p$  ( $N_e = 1$ ), then  $E$  is the  $N_p \times N_p$  identity matrix. Defining the  $N_a$  dimensional column vector  $\alpha$  by

$$\alpha = [\alpha_1, \alpha_2, \dots, \alpha_{N_a}]^T, \quad (27)$$

Eq. 24 can be written as  $\theta = E\alpha$ .



## Partial Subspace Procedure

Reynolds et al. (1995) have implemented subspace methods (Kennett and Williamson, 1988; Oldenberg et al., 1993; Oldenberg and Li, 1994) to significantly enhance the computational efficiency of the Gauss-Newton method. Here, we consider only a partial subspace procedure where  $\delta\theta^{l+1}$  in Eq. 18 is expanded as

$$\delta\theta^{l+1} = E\delta\alpha^{l+1} \quad (28)$$

at all Newton iterations. Using Eq. 28 in Eq. 18 and multiplying the resulting equation by  $E^T C_M$  gives

$$E^T(I + C_M C_\Theta^{-1})E\delta\alpha^{l+1} = E^T(m^l - m_{prior} - \theta^l) - E^T C_M C_\Theta^{-1}(\theta^l - \theta_0). \quad (29)$$

Eq. 28 indicates that  $\delta\theta^{l+1}$  is a linear combination of the columns of  $E$ , i.e., the columns of  $E$  represent the associated subspace vectors. If the initial guess for  $\theta$ ,  $\theta^0 = \theta_0$ , is also a linear combination of these subspace vectors, then by mathematical induction, it follows that for all  $l$ ,  $\theta^l$  is a linear combination of these subspace vectors. This result is apparent because if  $\theta^l$  is a linear combination of these subspace vectors, i.e.,  $\theta^l = E\alpha^l$ , it follows from Eqs. 20 and 28 that

$$\theta^{l+1} = E\alpha^l + \mu_l E\delta\alpha^{l+1} = E(\alpha^l + \mu_l \delta\alpha^{l+1}). \quad (30)$$

It now follows that when Eq. 18 is replaced by Eq. 29, Eq. 20 can be replaced by

$$\alpha^{l+1} = \alpha^l + \mu_l \delta\alpha^{l+1}, \quad (31)$$

and

$$\theta^{l+1} = E\alpha^{l+1}. \quad (32)$$

With this modification, the overall computational scheme for estimating the maximum a posteriori estimate (Eqs. 17 through 20) can now be written as

$$\begin{aligned} \delta m^{l+1} &= m_{prior} + \theta^l - m^l - C_M G_l^T (C_D + G_l C_M G_l^T)^{-1} \\ &\quad \times [g(m^l) - d_{obs} - G_l(m^l - m_{prior} - \theta^l)]. \end{aligned} \quad (33)$$

$$[E^T(I + C_M C_\Theta^{-1})E]\delta\alpha^{l+1} = E^T(m^l - m_{prior} - \theta^l) - E^T C_M C_\Theta^{-1}(\theta^l - \theta_0), \quad (34)$$

$$m^{l+1} = m^l + \mu_l \delta m^{l+1}, \quad (35)$$

and Eqs. 31 and 32. Eq. 33 was obtained from Eq. 17 by using basic matrix inversion lemmas (Tarantola, 1987; Chu et al., 1995a). The preceding subspace implementation of the Gauss-Newton iteration will converge to the so-called maximum a posteriori estimate  $(m_\infty, \theta_\infty)$ , which is commonly referred to as the most probable model. However, as noted previously, our

objective is not to simply generate the most probable estimate of  $\hat{m}$ , but to generate a suite of realizations which represent a correct sampling of the pdf of Eq. 9. The sampling procedure we use is presented in the following section.

## SAMPLING THE A POSTERIORI DISTRIBUTION

Markov chain Monte Carlo (MCMC) methods provide theoretical techniques which are guaranteed to produce a correct sampling of a given pdf if a sufficiently large number of states are generated. However, current implementations (Oliver et al., 1996b; Cunha et al., 1996) are too computationally intensive for practical applications when the goal is to generate realizations conditioned to production data and the generation of each state in the Markov chain requires a run of a reservoir simulator. Procedures based on approximating the a posteriori pdf by a Gaussian centered at the maximum a posteriori estimate require computing either the Cholesky decomposition or the square root of the a posteriori covariance matrix and do not always generate a correct sampling of the pdf (Oliver et al., 1996b; Cunha et al., 1996). Thus, we pursue a computationally efficient alternative. For the case where uncertainty in the prior mean is ignored, the basic procedure has been discussed by Oliver et al. (1996a) and relies on underlying theory developed by Oliver (1996). The basic procedure is technically correct only for the case where the data is linearly related to the model, however, Oliver et al. (1996a) have presented arguments which suggest that the procedure should give an approximately correct sampling in the nonlinear case.

### Linear Case

Here, we extend the results of Oliver (1996) and Oliver et al. (1996a) to the case where we incorporate uncertainty in the prior mean. We consider the case where the data is linearly related to the model, so Eq. 8 can be written as

$$d = Gm, \quad (36)$$

where  $G$  is an  $N_d \times N_p$  matrix. For this case, the maximum a posteriori estimate can be obtained by solving the following two equations:  $\nabla_\theta O(\hat{m}) = 0$  and  $\nabla_m O(\hat{m}) = 0$  (see Eqs. 12 and 13) to obtain  $m_\infty$  and  $\theta_\infty$ . It is easy to show that this solution satisfies

$$\begin{bmatrix} G^T C_D^{-1} G + C_M^{-1} & -C_M^{-1} \\ -C_M^{-1} & C_M^{-1} + C_\Theta^{-1} \end{bmatrix} \begin{bmatrix} m_\infty \\ \theta_\infty \end{bmatrix} = \begin{bmatrix} C_M^{-1} m_{prior} + G^T C_D^{-1} d_{obs} \\ -C_M^{-1} m_{prior} + C_\Theta^{-1} \theta_0 \end{bmatrix}. \quad (37)$$

Note that the coefficient matrix on the left side of Eq. 37 is the Hessian matrix defined in Eq. 15. Moreover, when Eq. 36 applies it is easy to show that the a posteriori pdf for  $\hat{M}$  (Eq. 9) is Gaussian with covariance matrix given by  $H^{-1}$  and expectation given by  $(m_\infty, \theta_\infty)$  (Tarantola, 1987).

Next, we present a procedure for sampling  $\pi(m, \theta)$  which does not require the generation and Cholesky or square root decomposition of  $H^{-1}$ . To construct a realization, we generate an unconditional simulation of  $m$ , which is denoted by  $m_{uc}$  and is given by

$$m_{uc} = m_{prior} + C_M^{1/2} Z, \quad (38)$$

where the components of the  $N_p$ -dimensional column vector  $Z$  are independent standard random normal deviates. Similarly, unconditional simulations of the data and the correction to the prior mean, respectively, are generated by

$$d_{uc} = d_{obs} + C_D^{1/2} Z_D, \quad (39)$$

and

$$\theta_{uc} = \theta_0 + C_\theta^{1/2} Z_\theta, \quad (40)$$

where again the components of  $Z_D$  and  $Z_\theta$  are independent standard random normal deviates. The  $1/2$  superscript on the matrices in the preceding three equations represent the square root of the matrix, but the square roots could also be replaced by the lower triangular matrix arising from the  $LL^T$  decomposition of the matrix. However,  $C_D$  and  $C_\theta$  are diagonal matrices, thus, it is trivial to compute their square root. Because we wish to avoid explicit factorization of  $C_M$ , in our computer implementation, we actually use sequential Gaussian cosimulation (e.g., Gomez-Hernandez and Journel, 1993) in place of Eq. 38 to generate  $m_{uc}$ . If we replace,  $m_{prior}$  by  $m_{uc}$ ,  $d_{obs}$  by  $d_{uc}$  and  $\theta_0$  by  $\theta_{uc}$  in Eqs. 12 and 13, set both equations to zero and solve to obtain the solution denoted by  $(m_s, \theta_s)$ , then similar to Eq. 37, we find that

$$\begin{bmatrix} G^T C_D^{-1} G + C_M^{-1} & -C_M^{-1} \\ -C_M^{-1} & C_M^{-1} + C_\theta^{-1} \end{bmatrix} \begin{bmatrix} m_s \\ \theta_s \end{bmatrix} = \begin{bmatrix} C_M^{-1}(m_{prior} + C_M^{1/2} Z) + G^T C_D^{-1}(d_{obs} + C_D^{1/2} Z_D) \\ -C_M^{-1}(m_{prior} + C_M^{1/2} Z) + C_\theta^{-1}(\theta_0 + C_\theta^{1/2} Z_\theta) \end{bmatrix}. \quad (41)$$

Subtracting Eq. 37 from 41, we see that the conditional simulations,  $m_s$  and  $\theta_s$  satisfy

$$\begin{bmatrix} G^T C_D^{-1} G + C_M^{-1} & -C_M^{-1} \\ -C_M^{-1} & C_M^{-1} + C_\theta^{-1} \end{bmatrix} \begin{bmatrix} m_s - m_\infty \\ \theta_s - \theta_\infty \end{bmatrix} = \begin{bmatrix} C_M^{-1} C_M^{1/2} Z + G^T C_D^{-1} C_D^{1/2} Z_D \\ -C_M^{-1} C_M^{1/2} Z + C_\theta^{-1} C_\theta^{1/2} Z_\theta \end{bmatrix} = B, \quad (42)$$

where the last equality of Eq. 42 serves to define  $B$ . The random vector  $\hat{M}_s$  is defined by

$$\hat{M}_s = [m_s^T, \theta_s^T]^T. \quad (43)$$

Since the expected values of  $Z$ ,  $Z_D$  and  $Z_\theta$  are all zero, it is clear that the expected values of  $\hat{M}_s$  is given by

$$E[\hat{M}_s] = \begin{bmatrix} m_\infty \\ \theta_\infty \end{bmatrix}, \quad (44)$$

i.e.,  $E[m_s] = m_\infty$  and  $E[\theta_s] = \theta_\infty$ . The covariance of the random vector  $\hat{M}_s$  is given by

$$E[(\hat{M}_s - E[\hat{M}_s])(\hat{M}_s - E[\hat{M}_s])^T] = H^{-1}E[BB^T]H^{-1}, \quad (45)$$

where  $B$  is defined by the last equality of Eq. 42. Using the fact that  $Z$ ,  $Z_D$  and  $Z_\theta$  are independent vectors, with components of each vector representing independent standard random normal deviates, it is straightforward to show that  $E[BB^T] = H$  and thus, Eq. 43 reduces to

$$E[(\hat{M}_s - E[\hat{M}_s])(\hat{M}_s - E[\hat{M}_s])^T] = H^{-1}. \quad (46)$$

Thus, we have shown that the covariance and expectations of  $\hat{M}$  and  $\hat{M}_s$  are the same. Since both random vectors satisfy Gaussian distributions when Eq. 36 applies, we can generate a sampling of  $\hat{M}$  by sampling the distribution for  $\hat{M}_s$ . Samples of  $\hat{M}_s$  can be generating by solving Eq. 41 for  $m_s$  and  $\theta_s$  for a set of independent unconditional simulations,  $m_{uc}$ ,  $d_{uc}$  and  $\theta_{uc}$ .

### Basic Sampling Procedure, Nonlinear Case

For the nonlinear case of interest, the same type of procedure is applied except we restrict  $\theta$  by introducing a subspace method, i.e, samples are generated by the computational algorithm of Eqs. 33, 34, 35, 31 and 32 with  $m_{prior}$  replaced by  $m_{uc}$ ,  $d_{obs}$  replaced by  $d_{uc}$  and  $\theta_0$  replaced by  $\theta_{uc}$ . Note this simulation procedure represents automatic history matching of the pressure data with prior information used as a regularization term.

In this process,  $\theta_{uc}$  must be generated so it lies in the appropriate subspace. To do this, recall that  $C_\Theta$  is a block diagonal matrix where the  $j$ th diagonal block is given by  $\sigma_{\theta,j}^2 I$  and introduce the associated covariance matrix  $C_\alpha$ , which is related to  $C_\Theta$  by

$$C_\alpha^{-1} = E^T C_\Theta^{-1} E. \quad (47)$$

$C_\alpha$  is an  $N_\alpha \times N_\alpha$  diagonal matrix with  $j$ th diagonal entry denoted by  $\sigma_{\alpha,j}^2$ . We compute

$$\alpha_{uc} = \alpha_0 + C_\alpha^{1/2} Z_\alpha, \quad (48)$$

where the components of the  $N_\alpha$  dimensional column vector are independent standard random normal deviates and set

$$\theta_{uc} = E\alpha_{uc}. \quad (49)$$

### COMPUTATIONAL EXAMPLE

The example considered pertains to a reservoir containing nine completely-penetrating wells. A simulation grid with 25 gridblocks in the x and y directions and 10 gridblocks in the z direction is used, i.e., 6,250 gridblocks are used. Since we wish to generate realizations of the

log-permeability and porosity fields, there are 12,500 model parameters. The areal grid is 400 ft by 400 ft and all gridblocks in the  $z$  directions are of thickness (height) 10 feet. Fig. 1 shows the areal grid and well locations.

The reservoir is areally isotropic  $k_x = k_y = k$  and we require that  $k_z = 0.1k$ . Thus, determination of a distribution for  $k$  automatically determines the vertical permeability at each gridblock. An anisotropic spherical variogram for  $\ln(k)$  is used with the range in the  $x$ -direction equal to 3,200 ft, the range in the  $y$ -direction equal to 1,600 ft and the range in the  $z$ -direction equal to 30 feet. The variance of  $\ln(k)$  (sill of the variogram) is specified as  $\sigma_k^2 = 0.5$ . The anisotropic variogram for porosity is identical to the one for  $\ln(k)$  except the variance for porosity is specified as  $\sigma_\phi^2 = 0.002$ . The correlation coefficient between log-permeability and porosity is specified as  $\rho_{k,\phi} = 0.7$ .

The true log-permeability is shown in Fig. 2. This truth case was obtained by unconditional simulation (Eq. 38) using  $m_{prior,k} = 4.0$  and  $m_{prior,\phi} = 0.20$ . This unconditional simulation also yields the true porosity field. For convenience, we refer to  $m_{prior,k} = 4.0$  and  $m_{prior,\phi} = 0.20$  as the true prior means. Synthetic well-test pressure data were generated by running the simulator using the true permeability and porosity fields. Well-test pressure data were collected at wells 2, 4, 5, 6 and 8 (see Fig. 1) during a period when the other four wells were produced at a specified rate. At the center well (well 5), a two-day drawdown followed by a one-day buildup test was run. At the other four tested wells (wells 2, 4, 6 and 8) pressure data were measured during three day drawdown tests. This synthetic pressure data is referred to as measured pressure data from this point onward.

In the following, we apply our procedures for sampling the a posteriori pdf (Eq. 9). We consider a case where we use  $m_{prior,k} = 5.0$  and  $m_{prior,\phi} = 0.25$  (referred to as the incorrect prior means) with and without allowing for uncertainty (errors) in the prior means.

Fig. 3 shows an unconditional simulation of the log-permeability field generated from Gaussian cosimulation using the true prior mean. Fig. 4 shows an unconditional simulation of the log-permeability obtained from Gaussian cosimulation using the incorrect prior means. As expected the gridblock values of log-permeability tend to be much higher when the incorrect mean is used; compare Figs. 3 and 4. Similar results were obtained for the porosity field since the incorrect mean for porosity is higher than its true mean.

Fig. 5 shows a conditional simulation of the log-permeability field obtained by applying the method of Oliver et al. (1996a) using true prior means for  $\ln(k)$  and porosity. This is equivalent to our basic procedure with  $\theta$  set equal to zero at all iterations, i.e., we do not incorporate uncertainty in the prior mean. Fig. 6 shows a conditional simulation obtained by the same procedure except in this case, the incorrect prior means were used. Note that the log-permeability values obtained in Fig. 6 tend to be much higher than those obtained in Fig. 5. This is the expected result because the incorrect prior means are much higher than the true values.

Fig. 7 shows a conditional realization obtained by our basic procedure. In this case, we used the incorrect prior means, but accounted for uncertainty in the prior means, where the  $2 \times 2$  diagonal covariance matrix  $C_\alpha$  (see Eq. 47) has as its two entries  $\sigma_{\alpha,1}^2 = 0.001$  and  $\sigma_{\alpha,2}^2 = 0.2$ . Note the realization in Fig. 7 is almost identical to the one of Fig. 5 which was generated with the true prior means by assuming no errors in the prior means. Although they are not presented here, similar results were obtained for the porosity field.

The results of Figs. 5 through 7 and the corresponding results for porosity (not shown) illustrate that our procedure for accounting for uncertainty in the prior means is viable and yields reasonable realizations of the rock property fields. The values of  $\theta$ , obtained by our basic procedure which gave the results of Fig. 7 indicate that the correction to the prior mean for  $\ln(k)$  was  $-1.041$  and the correction to the prior mean for porosity was  $-0.047$ . Note these values are very close to the true error in the incorrect prior means.

The permeability values corresponding to the results of Fig. 7 and associated porosity values were input to the simulator to predict pressure data at the five wells tested. Fig. 8 shows that the pressure data predicted at well 5 from this realization is in good agreement with the measured pressure data. Equally good agreement was obtained at the other tested wells. The dashed curve in Fig. 8 represents the pressure data predicted using the corresponding unconditional simulation,  $m_{uc}$ , as input in the reservoir simulator. As this  $m_{uc}$  was used as the initial guess in the Gauss-Newton method when constructing the conditional simulation by our basic simulation method, the results of Fig. 8 give a qualitative measure of how the incorporation of pressure data changes estimates of rock property fields obtained solely from the prior model.

We also generated 50 conditional simulations of the rock property fields using our basic simulation procedure. As discussed previously, this suite of realizations of the rock property fields represents an approximate sampling of the a posteriori pdf of Eq. 9. For each realization, we simulated reservoir performance for 1,000 days where each of the nine wells was produced at a specified bottom-hole pressure. Reservoir performance was also predicted from the set of  $m_{uc}$  values generated by Gaussian cosimulation. The lower set of curves in Fig. 9 represent the field cumulative oil production predicted from the 50 history-matched realizations, i.e., illustrates the uncertainty in predicted reservoir performance. The curve through the solid dots represents the field cumulative oil production generated using the true permeability and porosity fields as simulator input. The top set of curves in Fig. 9 represent the predictions of cumulative oil production obtained from the set of 50  $m_{uc}$  models which were used as initial guesses in the Gauss-Newton procedure. Note these realizations predict erroneously high values of cumulative oil production since the incorrect prior means are much higher than the true prior means.

A histogram of the cumulative oil production at 1,000 days and associated cumulative distribution function are shown in Fig. 10. The expected value (mean) is  $5.70 \times 10^6$  STB, the median is  $5.74 \times 10^6$  STB, and the standard deviation is  $1.68 \times 10^5$  STB. Note the bar in the histogram over  $5.80 \times 10^6$  STB represents the number of outcomes (15) between  $5.7 \times 10^6$  STB

and  $5.80 \times 10^6$  STB. The cumulative oil production at 1,000 days predicted using the true rock property fields was  $5.68 \times 10^6$  STB.

## CONCLUSIONS

Errors in the prior means can be properly taken into account by using the partially doubly stochastic model developed here. Based on the model, we have presented an automatic history procedure which can be applied to generate a set of realizations conditioned to pressure data and a prior geostatistical model. This set of realizations represents an approximate sampling of the a posteriori probability density function for the rock property fields. It has been proven rigorously that the basic procedure for sampling the pdf is correct if measured data are linearly related to the model. It has been shown that if estimates of prior means are inaccurate and the errors in the prior means are not accounted for, one can not obtain a correct sampling of the pdf for the rock property fields.

Using our basic procedure for sampling the pdf, one can predict reservoir performance for each realization to evaluate the uncertainty in predicted reservoir performance.

## REFERENCES CITED

- Chu, L., A. C. Reynolds, and D. S. Oliver, 1995a, Computation of sensitivity coefficients for conditioning the permeability field to well-test pressure data, *In Situ* v. 19, p. 179-223.
- Chu, L., A. C. Reynolds, and D. S. Oliver, 1995b, Reservoir description from static and well-test pressure data using efficient gradient methods, paper SPE 29999, presented at the 1995 SPE International Meeting on Petroleum Engineering, Beijing, Nov. 14-17.
- Cunha, L. B., D. S. Oliver, R. A. Redner, and A. C. Reynolds, 1996, A hybrid Markov chain Monte Carlo method for generating permeability fields conditioned to multiwell pressure data and prior information, paper SPE 36566, presented at the 1996 SPE Annual Technical Conference and Exhibition, Denver, Oct. 6-9.
- Fletcher, R., 1987, *Practical Methods of Optimization*, John Wiley & Sons, Inc., New York.
- Gomez-Hernandez, J. J. and A. G. Journel, Joint sequential simulation of multi-Gaussian random variables, 1993, in Soares, A., editor, *Geostatistic Troia 92*, Kluwer, p. 133-144.
- He, N., A. C. Reynolds, and D. S. Oliver, 1996, Three-dimensional reservoir description from multiwell pressure data, paper SPE 36509, presented at the 1996 SPE Annual Technical Conference and Exhibition, Denver, Oct. 6-9.
- Journel, A. G. and Ch. J. Huijbregts, 1978, *Mining Geostatistics*, Academic Press Limited, London.
- Kennett B. L. N. and P. R. Williamson, 1988, Subspace methods for large-scale nonlinear inversion, in *Mathematical Geophysics: A Survey of Recent Developments In Seismology and Geodynamics*, eds. Vlar, N. J. et al., D. Reidel Publishing Company, Dordrecht, p. 139-154.

- Oldenberg, D. W., P. R. McGillivray, and R. G. Ellis, 1993, Generalized subspace methods for large-scale inverse problems, *Geophysics J. Int.*, v. 10, p. 12-20.
- Oldenberg, D. W. and Y. Li, 1994, Subspace linear inverse method, *Inverse Problems*, v. 10, p. 915-935.
- Oliver, D. S., 1994, Incorporation of transient pressure data into reservoir characterization, *In Situ* v. 18, p. 243-275.
- Oliver, D. S., 1996, On conditional simulation to inaccurate data, *Math. Geology*, v. 28, p. 811-817.
- Oliver, D. S., N. He, and A. C. Reynolds, 1996a, Conditioning permeability fields to pressure data, Proceedings of at the 5th European Conf. on the Mathematics of Oil Recovery, p. 259-269.
- Oliver, D. S., L. B. Cunha, and A. C. Reynolds, 1996b, Markov chain Monte Carlo methods for conditioning a permeability field to pressure data, to appear in *Math. Geology*.
- Peaceman, D. W., 1983, Interpretation of well-block pressures in numerical reservoir simulation with non-square grid blocks and anisotropic permeability," *Soc. Pet. Eng. J.*, v. 23, p. 531-543.
- Reynolds, A. C., N. He, L. Chu, and D. S. Oliver, 1995, Reparameterization techniques for generating reservoir descriptions conditioned to variograms and well-test pressure data, paper SPE 30588, presented at the 1995 SPE Annual Technical Conference and Exhibition, Dallas, Oct. 22-25, to appear in *Soc. Pet. Eng. J.*
- Tarantola, A., 1987, *Inverse Problem Theory, Methods for Data Fitting and Model Parameter Estimation*, Elsevier Science Publishers, Amsterdam.
- Tjelmeland, H., H. Omre, and B. J. Hegstad, 1994, Sampling from Bayesian models in reservoir characterization, Technical Report Statistics No. 2, University of Trondheim.
- Xu, W., T. T. Tran, R. M. Srivastava, and A. G. Journel, 1992, Integrating seismic data in reservoir modeling: the collocated cokriging approach, paper SPE 24742, presented at the 1992 SPE Annual Technical Conference and Exhibition, Washington D.C., Oct. 4-7.



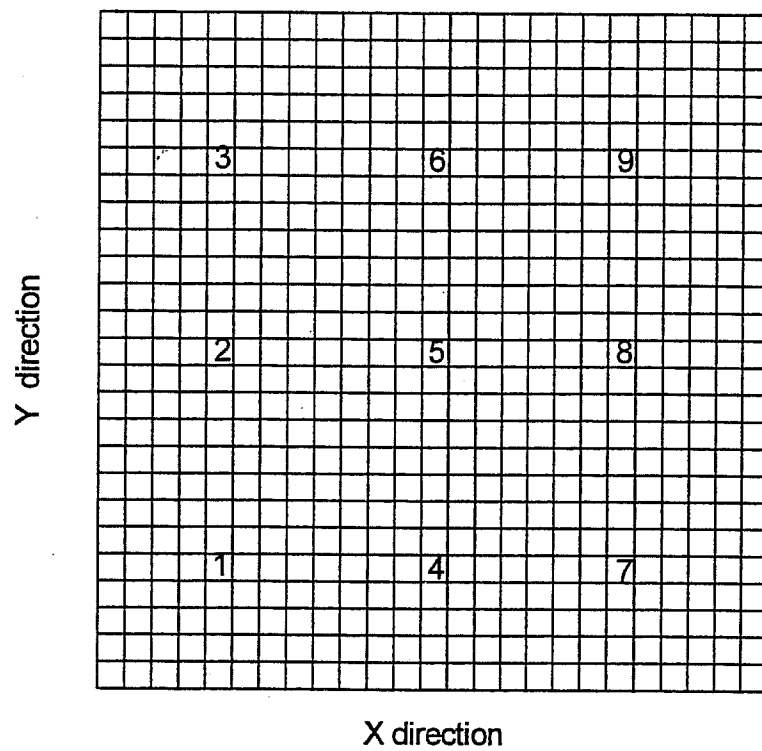


Fig. 1 - Areal grid, well locations and well numbers.

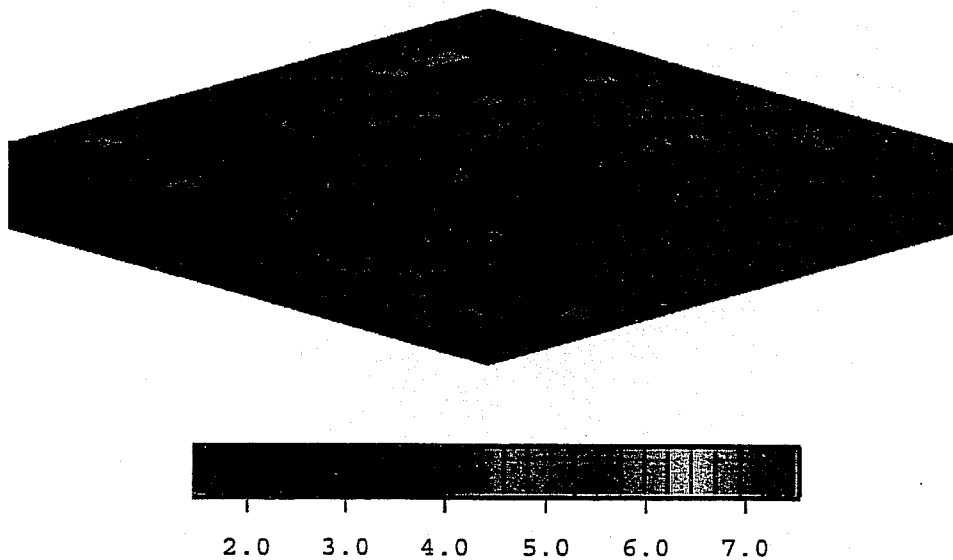


Fig. 2 - True log-permeability field.

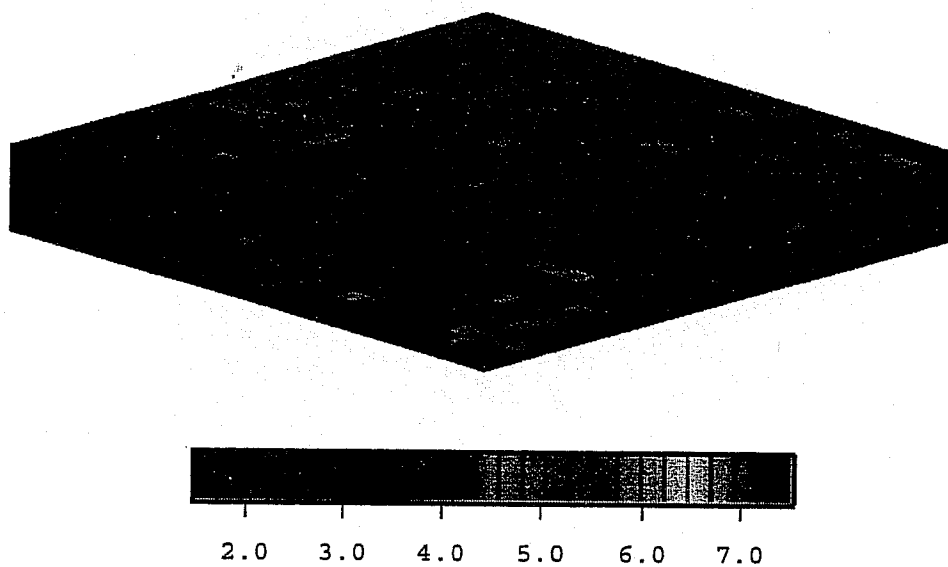


Fig. 3 - Unconditional realization of log-permeability field with true prior means.

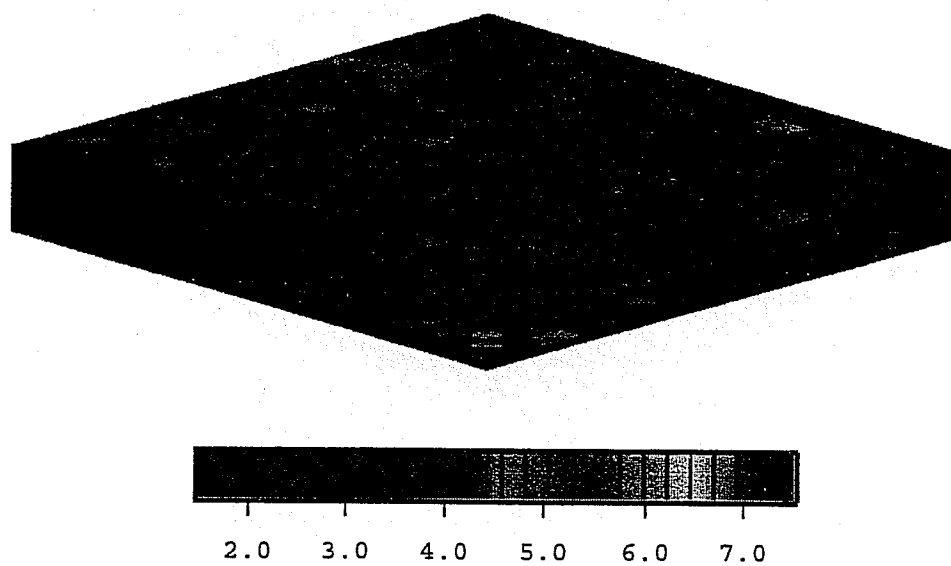


Fig. 4 - Unconditional realization of log-permeability field with incorrect prior means.

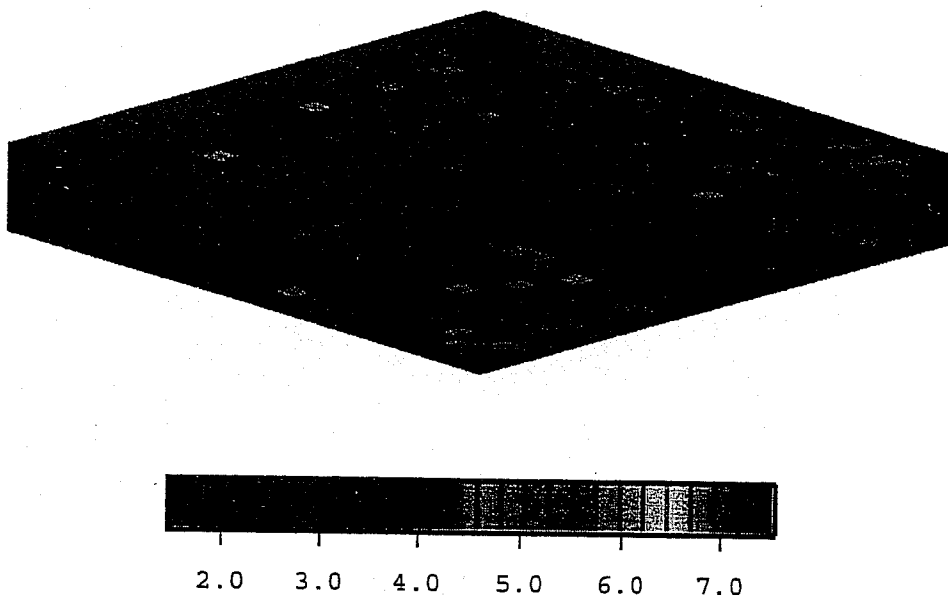


Fig. 5 - Realization of log-permeability field conditioned to pressure data using true prior means.

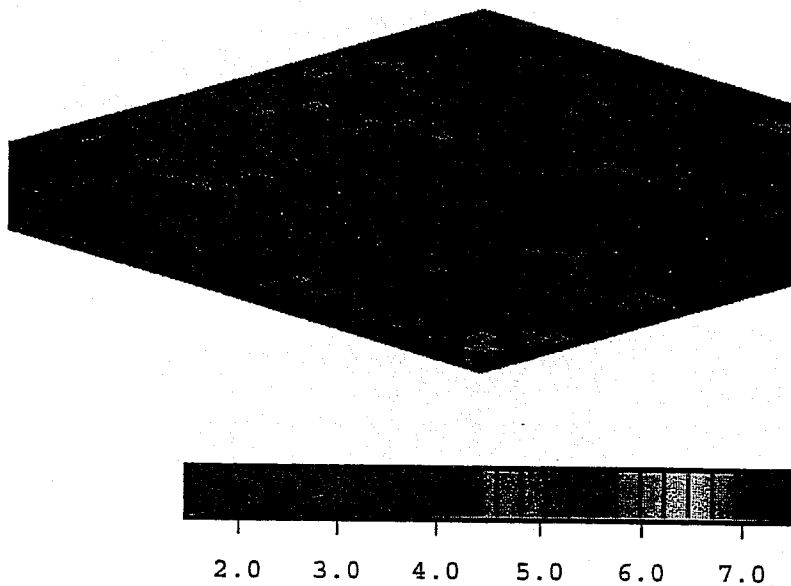


Fig. 6 - Realization of permeability field conditioned to pressure data using incorrect prior means without correction to prior means.

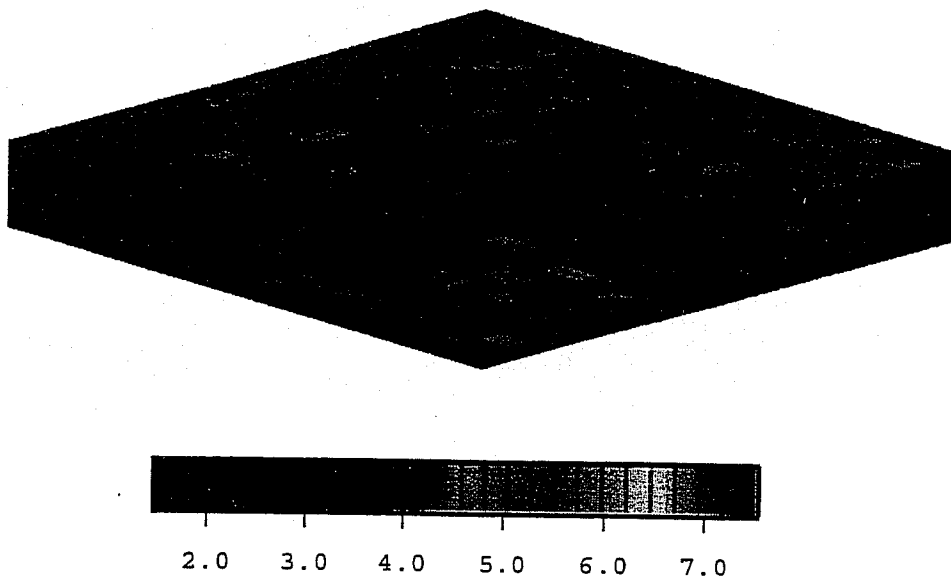


Fig. 7 - Realization of log-permeability field conditioned to pressure data with correction to incorrect prior means.

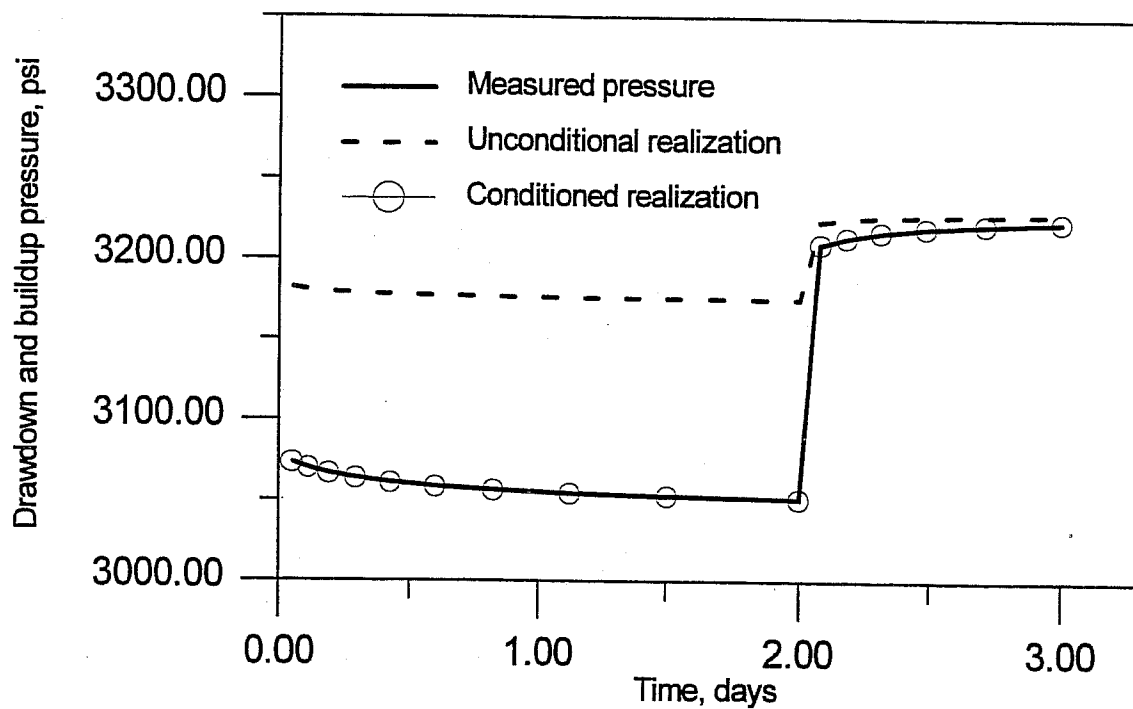


Fig. 8 - Pressure data predicted at well 5 from conditional and unconditional simulations of rock property fields compared to measured pressure data.

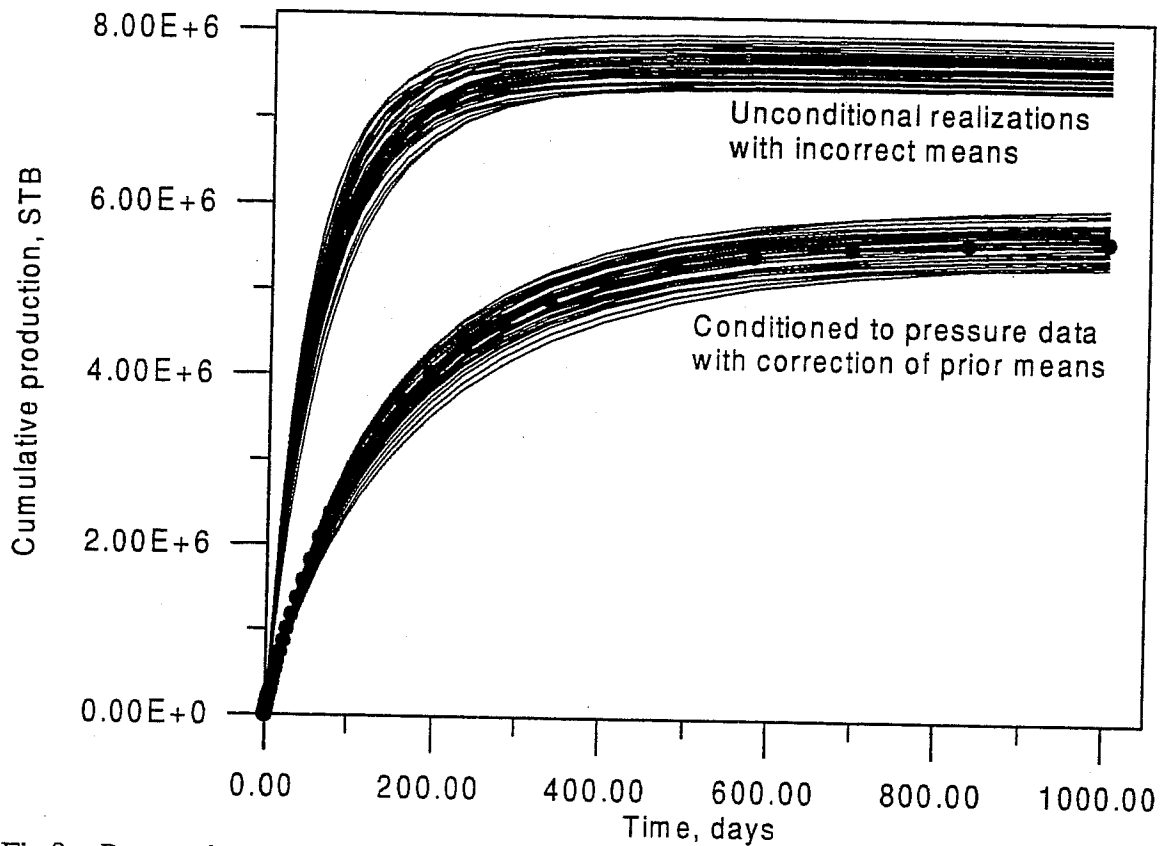


Fig.9 - Reservoir performance predicted from a suite of unconditional simulations and a suite of conditioned simulations.

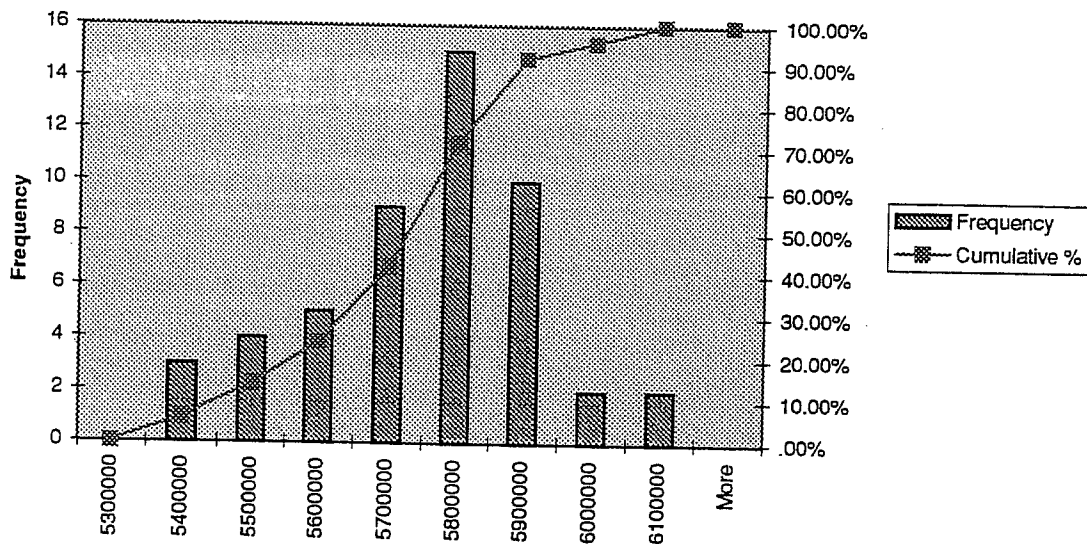


Fig 10 - Histogram and cumulative distribution of cumulative oil production at 1,000 days.

# A QUANTITATIVE METHOD FOR MEASURING THE QUALITY OF HISTORY MATCHES

Tom S. Shaw, Kerr-McGee Corporation, Oklahoma City, OK

Roy M. Knapp, University of Oklahoma, Norman, OK

## Abstract

History matching can be an efficient tool for reservoir characterization. A "good" history matching job can generate reliable reservoir parameters. However, reservoir engineers are often frustrated when they try to select a "better" match from a series of history matching runs. Without a quantitative measurement, it is always difficult to tell the difference between a "good" and a "better" matches. For this reason, we need a quantitative method for testing the quality of matches. This paper presents a method for such a purpose.

The method uses three statistical indices to (1) test shape conformity, (2) examine bias errors, and (3) measure magnitude of deviation. The shape conformity test insures that the shape of a simulated curve matches that of a historical curve. Examining bias errors assures that model reservoir parameters have been calibrated to that of a real reservoir. Measuring the magnitude of deviation assures that the difference between the model and the real reservoir parameters is minimized.

The method was first tested on a hypothetical model and then applied to published field studies. The results showed that the method can efficiently measure the quality of matches. It also showed that the method can serve as a diagnostic tool for calibrating reservoir parameters during history matching.

## 1. Introduction

A numerical reservoir model can be envisioned as a sophisticated instrument. The instrument must be properly calibrated before it can give accurate readings. History matching thus can be conceived as a model calibration process. The process involves adjusting the reservoir parameters of a numerical model to produce a "*best*" match between the simulated results and the observed reservoir performance data. The objective of a history matching process is to devise a set of reservoir data to properly describe the reservoir being simulated.

Reservoir simulation assumes that a numerical model which works during history matching mode will also work during the prediction mode. This implies that a model must be valid during history matching to be valid during prediction. The reliability of the predicted reservoir performance thus depends on the quality of the reservoir description data used to build the model. It is thus very important that the reservoir description data used in a model be the one that can best describe the reservoir being simulated.

What is considered the best data that can describe a reservoir? Theoretically, the set of reservoir description data that produces the "*best*" match between the simulated results and the observed reservoir performance data is presumed to be the one that can best describe the reservoir. In practice, however, it is difficult to tell when the best match has been achieved, unless a quantitative measure is provided for comparing the quality of matches. Unfortunately, to date, there is still no efficient quantitative method for measuring the quality of history match. Qualitative description such as "good matches", "excellent matches" or "poor matches" are often used to describe the quality of matches. This paper will present a quantitative method for measuring the quality of history matches.

## 2. Scope of This Paper

Because history matching is an ill-conditioned problem, different sets of reservoir parameters can result in the same quality of match. Evaluation of the quality of matches thus must include addressing two fundamental questions: (1) the quality of matches between simulated results and observed data; and (2) the uniqueness of the solution. Although knowing whether the estimated reservoir parameters represent the true solution is very important, solution nonuniqueness is an inherent problem to the history matching process that can not be readily resolved. The scope of this paper will focus on examining the quality of matches between simulated results and observed data.

## 3. Statistical Interpretation of The Quality of History Matches

During the past several decades, much work in reservoir simulation has been devoted to developing history matching algorithms and improving computation efficiency. Associated with these developments, various statistical indices have also been used to test the quality of history matches. Jahns (1966) used the standard deviation to test the reliability of reservoir properties estimated from regression analyses. Slater and Durrer (1971) suggested using the multiple correlation coefficient and the F-test for measuring the quality of matches. Dixon, *et al* (1973) applied the student-t test to express confidence limits on reservoir parameters estimated from history matches. Dogru and Knapp (1975) extended the student-t test to analyze the reliability of reservoir parameters estimated from history matching drawdown test data. Watson, *et al* (1984) used the chi-square test in an analytic study to express the confidence levels of reservoir parameters estimated from history matching.



Although application of the statistical tests described above requires that errors be randomly distributed and uncorrelated, this necessary condition was never addressed. If errors occurred in a certain pattern and were correlated, it indicated that the model reservoir properties had not been calibrated to match the "true" reservoir properties. Watson, *et al* (1989) incorporated residual analyses and the Durbin-Watson (D-W) Test (Draper and Smith, 1981) into the history matching process to examine error distribution and correlation. These two tests insured that the residuals were randomly distributed, a necessary condition for any least-squares minimization algorithm. However, the D-W test is a parametric method that requires the identification of the number of variables used to describe the model. In history matching problems, the number of variable used to model the reservoir system being simulated cannot be readily identified.

Although limited work has specifically been directed to the problems of quantitative measurement of the quality of history matches, there is still no efficient method developed for such a purpose. This can be attributed to the following reasons:

- (1) Methods such as the chi-square method and correlation coefficient can only provide a indication of overall fit between simulated and observed values. Overall fit is a necessary but not a sufficient condition for measuring the fit between model calculated and observed values (Draper and Smith, 1981).
- (2) Methods such as the F-test and Durbin-Watson test are parametric methods which require knowing the number of variables used to build the model being studied (Chatterjee and Price, 1977). In history matching, the number of variables used to build the numerical model is not readily identifiable. Therefore, parametric methods are not suitable for measuring the quality of history matches.

#### 4. Factors Affecting The Quality of History Matches

There are three types of errors that can affect the quality of reservoir parameters estimated from a history matching process: (1) simulator errors ( $e_s$ ) arise from the failure of the simulator to properly represent the physics of fluid flow process occurring in the reservoir, and failure to numerically integrate the descriptive equations accurately; (2) measurement errors ( $e_m$ ) result from incorrect sampling procedures, measurement errors or instrument malfunctions, etc.; and (3) history matching errors ( $e_h$ ) attributed to assigning incorrect reservoir parameter values to the numerical model representing the reservoir being studied. The total error ( $e_t$ ) in a history matching run may include all three error types, or

$$e_t = e_s + e_m + e_h \quad (1)$$

Where  $e_s = 0$  since it is generally assumed that: (1) the simulator accurately represents the physics of fluid flow process occurring in the reservoir system being studied and, (2) care has been taken to minimize the effects of truncation errors in the finite difference approximation process that their impact on the simulated results will be small. The  $e_m$  term contains only random errors since, in practice, it is generally assumed that all testing instruments function properly and correct sampling and measurement procedures have been taken to avoid adding patterned errors to  $e_m$ . The  $e_h$  term contains errors resulting from assigning incorrect reservoir parameter values to the numerical model representing the study reservoir system. Assigning incorrect reservoir parameters to a numerical model will cause the simulated reservoir performance to deviate from observed reservoir performance. Under such a condition, the  $e_h$  will be biased. With actual data, it is difficult to identify the exact contributions of each

type to the errors in the estimated reservoir parameter values.

## 5. Statistical Properties of Errors

Let  $R$  denote the model representing the system of governing equations plus the boundary and the initial conditions necessary to describe the reservoir system being simulated;  $y$ ,  $x$ ,  $b$  denote the dependent variables, independent variables and parameters of the model, respectively, then the reservoir model can be written as

$$Model = R(y, x, b) \quad (2)$$

In a simulator where the  $y$  terms represent the state variables, e.g., pressure and saturation; the  $x$  terms represent the spatial and time variables, e.g., grid block location and time step; and the  $b$  terms represent the coefficients of the finite difference equations to be solved, e.g., porosity and permeability. When  $R$  has a unique solution, then the postulated model can be expressed by

$$y = f(x, b) \quad (3)$$

If  $y^o$  denotes the observed data and  $y^*$  denotes the solution calculated from the postulated model, then  $y^*$  can be related to  $y^o$  by

$$y_i^* = y_i^o + e_i \quad (4)$$

In regression analysis, the  $e_i$  are generally referred to as residuals. They contain all the available

information which the model fails to properly explain for the observed variations in the dependent variables. Draper and Smith (1981) stated that the residuals contained two types of errors: random errors,  $e_{ri}$ , and bias errors,  $e_{bi}$ , that is:

$$e_i = e_{ri} + e_{bi} \quad (5)$$

They stated that: (1) the quantity  $e_{ri}$  is a random variable that has zero mean whether the model is correct or not; and (2) the quantity  $e_{bi}$  is zero if the model is correct and  $e_{bi}$  is not zero, but has a value that depends on the true model if the model is not correct. These statements imply that, when the model is correct, the bias errors are eliminated, i.e.,

$$\sum_{i=1}^n e_{bi} = 0 \quad (6)$$

and the sum of residuals is zero since the residuals contain only random errors. Under such a condition, the residuals are randomly distributed. However, if the model is not correct, then the residuals contain random and bias errors, i.e.,

$$\sum_{i=1}^n e_i = \sum_{i=1}^n e_{ri} + \sum_{i=1}^n e_{bi} \quad (7)$$

and the residuals are no longer randomly distributed. Under such a condition, the sum of the residuals equals the bias errors because the sum of random errors is zero whether the model is correct or not. The objectives of a history match process are not only to ensure a good match between the simulated

results and the observed data, but must also include eliminating bias errors in the residuals. If the bias errors can not be eliminated, then the sum of the residuals should be minimized.

## **6. Procedures for Measuring The Quality of History Matches**

The above discussions indicate that measuring the quality of history match requires not only testing the degree of match between the simulated results and the observed reservoir performance data, but also examining of the randomness of the residuals and a measuring of the magnitude of the residuals. Measuring the quality of history matches thus requires the following steps:

- (1) **test the goodness of fit** between the simulated results and the observed data to see whether there is a similarity between the shape of the simulated and the observed reservoir performance curves;
- (2) **examine the randomness of residuals** to see whether the residuals are randomly distributed and bias errors are eliminated; and
- (3) **measure the magnitude of residuals** to see whether bias errors are minimized if a perfect match can not be achieved and the bias errors can not be eliminated.

### **6.1 Testing The Goodness of Fit**

Goodness of fit is used in regression analysis to describe the degree of fit between the results calculated by a model and the observed data. Statistically, a close fit indicates that it is likely that the theoretical outcomes and the observed values have occurred under the same conditions and the shapes of the theoretical and the observed curves will be similar. Reservoir performance curves

represent the records of behavior as a reservoir reacts to fluid production and/or injection. A close similarity between the shape of the simulated and the observed reservoir performance curves indicates there is a similarity between the model and the actual reservoir behavior. A good fit between the simulated and the observed curves thus reflects how close a reservoir model represents the reservoir system being studied. A lack of fit between the simulated and the observed curves indicates that differences exist between the actual reservoir properties and the model input data. Thus testing the goodness of fit to see whether there is a similarity between the shape of the simulated and the observed reservoir performance curves becomes the first step in measuring the quality of history matches.

## **6.2 Examining Residuals for Bias Errors**

Residuals can be considered as the amount of observed values by which a model fails to account for. If the model is correct, there should be no discernible pattern to the distribution of residuals; that is, the residuals do not occur in a systematic way. Any pattern of variation present in the residuals indicates that the model input data have not been calibrated to reflect the "true" reservoir description data. Thus a "good fit" between the simulated and observed reservoir performance curves can be meaningful only insofar as the assumptions concerning the residual terms in the model are satisfied. Consequently, analyzing residuals for randomness to see whether bias errors are eliminated is the second step in measuring the quality of history matches.

## **6.3 Measuring the Magnitude of Residuals**

If a model has been calibrated to reflect the "true reservoir" under study, then there

should be no discernible pattern to the distribution of residuals. Since it is often impossible, if not impractical, to obtain a "perfect" match between the simulated results and observed data, a set of data that provides the "best" match is generally selected to describe the reservoir. However, for an "imperfect match" condition, residuals can contain bias and random errors, i.e.,  $e_i = e_{r,i} + e_{b,i}$ . The magnitude of the  $e_i$  increases with the increase in  $e_{b,i}$  since the  $e_{r,i}$  are randomly distributed and the sum of  $e_{r,i}$  is zero. The magnitude of the residuals represents the bias errors and measuring the magnitude of residuals becomes another necessary task in evaluating the quality of history matches.

## 7. Three Indicators for Measuring the Quality of Matches

As discussed in Section 3, there is still no efficient quantitative method for measuring the quality of history match. Today, qualitative phrases are often used to describe the quality of history matches. This is because methods proposed in the past were either inefficient or cumbersome to use. To avoid these shortcomings, the following non-parametric indicators were selected for measuring the goodness of fit, the randomness of residuals and the magnitude of residuals:

### 7.1 Kolmogorov-Smirnov (K-S) Statistic

The K-S statistic involves comparing the cumulative frequencies of a theoretical distribution,  $E(X)$ , with the observed cumulative frequency distribution,  $O(X)$ , of  $N$  random samples and possible score  $X$ . The point at which the two distributions show the maximum divergence determines how close the observed values fit the theoretical distribution. The maximum divergence,  $MD$ , is defined as:

$$MD = \text{maximum } | O(X) - E(X) | \quad (8)$$

The goodness of fit is measured by the significance level (  $\alpha$  ) of the K-S statistic associated with the calculated MD value (Smirov, 1948). Approximate values of  $\alpha$  of the K-S statistic can be calculated by the following equation given by Birnbaum (June, 1952):

$$\alpha = \exp ( - 2 \cdot N \cdot MD ) \quad (9)$$

Since  $O(X)$  and  $E(X)$  are dimensionless, this property makes the K-S statistic suitable for testing the goodness of fit for history matching problems because the matches can be done on any unit or scale without distorting the test results.

## 7.2 The Runs Test

The randomness of the sequence in which the residuals occur can be examined by the Runs Test. A run is defined as a succession of identical symbols which are preceded or followed by different symbols. The test examines the order of the symbols to determine the number of runs that a sample exhibits. The total number of runs in the sample gives the indication of whether the sample occurs in random sequence. If very few or a great many runs occur, it may suggest that a trend due to lack of independence exists in the residuals. A good approximation to the sampling distribution of  $r$  is the normal distribution, with mean



$$u = \frac{2 n_1 n_2}{n_1 + n_2} + 1 \quad (10)$$

and standard deviation

$$s = \sqrt{\frac{2 n_1 n_2 (2 n_1 n_2 - n_1 - n_2)}{(n_1 + n_2)^2 (n_1 + n_2 - 1)}} \quad (11)$$

and the probability of a normal distribution with  $u$  and  $s$

$$z = \frac{r - u + 0.5}{s} \quad (12)$$

where 0.5 is the usual continuity correction factor to compensate for the fact that a continuous distribution is being used to approximate a discrete distribution (Draper and Smith, 1981). The computed  $z$  value is compared to the normal distribution table to determine whether the residuals are randomly distributed. The significance level at which the computed  $z$  value equals the tabulated value indicates the degree of randomness in the sequence in which the residuals occur.

If the runs test reveals a lack of randomness in the residuals sequence, graphic procedures can be used to analyze the residuals for patterns of errors. Draper and Smith (1981) believed that more information could be obtained from an informal examination of a residual plot than from a formal test of statistical significance of some limited null-hypothesis. They suggested that a detailed examination of a residual plot could generally reveal error patterns which could be used as the

basis for correcting model deficiencies. However, interpreting residual plots requires insight and skill. Consequently, interpretation can be very subjective and formal statistical tests are still needed for quantitatively measuring residuals randomness.

### 7.3 Mean Absolute Error

The mean percentage error, MAE, which is defined as:

$$MAE = \frac{1}{n} \sum_{i=1}^n \left| \frac{e_i}{y_i^o} \right| \quad (13)$$

where the absolute values of  $e_i / y_i^o$  are used to avoid cancellation between positive and the negative residuals. The magnitude of each  $e_i$  is still compared to its corresponding value of  $y_i^o$  to show the importance of the deviation at that time step. Since the residuals contain bias and random errors, therefore

$$MAE = \frac{1}{n} \sum_{i=1}^n \left| \frac{e_{bi}}{y_i^o} \right| + \frac{1}{n} \sum_{i=1}^n \left| \frac{e_{ri}}{y_i^o} \right| \quad (14)$$

The mean absolute error approaches infinity when any  $y_i^o$  approaches zero. The following procedures are used to correct this problem:

- (1) When both the simulated and the observed values at any time step are zero, then the residual at that time step will be treated as zero.

- (2) When any observed value is zero, for instance,  $y_j^o = 0$ , but the corresponding model value,  $y_j^*$  is not zero, then an  $y_{j+0.25}^o$  and an  $y_{j+0.25}^*$  are interpolated for  $t_j + 0.25(t_{j+1} - t_j)$  to substitute for  $y_j^o$  and  $y_j^*$ , respectively. A new  $e_{j+0.25}$  is calculated as a substitute for  $e_j$ . The constant 0.25 is an arbitrary number used to account for the fact that the  $y_{j+0.25}^o$  is interpolated as a substitute for  $y_j^o$  rather than  $y_{j+1}^o$ . The interpolation process can also be carried backward to point  $t_{j-1}$  if preferred. If  $y_{j+1}^o = 0$ , then the interpolation is carried on to the time step until where the observed value is greater than 0.

The interpolation process is justified because when there is a good fit between the simulated and the observed curves,  $y_j^o$  will be close to  $y_j^*$  and the interpolated values will also be close to each other. Therefore, the error introduced by the interpolation process will be small. If there is not a good fit, then there is no need to worry about the magnitude of residuals, since the match will have been rejected.

## 8. Evaluation of The Efficiency of The Method

A hypothetical reservoir model was used to generate "observed" data. Six sets of simulated results were generated by setting porosity and permeability values 5%, 10% and 20% above and below the true values. All other reservoir and well control parameters were unchanged. The simulated BHP, GOR and WOR data were compared with the "observed" data. The K-S statistic, the runs test and the mean absolute error were used to evaluate the quality of the six sets of simulated results. The results, given in Figure 1, show that the three statistical indicators are effective for measuring the quality of matches:

- (1) The match quality improved with decreases of errors in the porosity and permeability.

This shows that the proposed method can effectively detect the changes in the quality

of reservoir description data.

- (2) The best fit, the highest randomness of residual and the lowest magnitude of residuals of the matches occurred for the cases with the smallest errors in the porosity and permeability. This further confirms that the K-S statistic, the runs test and the mean absolute error are effective methods to measure the quality of history matches.
- (3) Generally, when the K-S statistic showed a good fit and the mean absolute error showed a small magnitude of residuals, the runs test still showed a low level of residuals randomness. This indicates that the runs test is highly sensitive to bias errors in the residuals.

## **9. Application of The Method**

The three statistical indicators were applied to analyze the quality of 44 reported history matches from seven published field studies. The data were obtained from digitizing the published graphs (Ader and Stein, 1982; Kuo, et al, 1990; Grantz, 1980; Hopkins and Lancaster, 1991; Moltz, 1991; Kansas Corporation Commission Docket C-164, 1985), except one that was supplied by the author (Young and Paul, 1993). The results indicate that a good fit only indicates a close conformity between the shapes of the simulated and the observed curves. It does not guarantee that bias errors, as indicated by the randomness of residuals, do not exist in the residuals. Figure 2 compares the goodness of fit, the randomness of residuals and the magnitude of residuals of the 44 matches analyzed. Note that the matches are arranged according to the goodness of fit values in an ascending order. The figure shows most of the matches that had a low residual randomness also had a low goodness of fit. Only eight of the 22 matches tested with greater than 5% residual randomness

occurred to the matches that had a better than 90% goodness of fit. This shows that residuals can contain bias errors even when the simulated performance curve appears to closely conform to the observed curve. The distribution of the magnitude of residuals for the 44 matches shows a distinct trend when compared to the goodness of fit values, only in inverted order. Most of the matches tested with lower than 90% goodness of fit had a 10% or higher in residual magnitude. This indicates that conformity in the shapes of the simulated and the observed curves generally reduced the magnitude of residuals, although this may not be true in every match. However, these two indicators together do not guarantee a good match quality. For instance, two curves having a close similarity in shapes may show a high goodness of fit with small residual magnitude, yet the runs test may still show a low level of residual randomness.

## 10. Conclusions

Application of the method to test the quality of history matches for published field studies confirms that the K-S statistic, the runs test and the mean absolute error are efficient indicators for measuring the quality of history matches. It is concluded that:

- (1) Quantitative measurement of the quality of history matches requires all three quality indicators: the goodness of fit, the randomness of residuals and the magnitude of residuals; no single indicator can be ignored.
- (2) The K-S statistic, the runs test and the mean absolute error are efficient indicators for testing the goodness of fit, examining randomness of residuals and measuring the magnitude of residuals, respectively.
- (3) An efficient history matching strategy should first be devoted to increasing the

goodness of fit and the randomness of residuals, then to minimizing the magnitude of residuals.

- (4) Residuals plots are effective tools for detecting and analyzing bias errors present in the residuals.

### ACKNOWLEDGEMENT

The authors would like to thank Advanced Resources International, Inc. of Lakewood, Colorado for providing a portion of the data used in this study.

### REFERENCES CITED

Ader, J. C. and Stein, M. H., 1982: Slaughter Estate Unit CO<sub>2</sub> Pilot Reservoir Description via a Black Oil Model Waterflood History Match, SPE #10727, Proceedings of the 3rd SPE/DOE Joint Symposium on Enhanced Oil Recovery, Tulsa, Oklahoma, April 4-7, 1982, pp. 817-838.

Birnbaum, Z. W., June, 1952: Distribution-Free Tests of Fit for Continuous Distribution Functions, Preprint of the Meeting of the Inst. of Mathematical Statistics in Eugene, Ore., June 21, 1952, pp. 1-8.

Birnbaum, Z. W., September, 1952: Numerical Tabulation of the Distribution of Kolmogorov's Statistic for Finite Sample Size, American Statistical Association Jour., September 1952, pp. 425-441.

Chatterjee, S. and Price, B., 1977: Regression Analysis by Examples, John Wiley & Sons, N.Y., 1977.

Dixon, T. N., Seinfeld, J. H., Startzman, R. A. and Chen, W. H., 1973: Reliability of Reservoir Parameters from History Matched Drill Stem Tests, SPE #4282, Proceedings of the 3rd SPE Numerical Simulation of Reservoir Performance Symposium, Houston, Tx, January 10-12, 1973.

Dogru, A. H. and Knapp, R. M., 1975: The Reliability of the Predicted Performance of Natural Gas Reservoirs using Reservoir Parameters from Well Test Data Containing Errors, Preprint of the Rocky Mountain Regional Meeting of SPE, Denver, Co., April 7-9, 1975.

Draper, N.R. and Smith, H., 1981: Applied Regression Analysis, 2nd ed., John Wiley & Sons, N.Y., 1981.

- Grantz, R. E., 1980: Waterflood History Match Study of the Torchlight Tensleep Micellar Pilot, SPE #9046, Preprint of the SPE Rocky Mountain Regional Meeting, Casper, Wyoming, May 14-16, 1980.
- Hopkins, C. W. and Lancaster, D. E., 1991: History Match Analysis of Production and Well Test Data from Mitchell Energy Corporation's Stella Young 4 Well, Topical Report on Reservoir Engineering and Treatment Design Technology, GRI Contract #5086-213-1446, November 1991.
- Jahns, H. O., 1966: A Rapid Method for Obtaining a Two-Dimensional Reservoir Description from Well Pressure Response Data, SPEJ, December 1966, pp. 315-327.
- Kansas Corporation Commission Docket C-164, 1985: Direct Opening Testimony and Rebuttal Testimony Exhibits: Application of Cities Service Oil and Gas Company for an Order Amending the Basic Proration Order for the Kansas Hugoton Field before the State of Kansas, February - April, 1985.
- Kuo, M. C. T. and Dulaney, J. P., Deer, M. W. and Evans, B. S., 1990: Optimization of Waterflood Performance and CO<sub>2</sub>-Flood Design Using a Modeling Approach, Mallet Unit, Slaughter Field, Proceeding of the 65th Annual Technical Conference & Exhibition of SPE, New Orleans, La., September 23-26, 1990, pp. 609-620.
- Slater, G. E. and Durrer, E. J., October, 1971: A Statistical Method for Judging the Adequacy of a Numerical Reservoir Simulation, SPE #3182, Preprint of the 46th SPE Annual Fall Meeting, New Orleans, La., October 3-6, 1971.
- Watson, A. T., Gavalas, G. R. and Seinfeld, J. H., 1984: Identifiability of Estimates of Two-Phase Reservoir Properties in History Matching, SPEJ, December. 1984, pp. 697-706.
- Watson, A. T., Gatens, J. M, III, Lee, W. J. and Rahim, Z., 1989: An Analytical Model for History Matching Naturally Fractured Reservoir Production Data, Proceeding of the SPE Production Operations Symposium, Oklahoma City, OK, March 13-14, 1989, pp. 295-305.
- Young, G.R.C. and Paul, G.W., 1993: Reservoir Characterization of Mary Lee and Black Creek Coals at the Rock Creek Field Laboratory, Black Warrior Basin, GRI Topical Report, Contract #5091-214-2316, August 1993.

Figure 1. Quality of Matches vs. Errors in Porosity and Permeability.

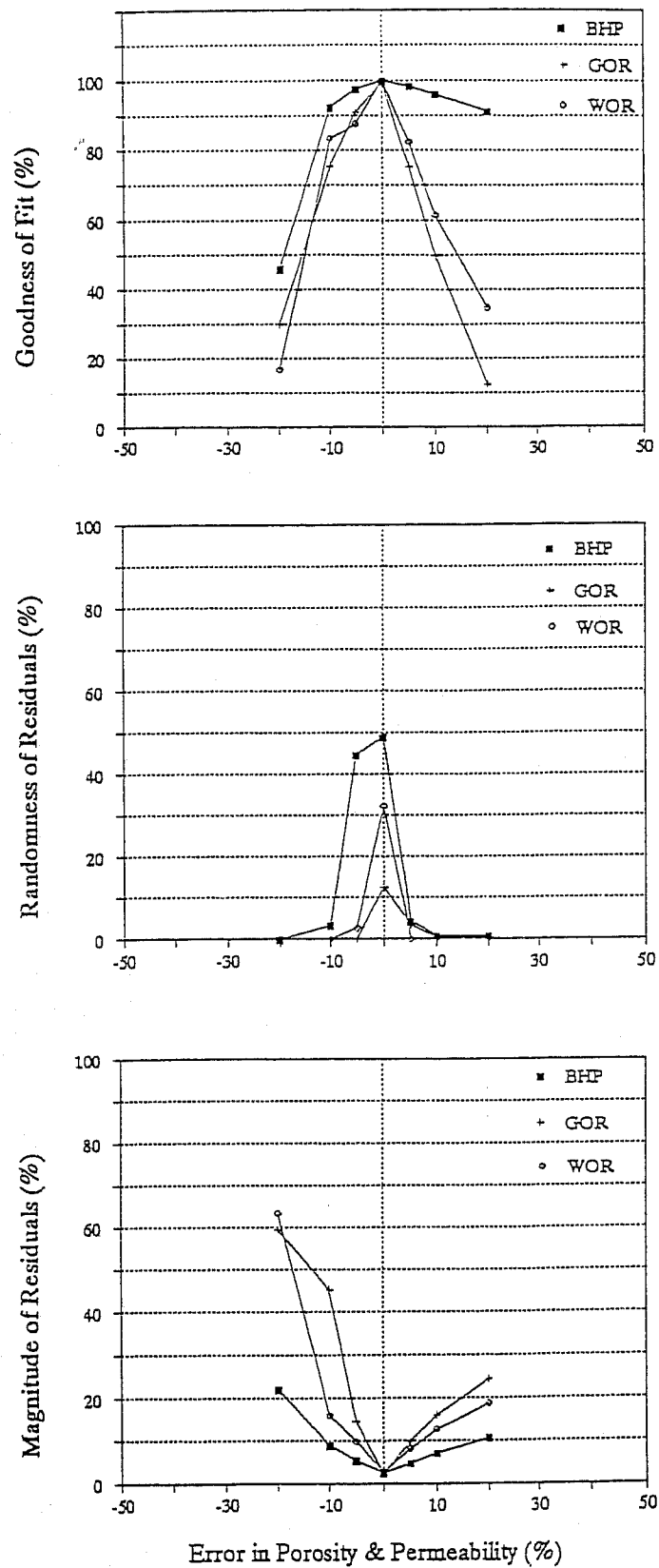
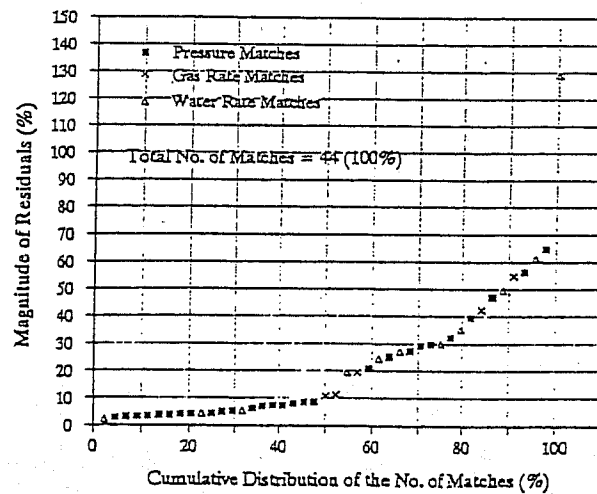
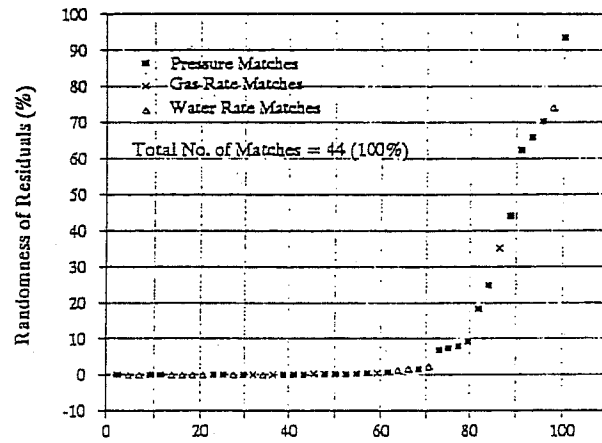
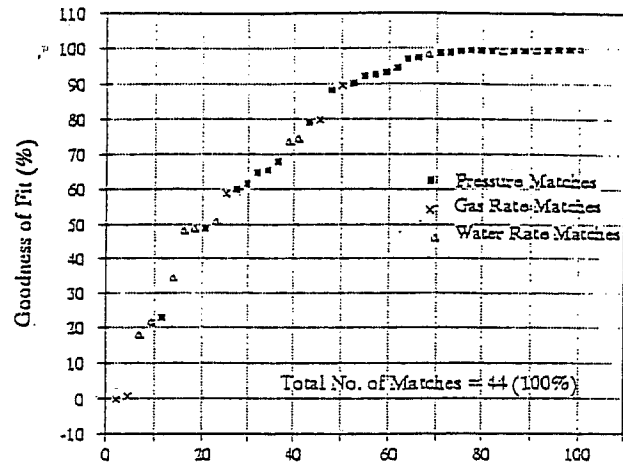




Figure 2. Quality of Matches on Published Studies.



# Study on Fine Geological Modelling of the Fluvial Sandstone Reservoir in Daqing Oilfield

Zhoa Han-Qing  
Daqing Research Institute  
of Exploration and Development  
Ranghulu, Daqing  
Helongjiang 163712 P.R. China

## ABSTRACT

These paper aims at developing a method for fine reservoir description in maturing oilfields by using close spaced well logging data.

The main productive reservoirs in Daqing oilfield is a set of large fluvial-deltaic deposits in the Songliao Lake Basin, characterized by multi-layers and serious heterogeneities. Various fluvial channel sandstone reservoirs cover a fairly important proportion of reserves. After a long period of water flooding, most of them have turned into high water cut layers, but there are considerable residual reserves within them, which are difficult to find and tap. Making fine reservoir description and developing sound a geological model is essential for tapping residual oil and enhancing oil recovery.

The principal reason for relative lower precision of predicting model developed by using geostatistics is incomplete recognition of complex distribution of fluvial reservoirs and their internal architecture's. Tasking advantage of limited outcrop data from other regions (suppose no outcrop data available in oilfield) can only provide the knowledge of subtle changing of reservoir parameters and internal architecture. For the specific geometry distribution and internal architecture of subsurface reservoirs (such as in produced regions) can be gained only from continuous infilling logging well data available from studied areas. For developing a geological model, we think the first important thing is to characterize sandbodies geometries and their general architecture's, which are the framework of models, and then the slight changing of interwell parameters and internal architecture's, which are the contents and cells of the model. An excellent model should posses both of them, but the geometry is the key to model, because it controls the

contents and cells distribution within a model. Inaccurate framework geometry results in complete failure of modelling, but inaccurate contents and cells can only bring about partial error.

Relying on sedimentological knowledge of modern deposits, using close spaced well logging curves which are available in large areas, we have succeeded in seeking out a new method for fine and accurate description of the framework and geometry of fluvial reservoirs. According to sedimentary rules which are unique in the various channels and the sedimentary facies preserved in the sandbodies, we studied the sandbody geometries, internal architecture and heterogeneities at different levels, in order to finally develop fluvial reservoir sedimentation models, to describe the reservoir heterogeneity. By largely applying this thought to subsurface study, we have got a great success.

The first step is according to close spaced well curves, subdividing the sedimentary units of fluvial reservoir into single channel sedimentary units (single fluvial cycle) and then drawing the unit microfacies map based on the accurate recognition of sedimentary microfacies.

The second is recognizing the single channel sandbody from complex channel sandbody extending widely in lateral, and judging the genetic type of each channel, and finally predicting boundary positions between wells, describing geometry, scale and associated pattern.

In the third step, the thickness distribution pattern of each single channel sandbody is finally described. The results can be further used to reveal the thickness distribution pattern, geometry, scale orientation and Marco-architecture of the river bar and the filling body. Then such kind of structure model is used to direct the modelling study of permeability distribution of channel sandbodies in different horizons. As to more detailed reservoir heterogeneities, such as the lateral accretion bodies of point bar and the lateral accretion baffles between them should be predicted with the help of outcrop knowledge and modern sedimentation study.

Utilizing this method, four types of fluvial channel sedimentation models in Daqing oilfield, such as sandy braided channel, high sinuosity distributary channel, low sinuosity distributary channel, and straight distributary channel have been developed. Those models systematically represent the main heterogeneous characteristics including the sedimentary associated

features of various channel sandbodies, geometry internal architecture, permeability distribution rule, even the baffles distribution pattern of each single sandbody.

Credible accuracy and wide adaptability of these models have been proved by infilling well data and production performance. These models are particularly applied to oilfields like Daqing which have taken the technique of selective production of multizones in a single well. Meanwhile, they also provide framework models for the predicting of interwell reservoir parameters by using geostatistic and developing high resolution reservoir predicting models.



# **A Combination of Streamtube and Geostatistical Simulation Methodologies for the Study of Large Oil Reservoirs**

Dr. Avi Chakravarty; A. S. Emanuel; J. A. Bernath  
Chevron Petroleum Technology Company  
1300 Beach Boulevard  
LaHabra, CA 90631

## **ABSTRACT**

The application of streamtube models for reservoir simulation has an extensive history in the oil industry. Although these models are strictly applicable only to fields under voidage balance, they have proved to be useful in a large number of fields provided that there is no solution gas evolution and production. These models combine the benefit of very fast computational time with the practical ability to model a large reservoir over the course of its history. These models do not, however, directly incorporate the detailed geological information that recent experience has taught is important.

This paper presents a technique for mapping the saturation information contained in a history matched streamtube model onto a detailed geostatistically derived finite difference grid. With this technique, the saturation information in a streamtube model, data that is actually statistical in nature, can be identified with actual physical locations in a field and a picture of the remaining oil saturation can be determined. Alternatively, the streamtube model can be used to simulate the early development history of a field and the saturation data then used to initialize detailed late time finite difference models.

The proposed method is presented through an example application to the Ninian reservoir. This reservoir, located in the North Sea (UK), is a heterogeneous sandstone characterized by a line drive waterflood, with about 160 wells, and a 16 year history. The reservoir was satisfactorily history matched and mapped for remaining oil saturation. A comparison to 3-D seismic survey and recently drilled wells have provided preliminary verification.



# Sedimentology, Statistical Representivity, and Flow Upscaling.

Philip Ringrose, Gillian Pickup, Jerry Jensen, and Margaret Forrester  
Dept. Petroleum Engineering, Heriot-Watt University,  
Edinburgh, EH14 4AS, UK.

**Acknowledgements:** This work has been funded by sponsors of the Reservoir Heterogeneity Project: Amerada Hess, British Gas, Chevron, Conoco, Deminex, UK Dept. of Trade and Industry, Elf, Esso, Fina, Mobil, Pan Canadian, Petrobras, Phillips, Shell, Statoil, Talisman. We thank our colleagues in the Reservoir Description Group for advice and discussion, especially Patrick Corbett, Ken Sorbie. Yaduo Huang kindly provided the lab-sample permeability data.

## Abstract

We have used a reservoir gridblock-sized outcrop (10m by 100m) of fluvio-deltaic sandstones to evaluate the importance of internal heterogeneity for a hypothetical waterflood displacement process. Using a dataset based on probe permeameter measurements taken from two vertical transects representing “wells” (5cm sampling) and one “core” sample (exhaustive 1mm-spaced sampling), we evaluate the permeability variability at different lengthscales, the correlation characteristics (structure of the variogram function), and larger-scale trends. We then relate these statistical measures to the sedimentology.

We show how the sediment architecture influences the effective tensor permeability at the lamina and bed scale, and then calculate the effective relative permeability functions for a waterflood. We compare the degree of oil recovery from the formation: (a) using averaged borehole data and no geological structure, and (b) modelling the sediment architecture of the interwell volume using mixed stochastic/deterministic methods.

We find that the sediment architecture has an important effect on flow performance, mainly due to bed-scale capillary trapping and a consequent reduction in the effective oil mobility. The predicted oil recovery differs by 18% when these small-scale effects are included in the model. Traditional reservoir engineering methods, using averages permeability values, only prove acceptable in high-permeability and low-heterogeneity zones. The main outstanding challenge, represented by this illustration of sub-gridblock scale heterogeneity, is how to capture the relevant geological structure along with the inherent geo-statistical variability. An approach to this problem is proposed.



The effects of sedimentary architecture on flow in petroleum reservoirs have been widely studied (e.g., Weber, 1982; van de Graaff & Ealey, 1989; Corbett et al., 1992; Jones et al., 1993; Kjønsvik et al., 1994; Saad et al. 1995). In most of these studies, the importance of considering the sedimentary architecture at a lengthscale relevant to the fluid flow problem (e.g., connectivity between wells versus sweep efficiency within flow units) has been stressed. But very often, the uncertainties associated with permeability estimation, inter-well variability, and relevance to effective flow behaviour at different lengthscales are un-differentiated. Thus, a general flow estimation problem, with large uncertainties, emerges. In this paper, we illustrate how sedimentary variability at different scales can be separated out into lithology-dependent components, to provide a better means of accurately judging effective flow properties of a reservoir unit. We base the illustration on a study of an outcrop the size of a typical reservoir gridblock.

The Ardross Cliff, an outcrop of Lower Carboniferous deltaic and fluvial sandstones, lies on the south coast of Fife, in eastern Scotland. This outcrop was chosen because it contains a variety of sediment architecture types which illustrate the heterogeneity which typically occurs at the sub-gridblock scale within reservoir simulation models. The main exposure is a 10 x 100m cliff, comprising two sandstone units - the Upper and Lower Ardross Castle Sand Units - separated by a prominent coal stratum (Figures 1 and 2). The lower unit is underlain by heterolithic sand and shale units, and the upper unit is overlain by a Limestone bed; both are assumed to be no-flow boundaries. The lower unit is characterised by ripple lamination, manifested in parts by well-preserved climbing ripple sets, and related to the building out of a delta front. The upper unit contains abundant trough crossbedding formed within a fluvio-deltaic channel.

### **Analysis of permeability measurements**

Two types of probe permeameter measurements have been taken in the Ardross units. Firstly, two vertical transects of 5cm-spaced measurements were taken in the field using a steady-state field permeameter calibrated against known samples. The two transects are 70m apart and represent "wells" at either end of the "gridblock" analogue. The probe tip used had a 4mm inner radius and a 24mm outer radius (implying a hemispheric volume of investigation of about 2cm diameter). Surface preparation comprised chipping rock edges to expose a fresh surface 1 to 2cm beneath the natural surface. This avoided most of the effects of the weathered crust, although no systematic study of surface effects was conducted. Secondly, measurements were made in the laboratory, using a pressure-decay permeameter on a block sampled from the logged section, representing a "whole core" sample for determination of relative permeability and capillary pressure curves. Exhaustive 1mm-spaced

inner radius and a 6mm outer radius (implying a hemispheric volume of investigation of about 1.5cm diameter). These data thus represent higher resolution and more accurate measurements (as the pressure decay device has a higher dynamic range). The calibration established for the field permeameter appears to give a consistent dataset, with no major systematic error.

The two probe-measurement transects taken in the field are shown in Figure 2. The upper sand unit has high permeabilities, average 566md, whereas the lower unit is less permeable, average 266md. The main features of permeability variation in the two wells (e.g. high permeability layer at 2.0m below datum) can be correlated between wells.

Figure 3 shows permeability histograms for the two sand units and the lab sample. The whole formation has an approximately log-normal distribution spanning over 3 orders of magnitude (1mD to 1.4D) with a mode at 100mD. The arithmetic averages for the two units are statistically different at the 95% level. Furthermore, the high-end tail to the permeability distribution for the Lower Sand Unit can be associated with a thin cross-bedded unit (at around -2.0m on well 1 and at -2.3m on well 2, Figure 2), and the lower values in the Upper Sand Unit can be associated with ripple bedding at the base (between 0.0 and 1.0m, Figure 2). Thus, the field permeability data can be separated into two distinct groups on the basis of lithology.

At the core-scale, one can resolve the sedimentological components (lamina and beds), whose effects are aggregated in the larger-scale dataset. Figure 4 shows two of five permeability profiles collected on the core sample and a histogram of all the data. The profiles show a marked oscillatory pattern as the sand-rich and mica-rich laminae alternate, and these laminae are clearly seen on the core surface. The lamina spacing is around 2cm. Despite a drift in the precise location and permeability of these laminae as successive permeability profiles are acquired, the lamina-scale fabric is persistent and evident in the bi-modal permeability histogram (Figure 4). The permeability contrast between sand-rich and mica-rich laminae varies between about 2:1 and 5:1. In a similar manner, the upper crossbedded sand unit reveals lamina and bed-scale patterns in permeability. These patterns are used for bed-scale permeability models for each lithofacies in the following section.

Semi-variogram analysis (Jensen et al., 1996) of the 5cm-spaced well data (Figure 5) reveals the presence of holes at lags of around 0.3m, 0.9m and 1.2m. By inspection of the outcrop, we relate this evidence of cyclicity to bed-scale repetitions in the ripple-bedded lithofacies. The large nugget reflects the undersampling of lamina-scale heterogeneity by the 5cm-spaced data. The Upper Sand Unit does not display strong vertical cyclicity, but an average crossbed thickness can be identified. These lengthscales of cyclicity are used as a guide to defining the bed-scale grid dimensions used in the flow

permeability is captured as an effective flow property.

## Single-phase permeability estimation

Using the field and lab permeability data, we constructed lamina-scale permeability models for the ripple-laminated Lower Sand Unit and the crossbedded Upper Sand Unit. These deterministic templates were designed to portray the characteristic permeability structure of each bed type (i.e. permeability contrast, lamina spacing, lamina shape, lamina continuity and internal grading). Variations in these characteristics, such as drift of the average between the two wells and vertical variations within the same facies, were treated by imposing stochastic variations and interwell trends on these templates. The models are illustrated in Figure 6. Two end-member cases were considered for the ripple model by allocating higher or lower permeability values for the bottomset to reflect observed variations. These end-members also represent well-connected and poorly connected extremes as far as flow is concerned. The lamina-scale ripple models were then scaled-up and assembled into stochastic bed-scale templates to capture the range of variability observed in the the wells.

A comparison of model statistics with well data is given in Table 1. A reasonable match of model to data is achieved. This could be improved on by detailed adjustment of the model values; however, our aim has been to honour the sedimentary architecture (especially lamina permeability contrasts) as much as the measured well data, so this match is quite acceptable given the uncertainties inherent in sampling.

The tensor effective permeabilities for the models were determined (Pickup et al., 1995; Pickup & Sorbie, 1996), using the Periodic Boundary Condition method, and these are shown in Table 2. The ripple lamina-scale models and the crossbed model have off-diagonal terms that are about 4% of the diagonal term, due to their cross-laminated architecture. The bed-scale ripple model, however, has negligible off-diagonal terms. This is because, at this scale, the effects of smaller-scale cross-lamination are masked by the effects of the approximately layered bed-scale architecture. The tensor permeability values also differ significantly from the arithmetic ( $k_a$ ) and harmonic averages ( $k_h$ ), which one might have used to estimate effective permeability. The crossbed model has  $k_{xx} = 0.92 k_a$ . The actual size of the off-diagonal term depends on the crossbed geometry and lamina permeability contrast. For example, an idealised crossbed unit with layers of 10:1 permeability contrast, an angle of 26.565 (arctan 0.5) and no bottomset would have  $k_{xx} = 0.866 k_a$  (a reduction of about 13%). Thus, the lithofacies model geometries impose a small but significant control on the effective single-phase

## Waterflood scale-up of the Lower Ardross Sand Unit

The lithofacies models of the Ardross Cliff have been evaluated in terms of their likely impact on a waterflood displacement, using the geopseudo method (Corbett et al., 1992, Ringrose et al., 1993, Pickup et al., 1994). This approach attempts to capture the impact of small-scale permeability architecture on multiphase flow, using some form of pseudofunction numerical scheme. For this illustration we use the Kyte & Berry (1975) method. We have evaluated the potential errors implicit to the pseudofunction scheme by comparison with other methods (e.g. Pc-equilibrium steady state). The differences can be significant but do not alter the overall conclusion, which is more influenced by the choice of rock and fluid properties than by the numerical scheme.

In the case of the crossbed model, one scale-up step is sufficient to define pseudo relative permeability functions for the gridblock model (0.3m high gridcells). However, in the case of the ripple-bedded model, pseudofunctions were first defined at the laminaset scale (3cm high model) for the high bottomset and low bottomset models. These pseudos were then applied to the stochastic bed-scale model (Figure 6) to define pseudofunctions for the gridblock model (0.3m high gridcells). Simulations at all scales are done at a flow rate of 0.2m/day, and assume a water-wet system with an endpoint mobility ratio of 1.76 (details of modelling assumptions are given in Ringrose et al., 1993). All models are 2D vertical sections.

Results for these models are given in Table 3. As a measure of the significance of these calculated recovery factors, the lithofacies-based model of the Lower Ardross Sand Unit has been compared with a model using 30cm layers defined using 30cm averages of the permeability data from Well 2. This case represents a common approach of only upscaling the permeability data (usually by averaging) and assuming the core scale relative permeability functions apply directly to the upscaled gridcell. The difference in recovery is 18%. This appreciable difference can be attributed mainly to the process of capillary oil retention within the small-scale cross-lamina and cross-bed architecture of the two lithofacies present in this section. In other work, Huang et al. (1995) and Honarpour et al. (1995) have conducted core-scale laboratory waterfloods to demonstrate that these small-scale capillary trapping phenomena do indeed occur. We are therefore confident that this degree of systematic difference in recovery (c. 20%) between models which capture and ignore the effects of lamina architecture is reasonable.

Sand Unit with the 30cm average model. Not only is the recovery much poorer for the geopseudo model, but the watercut has earlier breakthrough and a steeper rise. Clearly, the effects of sediment architecture in this formation could have important economic significance if this formation were an oil reservoir. A cross-sectional model based on 30cm averages (1 foot spacing) would over-estimate recovery and field performance considerably. In practice, averaging as a basis for upscaling is often done at a much larger scale (c. 10m) and so the errors may be even larger.

## Discussion

This study of the sedimentary architecture, permeability data, and flow property calculation serves to illustrate the potential effects of internal rock structure and variability on flow at the scale of a single reservoir model gridcell. Other studies have evaluated the impact of sedimentary architecture on waterflood over a wider range of scales (e.g. Corbett et al., 1992; Jones et al., 1993; Kjønsvik et al., 1994; Ciammetti et al., 1995; Saad et al., 1995). The general conclusion that can be drawn from these integrated studies is that small-scale heterogeneity can be important for multiphase flow, but exactly how much depends on the specific details of the sedimentary and reservoir architecture, and the displacement process being considered. One must consider the problem on a case-by-case basis. We have, however, developed some simple guidelines for assessing the potential influence of small-scale sedimentary structure on a waterflood. These are:

- 1) Are immiscible fluids flowing (rates <1m/day)?
- 2). Are significant small-scale heterogeneities present? Specifically:

Small-scale heterogeneity questions	Criterion
Is the permeability contrast	greater than 5:1 ?
Is the layer thickness pertaining to this contrast	less than 20cm ?
Is the mean permeability	less than 500md ?

If these criteria are all satisfied, then capillary/heterogeneity effects should be evaluated.

A further criterion, involves the relative importance of small-scale and large-scale reservoir architecture. Even if the small-scale structure is important, it may be that the large-scale reservoir connectivity issues are still the dominant uncertainty. Using the simple classification of reservoir heterogeneity proposed by Weber and van Guens (1990), we infer the following guidelines on this aspect of the problem:

- Layer cake reservoirs - small-scale structure will usually have primary importance.
- Jig-saw puzzle reservoir - small-scale structure may be important.
- Labyrinth reservoir - small-scale structure will usually be of secondary importance.

Once the potential importance of small-scale heterogeneities have been considered and a decision to proceed with a detailed evaluation has been made, we are then faced with detailed questions about how to go about the study. We have attempted to demonstrate an approach for doing this with the gridblock analogue described here. Figure 8 summarises the procedure we have used. The underlying problem is how to handle the uncertainties inherent in an incomplete dataset (the sampling and estimation problem) along with the scale-dependent flow-structure interactions. We advocate the importance of referring both the parameter estimation problem and the flow upscaling problem to the sedimentological lengthscales inherent in the reservoir system. The procedures for doing this include:

- 1) Considering the sample sufficiency of the well data. An important guide is the permeability  $C_v$  (Jensen et al., 1997, pp.150-153).
- 2) Evaluate the scales at which permeability variability is expressed. In this example, we compared an exhaustive permeability dataset acquired from one core sample with the well data to establish the degree of small-scale variability and importantly the typical lamina permeability contrasts. Wireline microscanner measurements could help to assess the permeability contrasts and small-scale sedimentary architecture.
- 3) Use correlation measures (e.g. semivariogram of well data) to identify inherent sedimentary lengthscales. In this example, we identified bed-cyclicity at the 30cm lengthscale and used this to guide the definition of the small-scale gridcells.
- 4) Apply a knowledge of sedimentology to define likely bed-scale architectural patterns. In this example, the ripple and crossbed architectures were found to have a significant effect on remaining oil. Where aspects of the architecture are uncertain, stochastic approaches can be used.
- 5) Use a flow upscaling framework based on the sedimentary hierarchy of lengthscales. In this example, we used two different schemes to define upscaled flow models for the two lithofacies present in the analogue (i.e. ripple bedding and cross-bedding).

This approach has been applied to a 3D reservoir study of a fluvio-aeolian system (Sylvester et al., 1996). This study shows that the approach is practicable within a realistic field development programme and has a significant impact on field performance predictions (in the case the geologically-based upscaling led to a 29% difference in recovery). However, more automated methods are needed in order to perform this type of study on a more routine basis.

The difficulties in actually detecting and modelling geological structure in the subsurface should not be under-estimated (Jensen et al., 1996). However, a greater emphasis on the smaller scale aspects of reservoir architecture is warranted in view of their potentially significant impact on flow. Conventional geostatistical approaches (modelling the reservoir at a single scale using correlation functions) may fail to account for the reservoir architecture that actually affects flow.

Finally, there is considerable uncertainty about the choice of multiphase flow function to use as input to the scale-up procedure. We have not considered this problem here, but have argued elsewhere (Ringrose et al., 1996) that the lithofacies control is also vital when considering the choice of special core analysis sample, the laboratory method, and the procedure for applying it to the simulator model. We have also tested our upscaling approach against a whole core experiment to lend support to our choice of multiphase flow functions for input at the lamina scale (Huang et al., 1995).

## Summary

The Ardross analogue provides an illustration of flow-heterogeneity interactions at the reservoir gridblock scale. Although the analogue is a specific example from a deltaic sequence, the sediment structures involved (ripple and crossbed lamination) occur quite widely in many other sediment environments. Our studies of effective single-phase permeability and two-phase waterflood of the cliff have demonstrated some very significant effects of sediment structure:

1. The tensor effective permeability  $k_{xx}$  term can be 10% less than the arithmetic average.
2. Waterflood oil recovery could be 20% lower than that estimated from arithmetic averages of 30cm (1 ft) intervals.

The architectural characteristics of any particular reservoir unit can be established using well data, provided that the data sufficiency is evaluated and the true lengthscales and patterns of permeability variability are identified. The basic tools for doing this involve the comparison of data from different lengthscales, different sedimentological models and use of correlation measures. We have shown how spatial and scale-dependent variability can be captured using mixed deterministic/stochastic models which incorporate the sediment structure as well as known spatial variability. This small-scale sedimentary architecture is particularly important when assessing waterflood behaviour.

- Ciammetti, G., Ringrose, P.S., Good, T. R., Lewis, J. M. L., and Sorbie, K. S., 1995. Waterflood recovery and fluid flow upscaling in a shallow marine and fluvial sandstone sequence. SPE 30783, presented at the SPE Annual Technical Conference and Exhibition, Dallas, USA, 22-25 Oct., 1995.
- Corbett, P. W. M., Ringrose, P. S., Jensen, J. L., and Sorbie, K. S., 1992. Laminated clastic reservoirs - the interplay of capillary pressure and sedimentary architecture. SPE Paper 24699, presented at the SPE Annual Technical Conference, Washington, 4-7 October, 1992.
- Honarpour, M.M. Cullick, A.S., Saad, N. and Humphreys, N.V., 1995. Effect of rock heterogeneity on relative permeability: implications for scale-up. *Journal of Petroleum Technology*, November 1995, p.980-986.
- Huang, Y., Ringrose, P. S., & Sorbie, K. S., 1995. Capillary Trapping Mechanisms in Water-wet Laminated Rock. *SPE Reservoir Engineering*, November 1995, p.287-292.
- Jones, A., Doyle, J., Jacobsen, T., and Kjønsvik, D., 1993. Which Sub-seismic heterogeneities influence waterflood performance? A case study of a low net-to-gross fluvial reservoir. *Proceedings of the 7th European IOR Symposium*, Moscow, Russia, 27-29 October, 1993.
- Jensen, J. L., Corbett, P. W. M., Pickup, G. E. and Ringrose, P. S., 1992. Permeability semivariograms, geological structure and flow performance. *Mathematical Geology*, 28(4), p. 419-435.
- Jensen, J. L., Lake, L., Corbett, P. W. M., and Goggin, D. J., 1997. *Statistics for Petroleum Engineers and Geoscientists*. Prentice Hall PTR, New Jersey.
- Kjønsvik, D., Doyle, J., Jacobsen, T., and Jones, A., 1994. The effects of sedimentary heterogeneities on production from a shallow marine reservoir - What really matters? SPE paper 28445, presented at the European Petroleum Conference, London, 25-27 October, 1994.
- Kyte, J. R. and Berry, D. W., 1975. New Pseudo Functions to Control Numerical Dispersion. *Soc. Pet. Eng. J.*, August, 1975, 269-275.
- Pickup, G. E., Ringrose, P. S., Forrester, M. M., Jensen, J. L., & Sorbie, K. S., 1994. The Geopseudo Atlas: Geologically-Based Upscaling of Multiphase Flow. SPE Paper 27565 given at the SPE European Petroleum Conf., Aberdeen, 15-17 March 1994, p.277-289.
- Pickup, G. E., Ringrose, P. S., Corbett, P.W.M., Jensen, J. L., & Sorbie, K. S., 1995. Geology, geometry and effective flow. *Petroleum Geoscience*, 1(1), p.37-42.
- Pickup, G. E. and Sorbie, K. S., 1996. The Scaleup of Two-Phase Flow in Porous Media Using Phase Permeability Tensors. *Society of Petroleum Engineers Journal*, December 1996, in press.
- Ringrose, P. S., Sorbie, K. S., Corbett, P. W. M., and Jensen, J. L., 1993. Immiscible flow behaviour in laminated and cross-bedded sandstones. *Journal of Petroleum Science and Engineering*, 9, p.103-124.
- Ringrose, P. S., Jensen, J. L. and Sorbie, K. S., 1996. Use of geology in the interpretation of core-scale relative permeability data. *SPE Formation Evaluation*, Sept. 1996, p.171-176.
- Saad, N., Cullick, A.S. and Honarpour, M.M., 1995. Effective relative permeability in scaleup and simulation. Paper SPE 29592, presented at the 1995 SPE Joint Rocky Mountain Regional/Low-Permeability Reservoirs Symposium, Denver, CO., March 20-22.
- Sylvester, I. F., Carruthers, D., Ringrose, P. S., Bratvold, R. B., and Lia, O., 1996. Gas/water flow upscaling in a mixed fluvio-aeolian reservoir simulation model. SPE Paper 35492, presented at the European 3D modelling Conference, Stavanger, 16-17 April, 1996.
- van de Graff, W. J. E. and Ealey, P. J., 1989. Geological modelling for simulation studies. *American Association of Petroleum Geologists Bulletin*, 73(11), p.1436-1444.
- Weber, K. J., 1982. Influence of common sedimentary structures on fluid flow in reservoir models. *Journal of Petroleum Technology*, March 1982, p.665-672.
- Weber, K. J., and van Geuns, L. C., 1990. Framework for constructing clastic reservoir simulation models. *Journal of Petroleum Technology*, October 1990, p.1248-1297.



Figure 1. Photograph of part of the Ardross outcrop showing the nature of the two main sand units.

Figure 2. Stratigraphic logs and permeability data for the two wells sampled at either end of the outcrop. (The coefficient of variation,  $C_v$ , is defined as the standard deviation divided by the arithmetic mean).

Figure 3. Permeability histograms.

Figure 4. Permeability profiles from the core data revealing the presence of the alternating sand-rich and mica-rich laminae within the ripple-bedded facies.

Figure 5. Semivariogram of well data from well 1.

Figure 6. Flow model templates for (A) lamina-scale ripple model (3cm high by 15cm long), (B) bed-scale ripple model (0.3m high by 1.5m long), (C) bed-scale crossbed model (0.3m high by 1.5m long). Darker tones indicate lower permeabilities.

Figure 7. Simulated oil production and watercut for a cross-sectional model of the Lower Ardross Sand Unit: (A) using geopseudo upscaling (B) using pseudos of 30-cm averaged well data.

Figure 8. Illustration of the integrated approach to flow upscaling, accounting for sedimentology and statistical representivity.

Lithofacies model	Arithmetic average (standard deviation) of model	Arithmetic average (st. dev.) of corresponding well data
Crossbed model (for both wells)	664 (356)	566 (308)
Ripple model Well 1 high-k bottomset	308 (211)	329 (153)
Ripple model Well 1 low-k bottomset	213 (158)	
Ripple model Well 2 high-k bottomset	154 (106)	153 (97)
Ripple model Well 2 low-k bottomset	107 (79)	

Table 1. Comparison of permeability statistics for lithofacies models and well data.

Lamina-scale ripple model (low-k bottomset)			Lamina-scale ripple model (high-k bottomset)		
192	0	-9	289	0	-11
0	213	0	0	308	0
-9	0	124	-11	0	162
Bed-scale ripple model			Bed-scale crossbed model		
234	0	0.08	612	0	-20
0	259	0	0	664	0
0.08	0	139	-20	0	311
Key to tensor permeability terms					
$k_{xx}$	$k_{xy}$	$k_{xz}$			
$k_{yx}$	$k_{yy}$	$k_{yz}$			
$k_{zx}$	$k_{zy}$	$k_{zz}$			

Table 2. Permeability tensors for the ripple and crossbed lithofacies models (well 1).

	Small-scale (3cm high)	bed-scale (30cm high)	Field-scale
<b>Upper Ardross Sand Unit</b>			
Curved graded crossbed model		50.19	54.34
<b>Lower Ardross Sand Unit</b>			
Ripples: Low k bottomset	38.00		
Ripples: High k bottomset	44.54		
Ripple bed-scale model with stochastically distributed high and low bottomsets		41.36	44.29
Model using 30cm average permeability data in place of lithofacies models			52.52
Difference in recovery if small-scale sedimentary architecture is ignored (Lower Sand Unit)			+18.6%

Table 3. Waterflood recovery (percent of original oil in place) after injection of 1 pore volume for different models of the Ardross Cliff.

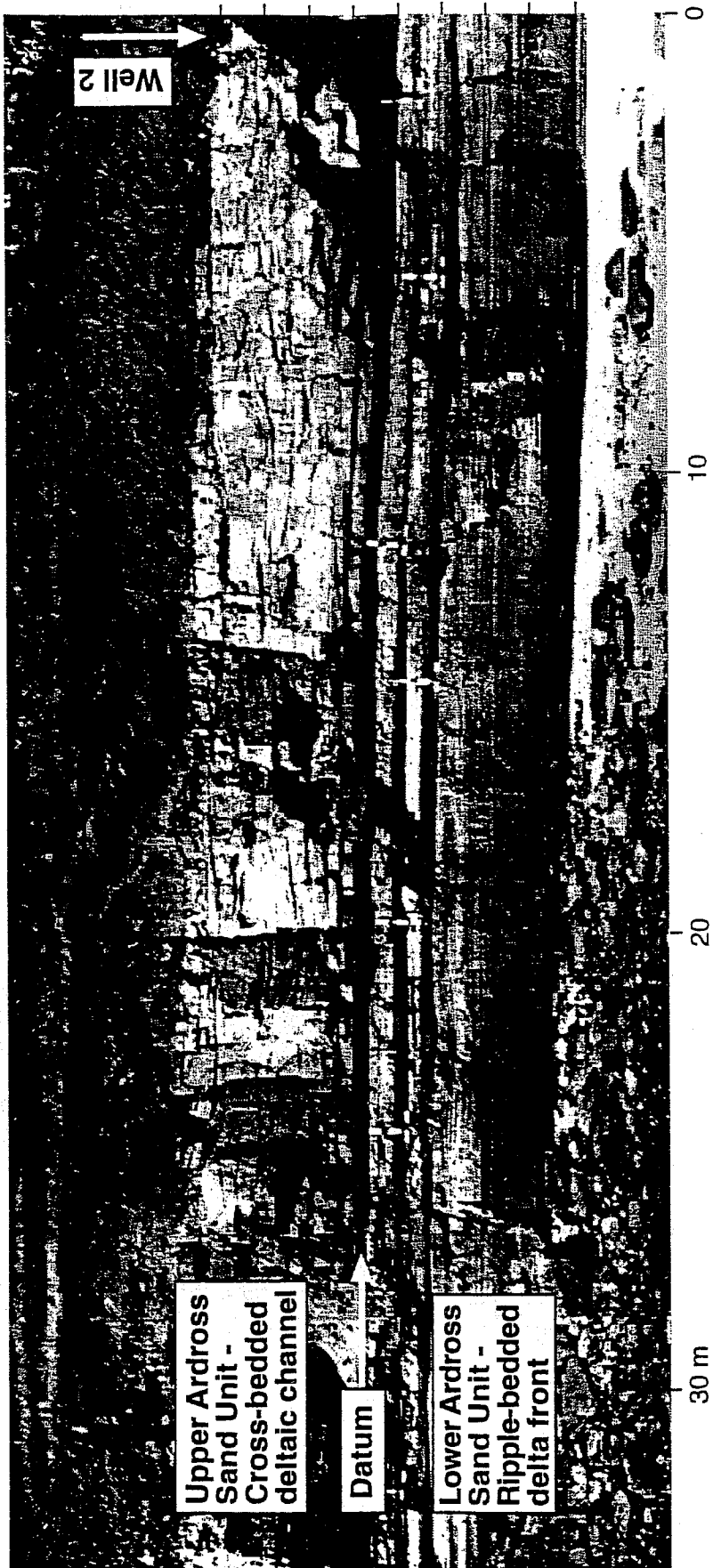
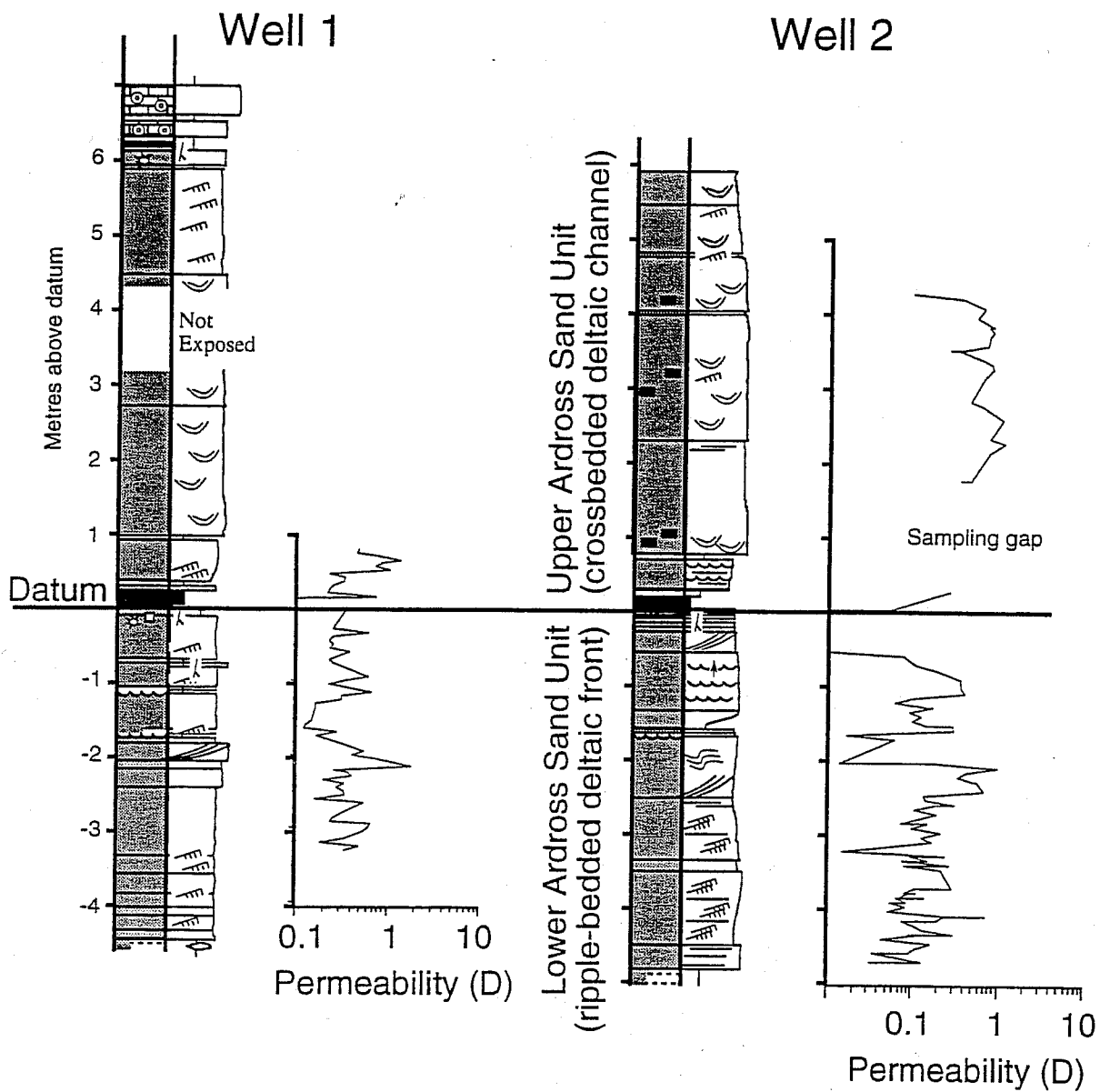


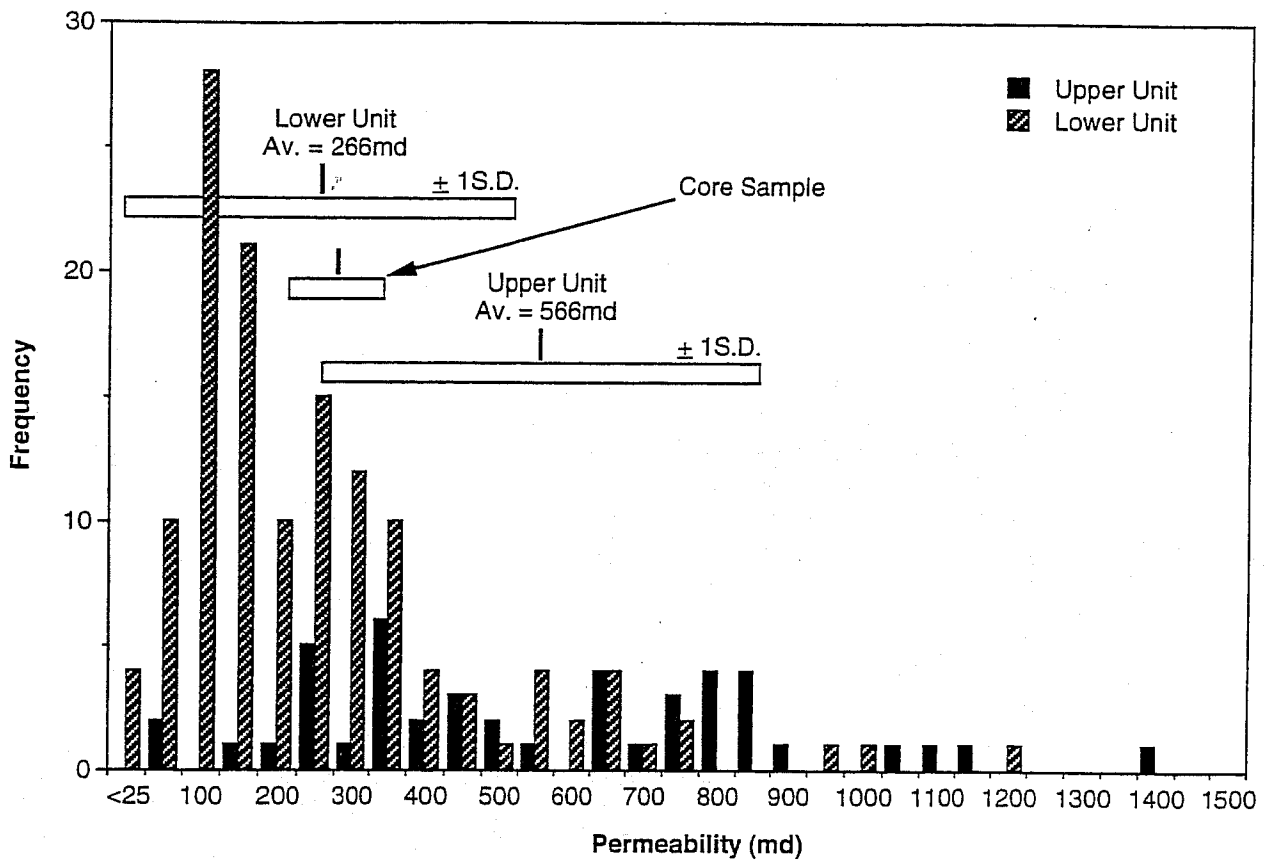
Figure 1



	Both Units	Lower Unit	Upper Unit
Well 1	N = 57	N = 43	N = 14
Arith Av	433.41	391.19	571.35
St. Dev.	313.40	290.98	353.64
Cv	0.72	0.74	0.62
Well 2	N = 115		N = 30
Arith Av	290.15	194.68	563.84
St. Dev.	272.08	189.82	288.84
Cv	0.94	0.97	0.51
Both Wells	N = 172		N = 44
Arith Av	341.09	266.01	566.34
St. Dev.	294.71	249.36	307.89
Cv	0.86	0.94	0.54

Figure 2

A) Histogram of field probe data from both wells separated into Lower and Upper Sand Units



B) Histogram of (exhaustive) lab probe data from one core sample from the Lower (ripple-bedded) Sand Unit

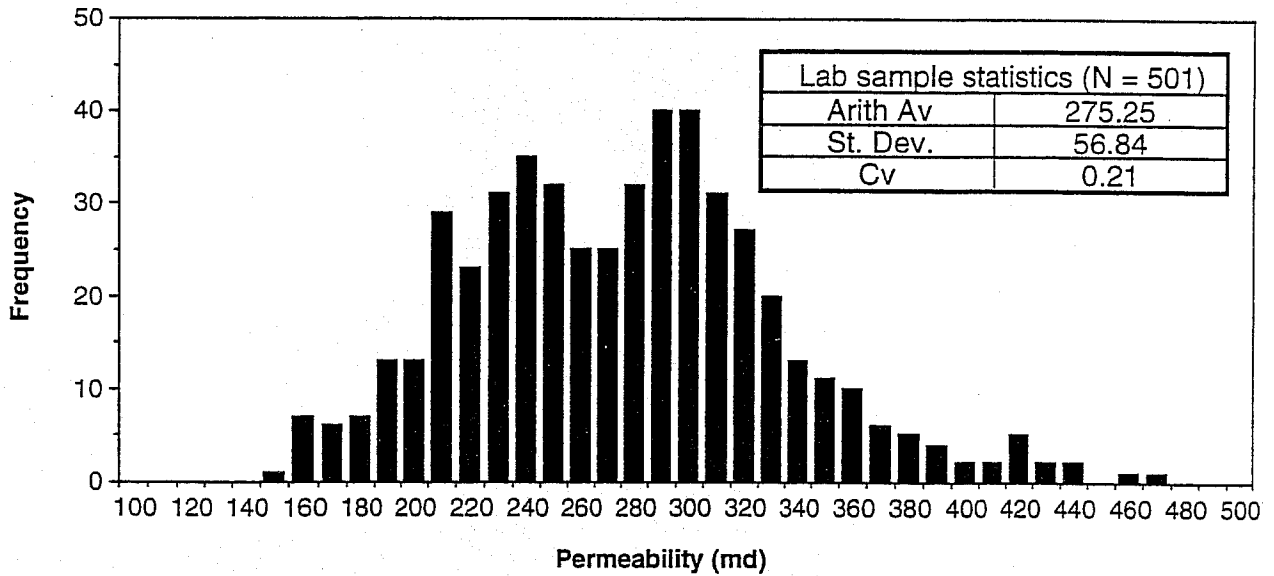


Figure 3

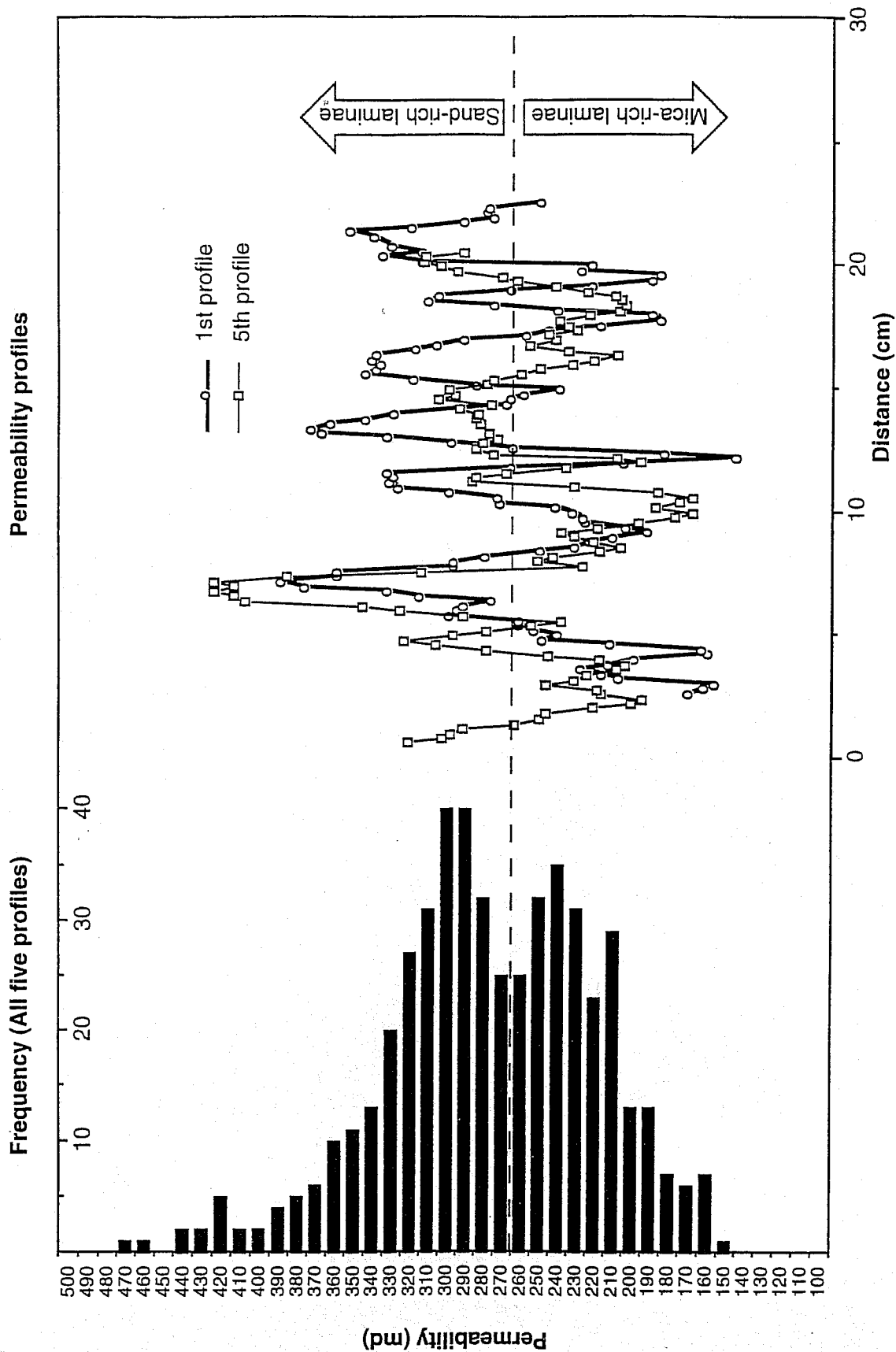


Figure 4

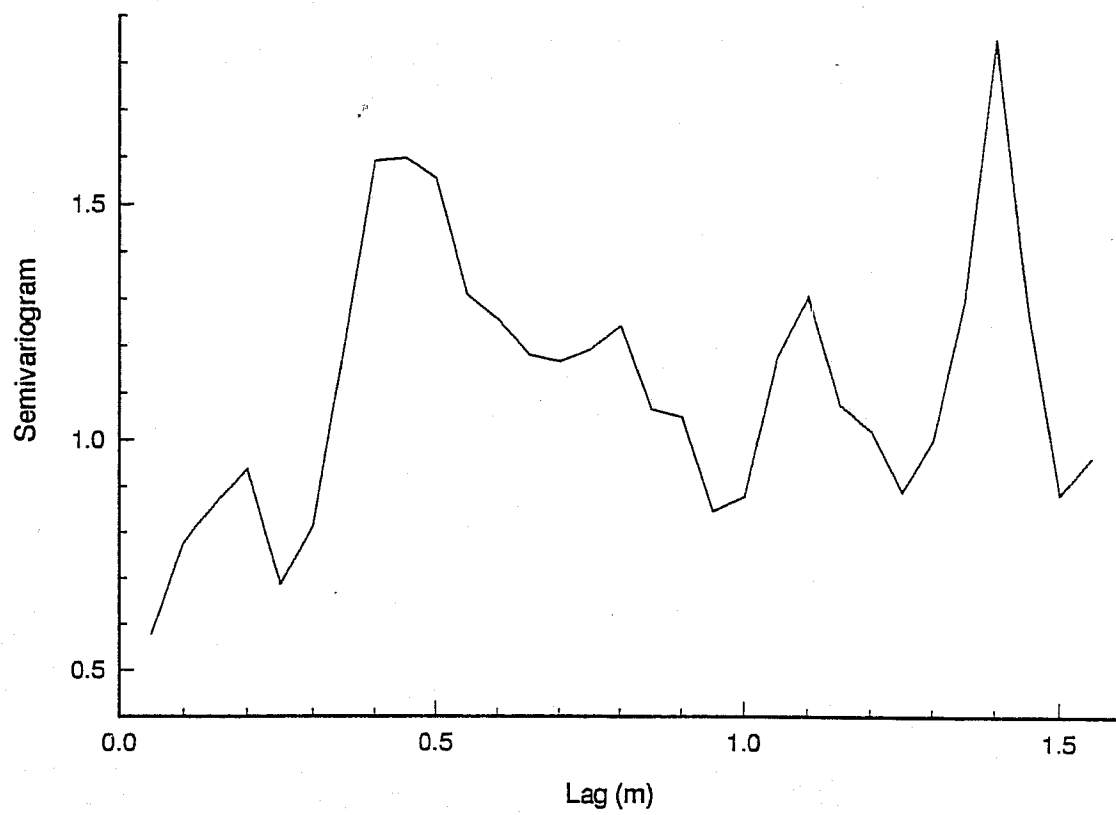
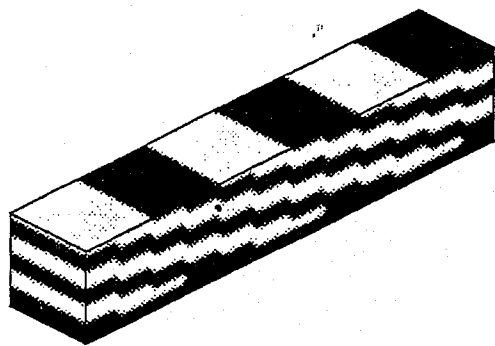


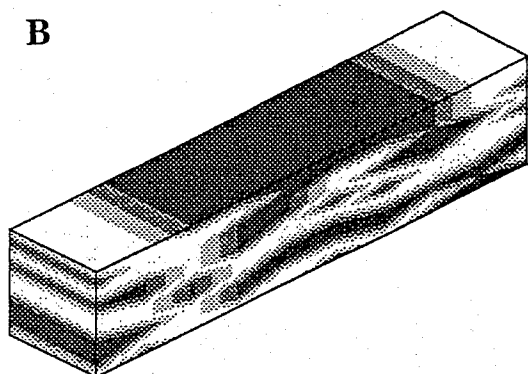
Figure 5



A



B



C

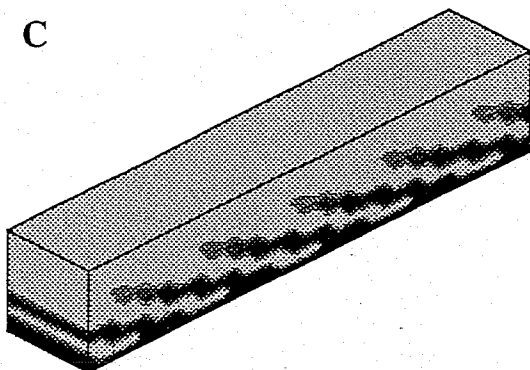


Figure 6

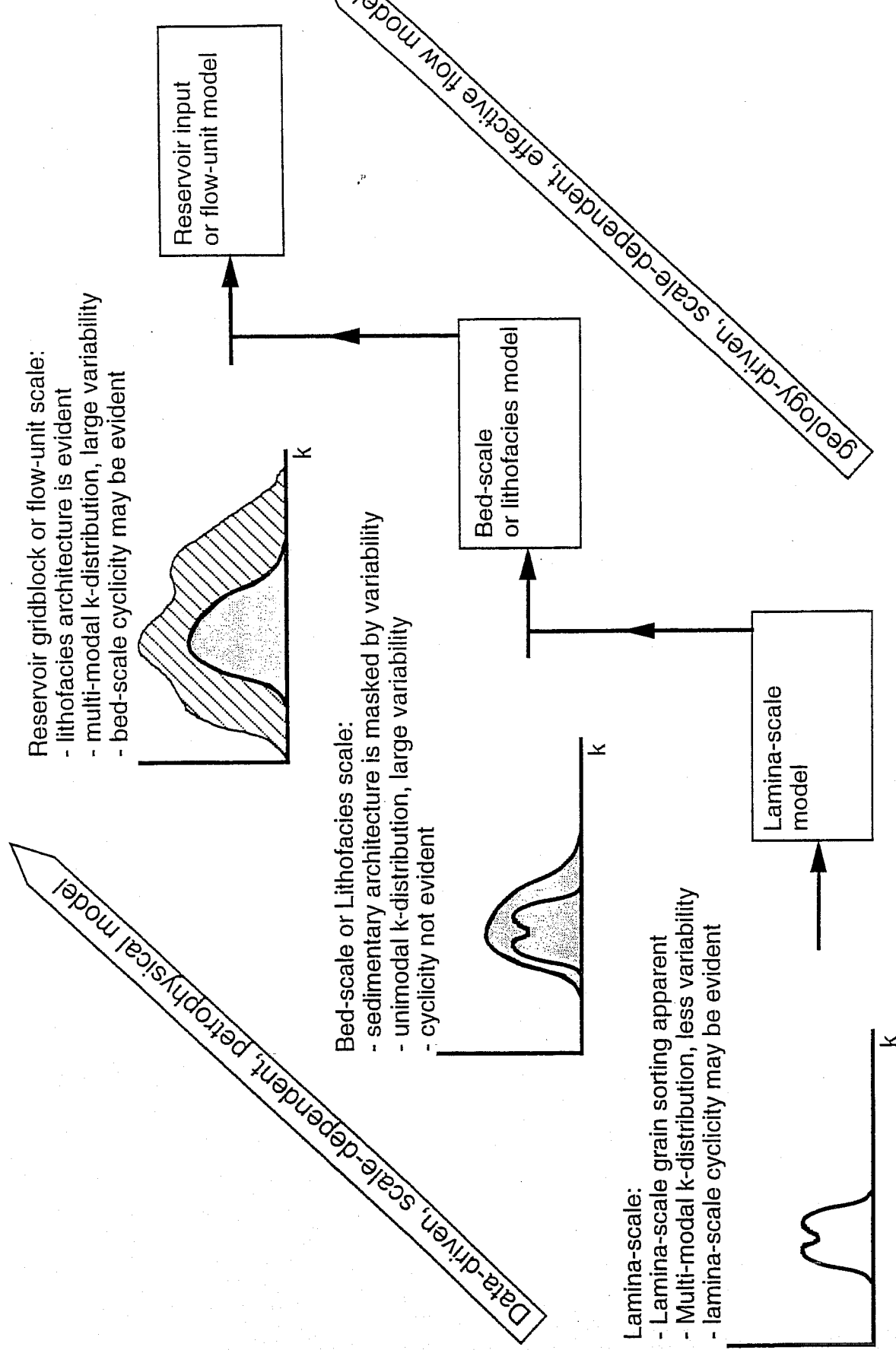


Figure 8

# Title: Use of Element Model to Evaluate Transmissibility Reduction Due to Barriers.

Authors: Tarald Svanes, Deborah South, Ole Magnar Drønen,

*Statoil, 5020 Bergen, NORWAY.*

## **ABSTRACT**

Water breakthrough has been observed a year earlier than expected in the productive Oseberg Formation in the Veslefrikk Field. Production data revealed extensive water override, whereas the opposite situation was expected based on a homogeneous and coarse flow simulation model.

A new model was developed to include geological heterogeneities using a simple upscaling method. The Oseberg Fm. consists of an upper homogeneous unit (zone 2) and a lower unit containing thin barriers of shale and calcite cemented sandstone (zone 1). The barrier content varies laterally. When barriers are distributed in a complex 3D pattern, they reduce the upscaled horizontal transmissibility more than what is obtained by multiplying the sand permeability by the net-to-gross ratio (N/G). However, the transmissibility reduction strongly depends on the spatial distribution of barriers and their geometry. Therefore, a fine scale element model was used to derive the average transmissibility reduction as a function of N/G for alternative geological descriptions of the barriers. A geo-statistical method called General Marked Point Process was used to generate the fine scale descriptions.

This work has resulted in a simple upscaling routine for horizontal transmissibility, which represents an effective bridge between geological evaluation of uncertainties and fluid flow simulation. The method combines geo-statistical and deterministic modelling in an elegant manner, recognising that most often these methods complement one another.

## **INTRODUCTION**

Nature is often more complex than the petroleum engineers account for, especially in the North Sea where the well spacing is large (more than 1 km) and

the reservoirs are heterogeneous. Predictions of production and spatial reservoir drainage, are often based on full field flow simulation models. The uncertainties regarding small scale heterogeneities and inter-well reservoir description, and the fact that full field models are too coarse to be able to incorporate the effect of such features, may result in poor predictions. For practical reasons, such as computing time, the full field models have to be coarse, and fine scale 3D models generated by geo-statistical techniques must be scaled up. Element models have a large potential in deriving suitable upscaling procedures applicable on the full field model, and in detailed studies of small scale heterogeneities (ref 1). The same idea has been widely used in flow simulation, for instance when generating pseudo relative permeability curves in order to incorporate effects related to the change in model resolution.

The Veslefrikk field (see figure 1) is situated in the Norwegian sector of the North Sea. The field is defined as a local horst block on the northwestern flank of the Horda platform. The most important reservoir is the Middle Jurassic deltaic Brent Group. Other reservoirs are the Early Jurassic Intra Dunlin Sand (equivalent to the Cook Fm.) and the Statfjord Fm. (ref 8). The Brent Group is subdivided into the Oseberg, Rannoch, Etive, Ness and Tarbert Formations. This study concentrates on the Oseberg Fm.

In this study, the barriers in zone 1 of the Oseberg Fm. have been of main focus as these are the most important sedimentological heterogeneities influencing fluid flow in the Oseberg Fm.. The barriers in this zone include both calcite cementations and shales. These heterogeneities in zone 1 are referred to as small scale. Zone 2 is described as homogeneous even though numerous smaller scale heterogeneities (e.g. laminations on centimetre scale) are present (see figure 2). Significant barriers to flow are lacking in zone 2.

---

References and illustrations at end of paper

## OSEBERG GEOLOGY

The Oseberg Fm. has been interpreted as being deposited as a sandy fan-delta prograding in a westerly direction during Middle Jurassic (ref 5). The main components of zone 1 and 2 are subaqueous, dipping fan-delta foresets comprising slump and grain flow deposits. Calcite layers are concentrated in zone 1, i.e. in the marine foreset deposits of the fan-delta.

A study done on the origin and extent of the calcite cemented intervals in the Oseberg Fm. (ref 11) showed that the geometry of the calcite cemented intervals reflected the original geometry of the distribution of calcareous bioclastic material. The calcite cemented intervals are classified into two main groups:

1. Cross bedded or massive cemented zones probably with an extent of less than a few hundred metres. These zones are not associated with laterally extensive surfaces of erosion or non-deposition, but are sourced either from evenly dispersed or isolated pockets of carbonate fossils. They occur as scattered concretions, continuous or discontinuous layers of concretions.
2. Intensely bioturbated zones probably with a lateral extent of upto a few kilometres. These layers may be correlatable between wells and represent surfaces of bioclastic concentrations as a result of prolonged non-deposition of siliciclastic material.

The calcite cemented layers occur in the lower part of the Oseberg Fm., often in direct association with fine-grained, shale rich layers. On the basis of this observation, a decision was made to model the barriers as a combination of both shale rich and calcite cemented layers, as both shale and calcite may act as a barrier alone or in combination.

## OVERRIDE IN OSEBERG - OBSERVATIONS

The fact that the uppermost part (zone 2) of Oseberg has been water flooded much sooner than the lower part, was revealed by a saturation log in A-1 and a production log in A-3. After this logging, A-17A was drilled, and open hole logs indicated that both zone 1 and zone 2 was flooded at this location (see figure 2). Water injector, A-10 (further to the north, see figure 1), supports the Oseberg producer A-3.

Formation pressure measurements indicate that none of the barriers in zone 1 act as field wide pressure seals. In addition to the contrast in barrier content between zone 1 and 2, there is a difference in quality of the sandy intervals. For instance, the average permeability in zone 2 is approximately 700 mD compared to 300 mD in zone 1.

## WHAT MAY CAUSE THE OVERRIDE?

The observed override in A-1 and A-3 may have alternative explanations:

1. A complex 3D pattern of small scale barriers in zone 1 may slow the water flooding compared to in the homogeneous zone 2 (see figure 6).
2. If the barriers dip downwards towards the injector (A-10), the water will be forced up into zone 2 (figure 6).
3. If most of the water is injected into zone 2 and there is an extensive barrier between zone 1 and 2, zone 2 will be flooded more efficiently. Due to the completion design in the injector A-10 the injection split in Oseberg cannot be measured.

Combinations of the 3 alternatives listed above may also cause override.

## MODELLING BARRIERS IN OSEBERG

The goal of the modelling was to include and evaluate the effect of the alternative geological explanations listed in the previous section. The geological uncertainty range is large and covered by generating numerous models. By flow simulation the range was restricted as not all models reproduced the observed override.

### Why Geo-Statistical Modelling?

Geo-statistical modelling involves computer based algorithms distributing heterogeneities in 3D (ref 4). The following advantages were crucial in this project:

1. These algorithms contain statistical correlation structures, controlled by user given input parameters, enabling heterogeneities smaller than the well spacing scale to be distributed - heterogeneities that ordinary mathematical interpolation routines are not able to generate. Hence the models become

more realistic.

2. Heterogeneity patterns could be hand-contoured by geologists. It is, however, time consuming to cover the geological uncertainty by generating alternative models - all conditioned to well observations and other input data. By varying the input parameters to geo-statistical routines, rapid generation of alternative models is possible, all consistent with input data.
3. The most commonly used geo-statistical routines are stochastic processes, which means that each run gives different outcomes (realizations) even though all input parameters are kept constant. This represents an additional level of variation in the uncertainty modelling, impossible to incorporate by any other method.

A geo-statistical modelling tool called General Marked Point Process was used to generate the fine scale barrier descriptions (ref 3). This routine is designed to model barrier structures with a large degree of flexibility.

### Why Element Model?

The main reasons for performing element instead of full field modelling are as follows:

1. The lateral extent of the barriers inducing the override (particularly the calcites) are believed to be of the same order of magnitude as the average grid cell size in the full field flow simulation model. Hence, the spatial distribution of these small scale barriers would not influence the behaviour of the upscaled full field model. On the other hand, the intensity and geometry of the barriers is extremely decisive regarding flow behaviour. Therefore, it is not necessary to distribute barriers in the full field, but the effect may be incorporated by using N/G to control the barrier intensity and alternative 3D element models to evaluate the geometrical aspect.
2. Evaluating alternative geological element models is much faster than working with detailed full field models. Both the model size and complexity are more practical as long as no conditioning data and structural maps are needed.
3. An important parameter in matching the Oseberg

production from wells where the override is not observed, has been the communication across the faults. As figure 3 illustrates, it would be time consuming to generate alternative full field models matching the history by tuning the fault communication differently for each model. This is one of the reasons why N/G was chosen as the correlative parameter when upscaling permeability for alternative geological cases to the full field model, see next section for more details.

### Method: N/G Scaling of Permeability

The rationale for this method is that when relatively small barriers are distributed in a complex 3D pattern, they reduce the upscaled horizontal transmissibility more than what is obtained by multiplying the averaged permeability in sand by the averaged N/G (which was used in the original flow simulation model which did not predict override). Figure 6 clearly illustrates this phenomenon, and also emphasizes that the amount of transmissibility reduction strongly depends on the spatial distribution of barriers and their geometry. Therefore, a fine scale element model was used to derive the average transmissibility reduction as a function of N/G for alternative geological descriptions of the barriers in zone 1, and the process is described step by step in the next section.

### Model Description

The following process is performed for each alternative geological case as defined by the geologists (see figure 4):

1. A fine scale realization is generated without conditioning to any well observations.
2. The realization is validated by geologists using 3D visualization.
3. The fine scale model is water flooded after assigning permeability (500 mD) and porosity (20%) to the non-barrier. The injection and production rates are given such that the pressure development is comparable with the full field model.
4. The fine scale model is upscaled into a coarse element model by using a Darcy based technique deriving the permeability vector, and arithmetic averaging deriving porosity and N/G.
5. The upscaled element model is water flooded using

the same well control as for the fine scale model, and pseudorized relative permeability curves to avoid numerical dispersion.

6. The two element simulations are compared focusing on water production, and if the match is poor, the upscaling is re-run using alternative methods until a satisfactory match is obtained (i.e. re-do step 4 to 6).
7. The upscaled permeability in X and Y direction for each coarse cell is plotted against the corresponding N/G, i.e. adding 15 points (number of coarse cells) to the plot.

Step 1 to 7 is re-run using the same geological model parameter setup, but varying the target volume fraction of barriers and the seed to the random number generator (i.e. generating many realizations), until the whole N/G range is covered and a clear trend is recognizable.

When using automatic routines to perform all the steps, each geological case is modelled and analysed in approximately 30 minutes.

## **Results**

Some of the geological alternatives for barrier distribution are illustrated in figure 5 with derived N/G plots. The "base case" was initially assumed to represent the most probable barrier distribution within zone 1. In each N/G plot a straight line is drawn from (N/G=0, Permeability=0) to (N/G=1, Permeability=500) representing how the upscaled N/G acts on permeability in the original model (see figure 6). Most of the alternative geological models represent a significant deviation from this straight line, except for the case Wide, since the barriers there are much larger than the coarse cell. For all anisotropic cases (i.e. when a direction is specified, e.g. the Dip and Ellips), the N/G plot is different for Kx and Ky. This was important to recognize when applying the results on the full field N/G matrix, as described in next section.

## **IMPLEMENTATION IN THE FULL FIELD MODEL**

The idea behind the element model described so far was to establish a simple upscaling routine for horizontal transmissibility taking into account the effect of small scale barriers (not correlatable between wells), and to evaluate the geological uncertainty in

their influence. However, there are other more extensive barriers present in the Oseberg Fm., most often related to zone boundaries since they are correlatable between wells. These barriers in combination with the smaller ones will reduce the vertical transmissibility, and to evaluate this an extended element model was established consisting of 3 homogeneous zone 2 layers overlying the heterogeneous zone 1 from alternative geological models already generated (see figure 7). This extended model proved to be useful concerning some additional aspects: It helped to eliminate those geological cases not reproducing the observed override, and it was used to optimize the strategy to drain the unswept oil in zone 1 (e.g. by horizontal producers).

The geo-statistical element modelling helped the geologists to evaluate their understanding of the reservoir by varying the input parameters and via 3D visualization. Based on this, and further evaluation in the extended element model, the case containing dipping barriers (Dip3) with some vertical transmissibility reduction between zone 1 and zone 2, seemed to be the most probable one. This element model was transferred into the full field model via the following steps:

1. The full field N/G matrix was updated based on a seismic lithology study which derived N/G maps from a correlation between seismic attributes and the concentration of calcite cemented barriers.
2. The field was divided into segments, and a barrier dip direction was assigned to each segment. Then the N/G plot from figure 5 (Dip3) was used to change the permeability matrix, both Kx and Ky.
3. Finally the vertical transmissibility between zone 1 and zone 2 was revised by the geologists based on well interpretations and the extended element model.

Figure 8 illustrates the difference between the new and the old permeability distribution in zone 1, and the resulting water-flood is shown in a vertical cross section. In addition, the improved history match is plotted both for the field production and the A-3 producer.

## DISCUSSION

The idea behind this study was to implement the geological uncertainty regarding small scale barriers, however there are other uncertain features not included, such as faults beyond seismic resolution. In addition, there are uncertainties regarding the validity and resolution of the input data used, e.g. the shale and permeability log curves, the saturation logs and the sedimentological analogues. Finally, the lack of data (e.g. the injection log in A-10) complicates the overall uncertainty picture. Hence, the conclusion that Dip3 (dipping small scale barriers) is the most probable one, is preliminary, and further analysis and data acquisition will be performed - particularly concerning the nature of the more lateral extensive barriers. In addition, the work on optimizing the strategy for draining reserves trapped by small scale heterogeneities using the extended element model, will continue, since these barriers are not explicitly included in the coarse model.

## CONCLUSION

A simple upscaling routine for horizontal transmissibility has been developed and tested. The method represents an effective bridge between geological evaluation of uncertainties and flow simulation. Geo-statistical modelling helps the geologists in evaluating their impression of the reservoir via 3D visualization of the models and by the generation of new models simply by modifying input parameters. Geological uncertainty is implemented by deriving transmissibility reduction functions for alternative barrier models in zone 1.

The extended element model was used to eliminate those geological cases not reproducing the observed override, and to evaluate the effect of various strategies, e.g. a horizontal well in zone 1 to produce the remaining reserves. When applying the transmissibility reduction function on the full field N/G matrix, an improved history match was obtained.

Transmissibility reduction as a function of N/G may very well be derived for other depositional environments and heterogeneity styles (if the heterogeneities are small compared to the cell size in the flow simulation model) and further improve the Veslefrikk model. The method combines geo-statistical and deterministic modelling approaches in

an elegant manner, recognising that most often they complement one another.

## Acknowledgments

The authors thank Statoil and the Veslefrikk partners for permission to publish this paper. We also thank our colleagues for contributing with ideas and input.

## NOMENCLATURE

$\Phi$	=	Porosity
K <sub>as</sub>	=	arithmetic averaged permeability in sand
K <sub>cell</sub>	=	permeability in grid cell
K <sub>x</sub>	=	Permeability in X-direction
mD	=	milli Darcy
N/G	=	Net/Gross ratio (sometimes NTG is used)
S-log	=	Saturation log
std	=	standard deviation
SWI	=	Initial water saturation
S <sub>w</sub>	=	Water saturation
Q	=	Production rate
3D	=	3 dimensional

## REFERENCES

1. Begg, S.H., Kay, A., Gustason, E.R., and Angert, P.F. (1996): "Characterization of a Complex Fluvial-Deltaic Reservoir for Simulation", SPE Formation Evaluation, Sept. 1996
2. Bjørkum, P.A. and Walderhaug, O. (1990): "Geometrical arrangement of calcite cementation within shallow marine sandstones". Earth Science Reviews, 29, P145-161
3. Bratvold, R.B., Holden, L., Svanes, T. and Tyler, K.J (1994): "STORM: Integrated 3D Stochastic Reservoir Modelling Tool for Geologists and Reservoir Engineers", paper

SPE 27563 presented at SPE 1994 European Petroleum Conference.

wegian North Sea", Marine and Petroleum Geology, 9, P308-318.

4. Damsleth, E. and Holden, L. (1994): "Mixed Reservoir Characterization Methods", paper SPE 27969 presented at the 1994 University of Tulsa Centennial Petroleum Engineering Symposium, Tulsa, Aug.
5. Graue, E., Helland-Hansen, W., Johnsen, J., Lømo, L., Nøttvedt, A., Rønning, K., Ryseth, A., and Steel, R. (1987): "Advance and retreat of the Brent delta system, Norwegian North Sea". Petroleum Geology of Northwest Europe, P915-937
6. Kjønsvik, D., Doyle, J., Jacobsen, T., and Jones, A. (1994): "The Effects of Sedimentary Heterogeneities on Production from a Shallow Marine Reservoir", paper SPE 28445 presented at the 1994 SPE European Petroleum Conference, London Oct.
7. Lia, O. et al (1995): "The Great Reservoir Uncertainty Study - GRUS", PROFIT Project Summary Reports, Norwegian Petroleum Directorate, Stavanger, P191-204.
8. Pedersen, P.Å., Hauge, R. and Berg, E. (1994): "The Veslefrikk Field". North Sea Oil and Gas Reservoirs - III, P51-73
9. Tyler, K.J., Svanes, T., Omdal, S. (1993): "Faster History Matching and Uncertainty in Predicted Production Profiles with Stochastic Modelling", paper 26420 presented at the Annual Technical Conference and Exhibition, Houston, Oct.
10. Walderhaug, O., Bjørkum, P.A. and Nordgård Bols, H.M. (1989): "Correlation of calcite cemented layers in shallow marine sandstones of the Fensfjord Formation in the Brage field". In: Correlation in hydrocarbon exploration (Ed. J. D. Collinson), Graham and Trotman, London, P367-375
11. Walderhaug, O. and Bjørkum, P.A. (1992): "Effect of meteoric water flow on calcite cementation in the Middle Jurassic Oseberg Formation, well 30/3-2, Veslefrikk field, Nor-

## FIGURES

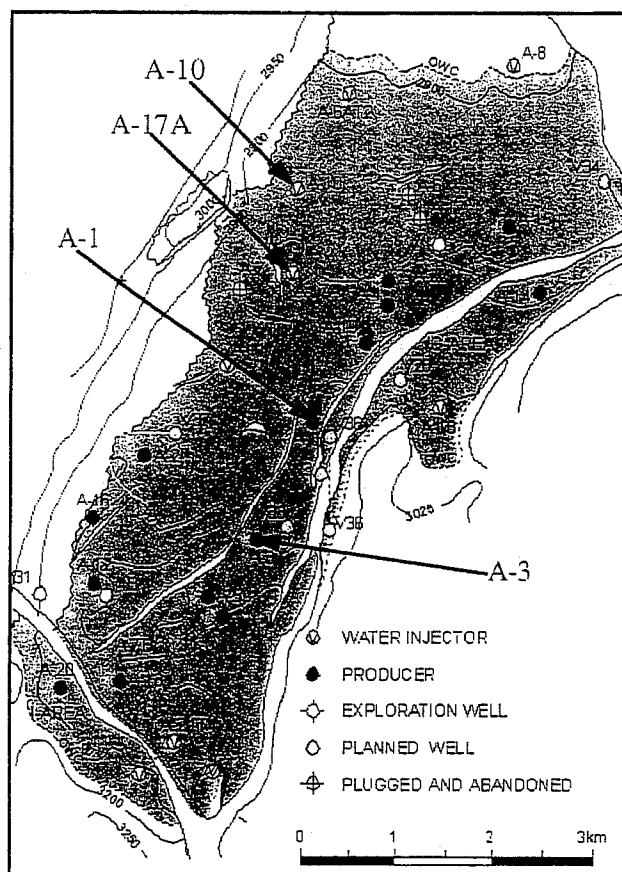


FIGURE 1 Field map with wells, top Etive Fm.



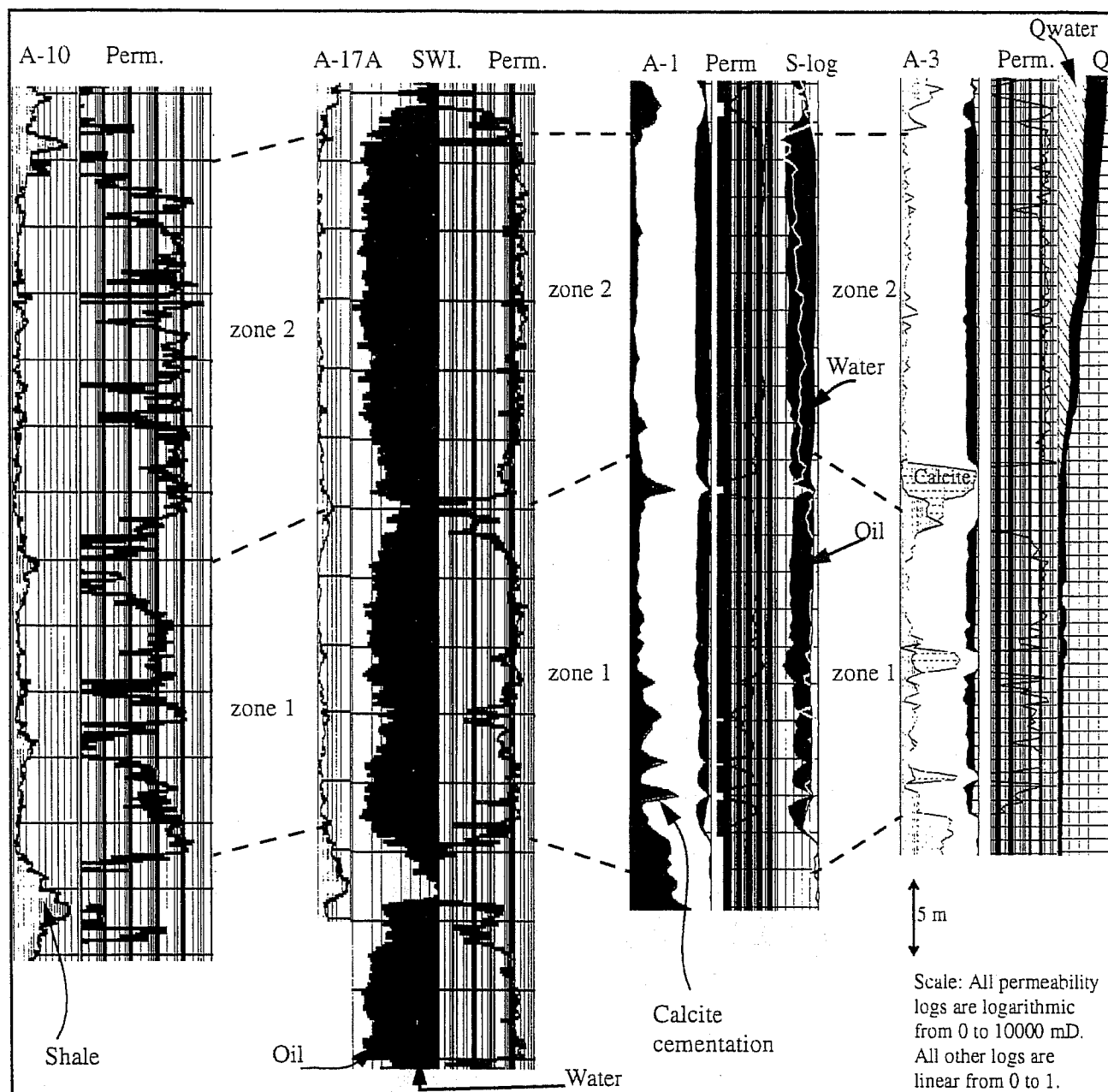


FIGURE 2 Observations: A-10, open-hole log in A-17A, saturation log in A-1, production log in A-3

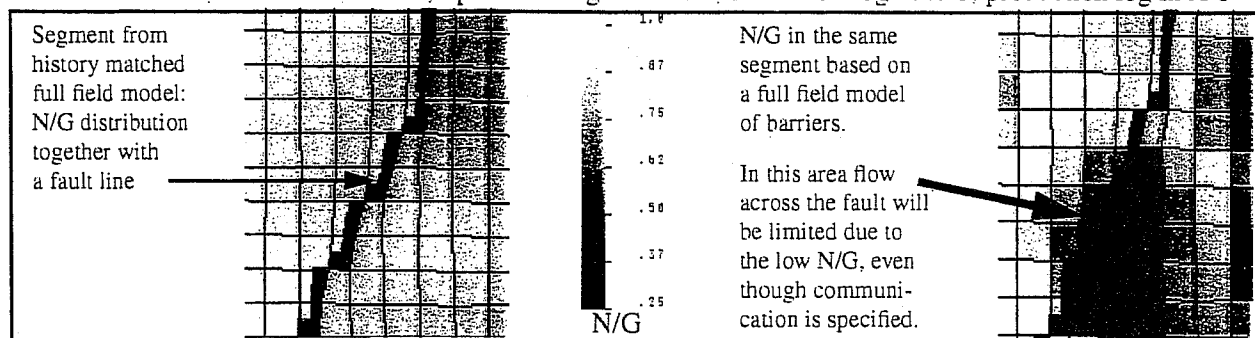


FIGURE 3 Possible disadvantage of geo-statistic full field barrier model regarding communication across faults.

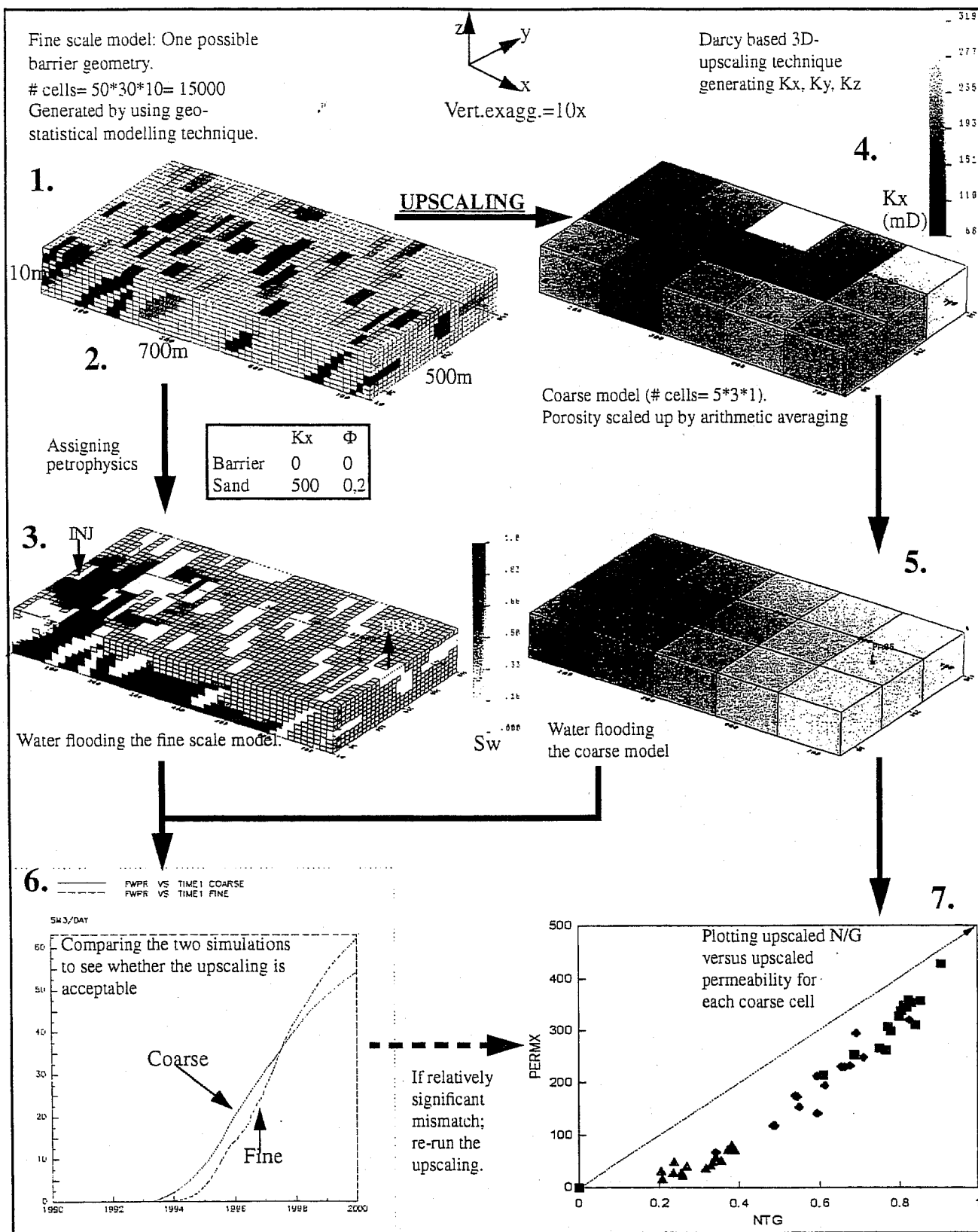


FIGURE 4 Method used to derive the relationship between N/G and permeability.

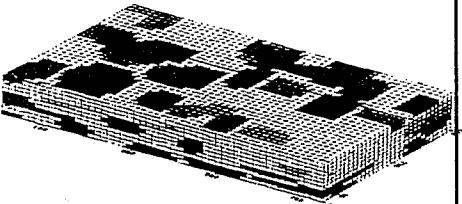
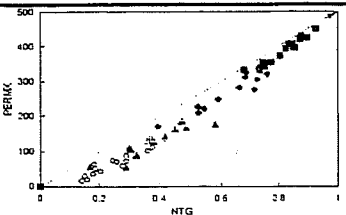
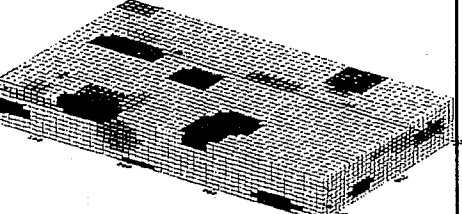
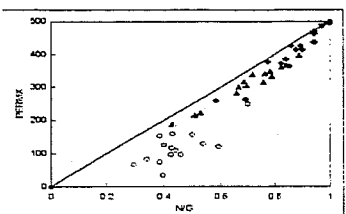
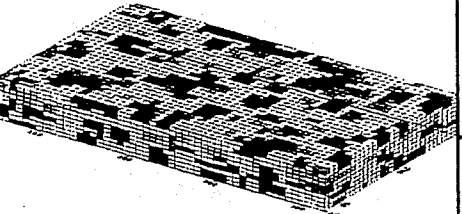
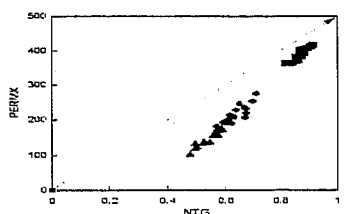
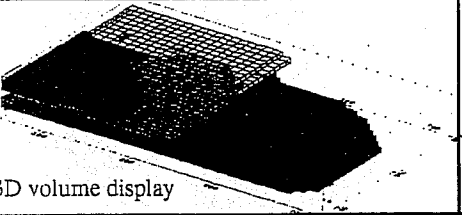
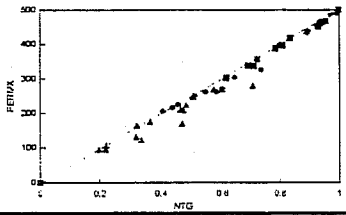
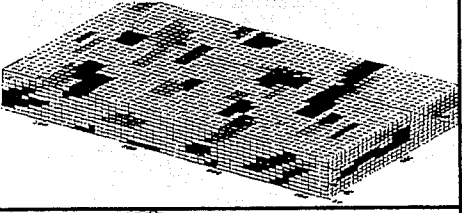
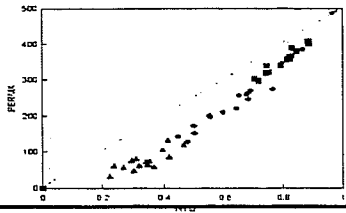
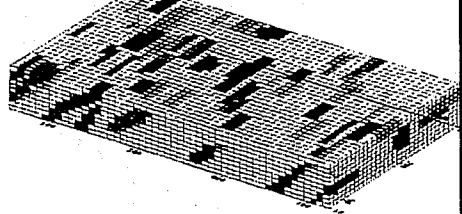
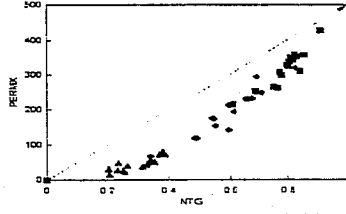
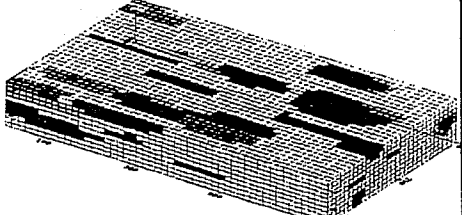
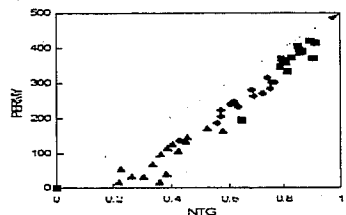
Model (brief description)	3D visualization (one example)	Resulting N/G-plot
Base case: Width=100m, std= 25m, thickness= 2m, no dip, circles, invers correlation between width and thickness		
Thick: As base case but with thickness= 4m		
Narrow: As base case but with width= 30m (std=15m)		
Wide: As base case but with width= 450m (std=100m)	 3D volume display	
Dip3: As base case but with dip angle= 3 deg. (std=1.5m)		
Dip6: As base case but with dip angle= 6 deg. (std=2)		
Ellips: As base case but with elliptical barriers, width= 50m and length= 175m		

FIGURE 5 Some alternative barrier models with corresponding N/G-PERM-relationship plots.

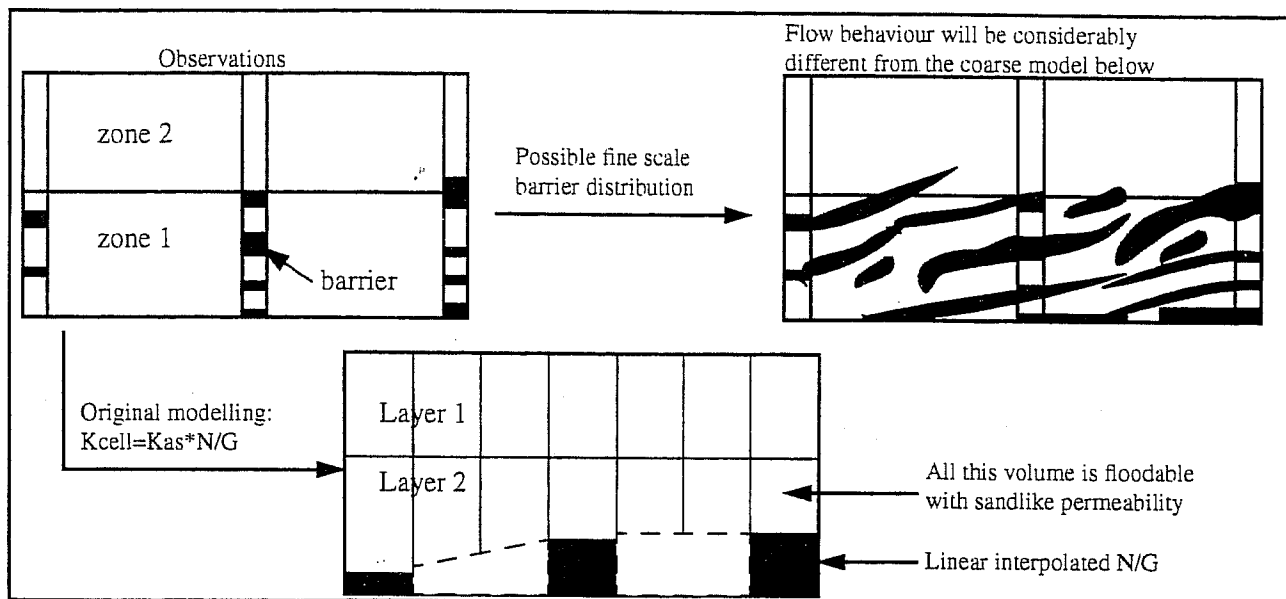


FIGURE 6 Comparison between original scaling of permeability and the effect of fine scale barriers.

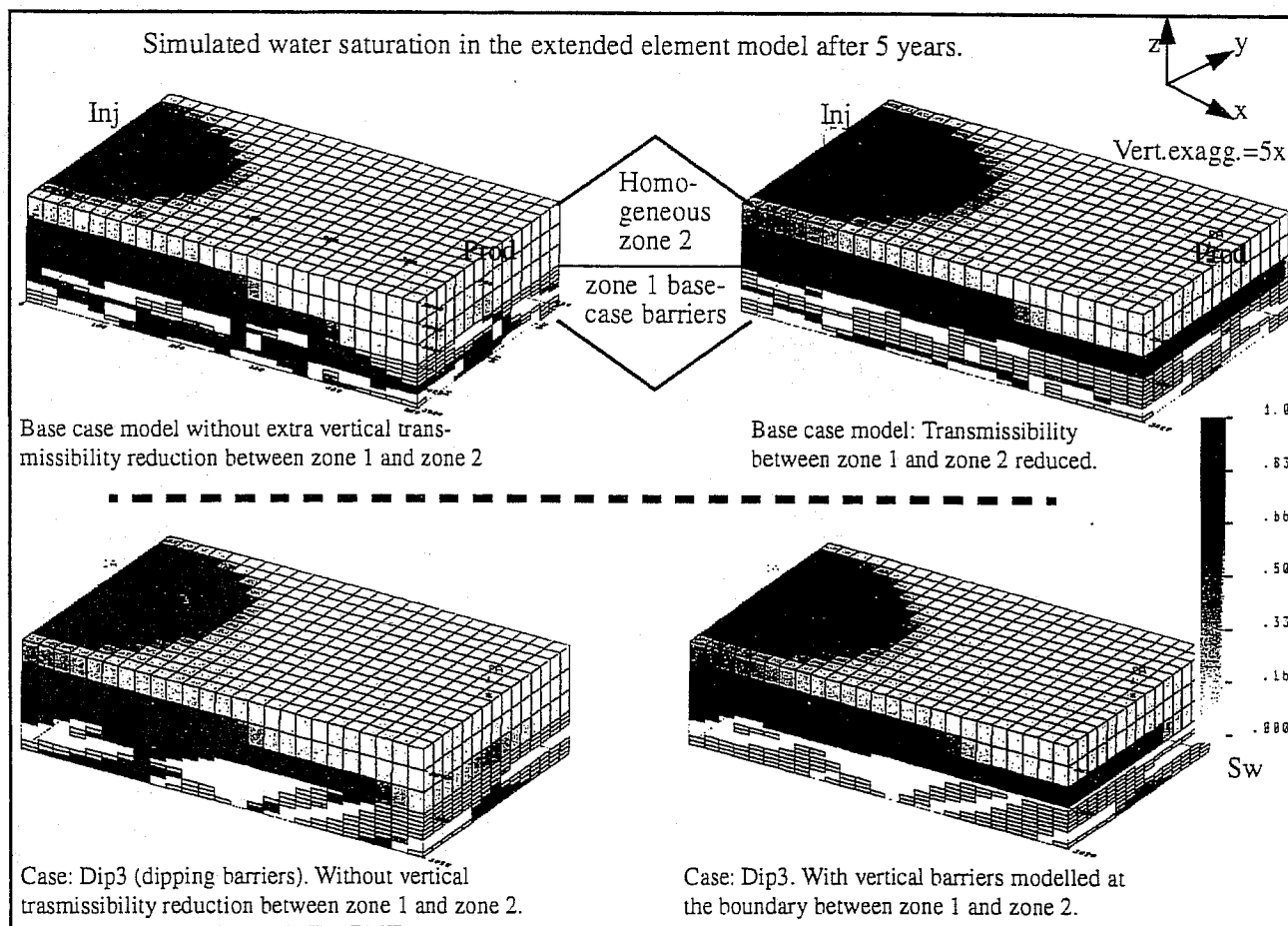


FIGURE 7 Flow simulations of the extended model: Two geological cases with varying vertical communication.

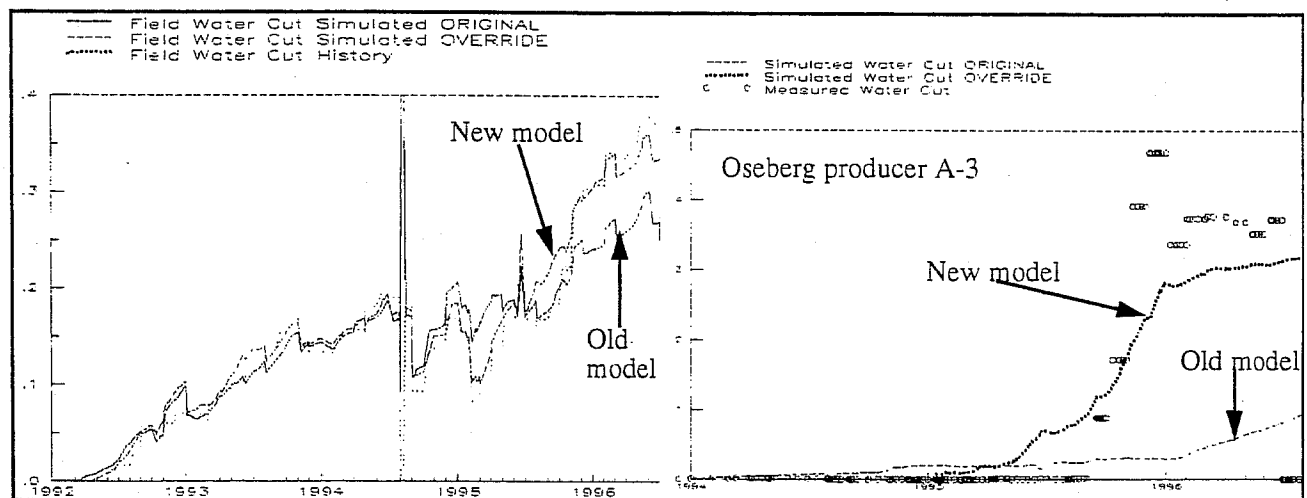
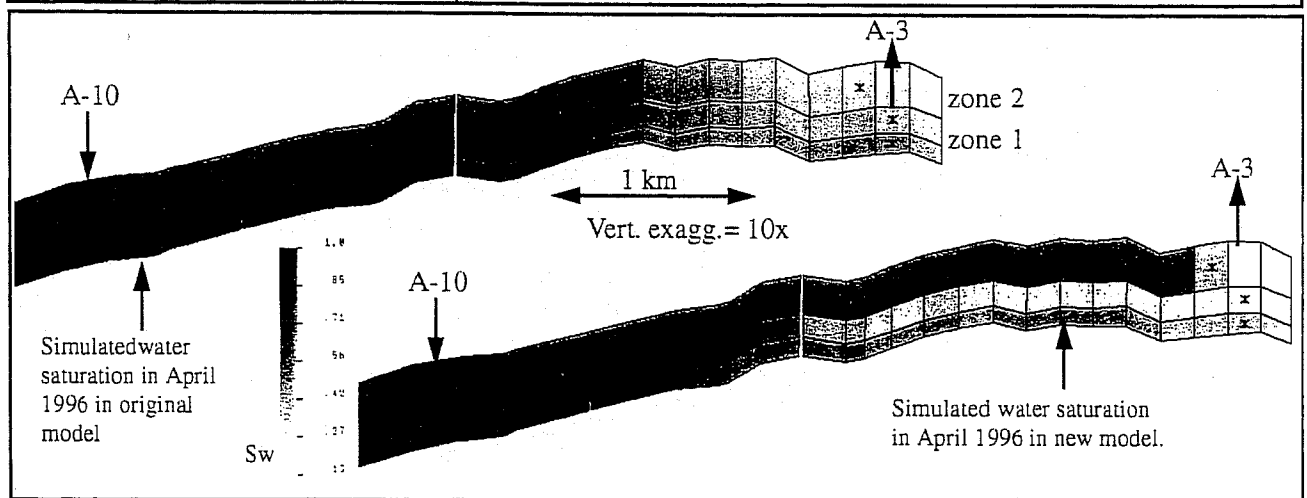
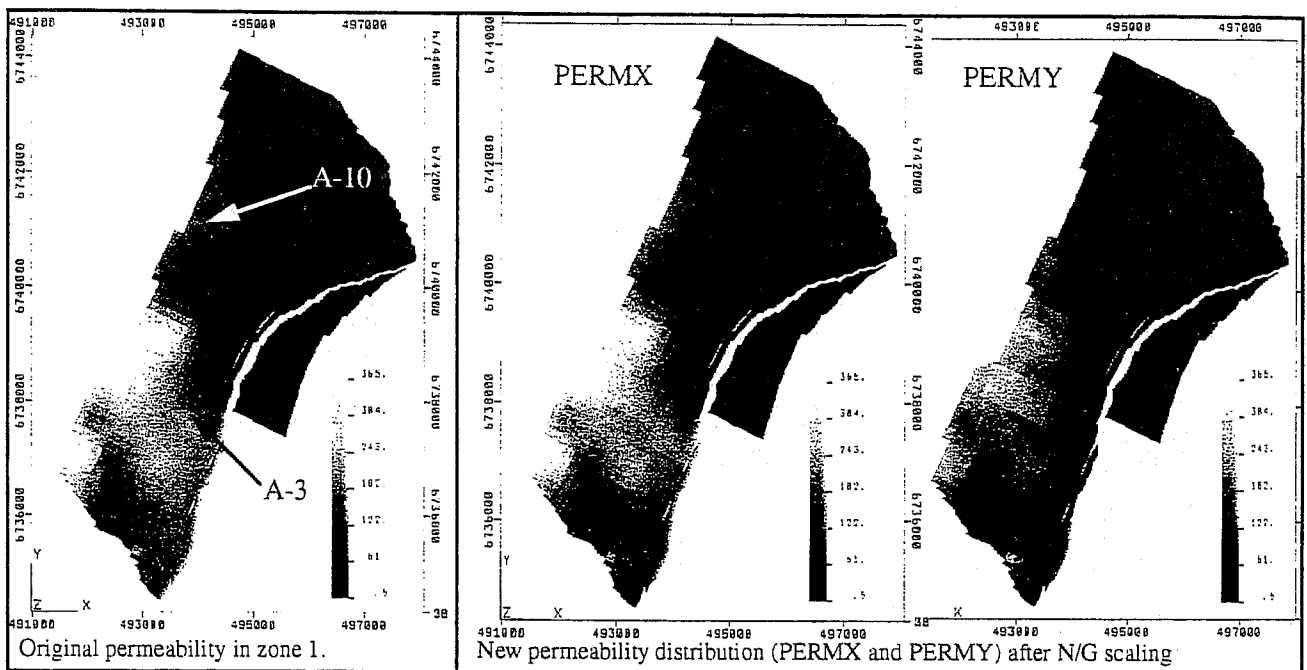


FIGURE 8 New full field model compared to the original (permeability, flooding and production).



P. LEMOUZY

INSTITUT FRANÇAIS DU PÉTROLE AND ELF/IFP HELIOS GROUP

PAU, FRANCE

## ACKNOWLEDGEMENTS

The author would like to thank the managements of the Institut Français du Pétrole and Elf for permission to publish this work performed within the Elf/IFP Helios Joint Research Group.

## ABSTRACT

In field delineation phase, uncertainty in hydrocarbon reservoir descriptions is large. To quickly examine the impact of this uncertainty on production performance, it is necessary to evaluate a large number of descriptions in relation to possible production methods (well spacing, injection rate, etc.). The method of using coarse upscaled models was first proposed by Ballin (1993). Unlike other methods (connectivity analysis, tracer simulations), it considers parameters such as PVT, well management, etc., .

After a detailed review of upscaling issues, applications to water-injection cases (either with balance or imbalance of production, with or without aquifer) and to depletion of an oil reservoir with aquifer coning are presented.

Much more important than the method of permeability upscaling far from wells, the need of correct upscaling of numerical well representation is pointed out. Methods are proposed to accurately represent fluids volumes in coarse models. Simple methods to upscale relative permeabilities, and methods to efficiently correct numerical dispersion are proposed.

Good results are obtained for water injection. The coarse upscaling method allows the performance of sensitivity analyses on model parameters at a much lower CPU cost than comprehensive simulations. Models representing extreme behaviors can be easily distinguished.

For depletion of an oil reservoir showing aquifer coning, however, the method did not work properly. It is our opinion that further research is required for upscaling close to wells.

We therefore recommend this method for practical use in the case of water injection.

## INTRODUCTION

### Need for fast evaluation of multiple geostatistical realizations

At delineation time, when only a few wells have been drilled, there remains a lot of uncertainty in the reservoir description:

- In the geometry of the reservoir, leading to uncertainty in the volume of hydrocarbon in place.
- In the amount of reservoir facies (which can be expressed as net/gross (N/G) ratio), leading also to uncertainty in the hydrocarbon in place volume.
- In the dimensions of geological bodies (i.e., channels, lobes) and of their internal heterogeneities, which control the connectivity of reservoir bodies, and thus the recovery.
- In the petrophysical characterization of the facies.

The major problem is to estimate the expected oil in place, the expected production profiles, and the attached uncertainties. If the value of expected production is below the economic standard of the operator, the decision will be to cancel any further development. When uncertainty is too large, additional data will be required (seismic, drilling) until a reasonable degree of certainty is reached, allowing the launching of a development. Determining the uncertainty is more critical offshore than onshore.

To estimate the uncertainty, two approaches are possible:

- One can determine scenarios (e.g., minimum, mode, maximum, or proven, probable, possible, etc.) for each factor participating in oil in place or in production profile computations (e.g., reservoir top depth map, porosity, N/G ratio), and combine them to obtain scenarios for the studied value. This approach can go from simple products of scenario values to more sophisticated Monte-Carlo computations, but it neglects possible interaction between factors.

- From a few wells, geological analysis can provide very realistic reservoir geological models. This knowledge can be expressed in terms of geostatistical parameters, used to build up very detailed reservoir models in lithofacies and/or petrophysics. The overall uncertainty is determined by the examination of the production behavior of a large number of realizations, letting uncertainty play for petrophysics, geometry, etc. The issue studied in the present paper is, therefore, the evaluation of the production behavior of a large number of realizations.

### Previous works

Guérillot et al. (1992) proposed a simplified flow simulator to sort several realizations. They used a single pressure field calculated once, and they computed the saturation evolution. This method is limited to cases when pressure has a limited impact on flow, e.g., for waterflood at a pressure above oil saturation pressure. It is exact for unit mobility ratio and negligible gravity and capillary effects, and inexact otherwise. Nevertheless it yields a satisfactory ranking of geostatistical realizations with respect to some production parameters (e.g., water breakthrough time) in its domain of validity.

Ballin et al. (1992) used tracer simulations to rank realizations. Similar to the previous method, it requires only a single calculation of the pressure field. Both methods have the same limitations. Saad and al (1996) confirmed that both methods are nearly equivalent with respect to cumulative oil production or water breakthrough time ranks.

Ballin et al. (1993) investigated how using the results of coarse upscaled model simulations can achieve a good ranking of multiple realizations. They proposed a methodology to approximate the cumulative distribution function (cdf) of production data which would be obtained through extensive simulations of fine models. Deutsch (1996) investigated statistical criteria and the use of coarse upscaled models, and concluded that the latter method is a valuable one.

The emergence of streamline-based computations (e.g., Thiele, 1996) is noteworthy. The method is similar to Guérillot's, as it uses a pressure field calculated once or a limited number of times. But it propagates 1D flow solutions along streamlines, making it faster and more general. Simplified simulations or streamline computations should present the same limitations concerning gravity and capillary effects, or strongly pressure dependent effects (e.g., gas liberation from oil).

The coarse upscaling approach is appealing because it is not restricted to a limited physical domain, as are the previous methods. It can handle cases with strong effects of pressure (three-phases flow, compositional). Moreover, sophisticated management of wells and reservoirs can be reproduced thanks to the possibilities of commercial simulators (e.g., a control of well flow-rate to limit the GOR can be handled automatically, a workover to plug a water-producing layer can be simulated).



## General

Upscaling must be performed considering the actual function of a reservoir simulator. First it processes data describing the reservoir (such as geometrical, petrophysical, PVT data), given as grid-block properties. The output of this pre-processing or initialization phase is a network composed of nodes (to which are attributed some grid-block data such as pore volume, pressure and saturation) and links (to which are attributed a transmissivity and a depth difference allowing to calculate gravitational potential differences). Flow equations are then solved for this network. This is not unfamiliar for people who worked with analog models made of resistors before the emergence of numerical models.

When upscaling flow models, it is better to define directly the components of the upscaled network, rather than the whole set of upscaled grid-block properties, which would be changed in the pre-processing phase. The coarser the model, the more critical it is to determine directly the network components, as the geometric approximations of pre-processing become inaccurate.

Another point to emphasize is that the upscaling problem in question is a pseudoization (calculation of properties depending on local conditions, as flow pattern and boundary conditions) rather than a homogenization (calculation of effective characteristics of an equivalent homogeneous medium).

## Permeability

As previously seen, we determined directly upscaled transmissivity, rather than upscaling block permeability and computing the transmissivity afterwards. This was proposed by Gomez-Hernandez (1990), who upscaled inter-block permeabilities. As the geometry of their model was regular, the geometric term within transmissivity (the ratio  $S/L$ ,  $S$  being the surface of the interface between two blocks, and  $L$  the distance between block centers) was constant, therefore upscaling either inter-block permeability or transmissivity was equivalent.

An explanation of the interest of direct upscaling of transmissivities may be found in Romeu et al. (1995). The authors investigated how numerical simulation gives the equivalent permeability of a block made of several sub-blocks with permeabilities obeying a spatially correlated distribution. They showed that the accuracy of numerical determination depends on the ratio of the size of the sub-block to the variogram range, and on the numerical method (finite difference (FD) underestimates equivalent permeability, while finite element (FE) overestimates it). The larger the sub-block size, the larger the error in the equivalent numerical permeability. They demonstrated that a special FD method, termed "direct", consisting in using permeability directly within the transmissivity term in place of the harmonic average of adjacent block permeabilities, yields equivalent numerical permeability closer to the value which would be obtained with an exact numerical method.

Attributing directly upscaled transmissivity is an application of this "direct" method. Upscaling implies that the ratio of block size to variogram range will be much larger in the coarse model, leading to large errors when using FD or FE methods. Using transmissivities directly allows for less error.

The upscaled transmissivities are computed by solving numerically for each coarse block small steady-state single-phase flow problems on fine scale models composed of the coarse block itself and of the existing neighboring blocks (up to 27 coarse blocks). Constant potential conditions are applied on two opposite faces of the model, and no-flow conditions on the remaining faces. One problem must be solved for each principal directions  $X$ ,  $Y$  and  $Z$ . Processing the results of the flow models (potential and flowrate) gives the interface transmissivities  $T$ . We have to sum up the flowrates  $q_i$  across each fine block interface composing a coarse block interface, and to calculate the average potential  $\Phi$  for each block separated by the interface.

The potentials are averaged by considering an arithmetic average of fine block potentials weighted by porous volume ( $V \phi$ ). This is obtained assuming that total compressibility is constant over fine blocks. Detailed derivation and discussion are presented in Appendix A.

$$\bar{\Phi} = \frac{\sum V_i \phi_i \Phi_i}{\sum V_i \phi_i} \quad (2)$$

## Initialization

Initialization of flow models consists in computing, for each block, its initial saturation and pressure, and attributing functions of pressure (PVT) or saturation (Kr-Pc). It requires the knowledge of the gravity center depths of blocks. In current use of FD numerical simulators, this gravity center depth is calculated from the geometrical description of the block, assuming the block is homogeneous. Thus the gravity center coincides with the geometric center of the block. When the coarse block is made of sub-blocks of different properties, these two points are not identical. When density of fluid is constant, the calculation detailed in appendix B leads to:

$$\bar{Z} \sum V_i \phi_i = \sum V_i \phi_i Z_i \quad (3)$$

Porous volume is also needed for the simulation. It is computed from fine scale models with equations A3 and A4.

Initial pressure is determined in the same way for coarse and fine blocks: given the initial reservoir pressure known at datum, PVT, and block depth, it is computed during the pre-processing phase of simulations. The same PVT is assumed to apply to the two scales. The question of whether to perform some kind of upscaling for PVT may be raised, as shown by the next equation expressing equivalence of oil in place volume at standard conditions for fine and coarse models:

$$\frac{\phi V S_o}{Bo(P)} = \sum \frac{\phi_i V_i S_{o_i}}{Bo(P_i)} \quad (4)$$

At initial equilibrium, pressure depends only on depth, and it is reasonable to keep the same PVT for coarse and fine blocks, as long as the dimensions of the coarse blocks are not too large.

To compute initial saturations, flow simulators consider the gravity-capillarity equilibrium, assuming that during migration, hydrocarbon displaced water by a drainage process. The saturation computation requires the definition of drainage capillary pressure ( $P_c$ ) curves, and of fluid contacts, which define the null  $P_c$  depth. Two methods have been tested:

- Upscaled drainage  $P_c$  curves may be determined, as explained in Appendix C. Using these curves for the coarse model initialization ensures that gravity-capillarity equilibrium is honored.
- Average saturations of coarse blocks resulting from the initialization of the fine model (equation C4) can be directly entered into the coarse model. In that case, if upscaled  $P_c$  curves are not provided to the coarse model, gravity-capillarity equilibrium will not be respected.

## Well representation

Wells are represented in numerical models by special nodes and links of the numerical network:

- A new node where well pressure is computed is added for each perforated reservoir block.
- The link between this node and the reservoir node representing the perforated block is characterized by a production index (PI) and by relative permeability functions, often those of the perforated block for a producing well.

When upscaling flow models, it is of prime importance to correctly upscale the characteristics of well functions (PI and Kr). The bottom hole pressure (BHP) is the most frequent pressure data available

accuracy. Moreover, the production operations (pumping, injecting, gas-lift) provide constraints for BHP and well flowrate. Their impact on the reservoir behavior can only be assessed if well functions are carefully computed. The radial flow pattern near wells is different from the nearly linear behavior far away from wells: therefore upscaling near wells is not the same as far from wells.

Classically, numerical PI is computed with the Peaceman (1978) equation. This equation has been established for centered vertical wells in a regular grid and homogeneous reservoir, far from reservoir limits and from other wells. Recently, Ding (1994) has proposed to process the results of a fine-scale simulation of steady-state single-phase flow around wells to compute upscaled PI, and upscaled transmissivities of interfaces of the perforated coarse blocks. This method takes into account, with the accuracy of the fine scale simulation, the following points:

- The true position of the well in the coarse block (not always centered).
- The deviation of the well from the vertical.
- Partial perforation of the coarse block.
- The effect of reservoir limits close to the well.
- Interference with another well (provided their flowrates keep the same ratio during simulation).
- The heterogeneity of reservoirs close to the well.

Practically, the steady-state single-phase simulation is performed on a fine scale model including the studied well and neighboring wells. In that model, the Peaceman equation is used. Well flowrates are set according to realistic values. Steady-state regime may be established when producing and injecting wells are present. For depletion, a pseudo steady-state may be simulated. From simulation results, the well flowrates  $q_i$  of perforated fine blocks composing a perforated coarse block are summed up to provide its flowrate  $Q$ . Average potentials of the perforated coarse block  $\Phi_b$ , and of surrounding blocks are obtained by a porous volume weighted average (Equation 2). Upscaled transmissivities near wells are calculated with equation 1. Finally, the upscaled PI is simply obtained from well potential  $\Phi_w$ :

$$\overline{PI} = \frac{\mu Q}{\Phi_b - \Phi_w} \quad (5)$$

Kr is needed to calculate the phase productions into the well. Due to the radial flow around the well, it is clear that saturation within fine blocks close to the well influences very much the overall mobility between the block and the well. That saturation detail is lost in the coarse block, where only average saturation is considered. Therefore, specific well Kr should be built-up. Furthermore, PVT must not be forgotten: one can imagine a case where only a few fine blocks around well have pressures below oil saturation pressure. The presence of gas close to the well has an impact on Kr, and thus on phase flows. But no gas appears in the coarse block if its average pressure is above saturation pressure: therefore significant differences between fine and coarse model results should occur. These PVT and Kr points have not been tackled in the present work, but we think they deserve further work.

## Relative Permeability

Relative permeability (Kr) may be upscaled in two steps:

- First, a physical upscaling gives the coarse scale Kr.
- Then, a correction of numerical dispersion is applied

### *Physical upscaling*

Upscaled Kr depends on relative magnitude of gravitational, capillary and viscous forces. When one force prevails, upscaling may be performed rather quickly, as the saturation distribution at fine scale may be obtained without any flood simulation. Then applying permeability upscaling techniques to the phase permeabilities provides upscaled Kr. Otherwise, the current practice is to use fine scale flow simulations and to process their results (e.g., KYTE & BERRY, 1975). This is obviously impractical when evaluating multiple realizations at the lowest computer time possible.

The set of end points (saturation and Kr).

- The set of Kr shapes, obtained by normalizing these curves in the [0, 1] range for both saturation and Kr axes with linear transformations.

Kr may be preserved through scales for some physical situations, and their preservation has been established in some practical cases by Kossak (1990). We only upscaled end points, and we kept the fine scale Kr shapes at the coarse scale. This choice is obviously erroneous in general cases, but we do hope that ranking capability of upscaled models will not be affected.

One issue is to select an average Kr shape when lithotypes show different shapes. In this case, we privileged the Kr shape of the most permeable lithotype, as it will dominate the flow capacity.

For saturation end points, we recalculated effective residual saturation, considering the initial saturation status in the fine model. When aquifer crosses a coarse block, the fine blocks below contact show a null oil saturation. Thus residual oil saturation for these blocks is set to zero. Once corrected, end point saturations are upscaled by a pore volume weighted average (equation C4).

For Kr end points, we considered permeability upscaling methods applied to phase permeability (K Kr). Algebraic methods are preferable, being faster than numerical ones. Among them, the power average method is useful, provided the exponent  $\omega$  characteristic of the reservoir is known. The upscaled Kr is obtained knowing the proportions of lithotypes  $x_i$ :

$$\bar{K}_r = \frac{\left[ \sum x_i \left( K_i K_r^i \right)^\omega \right]^{\frac{1}{\omega}}}{\left[ \sum x_i K_i^\omega \right]^{\frac{1}{\omega}}} \quad (6)$$

The determination of  $\omega$  requires a calibration step. As we did not perform this step, we assumed  $\omega = 1$ . This exponent corresponds to a layered reservoir, that is obviously often far from the actual configuration. Moreover, when a lithotype permeability is much larger than others, the end point Kr of this lithotype is recovered. Thus, we also tested the use of a proportion weighted average of Kr which gives a lower Kr:

$$\bar{K}_r = \sum x_i K_r^i \quad (7)$$

### *Correction of numerical dispersion*

Once the physical upscaling is done, one must tackle the problem of numerical dispersion. Use of coarse grids spreads displacing fluid fronts with usual FD methods. The analysis of this artefact is well known in 1D displacements (Lantz, 1971). To correct numerical dispersion in 1D, we can compute pseudo Kr from pressures and flowrates of a fine scale 1D flood simulation. They can be obtained for different aggregation ratios of fine blocks into coarse blocks. They depend on several factors: viscosity ratio, distance to injection block, capillary number. Nevertheless, a single Kr pseudo computed at half the mean distance between injector and producer, for the viscosity, capillary and velocity mean conditions prevailing in the reservoir, enables a reasonable reproduction of fluid rates at the producer.

It is thus attractive to use pseudo Kr computed in 1D to correct the numerical dispersion in 2D or 3D cases. As vertical velocity is usually low in reservoirs, we assume that correction of dispersion in 3D can be achieved by a 2D correction considering an areal flow.

The aggregation ratio to apply to 1D flow results must be chosen. To do this, we compared 2D areal flood simulations for a flood direction parallel or diagonal to the grid, and for favorable and unfavorable mobility ratios. We also calculated pseudo Kr in 1D for different aggregation ratios, and looked at the best choice of this ratio to reproduce the results of fine 2D simulations on coarse 2D grids.

From these simulations, the following conclusions may be drawn:

- When the mobility ratio is favorable, floods parallel to the grid direction show higher dispersion than floods along the diagonal direction of the grid.
- The best aggregation ratio for floods parallel to the grid is the actual aggregation ratio: e.g., if fine blocks are grouped into 5 x 5 to give a coarse block, a satisfactory pseudo Kr is obtained from 1D flow with an aggregation ratio of 5:1.
- The best aggregation ratio for floods along the diagonal direction of the grid is half the actual aggregation ratio. For a 4 x 4 grouping of fine blocks, a pseudo Kr from 1D flow with an aggregation ratio of 2:1 is efficient to recover results of the fine grid on the coarse grid.

## PRESENTATION OF CASE STUDIES

### First case: waterflooding a reservoir without active aquifer

This case, C1, deals with a turbiditic reservoir with two drilled wells. The study was aimed at determining the impact on production forecasts of the uncertainty on geostatistical parameters. Four lithotypes were described:

- Two types of channels (facies 1 and 2), of different petrophysical characteristics.
- A less permeable lithotype (facies 3), corresponding to levees.
- A shaly lithotype (facies 4), filling the remaining volume of the valley in which the turbiditic system was deposited.

A portion of this reservoir was represented by a rectangular box, elongated along the principal axis of the system. Geological uncertainty was thought to be important for two factors:

- The proportions of the facies. These data were simplified, considering the relations between the proportions of different facies, and reduced to a single factor, the proportion of channel 1.
- The dimensions of the reservoir bodies (facies 1 to 3). These dimensions are indirectly modeled thanks to variogram ranges (spherical model). As for proportions, the variogram range of channels 1 in the X direction perpendicular to the principal direction of the system (Y) is the single factor considered.

The possible value ranges of these factors was determined by a geologist. Applying experimental design techniques, five sets of geostatistical data (table 3) were compiled:

- The first set  $S_0$  corresponded to what the geologist thought was the most probable. It is the central point of the experimental plan, used to validate the model derived from the others sets.
- The four others sets  $S_1$  to  $S_4$  were build according to a complete factorial plan, each factor being fixed at one of the two limits of its range.

The parameter sets were used as input of the SISIMPDF routine of GSLIB (Deutsch, 1992) to obtain several facies simulations for each set. The chosen grid is shown in table 1. The block dimensions were 25 m in X, 60 m in Y and 1 m in Z. Each facies was given constant petrophysical data (table 2). Kr end points and shapes were different for each lithotype. Aquifer being far from this reservoir part, Pc was neglected ( $P_c = 0$  during simulations) and initial water saturation was at its irreducible value.

A waterflood with the two existing vertical wells and two new wells was simulated (Fig. 1). A perforation method for new wells was determined: the blocks of channel facies were systematically perforated. To maximize the impact of varying geostatistical parameters, high liquid production rates were imposed at producing wells. Injection rates were set to balance the total production, as long as injection pressure did not reach an upper limit. This led to an unbalanced waterflood, as the producing rate was not always able to balance production. Thus, depletion below bubble point pressure occurred near producing wells, making the GOR increase. The GOR was controlled by decreasing the liquid rate when an upper GOR limit was reached. Results were recorded at two different times: at 500 days,

## Second case: depleting or waterflooding a reservoir with active aquifer

The reservoir was an anticline structure, with a thickness of 40 m, an oil leg of about 60 m above an active aquifer. Two wells were drilled, and the study was aimed at determining the uncertainty of production either under balanced waterflood, or under depletion. Forty-nine geostatistical simulations of horizontal permeability conditioned to the two existing wells were performed in a grid presented in table 4. The block dimensions were 50 m by 50 m by 2 m. Porosity was attributed through a correlation between logarithm of horizontal permeability and porosity. A vertical to horizontal permeability ratio was assigned according to the level of horizontal permeability. The same Kr curves applied on all blocks.

For the waterflood case, two producing wells (P1 and P2) and four injecting wells (I1 to I4) were considered (Fig 2). P1 and I4 were the drilled wells, and they were perforated in the same way for all realizations. The other wells were perforated according to depth and permeability criteria. Liquid rates were fixed at producing wells. The sum of injection rates compensated the total fluid production of producers. As the total rate was moderate, no imbalance occurred during simulations, and reservoir pressure was above saturation pressure. The production results were recorded at two times: first when reservoir water-cut was at 5 %, and secondly at the end of production (20 years).

For the depletion case, seven producing wells (P1 to P7) were implemented in the oil zone (Fig. 3). P1 and P2 were the two drilled wells. The other wells were perforated according to depth and permeability criteria.

The production results are presented at end of production (20 years).

## ANALYSIS OF COMPARISON TESTS BETWEEN FINE AND COARSE SIMULATIONS.

### General

To test the value of upscaling to rank multiple realizations, a comparison between simulated productions results (termed X) of fine and upscaled models is performed. This yields the error  $\delta X$ :

$$\delta X = X_f - X_u$$

$\delta X$  is composed of two parts: its mean is the systematic error of using upscaled models, and is meaningless with respect to ranking. The important part of  $\delta X$  is its standard deviation, which gives the magnitude of random-like fluctuations around the mean: in the event of this standard deviation being null, one would obtain a perfect ranking of X, even if  $\delta X$  is far from being null. As the value of  $\delta X$  in itself is not sufficient to compare the ranking capability for different production results  $X^i$ , we propose to look at:

$$\varepsilon_1^i = \frac{\sigma(\delta X^i)}{\mu(X_f^i)} \text{ and } \varepsilon_2^i = \frac{\sigma(\delta X^i)}{\sigma(X_f^i)}$$

$\varepsilon_1$  represents the normalized accuracy of the "random" part of the error.  $\varepsilon_2$  represents the ranking capability: the smaller this figure, the better the ranking. A good ranking capability can be obtained either with small upscaling "random" errors, or because of a large variability of X. Conversely, if X has a small variability, ranking will be difficult, but in this case, uncertainty is not much of concern.

Another way to analyze ranking capability is to compute linear correlation coefficients. Exact scaling-up methods would provide a perfect linear correlation:  $X_u = X_f$ . As upscaling is not exact, one should expect a departure from this linear behavior, reasonably approximated by a linear correlation. Correlation coefficients between fine and upscaled simulation results will thus be calculated for both production parameters ( $\rho_X$ ) and their ranks ( $\rho_r$ ).

- Cumulative data: produced volumes of oil ( $N_p$ ), gas ( $G_p$ ), water ( $W_p$ ), and oil recovery factor. These data are smooth functions of time. Volumes produced are crucial for economic calculations (e.g., net present value). Normalized data such as recovery factor are important from a technical point of view to compare performances of different reservoirs.
- Instantaneous rates or rate ratios: oil flow-rate ( $Q_o$ ), gas-oil ratio (GOR), water-cut ( $F_w$ ). These data may vary a lot versus time and are the most difficult to recover through upscaled models.

### Tests of case C1

The tests (w1 to w5) differ according to the following options (see table 7):

- Coarse grid used.
- Method to upscale well functions:
  - 1: A simple method is used to compute upscaled PI. The Peaceman equation is applied to perforated coarse blocks, attributing a permeability which is the arithmetic average of the perforated fine blocks. No correction of transmissivities close to wells is done.
  - 2: Only PI is upscaled (equation 5), without any correction of transmissivities close to wells.
  - 3: PI and near well transmissivities are upscaled from fine scale well steady-state simulations.
- Aggregation ratio for computing corrected Kr shapes.
- Processing of end points:
  - 1: with equation 6 ( $\omega = 1$ ).
  - 2: with equation 7.

### Tests of case C2, waterflood

The tests (w1 to w6) differ according to the following options (see table 8):

- Coarse grid used.
- Aggregation ratio for computing corrected Kr shapes.
- Initialization of saturation:
  - 1: With a transfer of saturation from fine scale model initialization, and no Pc considered during waterflood.
  - 2: By using upscaled drainage Pc curves, used also during the imbibition phase.
- Using a correction of gravity term close to producing wells. As these wells are perforated close to aquifer, water coning or cusping occurs during production. To accurately describe the potential variation in the oil phase close to the well, a fine grid is necessary. When the grid is coarse, the driving potential difference that builds up the water cone is underestimated. This can be tackled in our numerical simulator by increasing the driving gravity term ( $g(\rho_w - \rho_o)$ ) applied in the blocks close to the well. A constant multiplying factor has been used in all realizations for all producing wells.

### Tests of case C2, depletion

The tests (d1 to d3) differ according to the following options (see table 9):

- Method to upscale well functions:
    - 1: Only PI is upscaled (equation 5), without any correction of transmissivities close to wells.
    - 2: PI and near well transmissivities are upscaled from fine scale well steady-state simulations.
  - Using a correction of gravity term close to producing wells, as for the waterflood case.
- The finest coarse grid was always used.

### Influence of correction of numerical dispersion

This influence is shown when comparing the following waterflood tests of case 2 (table 5):

- w1: Kr curves are not corrected for numerical dispersion.

- w4: Kr curves are corrected with an aggregation ratio 2:1.

Test w4 exhibits the best ranking performance for both intermediate and final production data. This observation confirms the conclusion of the 2D numerical dispersion investigation. The aggregation factor for computing corrected Kr curve (2:1) is close to half the 1D block aggregation factor (5:1).

### **Influence of Kr physical upscaling**

It is shown when looking at tests w3 and w5 of case 1 (table 10). The option to compute Kr end point in w5 gives better overall results for intermediate and final times. This shows that upscaling Kr is important to improve ranking. Methods used here are simplistic, and better ones should be developed. Li et al. (1995) recently proposed a promising method which seems accurate though not CPU expensive.

### **Influence of upscaling well parameters**

This influence is shown when comparing the following depletion tests of case 2 (table 6):

- d2: Only PI is upscaled.
- d1: PI and near well transmissivities are upscaled.

The results of test d2 are clearly worse than those of test d1, and the necessity of accurately computing near well transmissivities is clear.

### **Influence of saturation initialization**

This influence is shown when comparing the following waterflood tests of case 2 (table 5)

- w3: coarse models are initialized with upscaled Pc drainage curves.
- w4: coarse models are initialized with initial saturation computed on the fine scale models.

These tests do not show significant differences whether in correlation ( $\rho$ ), or accuracy ( $\epsilon$ ) coefficients. Thus, the simplest method is preferable in practical cases.

### **Influence of grid size**

This influence is shown when comparing:

- Tests w3 and w4 of case 1 (table 10).
- Tests w4 and w5 of case 2 (table 5).

Correlation coefficients are improved at final times for finest grids. They are also improved near breakthrough for case C1. For case C2 near BT, the accuracy ( $\epsilon_1$ ) is improved, though the correlation coefficient is not.

### **Coning**

Coning is present in case C2, especially for depletion. It can be better represented either with a finer grid (test w4), or by the trick on gravity coefficient (test w5, d3). The results show effectively an improvement of correlation coefficients when these options are chosen. This emphasizes the importance of correctly upscaling near wells.

The depletion case is demonstrative: if aquifer was not active, the depletion would be completely controlled by porous volume and well PI, which are well represented by the methods used in this study. Coning, which occurs in the vicinity of wells, deteriorates dramatically the results of upscaled models. Our present methods of Kr upscaling have to be improved and extended. We feel that the well PVT and Kr issues touched on in the discussion about upscaling methods are critical.

### **Additional results**

The upscaling method appears to be effective for waterflood cases, either when aquifer is present or not, or when injection balances production or not. It is possible to pick up realizations exhibiting extreme behaviors (Fig. 4, 6, 8, 9). Cumulative data appear easier to recover through upscaled models.



variability of this parameter, although recovery is obtained with the same precision as cumulative oil production. Instantaneous data (flowrates or rate ratios) are less easily captured. But yearly flowrates used in NPV calculations can be satisfactorily derived from cumulative data.

Depletion in the presence of an active aquifer cannot be accurately simulated with the present upscaling methods (Fig. 11), making this approach ineffective.

Fig. 5 represents the mean final oil production computed for each geostatistical set of case1. The mean values of fine scale models are satisfactorily approximated by upscaled models. In the preliminary phase of a sensitivity study, when the most important factors are not known, it is interesting to use upscaled models to investigate the relative importance of factors, and then to use fine models in a second phase focused on the controlling factors.

Fig. 7 depicts how the variation coefficients of several simulated productions parameters are approximated with upscaled models: their relative magnitude is preserved, thereby allowing the focus to be on the uncertainty of the most variable ones.

## COMPARISON OF COMPUTATIONAL COSTS

The mean performances for the case C1, compared to a mean computer time of 100 for the comprehensive simulation, are as follows:

Task	Computer time
Computation of pore volume, depth, saturation	0.24
Computation of transmissivities	1.19
Well model for PI computation	0.40
Upscaled flow simulation	0.79
Total	2.62
Ratio Upscaled Model / Fine Model	1: 38

Under some conditions (moderate permeability anisotropy and variance of the permeability field), the numerical solutions used for transmissivities and for well representations could be replaced by algebraic solutions, leading to smaller ratios of total time for upscaled simulation to fine scale simulation time. With the present options, smaller ratios would also be obtained for larger fine scale models.

## CONCLUSIONS

- We have successfully used upscaling to rank multiple geostatistical realizations, for waterflood cases. Upscaling with a large aggregation ratio is thus a practical method, which dramatically speeds up sensitivity studies, which would otherwise be precluded by business constraints.

- When depletion is controlled by aquifer coning, the upscaling techniques we used failed to provide a correct ranking of the realizations. Upscaling close to the well appears to be a critical point. A practical recommendation is to use fine grid-blocks around wells when upscaling from a geological model to a flow model.

- Upscaling of relative permeability is also a critical point. We recognize that we used over-simplified  $K_r$  upscaling methods for the sake of rapidity, and that further progress is necessary.

- When working with a regular coarse grid, correction of numerical dispersion seems necessary. A practical method consisting of computing a correction for 1D flow and applying it in 3D worked well. This correction depends on the respective directions of flow and of grid.

## Nomenclature

$c^t$	= total compressibility, $m^{-1}Lt^2, m^3/m^3/Pa$
$K$	= permeability, $L^2, m^2$
$Kr$	= relative permeability
$n_1:n_2$	= aggregation ratio, $n_1$ fine blocks grouped into $n_2$ coarse blocks
$P$	= pressure, $mL^{-1}t^{-2}, Pa$
$Pc$	= capillary pressure, $mL^{-1}t^{-2}, Pa$
$q$	= flowrate, $L^3t^{-1}, m^3/s$
$S$	= saturation, $L^3/L^3$
$t$	= time, $t, s$
$V$	= volume, $L^3, m^3$
$X$	= upscaled or averaged property $X$
$x$	= proportion, adimensional
$Z$	= depth, $L, m$
$\phi$	= porosity, $L^3/L^3$
$\Phi$	= potential, $mL^{-1}t^{-2}, Pa$
$\mu$	= viscosity, $mL^{-1}t^{-1}, Pa.s$
$\mu(X)$	= mean of $X$
$\sigma(X)$	= standard deviation of $X$

## Subscripts

$f$	= fine
$i$	= index
$o$	= oil
$u$	= upscaled
$w$	= water

## APPENDIX

### A. Computation of average potential

In transient regime, the discretized equation of conservation of volume (assuming that density of fluid is constant), is written as follows for either fine or coarse blocks:

$$\frac{V\phi c^t(\Phi^{n+1} - \Phi^n)}{\Delta t} = \sum_{i \in I} q_i, \quad I = \text{set of interfaces of the block} \quad (A1)$$

As the sum of all flowrates across interfaces of fine blocks is equal to the sum of flowrates across interfaces of the coarse block, we have:

$$\frac{\overline{V\phi c^t}(\overline{\Phi}^{n+1} - \overline{\Phi}^n)}{\Delta t} = \sum_{i \in B} \frac{V_i \phi_i c_i^t(\Phi_i^{n+1} - \Phi_i^n)}{\Delta t}, \quad B = \text{set of fine blocks} \quad (A2)$$

Total volume and porous volume of the coarse block are computed thanks to simple equivalence equations:

$$\overline{V} = \sum_{i \in B} V_i \quad \text{and} \quad \overline{V\phi} = \sum_{i \in B} V_i \phi_i \quad (A3, A4)$$

Equation A2 shows that averaging of compressibility and potential are not independent. One possibility is to compute average potential with porous volume weighting.

It follows that average compressibility is computed according to:

$$\overline{c^t} \sum_{i \in B} V_i \phi_i \Delta \Phi_i = \sum_{i \in B} V_i \phi_i c_i^t \Delta \Phi_i \quad (\text{A6})$$

Equation A6 means that average compressibility varies with time, as boundary conditions on the coarse block evolve in transient regime.

A second possibility is to compute the average compressibility as follows:

$$\overline{V \phi c^t} = \sum_{i \in B} V_i \phi_i c_i^t \quad (\text{A7})$$

The average potential resulting from the choice of compressibility averaging is given by the following equation:

$$\overline{V \phi c^t \Phi} = \sum_{i \in B} V_i \phi_i c_i^t \Phi_i \quad (\text{A8})$$

In the special case where total compressibility is constant, the average compressibility is equal to the small-scale compressibility for both choices, and the potential is simply averaged with porous volume weighting. This occurs when the total compressibility is composed of a negligible rock term, and a prominent constant fluid term. For cases where small-scale compressibility varies, further work is needed to determine which formulation is the best.

## B. Computation of gravity center depth

From the equivalence of gravitational potential between fine and coarse scale we obtain the following equation:

$$\overline{\rho V \phi g Z} = \sum \rho_i V_i \phi_i g Z_i \quad (\text{B1})$$

From equivalence of mass we have:

$$\overline{\rho V \phi} = \sum \rho_i V_i \phi_i \quad (\text{B2})$$

And finally:

$$\overline{Z} = \frac{\sum \rho_i V_i \phi_i Z_i}{\sum \rho_i V_i \phi_i} \quad (\text{B3})$$

When the specific gravity  $\rho$  is constant, it is a porous volume weighted average of block center depths:

$$\overline{Z} = \frac{\sum V_i \phi_i Z_i}{\sum V_i \phi_i} \quad (\text{B4})$$

## C. Computation of upscaled drainage capillary pressure curve

This is going to be done for a water-oil case. Before production starts, the reservoir is in equilibrium between capillary and gravity forces, resulting in a saturation vertical profile honoring the drainage Pc curve. The Pc in a fine block  $i$  may be expressed versus the small-scale Pc at the gravity center of the coarse block:

$$P_{c_i} = P_c(\overline{Z}) + \varepsilon g (\rho_w - \rho_o) (\overline{Z} - Z_i), \quad \varepsilon = \pm 1 \text{ depending on vertical axis orientation} \quad (\text{C1})$$

The average Pc in the coarse block is obtained thanks to a volume average:

$$\sum \phi_i V_i \quad \sum \phi_i V_i \quad \sum \phi_i V_i \quad (C2)$$

From equation B4, it follows that

$$\overline{Pc} = Pc(\overline{Z}) \quad (C3)$$

The appropriate choice of the gravity center of the coarse block leads to that simple relation, allowing to build up an upscaled drainage curve for a coarse block:

- i) Choose a value for  $\overline{Pc} = Pc^*(\overline{Z})$
- ii) Compute  $Pc_i$  for each fine block (C1), and the corresponding water saturation  $S_w^i$  from the drainage  $Pc$  curve.
- iii) Average water saturation for the coarse block:

$$\overline{S_w} = \frac{\sum V_i \phi_i S_w^i}{\sum V_i \phi_i} \quad (C4)$$

- iv) Join the new point  $(\overline{S_w}, \overline{Pc})$  to the upscaled drainage  $Pc$  curve, and iterate the sequence.

The fine-scale  $Pc$  curve is characterized by a maximum  $S_w$ , for which  $Pc = Pc_{\min}$ , and a minimum  $S_w$  for which  $Pc = Pc_{\max}$ . This curve has to be extended outside this  $Pc$  range as follows:

$$Pc > Pc_{\max} \Rightarrow S_w = S_{w\min}; Pc < Pc_{\min} \Rightarrow S_w = S_{w\max}$$

To completely define the upscaled  $Pc$  curve, the value picked up in step i must vary in the range between  $Pc_{\min} - \varepsilon g(\rho_w - \rho_o)(Z - z_{\text{top}})$  and  $Pc_{\max} - \varepsilon g(\rho_w - \rho_o)(Z - z_{\text{bot}})$ , where  $z_{\text{top}}$  and  $z_{\text{bot}}$  are the depths of the uppermost and lowermost fine blocks inside the coarse one. This results in an upscaled drainage  $Pc$  curve with a range of negative  $Pc$  values.

This method may be applied to homogeneous blocks, to initialize their saturation according to the capillary vertical profile, and to cases of pure gravity segregation when the capillary transition zone has a negligible thickness (the drainage  $Pc$  curve is then defined by:  $Pc \geq 0 \Rightarrow S_w = S_{w\min}$ ;  $Pc < 0 \Rightarrow S_w = S_{w\max}$ ).

## REFERENCES

- BALLIN, P. R., JOURNAL, A. G., AZIZ, K., 1992, Prediction of uncertainty in reservoir performance forecast: Journal of Canadian Petroleum Technology, Vol. 31, No. 4, p 52-62, April 1992.
- BALLIN, P. R., AZIZ, K., JOURNAL, A. G., 1993, Quantifying the impact of geological uncertainty on reservoir performing forecasts, Paper SPE 25238 in Proceedings of the 12th SPE Symposium on Reservoir Simulation held in New Orleans, LA, USA, February 28-March 3, 1993.
- DEUTSCH, C. V., JOURNAL A. G., 1992, GSLIB, Geostatistical Software Library and User's Guide, Oxford University Press editor, p 167-170.
- DEUTSCH, C., SRINIVASAN S., 1996, Ranking stochastic reservoir models, Paper SPE/DOE 35411: in Proceedings of 10th Symposium on Improved Oil Recovery, Tulsa, OK, USA, April 21-24, 1996.
- DING Y., 1995, Scaling-up in the vicinity of wells in heterogeneous fields: paper SPE 29137, in Proceedings of 13 th SPE Symposium on Reservoir Simulation, San Antonio, Feb. 1995.
- GOMEZ-HERNANDEZ, J. J., JOURNAL, A. G., 1990, Stochastic characterization of grid-block permeabilities: from point values to block tensors, in D. Guérillot and O. Guillon editors, Second European Conference on the Mathematics of Oil Recovery, Paris, Editions Technip, p83-90.

- KYTE, J.R., and BERRY, D.W., 1975, New Pseudo Functions to Control Numerical Dispersion, in SPE Journal (Aug. 1975), p 269-275.
- LANTZ, R. B., 1971, Quantitative evaluation of numerical diffusion (Truncation error): SPE Journal, Sept. 1971, p315-320.
- LI, D., CULLICK, A.S., LAKE, L. W. , 1995, Scale-up of reservoir models relative permeability using a global method: paper SPE 29872 in Proceedings of 9th Middle East Oil Show and Conference, Bahrain, March 1995.
- PEACEMAN, D. W., 1978, Interpretation of well-block pressures in numerical reservoir simulation: in Transactions of AIME, 1978, p253.
- ROMEU R.K., NGETINGER B., 1995, Calculation of internodal transmissibilities in finite-difference models of flow in heterogeneous media: Paper 94WR02422, in Water Resources Research, Vol. 31, n°4, April 1995, p943-959.
- SAAD, N., MAROONGROGE V., KALKOMEY, C. T., 1996, Ranking geostatistical models using tracer production data: Paper SPE 35494, Proceedings of European 3D Reservoir Modelling Conference, p 131-142, Stavanger, Norway, April 16-17, 1996.
- THIELE, M. R., BATICKY, R. P., BLUNT, M. J., ORR, F. M., 1996, Simulating flow in heterogeneous systems using streamtubes and streamlines: SPE Reservoir Engineering, Volume11, No. 1, p5-12, February 1996.

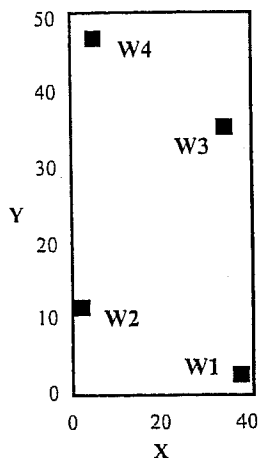


Fig. 1: Well implementation, case C1.

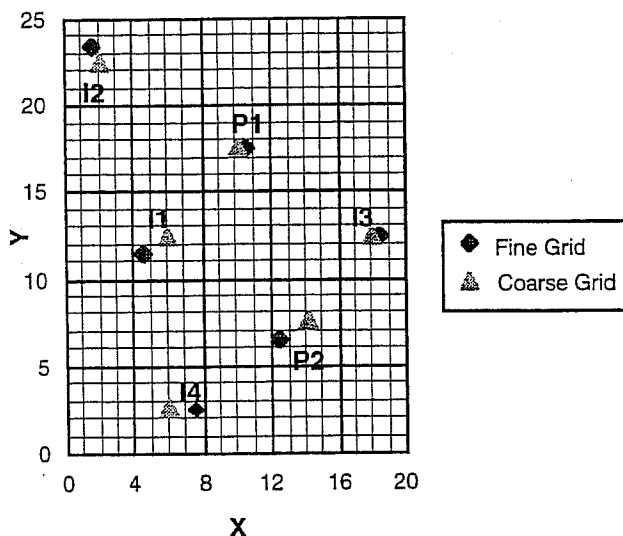


Fig. 2: Well implementation and grids, case C2 waterflood.

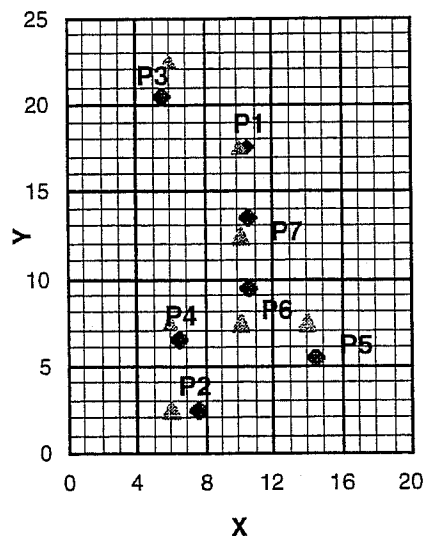


Fig. 3: Well implementation and grids, case C2 depletion.

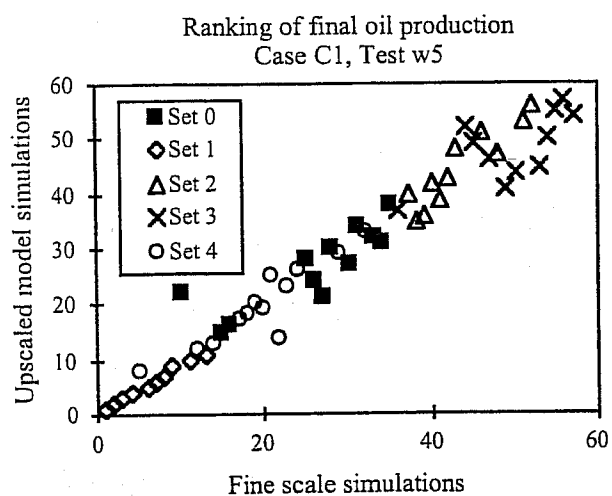


Fig. 4: Ranking of final oil production case C1, test w5.

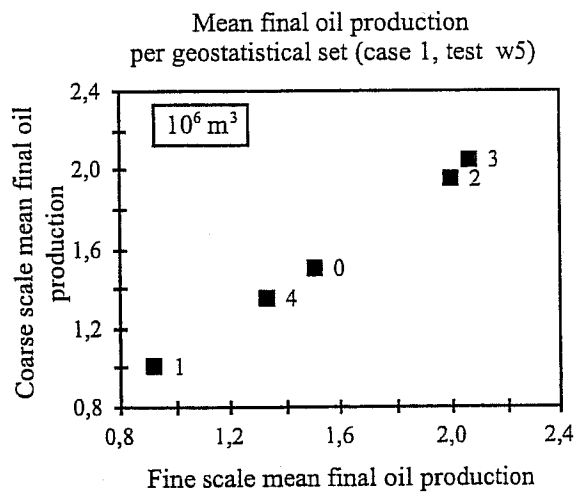


Fig. 5: Comparison of experimental planning results on fine and coarse models.

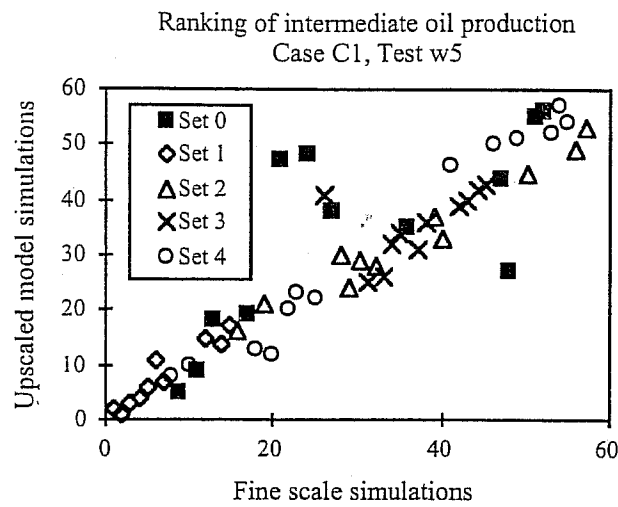


Fig. 6: Ranking of intermediate oil production case C1, test w5.

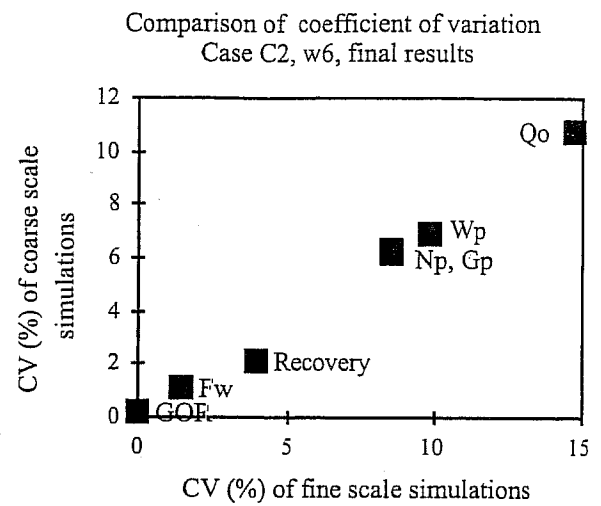


Fig. 7: Comparison of coefficients of variation for fine and coarse models.

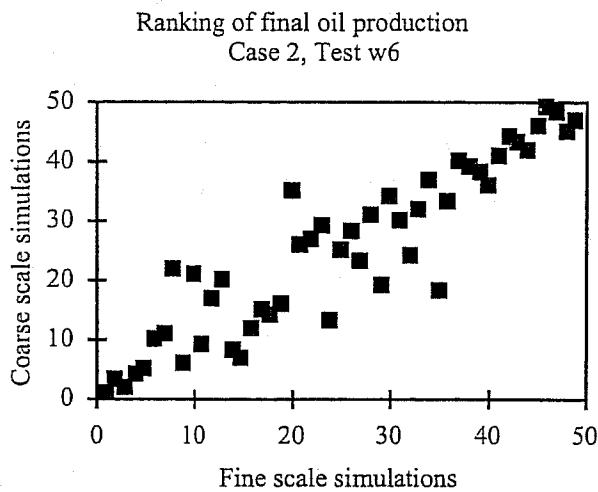


Fig. 8: Ranking of final oil production, case C2, test w6.

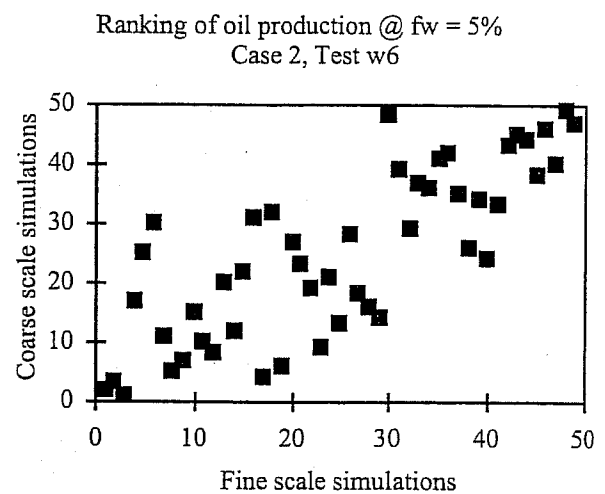


Fig. 9: Ranking of intermediate oil production, case C2, test w6.

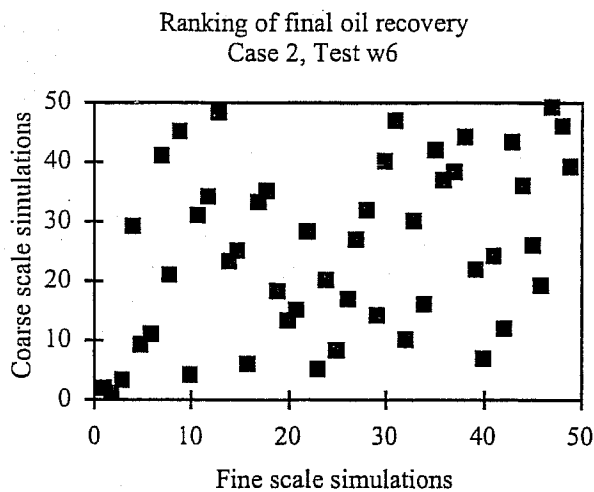


Fig. 10: Ranking of final oil recovery, case C2, test w6.

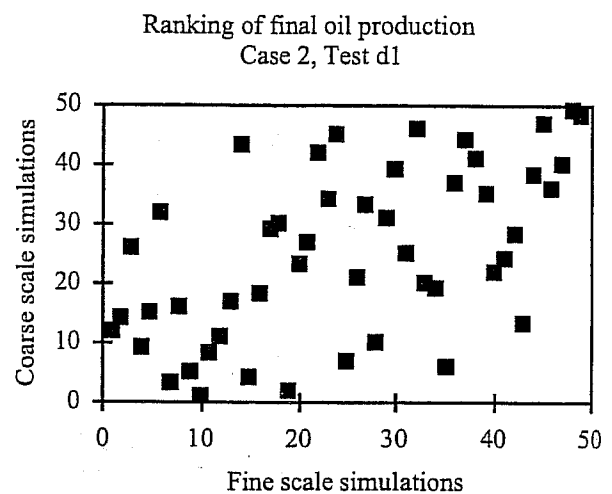


Fig. 11: Ranking of final oil production, case C2, test d1.

**Table 1: Grid description case C1.**

Grid	Block number / Aggregation ratio			
	X	Y	Z	Total
Fine	41	51	20	41820
Coarse 1	8 / ~5:1	10 / ~5:1	4 / ~5:1	320 / ~130:1
Coarse 2	10 / ~4:1	13 / ~4:1	5 / ~4:1	650 / ~64:1

**Table 2: Grid description case C2.**

Grid	Block number / Aggregation ratio			
	X	Y	Z	Total
Fine	20	25	20	10000
Coarse 1	5 / 4:1	5 / 5:1	2 / 10:1	50 / 200:1
Coarse 2	5 / 4:1	5 / 5:1	4 / 5:1	100 / 100:1

**Table 3: Petrophysical characteristics of facies, case C1.**

Facies	Permeability		Porosity	Swi	Sor	Krwmax
	Horizontal (mD)	Kv/Kh				
1	3000	0.1	0.30	0.15	0.20	0.40
2	300	0.01	0.26	0.30	0.17	0.20
3	25	0.001	0.06	0.35	0.18	0.15
4	1	0.00001	0.022	0.45	0.15	0.11

**Table 4: Definition of geostatistical sets, case C1.**

Set	Proportions	Variogram range (m)
S <sub>0</sub>	0,15	100
S <sub>1</sub>	0,10	50
S <sub>2</sub>	0,20	50
S <sub>3</sub>	0,20	200
S <sub>4</sub>	0,10	200

**Table 5: Case C2 - Waterflood Production Results**

		End of production (20 years)						fw = 5%						mean
		Data	w1	w2	w3	w4	w5	w6	w1	w2	w3	w4	w5	w6
Px	Np	0.93	0.96	0.95	0.95	0.94	0.95	0.63	0.63	0.65	0.64	0.76	0.71	0.81
	Qo	0.45	0.42	0.47	0.47	0.58	0.51	0.05	0.09	0.02	0.01	0.04	0.11	0.27
	Gp	0.93	0.96	0.95	0.95	0.93	0.95	0.64	0.63	0.65	0.64	0.76	0.71	0.81
	Wp	0.93	0.94	0.95	0.95	0.94	0.95	0.23	0.27	0.15	0.20	0.08	0.02	0.55
	Fw	0.45	0.19	0.48	0.28	0.57	0.50	0.08	0.04	0.10	0.06	0.08	0.07	0.24
	Recov.	0.55	0.59	0.57	0.58	0.74	0.55	0.51	0.49	0.52	0.51	0.69	0.61	0.58
	mean	0.71	0.68	0.73	0.70	0.78	0.74	0.36	0.36	0.35	0.34	0.40	0.37	
Pr	Np	0.87	0.93	0.91	0.90	0.90	0.92	0.76	0.78	0.77	0.79	0.71	0.79	0.84
	Qo	0.41	0.45	0.46	0.45	0.53	0.49	0.12	0.03	0.22	0.24	0.00	0.07	0.29
	Gp	0.87	0.93	0.91	0.90	0.91	0.92	0.76	0.78	0.77	0.79	0.71	0.80	0.84
	Wp	0.87	0.94	0.91	0.93	0.90	0.92	0.09	0.07	0.11	0.02	0.05	0.02	0.49
	Fw	0.43	0.41	0.51	0.40	0.57	0.50	0.11	0.05	0.20	0.10	0.05	0.17	0.29
	Recov.	0.31	0.35	0.33	0.32	0.63	0.37	0.64	0.64	0.65	0.67	0.64	0.70	0.52
	mean	0.63	0.67	0.67	0.65	0.74	0.68	0.41	0.39	0.45	0.43	0.36	0.42	
ε <sub>1</sub> %	Np	5.3	3.4	3.9	2.5	2.7	3.1	12.8	36.5	18.0	23.3	15.1	18.9	12.1
	Qo	13.5	20.0	13.7	11.8	12.8	10.5	746	0.3	0.4	0.3	0.3	0.5	69.1
	Gp	4.2	4.8	3.9	2.6	2.3	2.6	13.1	38.4	18.0	24.5	15.7	18.9	12.4
	Wp	6.1	4.1	4.5	2.7	3.1	3.6	16.8	40.8	62.3	35.3	39.4	48.6	22.3
	Fw	1.4	2.1	1.4	1.3	1.3	1.1	51.3	5.8	6.2	5.7	5.9	9.8	7.8
	Recov.	5.3	3.5	3.9	2.5	2.7	3.1	15.3	37.1	18.2	23.8	15.3	19.6	12.5
	mean	6.0	6.3	5.2	3.9	4.1	4.0	143	26.5	20.5	18.8	15.3	19.4	
ε <sub>2</sub> %	Np	33.8	29.7	28.0	22.5	24.7	24.2	46.2	70.8	42.1	67.9	49.6	72.3	42.6
	Qo	63.2	81.6	66.3	63.7	64.3	54.2	2460	106	226	189	109	186	306
	Gp	30.0	31.9	28.0	25.6	21.9	21.7	47.3	70.5	42.1	68.8	51.2	72.3	42.6
	Wp	33.9	32.8	28.0	22.1	24.6	24.2	84.9	88.7	80.6	60.8	75.1	114	55.8
	Fw	62.7	93.7	65.1	78.8	68.4	54.7	235	84.3	186	157	90.9	168	112
	Recov.	69.2	70.2	57.5	50.8	55.2	50.9	53.6	83.4	48.2	79.2	56.2	83.6	63.2
	mean	48.8	56.7	45.5	43.9	43.2	38.3	488	83.9	104	104	72.1	116	



**Table 6: Case C2 - Depletion Production**

Results					
		End of production (20 years)			
	Data	d1	d2	d3	mean
Px	Np	0.57	0.22	0.57	0.45
	Qo	0.10	0.00	0.28	0.13
	Gp	0.63	0.29	0.63	0.52
	GOR	0.09	0.00	0.12	0.07
	Wp	0.54	0.19	0.47	0.40
	Fw	0.04	0.00	0.13	0.06
	Recov.	0.37	0.02	0.36	0.25
	mean	0.33	0.10	0.37	
Pr	Np	0.56	0.23	0.55	0.45
	Qo	0.26	0.20	0.15	0.20
	Gp	0.61	0.26	0.65	0.51
	GOR	0.23	0.40	0.20	0.27
	Wp	0.49	0.13	0.51	0.38
	Fw	0.13	0.27	0.13	0.18
	Recov.	0.38	0.09	0.34	0.27
	mean	0.38	0.23	0.36	
$\varepsilon_1$ %	Np	36.3	77.8	29.5	47.9
	Qo	86.0	100	83.3	89.8
	Gp	9.0	72.3	8.6	30.0
	GOR	60.3	100	64.5	74.9
	Wp	34.5	94.2	34.0	54.2
	Fw	129	100	171	133
	Recov.	36.1	77.8	29.4	47.8
	mean	55.8	88.9	60.1	
$\varepsilon_2$ %	Np	103	97.5	102	101
	Qo	98.5	100	82.5	93.7
	Gp	70.7	95.8	70.5	79.0
	GOR	97.5	100	96.6	98.0
	Wp	75.4	99.6	68.2	81.1
	Fw	103	100	113	106
	Recov.	115	102	114	110
	mean	94.9	99.2	92.4	

**Table 7: Test specifications case C1**

Test	Grid	Wells	Correction of Kr	
			Shape	E. P.
w1	CG1	1	1:1	1
w2	CG1	2	5:1	1
w3	CG1	3	5:1	1
w4	CG2	3	5:1	1
w5	CG1	3	5:1	2

**Table 8: Test specification case C2 waterflood**

Test	Grid	Wells	Kr shape	Saturation initializ.	Gravity correction
w1	CG1	1	1:1	1	No
w2	CG1	1	5:1	1	No
w3	CG1	1	2:1	2	No
w4	CG1	1	2:1	1	No
w5	CG2	1	2:1	1	No
w6	CG1	1	2:1	1	Yes

**Table 9: Test specification case C2 depletion**

Test	Grid	Wells	Gravity correction
d1	CG2	1	No
d2	CG2	2	No
d3	CG2	1	Yes

Table 10: Case C1 - Waterflood Production Results

	Data	2000 days					500 days					mean
		w1	w2	w3	w4	w5	w1	w2	w3	w4	w5	
pX	Np	0.98	0.99	0.98	0.98	0.98	0.93	0.95	0.92	0.93	0.95	0.96
	Qo	0.28	0.07	0.44	0.25	0.75	0.97	0.96	0.95	0.95	0.96	0.66
	Gp	0.96	0.96	0.93	0.96	0.96	0.80	0.90	0.82	0.84	0.87	0.90
	GOR	0.28	0.65	0.17	0.31	0.67	0.91	0.94	0.92	0.90	0.92	0.67
	Wp	0.68	0.74	0.66	0.84	0.88	0.73	0.24	0.17	0.50	0.16	0.56
	Fw	0.50	0.49	0.24	0.49	0.90	0.44	0.11	0.37	0.61	0.08	0.42
	Recov.	0.56	0.76	0.60	0.65	0.79	0.74	0.89	0.82	0.83	0.86	0.75
	mean	0.61	0.67	0.57	0.64	0.85	0.79	0.71	0.71	0.80	0.68	
Pr	Np	0.97	0.98	0.97	0.97	0.98	0.85	0.90	0.84	0.87	0.91	0.92
	Qo	0.38	0.38	0.55	0.36	0.77	0.86	0.85	0.79	0.81	0.88	0.66
	Gp	0.94	0.95	0.92	0.94	0.96	0.73	0.80	0.76	0.74	0.80	0.85
	GOR	0.41	0.64	0.38	0.42	0.70	0.89	0.90	0.82	0.86	0.87	0.69
	Wp	0.77	0.78	0.75	0.86	0.90	0.77	0.57	0.49	0.60	0.46	0.70
	Fw	0.72	0.70	0.62	0.72	0.87	0.84	0.63	0.60	0.71	0.60	0.70
	Recov.	0.61	0.70	0.59	0.61	0.79	0.70	0.89	0.83	0.83	0.85	0.74
	mean	0.69	0.73	0.68	0.70	0.85	0.81	0.79	0.73	0.77	0.77	
ε1 %	Np	9.2	5.0	6.2	6.1	4.2	7.6	5.1	6.9	6.3	6.2	6.3
	Qo	33.5	37.6	41.6	37.4	23.1	6.3	6.4	8.5	7.2	6.7	20.8
	Gp	8.4	5.9	7.7	6.0	5.8	10.7	6.8	8.9	8.1	8.1	7.7
	GOR	27.3	20.9	30.1	24.5	18.9	7.8	5.0	5.8	6.0	6.8	15.3
	Wp	64.7	43.1	55.0	43.9	23.9	157	87.6	89.3	71.1	89.4	72.5
	Fw	38.0	31.6	38.4	30.6	15.4	102	97.3	88.4	74.5	93.4	61.0
	Recov.	9.3	5.1	6.4	6.3	4.5	9.9	6.2	8.5	7.7	7.5	7.1
	mean	27.2	21.3	26.5	22.1	13.7	43.0	30.6	30.9	25.8	31.1	
ε2 %	Np	19.4	12.5	15.6	16.1	13.0	40.2	32.1	41.7	39.4	36.1	26.6
	Qo	82.4	100	80.8	85.5	49.0	23.5	24.9	27.9	26.1	23.8	52.4
	Gp	24.8	19.3	26.9	21.6	19.0	56.3	38.3	48.4	47.9	44.9	34.7
	GOR	91.8	74.2	128	95.6	62.8	41.4	29.5	31.9	37.5	35.0	62.7
	Wp	56.0	55.8	58.2	45.1	39.0	139	92.4	94.5	80.0	94.6	75.4
	Fw	73.8	75.7	88.8	76.8	38.7	120	99.9	94.5	76.2	99.3	84.4
	Recov.	47.7	38.0	47.7	46.3	41.3	69.4	45.3	62.3	55.7	52.1	50.6
	mean	56.6	53.6	63.7	55.3	37.5	69.9	51.8	57.3	51.8	55.1	

- FIGURES ON PAGES
- Fig. 1: Well implementation, case C1.
  - Fig. 2: Well implementation and grids, case C2 waterflood.
  - Fig. 3: Well implementation and grids, case C2 depletion.
  - Fig. 4: Ranking of final oil production case C1, test w5.
  - Fig. 5: Comparison of experimental planning results on fine and coarse models.
  - Fig. 6: Ranking of intermediate oil production case C1, test w5.
  - Fig. 7: Comparison of coefficients of variation for fine and coarse models.
  - Fig. 8: Ranking of final oil production, case C2, test w6.
  - Fig. 9: Ranking of intermediate oil production, case C2, test w6.
  - Fig. 10: Ranking of final oil recovery, case C2, test w6.
  - Fig. 11: Ranking of final oil production, case C2, test d1.



# Effect of Wettability on Scale-up of Multiphase Flow from Core-Scale to Reservoir Fine-Grid-Scale

Y. C. Chang, V. Mani & K. K. Mohanty

Department of Chemical Engineering

University of Houston

Houston, TX 77204-4792

## ABSTRACT

Typical field simulation grid-blocks are internally heterogeneous. The objective of this work is to study how the wettability of the rock affects its scale-up of multiphase flow properties from core-scale to fine-grid reservoir simulation scale ( $\sim 10' \times 10' \times 5'$ ). Reservoir models need another level of upscaling to coarse-grid simulation scale, which is not addressed here. Heterogeneity is modeled here as a correlated random field parameterized in terms of its variance and two-point variogram. Variogram models of both finite (spherical) and infinite (fractal) correlation length are included as special cases. Local core-scale porosity, permeability, capillary pressure function, relative permeability functions, and initial water saturation are assumed to be correlated. Water injection is simulated and effective flow properties and flow equations are calculated. For strongly water-wet media, capillarity has a stabilizing/homogenizing effect on multiphase flow. For small variance in permeability, and for small correlation length, effective relative permeability can be described by capillary equilibrium models. At higher variance and moderate correlation length, the average flow can be described by a dynamic relative permeability. As the oil wettability increases, the capillary stabilizing effect decreases and the deviation from this average flow increases. For fractal fields with large variance in permeability, effective relative permeability is not adequate in describing the flow.

## INTRODUCTION

Heterogeneities exist at several length scales in naturally-occurring porous media. Variations in properties such as permeability and porosity can occur in core scale, stratum scale, bedding scale, well-log scale, and interwell scale (Worthington, 1991). Reservoir heterogeneity at different scales has different impacts on ultimate oil recovery in displacement processes. In the last decade, much progress has been accomplished on the characterization of detailed heterogeneities in oil reservoirs and the integration of these heterogeneities into the flow calculations (Wolcott and Chopra, 1993). Geostatistical techniques have been developed for estimation of the heterogeneities (Journel, 1990). Emerging parallel computers and new numerical techniques are increasing the power of reservoir simulation (Thiele et al., 1994; Bhogeswara and Killough, 1993). However,

typical reservoir-scale simulation models still do not have the resolution to incorporate fine-scale heterogeneities directly and rely on the use of effective properties to represent the effect of small-scale heterogeneities in large-scale numerical grids (Edwards and Christie, 1993).

Upscaling techniques have been developed to estimate effective flow properties in heterogeneous media (Warren, J. E. and Price, 1961; Gelhar, 1984; King, 1989; Durlofsky, L. J. et al., 1995; Glimm et al., 1993). The techniques developed for single phase flow are accurate and range from simple statistical estimates to detailed numerical simulations. The upscaling of multiphase flow has proven to be difficult. Multiphase flow in porous media is governed by functions such as relative permeability ( $k_r$ ) and capillary pressure ( $P_c$ ). Barker and Thiebaut (1996) have reviewed the pseudo relative permeability method and point out its lack of generality. Capillary-equilibrium method has been professed by many (Smith et al. 1989), but is applicable in water-wet rocks at small scales (e.g. laboratory-scale) at low flow rates. The homogenization method proposed by Quintard et al. (1996) and others is valid for small correlation lengths. The stochastic method proposed by Butts (1991) and Gelhar (1984) is valid for small permeability variations. The effective relative permeability approach has been proposed by many (Muggeridge et al., 1991; Hewett and Behrens, 1991) to take into account the dynamic effects of flow. It can be calculated by many methods: fine-grid simulation (Muggeridge et al., 1991), space renormalization (King et al., 1993) or heuristic methods (Li et al., 1996).

The applicability of the effective relative permeability approach for core-to-numerical grid (in typical pattern simulations) scaleup was tested for water-wet media by Chang and Mohanty (1997). This issue involves two questions. First, can the flow at a larger scale be adequately described by the multiphase Darcy's law involving an effective relative permeability (and an effective capillary pressure)? Second, if the Darcy's law is adequate, what is the effective permeability (and is effective capillary pressure) as a function of intrinsic relative permeability and heterogeneity? Chang and Mohanty (1997) found that in water-wet rocks the average flow can be described by an effective relative permeability if the permeability variance and correlation lengths are not very large. Such a formulation is not valid if the permeability variance is large and the spatial correlation is fractal. Water-wet capillary pressure plays an important role in stabilizing the waterflood displacement fronts.

Many reservoirs are not water-wet. The objective of this work is to study how the wettability of the rock affects its scale-up of multiphase flow properties from core-scale (~2") to pattern simulation grid-scale (~10'). Reservoir models need another level of upscaling to coarse-grid simulation scale (Li et al., 1996; Barker & Thibeau, 1996), which is not addressed here. Two key simplifying assumptions are used in this paper: effects of gravity are neglected and two-dimensional flow regions are considered. The scale-up of flow in only the horizontal direction is considered in several permeability fields. The anisotropic nature of the scaled-up relative

permeability is outside the scope of this paper. Also, the scale-up of the capillary pressure is not considered here. In the following section, the methodology used to represent reservoir wettability, heterogeneity and flow is summarized. The results are described in the following section.

## METHODOLOGY

Heterogeneity is modeled here by a spatially correlated random permeability field parameterized in terms of its variance and two point variogram, similar to our earlier work (Chang & Mohanty, 1997). Local porosity, permeability, capillary pressure, relative permeability and initial water saturation are assumed to be correlated to one another. High resolution reservoir simulation of water/oil displacement is conducted to understand the effect of heterogeneity on detailed multiphase flow. The saturation fronts and pressure drops were monitored and the JBN method (Johnson et al., 1959) is used to compute the effective relative permeabilities from these simulation data.

The computational flow field is taken to be 16 ft by 8 ft, about the size of a typical grid block in a reservoir pattern simulator. This system is modeled by a 100x50 grid of uniform size. The individual grid blocks are 0.16 ft by 0.16 ft, about the size of typical laboratory systems on which relative permeability and capillary pressure functions are measured. Each grid block is assumed to be homogeneous with prescribed intrinsic multiphase flow functions. Darcy's law for multiphase flow and capillary pressure-saturation relations are presumed to be valid at each grid block scale.

The permeability heterogeneity is specified by its probability distribution function and its two-point variogram. The probability distribution function for permeability is assumed to be log-normal with the average of 100 md and a standard deviation of  $\sigma_{\log k}$ .  $\sigma_{\log k}$  is varied from 0.2 to 0.8. Both spherical variograms with correlation lengths of 0.05 to 0.2 the system length and fractal variograms with Hurst dimension 0.87 are considered. The correlation length in the horizontal direction is considered to be twice the correlation length in the vertical direction. Thus the flow field is anisotropic, but only the overall flow in the horizontal direction is calculated in this work. The porosity was correlated to the permeability by the equation,

$$K = a \cdot 10^{b\phi} \quad (1)$$

where  $a$  and  $b$  are set to 0.001 and 25, respectively (Beier and Hardy, 1993).

## Water-Wet System

The water-wet media were modeled similar to our earlier work (Chang & Mohanty, 1997). Model parameters are listed in Table 1. The intrinsic relative permeability function is given by the Corey model (Honarpour et al., 1982) as

$$k_{ro} = k_{ro}^0 \left( \frac{S_o - S_{or}}{1 - S_{or} - S_{wr}} \right)^{n_o} \quad (2)$$

$$k_{rw} = k_{rw}^0 \left( \frac{S_w - S_{wr}}{1 - S_{or} - S_{wr}} \right)^{n_w} \quad (3)$$

The residual oil saturation ( $S_{or}$ ) and initial oil saturation ( $S_{oi}$ ) are related by the correlation (Land, 1968)

$$S_{or} = \frac{S_{oi}}{1 + c \cdot S_{oi}} \quad (4)$$

The irreducible water saturation  $S_{wr}$  is assumed to be a constant for all grid points and equal to 0.2. The initial oil saturation ( $S_{oi}$ ) depends on the initial capillary pressure of the system. The permeability, the porosity, and the primary drainage capillary pressure functions are correlated by the use of the J-function (Lake, 1989). Since the J-function depends on only the effective saturation, the capillary pressure function can be expressed in terms of permeability, porosity, and effective saturation and is given by

$$P_c^{Dr}(S) = \Gamma \sigma (K/\phi)^{1/2} S^{-1/\beta} \quad (5)$$

where  $\Gamma$  and  $\beta$  are constants and  $S$  is given by

$$S = \frac{S_w - S_{wr}}{1 - S_{wr}} \quad (6)$$

The imbibition capillary pressure,  $P_c^{Im}$ , is given by an equation similar to Eq. 5 but with a different constants  $\Gamma$  and  $\beta$  and the effective saturation  $S$  is defined as

$$S = \frac{S_w - S_{wr}}{1 - S_{or} - S_{wr}} \quad (7)$$

Capillary pressure hysteresis and relative permeability hysteresis are assumed to follow the model developed by Killough (1976).

### Mixed-Wet System

For mixed-wet media, the wettability is heterogeneous and strongly depends on initial water saturation. Jadhunandan and Morrow (1995) have studied the initial water saturation effect on wettability and the effect of wettability on oil recovery for oil/brine/rock system. They found that the initial water saturation increases as the wettability changes from oil-wet to water-wet. The wettability index  $I_{w-o}$  obtained from Amott tests is linearly related to initial water saturation. The relation can be described by

$$I_{w-o} = S_{wi} \cdot m + I_{w-o}^* \quad (8)$$

The slope ( $m$ ) and the intercept ( $I_{w-o}^*$ ) depend on brine composition and crude oil. They also demonstrated that the residual oil saturation decreases as the wettability changes from strongly water-wet to a neutral wettability, then it increases as wettability changes to strongly oil-wet. Residual oil saturation,  $S_{or}$  and wettability index,  $I_{w-o}$  can be expressed by

$$S_{or} = a \left( \left| I_{w-o} - I_{w-o}^{\min} \right| \right)^b + S_{or}^{\min} \quad (9)$$

By substituting Eq. 9 into Eq. 10, the initial water saturation and residual oil saturation can be



explicitly related by

$$S_{or} = a \left( \left( S_{wi} \cdot m + I_{w-o}^* - I_{w-o}^{\min} \right) \right)^b + S_{or}^{\min} \quad (10)$$

The model parameters are listed in Table 1. Depending on the initial water saturation, we classify the grid blocks into three categories: strongly water-wet ( $S_{wi} \geq 0.4$ ); mixed-wet ( $0.2 < S_{wi} < 0.4$ ); strongly oil-wet ( $S_{wi} \leq 0.2$ ). For strongly water-wet system,  $S_{or}$  and  $S_{wi}$  can be related by Land's correlation. Figure 1 shows the relation between  $S_{wi}$  and  $S_{or}$  in such mixed-wet systems.

The relative permeability is also given by the Corey model (Eqs. 2 & 3), but the parameters,  $k_{rw}^0$ ,  $k_{ro}^0$ ,  $n_w$ ,  $n_o$  are assumed to depend on the wettability (which depends on the initial water saturation). For mixed-wet media, the parameters are interpolated between the values of strong water-wettability and strong oil-wettability, according to the initial water saturation. Table 2 shows the parameters for relative permeability model in grids of different wettability. Figure 2 shows the relative permeability curves at different initial water saturations.

Imbibition capillary pressure function also depends on wettability. For water-wet grids ( $S_{wi} \geq 0.4$ ), capillary pressure is positive at all saturations, while capillary pressure is negative at all saturations for oil-wet grids ( $S_{wi} \leq 0.2$ ). For mixed-wet grids ( $0.2 < S_{wi} < 0.4$ ), capillary pressure is positive at low water saturation and negative at higher saturation. The imbibition capillary pressure for mixed-wet grids is described by

$$P_c = P_c^{ww} - F_{mw} (P_c^{ww} - P_c^{ow}), \quad (11)$$

where

$$F_{mw} = \begin{cases} 1, & \text{for } S_{wi} \leq S_{wi}^{ow}, \\ \frac{1}{(S_w - S_{wi}) \cdot (S_{wi}^{ww} - S_{wi}) + \varepsilon} - \frac{1}{\varepsilon}, & \text{for } S_{wi}^{ow} < S_{wi} < S_{wi}^{ww}, \\ \frac{1}{(S_{wi}^{ww} - S_{wi}^{ow}) \cdot (S_w - S_{wi}^{ow}) + \varepsilon} - \frac{1}{\varepsilon}, & \text{for } S_{wi} \geq S_{wi}^{ww}, \\ 0, & \text{for } S_{wi} \geq S_{wi}^{ww}, \end{cases} \quad (12)$$

and  $S_{wi}^{ww}$ , the critical initial water saturation for water-wet media, is set to 0.4;  $S_{wi}^{ow}$ , the critical initial water saturation for oil-wet media, is equal to 0.2;  $\varepsilon$  is a given parameter. Here water-wet capillary pressure,  $P_c^{ww}$  and oil-wet capillary pressure,  $P_c^{ow}$  are given by

$$P_c^{ww} = P_c^{\text{init}} \cdot \left( \frac{S_w - S_{wcp}}{S_{wi} - S_{wcp}} \right)^{-1/\lambda_p} \quad (13)$$

and

$$P_c^{ow} = -\Gamma \cdot \left( \frac{S_o - S_{ocm}}{1 - S_{ocm} - S_{wcm}} \right)^{-1/\lambda_m}, \quad (14)$$

where  $P_c^{\text{init}}$  is the equilibrium capillary pressure at  $S_{wi}$ ;  $\lambda_p$ ,  $\lambda_m$ ,  $S_{wcp}$ ,  $S_{wcm}$ ,  $S_{ocm}$  and  $\Gamma$  are given parameters. Figure 3 shows the capillary pressure at different initial water saturation.

## Oil-Wet System

The intrinsic relative permeability and capillary pressure of the oil-wet system are represented by functions similar to those of the water-wet system. The relative permeabilities are described by Eqs. 2 and 3, but with parameters listed in Table 1. Capillary pressure is denoted by

$$P_c(S) = \Gamma \sigma (K/\phi)^{1/2} S^{-1/\beta} \quad (15)$$

where  $\Gamma$  and  $\beta$  are constants and  $S$  is given by

$$S = \frac{S_o - S_{oc}}{1 - S_{oc} - S_{wc}} \quad (16)$$

For simplicity, no hysteresis in relative permeability and capillary pressure was assumed for oil-wet media.

## Waterflood Simulation

Two-dimensional fine grid simulations of waterflood were conducted to investigate the impact of heterogeneity on two-phase flow. A two-phase, immiscible, third-order, finite difference simulator with flux limiters was used. The numerical scheme is implicit in pressure and explicit in saturation. Water was injected at the left boundary at a specified total rate. The pressure at the right boundary was specified. The top and bottom were no-flow boundaries. Gravitational effects were neglected. The following parameters affect waterflood, but were kept constant in this study at the values listed.  $\Delta\rho = 0$ ,  $\mu_o = 10$  cp,  $\mu_w = 1$  cp, velocity =  $0.49 \times 10^{-2}$  cm/s,  $N_{gv} = 0$ ,  $N_{cv} \sim 3$ ,  $R_l = 2$ . The effect of these parameters is discussed elsewhere (Li & Lake, 1993; Chang & Mohanty 1997).

From computed 2-D saturation distributions, cross-sectionally averaged 1-D saturation fronts are calculated and monitored. The objective in scale-up is to relate the flux of a certain phase to its average saturation around any location and thus predict approximate 1D saturation distributions at any time. In this work, we determine whether the relative permeability formulations can be used to estimate these average saturations and the effective relative permeabilities. For homogeneous media and 1-D flow, Darcy's law leads to the traditional fractional flow theory (Lake, 1989). When the capillary pressure term is negligible, fractional flow theory dictates that each saturation,  $S_w$ , has its own constant characteristic velocity given by  $df_w/dS_w$ . Even when the capillary pressure term is not negligible, the characteristic velocity of each saturation depends only slightly on time. If a heterogeneous system can be averaged to a 1-D homogeneous system, the plot of  $S_w$  vs its characteristic velocity ( $x/t$ ) must be independent of time. Only then, can the Darcy's law with relative permeability be used to describe multiphase flow in a large scale heterogeneous system and appropriate effective relative permeability functions be identified. We will call such systems "k<sub>r</sub>-formulation adequate". If, however, the characteristic velocity of each

saturation depends on time strongly, i.e. the plots of  $S_w$  vs velocity ( $x/t$ ) do not fall on one line, the system will be identified as “ $k_r$ -formulation inadequate”. These systems cannot be described by a traditional relative permeability at the large scale. New flow equations need to be developed for effective multiphase flow of these systems.

Effective relative permeabilities were calculated by the JBN method (Johnson et al., 1959) by monitoring the effluent fractional flow and pressure drop during waterflood simulations. This method is commonly used to determine relative permeabilities from coreflood experiments.

## RESULTS

Three typical heterogeneous permeability fields are illustrated in Figure 4. Figure 4(a) shows the permeability distribution for the case of a small standard deviation and a small correlation length, e.g.  $\sigma_{\log k}=0.2$  and  $\lambda=0.05$ . Figure 4(b) shows the permeability distribution for the case of a large standard deviation and a large correlation length, e.g.  $\sigma_{\log k}=0.8$  and  $\lambda=0.2$ . Figure 4(c) shows the permeability distribution for the case of the fractal model with a large standard deviation, e.g.  $\sigma_{\log k}=0.8$  and  $H=0.87$ . As discussed earlier, three kinds of wettability scenarios are studied: completely water-wet, mixed-wet and oil-wet. In the mixed-wet scenario, the grids with  $S_{wi}>0.4$  (black in Figure 4 (d-f)) are water-wet, those with  $0.2<S_{wi}<0.4$  are mixed-wet, and those with  $S_{wi}<0.2$  are oil-wet. The distribution of the water-wet region depends on the correlation length of the permeability field.

The results for strongly water-wet media has been presented elsewhere (Chang & Mohanty, 1997). We have conducted numerical simulations for mixed-wet media and oil-wet media in this work. For the mixed-wet media, the wettability is heterogeneous and capillary pressure and relative permeability depend on initial water saturation as described earlier. Figures 5(a)-(b) shows saturation-velocity profiles for mixed-wet systems at  $\sigma_{\log k} = 0.2$  with  $\lambda=0.05$  and  $\lambda=0.20$ . As discussed earlier, these profiles were obtained by averaging the simulated 2-D saturation profile in the vertical direction and plotting them against the ratio of the distance over time. The shock fronts are more dispersive and the fluctuations of characteristic velocity are larger than those for water-wet media with similar heterogeneity. This is due to wettability heterogeneity and more oil-wet characteristics. Saturation-velocity curves at large times fall on top each other, so  $k_r$ -formulation is adequate for small standard deviation and finite correlation length cases. For the fractal field as shown in Figure 5(c), the saturation-velocity curves do not follow together, so  $k_r$ -formulation is inadequate for this case.

Figures 6(a)-(c) shows saturation profiles for mixed-wet systems at  $\sigma_{\log k} = 0.8$  with different  $\lambda$ . The saturation-velocity profiles are similar to those for water-wet system, except that the fluctuations are larger. For  $\lambda=0.05$  and  $0.20$ , the average characteristic velocity is a function of saturation alone, thus  $k_r$ -formulation is adequate at large  $\sigma_{\log k}$ . For the fractal field, the saturation

velocity profile does not fluctuate around an average. The average characteristic velocity is not a function of saturation alone, thus  $k_r$ -formulation is not adequate at for fractal fields at large  $\sigma_{\log k}$ .

Figure 7 illustrates the effective relative permeabilities at  $\sigma_{\log k}=0.2$ . The effective relative permeabilities at small permeability deviation with  $\lambda=0.05$  and  $\lambda=0.2$  are almost identical, while the effective relative permeabilities for the fBm fractal field are a little lower than those for small correlation ones. Since the relative permeability depends on initial water saturation, the intrinsic relative permeability chosen was based on the initial average saturation of the whole medium. All the effective relative permeabilities at this small permeability heterogeneity are comparable to intrinsic relative permeability. As permeability variance increases, the deviation between effective relative permeability and intrinsic relative permeability increases as shown in Figure 8, especially for water relative permeability. All effective relative permeabilities to water at large  $\sigma_{\log k}$  are higher than the intrinsic one.

Figure 9 shows the saturation-velocity profiles for oil-wet systems at  $\sigma_{\log k}=0.8$ . The saturation-velocity profiles for oil-wet systems at  $\sigma_{\log k}=0.2$  are very similar to those of the mixed-wet systems. The fluctuations of saturation-velocity at large  $\sigma_{\log k}$  and finite  $\lambda$  are much larger than those for mixed-wet and water-wet systems. However, the characteristic velocities after break through for the fBm fractal field are more smooth and close to each other at large times compared to those for mixed-wet and water-wet media. This is due to the constant initial water saturation assumed in this oil-wet system. The situation is similar to stratified layer system with constant initial water saturation and the saturation fronts move at the same velocity at each layer. Therefore, the 1D cross-sectionally averaged saturations are more smooth than those of nonuniform initial water saturations. Figure 10 shows the effective relative permeabilities at  $\sigma_{\log k}=0.2$ . The effective relative permeabilities at small permeability variance are close to intrinsic relative permeability. However, at large permeability variance, the effective relative permeabilities for various correlation lengths are quite different, as illustrated in Figure 11. Intrinsic oil relative permeability overestimates all the oil effective relative permeabilities while intrinsic water relative permeability underestimates the water effective relative permeabilities at low water saturation. The water effective relative permeability at  $\sigma_{\log k}=0.8$  and  $\lambda=0.2$  is higher than the other two with distinct  $\lambda$ , while oil effective relative permeability is lower than the other two. The flow in this large permeability variance and large correlation length media has the earliest breakthrough. The effect of correlation length of permeability field on effective relative permeability increases as the medium become more oil-wet.

From the above simulation results, we realize that permeability variance has more significant impacts on the fluctuation of saturations-velocity than correlation length for permeability fields with finite length autocorrelation model. To quantify the effect of the permeability variance on the fluctuation of saturation velocity, the average saturation velocity was first determined based

on the saturation-velocity profiles after breakthrough using a weighted least square method, then the deviation between average saturation velocity and saturation velocity was calculated. Figure 12 shows the relation between the standard deviation of fluctuation of saturation-velocity,  $\sigma_F(S_w)$  and standard deviation of permeability field,  $\sigma_{\log k}$  at  $\lambda=0.05$ . The variance of fluctuations of saturation velocity for both water-wet and oil-wet systems increase almost linearly with the permeability variance. The velocity fluctuation is larger for oil-wet systems than for water-wet systems at the same intensity of heterogeneity. Therefore, the heterogeneity region for which the  $k_r$ -formulation is adequate is larger for the water-wet media than for the oil-wet media.

In-situ water saturations provide insights to understand the effect of wettability on multiphase flow in heterogeneous media. Figure 13 compares the in-situ water saturations at  $\sigma_{\log k}=0.8$  and  $\lambda=0.2$  for water-wet and oil-wet media. The constant initial water saturation is assumed in the oil-wet media. The right hand side of the figure is the flow distributions at different injected pore volumes for the oil-wet medium. As water flows through the oil-wet medium, water first move to high permeability grids as illustrated in the figure at 0.05 PV, 0.1 PV and 0.2 PV. Capillary pressure in the oil-wet medium resists the water to flow through low permeability grids. Water can move through the low permeability grids only when the viscous force overcomes the capillary force. Even at 1.0 PV, a lot of low permeability regions are still bypassed. The capillary pressure term in the oil-wet medium tends to destabilize front movement. In water-wet media, capillary pressure helps imbibe water into low permeability grids while viscous pressure drop tends to move water into high permeability grids. As shown on the left hand side of the figure at 0.05 PV, 0.1 PV and 0.2 PV, the saturation fronts in the water-wet medium are more uniform than those of oil-wet case. The medium is almost completely swept at 1.0 PV. The capillary pressure term in the water-wet medium will help to stabilize front movement.

## Conclusions

This study has looked at upscaling of relative permeability from the laboratory scale (several centimeters) to fine grid field scale (several meters). The effect of various wettability, permeability variation and correlation length scale are studied. Only the flow in the horizontal direction is considered. Gravitational effects and three-dimensional flow are neglected.

- For strongly water-wet media, capillarity has a stabilizing/homogenizing effect on multiphase flow. As the oil wettability increases, the capillary stabilizing effect decreases and the deviation from this average flow increases.
- For small variance in permeability, and for small correlation length, effective relative permeability can be described by intrinsic relative permeability models. At higher variance and moderate correlation length, the average flow can be described by a dynamic relative permeability. The deviation from this average increases with increasing oil wettability.

- For fractal fields with large variance in permeability, effective relative permeability is not adequate in describing the flow.

## ACKNOWLEDGEMENTS

This work was partially funded by the Energy Lab, ARCO, Chevron and Mobil.

## REFERENCES CITED

- Barker, J. W. & Thibeau, S.: "A Critical Review of the Use of Pseudo Relative Permeabilities for Upscaling," SPE 35491, presented at the European 3D Reservoir Modelling Conf., Stavanger, Norway, April 16-17, 1996.
- Beier, R. A. and Hardy, H. H.: "Comparison of 2D and 3D Fractal Distribution in Reservoir Simulation," SPE 25236, SPE 12th Symposium on Reservoir Simulation, New Orleans, LA, Feb. 28-March 3, 1993.
- Bhogeswara, R. and Killough, J. E.: "Parallel Linear Solvers for Reservoir Simulation: A Generic Approach for Existing and Emerging Computer Architectures," SPE 25240, SPE 12th Symposium on Reservoir Simulation, New Orleans, LA, Feb. 28-March 3, 1993.
- Butts, M.B.: "A Stochastic Model for Two-phase Flow in Heterogeneous Porous Media," Prog. Rep. 73, Inst. Hydrodyn. and Hydraulic Eng., Tech. Univ. Denmark, (1991) 31-54.
- Chang, Y.C. & Mohanty, K. K.: "Scale-up of Two-Phase Flow in Heterogeneous Porous Media," to be published in J. Petrol. Sci. & Eng. (1997).
- Durlofsky, L. J. et al.: "Scale-up of Heterogeneous Three Dimensional Reservoir Descriptions," SPE 30709, ATCE of SPE, Dallas, TX, Oct. 22-25, 1995.
- Edwards, M. and Christie, M. A.: "Dynamically Adaptive Gudonov Schemes with Renormalization in Reservoir Simulation," SPE 25268, SPE 12th Symposium on Reservoir Simulation, New Orleans, LA, Feb. 28-March 3, 1993.
- Gelhar, L. W.: "Stochastic Analysis of Flow in Heterogeneous Media," Fundamentals of Transport Phenomena in Porous Media, J. Bear and M. Y. Corapcioglu (eds.), Martinus Nijhoff Publishers, Boston, 1984, 673-718.
- Glimm, J., Lindquist, W. B., Pereira, F. and Zhang, Q.: "A Theory of Macrodispersion for the Scale-Up Problem," Transport in Porous Media, 13, 97-122, 1993.
- Hewett, T. and Behrens, R.: "Scaling Laws in Reservoir Simulation and Their Use in a Hybrid Finite Difference / Streamtube Approach to Simulating the Effects of Permeability Heterogeneity," *Reservoir Characterization II*, edited by Lake et al., Academic Press, 1991, 402-441.
- Honarpour, M., Koederitz, L. F., and Harvey, H. A.: "Empirical Equations for Estimating Two-Phase Relative Permeability in Consolidated Rock," *J. Petrol. Tech.* (1982) 34, 2905-2908.

- Jadhunandan, P. P. & Morrow, N. R.: "Effect of Wettability on Waterflood Recovery for Crude-Oil/Brine/Rock Systems," *SPE*, 40-48, 1995.
- Johnson, E.F., Bossler, D.P. and Naumann, V.O.: "Calculation of Relative Permeability from Displacement Experiments," *Transactions of the AIME*, (1959) 216, 370-372.
- Journel, A. G.: "Geostatistics for Reservoir Characterization," *SPE* 20750, 65th ATCE of SPE, New Orleans, LA, Sep. 23-26, 1990.
- Killough, J. E.: "Reservoir Simulation with History-Dependent Saturation Function," *SPE J.* (1976) 16, 37-48.
- King, P. R.: "The Use of Renormalization for Calculating Effective Permeability," *Transport in Porous Media*, 4, 37-58, 1989.
- King, P.R., Muggeridge, A. H. and W. G. Price.: "Renormalization Calculation of Immiscible Flow," *Transport in Porous Media* (1993) 12, 237-260.
- Kossack C. A., Aasen, J. O. and Opdal S.T.: "Scaling up Heterogeneities with Pseudofunctions," *SPEFE*, 226-232, Sept. 1990.
- Lake, L. W.: *Enhanced Oil Recovery*, Prentice Hall (1989).
- Land, C. S.: "The Optimum Gas Saturation for Maximum Oil Recovery from Displacement by Water," *SPE* 2216, 43rd ATCE of SPE, Houston, TX, Sep.29-Oct.2, 1968.
- Li, D., Cullick, A.S., Lake, L. W.: "Scale-up of Reservoir Model Relative Permeability With a Global Method," *SPE*, 149-157, 1996.
- Muggeridge, A. H.: "Generation of Effective Relative Permeabilities from Detailed Simulation of Flow in Heterogeneous Porous Media," *Reservoir Characterization II*, edited by Lake et al., Academic Press, 1991, 197-225.
- Quintard, M. and Whitaker, S.: "Two-Phase Flow in Heterogeneous Porous Media I: The Influence of Large Spatial and Temporal Gradients," *Transport in Porous Media* (1990) 5, 341-379.
- Smith, E. H.: "The Influence of Small-Scale Heterogeneity on Average Relative Permeability," *Reservoir Characterization II*, edited by Lake et al., Academic Press, 1991, 52-76.
- Thiele, M. R., Blunt, M. J., and Orr, F. M.: "A New Technique for Predicting Flow in Heterogeneous Systems Using Streamtubes," *SPE/DOE* 27834, *SPE/DOE* 9th Symposium on Improved Oil Recovery, Tulsa, OK April 17-20, 1994.
- Warren, J. E. and Price, H. S.: "Flow in Heterogeneous Porous Media," *JPT*, Sept. 1961, 153-169.
- Wolcott, D. S. and Chopra, A. K.: "Incorporating Reservoir Heterogeneity with Geostatistics to Investigate Waterflood Recoveries," *SPEFE*, March 1993, 26-32.
- Worthington, P. F.: "Reservoir Characterization at the Mesoscopic Scale," *Reservoir Characterization II*, edited by Lake et al., Academic Press, 1991, 123-165.

Table 1 Model Parameters

Water-Wet System

<u>Parameter</u>	<u>Value</u>	<u>Equation</u>	<u>Parameter</u>	<u>Value</u>	<u>Equation</u>
$k_{ro}^0$	1	2	$k_{rw}^0$	0.16	3
$n_o$	2	2	$n_w$	3	3
$c$	1.5	4	$\sigma$	30	5
$\Gamma$ (Drainage)	1.537	5	$\Gamma$ (Imbibition)	0.461	5
$\beta$ (Drainage)	2	5	$\beta$ (Imbibition)	2.76	5
$S_{wr}$	0.2	2,3,6,7			

Mixed-Wet System

<u>Parameter</u>	<u>Value</u>	<u>Equation</u>	<u>Parameter</u>	<u>Value</u>	<u>Equation</u>
$m$	7.5	8	$I_{w-o}^*$	2	8
$a$	0.3	9	$b$	2	9
$I_{w-o}^{min}$	0.25	10	$S_{or}^{min}$	0.15	10
$\varepsilon$	0.05	12	$P_c^{init}$	13 psi	13
$S_{wcp}$	0.1	13	$\lambda_p$	0.5	13
$S_{ocm}$	0	14	$\lambda_m$	0.5	14
$S_{wcm}$	0.2	14	$\Gamma$	3	14

Oil-Wet System

<u>Parameter</u>	<u>Value</u>	<u>Equation</u>	<u>Parameter</u>	<u>Value</u>	<u>Equation</u>
$k_{ro}^0$	1	2	$k_{rw}^0$	0.5	3
$n_o$	4	2	$n_w$	2	3
$\sigma$	30	15	$\Gamma$	0.745	15
$\beta$	0.7	15	$S_{oc}$	0	16
$S_{wc}$	0.2	16			

Table 2 Parameters of relative permeability model for mixed-wet media

	Oil-Wet Grid	Mixed-Wet Grid	Water-Wet Grid
$S_{wi}$	$\leq 0.2$	0.2~0.4	$\geq 0.4$
$S_{or}$	Eq. 4	Eq. 10	Eq. 4
$k_{rw}^0$	0.5	Interpolation	0.1
$k_{ro}^0$	1.0	1.0	1.0
$n_w$	2.0	Interpolation	4.0
$n_o$	4.0	Interpolation	2.0



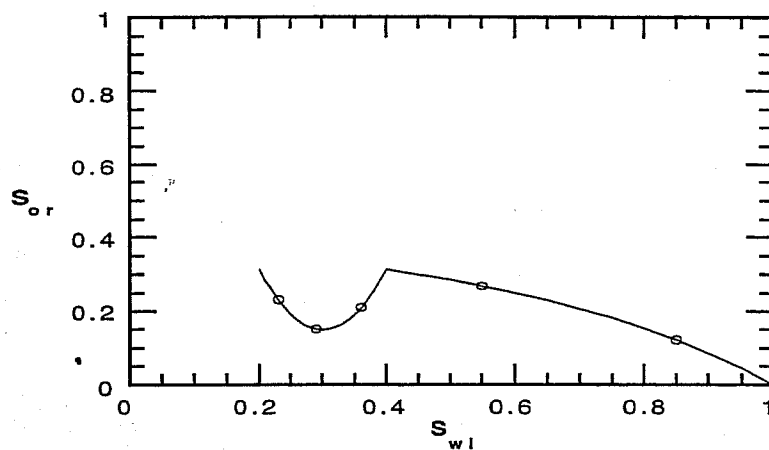


Figure 1 Relation between  $S_{oi}$  and  $S_{or}$  in mixed-wet system.

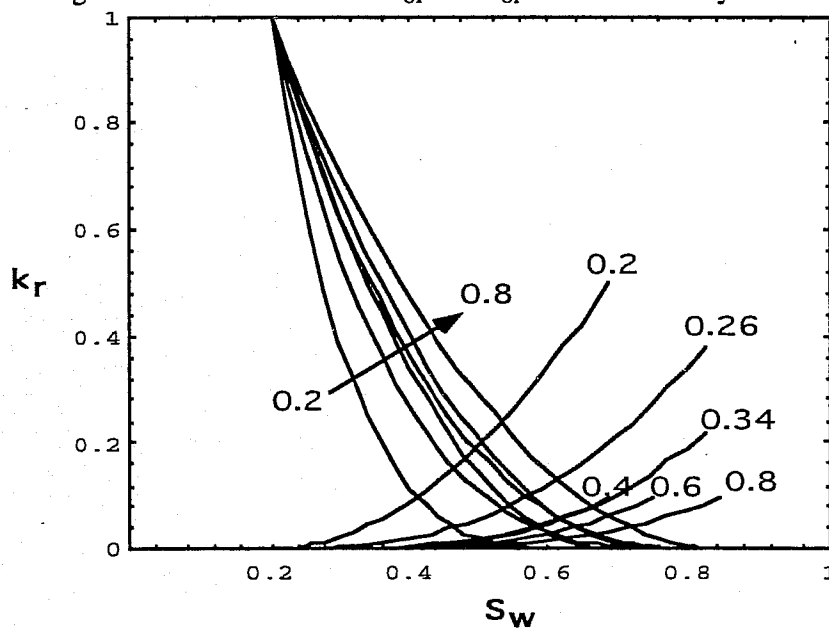


Figure 2 Relative permeability at different initial water saturation in mixed-wet system.

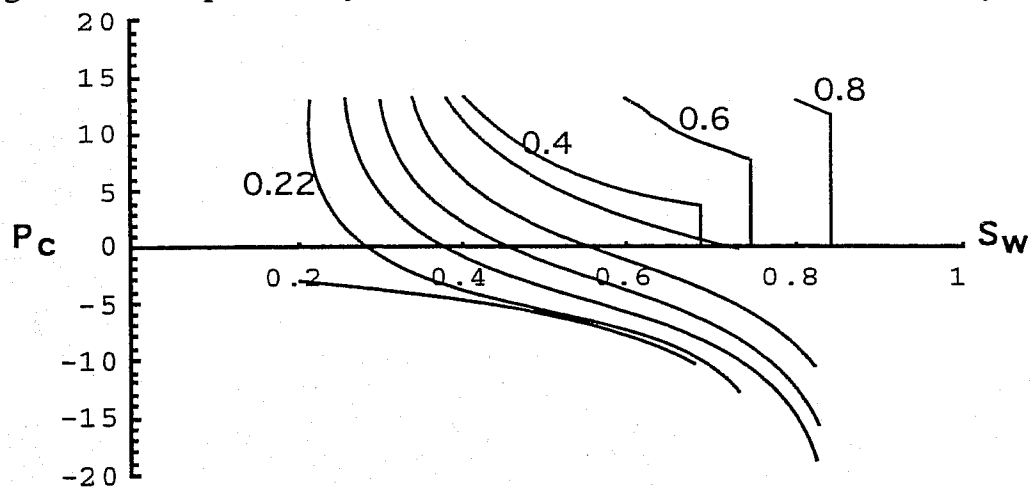
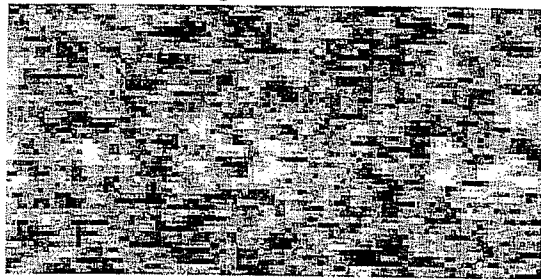
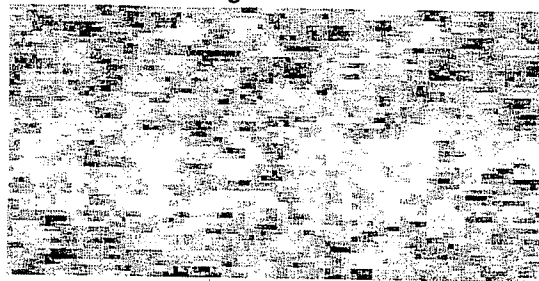


Figure 3 Capillary pressure at different initial water saturation in mixed-wet system.

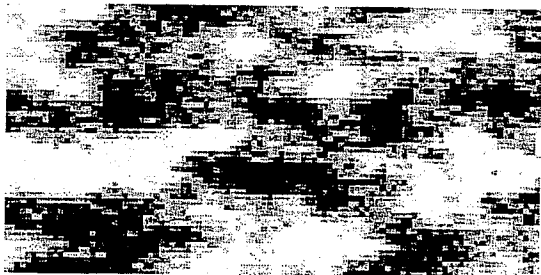
(a)  $\sigma_{\log k} = 0.2, \lambda = 0.05$



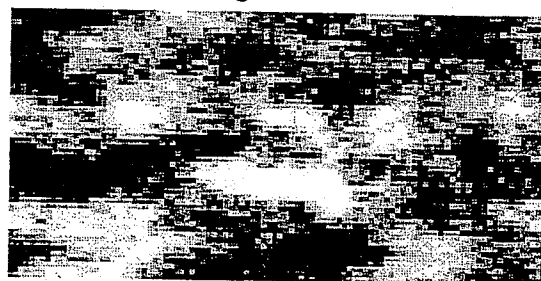
(d)  $\sigma_{\log k} = 0.2, \lambda = 0.05$



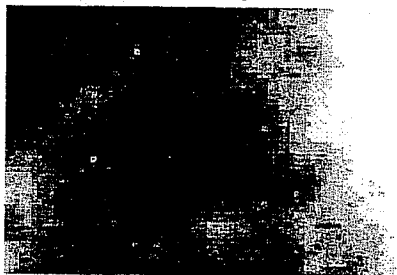
(b)  $\sigma_{\log k} = 0.8, \lambda = 0.2$



(e)  $\sigma_{\log k} = 0.8, \lambda = 0.2$



(c) FBM,  $\sigma_{\log k} = 0.8, H = 0.87$



(f) FBM,  $\sigma_{\log k} = 0.8, H = 0.87$



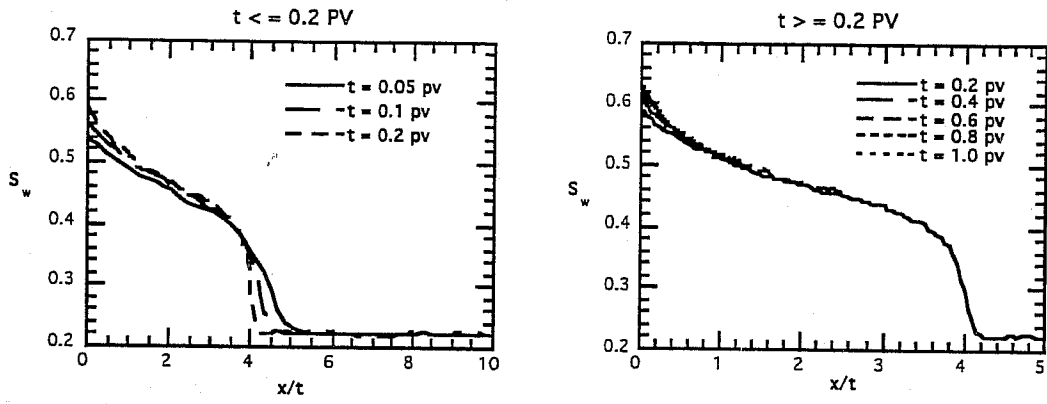
10D  
2mD

Permeability Distribution

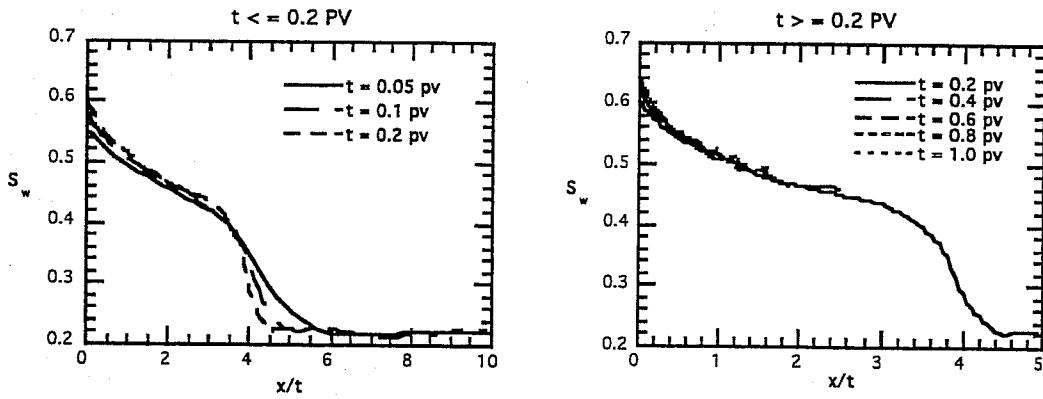
Swi Distribution

0.86  
0.2

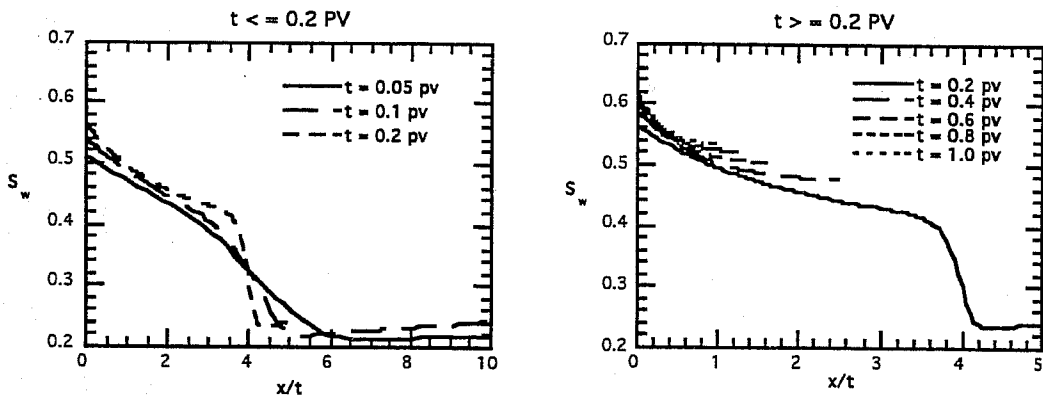
Figure 4 Permeability and Swi Distribution



(a)  $\sigma_{\log k}=0.2$  and  $\lambda=0.05$

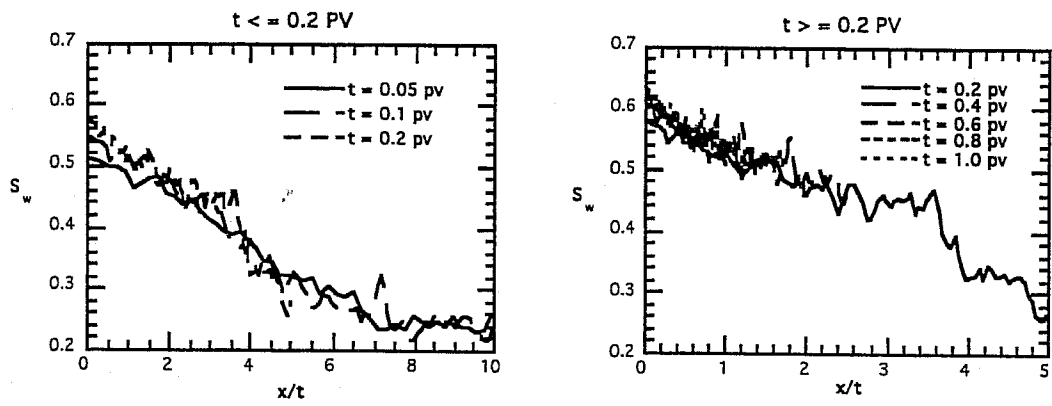


(b)  $\sigma_{\log k}=0.2$  and  $\lambda=0.20$

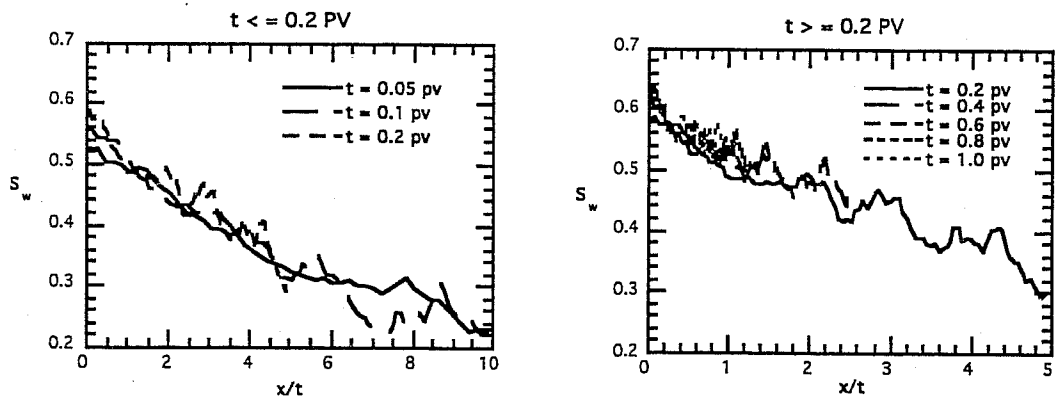


(c) FBM,  $\sigma_{\log k}=0.2$ ,  $H=0.87$

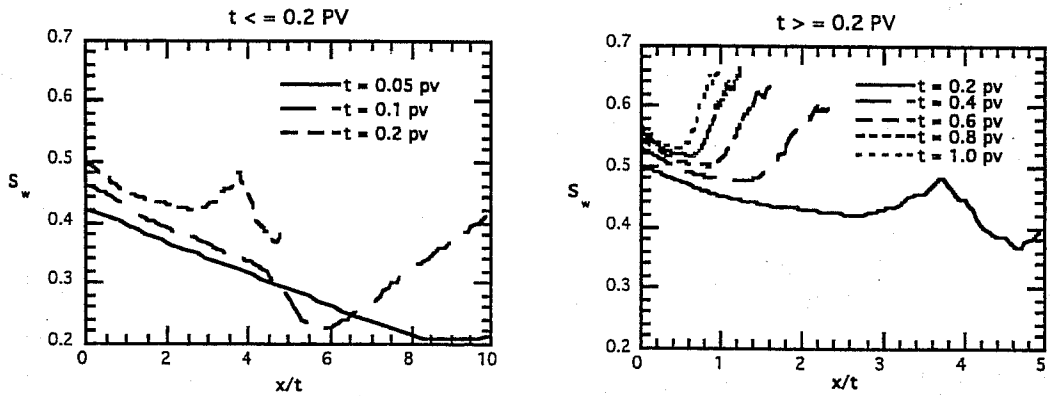
Figure 5 Saturation-velocity profiles at  $\sigma_{\log k}=0.2$  for mixed-wet system.



(a)  $\sigma_{\log k}=0.8$  and  $\lambda=0.05$



(b)  $\sigma_{\log k}=0.8$  and  $\lambda=0.20$



(c) FBM,  $\sigma_{\log k}=0.8$ ,  $H=0.87$

Figure 6 Saturation-velocity profiles at  $\sigma_{\log k}=0.8$  for mixed-wet system.

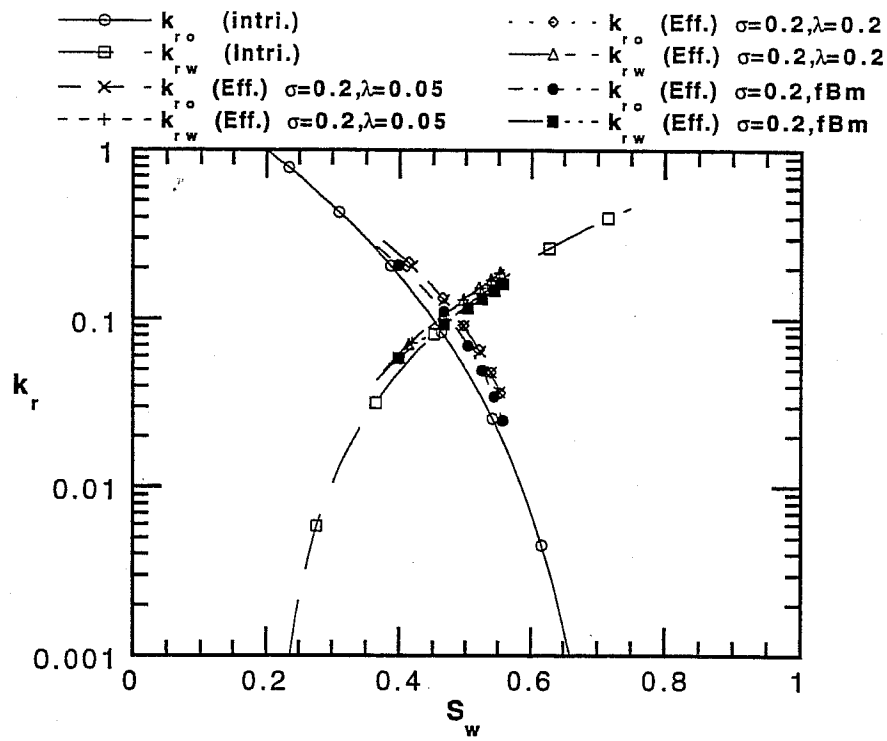


Figure 7 Relative permeability at  $\sigma_{\log k}=0.2$  for mixed-wet system.

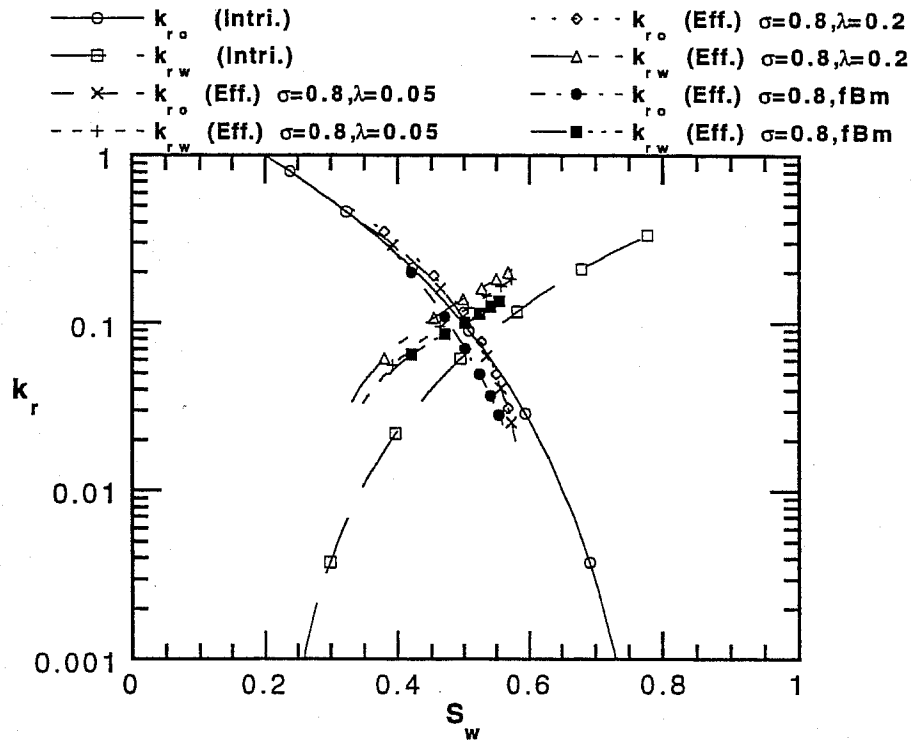
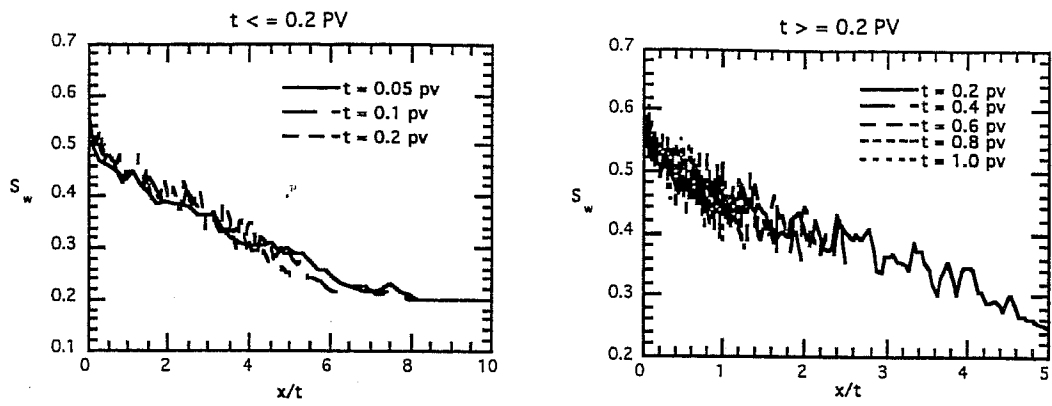
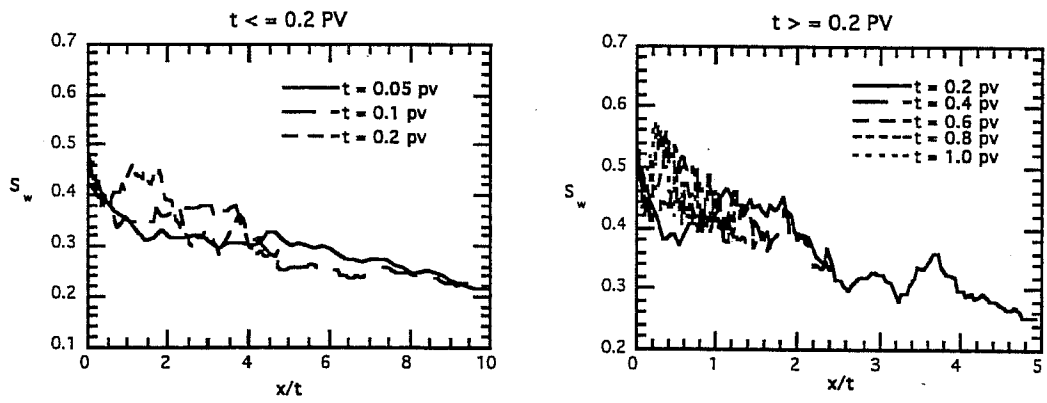


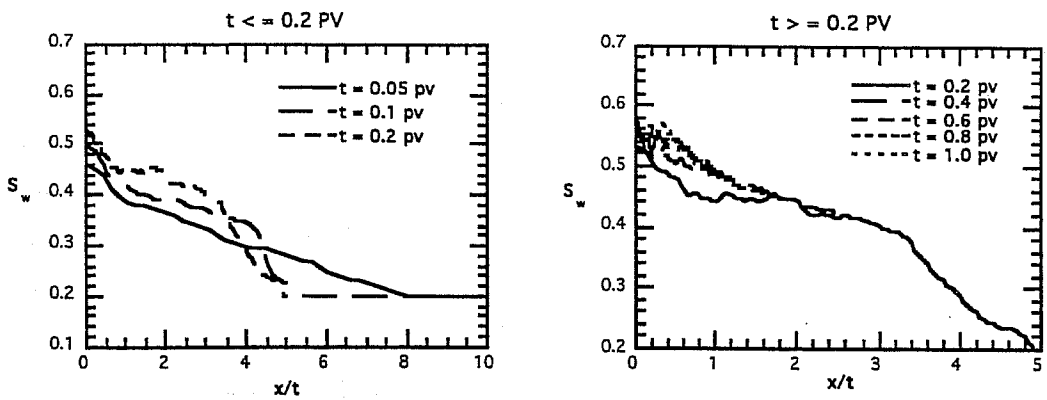
Figure 8 Relative permeability at  $\sigma_{\log k}=0.8$  for mixed-wet system.



(a)  $\sigma_{\log k}=0.8$  and  $\lambda=0.05$



(b)  $\sigma_{\log k}=0.8$  and  $\lambda=0.20$



(c) FBM,  $\sigma_{\log k}=0.8$ ,  $H=0.87$

Figure 9 Saturation-velocity profiles at  $\sigma_{\log k}=0.8$  for oil-wet system.

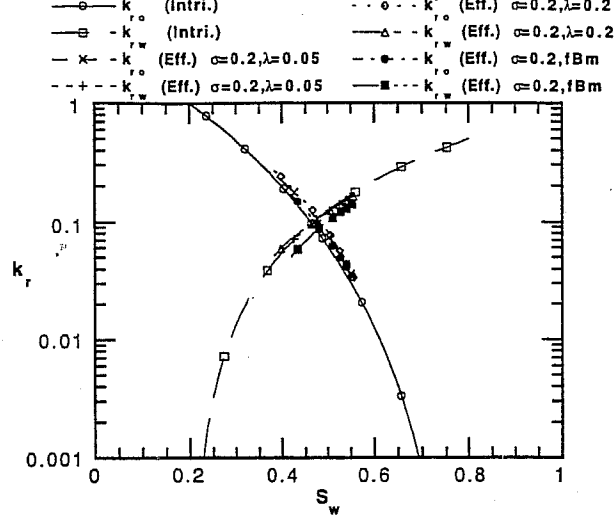


Figure 10 Relative permeability at  $\sigma_{\log k} = 0.2$  for oil-wet system.

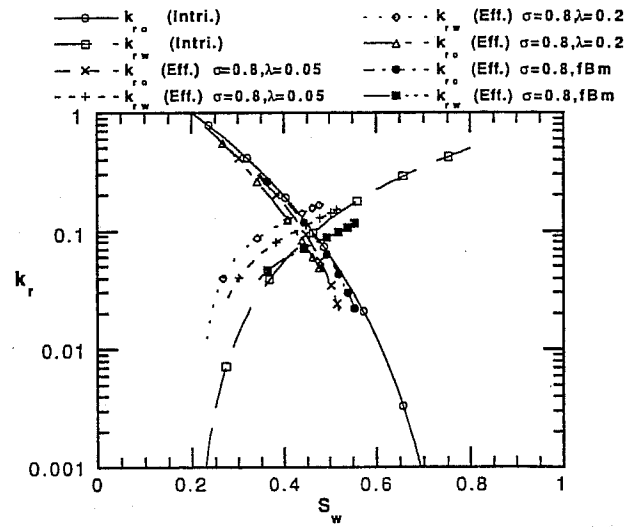


Figure 11 Relative permeability at  $\sigma_{\log k} = 0.8$  for oil-wet system.

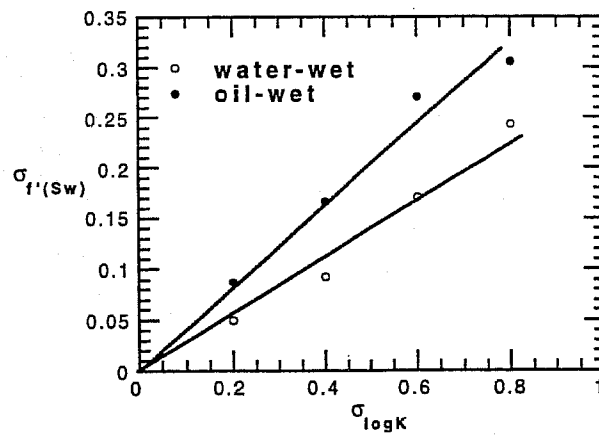
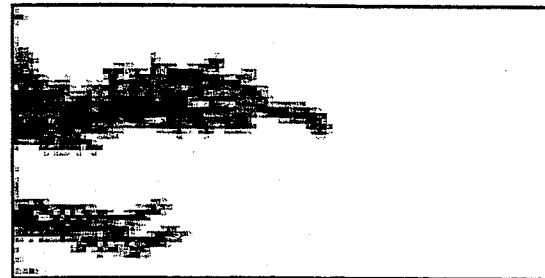
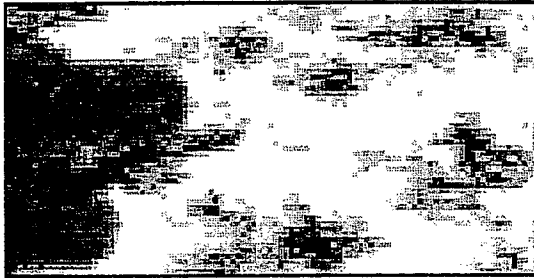


Figure 12 The effect of standard deviation of permeability on the fluctuation of saturation-velocity for  $\lambda = 0.05$ .

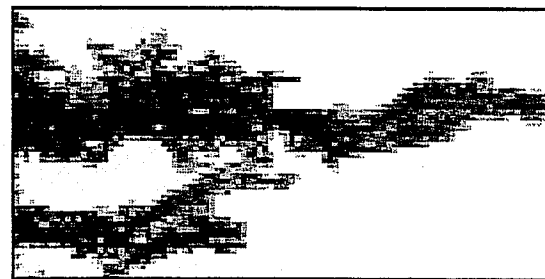
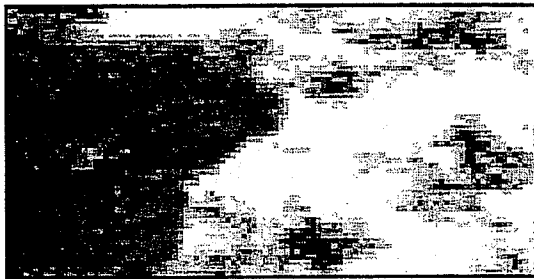
Water-wet

Oil-wet

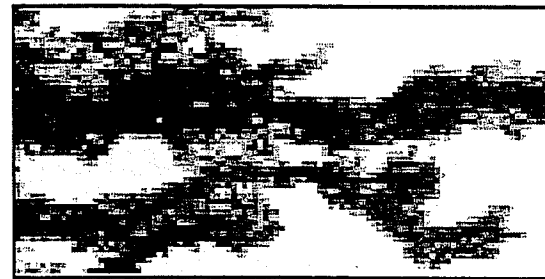
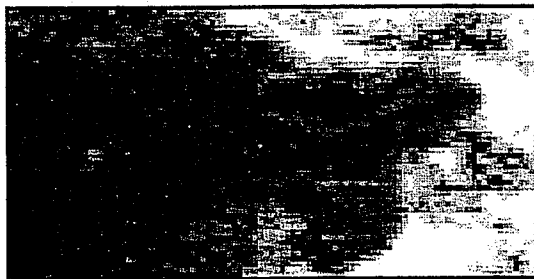
$t = 0.05$  PV



$t = 0.1$  PV



$t = 0.2$  PV



$t = 1.0$  PV



Figure 13 In-situ water saturations for water-wet and oil-wet media  
at  $\sigma_{\log k}=0.8$ ,  $\lambda=0.2$ .



# Adaptive Upscaling with the Dual Mesh Method

*Dominique Guérillot<sup>1</sup>*

*Sophie Verdière<sup>1,2</sup>*

**1: Institut Français du Pétrole**

**2: Université de Pau et des Pays de l'Adour**

## ABSTRACT

The objective of this paper is to demonstrate that upscaling should be calculated during the flow simulation instead of trying to enhance the a priori upscaling methods. Hence, counter-examples are given to motivate our approach, the so-called Dual Mesh Method. The main steps of this numerical algorithm are recalled. Applications illustrate the necessity to consider different average relative permeability values depending on the direction in space. Moreover, these values could be different for the same average saturation. This proves that an a priori upscaling cannot be the answer even in homogeneous cases because of the "dynamical heterogeneity" created by the saturation profile. Other examples show the efficiency of the Dual Mesh Method applied to heterogeneous medium and to an actual field case in South America.

## I Motivations

Darcy's equations give a simple relation between the speed  $\vec{Q}_\phi$  of a phase  $\phi$  and the pressure gradient  $P_\phi$  in this phase. When only one phase is present, this relation is fully determined by the introduction of the absolute permeability tensor  $\vec{k}$ , the viscosity  $\mu$ , the density  $\rho$  of the fluid and the height  $z$ , i.e.:

$$\vec{Q} = -\frac{\vec{k}}{\mu} \vec{\text{grad}}(P - \rho g z).$$

When several phases are considered, the relative permeability curves  $k_{r\phi}$  allow to consider the same type of equation for each phase:

$$\vec{Q}_\varphi = -\frac{k}{\mu} k_{r\varphi} \vec{\text{grad}}(P_\varphi - \rho_\varphi g z).$$

These relative permeability curves are very convenient because they incorporate different phenomena in one single curve depending only on one parameter: the saturation  $S_\varphi$  of the phase  $\varphi$ . The capillary pressure curves are considered also to depend only on the saturation.

The following remarks showt why we propose to calculate the upscaled relative permeability during the flow simulation.

At the laboratory scale, the above equations allow to explain the observations and relative permeability curves can be obtained by different methods ("Pen State", "Hassler", etc... ; see for instance [Marle, 1972]). Relative permeabilities, and capillary pressures, depend obviously on the phase distribution at the pore level. There are several distributions of phases for the same saturation. Hence, several relative permeabilities may correspond to these different cases.

For three-phase sytems, (see for instance [Kalaydjian, 1993]) current research is focused on the impact of the phase distribution on the relative permeability and capillary values.

In reservoir simulations, the flow behaviour is also modeled by this concept of relative permeability equations and the reservoir is described by a set of cells.

usually, the main question is: *"what curve should be used at the scale of one cell to reproduce properly the behaviour of the flow in the reservoir ?"*.

One approach is to find out situations where assumptions can be made to consider that an average saturation is sufficient. This is the case for instance when in the reservoir the saturation profile along the vertical is nearly always the same, i.e. when there is an equilibrium between gravity and capillary forces. "Vertical Equilibrium" pseudos can be calculated by the method of [Coats et al, 1971].

However in many reservoirs, the saturation distribution depends on the production history, i.e. on the location of the wells and their perforations, their flow rates and pressures (boundary conditions). Hence the relative permeabilities and capillary pressures will depend on this history. This is why "dynamic pseudo relative permeabilities" are currently considered in practice (see the critical review: [Barker & Thibeau, 1996]). The principle is to calculate these curves by running

flow simulations with a detailed description of the porous media and with the relative permeability and the capillary pressure curves obtained at the laboratory scale. The principle is very similar to the one used at the laboratory scale. Instead of measurements, a fluid flow simulator is used to "calculate" the flow rate of the different phases coming out from one or a group of cells submitted to different boundary conditions. Our point of view is that approach may be very heavy in cases when this distribution may vary widely depending on the location in space (distance from the wells for instance) and the boundary conditions.

*So instead on trying to uncouple the saturation distribution calculation and the averaging process, we propose to upscale during the fluid flow simulation.*

## II Difficulties of the "a priori" methods

The following example illustrate some major difficulties of the "a priori" methods or "dynamic relative permeabilities" with two counter-examples for a two phase system ( $\phi = w, o$ ).

The total mobility  $m(s)$  is defined as:

$$m(s) = \frac{k_{rw}}{\mu_w} + \frac{k_{ro}}{\mu_o}$$

### II.1 First Counter-example

With an IMPES scheme (see for instance [Aziz & Setari, 1979]), the average value of the product of absolute permeability by the total mobility ( $\overline{\overline{k m(s)}}$ ) is needed for the pressure equation. With the "a priori" approaches, the averages  $\overline{\overline{k}}$  and  $\overline{\overline{m(s)}}$  are calculated separately, where  $\overline{s}$  is for instance the average water saturation.

One difficulty is that the following inequality may occur:

$$\overline{\overline{k m(s)}} \neq \overline{\overline{k}} \overline{\overline{m(s)}}$$

For instance, in a 1D example (cf. Figure 1).

$$\begin{cases} k_{rw}(s) = s & (s = s_w) \\ k_{ro}(s) = 1 - s \\ S_{wi} = S_{or} = 0 \end{cases}$$

The aim is to determine  $\overline{k m(s)}$  and  $\overline{k m(\bar{s})}$  over the homogeneized cell containing the cells 1 and 2. Cell 1 (resp. cell 2) is supposed to have a saturation equal to  $1 - S_{or}$  (resp.  $S_{wi}$ ) and an absolute permeability  $k_1$  (resp.  $k_2$ ).

$$\overline{k m(s)} = \frac{2k_1 m(s_1)k_2 m(s_2)}{k_1 m(s_1) + k_2 m(s_2)} = \frac{2k_1 k_2}{\mu_o k_1 + \mu_w k_2}$$

$$\overline{k m(\bar{s})} = \frac{2k_1 k_2}{k_1 + k_2} * m\left(\frac{S_{wi} + 1 - S_{or}}{2}\right) = \frac{k_1 k_2}{k_1 + k_2} * \left(\frac{1}{\mu_w} + \frac{1}{\mu_o}\right)$$

These 2 values are often different. So, even if an homogeneous case is considered ( $k = k_1 = k_2$ ), we have, for  $\mu_o = 10 \mu_w$ :

$$\overline{k m(s)} = \frac{2k}{11\mu_w} \neq \frac{11k}{20\mu_w} = \overline{k m(\bar{s})}, \text{ it means } \frac{\overline{k m(s)}}{\overline{k m(\bar{s})}} \cong \frac{1}{3}$$

The difference increases with the contrast of permeability between the two cells.

## II.2 Second Counter-example in 2D (xy)

Let us now consider a 2 D example (cf. Figure 9). An homogeneous absolute permeability is also supposed. Even if the average saturation of the cells (1,5) and (5,1) are the same, these one should not have the same directional total mobilities to the extent that the directions of the flow of each cell are completely different and influence the calculation of the pseudo function.

## II.3 Solutions

Considering more parameters to characterise the flow behaviour. For instance, one way of thinking is to consider the distribution of the saturation in the cell.

One can consider other equations to modelize the flow, with the MHD method for instance [Lenormand, 1996].

It is also possible to keep a level of detail in the saturation such that the permeability and the capillary curves are valid and to transfer the problem of upscaling on the numerical scheme side.

It is the latest option that has been considered. In fact, even if the other options may give good answers, they will be very difficult to implement on a practical way.

### **III Dual Mesh Method**

#### **III.1 General Remarks**

The Dual Mesh Method, early proposed by the authors (cf. [Guérillot and Verdière, 1995]) allows to adapt in time and space the discretization for each unknown. So, for a typical two phase problem, the saturation equation will be solved over the geological mesh, and the pressure equation over a lower resolution grid, like in a classical simulator (which corresponds to the upscaled flow model).

This method enables to make "adaptive upscaling". Indeed, it is possible to upscale the parameters necessary to the pressure equation by taking into account the evolution of the saturation during time. So, there is no more problem due to:

- boundary conditions over each lower resolution grid,
- the opening and closing of a well, during the simulation, which would require new calculation of pseudos functions.

#### **III.2 Description of the Algorithm**

Let us briefly summarize the principle of the Dual Mesh Method. For that, 2 different grids are introduced: a Low Resolution Grid (called LR Grid) and a High Resolution Grid (called HR Grid). A time step is associated to each grid [Verdière et al, 1996]. We consider the update of the unknowns (pressure and saturation) for a LR time step:

**Step 1** - Calculation of the LR time step,

**Step 2** - Calculation of the parameters necessary to solve the pressure equation by using an adaptive homogeneization from the HR to the LR grid,

**Step 3** - Calculation of the pressure over the LR Grid, with the LR time step,

**Step 4** - Reconstruction of the flow-rate over the HR grid at each HR time step by using the pressure over the LR grid,

**Step 5** - Resolution of the saturation equation over the HR grid for each HR time step.

## IV Numerical Results

### IV.1 Description of the Test Cases

A quarter of five spot is considered (cf. Figure 4). The HR and a LR grids are different according to the simulations. For each test-case, the HR grid is considered as the reference.

In order to avoid differences between numerical results due to Productivity Indices (PI) problems, boundary conditions have been considered rather than well conditions (cf. Figure 3).

Three different types of permeability maps are generated:

- the first case is an homogeneous case with  $K=100$  mD (over a  $90 \times 90$  grid);
- the second case (called **heter. case 1**) is an heterogeneous porous medium with a lognormal distribution (see Figure 4). With these choices, an algebraic estimator [Guérillot, 1988] is used to estimate averaged permeability maps over lower resolution grids ( $10 \times 10$ ,  $30 \times 30$  and  $90 \times 90$ );
- the third case (called **heter. case 2**) comes from a field case study in South America. The reservoir (Albian/Cenomanian) deposited in an overall transgressive context, produces from turbidite sandstones and is composed of massive sandstones, classical Bouma turbidites, marls and shales. The lithofacies map (cf. Figure 5) was generated in a sequential stratigraphic context. It corresponds to an horizontal cross section. The lithofacies 1, 2, 3, 4 are respectively very porous sandstone (1), sandstone (2), thin bedded turbidite sandstone (3) and carbonate rock (4). For each lithofacies, the permeability are measured on plugs ( $k_1=2779$  mD,  $k_2=177$  mD,  $k_3=14$  mD,  $k_4=1$  mD).

The relative permeabilities used are of the Corey type [Brooks & Corey, 1966] as follows:

$$k_{rw}(S) = k_{wm} S^{*n_w} \text{ and } k_{ro}(S) = k_{om} (1 - S^*)^{n_o}$$

$$\text{with } S^* = \frac{S - S_{wi}}{1 - S_{wi} - S_{or}}$$

The fractional flow is noted  $f_w$ .

The tests are built with three mobility cases:

- a linear case (cf. Figure 6);
- an unfavourable case; the mobility ratio is equal to 2 (cf. Figure 7);
- a favourable case; the mobility ratio is equal to 0.16 (cf. Figure 8).

## **IV.2 Importance of Saturation Profile for the Upscaling**

An homogeneous case with the favourable mobility ratio is simulated ( $M=0.16$ , see Figure 8). The LR grid is  $10 \times 10$  and the HR grid is  $90 \times 90$  (cf. Figure 9)

For each time step, and for each lower cell, the algebraic method of upscaling allows to calculate the product of the absolute permeability and the total mobility, for each direction of the flow, called  $k_{mx}$  and  $k_{my}$ . This product corresponds to the coefficients of the pressure equation (see II).

By considering in particular the cells (1,5), (2,2) and (9,9) (Figure 9),  $k_{mx}$  and  $k_{my}$  are plotted, function of the average saturation calculated with the average saturation obtained over the HR Grid. The "fine km" of the Figure 9 corresponds to the analytical function of  $k_m$  with the Corey's law, supposed to be over the HR Grid.

The different saturation profiles for each cell give different averaged total mobility.

The cells (2,2) and (9,9) give similarly the same pseudo function to the extent that boundary conditions are the same. Besides,  $k_{mx}=k_{my}$  because of the symmetry of the problem.

On the other hand, we find different curves for  $k_{mx}$  and  $k_{my}$  in the cell (1,5). If we consider a 1D problem along the west boundary,  $k_{my}$  should be equal to a harmonic mean of  $k_m$  over the HR Grid. This result is approximately found for  $k_{my}$  of the cell 1,5, which is close to a 1D flow.

So, we can say that the Dual Mesh Method allows really to make adaptive upscaling. The real boundary conditions, and also the real saturation profile over the geological model are used to dynamically upscale the needed coefficients for the pressure equation

## **IV.3 Quality of the Results and Efficiency of the Dual Mesh Method**

The heterogeneous case 1 (Figure 4) with the unfavourable mobility ratio ( $M=2$ , see Figure 7) is simulated. Three different grids are considered:  $10 \times 10$ ,  $30 \times 30$  and  $90 \times 90$ .

The comparison of watercut (Figure 15) for each simulation reveals that the result obtained with a fully HR grid simulation are similar to the one obtained with the Dual Mesh Method with a resolution of the pressure equation over the  $10 \times 10$  grid and a resolution of the saturation equation over the finer grid ( $30 \times 30$  or  $90 \times 90$  according to the case).

The Table 1 shows the Cpu-Time of the different simulations. Computing cost using DMMs is of the same order as the LR method, even if it is more important (about three times), while the HR grid method requires a very long simulation.

#### **IV.4 Field Case Study**

The heterogeneous case 2 (Figure 5) in constant total mobility ( $M=1$ , see Figure 6) is simulated. Two different grids are considered:  $16 \times 16$  and  $256 \times 256$ .

The different saturation maps (Figures 11 to 14) show qualitatively the capability of the Dual Mesh Method to integrate the fine ( $256 \times 256$ ) grid petrophysical information, even though the pressure equation is solved over a LR grid ( $16 \times 16$ ). More details of this field will be described elsewhere.

#### **V Conclusion**

This paper demonstrates it is possible to upscale the relative permeability curves during the flow simulation for a two phase flow problem.

The efficiency of the Dual Mesh Method is proven for an oil field case produced by water injection. It is straightforward to add gravity and capillary forces for this two phase problem. Current research focus on the ability to consider phase exchanges, to apply this approach to basin modeling and to integrate the capacity of parallel computers.

#### ***Acknowledgements***

The authors thank the "Institut Français du Pétrole" for permission to publish this work. They also thank Eric Delamaide, Patrick Lemonnier for their useful comments.



## *Références*

- Aziz, K., Setari, A.: "Petroleum Reservoir Simulation", Applied Science Publisher LTD, 1979
- Barker, J., Thibeau, S., "A Critical Review of the Use of Pseudo Relative Permeabilities for Upscaling", European 3-D Reservoir Modelling Conference, Stavanger, April 16-17 1996
- Brooks, R.H., Corey, A.T., "Properties of Porous Media Affecting Fluid Flow", Journal of the Irrigation and Drainage Division, Proceedings of ASCE (1966), Vol. 92, NO IR2
- Coat, K.H., Dempsey, J.R., Henderson, J.H.: "the Use of Vertical Equilibrium in Two-Dimensional Simulation of Three -Dimensional Reservoir Performance", SPEJ, March 1971, pp. 63-71
- Guérillot, D., Rudkiewicz, J.L., Ravenne, C., Renard G., : "An Integrated Model for Computer Aided Reservoir Description from Outcrop Study to Fluid Flow Simulation", 5th European Symposium on Improved Oil Recovery, Budapest, April 25-27 1989, Rev IFP, Vol 45-1, 71-77
- Guérillot, D., Verdière, S.: "Different Pressure Grids for Reservoir Simulation in Heterogeneous Porous Media", Proceedings of 13th SPE Symposium on Reservoir Simulation, SPE 29148, San Antonio, Fév. 1995
- Kalaydjian, F., Moulu, J.-C., Vizika, O., Munkerund, P.K., "Three-Phase Flow in Water-Wet Porous Media: Determination of Gas/Oil Relative Permeabilities Under Various Spreading Conditions", SPE 26671, presented at the 68th Annual Technical Conference and Exhibition of the SPE, Houston, Texas, 3-6 Oct. 1993, to appear in the Journal Science and Engineering 554 (1996)
- Marle, C.-M., "Les écoulements polyphasiques en milieux poreux", Editions Technip, 1972
- Ramé, M., Killough, J., "A New Approach to the Simulation of Flows in Highly Heterogeneous Porous Media", 11th SPE Symposium on Reservoir Simulation, Anaheim, February, 1991
- Verdière, S., Guérillot, D., Thomas, J.M. : "Dual Mesh Methods in Heterogeneous Porous Media", "Proceedings of the 5th European Conference on the Mathematics of Oil Recovery", Leoben, Sept 1996

## Figure Captions

**Figure 1: 1D Counter-Example**

**Figure 2: Dual Mesh Representation**

**Figure 3: Geometrical Characteristics of the Test Case**

**Figure 4: Permeability Map - Heter. Case 1**

**Figure 5: Lithofacies Map - Heter. Case 2**

**Figures 6 7 and 8: Fluid Properties for the Different Mobility Ratios**

**Figure 9: Counter-Example 2**

**Figure 10: Comparison of Averaged Total Mobilities**

**Figure 11: Saturation Map - Heter. Case 2 -  $M=1$  - Time = 200 days**

**Figure 12: Saturation Map - Heter. Case 2 -  $M=1$  - Time = 400 days**

**Figure 13: Saturation Map - Heter. Case 2 -  $M=1$  - Time = 600 days**

**Figure 14: Saturation Map - Heter. Case 2 -  $M=1$  - Time = 800 days**

**Figure 15: Comparison of Watercut - Heter. Case 1 -  $M=2$**

**Table 1: Comparison of the Cpu-Time (s) Heter. Case -  $M=2$**

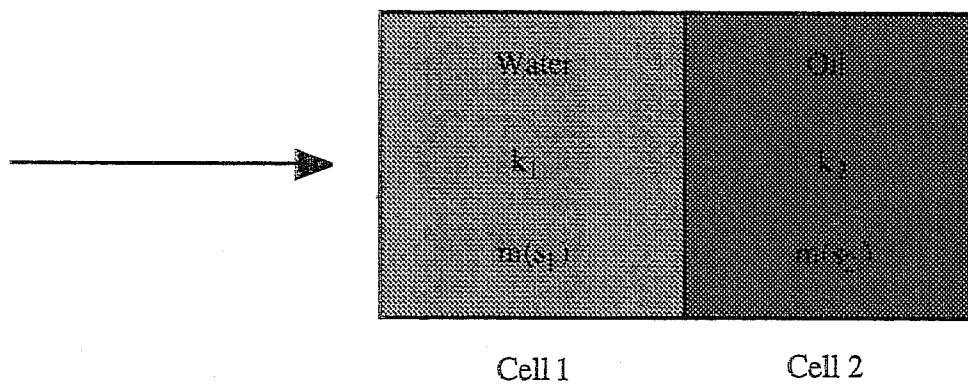


Figure 1: 1D Counter-Example

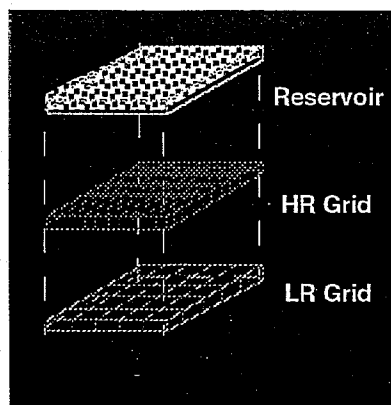


Figure 2: Dual Mesh Representation

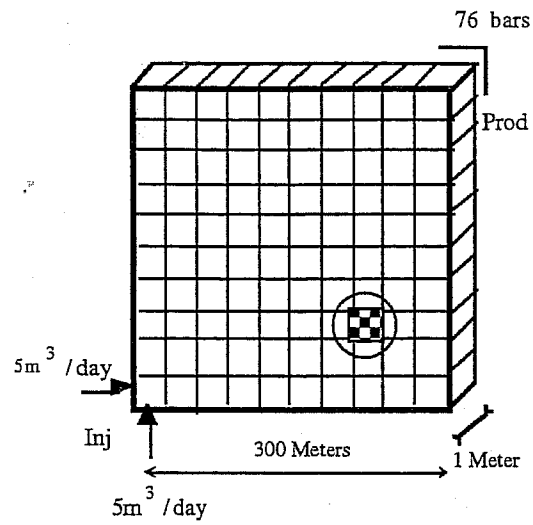


Figure 3: Geometrical Characteristics of the Test-Cases

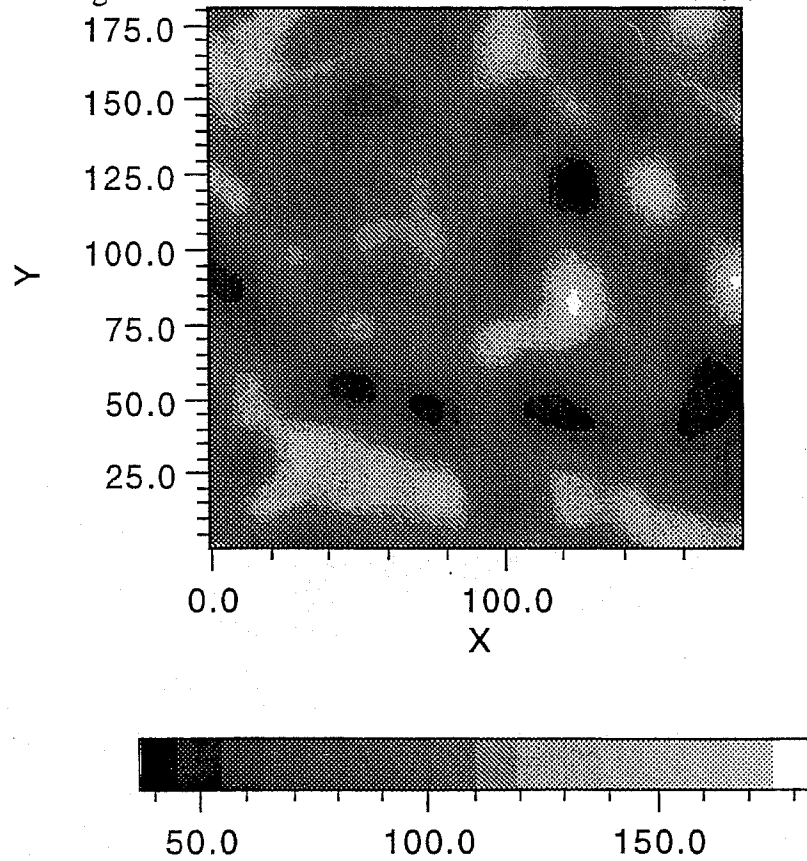


Figure 4: Permeability Map - Heter. Case 1

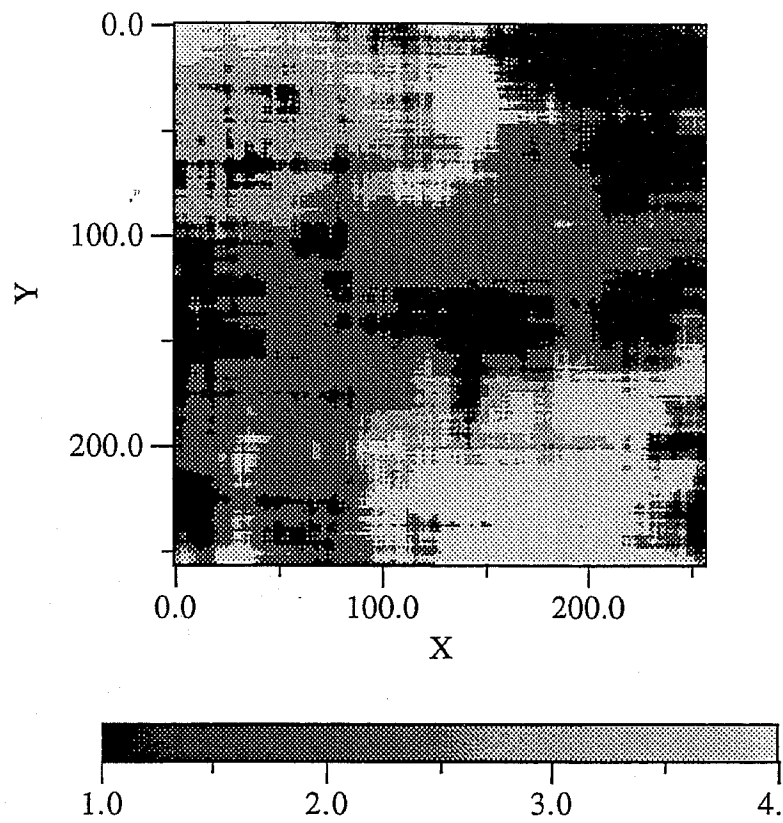
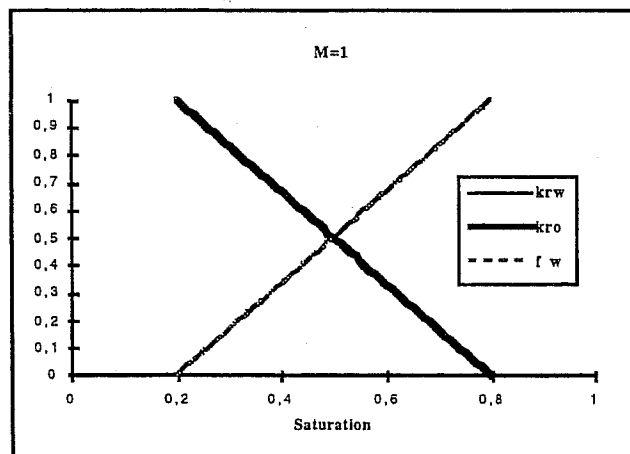
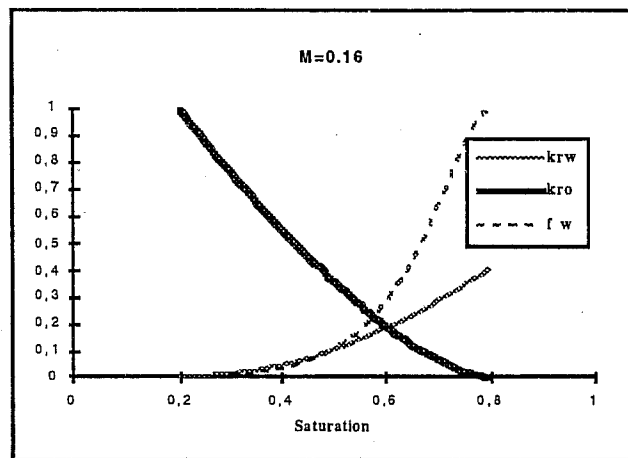
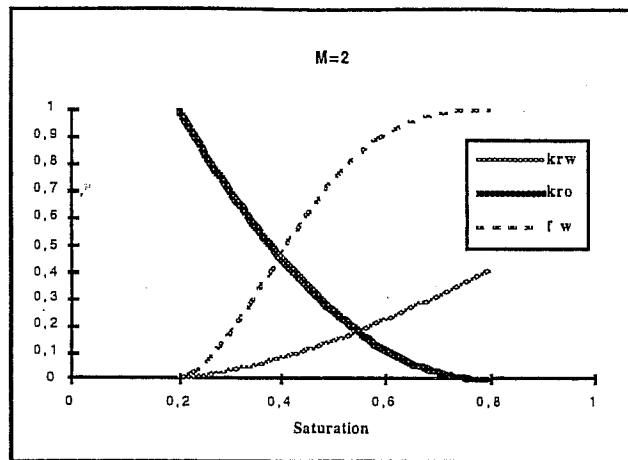


Figure 5: Lithofacies Map - Heter. Case 2





Figures 6, 7 and 8: Fluid Properties for the Different Mobility Ratios

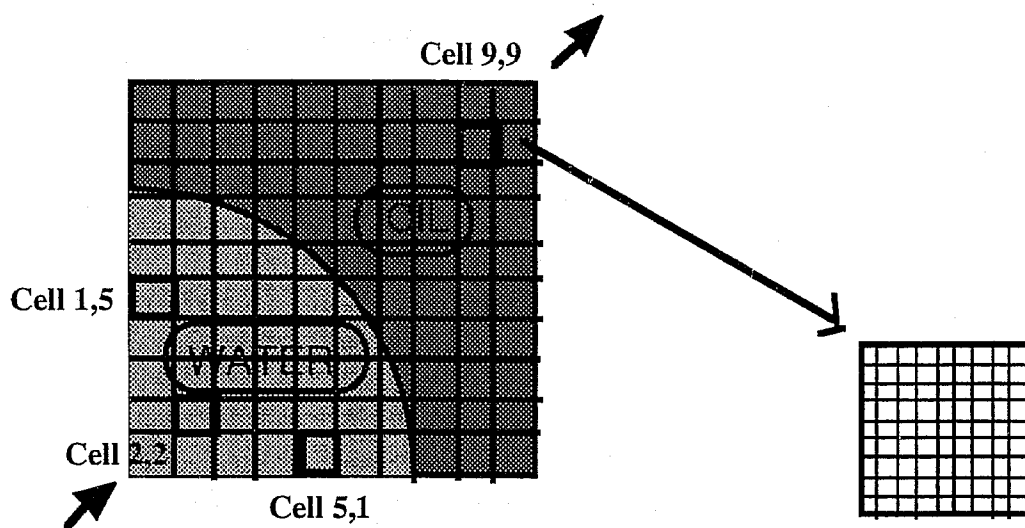


Figure 9: 2D Counter-Example

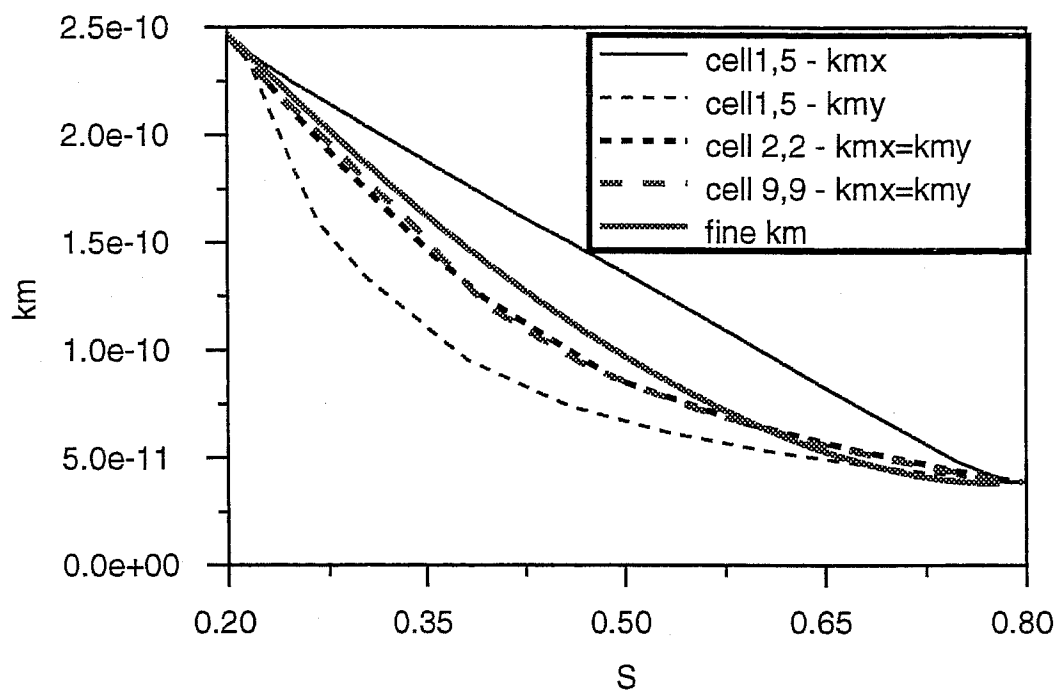


Figure 10: Comparison of Averaged Total Mobilities

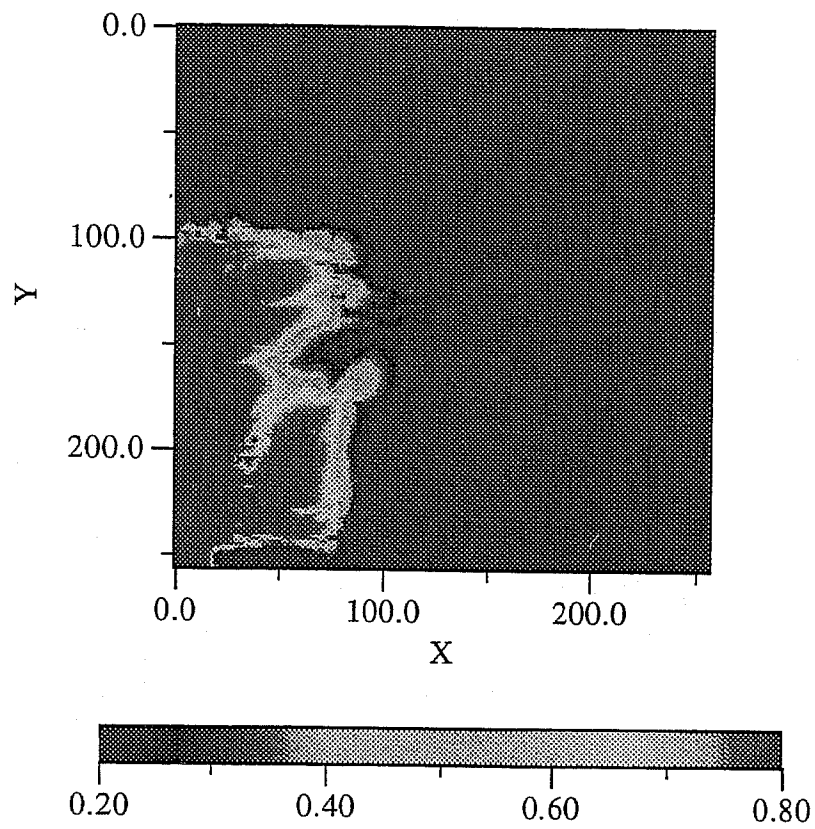


Figure 11: Saturation Map - Heter. Case 2 - M=1 - Time = 200 days



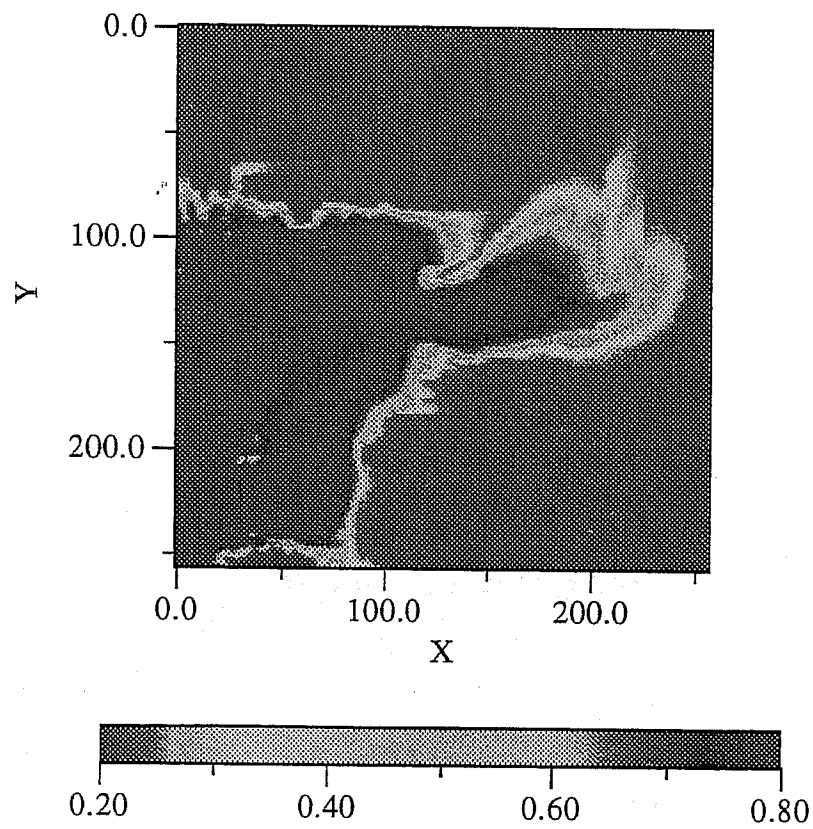


Figure 12: Saturation Maps - Heter. Case 2 -  $M=1$  - Time = 400 Days

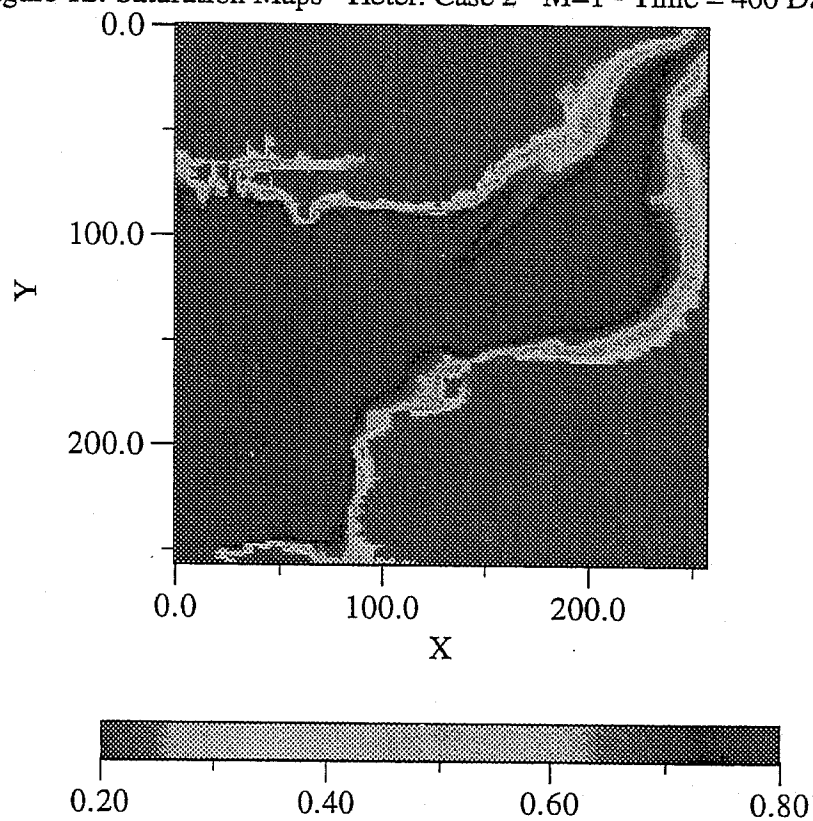


Figure 13: Saturation Map - Heter. Case 2 - M=1 - Time = 600 Days

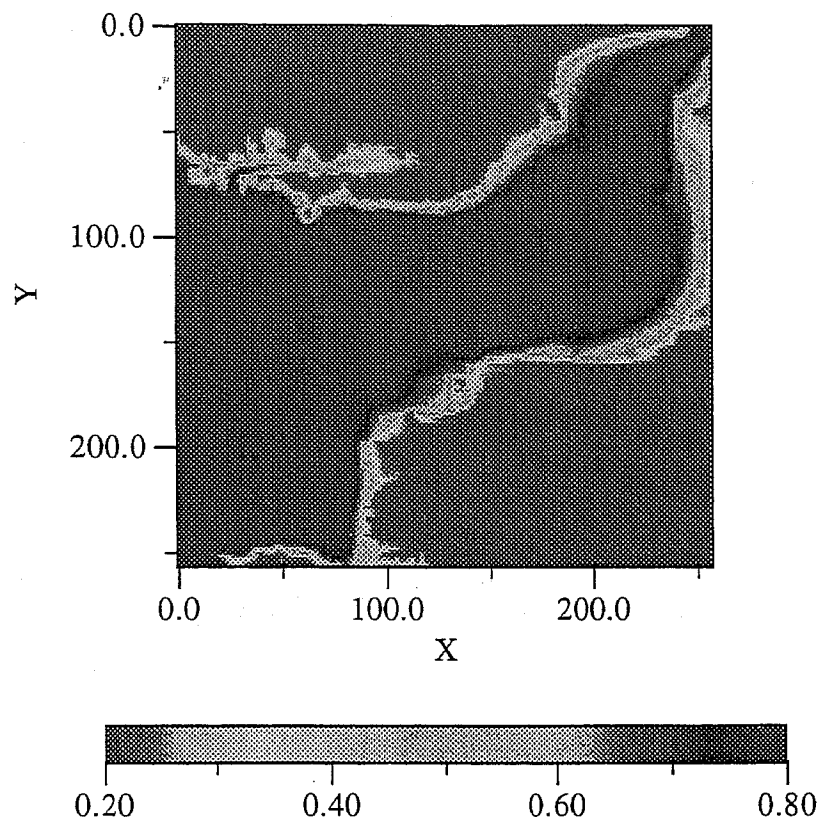


Figure 14: Saturation Map - Heter. Case 2 - M=1 - Time = 800 Days

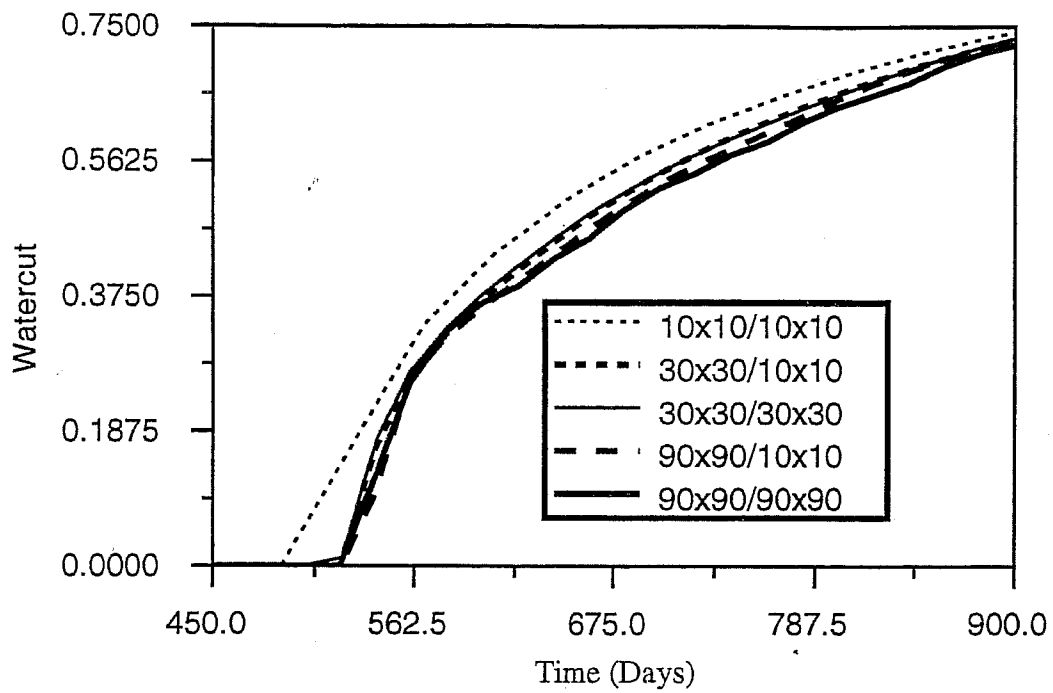


Figure 15: Comparison of Watercut - Heter. Case 1 - M=2

Pressure Grid → Saturation Grid ↓	10x10	30x30	90x90
10x10	11	XXXX	XXXX
30x30	52	293	XXXX
90x90	797	1350	18052

Table 1: Comparison of the Cpu-Time (s) - Heter. Case - M=2



# UPSCALING VERTICAL PERMEABILITY WITHIN A FLUVIO-AEOLIAN RESERVOIR

S.D. Thomas, P.W.M. Corbett and J.L. Jensen  
Department of Petroleum Engineering, Heriot-Watt University,  
Edinburgh, Scotland. EH14 4AS

## Abstract

Vertical permeability ( $k_v$ ) is a crucial factor in many reservoir engineering issues. To date there has been little work undertaken to understand the wide variation of  $k_v$  values measured at different scales in the reservoir. This paper presents the results of a study in which we have modelled the results of a downhole well tester using a statistical model and high resolution permeability data. The work has demonstrated and quantifies a wide variation in  $k_v$  at smaller, near wellbore scales and has implications for  $k_v$  modelling at larger scales.

## Introduction

Vertical permeability has been identified as a critical factor in the reservoir engineering concerns of the Morecambe Gas Fields (Wannell et al, 1992,1993). These concerns include maximising low saturation gas recovery from beneath gas-water contacts, producing from high angle deviated wells in thin high permeability aeolian sands and maximising small satellite field production with strong aquifer support.

The low saturation gas beneath the gas-water contact of the North Morecambe Field constitutes reserves in excess of 300bcf in-place. Simulation has indicated that a vertical permeability ( $k_v$ ) of 0.02mD would allow 50% of this gas to migrate upwards into the main gas cap for recovery (McCulloch, 1994). However, a  $k_v$  of 0.002mD would allow just 6% to migrate to the gas cap. The small satellite gas fields identified surrounding the

Morecambe Fields amount to 500bcf of total gas-in-place with individual fields of 15-150bcf. The presence of a strong aquifer beneath these reservoirs means that both high and low extremes in  $k_v$  will have detrimental effects on gas recovery.  $k_v$  must be high enough to allow this gas to migrate upwards from unperforated intervals while also being low enough to prevent the encroaching water front from trapping gas behind it. Simulation indicates that gas recovery is maximised where the vertical - to - horizontal permeability ratio ( $k_v/k_h$ ) is approximately 0.004 (Wannell, 1993). Although  $k_v$  is commonly estimated from production data, there is clearly a good case for its early prediction in order to estimate the financial viability and facility size of a field before production data become available.

Field  $k_v/k_h$  measurements derived from 1" core plugs reveal  $k_v/k_h$  values of approximately 0.3-0.5 while larger scale estimates derived from wireline test tools indicate values of around 0.01. The range of vertical resolution for these tools is from 1-10ft (Wannell et al, 1993). Production and vertical pressure profiles indicate a further reduction in anisotropy for the reservoir scale to ~0.002. While these measurements provide accurate anisotropy estimates for their respective scales of investigation, they do not necessarily offer any indication as to the geological controls on its variability (Figure 1).

Numerical methods provide ways of quantifying the reservoir  $k_v/k_h$  variation at all scales by calculation of effective permeabilities ( $k_{eff}$ ) from reservoir models. However, these methods require a thorough understanding of the reservoir architecture and the permeability distribution within it. Although these numerical techniques are well documented, they are commonly misinterpreted for  $k_v$  and  $k_v/k_h$  estimation due to the quality of the data used in them (Bourdarot et al, 1989). The need for high resolution data is essential for numerical modelling of  $k_{eff}$  (Hurst, 1993; Corbett et al, 1992, 1993; Pickup et al 1995; Thomas et al, 1996; Jensen et al, 1997).

This paper describes how  $k_{\text{eff}}$  estimates derived from the simplest of these numerical methods are improved through use of sufficiently high resolution data. This model is used to determine upscaled permeability anisotropy for comparison with  $k_v/k_h$  estimates derived from the wireline tester. This paper also demonstrates how this model is able to quantify the permeability structure and assess the geological controls on the relationship between  $k_v$  and scale in Figure 1. Guidelines are also established for the larger  $k_v/k_h$  variation and suitable grid-block thicknesses for reservoir simulation.

### **Numerical Permeability Upscaling**

For a simple layered reservoir model, harmonic and arithmetic averages of the layer permeabilities (Figure 2) maybe used to estimate layer normal ( $k_v$ ) and layer parallel ( $k_h$ ) flow respectively (Muskat, 1937 p. 403-404). In this case, each layer within the model are assumed to be isotropic. Numerical estimates of  $k_v$  and  $k_h$  derived from this method are supported by the results of simulation.

Data input to these models are commonly derived from core plug measurements, made at 1ft intervals, or from well log predictions of permeability, at 0.5ft interval but with substantial volumes of investigation. It is an unfortunate result that these measurements frequently undersample the reservoir and this undersampling may lead to over-estimation of vertical permeability (Bourdarot, 1989, Corbett & Jensen, 1992) for three reasons. Firstly, because thin low permeability reservoir intervals, such as fluvial channel clay drapes or aeolian toe-sets, are commonly missed by the sampling program. These intervals, while not greatly affecting horizontal fluid flow, do affect vertical fluid flow. Since these intervals are not included in the model, vertical permeability will be over-estimated. Secondly, the population means are only approximated by the respective averages. These sample averages require sufficient sampling to ensure that they lie within acceptable limits of the true means. The method employed to ensure sample sufficiency is the so-called No

technique (Hurst & Rosvoll, 1991; Corbett & Jensen, 1992; Jensen et al., 1997). This method defines the number of samples required to estimate the arithmetic and harmonic means within  $\pm 20\%$  for 95% of cases and is defined as:

$$N_0 = (10C_v)^2$$

where  $C_v = \frac{\text{Standard Deviation}}{\text{Arithmetic Average}}$

Therefore the more heterogeneous the reservoir, the larger is the  $C_v$  and the more samples which are required. As demonstrated later, routine core plugging and well logging may undersample the reservoir heterogeneity (e.g., Ball et al., 1994). Both core plugs and well logs have the added problem that they are both upscaled measurements in themselves and represent average reservoir properties, for a particular set of boundary conditions, at the scale of their measurement (Corbett et al, 1996). Finally, in contrast to the arithmetic average, the harmonic average has a positive statistical bias associated with it. This results in overestimation of the harmonic mean, especially within heterogeneous or undersampled intervals. This bias has been quantified and may be corrected (Jensen et al, 1997):

$$\bar{X}_h^* = \bar{X}_h \left( 1 + \frac{C_v^2}{n} \right)$$

$\bar{X}_h^*$  = Bias Corrected Harmonic Average  
 $\bar{X}_h$  = Harmonic Average &  
 $n$  = Sample Number

The advent of fine-scale reservoir measurement techniques, notably the probe permeameter (Robertson & McPhee, 1990; Corbett & Jensen, 1992,1993; Goggin 1993; Halvorsen, 1990; Sutherland et al, 1993) and micro-scanner tools (Bourke, 1992, 1993; Ekstrom et al, 1987; Hackbarth et al, 1988; Lovell et al, 1991; Safinya et al, 1991; Troullier et al, 1989; Thomas et al, 1996) now enable the collection and prediction of extensive, small-scale permeability datasets which reduce the problems brought about by undersampling and



outlined above. The following case study uses probe permeability data to successfully upscale both  $k_v$  and  $k_h$  for cross-scaling with a wireline measurement of anisotropy over the same interval.

### **Case Study Location & Dataset**

The location of the study well, 110/8a-5, is shown in Figure 3. It lies within the East Irish Sea Basin off the west coast of the UK and south of the South Morecambe Gas Field. The reservoir interval in this area is the Sherwood Sandstone Group (Stuart & Cowan, 1991; Cowan, 1993) which comprises mixed fluvio-aeolian facies associations. These associations are dominated by seven major facies types: wet sabkha, dry sabkha sandsheet, ephemeral channel/ sheetflood, stacked fluvial channel, channel abandonment, playa/playa margin and aeolian dune/dune remnant.

Along with core plug permeability and probe permeability, both resistivity micro-scanner and wireline tester data were also available for this well. Four wireline tester measurements were obtained, all located within an interval of stacked fluvial channel deposits and set between major channel abandonments. Their aim was to establish the lateral abandonments as local no-flow barriers and to determine the permeability anisotropy in the fluvial channel sand between them. The responses of these measurements are all remarkably consistent with an average  $k_v/k_h$  of 0.02 (Figure 4). Only one test was taken within a cored interval, WT4. Its position alongside the core plug and probe permeability data is shown in Figure 5. The plug data were taken at 1ft intervals and the probe data at 0.05ft intervals. The permeability data statistics are summarised in Table 1.

## Modelling Wireline Tester Scale Estimates of $k_v/k_h$

The large lateral continuities of the fluvial channel facies types, a product of their environment of deposition, allows for the assumption of a simple layered model of the near wellbore region. Harmonic and arithmetic averages of the model's layer permeabilities is therefore appropriate for estimation of  $k_v$  and  $k_h$  respectively. Recent numerical simulation of the wireline tester behaviour (Atherton, 1993; Hollinshead, 1994) has demonstrated that its response is most sensitive to the formation permeability directly between the pressure probes of the tool. Numerical models of  $k_v/k_h$  were therefore constrained to thicknesses of approximately 7ft, the separation of the probes.

The permeability anisotropy estimates derived using both plug and probe data in these numerical models are shown in Figure 6 with the  $k_v/k_h$  estimate from WT4. Both numerical estimates have been corrected for harmonic average bias. Using probe data, the numerical model closely matches the tester  $k_v/k_h$  of 0.008. Using plug data, the model overestimates permeability anisotropy by a factor of 50. This overestimation is the result of insufficient sampling by the plug dataset (Table 1) and the failure of plugs to capture the low permeability clay drape at 4242ft (Figure 5).

The success of this simple numerical model allows us to assess the near wellbore  $k_v/k_h$  variability throughout the fluvial section (Figure 7). For this calculation, the 7ft window was retained and  $k_v/k_h$  was modelled over the interval of fluvial deposits between the channel abandonments at 4235 and 4255ft (Figure 5). Figure 7 demonstrates the wide range of  $k_v/k_h$  estimates for this scale of measurement even over this relatively thin reservoir interval. The estimates of  $k_v/k_h$  have a range of nearly three orders magnitude with probe data model variability clustering into two groups; one of  $k_v/k_h \approx 0.3$  and the other of  $k_v/k_h \approx 0.01$ . The small group with relatively high  $k_v/k_h$  represents those

estimates made within the channel sand units with relatively little internal heterogeneity (e.g., 4250ft), while the much larger and more variable cluster of  $k_v/k_h$  estimates represents those intervals affected by low permeability clays and silts (e.g., 4242ft). The presence of clustering is a reflection of geological structure in the interval which controls the observed variation of  $k_v/k_h$  with scale. This also suggests that the 7ft probe spacing of the wireline test is not estimating  $k_v/k_h$  at a representative scale for this fluvial channel facies type. As we will shortly explain, the 7ft probe spacing may not give a reliable indication of the permeability anisotropy for the sand located between the major channel abandonments. This has important implications for upscaling  $k_v/k_h$  away from the near wellbore region.

### **Structural Analysis and Representative Scales**

The understanding and capture of reservoir permeability structure in our models is crucial since it often plays a fundamental role in the control of fluid flow during production e.g., fining upwards sequences, distributions of shales, or the presence of high permeability streaks. Structural analysis of log and permeability data has traditionally been undertaken using the semivariogram (Hohn, 1988). This method analyses the average difference between data separated by increasing distances or lag (Figure 8). Simple theoretical models which maybe fitted to the semivariogram include the linear, spherical, exponential, gaussian and 'holed'. Each of these types models the phenomenon of decreasing data correlation with increasing separation. The 'holed' model (Figure 8) attempts to capture the increasing degree of correlation at certain lag distances within structured data. However, the semivariogram has a number of limitations. Firstly, semivariograms are sensitive to the distribution of the data and problems occur with highly skewed data, a problem which may be overcome by data transformation prior to the calculation of the semivariogram. Secondly, the experimental semivariogram commonly requires 'nested' or multiple models to achieve a fit, a process prone to ambiguous results. Finally, the method gives no

quantification of the permeability within the structure other than its similarity/variability at certain separations.

Another method for analysing data structure is the Representative Elementary Area/Volume (REA/V) method (Bear, 1972; Haldorsen, 1986; Norris & Lewis, 1991). This method simply calculates or measures reservoir properties at increasing scales over intervals of the reservoir, thus allowing the property variability to be assessed at different scales (Figure 8). A representative scale within a reservoir is one at which the sample variability is reduced to a local minimum. In a structureless, random reservoir model a representative scale would be purely defined as a function of the variability of the data. Therefore the more variable and/or skewed the data in the model, the larger the scale of representivity will be. The determination of representative scales is made more complex in the presence of sedimentary structure, especially in heterogeneous reservoirs such as those at Morecambe. In many cases there may be multiple representative scales.

Figures 9-11 display the range of upscaled  $k_v$  and  $k_h$  (and therefore  $k_v/k_h$ ) over a range of scales from 0.5 - 20ft within the stacked fluvial channel section of 110/8a-5. The envelopes shown in Figures 9 and 10 define the behaviour of the same permeability data randomly distributed throughout the interval. Actual permeability estimates become less variable at approximately 12ft due to the presence of thick, low permeability channel abandonment deposits occurring at this length scale. Beyond this scale, permeability estimates vary by less than an order of magnitude,  $k_h$  between 10 - 80mD,  $k_v$  between 0.1 - 1mD and  $k_v/k_h$  between 0.003 - 0.02. Below this scale,  $k_h$  estimate variability steadily increases with only a minor reduction in at 3ft (Figure 9). However variability in the estimates of  $k_v$  rapidly increases (Figure 10), not uniformly but by clustering into intervals where  $k_v \approx 30\text{mD}$  and those where  $k_v \approx 0.3\text{mD}$ . Similarly,  $k_v/k_h$  estimates cluster between 3ft - 12ft into intervals where  $k_v/k_h \approx 0.3$ , 0.02 and 0.002 (Figure 11). Analysis

of core and image data shown in Figure 5 reveals that these clusters are due to distinct intervals of clean sand, sand containing intrachannel clay drapes and those with channel abandonment features.

The semivariograms of these data indicate 'nested' structure (Figure 12). The semivariogram of the raw data contains a large nugget effect and appears to indicate structure at approximately 3ft, while the semivariogram of the log transformed data has a smaller nugget and structure identified at approximately 10ft. The strength of the representative volume method, as compared with the semivariogram of this dataset, is its ability to identify that structure which influences horizontal and vertical fluid flow. For example, Figures 9-10 clearly show that, while the structure at 12ft controls  $k_h$  it is the structures at approximately 3-12ft which are controlling  $k_v$ . This method also quickly quantifies the permeability variability present at these scales for incorporation in larger scale models. For example, at the scale of the wireline tester, 7ft, the range in  $k_v/k_h$  is between 0.002 and 0.2. This degree of variability clearly shows that this tool is not measuring a representative volume. Therefore, when constructing a larger scale model for permeability upscaling, this must be taken into consideration and these higher  $k_v/k_h$  intervals included.

Figure 13 demonstrates the estimation of  $k_v$  using the same technique applied to an interval of aeolian deposits from within 110/8a-5. The high resolution permeability data were derived from micro-resistivity image data (Thomas et al, 1996). The patterns of permeability variability and clustering occurring in these data differ in scale and magnitude from the previous fluvial example. Permeability anisotropy is far greater in this setting due to the interbeddedding of high permeability aeolian dune sands with clay rich and evaporitic sabkha deposits. This behaviour contrasts with the usual assumption that fluvial deposits are more heterogeneous than aeolian sediments. This permeability dataset shows estimate variability reduction at approximately 15ft with clustering occurring between 4ft and 15ft.

This clustering represents those intervals containing thin evaporite cemented laminae and those intervals of aeolian dune where no evaporitic cement exists.

These results also suggest that, when developing a reservoir scale numerical model, the gridding should differ between the aeolian and fluvial regions. Grid blocks should be approximately 10ft thick in the fluvial regions, with two element types. The first with  $k_v \approx 0.3\text{mD}$  and allowed to vary for a history match by no more than one order of magnitude, and the second with  $k_v \approx 30\text{mD}$  and with little or no variation. For the aeolian region, two element types are also necessary, one where  $k_v \approx 0.009\text{mD}$  with one and a half orders of magnitude variation and the other where  $k_v \approx 30\text{mD}$  and with a permitted variation of one order of magnitude. Lateral extent of these elements would be derived from outcrop analogue studies.

## Summary and Conclusions

In this work we have demonstrated that, with adequate sampling, simple averages of probe permeability data may be used to model the vertical and horizontal permeability of the near wellbore region. The work has also shown that care must be taken when applying the permeability estimates of wireline testers to larger scale models since they may not be giving a reliable estimate for that scale. This work has also shown that the use of representative elementary units is a useful tool when defining structure within complex, heterogeneous reservoir intervals. Finally we have demonstrated that, while  $k_v$  vs. scale plots reflect geological and petrophysical architecture, semivariograms help elucidate the controlling structure.

## Acknowledgements

The authors would like to thank British Gas for their data and support of this work.

## References Cited

Atherton, G.M., (1993). An investigation into the use of the MDT\* tool for layer permeability identification. Unpublished MEng. Thesis, Heriot-Watt University, Edinburgh.

Ball L.D, P.W.M. Corbett, J.L. Jensen and J.J.M. Lewis, (1994) The Role of Geology in the Behaviour and Choice of Permeability Predictors, SPE 28447, Presented at: 69th SPE Annual Technical Conference, New Orleans, September 25-28, p. 867-879.

Bear, J., (1972). Dynamic of fluids in porous media: New York, Elsevier Publishing Company.

Bourdarot, G. and F. Daviau, (1989). Vertical Permeability: Field Cases: SPE 19777 presented at: 64th SPE Annual Technical Conference, San Antonio, October 8-11, p. 53-68.

Bourke L.T., (1992). Sedimentological borehole image analysis in clastic rocks: a systematic approach to interpretation. In: A. Hurst, C.M. Griffiths and P.F. Worthington, Geological applications of wireline logs II Geological Society Special Publication, 65, 31-42.

Bourke L.T. (1993). Core Permeability Imaging: Its Relevance to Conventional Core Characterisation and Potential Application to Wireline Measurement, Marine and Petroleum Geology, August, 1993, 318-324.

Corbett P.W.M. and J.L. Jensen, (1992). Estimating mean permeability: How many measurements do you need?. First Break, v. 10, p. 89-94.

Corbett, P.W.M. and J.L. Jensen, (1993). Quantification of variability in laminated sediments: A role for the probe permeameter in improved reservoir characterisation, in C.P. North and D.J. Prosser. Characterisation of Fluvial and Aeolian Reservoirs, Geological Society Special Publication, v. 73, p. 433-442.

Corbett, P.W.M., J.L. Jensen and K.S. Sorbie, (1996). Up-scaling and cross-scaling of core and log data for interpretation and prediction, presented at Geological Society/London Petrophysical Society "Core-log Integration" Meeting, September 17-18.

Cowan, G., (1993). Identification and significance of aeolian deposits within the dominantly fluvial Sherwood Sandstone Group of the East Irish Sea Basin UK. In : C.P. North and D.J. Prosser, Characterisation of Aeolian and Fluvial Reservoirs, Geological Society Special Publication, v. 73, p. 231-245.

Ekstrom M.P., C.A. Dahan, M.Y. Chen, P.M. Lloyd and D.J. Rossi, (1987). Formation Imaging with Microelectrical Scanning Arrays. The Log Analyst, v. 28(3), p. 294-306.

Goggin, D.J., (1993). Probe permeametry: Is it worth the effort? Marine and Petroleum Geology, v. 10, p. 299-308.

Hackbarth, C.J. and B.J. Tepper., (1988). Examination of BHTV, FMS and SHDT images in very thinly bedded sands and shales. SPE 18118 presented at: 63rd SPE Annual Technical Conference, Houston, October 2-5, p. 119-127.

Haldorsen, H.H., (1986). The problem of scale in reservoir engineering, in L.W. Lake and H.B. Carroll., Reservoir Characterisation, Orlando, Academic Press.

Halvorsen, C. and A. Hurst., (1990). Principles, practice and applications of laboratory permeametry, in P.F. Worthington. Advances in core evaluation, accuracy and precision in reserves estimation. Amsterdam, Gordon and Breach, p. 521-549.

Hohn, M.E. (1988)., Geostatistics and Petroleum Geology. New York, Van Nostrand Reinhold, 264 p.

Hollinshead, M., (1995). A comparison between probe permeability and MDT\* determined Anisotropy. Unpublished MEng. Thesis, Heriot-Watt University, Edinburgh.

Hurst, A. (1993)., Sedimentary flow units in hydrocarbon reservoirs: some shortcomings and a case for high-resolution permeability data, in S. Flint and I. D. Bryant. Quantitative description and modelling of clastic hydrocarbon reservoirs and outcrop analogues: International Association of Sedimentologists Special Publication. v. 15. p. 191-204.



Hurst, A. and K. Rosvoll., (1991). Permeability variations in sandstones and their relationship to sedimentary structures, in L.W. Lake, H.B. Carroll. Jr. and T.C Wesson, Reservoir Characterisation II: San Diego, Academic Press, p. 166-196.

Jensen, J.L., S. D. Thomas and P.W.M. Corbett., (1997). On the bias and sampling variation of the harmonic average. Mathematical Geology, v. 29, no. 2 (in press).

Lovell, M.A. and P.D. Jackson., (1991). Electrical flow in rocks: The application of high resolution electrical core measurements. Presented at the Society of Professional Well Log Analysts 32nd Annual Logging Symposium, June 16-19.

McCulloch, N., (1994). Unlocking North Morecambe's Trapped Gas: Prediction and enhancement of recovery. Unpublished MEng. Thesis, Heriot-Watt University, Edinburgh.

Muskat, M., 1937, Flow of homogeneous fluids: New York, McGraw-Hill, 763 p.

Norris, R, J, and J.J.M. Lewis., (1991). The geological modelling of effective permeability in complex heterolithic facies: SPE 22692 presented at: 66th Annual Technical Conference and Exhibition, Dallas, October 6-9, p. 359-374.

Pickup, G.E., P.S. Ringrose, P.W.M. Corbett, J.L. Jensen and K.S. Sorbie., (1995). Geology, geometry and effective flow. Petroleum Geoscience, v. 1, p. 37-42.

Robertson, G.M. and C.A. McPhee., (1990). High resolution probe permeametry: an aid to reservoir description. In P.F. Worthington, Advances in Core Evaluation: Accuracy and Precision in Reserves Estimation, London, Gordon and Breach, p. 495-520.

Stuart I.A. and G. Cowan, (1991)., The South Morecambe Field, Blocks 110/2a, 110/3a, 110/8a, UK East Irish Sea. In I.L. Abbotts, 25 Years Commemorative Volume, Geological Society Memoir, v. 14, p. 527-541.

Sutherland, W.J., C. Halvorsen, A. Hurst, C.A. McPhee, G. Robertson, P.R. Whattler and P.F. Worthington. Recommended practice for probe permeametry. Marine and Petroleum Geology, v. 10, p. 309-318.

Safinya K.A., P. Le Lan, M. Villegas, and P.S. Cheung., (1991). Improved formation imaging with extended microelectrical arrays. SPE 22726 presented at 66th ATC, Dallas, October 6-9, p. 653-664.

Thomas, S.D., P.W.M. Corbett and J.L. Jensen., (1996). Characterisation of Permeability and Permeability Anisotropy Characterisation in the Near Wellbore: A Numerical Model using the Probe Permeameter and Micro-Resistivity Image Data. Presented at the Society of Professional Well Log Analysts 37th Annual Logging Symposium, June 19-22.

Trouiller, J-C, and J-P. Delhomme., (1989). Thin-bed reservoir analysis from borehole electrical images: SPE 19578 presented at: 64th Annual Technical Conference and Exhibition, San Antonio, October 8-11, p. 217-228.

Wannell, M, J, and E.C. Ezekwe., (1992). The use of Observation Wells in reservoir management: SPE 24671 presented at: 67th Annual Technical Conference and Exhibition, Washington DC, October 4-7, p. 89-100.

Wannell, M, J, and N.M. Colley., (1993). The use of a new technique to determine Permeability Anisotropy: SPE 26801 presented at: Offshore European Conference, Aberdeen, September 7-10, p. 489-495.

## Figure Captions

**Figure 1.**  $k_v/k_h$  decrease with increasing scale observed from different measurement types.

**Figure 2.** Simple numerical model for estimation of  $k_v$  &  $k_h$  using harmonic and arithmetic averages respectively.

**Figure 3.** Location of the study well, 110/8a-5.

**Figure 4.** Similar values for vertical and horizontal mobility given by the wireline tool within the fluvial channel facies association of 110/8a-5.

**Figure 5.** Permeability data collected with core plugs and the probe permeameter over the ~50ft interval from around WT4 in 110/8a-5. Note the improvement in resolution given by the probe permeability data over the plug data (left), the reflection of this permeability heterogeneity in the electrical images (middle) and the position at which WT4 was set.

**Figure 6.** Estimates of  $k_v/k_h$  from core plug and probe datasets at location of WT4.

**Figure 7.** Estimates of  $k_v/k_h$  for core plug and probe datasets over 7ft windows within a fluvial channel sand unit, 4235-4255ft.

**Figure 8.** Methods for structural analysis: the Representative Elementary Volume and Semivariogram.

**Figures 9 - 11.** Numerical estimates of  $k_h$ ,  $k_v$  and  $k_v/k_h$  determined using probe permeameter dataset from the stacked fluvial channel core. The envelope in these figures indicates the expected reduction in upscaled permeability for a randomly distributed permeability field.

**Figure 12.** Semivariograms of raw and log transformed probe permeability data from fluvial channel core.

**Figure 13.** Numerical estimates of  $k_v$  determined using predicted permeability dataset from aeolian deposits within 110/8a-5.

	Plug Data	Probe Data
Cv	1.9	2.0
Samples	38	435
No	379	403
Do (=No/Samples)	0.1	1.1
Arithmetic Avg. (mD)	64.7	46.2
Harmonic Avg. (mD)	0.426	0.218
(Bias Corrected)	(0.467)	(0.220)
Anisotropy	0.007	0.005
(Bias Corrected)	(0.007)	(0.005)

Table 1.

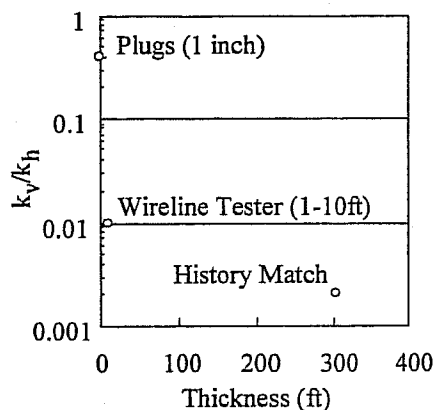
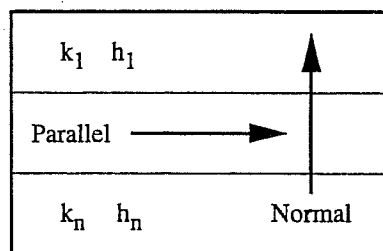


Figure 1.



$$k_{parallel} = \frac{\sum_{i=1}^n k_i h_i}{\sum_{i=1}^n h_i} = k_h \quad k_{normal} = \left( \frac{\sum_{i=1}^n \frac{h_i}{k_i}}{\sum_{i=1}^n h_i} \right) = k_v$$

Figure 2.

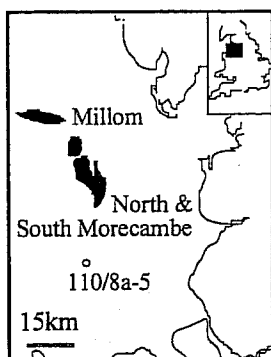


Figure 3.

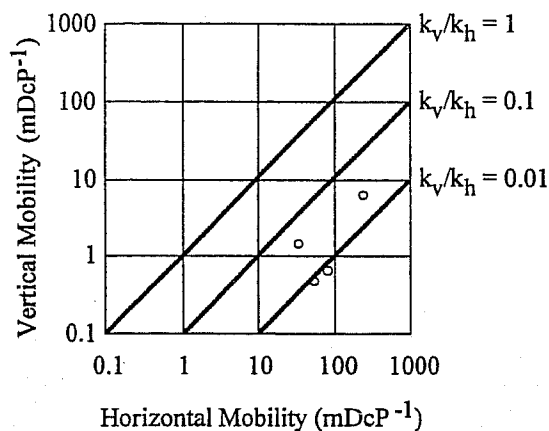


Figure 4.

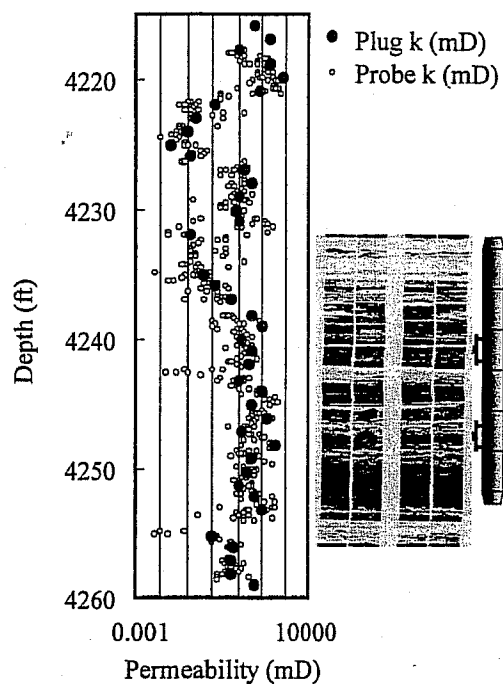


Figure 5.

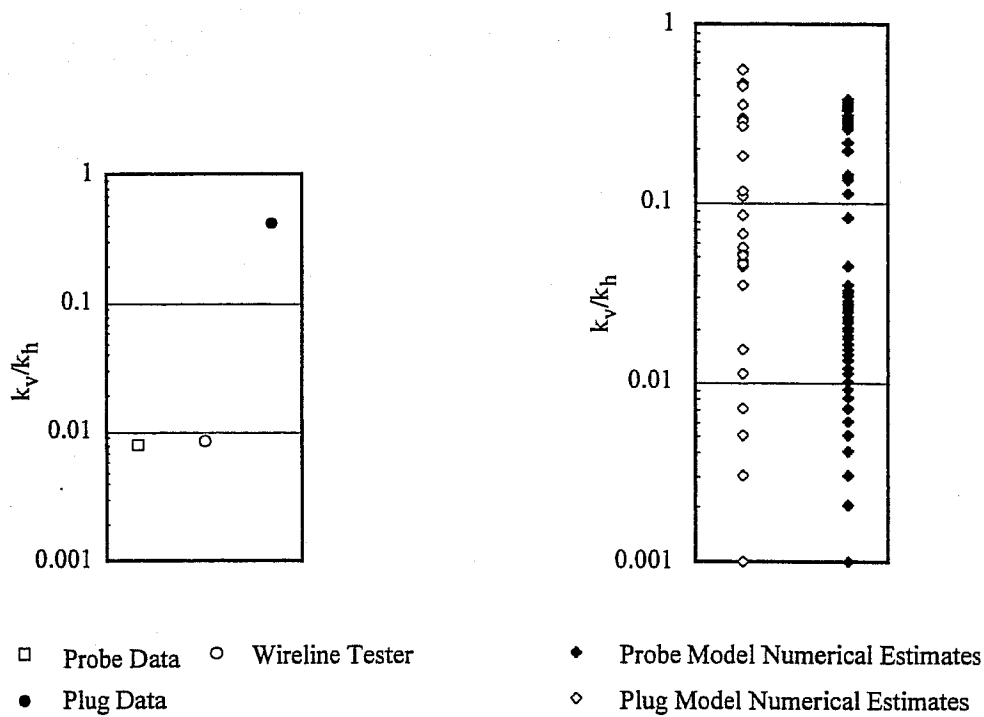


Figure 6.

Figure 7.

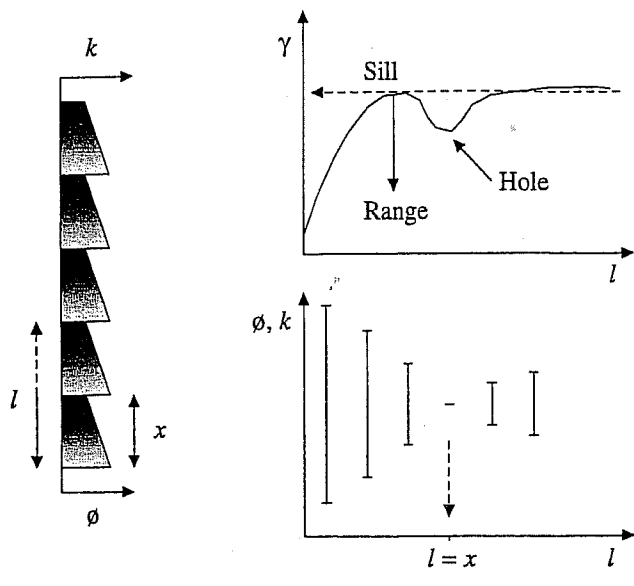


Figure 8.

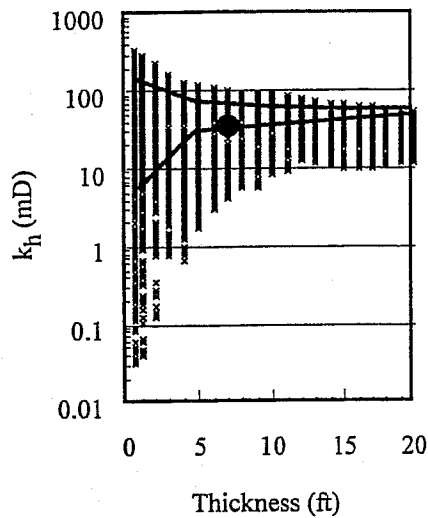


Figure 9.

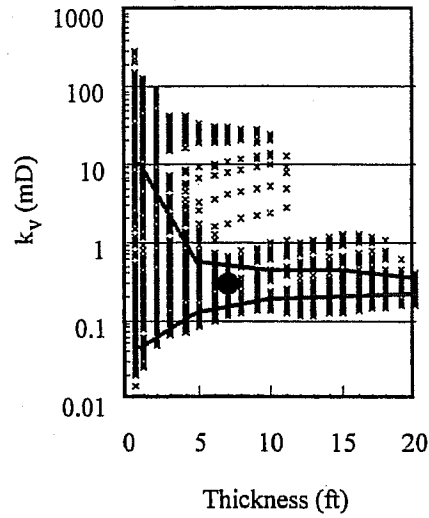


Figure 10.

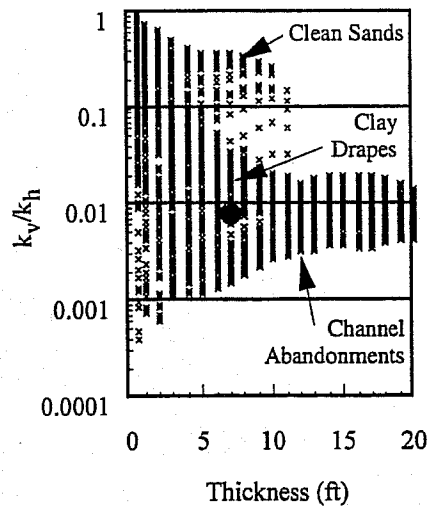
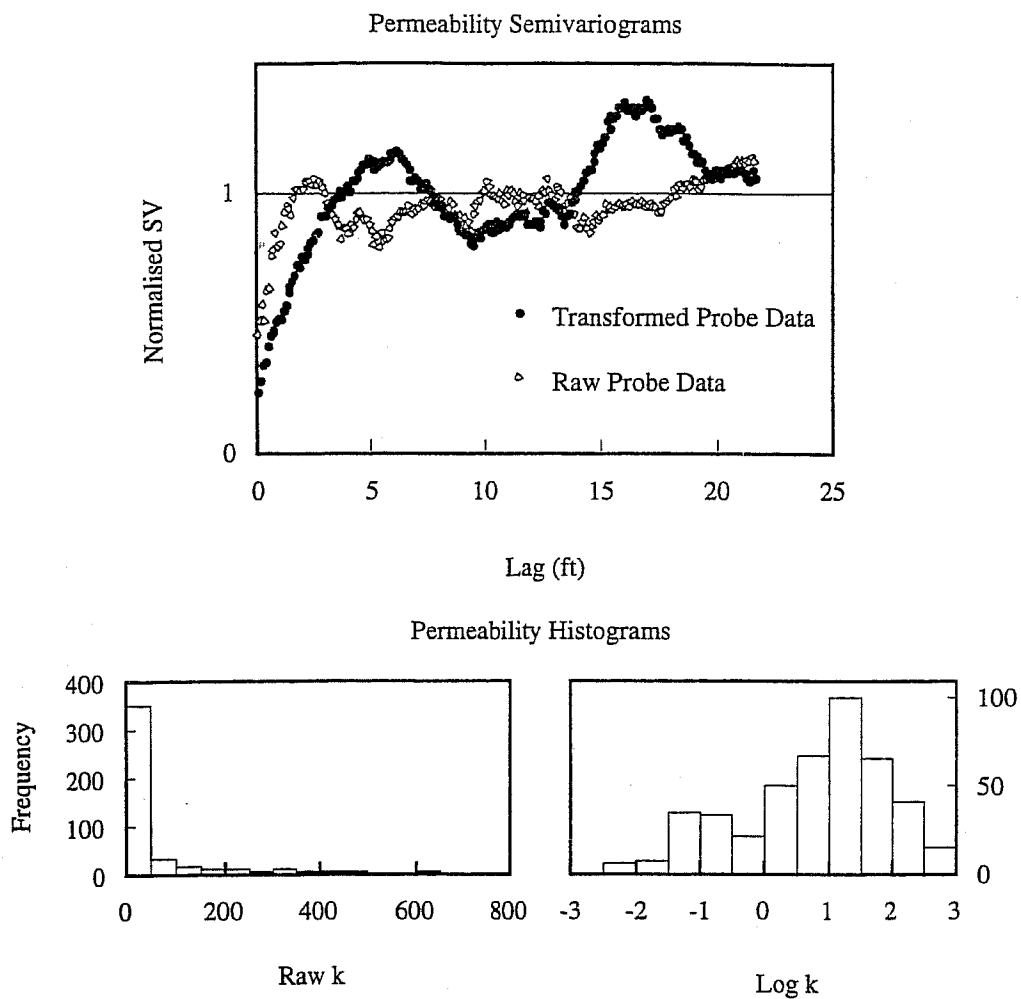
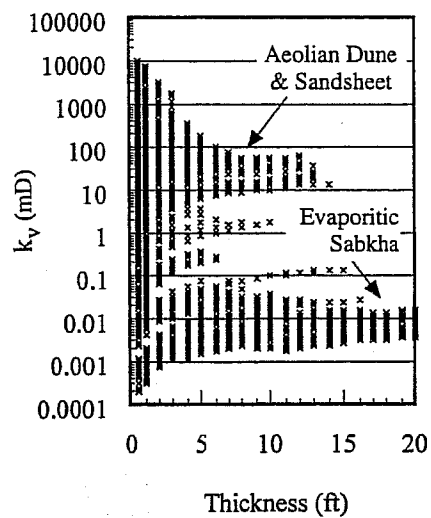


Figure 11.



**Figure 12.**



**Figure 13.**





**Use of Geostatistic Techniques to Describe a Reservoir to be  
Submitted into a Secondary Recovery Process  
Field Case: "Eocene B-Inferior/VLG-3659, Ceuta, Venezuela"**

Thamera Hernandez; Walter Poquioma  
Maraven, S.A.  
LaEstancia Avenue Chuao  
Caracas, Venezuela

**ABSTRACT**

This study presents the results of an integrated reservoir study of the Eocene B-Inferior/VLG-3659, Area 7, Ceuta filed. This field located in the Maracaibo Lake in the western side of Venezuela. The objective was to evaluating the feasibility to implement a secondary recovery project by means of water flooding. Core information was used for this study (194 ft), PVT analysis, RFT, build-up and statistic's pressure analysis, modern logs and production history data.

Using geostatistical techniques (Kriging) it was defined a low uncertainty geological model that was validated by means of a black oil simulator (Eclipse). The results showed a good comparison of historical pressure of the reservoir against those obtained from the model, without the need of "history matching". It means without modifying neither the initial rock properties nor reservoir fluids. The results of this study recommended drilling in two new locations, also the reactivation of four producing wells and water flooding under peripheral array by means of four injection wells, with the recovery of an additional 30.2 MMSTB. The economical evaluation shows an internal return rate of 31.4%.



# How Incorporating More Data Reduces Uncertainty in Recovery Predictions

Fernando P. Campoza\*

Larry W. Lake\*

Kamy Sepehrnoori\*

\* Center for Petroleum and Geosystems Engineering

The University of Texas at Austin

## ABSTRACT

From the discovery to the abandonment of a petroleum reservoir, there are many decisions that involve economic risks because of uncertainty in the production forecast. This uncertainty may be quantified by performing stochastic reservoir modeling (SRM); however, it is not practical to apply SRM every time the model is updated to account for new data.

This paper suggests a novel procedure to estimate reservoir uncertainty (and its reduction) as a function of the amount and type of data used in the reservoir modeling. Two types of data are analyzed: conditioning data and well-test data. However, the same procedure can be applied to any other data type. Three performance parameters are suggested to quantify uncertainty.

SRM is performed for the following typical stages: discovery, primary production, secondary production, and infill drilling. From those results, a set of curves is generated that can be used to estimate (1) the uncertainty for any other situation and (2) the uncertainty reduction caused by the introduction of new wells (with and without well-test data) into the description.

## INTRODUCTION

Reservoir uncertainty is the result of a lack of information. Sample data taken at well locations (cores and well logs) are too scarce to allow a detailed description. Other types of information such as (1) seismic data, (2) geological interpretation, (3) outcrop analogs, and (4) tracer, well-test, and production data can reduce, but not eliminate, uncertainty in reservoir description. As a result, multiple, equiprobable models of the same reservoir can be generated, all of them honoring the available information. This process, called stochastic reservoir modeling (SRM), allows one to (1) quantify reservoir uncertainty (2) verify fluctuations in the cash flow of projects (3) find where unswept areas of the reservoir are probably located, and (4) better manage improved oil recovery projects or infill drilling.

To stochastically simulate reservoir performance, one generally needs to build a probability density function (pdf) for each of the reservoir simulation parameters. Assuming independence among all parameters, this can be achieved by performing the following steps<sup>1</sup>:

- define a reference or most probable reservoir model;
- generate multiple realizations of each reservoir parameter of the reservoir model;
- perform repeated flow simulations varying only one reservoir parameter, keeping unchanged the others from the reference model parameters; and
- define a performance parameter such as oil recovery at a given time, water cut, or breakthrough time to build the pdf of the parameters.

The procedure outlined above provides an estimate of how reservoir performance varies with each parameter. This information is useful to determine the degree of accuracy necessary for each reservoir parameter. After estimating the pdfs of the reservoir parameters, multiple reservoir models can be obtained by applying the Monte-

Carlo method, as shown in Fig. 1. Each reservoir model is defined by randomly selecting the reservoir parameters from their pdfs. Reservoir uncertainty is then quantified by using each reservoir model as input to a numerical flow simulator. Based on performance parameters obtained from the simulation results, a pdf can be built similarly to what was done for each individual reservoir parameter.

Stochastic reservoir modeling can be time-consuming and sometimes computationally prohibitive. Since no satisfactory numerical simulator based on stochastic differential equations has yet been developed, each reservoir model must be input one at a time. To overcome this limitation, a number of techniques have been suggested. First, the sampling process can be minimized without losing information by using either the Stratified Sampling Method or Latin HyperCube Sampling<sup>2</sup>; second, subjective pdfs (like triangular distributions) can be considered for those parameters that practical experience or previous sensitivity analysis have shown not to be critical<sup>3</sup>; and, finally, one can perform simplified numerical simulations to rank each reservoir description and then select those that correspond to the most important quantiles to run full numerical simulations<sup>4</sup>. The fast, simplified numerical simulations are usually done by using a coarse grid simulation, a tracer simulator, or a simplified flow model such as a streamline simulator.

It must be pointed out that, usually, reservoir parameters exhibit multivariate dependence and application of multivariate statistics is necessary. The calculated variance of production profiles, assuming independence among the variables, can be very different from that calculated considering multidependence. However, a complete study on the dependence of all variables is rarely feasible because it requires information that is not available. Bivariate statistics considering, for example, dependence between porosity and permeability, is strongly suggested.

Applying SRM every time new information is added to the reservoir description is not viable, even with the sampling techniques described above. In this work, a

procedure is suggested that allows one to infer uncertainty in production performance for any data configuration, as well as the uncertainty reduction caused by the incorporation of new data into the model, with a reasonable computational effort.

## THE APPROACH

The more data are considered in a description, the better a model should represent reality. Reservoir uncertainty should decrease. To quantify reservoir uncertainty as a function of the amount and type of data used in the model without applying SRM after every model update the following procedure is suggested:

- generate a reference model that accounts for as much data as possible and use it as input of a numerical simulator to obtain a production forecast;
- perform some samplings from the reference model (say, four) to mimic a typical sequence of data acquisition obtained from equally spaced wells (as in the example shown in Fig. 2);
- perform SRM for each data configuration assuming the only information known about the reference model is that provided by the samples;
- choose one or more performance parameter(s) to rank the realizations and quantify the uncertainty in the recovery for each data configuration; and
- plot the performance parameter versus the number and type of data.

The uncertainty related to the reference model is bounded by two extremes: when no data are available it is a maximum and when all block values of the reference model are known it is zero. With this information, plus the points obtained using the procedure above, a curve that describes reservoir uncertainty versus number of wells can be generated. Interpolation may be used to estimate uncertainty for any number of wells.

Many performance parameters have been suggested in the literature<sup>5</sup>; most of them require the use of numerical flow simulation. An interesting parameter that does not rely on numerical simulation is the visual likeness factor<sup>6</sup>. It is defined as

$$\Gamma = \frac{\sum_i (Z_i - \bar{Z})(Y_i - \bar{Y})}{\sqrt{\sum_i (Z_i - \bar{Z})^2 \sum_i (Y_i - \bar{Y})^2}} \quad (1)$$

where  $Z_i$  and  $Y_i$  are, respectively, the values of the variable at the  $i^{\text{th}}$  block of the simulated image and the reference or base case.  $\bar{Z}$  and  $\bar{Y}$  are the average values. A perfect match gives  $\Gamma = 1$ , while  $\Gamma = 0$  means that there is no correlation between the base case and the generated image. The visual likeness factor is very similar to the well-known correlation coefficient, the difference being that  $\Gamma$  considers the spatial location of the samples. This is why  $\Gamma$  is sometimes called spatial correlation coefficient.

Given a set of simulations, the uncertainty in the recovery prediction ( $URP$ ) can be expressed as

$$URP_i^j = \left( RF_{opt} - RF_{pess} \right)_i^j / RF_{base} \quad (2)$$

where the subscript  $i$  refers to the number of conditioning wells, the superscript  $j$  refers to the algorithm used to generate the set of images, and  $RF_{opt}$ ,  $RF_{pess}$ , and  $RF_{base}$  are, respectively, the most optimistic, the most pessimistic and the base-case recovery factors after a given time of production. If the reference model is updated, this parameter can be adjusted accordingly.

Analyzing the boundaries,  $URP = 0$  if all  $i$  realizations match the reference case perfectly since both  $RF_{opt}$  and  $RF_{pess}$  coincide with  $RF_{base}$ . The upper bound of  $URP$  is obtained from Eq.2 for the set of realizations that gives the largest or maximum recovery

range:  $URP_{\max} = \left( RF_{opt} - RF_{pess} \right)_{i \max}^j / RF_{base}$ . Generally, this set is the one that accounts for less data. A set of unconditional simulations could be used for this purpose. An alternative expression,  $URP^*$ , is independent of the base-case recovery and varies between 0 and 1:

$$URP_i^{*j} = URP_i^j \frac{RF_{base}}{(RF_{opt} - RF_{pess})_{\max}} = \frac{(RF_{opt} - RF_{pess})}{(RF_{opt} - RF_{pess})_{\max}} \quad (3)$$

A plot of  $URP$  versus the number of wells gives an estimate of the recovery range one would obtain for a generic configuration of wells, provided that they are approximately equally spaced. Obviously, if the wells are clustered, they will not reduce uncertainty as much as if they were equally spaced.

A third parameter measures the reduction of the uncertainty in the recovery prediction ( $RURP$ ) as more data are added to the description:

$$RURP_i^j = (URP_{\max} - URP) / URP_{\max} = 1 - URP_i^{*j} \quad (4)$$

A plot of  $RURP$  versus the number of wells quantifies the impact of new data on reservoir uncertainty.

#### AN EXAMPLE APPLICATION

A hypothetical reservoir submitted to waterflooding is stochastically modeled to observe how reservoir uncertainty decreases as more conditioning data and well-test information are added to the description. For the sake of simplicity, only absolute permeability is allowed to vary. All other reservoir parameters are assumed to be perfectly known. A synthetic base case is generated and used as input to the commercial ECLIPSE 100 numerical simulator<sup>7</sup> to obtain dynamic data (well-test permeability and



oil recovery). The results are compared to those obtained using several sets of geostatistical realizations that honor different amounts of conditioning and well-test data.

### The Base Case

A two-dimensional permeability field was generated using the matrix decomposition method (MDM)<sup>8,9</sup>. The hypothetical reservoir is a square of 4500'x4500' divided into 45x45 square gridblocks of 100'x100' each. For purposes of numerical simulation, nine equally spaced wells are active in the field: four are water injectors and five are oil producers. Their location and rates are shown in Fig. 3. The grayscale map of the base-case permeability field is shown in Fig. 4. The semivariogram model is isotropic, spherical, with no nugget, and has a range of 2,250' (half of the side length of the reservoir). The reservoir properties are given in Table 1.

The base case was then used as input to ECLIPSE 100. Two types of flow simulation were performed: a production forecast and well tests. The radius of investigation of the well-test simulations is equal to 1500'. These synthetic data are considered as reference or the *truth* case.

### Stochastic Modeling

Three geostatistical algorithms were used to generate realizations conditioned to different types of data: turning bands method<sup>10</sup> (TBM), simulated annealing<sup>11-13</sup> (SA), and MTWELL<sup>14</sup>. The TBM algorithm was used to generate a set of unconditional simulations that was constrained only by the semivariogram. The SA algorithm was used to generate four sets of realizations conditioned to different numbers of wells (1, 5, 9, and 25) and to the semivariogram. Finally, the MTWELL algorithm was used to obtain four more sets of realizations conditioned to the semivariogram, to the same wells used in the SA realizations, and their respective well-test permeabilities derived from

pressure-transient analysis. Each set is composed of 30 two-dimensional, 45x45 permeability realizations.

The configurations of the conditioning data used in the SA and MTWELL realizations are shown in Fig. 2. These configurations can be associated with the discovery, primary production, secondary production, and infill drilling phases of the reservoir. Each well is representative of the block in which it is located. The semivariogram used in all realizations is identical to that of the base case. Therefore, uncertainty in the semivariogram model is not being considered in this application.

A statistical procedure was followed to verify if 30 realizations were enough to give meaningful results<sup>14</sup>. All sets of realizations were submitted to several samplings without replacement and the recovery range ( $OR_{opt} - OR_{pess}$ ) was calculated for each sample. Figures 5 and 6 show how the recovery range varies with the number of SA and MTWELL realizations, respectively. Stable values are reached after 25 realizations for all sets, meaning that 30 realizations are enough for the present example.

Figures 7 to 11 show one TBM, two SA, and two MTWELL realizations randomly taken from their sets. Comparing these images with the base case (Fig. 4), there is improvement as (1) the number of conditioning data increases and (2) well-test data are incorporated into the description. This improvement will be quantified in the next sections.

### *The Visual Likeness Factor*

The visual likeness factor (see Eq. 1) was calculated for all realizations, as well as the mean value  $\bar{\Gamma}$  of each set. In the limiting case where all block values (2,025) are known,  $\bar{\Gamma} = 1$  for both the SA and MTWELL cases, since all realizations are identical to the base case. A plot of  $\bar{\Gamma}$  versus the number of wells ( $N_W$ ) is shown in Fig. 12. The visual likeness increases as  $N_W$  increases, but the impact of additional wells on  $\bar{\Gamma}$  becomes smaller as  $N_W$  increases. The sets of realizations conditioned to the well-test

data (MTWELL) have a greater  $\bar{\Gamma}$  than those conditioned only to the data points (SA). The TBM set had the lowest value of  $\bar{\Gamma}$ .

For the cases run, the data points are close to a straight line on a semilog plot, and  $\bar{\Gamma}$  can be reasonably well predicted for any number of equally spaced wells by using the equation  $\bar{\Gamma} = 0.258 \log N_w + 0.145$  for the SA realizations and the equation  $\bar{\Gamma} = 0.219 \log N_w + 0.281$  for the MTWELL realizations. Analyzing the difference between the two curves, one can see the improvement in  $\bar{\Gamma}$  caused by the incorporation of well-test information into the description. Although accounting for well-test data always improves the description, its contribution diminishes as the number of conditioning wells increases.

### *Uncertainty in the Recovery Prediction*

Numerical simulation was used to transfer uncertainty in the reservoir models to a production forecast. The nine sets of 30 permeability realizations described in the previous section were used as input to the commercial simulator ECLIPSE 100. All other reservoir properties were kept identical to those of the base case. Although the number of conditioning data varied from zero to 25, the number of active wells (injectors and producers) was kept unchanged during the numerical simulation (see Fig. 3).

The uncertainty in the recovery prediction ( $URP$ ) was calculated for all sets of realizations (see Eq. 2). Figure 13 shows that, like the behavior of  $\bar{\Gamma}$ ,  $URP$  decreases as  $N_w$  increases, but the impact of additional wells on  $URP$  decreases as  $N_w$  increases. Notice also the reduction in  $URP$  caused by the inclusion of well-test data into the description, especially for small values of  $N_w$ . If all 2,025 permeability block values are known,  $URP$  must be zero, since all realizations would be identical to the base case. Unlike  $\bar{\Gamma}$ ,  $URP$  is not linearly related to the logarithm of  $N_w$ .

The reduction of the uncertainty in the recovery prediction ( $RURP$ ) can now be analyzed in detail. Since the TBM realizations had the largest recovery range of all sets, Eq. 4 can be rewritten as

$$RURP = (URP_{TBM} - URP) / URP_{TBM}. \quad (5)$$

The results obtained using Eq. 5 are shown in Table 2 and plotted in Fig. 14. For  $N_w = 1$ , the  $RURP$  of the MTWELL set is 47 %, while that of the SA set is only 14 %. On the other hand, to get the same  $RURP$  of 47 % without considering well-test data, one needs five conditioning wells. Therefore, in this situation, testing the single well is as valuable as adding four wells to the description. However, for  $N_w = 25$ , the  $RURP$  of the MTWELL and SA realizations are not too different (89 % and 83 %, respectively).

## CONCLUSIONS

A method based on stochastic reservoir modeling has been proposed to estimate the reservoir uncertainty and its reduction as a function of the amount and type of data used in the description. This method allows one to assess (1) reservoir uncertainty for any data configuration and (2) the impact of new data on reservoir uncertainty. Three performance parameters are suggested to quantify geostatistical realizations. An application example shows how uncertainty decreases as more conditioning data and well-test data are incorporated into the model. The impact on reservoir uncertainty of adding well-test information to the description is larger in the early stages of a field development, when only a few wells are available.

## AKNOWLEDGEMENTS

We acknowledge the Enhanced Oil Recovery Research Program of the Center for Petroleum and Geosystems Engineering at The University of Texas at Austin for partial support of this work. We thank Geoquest for providing the ECLIPSE-100 simulator and the Deltas Industrial Affiliates Program of the Bureau of Economic Geology of The University of Texas for the computer time. Fernando Campoza thanks Petrobras for his financial support. Larry W. Lake holds the W. A. (Tex) Moncrief Centennial Chair.

## NOMENCLATURE

$N_w$	= number of wells
pdf	= probability density function
$RF$	= recovery factor (fraction)
$RURP$	= reduction of the uncertainty in the recovery prediction
SRM	= stochastic reservoir modeling
$URP$	= uncertainty in the recovery prediction
$Y_i$	= value of the stochastic variable at the $i^{th}$ block for a generalized realization
$\bar{Y}$	= mean value of the variable $Y_i$
$Z_i$	= value of the stochastic variable at the $i^{th}$ block for the the base case realization
$\bar{Z}$	= mean value of the variable $Z_i$
$\Gamma$	= visual likeness factor
$\bar{\Gamma}$	= mean value of the visual likeness factor
<u>Superscripts</u>	
$j$	= refers to the algorithm used to generate the realizations
*	= normalized

### Subscripts

base	= base case
i	= refers to the number of conditioning data used in the realizations
max	= maximum
opt	= optimistic
pess	= pessimistic
TBM	= turning bands method

### REFERENCES

1. Haldorsen, H.H. and Damsleth, E.: "Stochastic Modeling," J. Pet. Tech. (Apr. 1990), 404-412.
2. Ding, L.Y., Mehra, R.K., and Donnelly, J.K.: "Stochastic Modeling in Reservoir Simulation," paper SPE 18431, Proceedings of the 10<sup>th</sup> SPE Symposium on Reservoir Simulation, Houston, TX, Feb. 1989.
3. Øvreberg, O., Damsleth, E., and Haldorsen, H.H.: "Putting Error-bars on Reservoir Engineering Forecasts," paper SPE 20512, Proceedings of the 65<sup>th</sup> Annual Tech. Conf. and Exhib. of the SPE, New Orleans, LA, Sept. 1990.
4. Ballin, P.R.: "Approximation of Flow Simulation for Uncertainty Assessment," Ph.D. dissertation, Stanford University, CA (June 1992).
5. Ballin, P.R., Aziz, K., Journel, A.G., and Zuccolo, L.: "Quantifying the Impact of Geological Uncertainty on Reservoir Performing Forecasts," paper SPE 25238, Proceedings of the 12<sup>th</sup> SPE Symposium on Reservoir Simulation, New Orleans, LA, Feb. 1993.
6. Ouenes, A., and Saad, N.: "A New, Fast Parallel Simulated Annealing Algorithm for Reservoir Characterization," paper SPE 26419, Proceedings of the 68<sup>th</sup> Annual Tech. Conf. and Exhib. of the SPE, Houston, TX, Oct. 1993.
7. ECLIPSE-100, Exploration Consultants Ltd. - Highlands Farm, Oxfordshire (RG9-4PS), England.

8. Fogg, G.E. and Lucia, F.J.: "Stochastic Simulation of Interwell-Scale Heterogeneity for Improved Prediction of Sweep Efficiency in a Carbonate Reservoir," Proceedings of the NIPER/DOE Second International Reservoir Characterization Technical Conference, Dallas, TX, June 1989.
9. Young, A.P.: "Stochastic Heterogeneity and Dispersion," Ph.D. dissertation, the University of Texas, Austin, TX (1990).
10. Journel, A.G. and Huijbregts, C.J.: *Mining Geostatistics*, Academic Press, London, 1978.
11. Kirkpatrick, S., Gelatt, C.D., Jr., and Vecchi, M.P.: "Optimization by Simulated Annealing," *Science* (1983), 220, 671-680.
12. Farmer, C.L.: "The Mathematical Generation of Reservoir Geology," Proceedings of the Joint IMA/SPE European Conf. on the Math. Oil Recovery, Robinson College, Cambridge University, July 1989.
13. Otten, R. and Van Ginneken, L.: *The Annealing Algorithm*, Kluwer Academic Publishers, Dordrech 1989.
14. Campozana, F.P., Lake, L.W., and Sepehrnoori, K.: "Reservoir Modeling Constrained to Multiple Well-Test Permeabilities," paper SPE 36569, Proceedings of the 71<sup>th</sup> Annual Tech. Conf. and Exhib. of the SPE, Denver, CO, Oct. 1996.

#### LIST OF FIGURES

1. Monte-Carlo approach to stochastic reservoir modeling.
2. Four configurations of the conditioning data. From top to bottom and left to right: field discovery, primary recovery, secondary recovery, and infill drilling.
3. Well locations and water injection rates for all numerical simulations.
4. Base-case permeability distribution generated using sequential Gaussian simulation (SGS). The image is conditioned to the permeabilities at the nine wells in Fig. 3 and to a

spherical semivariogram. There is no nugget effect and the range of correlation is one-half of the reservoir horizontal length.

5. Variation of the recovery range with the number of SA realizations. The samplings are made in increments of 5.

6. Variation of the recovery range with the number of MTWELL realizations. The samplings are made in increments of 5.

7. Single realization randomly taken from the TBM set (unconditional).

8. Single realization randomly taken from the SA set conditioned to one well.

9. Single realization randomly taken from the SA set conditioned to five wells.

10. Single realization randomly taken from the SA set conditioned to nine wells.

11. Single realization randomly taken from the SA set conditioned to 25 wells.

12. Single realization randomly taken from the MTWELL set conditioned to one well plus its well-test permeability.

13. Single realization randomly taken from the MTWELL set conditioned to five wells plus their well-test permeabilities.

14. Single realization randomly taken from the MTWELL set conditioned to nine wells plus their well-test permeabilities.

15. Single realization randomly taken from the MTWELL set conditioned to 25 wells plus their well-test permeabilities.

16. Variation of the visual likeness factor with the number of conditioning wells and type of data.

17. Variation of the URP factor with the number of conditioning wells and type of data.



18. Variation of the RURP factor with the number of conditioning wells and type of data.

Table 1 - Reservoir Properties	
Reservoir dimensions, ft	4500 x 4500
Number of gridblocks ( $n_x, n_y, n_z$ )	45 x 45 x 1
Block dimensions ( $\Delta x, \Delta y, \Delta z$ )	100 x 100 x 20
Porosity, fraction	0.2
Wellbore radius, ft	0.25
Total compressibility, 1/psi	$4.7 \times 10^{-7}$
Initial water saturation	0.22
Oil formation volume factor, bbl/STB ( at initial pressure, 2200 psia)	1.15
Oil viscosity at 2200 psia, cp	0.8
Initial pressure, psia	2200

Table 2 - Numerical simulation results.				
Algorithm	$N_w$	RF range*	URP	RURP
TBM	0	0.133	0.284	0
SA	1	0.115	0.245	0.135
SA	5	0.07	0.149	0.474
SA	9	0.044	0.094	0.669
SA	25	0.022	0.047	0.835
MTWELL	1	0.071	0.151	0.466
MTWELL	5	0.04	0.085	0.699
MTWELL	9	0.022	0.047	0.835
MTWELL	25	0.014	0.030	0.895
-	2025**	0	0	1

\* Range of the recovery factor ( $RF_{opt} - RF_{pess}$ ).

\*\* Extrapolation.

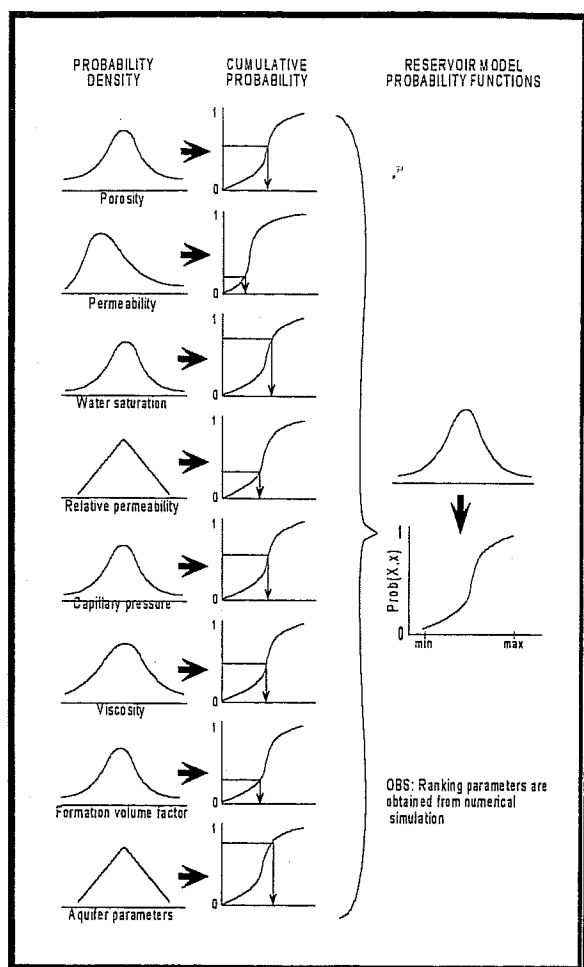


Figure 1. Monte-Carlo approach to reservoir stochastic modeling.

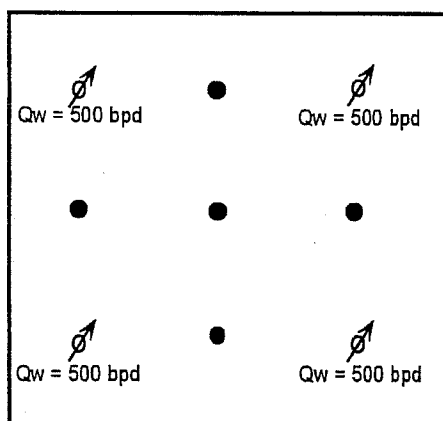
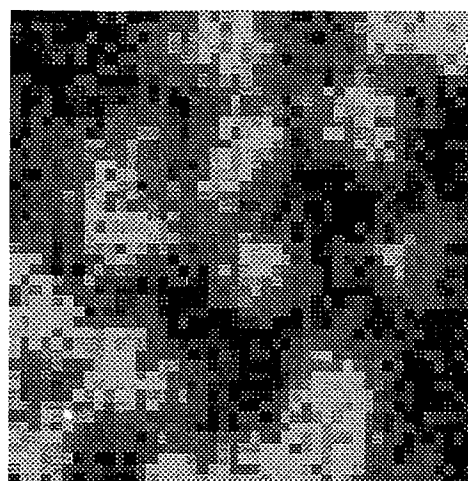


Figure 3. Well locations and water injection rates for all numerical simulations.



0 md  1500 md

Figure 4. Base-case permeability distribution generated using sequential Gaussian simulation (SGS). The image is conditioned to the permeabilities at the nine wells in fig. 3 and to a spherical semivariogram. There is no nugget effect and the range of correlation is one-half of the reservoir horizontal length.

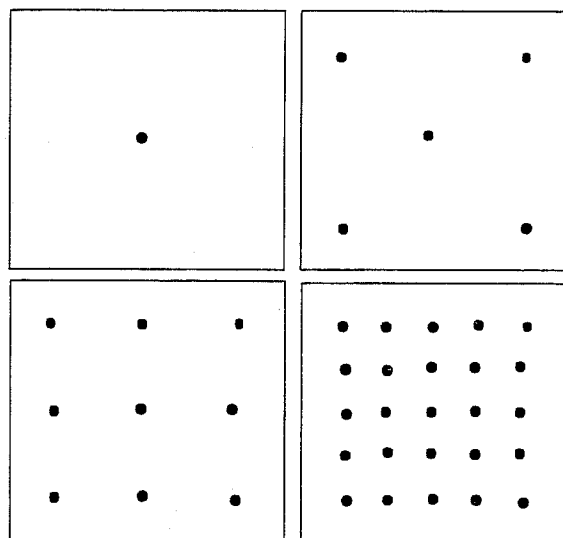


Figure 2. Four configurations of the conditioning data. From top to bottom and left to right: field discovery, primary production, secondary production, and infill drilling.

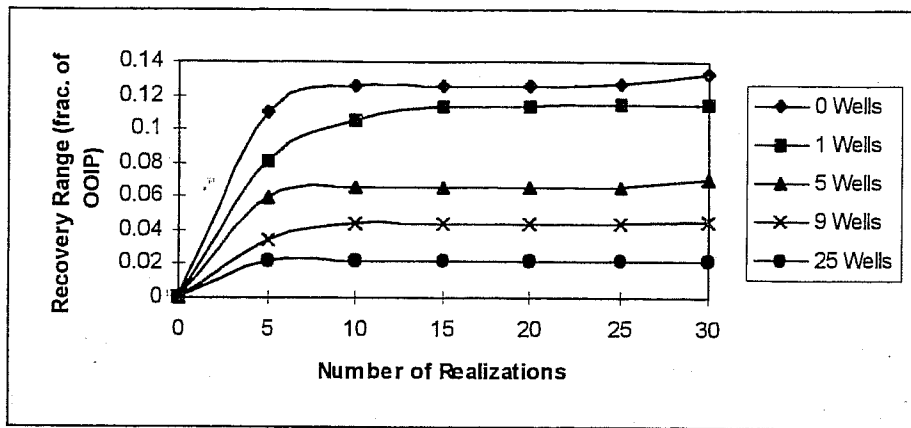


Figure 5. Variation of the recovery range with the number of SA realizations. The samplings are made in increments of 5.

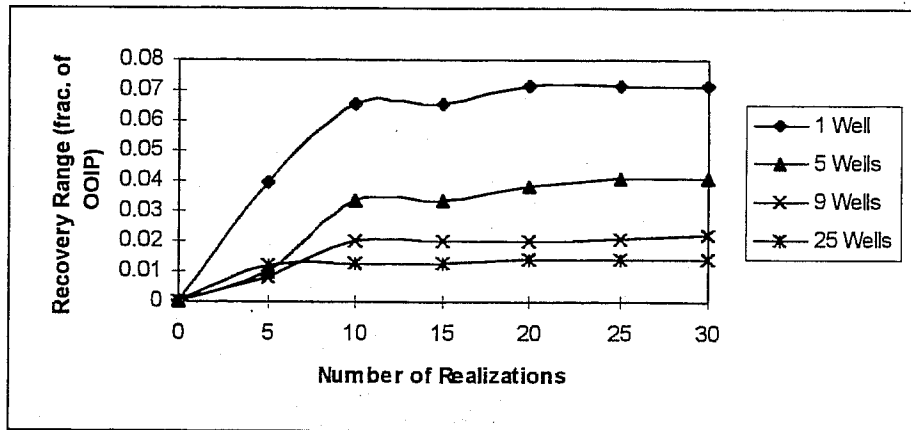


Figure 6. Variation of the recovery range with the number of MTWELL realizations. The samplings are made in increments of 5 without replacement.

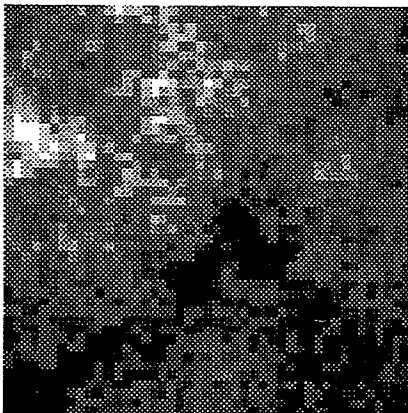


Figure 7. One realization randomly taken from the TBM set (unconditional).

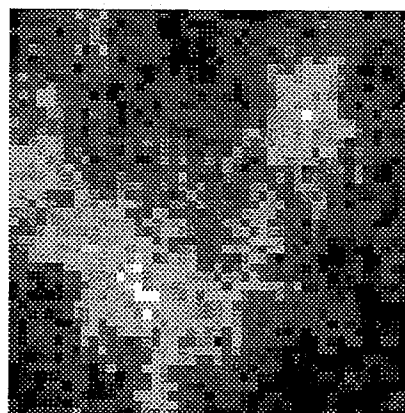


Figure 8. One realization randomly taken from the SA set conditioned to one well.

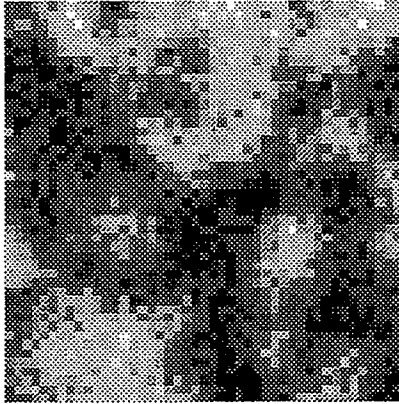


Figure 9. One realization randomly taken from the SA set conditioned to 25 wells.

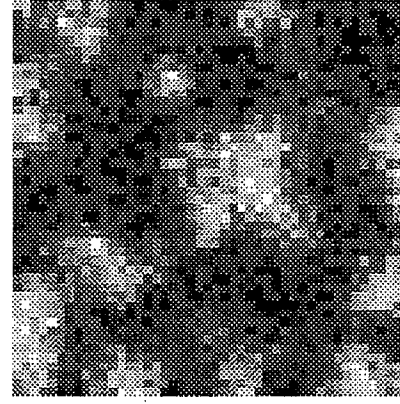


Figure 10. One realization randomly taken from the MTWELL set conditioned to one well plus its well-test permeability.

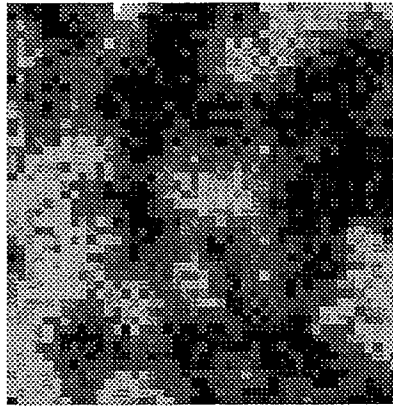


Figure 11. One realization randomly taken from the MTWELL set conditioned to 25 wells plus their well-test permeabilities.

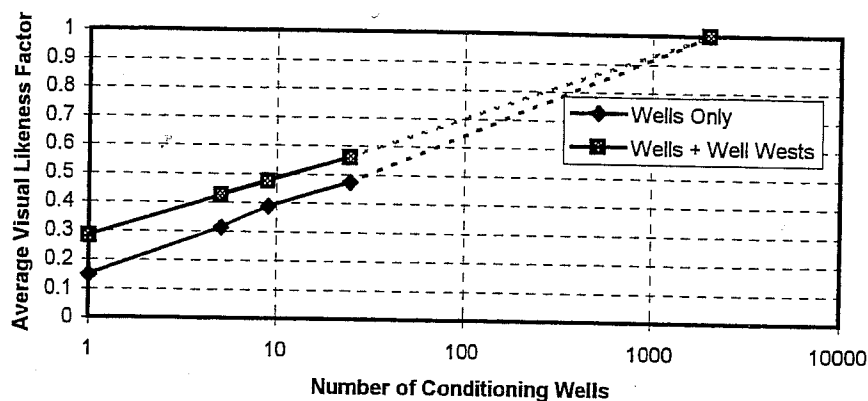


Figure 12. Variation of the visual likeness factor with the number of conditioning wells and type of data. The dotted lines are extrapolations.

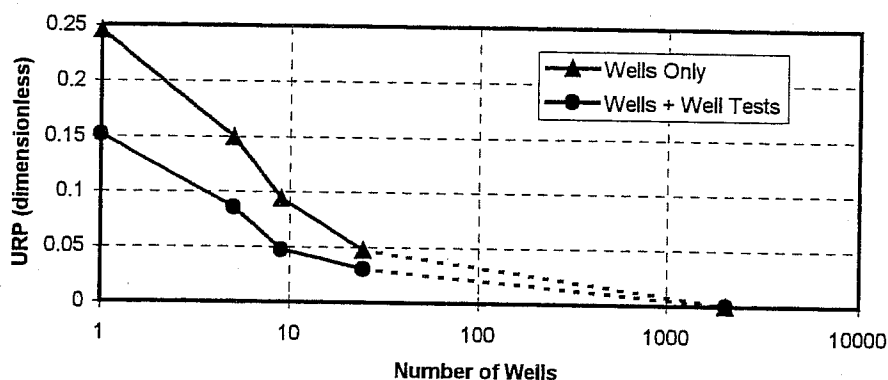


Figure 13. Variation of the uncertainty in the recovery prediction (*URP*) with the number of conditioning wells and type of data. The dotted lines are extrapolations.

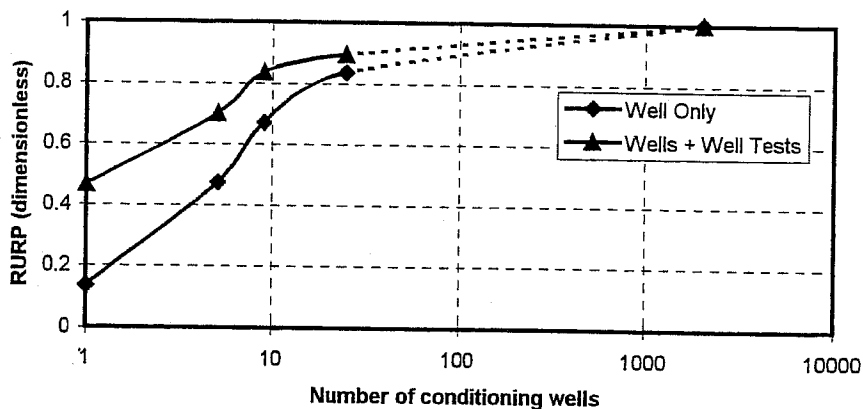


Figure 14. Reduction of the uncertainty in the recovery prediction (*RURP*) with the number of conditioning wells and type of data. The dotted lines are extrapolations.



# Evaluation of Field Development Plans Using 3-D Reservoir Modelling

D. Seifert<sup>1</sup>, J.D.H. Newbery<sup>2,3</sup>, C. Ramsey<sup>2,4</sup> and J.J.M. Lewis<sup>1,5</sup>

<sup>1</sup>Heriot-Watt University, Edinburgh, Scotland

<sup>2</sup>Conoco (UK) Ltd, Aberdeen, Scotland

<sup>3</sup>Present Address: Enterprise Oil Ltd, London, England

<sup>4</sup>Present Address: LASMO North Sea Plc, London, England

<sup>5</sup>Present Address: Landmark, Austin, Texas

## Abstract

Three-dimensional reservoir modelling has become an accepted tool in reservoir description and is used for various purposes, such as reservoir performance prediction or integration and visualisation of data. In this case study, a small Northern North Sea turbiditic reservoir was to be developed with a line drive strategy utilising a series of horizontal producer and injector pairs, oriented north-south. This development plan was to be evaluated and the expected outcome of the wells was to be assessed and risked.

Detailed analyses of core, well log and analogue data has led to the development of two geological "end member" scenarios. Both scenarios have been stochastically modelled using the Sequential Indicator Simulation method. The resulting equiprobable realisations have been subjected to detailed statistical well placement optimisation techniques. Based upon bivariate statistical evaluation of more than 1000 numerical well trajectories for each of the two scenarios, it was found that the wells inclinations and lengths had a great impact on the wells success, whereas the azimuth was found to have only a minor impact. After integration of the above results, the actual well paths were redesigned to meet external drilling constraints, resulting in substantial reductions in drilling time and costs.

## Introduction

Journel and Alabert (1990) stated that "the goal of detailed reservoir description is to provide a numerical model of the reservoir attributes for input into various flow simulators". Today, reservoir (flow) simulations form the basis of almost all economic decisions for a field development strategy (including IOR and EOR), and reservoir management (Haldorsen and van Golf-Racht, 1992). Even though flow simulation is probably still the most important application of numerical reservoir models, there are by now other very important applications, such as well

placement optimisation studies, the provision of a common database (forcing quantification and integration of data) and the three-dimensional visualisation of data.

This study is an example of one of these applications. Based on two-layer, single-phase flow simulation, a development plan was devised for this reservoir, utilising a series of horizontal injector and producer pairs, oriented north-south. The objective of this study was to develop a stochastic model of the reservoir, evaluate the planned drilling programme and transfer the technology to the operating environment.

To ensure the latter, the company seconded the development geologist to Heriot-Watt University for the duration of the entire study so he would gain "hands on" experience with every step within the study-process. The study-process was building on earlier work (Hern et al., 1996; Seifert et al., 1996) and involved quantitative sedimentological analysis, stochastic reservoir modelling and statistical well placement optimisation.

In this statistical well placement optimisation technique, a number of static measurements are used to identify the optimum trajectory for development wells. Based on these data, actual drilling trajectories are designed by developing "drilling diagrams" which envelope the potential range of drilling targets (Solomon et al., 1993). During the drilling process, newly developed LWD tools are able to provide new data every hour which may be quickly integrated into a deterministic framework of the models to help steer the drill bit in-between the "target boundaries" (Bryant and Baygün, 1996).

### **Geological Overview and Initial Development Plan**

The field under study is a small turbidite sandstone reservoir of late Palaeocene age located in the Northern North Sea. It comprises four way dipped closed structure which is relatively flat but has steep flanks along the channel margins. Prior to development, the field was delineated by four wells, all of which were comprehensively logged and cored.

A wide variety of facies has been identified in the core. These range from massively stacked channel sands representing high density turbidite flows to thinly interbedded very fine sands and shales that represent channel margin deposits. Relatively thick hemipelagic shales have also been identified in the core. Over parts of the field, some of the sediments have moved due to post-depositional liquefaction. This movement has caused load structures, sand injection features and where body shear has occurred, significant slumping.

The initial (Phase 1) development plan has been designed to access a proven, minimum reserves case. Three horizontal production wells have been targeted at areas where the likelihood of



encountering stacked submarine channel sands is highest, close to the existing appraisal wells. These areas also coincide with those parts of the field with the highest structural relief, and hence have the potential to achieve highest deliverability. Added together, the Phase 1 development areas are estimated to contain over half of the oil-in-place for the field.

In order to pursue a strategy which confirms the minimum reserves case while providing the potential to access additional economic reserves, the original development plan included a range of up to nine high angle/horizontal wells, comprising four producers and five injectors. The three producers drilled as Phase 1 prior to first oil, were to be followed by at least one further producer and up to five injectors comprising Phase 2.

The biggest concern regarding recovery efficiency, and the eventual Phase 2 well count, is pressure maintenance. Even in the Phase 1 development area where sand connectivity is assumed to be good, basal aquifer support has been considered to be a major uncertainty. As a result, the base case development strategy assumes that following an initial period of primary depletion during which formation pressure data will be obtained, a line drive waterflood may need to be implemented to maintain reservoir pressure above the bubble point and to improve sweep efficiency. This second phase of drilling is planned to commence once sufficient production data have been acquired to define the most appropriate water injection strategy.

#### **Data Acquisition and Analysis (Reservoir and Analogue)**

To perform any modelling work it is necessary to delineate the modelling elements and gain quantitative data on their form and spatial distribution. To acquire the appropriate data for the modelling process a multi-step approach has been employed which involves (i) identification of the lithofacies, (ii) definition of the genetic units, (iii) derivation of spatial statistics of the genetic units (proportion, geometry, size, orientation) and (iv) construction of a conceptual model.

**Identification of Lithofacies.** The sedimentological logs, probe-permeametry data, petrophysical data and core photographs were analysed with each probe-permeametry point being given a lithofacies indicator label. The probe-permeametry data gives significant control on this identification process (Hurst and Goggin, 1995). It appeared that a significant number of the sandstone "flow units" have an upward increasing permeability profile. Similar profiles have been identified in the Tabernas Basin (Kleverlaan, 1994) where it may be associated with dewatering structures. On identification of each lithofacies unit in the cored section, a full core viewing was held to calibrate the results.

On completion of the lithofacies identification from the core, petrophysical descriptors were applied to each type. These descriptors, or signatures, were then applied to the remainder of the reservoir zone in the uncored sections. In practise, this was difficult to do as the log characteristics did not allow for detailed facies identification. However, the hemipelagic shales could be identified from their "hot" gamma ray responses.

**Definition of the Genetic Units (GU's).** A genetic unit is defined as a body of rock that is distinct from other bodies on the basis of geometrical, petrophysical and spatial properties (Dreyer, 1993). This definition can be expanded to "...a genetic unit is an association of facies which are related by the same depositional process and which are distinct from other genetic units..." (Hern and Good, 1996, personal communication). Consequently, a genetic unit may contain several lithofacies types if it is believed they were deposited at the same time and have the same or similar spatial properties.

From core data, a total of seven genetic units were interpreted (Table 1). These relate to the depositional processes involved and the grain size of the resulting deposits.

**Derivation of Spatial Statistics.** The genetic units represent the basic building blocks of the reservoir model. It is therefore important to characterise the relevant GU's in terms of shape, size and orientation within the reservoir. Of fundamental importance is the proportion of a given GU at a given location within the reservoir. Some of these data can be derived from core and well data, such as proportions and thicknesses of the relevant GU's. Regional orientations on the reservoir scale will be most likely derived from regional geological interpretations, including data from nearby fields. Dipmeter data, however, may provide an indication of (local) orientation of, for example, fluvial GU's.

Other data, such as width and approximate length of GU's can only be deduced from outcrop analogue data. It is, of course, very difficult to find a "true" analogue for any reservoir (unless the very formation crops out in the "neighbourhood"). However, certain measures can be used to assess the similarity of the outcrop with the reservoir at hand (Hern and Good, 1996, personal communication). For example, thicknesses, aspect ratios and proportions of individual GU's can be compared, as well as the size of the entire depositional system.

For this study, the Eocene Ainsa II channel complex in the south-central Pyrenées was chosen as an analogue (Clark and Pickering, 1996). The Ainsa II is not a "true" analogue to the field under study. However, there are similarities between them in terms of turbidite system dimensions, channels and flow units. Integrating the quantitative sedimentological and petrophysical data from

the Ainsa II and published ancient and modern data, the key genetic units could be delineated. Data gathered included average thicknesses and proportions (from wells), and aspect ratios and estimated lengths (from outcrop) of the key GU's.

**Conceptual Reservoir Model.** Before any stochastic modelling is undertaken, it is essential that a conceptual geological model be developed. In this case, it was important to understand the stacking and channel fill patterns of the channels and flow units. Clark and Pickering (1996) have shown that in a typical upper fan channel fill, different stacking and channel fill patterns are to be expected. To capture this degree of complexity stochastically within one model is very difficult and it was therefore decided to model the two endpoints of the sedimentation process separately; "scour & fill" and "lateral accretion". The "scour & fill" model assumed the flow units to be horizontal, whilst the "lateral accretion" model had the units dipping at a low angle.

### **Reservoir Modelling Procedures**

**Modelling Technique.** The sequential indicator simulation (SIS) method (pixel-based stochastic simulation technique) was chosen over a boolean method (object-based simulation technique). The main advantage of this modelling method is its capability to reproduce very complex heterogeneity patterns, allowing for different orientations, aspect ratios and frequencies for each modelling category (discrete or continuous). This method also allows for reproduction of geological trends and facies associations through spatial cross-correlation between indicator variables. The flexibility comes from the use of one indicator variogram for each indicator variable to be modelled. Detailed discussions of the SIS technique have been provided by Deutsch and Journel (1992) and Alabert and Modot (1992). Numerous case studies have shown that SIS proves to be effective in modelling reservoir heterogeneities (Journel and Gómez-Hernández, 1989; Alabert and Massonnat, 1990; Journel and Alabert, 1990; Massonnat et al., 1992).

**Model Setup.** The aim of this study was not to produce a full field three-dimensional model for reservoir simulation purposes, but to model the reservoir heterogeneity as accurately as possible to understand its impact on well placement. As a result, stochastic modelling was only applied to model discrete variables, i.e. the key genetic units.

Geological uncertainty exists at two scales. Firstly, on a large scale, the possibility exists that there are two channel systems present within the reservoir, instead of only the one that has been found by Well A (Figure 1). To reduce this uncertainty, it was decided to focus on the northern part of the field where two of the three Phase 1 wells would be drilled. However, this model could also serve as a generic model for the southern channel system, if present. Secondly, on a smaller scale, uncertainty exists whether the sands within the channel system(s) are laterally accreted or represent

a "scour & fill" scenario (Figure 2). In order to account for this uncertainty, both possibilities, representing two sedimentological end members, have been modelled and subsequently analysed separately.

In addition, three general assumptions were made for the modelling:

- a) all structure has been removed, resulting in an orthogonal reservoir model;
- b) no faulting is present within the modelled area; and
- c) the thickness of the reservoir model was set to 80 ft even though the proven oil column is about 150 ft.

Assumptions (a) and (b) allow the model and subsequent well placement optimisation results to be adapted quickly to fit any geophysical interpretation. This was deemed important as this reservoir is currently in its earliest stage of development and the seismic interpretation is likely to be revised after more well data becomes available. Assumption (c) was made because (i) the top 20 ft of the reservoir was classed as non-pay to avoid potential poorly connected sand bodies which included sand injection features or thin, isolated turbidite flows, (ii) the uncertainty on the geophysical top structure map was about  $\pm 20$  ft and (iii) based on flow simulation studies it was decided that no producing well should go within 50 ft of the oil-water contact, to avoid water coning.

As a result the modelled area covered a volume of 4,600 x 4,300 x 80 ft. The size of the smallest genetic unit that needed to be modelled, the "slumped" GU, determined the cell size, resulting in a total model of 632,960 cells, each of which 50 x 50 x 1 ft in size.

**Sensitivity Testing.** Extensive sensitivity testing is an essential first step within the reservoir modelling procedure. In sensitivity testing, it is the aim to establish the proper parameters for both, technique specific (e.g. variogram type, search ellipsoid) and geological (e.g. lateral trends, correlation lengths) parameters. Up to thirty binary, ternary and four-component models were created for both depositional end members, using models that have a reduced total thickness of only 25 ft (to save computation time), but full lateral dimensions.

It was not possible to model all seven genetic units stochastically (Table 1) because each simulation run would take too long to complete. It was therefore necessary to group several GU's together appropriately into modelling categories. Therefore, after establishing the proper variogram parameters for each GU (e.g. variogram type, correlation lengths, anisotropies) and search neighbourhood (i.e. ellipsoid), it was investigated how well the heterogeneity would be represented using models with two, three and four modelling categories.

For the binary model, pay was modelled versus non-pay. Effectively, the clean sands were modelled versus the mixed sands and shales (Figure 3). For the ternary model, three different groupings were investigated. The most appropriate grouping modelled the shale GU versus the slumped GU versus the clean sand GU (Figure 4). For the four-component model, two different groupings were investigated. The most appropriate grouping modelled the shale GU versus the slumped GU versus the clean sand GU versus the sands with loaded structures GU (Figure 5).

By comparing Figures 4 and 5, it can be seen that the four-component model improved the level of heterogeneity by splitting the pay up into two different sand genetic units (white and light grey). If flow simulation had been the end product of this study, the four-component representation would have allowed for different effective properties within the pay sands and therefore yielded a more accurate description of the heterogeneity. This was, however, considered unnecessary, since only the intersection of sands with the wells was of interest, not their type. The binary model was not believed to be appropriate because it forced an amalgamation of the slumped GU and the shale GU into one modelling category. Because both have significantly different shapes and sizes, it would not have been possible to represent their presence appropriately within the channel sands. Their appropriate representation, however, is most crucial in this high N/G reservoir, as these govern the potential compartmentalisation of the channel sandbodies. Therefore, the approach taken in the ternary model (Figure 4, Table 1) was chosen as the optimum way to proceed.

A further complication was introduced when trying to reproduce the lateral deterministic trends as expected within this reservoir. The model was to extend beyond the main channel system to the north and south (Figure 1). Both edges are expected to have much lower N/G ratios than the channelised centre. Secondly, both edges would have different proportions of each GU, because the northern edge would represent the end of the turbidite system, exhibiting a very low proportion of hemipelagic shales but a fairly high proportion of slumped material, whereas the southern edge would represent a barrier or transition zone between two possible channel systems, therefore resulting in mixed proportions of hemipelagic shales and slumped materials. Finally, all deposits are expected to be flat lying within the edge volumes, even for the case that the channelised centre would be inclined to represent the lateral accretion system. As a result, these "edge" volumes would have had to be modelled differently from the main channelised section.

The stationarity principle in stochastic modelling ensures that a certain set of parameters, represented by indicator variograms and proportion statistics for the SIS method, will be applied and "honoured" throughout the entire model. Therefore, lateral non-stationarity could only be modelled by splitting up the model into three sections along the Y-axis, with a centre of 3000 ft, and a northern and southern edge of 650 ft each (Figure 6). Appropriate sets of statistical

parameters were defined for each section based on well data and geological assumptions with reference to the respective depositional end member to be modelled. The sections were then modelled sequentially, conditioning each section to the adjacent face of the neighbouring section.

This sequential process turned out to be complex. It became important in which order the sections were modelled. In the case of modelling the edges before the centre section, results looked much different from the case where the centre was modelled before the edges (Figure 7). This is an effect of the conditioning process using the adjacent face of the neighbouring section. When modelling the edges first, all GU's would be distributed "evenly" throughout the edge sections. This would result in a significant amount of slumped and shale GU's at the border to the centre section. These would then have to be honoured by the subsequently modelled centre section, drawing a lot of these GU's to the edge of the centre model, leaving much fewer of these behind within the centre of the centre section. The result was a sharp drop in N/G across the section boundaries (Figure 7a). When modelling the centre section first, all GU's would get distributed "evenly" and only a low proportion of the slumped and shale GU's would be placed at the border to the edges. These would then be honoured by the edge statistics, drawing a lot of the channel sands within these sections towards the centre section. The result was a transition zone of medium high N/G between the high N/G of the centre section and the lower N/G of the outer edges (Figure 7b). With respect to the geological model, the second approach was deemed more appropriate, because it resulted in a smooth transition across the boundaries of the sections. This illustrates how dependent the end result can be on the modelling approach. Hence, it is of crucial importance to check the results of each modelling step with respect to the geological model of the reservoir under study.

**Modelling and Model Descriptions.** Analysis of the geological data and the sensitivity testing, resulted in two different geological scenarios, representing the "scour & fill" and the "lateral accretion" end members. Each scenario was modelled by subdivision into three sections, the first section to be simulated (Section 1) being constrained by Well A, Sections 2 and 3 being conditioned to the adjacent faces of Section 1. For each scenario, a total of 15 equiprobable realisations were obtained.

Figure 8 shows a vertical cross-section through the "scour & fill" model. The centre has a very high proportion of channel sands (light grey) and very low proportions of slumped deposits (dark grey) and hemipelagic shale (black). It is obvious, that size and geometry information for the sand GU are of minor effect to this model. The slumped sands and shales are of much smaller size than the hemipelagic shales. The northern edge of the model (Section 2) representing the edge of the turbidite system where the channels are getting thinner and other deposits increase in proportion, is characterised by a medium N/G ratio, a slightly lower proportion of slumped deposits and a

relatively low proportion of hemipelagic shale. The ratio between the slumped and the hemipelagic shale is approximately 2:1. The southern edge of the model (Section 3), representing the area between two potential channel systems, is characterised by a medium N/G ratio and lower proportions of slumped deposits and hemipelagic shales (ratio of 1:1). Within the edge sections, the channel sands are generally situated near to the centre model, resulting in a gradual reduction of the sand proportions.

Figure 9, shows a vertical cross-section through the "lateral accretion" model. Notice the approximately 5° inclination (strong vertical exaggeration) of all genetic units in the centre model. The genetic units in the edges, however, have been modelled horizontally, as this was found more appropriate for the northern edge and southern transition zone.

To complete the visual representation of this reservoir, Figures 10 and 11 are showing areal cross-sections through both end member models. Notice the different proportions of the GU's in the northern and southern sections and the much narrower shales (black) in Figure 11, representing the thickness of the inclined shales. Further, in Figure 11, the boundaries for the sections and the well trajectories (below) have been superimposed.

**Assessment of Potential Object-based Modelling.** For the channel genetic unit, excellent geometry and size data was available from outcrop analogue. This would destine this genetic unit to be best modelled using an object-based approach. However, these geometries and sizes have lost importance due to the extremely high N/G ratio within the centre portion of the reservoir. Geometry and size data for the slumped and shale GU's are much more important as they govern the inter-connectivity of the sands. Since their sizes and geometries are only poorly known, they are likely to be modelled best using a pixel-based approach. In conclusion, this particular reservoir is likely to be modelled optimally with a pixel-based approach such as SIS. Object-based modelling would introduce geometrical artefacts based on assumed geometries that are not known. However, in cases where N/G ratios are significantly lower, a good knowledge of the channel geometries may elevate an object-based or combined modelling approach to be the method of choice.

### **Well Placement Optimisation Procedures**

The resulting 15 realisations per geological end member have been subsequently, but independently subjected to detailed statistical well placement optimisation techniques (Seifert et al., 1996). In essence, originating from eleven cluster locations (Figure 11), a variety of linear wells have been drilled at every 15° azimuth with varying well lengths (ranging from 1000 to 2250 ft) and inclinations (ranging from 0° to 5°). A total of 1,004 numerical wells were drilled through each of

the 30 realisations. Along each well trajectory, the amount of channel sand penetrated (SGUP's - "Sand GU Proportions") and the number of sand bodies intersected (SBI's) were extracted and analysed. The following bivariate statistical evaluation of these data resulted in a statistical database of 60,240 datapoints.

### **Analysis of Results**

Bivariate statistical analysis (SGUP's and SBI's) of the 2 x 15 realisations results in minimum, mean and maximum outcome values which need to be evaluated. The mean value represents the likely outcome and the difference between the minimum and the maximum values represents the range of the possible outcomes. The range of SGUP's and SBI's for each well trajectory can be quantified in terms of:

- location within the reservoir model;
- azimuth angles;
- angles of inclination; and
- well success versus well lengths.

Because this paper intends to show the procedure rather than actual results, the presentation of the analysis will focus on the results from Cluster 4 (located in the western centre of the centre section) and the 15 realisations with respect to the "scour & fill" scenario.

**Location within the Reservoir Model.** It is aimed to keep all development wells in the area of highest N/G which corresponds to the centre section of the model. Therefore, eight of the clusters have been placed all across the centre section, making sure that the wells do not extend beyond the edges (Figure 11). By analysing these clusters only, the outcomes evaluated will refer to the most likely case. However, in order to assess the impact on the wells success in the case that the actual wells will extend beyond the first channel system into the transition zone to the south, two clusters have been placed there, for analysis. Similarly, one cluster was placed in the very north to provide an outcome assessment for the case that the wells would reach the reservoir depth prematurely and drill through the edge of the turbidite system. These clusters could be analysed all together or separately, taking their locations into account.

**Azimuth Angle.** For each well cluster, 12 azimuth angles were analysed which covered the whole 360 degree spectrum on a 15 degree incremental basis. Figure 12 plots the sand genetic unit proportions (SGUP's) versus azimuth, for Cluster 4. All wells have the same inclination and length. As can be seen, the mean value remains almost the same throughout the dataset and the range of possible values displays only little variation. It is therefore obvious that azimuth (i.e. drilling across or along channel) will have a minor impact on the success of the wells. The reason



is that because of the very high N/G, channel bodies tend to lie next to each other and are not often separated by slumped material or hemipelagic shales. This is a very important result, particularly when considering that the drilling platform location is one of the external constraints on the drilling programme. Therefore, the azimuth of 15 degrees was considered optimum because it allowed to minimise the well length prior to entering the reservoir at target depth and azimuth.

**Angle of Inclination.** By changing the inclination angles from 0 degrees (horizontal) to 5 degrees (sub-horizontal) in 1 degree increments, it is apparent in Figure 13 (for optimum azimuth) that even though the mean value doesn't change much, the range of outcome values reduces significantly, as the inclination angle increases to about 3 degrees. For example, the minimum value for the 3 degree well is more than 20% greater than for the 1 degree well, therefore reducing the risk of drilling a poor well.

With increasing the inclination, one can also observe that the amount of bodies intersected increases (Figure 14). Compared to the horizontal well of 0 degrees inclination, the 3 degree inclined well almost triples the average (mean) number of sand bodies intersected, therefore significantly increasing the connected pay-volume. Upon further inclination, the average (mean) values remain very similar, only the range increases significantly. However, because of the very high N/G ratio in this reservoir, this indicator is of minor importance, especially when considering that the intervening shales may not act as barriers, therefore, not isolating one "sandbody" from another.

It has been concluded, that inclination of 3 degrees is the optimum drilling angle, because it allows a penetration of the target zone of up to 1500 ft. Upon further inclining the well, well length would have to be reduced in order to not extend into the 50 ft envelope of the oil-water contact. The outcome of such a well, however, would be similar to the 3 degree inclined well.

**Well Success as a Function of Well Length.** From reservoir simulation studies, it had been concluded that a certain amount of net pay intersected by each of the development wells was required for well deliverability. Therefore, six different well lengths have been investigated in this study. Figure 15 plots the cumulative pay intersected as a function of well length, for the optimum azimuth with respect to the location of the drilling platform. There appears to be a linear relationship between cumulative pay and well length. Using the slope of the lines connecting the values, one can identify what well length is likely to be needed to ascertain a minimum penetration of net pay.

It is further of importance for the drilling crew, how much shale (proportion and number of bodies) are likely to be encountered for a given well. Figure 16 gives an example of the likely proportions of each genetic unit to be encountered during drilling.

**General Comments.** It is important to note that the results of the well placement optimisation have to be analysed taking into account geometrical considerations when setting up the model and the well trajectories as well as the geological assumptions that led to the stochastic models. For example, the optimum inclination of 3 degrees is based on the assumption, that a linear well entering the target zone 20 ft below top structure is not to come within 50 ft of the oil-water contact in a 150 ft thick reservoir section. A well inclined at a greater angle would yield similar outcomes but violate the geometrical constraints of the reservoir model and is, therefore, considered only sub-optimum.

Secondly, this analysis is based upon only two static parameters, the amount (or proportion) and number of bodies of net pay intersected. Because of the high N/G, the second parameter is of minor importance. In order to make these interpretation results more robust, one should engage into multivariate statistical evaluations, taking dynamic parameters into account as well. This could be done, for example, by modelling the inflow performance of the best well trajectories and relating this to different well lengths. For example, using tensors for the dynamic properties, derived from lamina scale models of the genetic units, the azimuth at which the channel bodies are being intersected for drainage may become important.

Finally, taking such multivariate evaluations into account, wells could be ranked again and by assigning confidence intervals to the results, risk and uncertainty could be assessed more accurately.

### **Impact of Results on Drilling Plan**

The results from the above analysis showed that azimuth would have a minor impact on the success of the well. Because the drilling platform location is one of the given constraints, a target azimuth of 15 degrees was considered optimum as it reduces the well length prior to entering the reservoir at target depth (Figure 17), while keeping the well in the across-channel orientation. For the drilling process, this not only resulted in time savings per well but further reduced the amount of material used (i.e. pipe, drill-bit), ultimately resulting in reductions in drilling costs.

To date, three development wells (Phase 1) were drilled following the recommendations as closely as practical. The wells showed very high sand proportions as predicted. However, the wells also showed that some of the geological assumptions made prior to the modelling process are invalid.

For example, the edge of the sand prone part of the system is very abrupt whereas it was modelled as a smooth transition across the boundaries of the sections.

This proves that there is a need for much improved understanding of the sedimentological processes that generate turbidite reservoirs. Furthermore, detailed quantitative sedimentological data for a wide range of submarine channel systems is needed. Such data can be used in the modelling process to investigate sedimentological uncertainties and will result in greater geological control during the modelling process and in greater confidence in the stochastic end product.

### **Summary and Conclusions**

This paper describes the hybrid deterministic-stochastic modelling of genetic unit distributions within a deep marine clastic (turbidite) reservoir. Using Sequential Indicator Simulation (SIS), two end member scenarios have been modelled in a part of the reservoir in order to account for uncertainties associated with the geological model. Extensive sensitivity tests were run, in 2-D and 3-D, in order to derive the appropriate modelling parameters. A pixel-based modelling technique is believed to be best suited for modelling this particular reservoir, because of the lack of good geometry data on the most important elements of this reservoir, the slumped sands and the hemipelagic shales.

The objective of this study was to evaluate the existing development drilling plan, which consisted of pairs of horizontal injectors and producers, oriented parallel to the north. The resulting set of realisations for both end members, were subjected to detailed well placement optimisation and analysis techniques. The optimum wells were defined in terms of azimuth, inclination angle and well length. These results had to be put into context of the structural and bedding dip as well as existing external constraints in order to derive the optimum drilling trajectories for the reservoir. As a result, the existing drilling programme was revised, saving significant amounts of drilling time, materials and ultimately costs.

It is acknowledged that there still exists uncertainty within several elements of this study. This includes uncertainty as to the stacking and fill pattern of the channels, the identification of petrophysical GU-descriptors applied to the uncored sections of the wells, the stochastic modelling procedure and the static bivariate statistical analysis of the data. However, it is believed that these uncertainties have been dealt with appropriately considering the time constraints and objectives of the study.

Today, after drilling of three development wells, it can be concluded that azimuth, inclination and well length have a relatively minor impact on the wells which is largely due to the high N/G ratio

of the reservoir. The outcomes of the (successful) wells, however, raise questions about the validity of the stochastic model which is based on geological assumptions which in turn were derived from much fewer well data. It is evident that a better quantitative sedimentological understanding of this reservoir would have resulted in a more reliable reservoir model. Thus, this study should be seen as a stepping stone in the development process. The new wells provide quantitative data in lateral dimensions which incorporated into a new modelling study would yield a reservoir model which is much better constrained geologically, as this study could have been.

In summary, a thorough understanding of the sedimentology as well as the uncertainties associated with the stochastic modelling process are necessary prerequisites for developing appropriate stochastic reservoir models.

### **Acknowledgements**

The authors wish to thank C. Hern, J. Clark, K. Pickering, P. Sherwood and D. Macklon for their helpful comments during the duration of the project. Their expertise helped ensure that the data was obtained and interpreted in a way that could readily benefit the development of the field. Furthermore, the authors wish to thank John Warrender who critically reviewed the manuscript. Thanks are also due to the managements of Conoco (UK) Ltd and LASMO North Sea Plc for permission to publish this study. Finally, the authors are grateful to Landmark Graphics Ltd for the donation of their SGM software.

### **References Cited**

- Alabert, F.G. and Massonnat, G.J., 1990, "Heterogeneity in a Complex Turbiditic Reservoir: Stochastic Modelling of Facies and Petrophysical Variability", paper SPE 20604 presented at the 1990 SPE Annual Technical Conference & Exhibition, New Orleans, LA, Sept. 23-26, p. 775-790
- Alabert, F.G. and Modot, V., 1992, "Stochastic Models of Reservoir Heterogeneity: Impact on Connectivity and Average Permeabilities", paper SPE 24893 presented at the 1992 SPE Annual Technical Conference & Exhibition, Washington, DC, Oct.4-7, p. 355-370
- Bryant, I.D. and Baygün, B., 1996, Reservoir Description for Optimal Placement of Horizontal Wells, paper SPE 35521 presented at the 1996 SPE/NPF European 3-D Reservoir Modelling Conference, Stavanger, Norway, April 16-17, p. 301-305
- Clark, J.D. and Pickering, K.T., 1996, *Submarine Channels: Processes and Architecture*, Vallis Press, London, 231 p.
- Deutsch, C.V. and Journel, A.G, 1992, *GSLIB - Geostatistical Software Library and User's Guide*, Oxford, Oxford University Press, 340 p.

- Dreyer, T., 1993, "Quantified Fluvial Architecture in Ephemeral Stream Deposits of the Esplugafreda Formation (Palaeocene), Tremp-Gaus Basin, Northern Spain" *Alluvial Sedimentation*, IAS Special Publication No.17, p. 337-362
- Haldorsen, H.H. and van Golf-Racht, T., 1992, "Reservoir Management into the Next Century", SEG Investigations in Geophysics No.7, *Reservoir Geophysics*, R.E. Sheriff (ed.), Society of Exploration Geophysics, Tulsa, p. 12-24
- Hern, C.Y., Lewis, J.J.M., Seifert, D. and Steel, N.C.T., 1996, "Geological Aspects of Model Construction For Well Placement Optimization in a Mixed Fluvio-Aeolian Reservoir", presented at the 1996 AAPG Annual Meeting, San Diego, CA, May 19-22, Annual Convention Program (abs.), p. A64
- Hern, C.Y. and Good, T., 1996, personal communication
- Hurst A. and Goggin, D., 1995, "Probe permeametry: An overview and bibliography", *AAPG Bulletin*, Vol.79, No.3 (March), p. 463-473.
- Journel, A.G. and Gómez-Hernández, J.J., 1989, "Stochastic Imaging of the Wilmington Clastic Sequence", paper SPE 19857 presented at the 1989 SPE Annual Technical Conference & Exhibition, San Antonio, TX, Oct.8-11, p. 591-606
- Journel, A.G. and Alabert, F.G., 1990, "New Method for Reservoir Mapping, *Journal of Petroleum Technology*, Feb., p. 212-218
- Kleverlaan, K., 1994, "Architecture of a Sand-Rich Fan From The Tabernas Submarine Fan Complex, SE Spain", presented at the SEPM Gulf Coast Section 15th Annual Research Conference, Houston, TX, Dec.4-7, p. 209-216
- Massonnat, G.J., Alabert, F.G. and Giudicelli, C.B., 1992, "Anguille Marine, a Deepsea-Fan Reservoir Offshore Gabon: From Geology to Stochastic Modelling", paper SPE 24709 presented at the 1992 SPE Annual Technical Conference & Exhibition, Washington, DC, Oct.4-7, p. 477-492
- Seifert, D., Lewis, J.J.M., Hern, C.Y. and Steel, N.C.T., 1996, "Well Placement Optimisation and Risking using 3-D Stochastic Reservoir Modelling Techniques" paper SPE 35520 presented at the 1996 SPE/NPF European 3-D Reservoir Modelling Conference, Stavanger, Norway, April 16-17, p. 289-300
- Solomon, S.T., Ross, K.C., Burton, R.C. and Wellborn, J.E., 1993, "A Multi-Disciplined Approach to Designing Targets for Horizontal Wells", paper SPE 25506 presented at the 1993 SPE Production Operations Symposium, Oklahoma City, OK, March 21-23, p. 53-67

Category	Genetic Unit Description	Interpretation
<b>channel sand</b>	clean sandstones, often stacked	high density turbidites
	argillaceous sandstones, often stacked	low density turbidites
	clean sandstones, with mixed sandstones and shales at tops	high density turbidites topped by "load" structures and slumped materials
	clean sandstones, with mixed sandstones and shales at base	high density turbidites with "loaded" shales and sandstones at base
<b>slumped</b>	mixed sandstones and shales, often containing clastic injections	slump deposits and sandstone injections
	mixed sandstones and shales, often containing clastic injections	slump deposits and sandstone injections
<b>shale</b>	bioturbated mudstone	hemipelagic shales

Table 1: Modelling categories, GU description and interpretation.

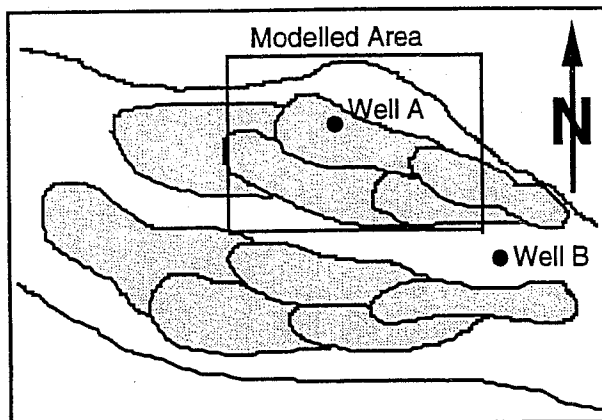


Figure 1: Channel model and modelled area.

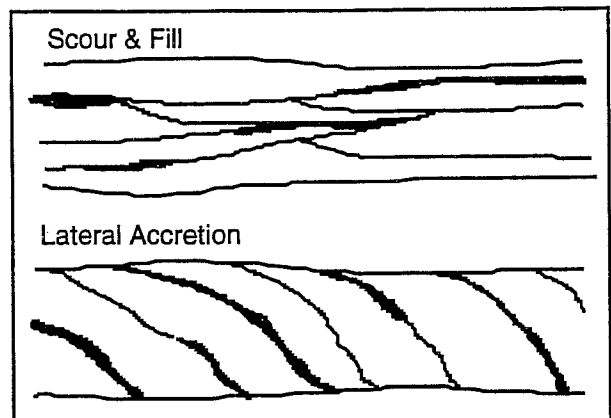


Figure 2: Channel fill scenarios.

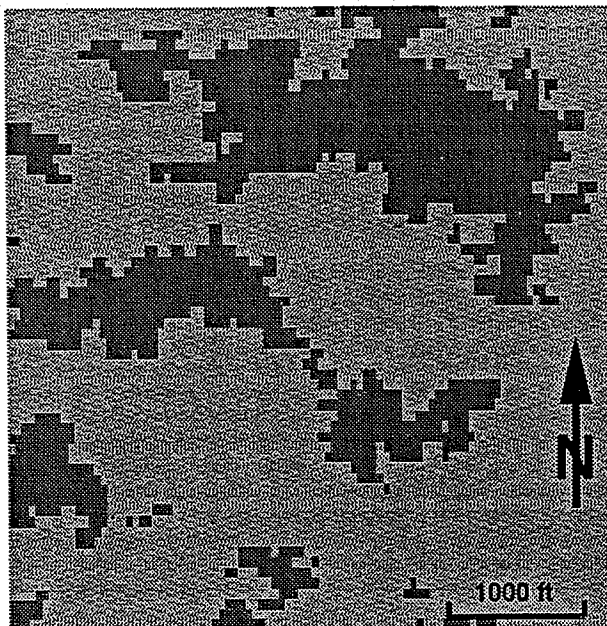


Figure 3: Binary model (areal cross-section). Sand (light) vs. non-pay (dark).

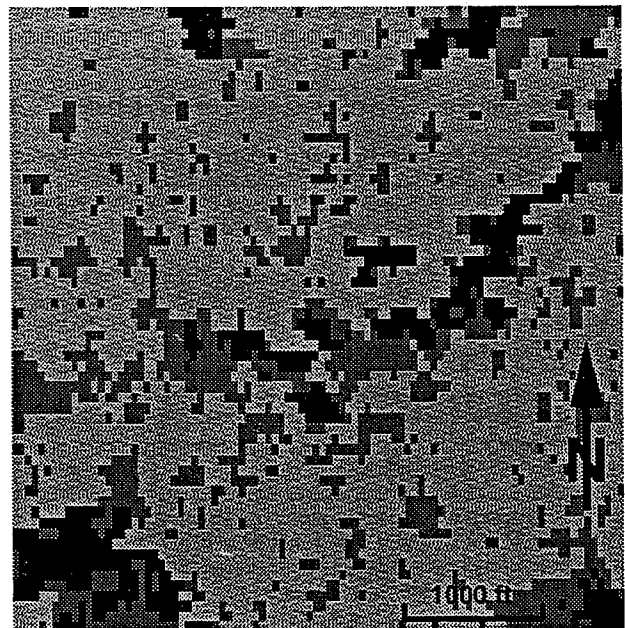


Figure 4: Ternary model (areal cross-section). Sand (light) vs. slumped (dark) vs. shale (black).

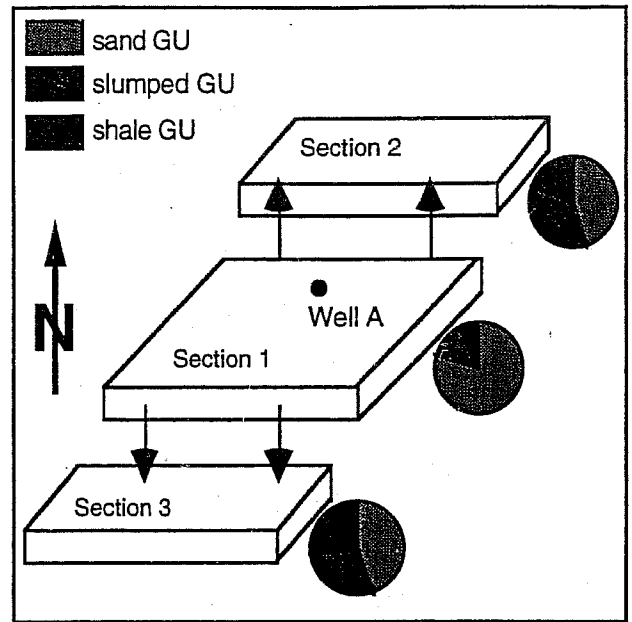
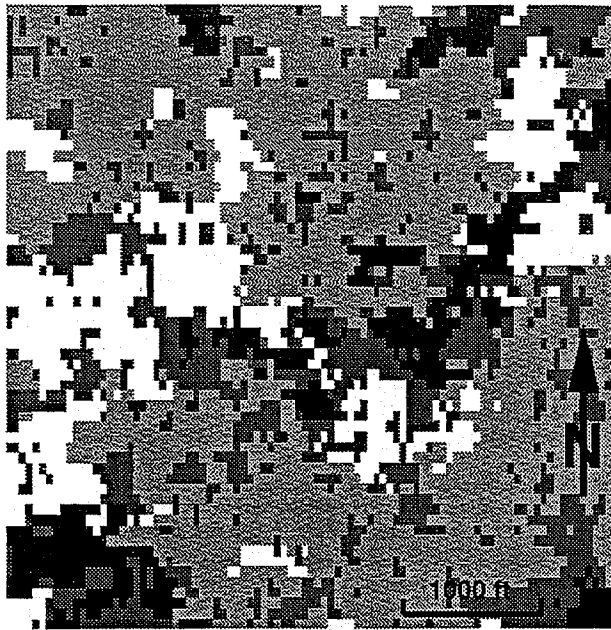


Figure 5: Four-component model (areal cross-section). Figure 6: Sub-division of model. Pie diagrams Sand A (white) vs. sand B (light) vs. slumped (dark) vs. shale (black). show proportions of GU's present within sections.

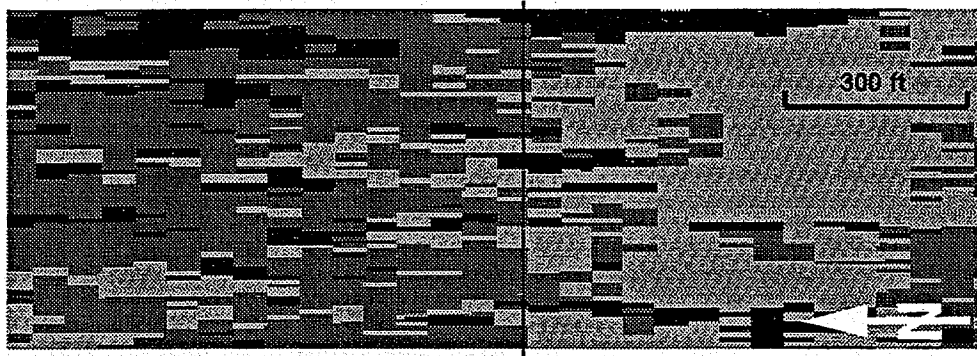


Figure 7a: Vertical cross-section (80 ft). Modelling the edge first (left) results in a sharp contrast across the boundary of the sections.



Figure 7b: Vertical cross-section (80 ft). Modelling the centre first (right) results in a smooth transition across the boundary of the sections.



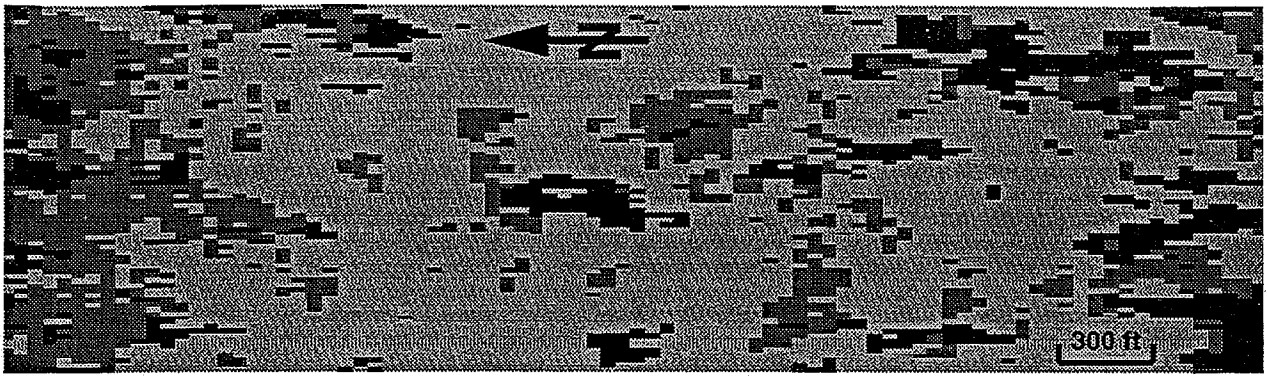


Figure 8: Vertical cross-section (80 ft) of the "scour & fill" scenario.

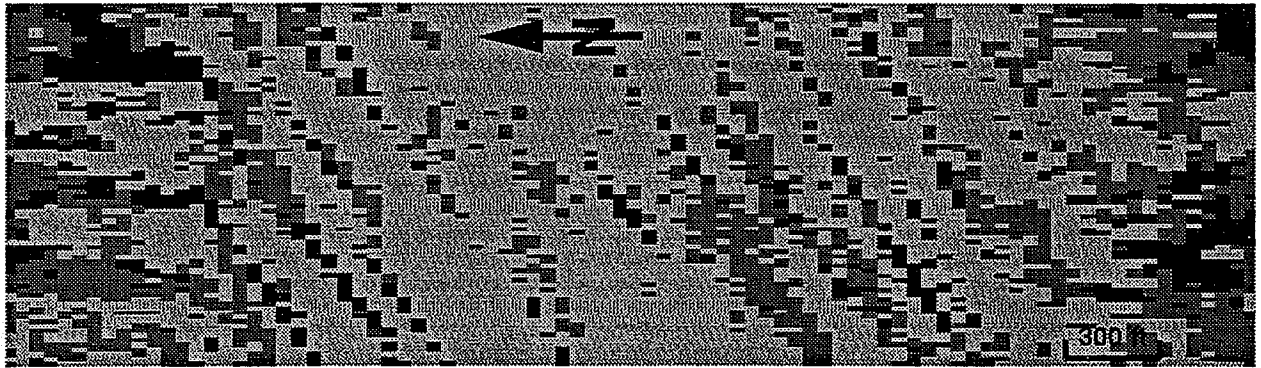


Figure 9: Vertical cross-section (80 ft) of the "lateral accretion" scenario.

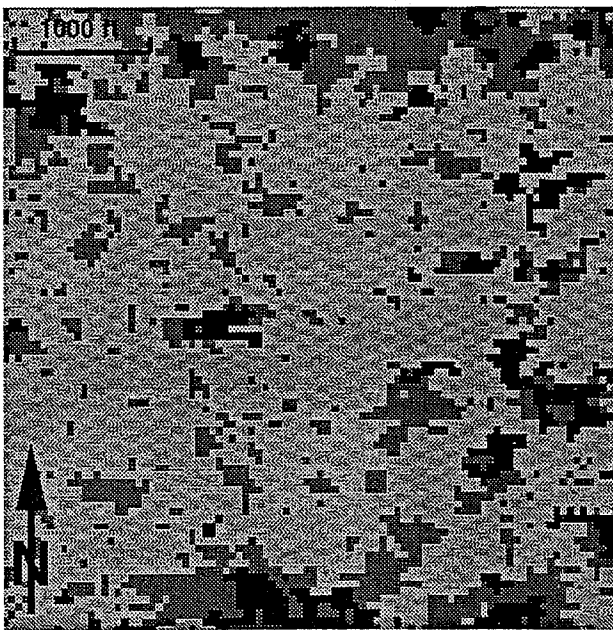


Figure 10: Areal cross-section of the "scour & fill" scenario.

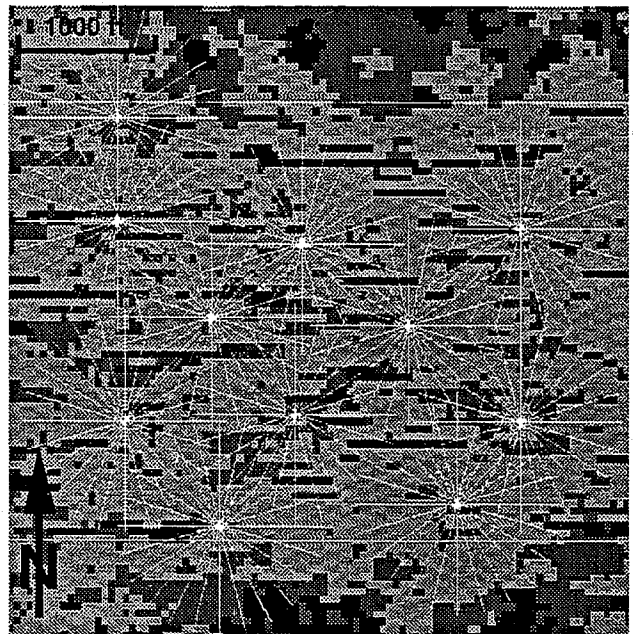


Figure 11: Areal cross-section of the "lateral accretion" scenario. Well trajectories and boundaries of sections are superimposed.



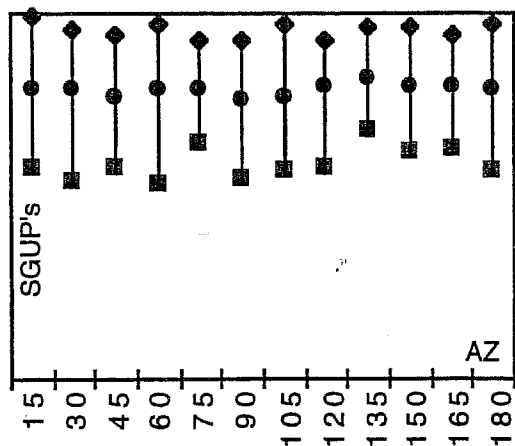


Figure 12: Cluster 4, "scour & fill" model, INC=3°; well length=1500 ft. Sand proportions vs. azimuth.

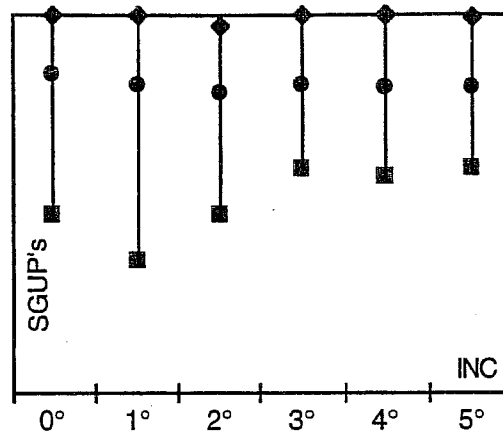


Figure 13: Cluster 4, "scour & fill" model, well length=1500 ft. Sand proportions vs. inclination.

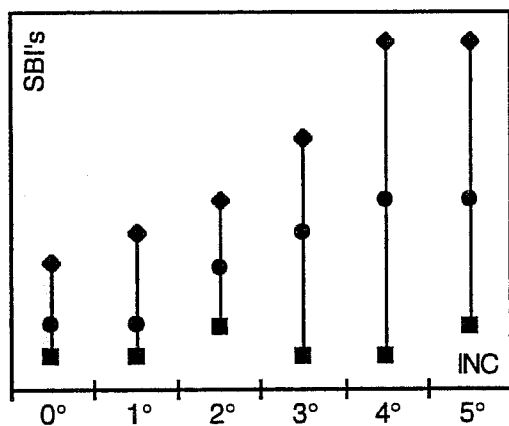


Figure 14: Cluster 4, "scour & fill" model, well length=1500 ft. Sand bodies intersected vs. inclination.

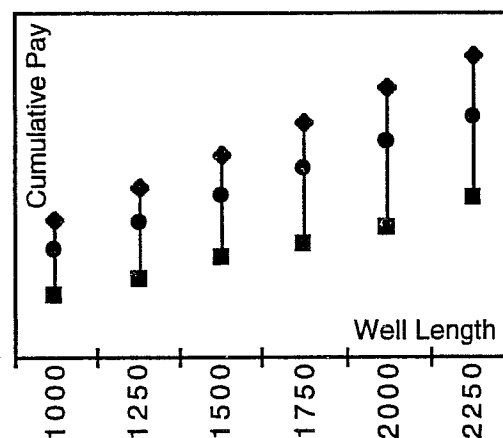


Figure 15: Cluster 4, "scour & fill" model. Cumulative pay vs. well lengths for optimum azimuth.

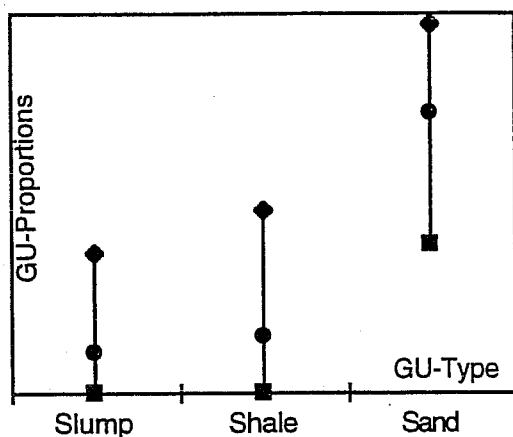


Figure 16: Cluster 4, "scour & fill" model, INC=3°, well length=1500 ft, AZ=30°. Genetic unit proportions by genetic unit type.

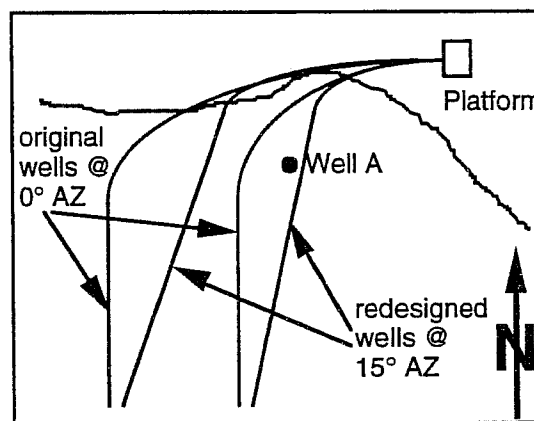


Figure 17: Original and revised drilling plan (schematic).



# Improved Characterization Of Reservoir Behavior By Integration Of Reservoir Performance Data And Rock Type Distributions

David K. Davies,<sup>1</sup> Richard K. Vessell,<sup>1</sup>  
Louis E. Doublet,<sup>2</sup> and Thomas A. Blasingame<sup>2</sup>

## ABSTRACT

An integrated geological/petrophysical and reservoir engineering study was performed for a large, mature waterflood project (>250 wells, ~80% water cut) at the North Robertson (Clear Fork) Unit, Gaines County, Texas. The primary goal of the study was to develop an integrated reservoir description for "targeted" (economic) 10-acre (4-hectare) infill drilling and future recovery operations in a low permeability, carbonate (dolomite) reservoir. Integration of the results from geological/petrophysical studies and reservoir performance analyses provide a rapid and effective method for developing a comprehensive reservoir description.

This reservoir description can be used for reservoir flow simulation, performance prediction, infill targeting, waterflood management, and for optimizing well developments (patterns, completions, and stimulations). The following analyses were performed as part of this study:

- Geological/petrophysical analyses: (core and well log data)
  - "Rock typing" based on qualitative and quantitative visualization of pore-scale features.
  - Reservoir layering based on "rock typing" and hydraulic flow units.
  - Development of a "core-log" model to estimate permeability using porosity and other properties derived from well logs. The core-log model is based on "rock types."
- Engineering analyses: (production and injection history, well tests)

- Material balance decline type curve analyses to estimate total reservoir volume, formation flow characteristics (flow capacity, skin factor, and fracture half-length), and indications of well/boundary interference.
- Estimated ultimate recovery analyses to yield movable oil (or injectable water) volumes, as well as indications of well and boundary interference.
- Well tests to provide estimates of flow capacity, indications of formation damage or stimulation, and estimates of drainage (or injection) volume pressures.

Maps of historical production characteristics (contacted oil-in-place, estimated ultimate recovery, and reservoir pressure) have been compared to maps generated from the geologic studies (rock type, permeability-thickness, hydrocarbon pore volume) to identify the areas of the unit to be targeted for infill drilling. Our results indicate that a close relationship exists between the rock type distribution and reservoir performance characteristics throughout the unit.

The reservoir performance data also suggest that this reservoir depletes and recharges almost exclusively according to the rock type distribution. This integration of "rock" data and the reservoir performance attributes uses existing data and can eliminate the need for "evaluation" wells, as well as avoiding the loss of production that occurs when wells are shut-in for testing purposes.

In short, a comprehensive analysis, interpretation, and prediction of well and field performance can be completed quickly, at a minimal cost. This analysis can be used to directly improve our understanding of reservoir structure and performance behavior in complex formations.

<sup>1</sup> David K. Davies & Associates, Inc., Kingwood, Texas

<sup>2</sup> Texas A&M University, College Station, Texas

## INTRODUCTION

This study was funded in part by the U.S. Department of Energy as part of the Class II Oil Program for improving development and exploitation of shallow-shelf carbonate reservoirs. According to the DOE, shallow-shelf carbonate (SSC) reservoirs in the USA originally contained >68 billion bbls of oil ( $10.81 \times 10^9$  m<sup>3</sup>)--or about one-seventh of all the oil discovered in the Lower 48 States. Recovery efficiency in such reservoirs is low, as only 20 billion bbls of oil have been produced, and current technology may only yield an additional 4 billion bbls (Pande, 1995).

The typical low recovery efficiency in SSC reservoirs is not restricted to the USA--it is a worldwide phenomenon. SSC reservoirs such as the North Robertson (Clear Fork) Unit (NRU) share a number of common characteristics (Pande, 1995), including:

- A high degree of areal and vertical heterogeneity, relatively low porosity and low permeability,
- Reservoir compartmentalization, resulting in poor vertical and lateral continuity of the reservoir flow units and poor sweep efficiency,
- Poor balancing of injection and production rates, and early water breakthrough in certain areas of the reservoir. This indicates poor pressure and fluid communication and limited repressuring in the reservoir, and
- Porosity and saturation (as determined from analysis of wireline logs) do not accurately reflect reservoir quality and performance.

Production at the NRU is from the Lower Permian Glorieta and Clear Fork Carbonates. The reservoir interval is thick, with a gross interval of approximately 1,400 ft (427 m), and more than 90% of the interval has uniform lithology (dolostone). Unfortunately, the interval is characterized by a complex pore structure that results in extensive vertical layering. The reservoir is characterized by discontinuous pay intervals and high residual oil saturations (35% to 60%, based on steady-state measurements of relative permeability). The most important, immediate problem in the field is that

porosity and saturation determined from logs do not accurately reflect reservoir quality and performance.

Given these reservoir characteristics, the ability to accurately target infill well opportunities is critical because blanket infill drilling will be uneconomic in most cases. For this particular study, the cost-effective, and readily available reservoir characterization tools outlined in this work allowed us to optimally target specific well locations. After implementing a targeted infill drilling program, the total production at the NRU increased over 30 percent, while the total well count increased by only 7 percent.

## HISTORICAL BACKGROUND

The NRU is located in Gaines County, west Texas, on the northeastern margin of the Central Basin Platform (Figure 1). The hydrocarbon-bearing interval extends from the base of the Glorieta to the base of the Lower Clear Fork, between correlative depths of approximately 6,160-7,200 ft (1,877-2,195 m). The unit includes 5,633 surface acres (2253 hectares, 22.8 km<sup>2</sup>) containing a total of 270 wells (November, 1996). This includes 156 active producing wells, 113 active injection wells, and 1 fresh water supply well.

### Development and Production History

Production from the North Robertson field area began in the early 1950s with 40-acre (16-hectare) primary well development. This 40-acre primary development resulted in 141 producing wells by 1965. The NRU was formed effective March, 1987 for the purpose of implementing waterflood and infill drilling operations and nominal well spacing was reduced from 40 acres to 20 acres (8 hectares). Secondary recovery operations were initiated after unitization and in conjunction with infill drilling. Most of the 20-acre infill drilling was completed between unitization and the end of 1991.

The contacted original oil-in-place from material balance decline type curve analysis is estimated to be 262 million bbls ( $41.66 \times 10^6$  m<sup>3</sup>), with an estimated ultimate recovery factor of approximately 15% (primary and secondary) based on the current production and workover schedule. Figure 2 presents the production and injection history of the unit from development in 1956 through November 1996.

The total oil and water volumes produced and injected since field development are tabulated below:

<u>Time Frame</u>	<u>Oil Produced</u> (mil. bbls)	<u>Water Produced</u> (mil. bbls)	<u>Water Injected</u> (mil. bbls)
As of 1987 (primary)	17.5	8.2	0.0
1987-1996 (secondary)	9.3	28.3	64.2

Prior to 10-acre (4-hectare) infill drilling, the total unit production rates were approximately 2,740 STBO/D (436 m<sup>3</sup>/day), 1,130 MSCF/D gas (32,000 m<sup>3</sup>/day), and 12,230 BW/D (1,945 m<sup>3</sup>/day). Water injection prior to the infill program was approximately 19,000 BWI/D (3,021 m<sup>3</sup>/day), with injection water comprised of produced water, and fresh water from the Ogallala aquifer obtained from a water supply well within the unit.

The eighteen (14 producers, 4 injectors) 10-acre infill wells that were drilled during the second and third quarters of 1996 have increased unit production rates to 3,600 STBO/D, 1,700 MSCF/D gas, and 13,500 BW/D. Current injection at the unit is approximately 19,600 BWI/D.

The well configuration at the NRU is an East-West line drive pattern (staggered five-spot) as shown in Figure 3, and was developed for optimum injectivity and pressure support. Sweep efficiency is difficult to quantify due to differences in depositional environments throughout the unit. Fortunately, these differences are easily identified on the basis of reservoir rock type.

## GEOLOGIC STUDY

This geological/petrophysical reservoir characterization of the NRU involved the following methodologies:

- Development of a depositional and diagenetic model of the reservoir,
- Definition of "rock types" based on pore geometry and development of the rock-log model,
- Rock type extension to non-cored wells using the rock-log model,
- Definition of flow units and cross-flow barriers, and

- Mapping of reservoir parameters (thickness,  $\phi h$ ,  $kh$ , and hydrocarbon pore volume) and rock type for each flow unit.

The purpose of the geological/petrophysical portion of this study was to identify and map individual hydraulic flow units (HFU's) to evaluate the potential for continued development drilling. Flow units had to be readily identified using wireline logs because core data are sparse (8 wells). Thus, the fundamental reservoir description is well log-based. However, because values of porosity and saturation derived from routine well log analysis do not accurately identify productive rock in most shallow-shelf carbonates, it is necessary to develop a core- and rock-log model that allows for the prediction of another producibility parameter--in this case formation permeability.

A geologic model is developed for the reservoir, based fundamentally on the measurement of pore geometrical parameters. Pore-level reservoir modeling allows for improved accuracy in the identification and prediction of rock types, permeability, and the identification of flow units. Pore geometry attributes were integrated with well log data to allow for log-based identification of intervals of rock with different capillary characteristics, as well as the prediction of permeability throughout the unit.

No new wells were drilled to aid the reservoir description. The existing database consisted of conventional cores from eight wells, and relatively complete log suites in 120 wells consisting of:

- Gamma ray, GR
- Photoelectric capture cross-section, PE
- Compensated neutron porosity,  $\phi_N$
- Compensated formation bulk density,  $\rho_b$
- Dual laterolog (LLD and LLS--deep/shallow resistivities)
- Borehole caliper

## Pore Geometry Modeling

At the NRU, no strong relationship exists among core derived values of porosity, permeability, and depositional environment, as indicated by the wide scatter of data points shown in Figures 4 and 5. Different environments exhibit similar ranges of

porosity and permeability which is not surprising as the carbonates have undergone significant diagenetic alteration of pore geometry after deposition. Thus, there is no fundamental relationship between depositional environment and permeability. This is a common problem in many diagenetically-altered reservoirs (sandstones and carbonates).

Analysis of 3D pore geometry data allows reservoir characterization efforts to be pore system oriented. The resulting reservoir models are based on characteristics of the pore system. Analysis of pore geometry involves identification of individual pore types and rock types.

Quantitative analysis of pore geometry is used to develop the vertical reservoir layering profile of the reservoir (*i.e.*, to identify vertical compartmentalization) at the NRU. Integration of pore scale observations with depositional and diagenetic data allows for the determination of the areal compartmentalization and permeability distributions within the reservoir.

**Pore Types:** The determination of pore types in a reservoir requires the use of rock samples (conventional core, rotary sidewall cores, and cuttings samples in favorable circumstances). In this study, analyses were based on the end-trims of 1 inch plugs removed from conventional cores. Individual pore types were classified in terms of the following parameters:

**Pore Body Size and Shape:** Determined using scanning electron microscope (SEM) image analysis of the pore system (Clelland and Fens, 1991).

**Pore Throat Size:** Determined through capillary pressure analysis and SEM analysis of pore casts (Wardlaw, 1976).

**Aspect Ratio:** The ratio of pore body to pore throat size. This is a fundamental control on hydrocarbon displacement (Wardlaw, 1980; Li and Wardlaw, 1986).

**Coordination Number:** The number of pore throats that intersect each pore (Wardlaw and Cassan, 1978).

**Pore Arrangement:** The detailed distribution of pores within a sample (Wardlaw and Cassan, 1978).

These parameters are combined to yield a classification of the various pore types in these rocks (Table 1). Pore types were identified in each

core sample (350 samples in this study). Commonly, each sample contained several different pore types. It was therefore necessary to group pore types into rock types.

For each sample, the volumetric proportion of each pore type was determined using SEM-based image analysis (Clelland and Fens, 1991). Because the pore throat size is known for each pore type, it is possible to develop a pseudo-capillary pressure curve for each sample using the well known relation (Thomeer, 1983):

$$p_c = \frac{214}{d} \dots \dots \dots (1)$$

for which  $p_c$  is mercury-air capillary pressure in psia and  $d$  is pore throat diameter in microns ( $10^{-6}$  m).

The validity of the geologically-determined rock types was evaluated using mercury capillary pressure analysis of selected samples. Our results reveal differences between the rock types in terms of the measured capillary characteristics (Figure 6 and Table 2). Such cross-checks allow for independent validation of the pore geometrical classification of rock types. Mercury capillary pressure data are also used to aid in the determination of pore throat sizes.

**Rock Types:** A "rock type" is an interval of rock characterized by a unique pore structure (Archer and Wall, 1986), but not necessarily a unique pore type. In this study, eight rock types were identified, based on the relative volumetric abundance of each pore type (Figure 7). Each rock type is characterized by a particular assemblage (suite) of pore types (Ehrlich and Davies, 1989). For example, Rock Type 1 is dominated by Pore Type A, while Rock Type 2 contains few pores of Type A and is dominated by Pore Types B and C (Figure 7). Identification of rock types is fundamentally important because porosity and permeability are related within a specific pore structure (Calhoun, 1960).

## Porosity-Permeability Relationship

At the NRU, the basic relationship between porosity and permeability exhibits a considerable degree of scatter (up to 4 orders of magnitude variation in permeability for a given value of porosity). In contrast, the porosity and permeability are closely related for each rock type (Figure 8).

Permeability calculations on the basis of rock type have an error range of less than one-half decade for most samples. Regression equations for permeability as a function of porosity were developed for each rock type to quantitatively define each relationship (using log-log plots to avoid zero porosity intercepts). These equations were used in the field-wide prediction of permeability using well logs (permeability being a function of porosity and rock type).

Average values of porosity and permeability are given for each rock type in Table 3. We immediately note that the highest porosity rocks at the NRU do not exhibit the highest permeability. The principal pay rock at the NRU is Rock Type 1. Rock Type 1 has significantly lower values of porosity than Rock Type 4 (flow barrier). This characteristic has important implications in terms of selecting zones to perforate. Given our observations, the zones with the highest porosity should not always be the principal targets in this field.

### Rock-Log Model

Analysis of pore geometries reveal that eight rock types occur in the NRU. Six of the rock types are dolostone, one is limestone (non-pay--structurally low and water-bearing in this field), and one is shale (Table 3). Individual rock types can be recognized using specific "cut-off" values based on analysis of environmentally corrected and normalized well log responses and using the comparison of core-based determination of rock type.

The well log responses used to isolate the eight different rock types for the NRU study were:

- $\rho_{maa}$  versus  $U_{maa}$  with gamma ray (Figure 9)
  - This data plot allows the discrimination of dolostone, limestone, anhydritic dolostone, siltstone, and shale
  - Can be used to identify "pay" vs. "non-pay" reservoir rock
- Shallow and deep laterolog resistivities and porosity (Figure 10)
  - Provides discrimination of "pay" Rock Types 1-3.

The rock-log model was first developed using data from only 5 cored wells. Subsequently the model was extended to include the 3 remaining

cored wells. Evaluation of cored intervals reveals successful discrimination (>80%) of each of the principal rock types (Rock Types 1-3) despite the fact that wells were logged by different companies at different times. Misidentification of Rock Type 1 results in identification of Rock Type 2, while misidentification of Rock Type 2 results in identification of Rock Type 1. Thus, there is no significant misidentification of the dominant rock types by logs over the cored intervals. The model has been extended to all wells with sufficient log suites in the field (120 wells in the NRU). Specific algorithms allow for rock type identification on a foot-by-foot basis in each well.

As we showed previously (Figure 8), permeability is a function of both rock type and porosity. We have established that rock type and porosity can be determined from well log responses alone. Therefore, permeability can, in principle, be predicted using only well log data. This gives us the ability to develop a vertical layering profile based on rock type and permeability in cored and non-cored wells.

### Hydraulic Flow Units

Individual HFU's were identified based on the integration of the data for the distribution of rock types, petrophysical properties (in particular, permeability and fluid content) and depositional facies. Evaluation of this data for 120 wells revealed that rock types are not randomly distributed, rather the principal reservoir rocks (Rock Types 1, 2, and 3) generally occur in close association, and typically alternate with lower quality rocks (e.g., Rock Types 4, 6, 7 and 8). Correlation of rock types between wells reveals an obvious layering profile in which 12 distinct layers, or HFU's, are distinguishable at the NRU (Figure 11). Correlation of these layers is aided by a knowledge of the distribution of depositional environments as there is a weak relationship between depositional environment and rock type. Better quality rocks (> 1 md permeability, > 10% porosity,) occur most commonly in the shoal deposits (Figure 4). Consequently, Rock Types 1 and 2 are more common in the high energy deposits (shoals). Rock Types 3 and 4 are more common in low energy deposits (supratidal, tidal flat, lagoon).

Maps were prepared for each of the HFU's to illustrate the distribution of important petrophysical parameters (Figure 12). The distribution of the principal rock types for each HFU is also mapped (Figure 13). This allows for rapid identification of areas of the field dominated by either high or low quality reservoir rock.

There is a general tendency at the NRU for the higher quality rocks (Rock Types 1 and 2) to occur in discrete trends on the NE (high energy) edge of the unit while relatively lower quality rocks (Rock Types 3 and 4) occur in SW (low energy) portions of the unit. Within these general trends, variations exist in the distributions of permeability. These variations are important as they result in compartmentalization of the reservoir. There are no faults in the NRU--compartmentalization is entirely stratigraphic and is the result of areal variations in the distributions of individual rock types within the reservoir.

## ENGINEERING STUDY

In order to verify the results of the rock-log modeling, long-term production and injection data were analyzed using material balance decline type curves, and the results were mapped for comparison to the petrophysical parameter and rock type maps generated from the work summarized above. In addition, the results of pressure transient tests (average reservoir pressure and flow characteristics) were also incorporated to help correlate the reservoir rock type and historical performance.

Other applications for the decline curve results are:

- Reservoir delineation, recovery and rate forecasting,
- Maps of reservoir performance potential,
- Estimating efficiency of reservoir drive mechanism(s),
- Analogy with offset properties, and
- Calibrating reservoir simulation models.

### Material Balance Decline Type Curve Analysis

An initial study of the 40- and 20-acre producing wells, and 20-acre water injection wells was performed using rigorous material balance decline type curve methods (Doublet et al., 1994; Doublet

and Blasingame, 1996). The goals of these analyses were:

- To analyze long-term production data as well as injection rate and pressure data to evaluate reservoir performance.
- To provide the same flow characteristics associated with the acquisition of field data and without well "downtime."

The results of these analyses include the following:

- In-place fluid volumes:
  - Contacted original oil-in-place,
  - Movable oil or injectable water at current conditions, and
  - Reservoir drainage or injection area.
- Reservoir properties (based on performance):
  - Skin factor for near-well damage or stimulation,  $s$ , and
  - Formation flow capacity based on production performance,  $kh$ .

Examples of the decline type curves for both unfractured and hydraulically-fractured wells are shown in Figures 14 and 15.

The results of the analyses performed on the 40-acre and 20-acre producing wells are presented in this work. We focused on using data that operators acquire as part of normal field operations (e.g., production rates from sales tickets and pressures obtained from permanent surface and/or bottomhole gauges). In most cases, these will be the only data available in any significant quantity, especially for older wells and marginally economic wells, where both the quantity and quality of any types of data are limited.

This approach of using production and injection data eliminates the loss of production that occurs when wells are shut in for pressure transient tests, and provides analysis and interpretation of well and field performance at little or no cost to the operator. This technique allows us to evaluate reservoir properties quickly and easily, and provides us with an additional method for locating the most productive areas of the reservoir.

The results of the decline type curve analyses were used to generate reservoir quality maps of contacted original oil-in-place (OOIP), permeability-thickness ( $kh$ ), and estimated ultimate



recovery (EUR) for both the original 40-acre (primary), and 20-acre (secondary) producing wells as shown in Figures 16-19.

### Pressure Transient Analysis

A unit-wide pressure transient data acquisition program was initiated prior to 10-acre infill drilling. The purpose of this study was to:

- Obtain sufficient data for a representative comparison with tests recorded prior to the initiation of water injection,
- Provide additional data for simulation history matching,
- Estimate completion/stimulation efficiency,
- Identify the best areas of the reservoir with regard to pressure support, and
- Identify any other major problems related to waterflood sweep efficiency.

Our data acquisition program consisted of taking 10 pressure buildup tests (on producing wells) and 13 pressure falloff tests (on injection wells). The locations for these tests were well distributed throughout the unit in order to obtain a representative, unbiased sampling.

The estimated formation flow characteristics (permeability, skin factor, fracture half-length) compare very well with the results from the pre-waterflood transient tests. The major difference we noted was the relative change in average reservoir pressure throughout the unit after eight years of continuous water injection. Reservoir pressure maps for the 1988 and 1995 tests (from pressure buildup and falloff tests) are shown in Figures 20 and 21.

### COMPARING GEOLOGICAL AND PETROPHYSICAL PROPERTIES WITH HISTORICAL PERFORMANCE

If the pore modeling and rock typing exercises are performed properly, the resulting rock type and permeability distributions associated with the reservoir should mirror the historical production performance. The petrophysical parameter and rock type maps resulting from our geological/petrophysical study were compared to the performance maps derived from the results of decline type curve analyses and pressure transient tests. This provided

us with a rapid, cost-effective, and accurate method for targeting infill well locations at the NRU. The results of these comparisons are outlined in the section below.

From Figure 12, we note that the thickest reservoir intervals in HFU #12 (Lower Clear Fork) lie in a NW-SE trend along the northern edge of the unit which correlates to the region in which high energy deposits (shoals, sand flat, forebank) dominated. Porosity is also well developed along this same trend (Figure 12B). There is moderate porosity development in discrete locations within the interior of the unit, primarily to the southwest where low energy deposits (supratidal, tidal flat, lagoon) dominate.

Looking at permeability development within this layer, we note a relatively low concentration of good permeability rock in the lower energy deposits, but very good permeability characteristics along the NW-SE trend in which the higher energy deposits dominate. Hydrocarbon pore volume (HPV) is most pronounced in the same area, however, there are also some fairly good accumulations within the unit's interior that correspond to porosity development.

It is worth noting that the primary reservoir rock types (Rock Types 1 and 2) are most prevalent along the same NW-SE trend on the northern edge of the NRU. Rock Type 3 is dominant in the southern interior of the unit along a roughly E-W trend, in an area of relatively poorer porosity and permeability characteristics (Figure 13).

Examining the reservoir performance maps generated from decline curve analyses (Figures 16-19), we note that the highest accumulation of contacted oil-in-place and the best regions with regard to ultimate recovery are in the same regions as those possessing good permeability and porosity characteristics and large volumes of Rock Types 1 and 2.

The producing mechanisms in the southwestern section of the unit in which Rock Type 3 is dominant are much more complex. We note from Figures 16-17 that there is a considerable volume of producible oil within this region although it is not as prolific as the trend along the northern edge of the unit. The flow capacity, ( $k_o h$ ), estimated from decline curve analysis of the 40-acre primary producing wells indicates a fairly continuous, moderate permeability trend across the southern part

part of the unit. The waterflood response in this area could have been predicted before water injection was initiated, based on the type of rock-log modeling used in this study. As can be seen in Figure 19, the ultimate recovery in the 20-acre producing wells due to water injection will be very good. We note from Figures 12B,D and Figures 16-17 that there were hydrocarbons initially in place, and Rock Type 3 does have sufficient permeability and porosity to contribute significantly to total production.

Producing wells in areas of the unit in which Rock Types 1 and 2 are prevalent usually produce at high total fluid rates with fairly high water cuts (60-90%). Producing wells in areas in which Rock Type 3 is dominant usually produce at fairly low total fluid rates with very low water cuts (20-40%). Based on this information, we are of the opinion that the producing characteristics of individual wells are also a direct function of the local rock type distribution.

Comparing the rock type maps made as part of the geologic study (Figure 13) with the average reservoir pressure maps, we note that the reservoir depleted (Figure 20) and recharged (Figure 21) along the same geologic trends noted above. The regions of the reservoir with the highest quality rock are at a relatively low pressure due to increased fluid production as a result of greater continuity and higher permeability. The converse is true in the areas of lower reservoir quality within the central regions of the unit where the reservoir was never really depleted due to a lack of continuity and overall reservoir quality. Therefore, we believe that the reservoir has depleted and recharged in accordance with its rock type distribution (*i.e.*, reservoir quality).

### **Optimizing Well Completions and Stimulations At The NRU**

Another benefit of the specific type of geologic analyses performed on the new and existing whole core was the more accurate targeting of discrete producing intervals within the 1,400 ft Glorieta/Clear Fork section. For the most part these intervals coincide with zones containing a predominance of Rock Type 1 (that this is the main pay rock type). These are zones of relatively high permeability and porosity, which are separated by larger intervals of

lower permeability and porosity rock that act as barriers or source beds for the higher quality reservoir sections. At North Robertson, these discrete productive intervals include:

- Lower Clear Fork:  $\pm 7,000-7,180$  ft
- Middle Clear Fork:  $\pm 6,350-6,500$  ft  
 $\pm 6,770-6,900$  ft
- Upper Clear Fork:  $\pm 6,160-6,250$  ft

Since all wells at the North Robertson Unit are hydraulically-fractured before they are placed on production or injection, knowledge concerning the distribution of porosity and permeability is of paramount importance. If the vertical extent of the completion interval can be reduced, then the completion efficiency can be increased and completion costs can be decreased.

The result of these improved completion techniques is shown in Figure 22. For the 18 10-acre infill wells drilled during 1996, total unit production has increased over 30 percent, while the total well count was increased by only 7 percent. The average three-month initial potential (IP's) for these new infill wells are two to three times greater than the IP's from the previous drilling and completion programs at the NRU.

### **CONCLUSIONS**

One of the principal objectives of this study is to identify useful and cost-effective methods for the exploitation of the shallow-shelf carbonate (SSC) reservoirs. The techniques presented herein for the formulation of an integrated reservoir description, can be applied in all oil and gas reservoirs. However, these techniques have proven particularly useful in the NRU, a heterogeneous, low permeability carbonate reservoir. Based on the results of this study, we conclude that:

1. Measurement of pore geometry parameters allows for the improved prediction of permeability and permeability distribution from wireline logs in partially cored intervals, and in adjacent uncored wells. This approach improves the prediction of reservoir quality in non-cored intervals and results in improved well completions and EOR decisions.

2. Detailed pore geometry attributes allow for better definition of hydraulic flow units. These attributes can be related to well log responses, which allows for the development of a field-wide, log-based reservoir model.
3. The material balance decline type curve techniques summarized in this work provide very good estimates of reservoir volumes (total and movable), and reasonable estimates of formation flow characteristics. Using this approach to analyze and interpret long-term production and injection data is relatively straightforward and can provide the same information as conventional pressure transient tests, without the associated costs of data acquisition, or loss of production.
4. Comparison of geological and petrophysical parameters with historical production performance data, reveals that the producing characteristics of individual wells are a direct function of the local rock type distribution. The reservoir depletes and re-pressures as a function of reservoir quality (rock type), throughout all areas of the unit.
5. We identified regions in the unit with additional reserves potential (accelerated or incremental), as well as those areas in which infill drilling is not likely to be economic.
6. Uniform infill drilling is neither prudent, nor warranted, given the stratigraphic compartmentalization and irregular permeability distributions in this, and similar reservoirs. Infill drilling should be restricted to:
  - a) Areas of the field that exhibit Rock Types 1, 2, and 3 as dominant, with good permeability and hydrocarbon pore volume (HPV) characteristics, high primary and secondary recovery, and
  - b) Areas of poor reservoir continuity with acceptable porosity and permeability values, with a significant abundance of Rock Types 1, 2, or 3, and good primary, yet poor secondary recovery characteristics.
7. If the productive intervals within the reservoir can be better defined based on core and well log analyses, then completion efficiency (initial po-

tential and reserves recovery) can be increased and completion costs can be decreased.

## REFERENCES CITED

- Archer, J.S. and Wall, C.G.: Petroleum Engineering Principles and Practice, Graham and Trotman, Ltd. (1986) 362.
- Calhoun, J.C.: Fundamentals of Reservoir Engineering, Univ. Oklahoma Press, Norman, Oklahoma (1960) 426.
- Clelland, W.D. and Fens, T.W.: "Automated rock characterization with SEM/Image analysis techniques", SPE Formation Evaluation (1991) v. 6, No. 4, 437-443.
- Doublet, L.E., Pande, P.K., McCollum, T.J. and Blasingame, T.A.: "Decline curve analysis using type curves--analysis of oil well production data using material balance time: application to field cases," SPE Petroleum Conference and Exhibition of Mexico, Veracruz, Mexico, Paper 28688 (1994).
- Doublet, L.E. and Blasingame, T.A.: "Evaluation of injection well performance using decline type curves," SPE Permian Basin Oil and Gas Recovery Conference, Midland, Texas, Paper 35205 (1996).
- Ehrlich, R. and Davies, D.K.: "Image analysis of pore geometry: relationship to reservoir engineering and modeling", Proc. SPE Gas Technology Symposium, Dallas, Texas, Paper 19054 (1989) 15-30.
- Li, Y. and Wardlaw, N.C.: "The influence of wettability and critical pore-throat size ratio on snap-off", J. Colloid and Interface Sci. (1986) v. 109, 461-472.
- Pande, P.K.: "The NRU-DOE prospectus", Fina Oil and Chemical Co., Midland, Texas (1995).
- Thomeer, J.H.: "Air permeability as a function of three pore-network parameters," Journal of Petroleum Technology (1983) v. 35, 809-814.
- Wardlaw, N.C.: "Pore geometry of carbonate rocks as revealed by pore casts and capillary pressure", AAPG Bull. (1976) v. 60, 245-257.
- Wardlaw, N.C. and Cassan, J.P.: "Estimation of recovery efficiency by visual observation of pore systems in reservoir rocks", Bull. Can. Pet. Geol. (1978) v. 26, 572-585.

Wardlaw, N.C.: "The effects of pore structure on displacement efficiency in reservoir rocks and in glass micro models", SPE Paper 8843, First Joint SPE/DOE Symposium on Enhanced Oil Recovery, Tulsa, Oklahoma (1980) 345-352.

**Table 1 - Pore Type And Classification At The NRU**

Pore Type	Size, $\mu\text{m}$	Shape	Coordination Number	Aspect Ratio	Pore Arrangement	Geologic Description
A	30-100	Triangular	3-6	50-100:1	Interconnected	Primary interparticle
B	60-120	Irregular	<3	200:1	Isolated	Shell molds and vugs
C	30-60	Irregular	<3	100:1	Isolated	Shell molds and vugs
D	15-30	Polyhedral	~6	<50:1	Interconnected	Intercrystalline
E	5-15	Polyhedral	~6	<30:1	Interconnected	Intercrystalline
F	3-5	Tetrahedral	~6	<20:1	Interconnected	Intercrystalline
G	<3	Sheet/slot	1	1:1	Interconnected	Interboundary sheet and intercrystalline pores

**Table 2 - Capillary Characteristics By Rock Type Based On Mercury Injection**

Rock Type	Entry Pore Throat Radius, $\mu\text{m}$	Displacement Pressure, psia	Ineffective Porosity (porosity invaded by Hg at $p_c > 500$ psia), %
1	7.6-53.3	2-10	8.2-29.6
2	2.7-3.6	30-40	23.1-49.5
3	0.4-1.3	80-300	61.6-72.3
4*	1.8	60	88
5	1.1-1.8	60-150	21.7-57.2
6*	0.1	800	100

\* - Only one (1) measurement

**Table 3 - Porosity, Permeability, And Lithology By Rock Type**

Rock Type	Median Porosity, %	Median Permeability, md	Lithology	Reservoir Quality	Cross-flow Barrier Quality
1	4.0	0.70	Dolostone	Excellent	Poor
2	5.6	0.15	Dolostone	Good	Poor
3	3.5	0.39	Dolostone	Moderate	Moderate
4	7.5	0.01	Dolostone	Poor	Moderate
5*	5.8	0.40	Limestone	Good (water-bearing)	Poor
6	1.0	<0.01	Anhydritic Dolostone	None	Good
7	2.3	<0.01	Silty Dolostone	None	Good
8	--	--	Shale and argillaceous dolostone	None	Good

\* - Structurally low and wet at the NRU

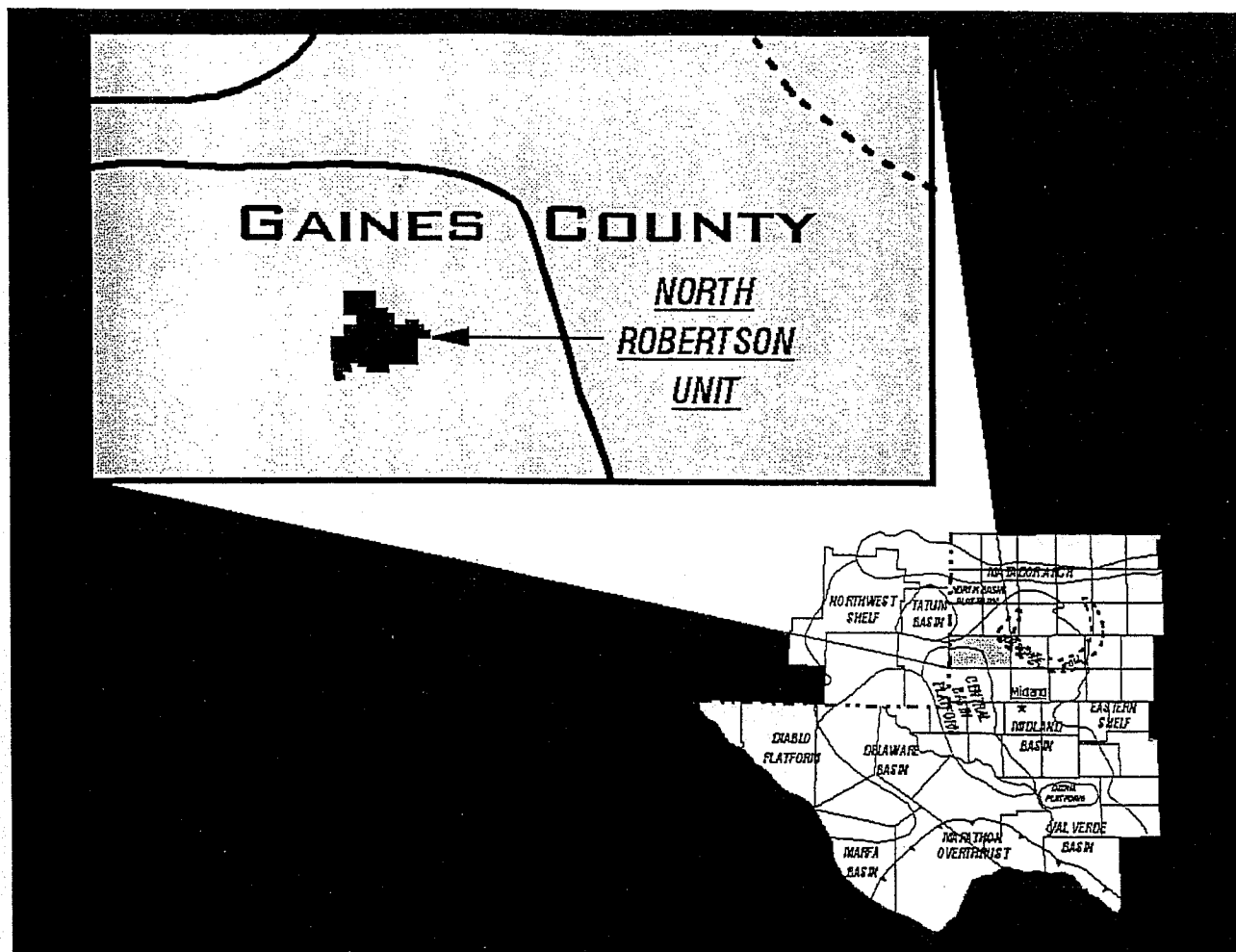


Figure 1 - Regional map showing location of the North Robertson (Clear Fork) Unit.

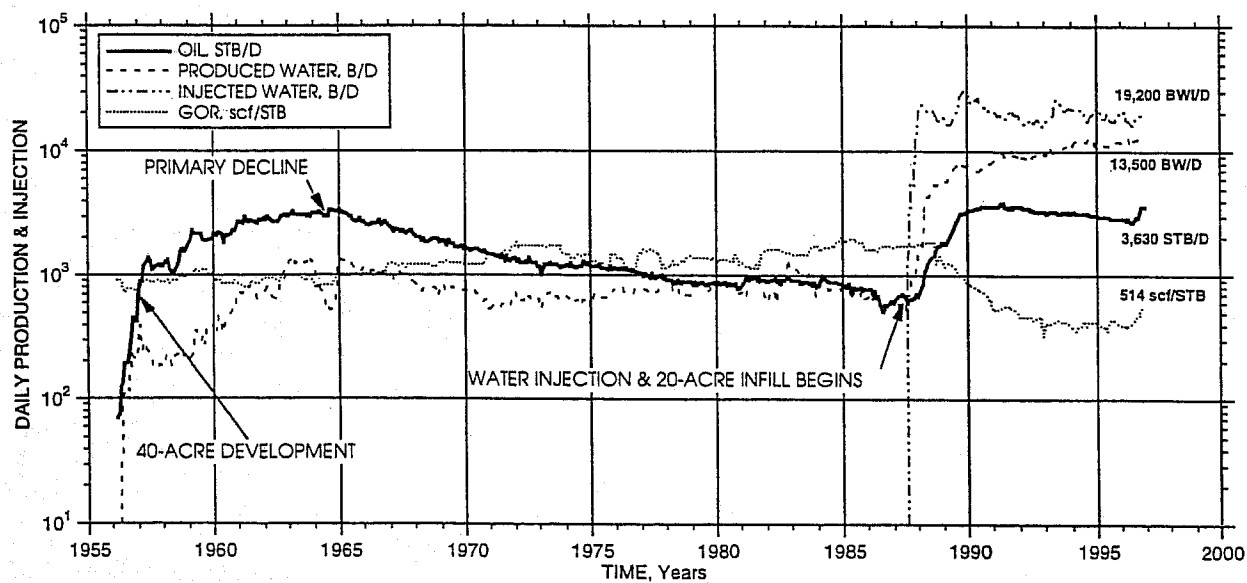


Figure 2 - NRU production and injection history.

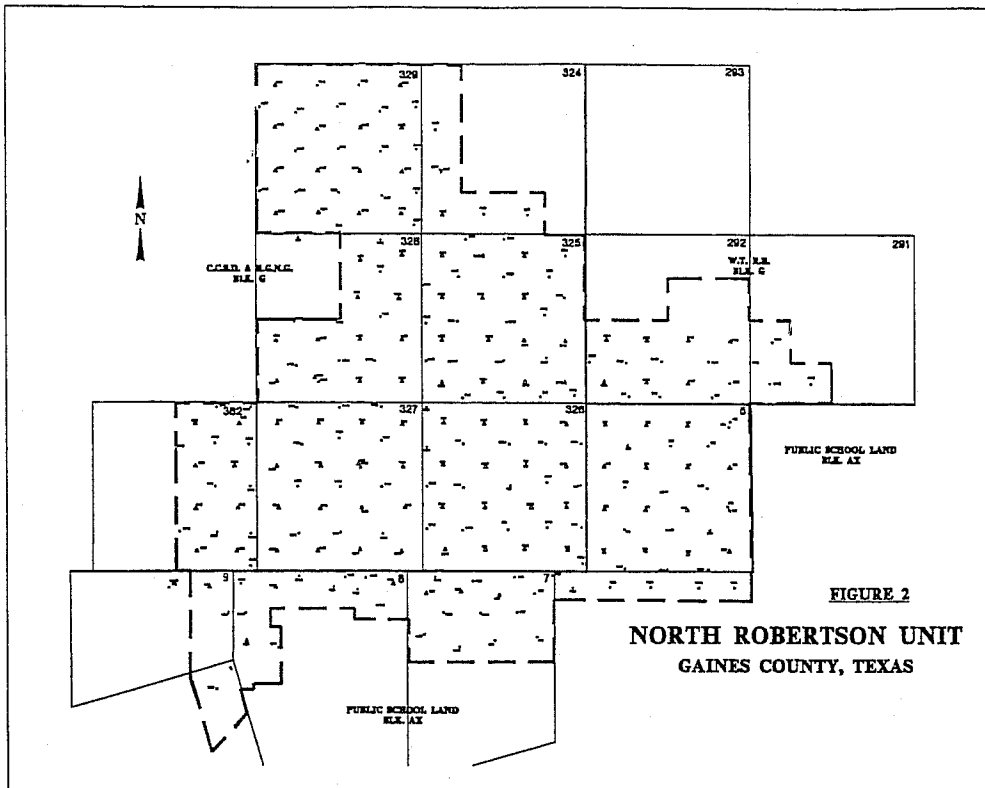


Figure 3 - North Robertson Unit - well configuration.

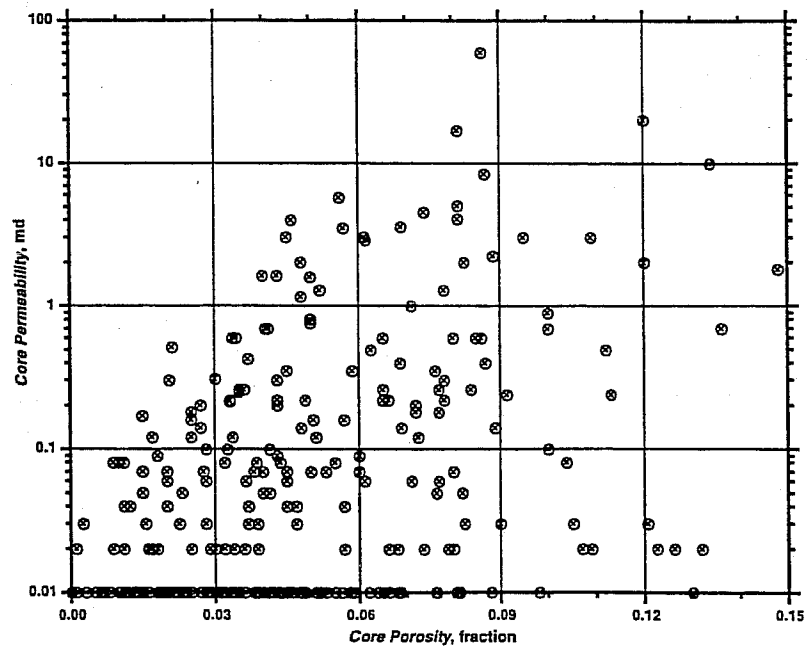


Figure 4 - Porosity-permeability relationships - all core data.

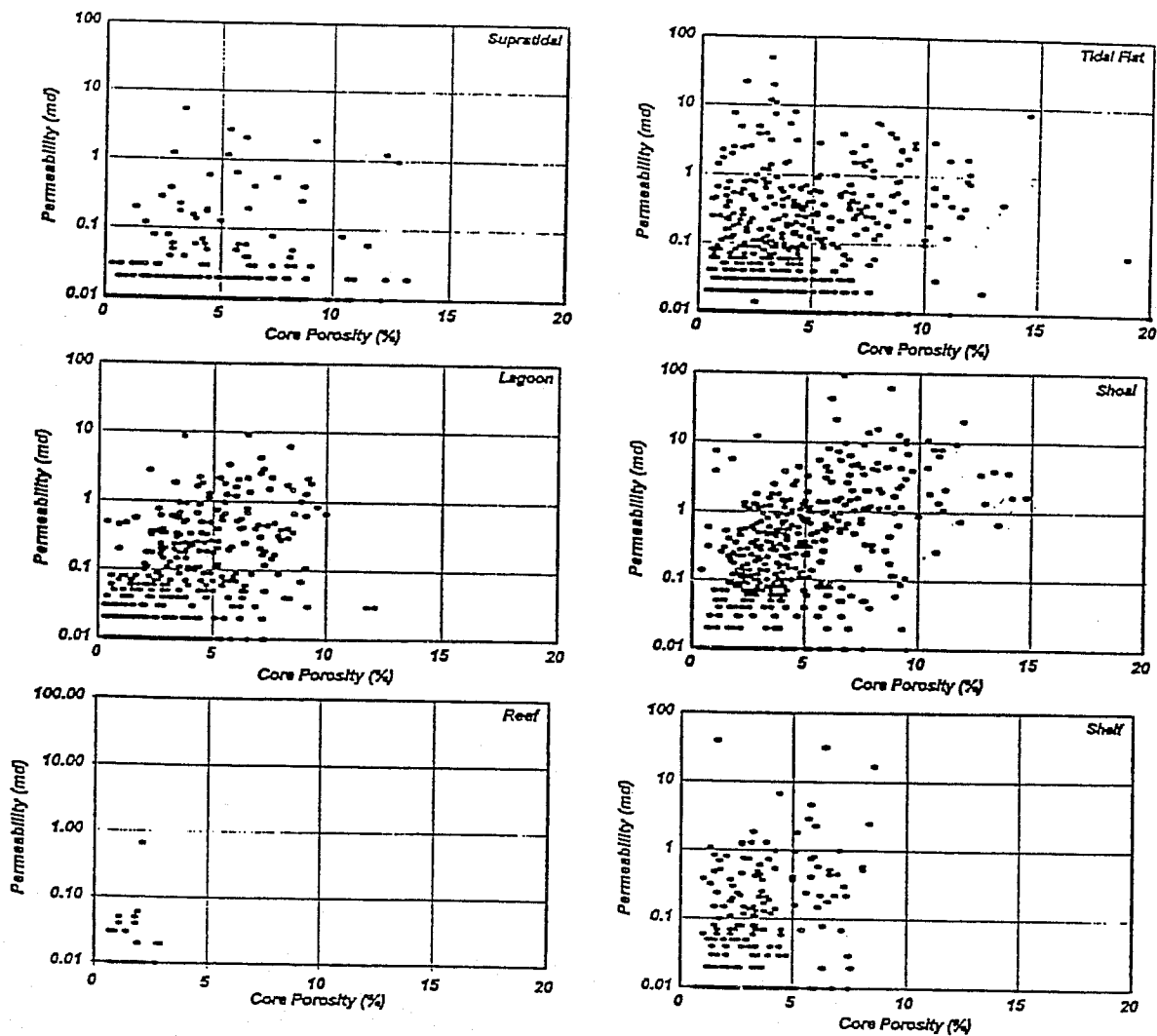


Figure 5 - Porosity and permeability for principal depositional environments.



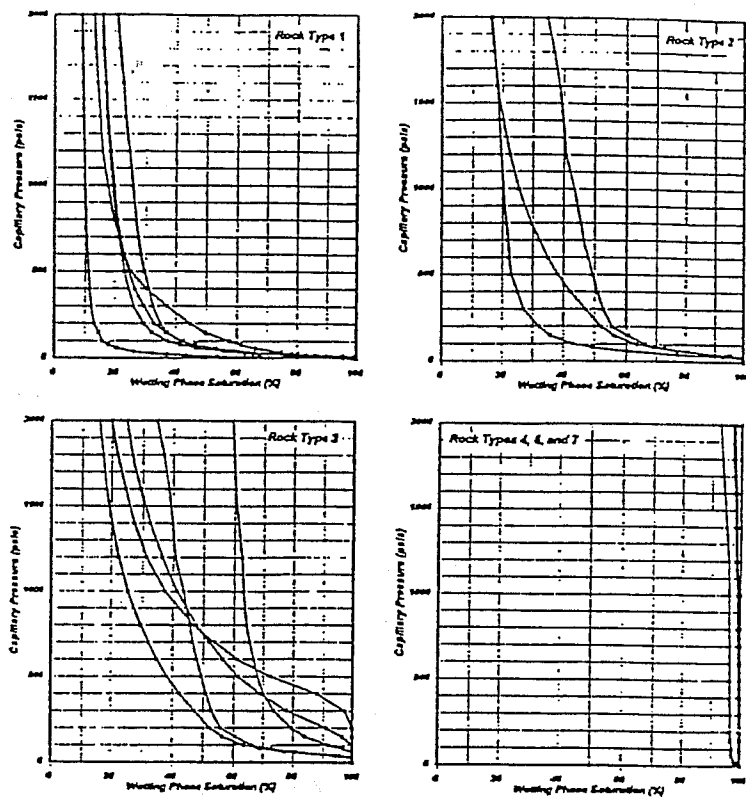


Figure 6 - Capillary pressure curves by rock type.

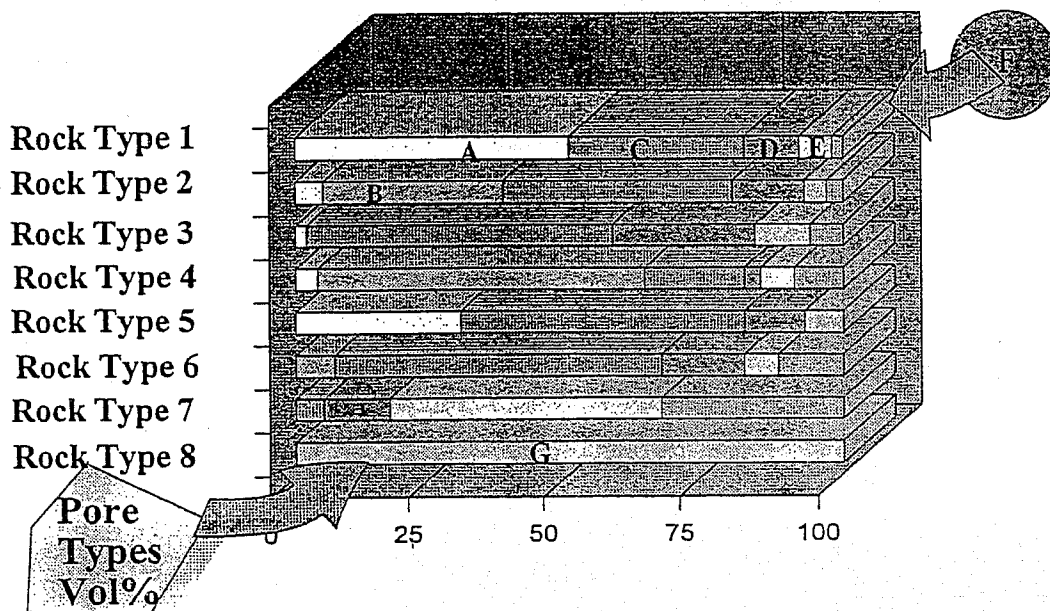


Figure 7 - Volumetric proportions of pore types in each rock type.

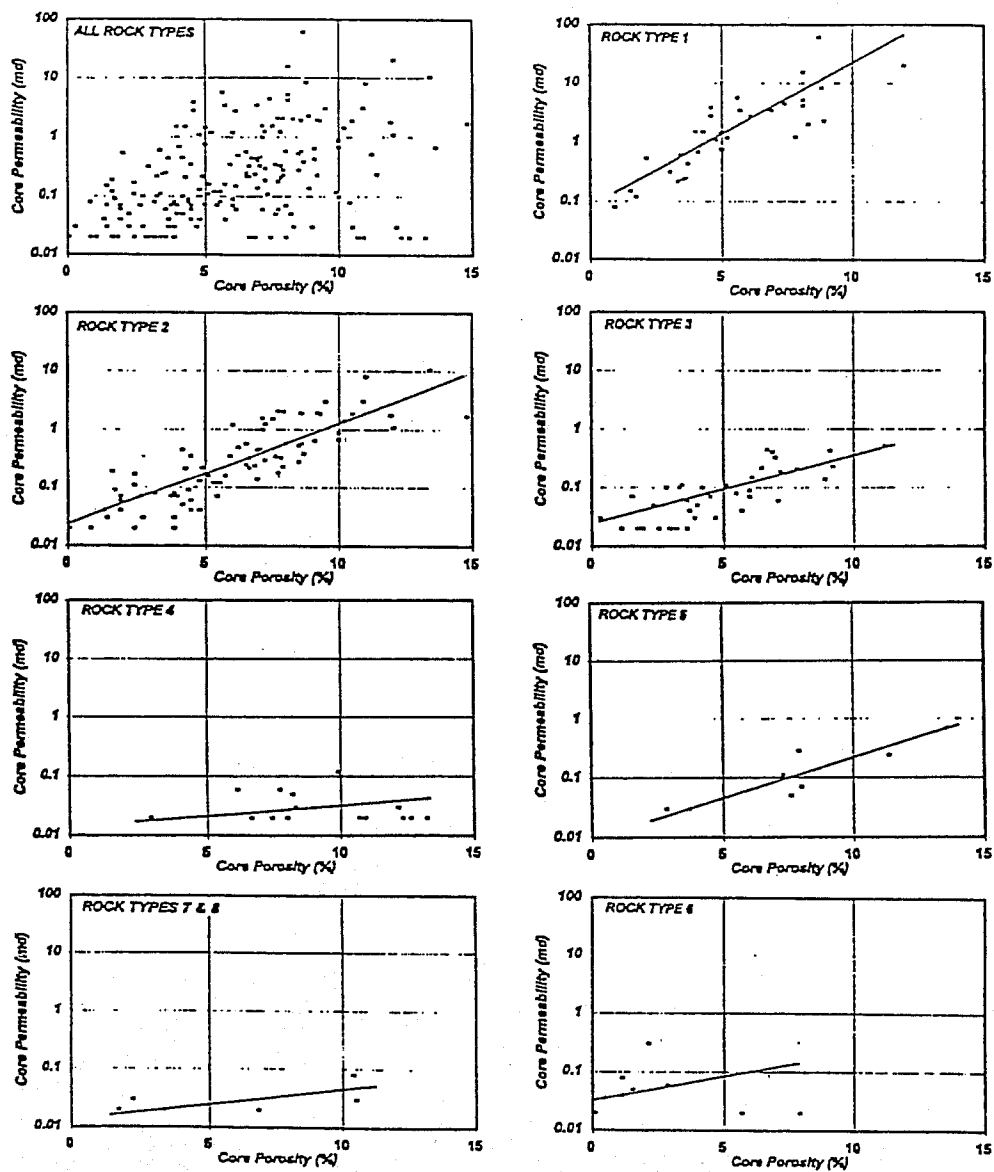


Figure 8 - Porosity and permeability by rock type

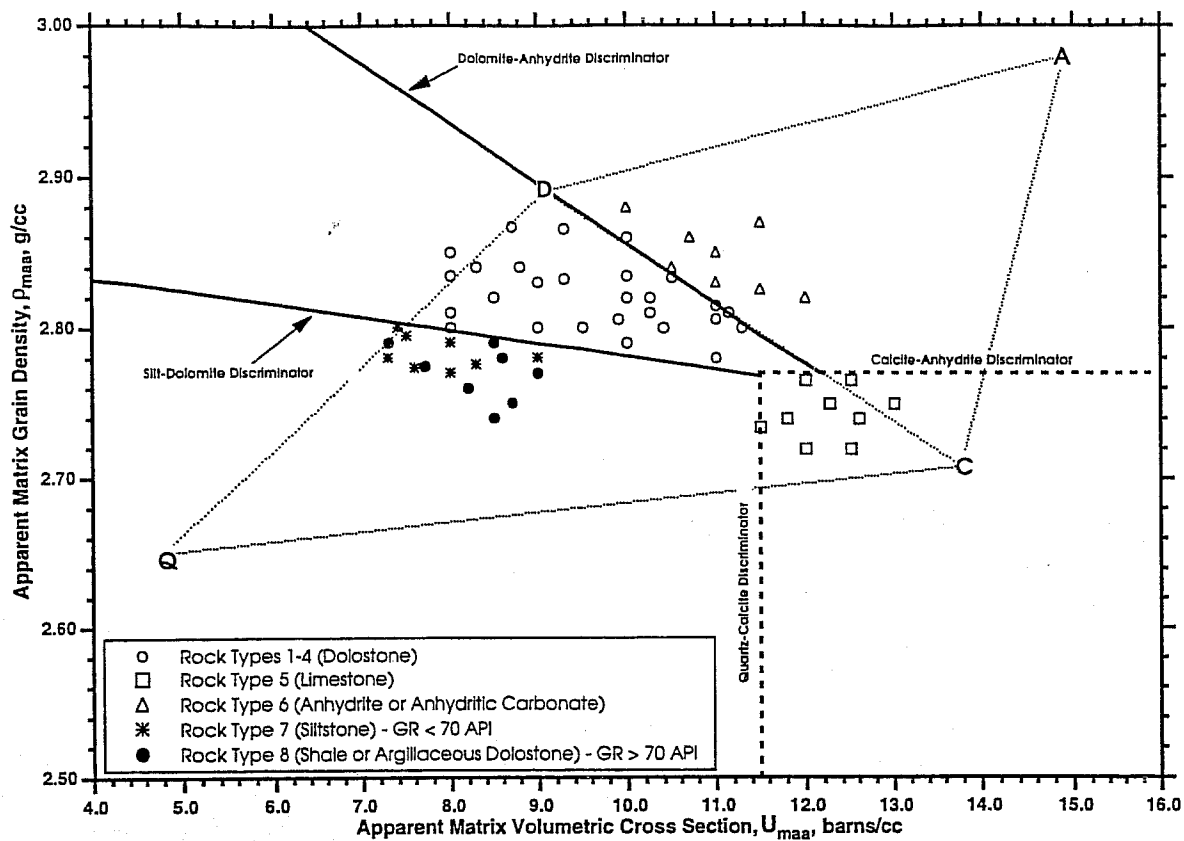


Figure 9 - Differentiating "pay" from "non-pay" reservoir rock.

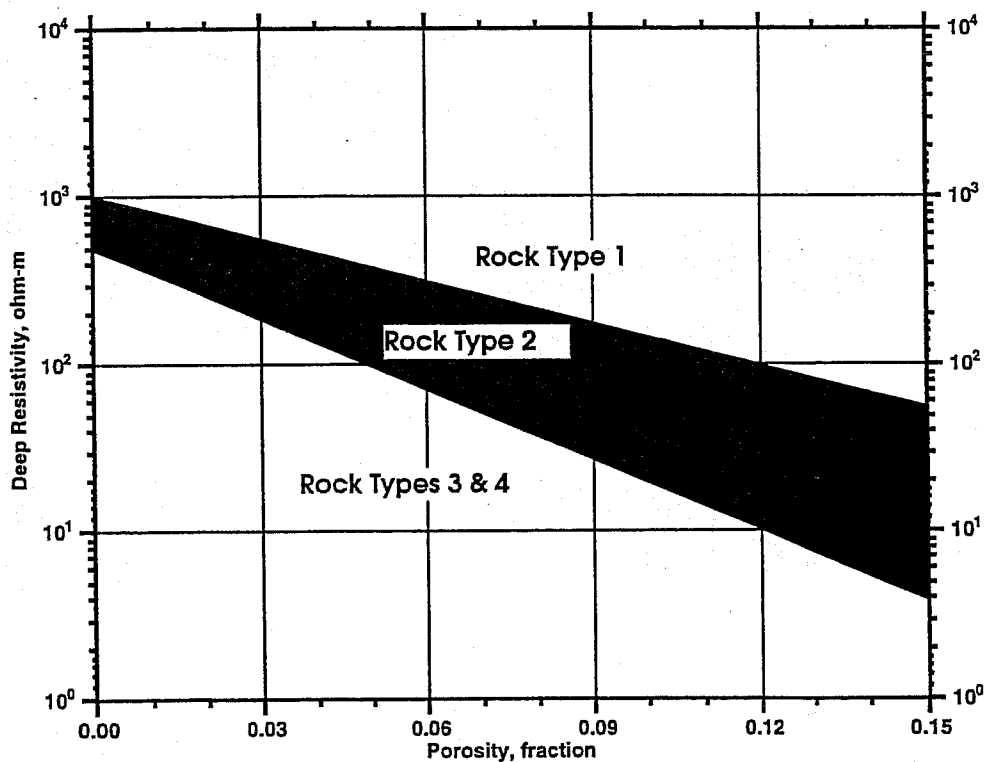


Figure 10 - Differentiating between "pay" rock types 1-3.

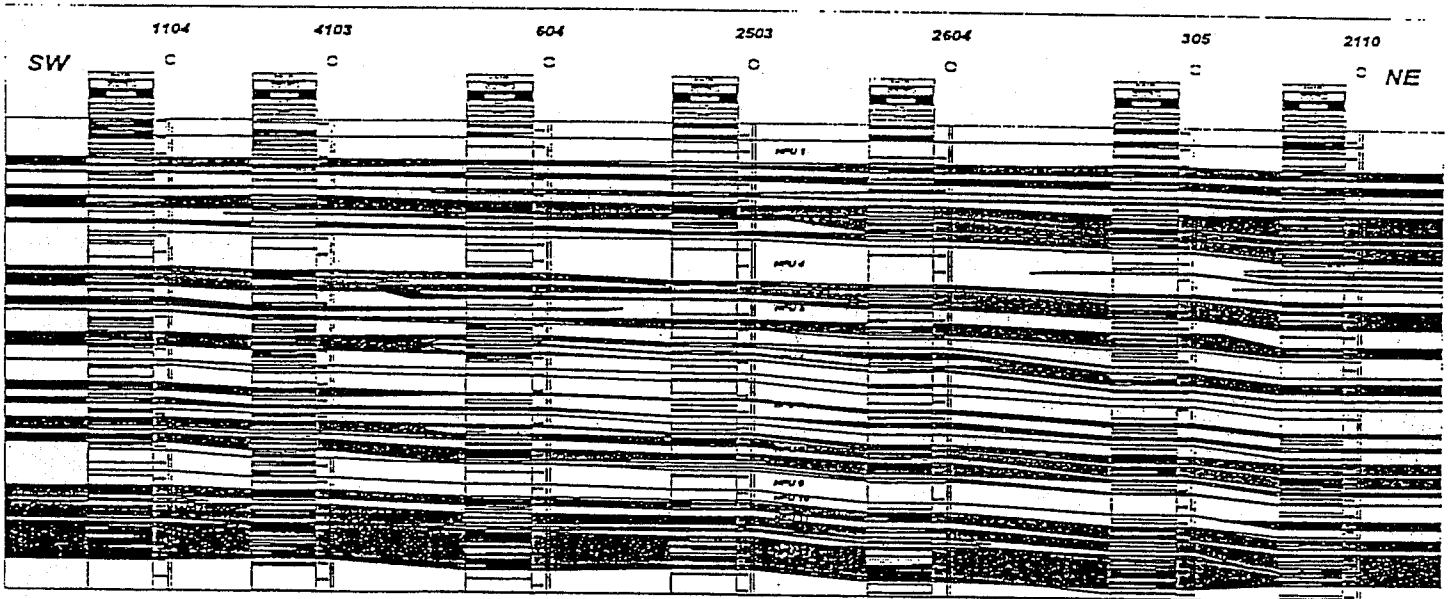


Figure 11 - Cross-section of NRU showing distribution of HFU's. Dark zones are Rock Types 1 and 2. Light zones are Rock Types 3, 4, 6, 7, and 8.



Figure 12 - Contour map of HFU #12 showing distribution of: (A) thickness, (B)  $\phi h$ , (C)  $kh$ , and (D) HPV.

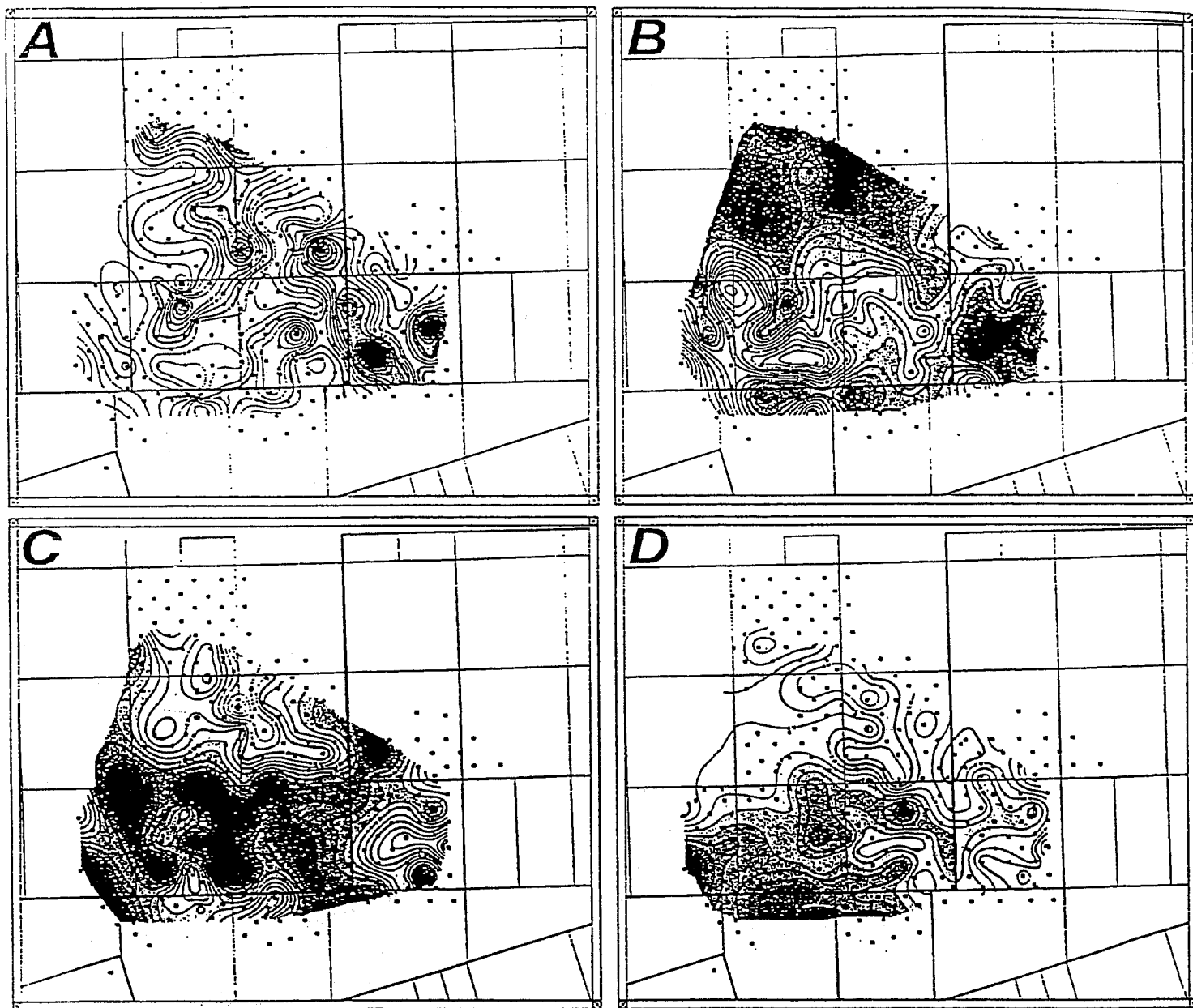


Figure 13 - Contour map of HFU #12 showing distribution of Rock Types 1-4. Note: Darker areas have higher values than lighter areas.

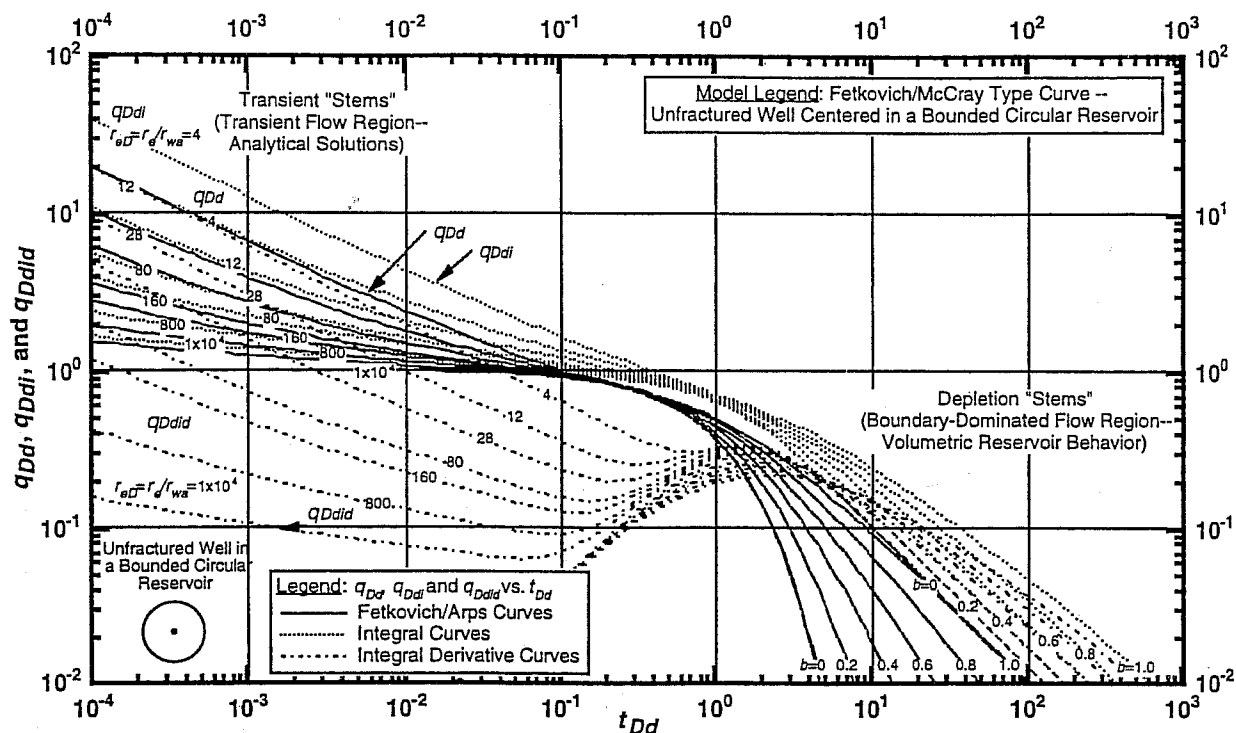


Figure 14 - Fetkovich/McCray decline type curve for an unfractured well ( $q_{Dd}$ ,  $q_{Ddi}$ , and  $q_{Ddid}$  versus  $t_{Dd}$  solutions).

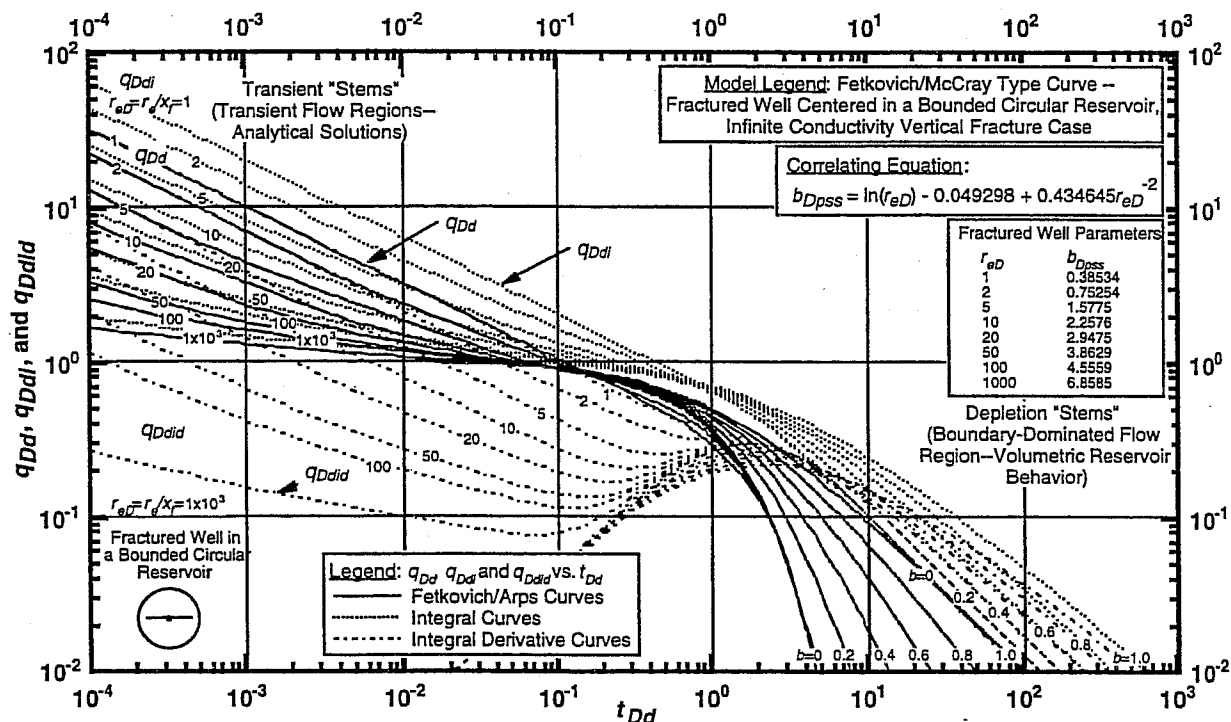


Figure 15 - Fetkovich/McCray decline type curve for a well with an infinite conductivity vertical fracture ( $q_{Dd}$ ,  $q_{Ddi}$ , and  $q_{Ddid}$  versus  $t_{Dd}$  solutions).





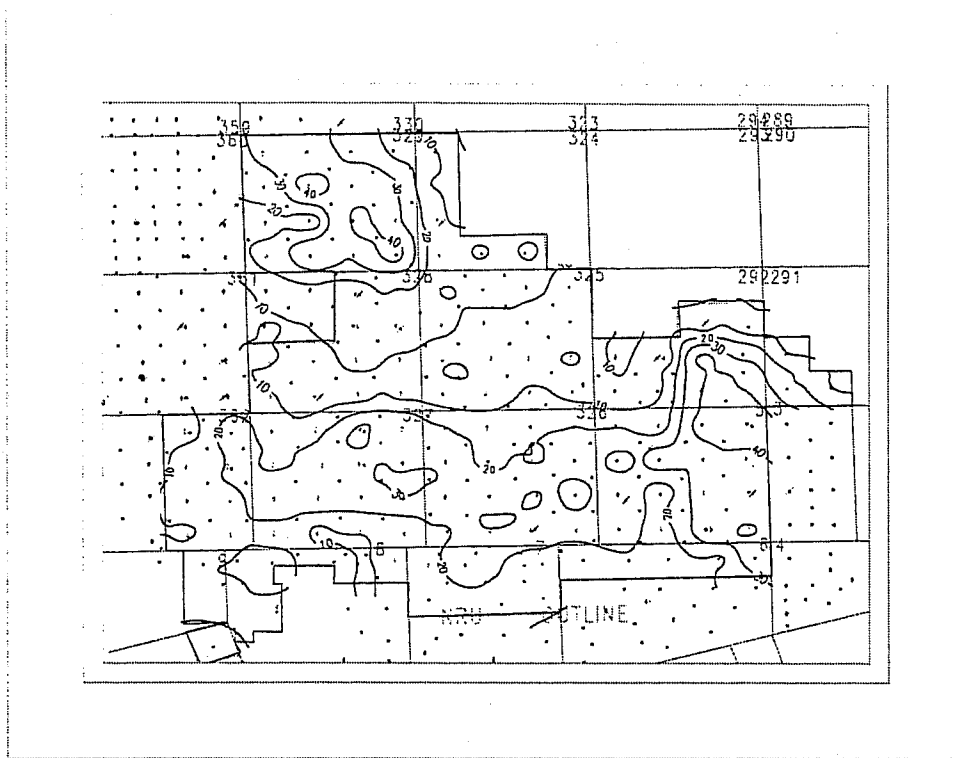


Figure 18 - Map of forty-acre well flow capacity ( $k_h$ ) from decline curve analysis (CI = 10md-ft).

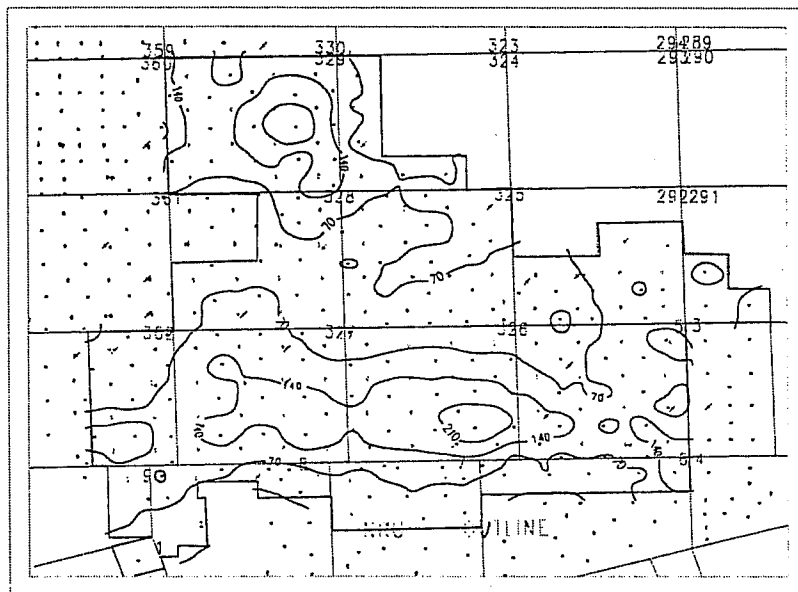
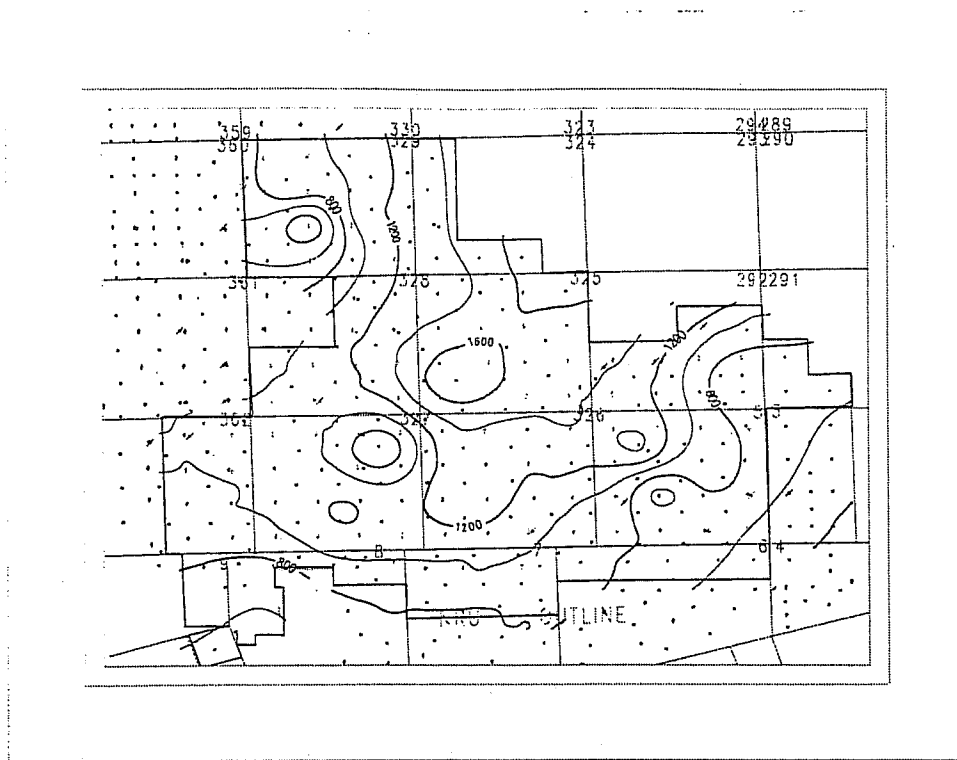
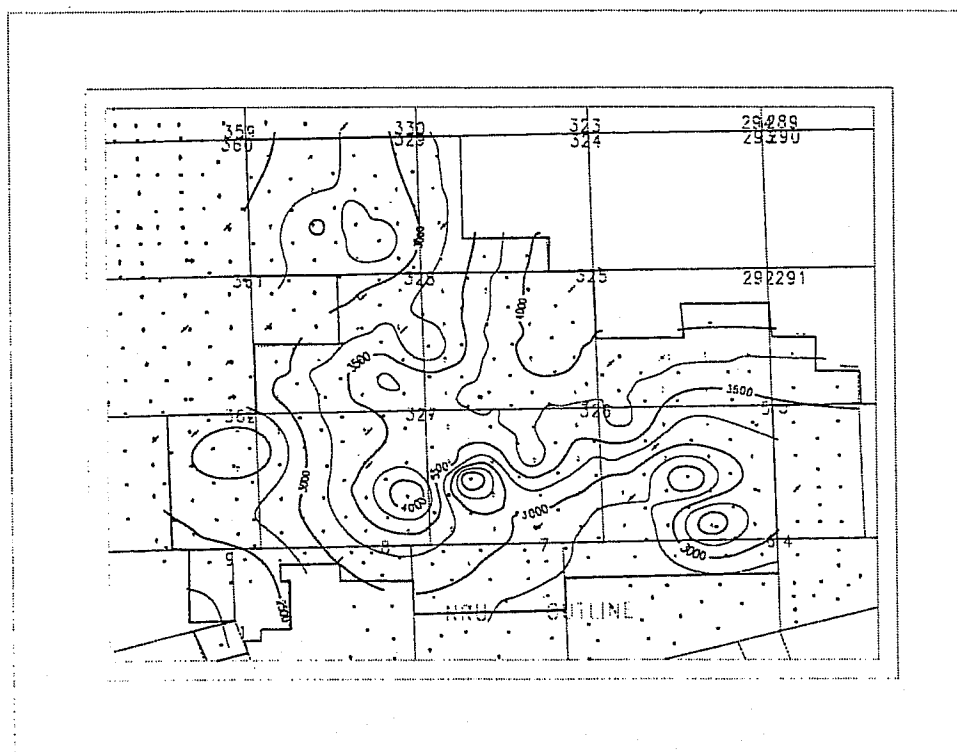


Figure 19 - Map of twenty-acre well est. ultimate recovery (EUR) from decline curve analysis (CI = 70x10<sup>3</sup> bbls).



**Figure 20- Map of 1988 average reservoir pressure from pressure transient tests (CI = 200 psia).**



**Figure 21- Map of 1995 average reservoir pressure from pressure transient tests (CI = 250 psia).**

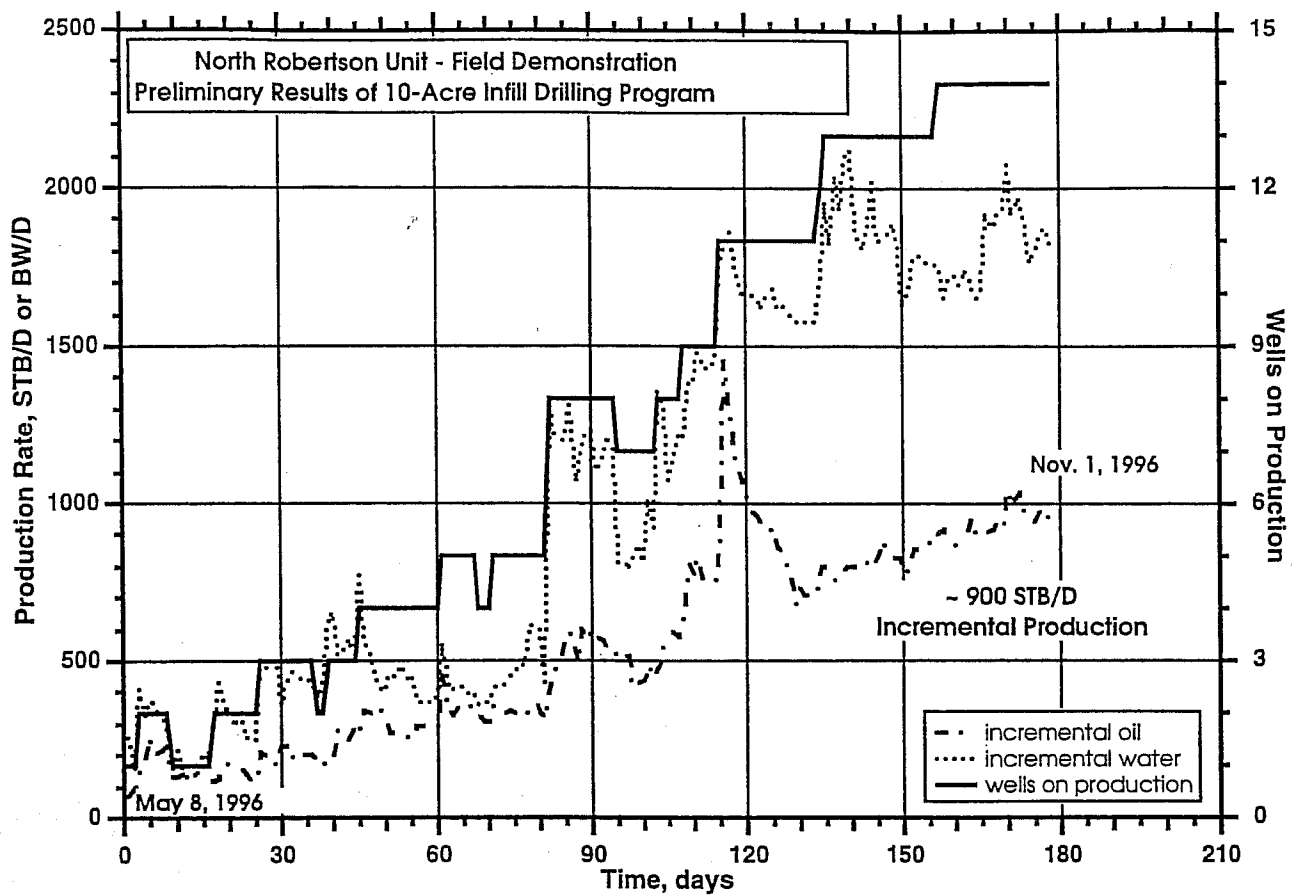


Figure 22 - Preliminary Ten-Acre Infill Well Results (November 1996).



# **The Role of Reservoir Characterization in the Reservoir Management Process (as Reflected in the Department of Energy's Reservoir Management Demonstration Program)**

Michael L. Fowler, BDM-Petroleum Technologies, P.O. Box 2543, Bartlesville, Oklahoma, 74005

Mark A. Young, Michael P. Madden, BDM-Oklahoma, P.O. Box 2565, Bartlesville, Oklahoma, 74005

E. Lance Cole, Petroleum Technology Transfer Council, P.O. Box 246, Sand Springs, Oklahoma, 74063

## **ABSTRACT**

Optimum reservoir recovery and profitability result from guidance of reservoir practices provided by an effective reservoir management plan. Success in developing the best, most appropriate reservoir management plan requires knowledge and consideration of (1) the reservoir system including rocks, fluids, and rock-fluid interactions (i.e., a characterization of the reservoir) as well as wellbores and associated equipment and surface facilities; (2) the technologies available to describe, analyze, and exploit the reservoir; and (3) the business environment under which the plan will be developed and implemented.

Reservoir characterization is the essential to gain needed knowledge of the reservoir for reservoir management plan building. Reservoir characterization efforts can be appropriately scaled by considering the reservoir management context under which the plan is being built. Reservoir management plans de-optimize with time as technology and the business environment change or as new reservoir information indicates the reservoir characterization models on which the current plan is based are inadequate.

BDM-Oklahoma and the Department of Energy have implemented a program of reservoir management demonstrations to encourage operators with limited resources and experience to learn, implement, and disperse sound reservoir management techniques through cooperative research and development projects whose objectives are to develop reservoir management plans. In each of the three projects currently underway, careful attention to reservoir management context assures a reservoir characterization approach that is sufficient, but not in excess of what is necessary, to devise and implement an effective reservoir management plan.

## INTRODUCTION

In discussing the definition of reservoir characterization at the first meeting of the organizing committee for the first International Reservoir Characterization Technical Conference in Dallas, Texas in 1985, the attendees, who represented a wide spectrum of technical backgrounds, decided on the following definition: "Reservoir characterization is a process for quantitatively assigning reservoir properties, recognizing geologic information and uncertainties in spatial variability." (Lake and Carroll, 1986). Traditionally, reservoir characterization has aimed at the quantitative transfer of information on reservoir property distribution with a sufficient level of detail and accuracy to a numerical simulator so that fluid flow simulation predictions would match reservoir performance. Through simulation, an appropriately detailed and accurate model of reservoir property distribution will allow the operator to avoid the deleterious effects of heterogeneities and/or exploit them to best economic advantage. To the extent that the information supplied to the simulator is incomplete, inaccurate, or at an inappropriate scale, the ability to predict reservoir performance and maximize economic returns will be lessened.

Reservoir characterization, when appropriately done, is recognized as a valuable tool to avoid costly errors in reservoir decision making. Powerful reservoir characterization tools and techniques have evolved since that first conference in 1985, and new tools and techniques continue to be developed, tested, and refined, but efficient and cost-effective reservoir characterization is still more commonly viewed as an art rather than as a science. Operators have often found it difficult to prescribe and construct at an acceptable cost an appropriate reservoir characterization model in terms of its degree of detail (resolution) and its associated degree of uncertainty.

Characteristics of the reservoir characterization model are a function of the purpose of the model, which in turn depends strongly on the reservoir management context in which the model is to be applied. A proper understanding of reservoir management is therefore fundamental to performing appropriate reservoir characterization. The primary goal of this paper will be to identify the role of reservoir characterization in reservoir management and to elucidate the factors that determine the type of reservoir characterization model necessary for a given reservoir management situation.

The relationship between reservoir characterization and reservoir management has been explored by the authors under the auspices of the Department of Energy's Reservoir Management Demonstration Program by review of extensive literature on reservoir management and by participation in program projects with a variety of small independent operators. Two of these projects will be used as examples to show appropriate scaling of reservoir characterization efforts in reservoir management. Much was also learned about the relationship between reservoir

characterization and reservoir management from observation and study of field demonstration projects being carried out under the Department of Energy's Reservoir Class Program and from the authors' experience in industry reservoir management and reservoir characterization projects performed in the context of major and independent oil companies.

## **RESERVOIR MANAGEMENT, PERCEPTIONS VS REALITIES**

Misconceptions about reservoir management abound. Some operators think of reservoir management as something done only to large reservoirs where large improved recovery targets can justify the large investments in time and dollars they see as necessary. Others think of reservoir management as the day-to-day reservoir problem solving activities of reservoir engineers. Yet others, usually those with limited familiarity with new technologies, view reservoir management as a strictly "high-tech" venture involving the application of state-of-the-art new techniques and technologies. And, of course, there are numerous operators of marginally profitable mature reservoirs who think only of reservoir management as an unaffordable expenditure. Fortunately, not all reservoir operators can be categorized with the above examples, but a general atmosphere of conservatism and reluctance prevails, and, as a consequence, the full potential of effective reservoir management has not been realized.

### **Definition of Reservoir Management**

Just as there are many publications on the subject, so are there many definitions of reservoir management to accompany them. Thakur (1991) defined reservoir management as the "judicious use of available resources to maximize economic recovery" Cole et al. (1993) went on to specify that "resources" in the above definition include people, equipment, technology, and money. Other definitions, such as that offered by Wiggins and Startzman (1990), that reservoir management is "application of state-of-the-art technology to a known reservoir system within a given management environment," take a slightly different view. Most definitions, however, focus on identification of the components of reservoir management much as if we were to define an automobile as consisting of engine, wheels, steering mechanism, etc.

Nearly all discussions of reservoir management agree on the following as general characteristics:

- It requires and makes use of resources.
- It is continuous and long-term, over the life of a reservoir.
- It concentrates on economic optimization.

From this, we can surmise that the main activity of reservoir management is a sequence of resource-deployment decisions made to maintain optimum economic recovery of petroleum.

## **The Plan as a Central Concept**

Definitions are valuable in that they serve to enlighten us to the important considerations that are critical to reservoir management activities, but taking a slightly different perspective may help us grasp the concept more completely. Let us assume that every reservoir being operated today, like every business being operated today, is being managed. Some are managed well, and some are without question poorly managed. We can think of well and poorly managed reservoirs and businesses as those that are and are not realizing their maximum potential to their operators, respectively. Every reservoir operator is taking some kind of approach, that is, has some kind of philosophy, guidelines, or strategy that is used to guide his interaction with the reservoir. Formulating these guidelines or plans and following them is the real essence of reservoir management (Cole et al., 1994).

The spectrum of possible approaches, strategies, or plans that might be employed in reservoir management is extremely wide. Some plans may be very simply conceived or literally just assumed. Such a simple and straightforward approach could amount to a stark "produce the reservoir until the total cost of production becomes greater than the revenue obtained, then quit," where "quit" implies either selling the property to an organization with lower overhead costs that can continue to operate the reservoir at a profit or simply abandoning the reservoir. The opposite extreme might be a case in which all the latest improved oil recovery technologies are periodically screened and selected technologies are carefully applied in the context of a complete and detailed 3-D description of the physical and chemical aspects of the subsurface reservoir in an attempt to retrieve substantial dollar amounts of oil in return. Intermediate between the extremes are plans that consist of informal guidelines that may or may not be regularly reviewed for appropriateness. Reservoir management can be thought of as the decision-making process that matches the approach or plan to the reservoir and its operator in such a way as to maximize the profitability of the reservoir to the operator.

## **Consequences of Plan Mismatch**

If close attention is not paid to developing reservoir management plans or guidelines, it is possible to get a poor match between the approach implemented and the reservoir's and/or operator's needs. The most likely consequence of a poor match is a less-than-optimum economic performance. Some common scenarios include:

- *Gambler's ruin* - A company invests capital it cannot afford to lose in a reservoir management project. Not only does the project fail to make a return, but the investment is



lost also.

- *Partial failure* - A moderately profitable reservoir management project is carried out. Returns, however, are not as good as predicted, and other investments available would have done better.
- *Partial success* - A reservoir management project makes a return as good or better than predicted. The reservoir, now depleted to its economic limit, is sold to another operator who makes a windfall from enhanced production.
- *Unrecognized failure* - A reservoir performs as expected under an implemented plan to the projected economic limit. It is then sold to a smaller operator with lower overhead who continues under the same approach. Only the reservoir knows about the millions of dollars of additional revenues that could have been obtained under a different approach.

Because a generally conservative attitude has prevailed toward reservoir management in the past, there is potential for increasing profitability in a large number of petroleum reservoirs. In a majority of cases, this increased profitability could be accompanied by increased recovery as well. Recognizing these facts and in keeping with its mission to increase profitability and recovery from domestic reservoirs to prevent or forestall their abandonment, the Department of Energy is funding a program of reservoir management demonstration projects. The program was initiated in 1995 with the primary objective of improving reservoir management understanding through demonstration and technology transfer. Program projects encourage operators, especially small independent operators, to learn, apply, and disseminate sound reservoir management techniques. Projects are now underway to develop reservoir management plans for a variety of reservoirs managed by small operators. Technology transfer plays a vital role in each of these projects.

## **CONSTRUCTING AN OPTIMUM RESERVOIR MANAGEMENT PLAN**

How can we match the vast number of possible reservoir management approaches to appropriate reservoir situations? The answer is "it is a matter of how well we know (1) the business environment, both internal and external to our company, under which the reservoir management plan will be constructed and implemented, (2) the availability and use of proven and developing technologies, and (3) the reservoir and its facilities (i.e., the reservoir system)" (Fowler et al., 1996). Of particular note is the concept that knowing the context under which reservoir management is to be performed is important as well as knowing about the reservoir itself. The importance of this contextual information will carry over to reservoir characterization planning as well.

## **Knowledge of the Reservoir Management Business Environment**

Reservoir management business environment factors fall into one of two categories: those that are external to the operator's organization (i.e., those that affect all operators equally), and those that are internal and perhaps unique to the operator's organization. No plan can be optimized without paying close attention to both types of factors, and some reservoir management projects fail due to oversights in this area. Furthermore, any of these factors is subject to change at any time, either during the formulation of a reservoir management plan or after it has been implemented. Maintaining an awareness of the consequences of such changes enables plans to be revised to maintain optimum performance.

Examples of external factors that need to be considered include market economics, taxes, operational laws and regulations, safety and environmental laws and regulations, and less tangible items such as public opinions. Internal factors include the organization's ability to raise and/or commit capital and a number of items related to the "corporate culture" of the organization. The latter include factors such as how the company measures value (i.e., is the objective to increase reserves?, to obtain a certain rate of return on investment?, or to achieve some other measure of success?). Other factors might include the organization's attitude toward risk, its organizational structure, and its ability to commit to long term plans (Cole et al., 1993; Wiggins and Startzman, 1990). Some of an organization's internal factors may be pliable and capable of being changed to accommodate the best interests of a reservoir management plan, but some factors may be difficult or impossible to alter. The structure of the reservoir management plan has to acknowledge those factors which cannot be altered.

### ***A Further Note on Organizational and Team Structure***

The larger structure of the organization may have a minimal direct impact on reservoir management activities, but there is a general consensus that successful reservoir management requires a team approach. Ideally the team will include all persons who have anything to do with the reservoir (Satter et al., 1992). An organizational structure that encourages the formation of multidisciplinary teams will be much more conducive to creation of optimal reservoir management plans than one that effectively dictates that plans be created by geologists, engineers, and others working sequentially and independently. Satter and Thakur (1994) present an excellent discussion on the structure and function of reservoir management teams.

At project inception, all members should share in developing common project goals and objectives and aid in developing and assigning project responsibilities for each team member. A team leader with the multidisciplinary insight and management skills to encourage cooperative participation in these and subsequent project activities is a necessity.

The dynamic interaction of the group comprising the reservoir management team is a strong contributor to the success of the effort. The team leader must be aware that the members of the team may have varying degrees of technical skill and experience in their own disciplines and may have varying experience in working closely with people from other disciplines. The leader must monitor and nurture the daily interaction of team members. To do so the team leader must be aware of individual personality traits and differences in rank, must be aware that certain team members may have commitments to other projects that may compete for their time and dedication at inconsistent and often inconvenient intervals (though management should do everything possible to minimize conflicts in priorities!), and must realize that occasional disruptions such as loss or addition of team members may inevitably occur.

### **Knowledge of Available Technologies**

A second contextual consideration necessary for creating optimal reservoir management strategies is a familiarity with existing and newly developing technologies that are available to improve hydrocarbon recovery, increase operational efficiencies, and characterize reservoirs. Maintaining an awareness of appropriate technologies in such diverse areas as recovery, wellbore and facilities, and reservoir characterization is a difficult task, especially for smaller organizations. The difficulty of the task is compounded by the rapid evolution of technology in almost every area. Membership and participation in professional societies, attendance at their meetings, and review of their publications may help, but it is not realistic to assume that any organization will have (or should have!) the necessary knowledge and experience in all areas that may be required. A realistic goal would be to obtain enough of a general or screening-level knowledge of available technologies to know when an expert should be consulted for in-depth evaluation. Professional societies and organizations like the regional offices of the Petroleum Technology Transfer Council can often provide contact with the appropriate consulting expertise.

### ***Improved Recovery Technologies***

It is important to be aware of routine applications techniques as well as new techniques and technologies associated with improved recovery. Secondary recovery techniques include injection of water or gas (immiscible) for pressure maintenance or displacement of hydrocarbons. Advanced secondary recovery techniques include those aimed at improving contact with mobile oil such as conformance and recompletion considerations, infill drilling using vertical, deviated, and horizontal wells, and employing polymers for profile modification and mobility control. Enhanced oil recovery techniques include application of processes to recover immobile oil such

as microbial, alkaline and alkaline-surfactant-polymer, surfactant, steam, in situ combustion, and miscible and immiscible gas-injection processes. A moderately comprehensive review of technologies associated with advanced secondary and enhanced recovery is presented by Cole et al. (1994).

### ***Wellbore and Facilities Technologies***

Familiarity with existing and evolving techniques and technologies associated with wellbore equipment and surface facilities can also bear on formulating an appropriate reservoir management plan. The ability of the mechanical equipment both within wells and on the surface to handle changes in fluid types, volumes, and relative volumes under different pressures and temperatures due to possible changes brought about by a reservoir management project can be critical to its success. New or different technologies and/or techniques may be required to accommodate such changes. In some instances, the focus of a reservoir management plan may be to incorporate new technologies or approaches just to improve performance of facilities and equipment.

### ***Reservoir Characterization Technologies***

Successful reservoir management is also dependent on a familiarity with existing and newly developing technologies that are available to characterize reservoirs. Technological knowledge related to the building of reservoir models from both analog and deterministic sources is appropriate, but it is becoming increasingly important to include technologies involved with the collection, handling, integration, and analysis of the large volumes of data that have become associated with reservoir characterization. This does not imply that a high-tech approach is necessarily the appropriate one to take. It is important to be aware of the wide range of both traditional and newly developing technologies available and to have some familiarity with economics involved in assessing and implementing those technologies.

### ***Knowledge of the Reservoir System***

The third consideration for reservoir management plan building is a knowledge of the reservoir system. The reservoir system is composed of subsurface reservoir rock, the reservoir's contained fluids, all its wellbores and downhole equipment, and its surface equipment and facilities. Man's activities may have affected any of the components of the reservoir system and should be considered also.

## ***The Physical Reservoir***

In the past, the terms “reservoir description” and “reservoir characterization” have been used almost interchangeably. Reservoir description perhaps more aptly connotes collection of descriptive or deterministic data from the reservoir itself. Reservoir characterization, on the other hand, might be thought of as a more comprehensive undertaking employing other information sources such as analog reservoirs, outcrops, and modern environments as well as directly measured data from the subsurface reservoir. The end result of reservoir characterization is a complete conceptual picture or model of the reservoir.

A reservoir characterization model is a representation or estimate of reservoir reality. It represents not only the three-dimensional extent or bounds of the reservoir, but the qualitative (presence or absence) and quantitative (magnitude) values of rock, fluid, and other reservoir parameters affecting fluid flow at every location in the volume of the reservoir. The degree of uncertainty associated with placement and magnitude of fluid-flow properties is an important facet of this model.

An important objective of reservoir characterization model construction is to accurately represent and minimize, as far as economically feasible, the uncertainty in our knowledge of reservoir parameters. In the past, the aim of reservoir characterization generally was to create a single “most probable” representation of the reservoir to be used as input to subsequent decision making, but the need for a small number of more extreme yet reasonably probable representations should be recognized as a useful if not critical addition. This approach allows bracketing the range of reasonably expected recovery and economic outcomes. We can think of the goal of reservoir characterization as the construction of a model or small number of models that will aid in predicting by simulation or other means the outcome or probable range of outcomes of potential reservoir management plans (i.e., projects, processes, or operating plans and procedures) in order to evaluate their relative economic merits.

Deterministic reservoir characterization data (i.e., data derived by actual measurement of reservoir properties rather than derived by analogy from similar reservoirs or deposits) can come from a wide variety of technologies and cover a wide range of scales. Although data are taken directly from the reservoir, uncertainties in many types of information gathered are inherent due to the resolving power of the tool used and the inability of many tools to measure desired properties directly. However, the degree of uncertainty associated with the deterministic, quantitative measurement of reservoir properties is often less than that associated with properties assigned by a model of conceptual or analog origin. Figure 1 schematically depicts the scale of measurement and associated resolving power associated with several common deterministic tools.

A number of geological and engineering tools are commonly available to gather deterministic information from which to formulate a reservoir model. Samples of reservoir rocks and fluids collected early in a reservoir's development history may be the best source of information available to predict fluid-flow patterns that may be critical when the reservoir reaches maturity. Reservoir production and injection data are often-overlooked and inexpensive sources of information on larger scale reservoir architecture and heterogeneities. A wide variety of geophysical wireline logging tools, in addition to having great utility in establishing structural and stratigraphic frameworks, are available to make direct measurements of reservoir properties such as rock composition, porosity, and fluid content. Single- or multiple-well pressure transient tests may be run for the purpose of qualitatively or quantitatively discerning variations in the properties of the reservoir's pore system. Tracer testing, i.e., the addition of small quantities of an easily detectable (often radioactive) material to an injected fluid and the subsequent monitoring of its temporal and/or volumetric appearance in the same or adjacent wells, results in direct measurements of critical well-to-well flow characteristics or estimates of residual oil saturation.

Among existing direct measurement techniques, approaches based on seismic methods perhaps have the greatest potential to provide reliable information on reservoir property variations in the interwell region. Recent advances in several areas of seismic technology are making this possible. The accuracy, resolution, and utility of 3-D seismic are being realized thanks to continuing improvements in data acquisition instrumentation, field procedures, data processing software, and 3-D data visualization techniques. Development of procedures for extracting useful information from attributes of the seismic signal such as amplitude, phase, and frequency facilitate the delineation of stratigraphic traps and other subtle geological features and make it possible to determine the distribution of porosity and fluid content in reservoir rocks. Developments in downhole seismic surveys like cross-well tomography and vertical seismic profiling are adding to resolution capabilities in the interwell area.

The deterministic tools discussed above do not constitute an all inclusive list by any means. Other tools and techniques include electromagnetic mapping, remote sensing, surface geochemical sampling surveys, and any of numerous other approaches that have potential to add to our knowledge of the distribution and movement or potential movement of fluids in the reservoir.

Because a single reservoir characterization model or a small number of such representations is the desired result, and because the necessary data are of both engineering and geological origin, the need for close cooperation between geoscientists, engineers, and other professionals (i.e., the members of the reservoir management team) in formulating such models is paramount. Data from various individual technological sources often suggest a number of nonunique interpretations of reservoir reality. It is the duty of the reservoir management team to

understand and use the various technological data types in complementary and supplementary fashions to arrive at the most probable range of possible reservoir realities upon which to base future reservoir performance predictions. Model construction is not a trivial task, and its successful completion requires continual cooperation and interchange of information and ideas among team members. The task cannot be efficiently accomplished (indeed it may not be accomplishable at all!) if geologists and engineers work on the task sequentially and independently.

### ***Reservoir Infrastructure and History***

An additional important aspect of reservoir knowledge is familiarity with the production/injection infrastructure. Natural processes in the subsurface can interact with wellbore equipment resulting in problems such as corrosion, scaling, paraffin deposition, etc. Surface processes, such as erosion or flooding can affect wells and facilities. Knowledge of the history of drilling, completion, recompletion, and workover practices employed in field development as well as familiarity with current surface and wellbore facilities is also necessary. Equally important is a knowledge of past production and injection practices.

Human development activities may certainly affect surface facilities and the use of wellbores. It is also important, however, to know of alterations in the natural properties of the reservoir that have resulted from past human activities. Human activities in development and depletion of a reservoir can have a profound influence on its basic characteristics and thus on its performance. In some cases, human activities are equivalent to introduction of whole new and often extreme episodes of diagenesis, tectonics, and/or fluid exchange. The nature of these changes is unexpected in many instances and can result in decreased reservoir performance and permanent reservoir damage if not considered. Examples might include situations where stimulation practices have led to communication between reservoir units behind pipe, or where long periods of water injection above formation parting pressure have led to channeling between injection and production wells.

### **Steps in Reservoir Management Plan Construction**

One of the key objectives in the Reservoir Management Demonstration Program being sponsored by the Department of Energy has been to resolve the sequence of considerations that goes into the development of an effective reservoir management plan. At this time, only the broadest categories have been identified, but it is hoped that subsequent work on a variety of reservoir management projects under different contexts will enable the procedures to be defined in greater detail with time.

As currently recognized, the primary steps in plan construction are:

Defining the target size

Locating the target

Identifying appropriate technologies

Optimizing technology implementation

Optimizing operational procedures and technologies

An ideal plan will also specify its own limitations based on the conditions and assumptions that were incorporated into its development. The plan may project expected performance by simulation or by other means of all aspects of reservoir performance over the plan's duration (e.g., reservoir wellbore injection and production performance, facilities and equipment usage, environmental and other regulatory compliance, etc.). The plan may specify surveillance and monitoring activities, including data types, collection protocol, database construction, data processing and analysis, and performance variance to be tolerated. The plan may also specify or recommend future plan revisions based on specific criteria such as timing or volume performance of reservoir fluid production or injection. In any event, the plan should be developed so that it is not so rigid as to be inflexible to potential modifications.

These steps are very general and should be applicable whether or not improved recovery is being considered as a reservoir management option. In each step careful attention must be paid to the complete context of reservoir management, i.e., the reservoir system, available technologies, and the business environment. Specific objectives of any plan will depend on the context in which the plan is developed as discussed above, including consideration of the current stage of reservoir development and the type and scale of the decisions required (e.g., evaluation of a potential new process implementation, local production and injection optimization, new facilities or equipment technologies, etc.). A comprehensive reservoir management plan initiated at the time of reservoir discovery will assure early collection of native-state reservoir data vital to implementation of advanced recovery processes many years in the reservoir's future. On the other hand, reservoirs in which data collection has been neglected and reservoirs acquired without adequate accompanying data require a reservoir management plan designed to correct or alleviate the effects of information deficiencies. Ideally, a reservoir management plan or series of plans will provide guidelines over the life of the reservoir.

### ***Target Definition***

Defining the target size, whether that target may be the recovery of additional petroleum resources or merely saving dollars associated with addressing chronic production problems or spent on inefficient operating procedures, will help to determine the scale and scope of the plan



being developed as well as help scale the effort expended in constructing the plan. Multiple targets of the same or different types may be addressed by the same reservoir management plan. In fact, this approach should lead to a plan that will optimize the profitability of the reservoir to the operator on several fronts. Often the target or targets can be defined adequately with existing data, but there are instances in which additional information may have to be collected to reduce uncertainty about the target size to an acceptable level. If the target (or one of the targets) is additional recovery, reservoir characterization at least at some general level, will be needed to estimate the quantity of petroleum that might potentially be present unless this information is already available and reliable from previous work.

### ***Target Location***

In some cases, the focus of the reservoir management plan will include the entire field, but more often, certain zones or areas of the field will present the best development of the target situation. Additional data may have to be gathered on a field-wide scale to locate the target or targets accurately. If additional recovery is the target, questions such as whether the oil is mobile or immobile may also have to be addressed. Reservoir characterization required to answer the questions posed at this stage in plan development will probably be more detailed than that required to estimate the size of the recovery target in the previous step.

### ***Technology Selection***

Identifying appropriate technologies to achieve the target may involve gathering yet more information in order to evaluate not only the technical appropriateness of potential technologies, but to arrive at an economic prioritization of potentially acceptable technologies as well. For example, when the target is improved recovery, this step will include a first-pass screening evaluation of a wide variety of technologies followed by an in-depth evaluation of the appropriateness of the resulting top-ranking recovery technologies.

### ***Technology Optimization***

Optimizing an implementation scheme for selected technologies can require major data collection and analysis efforts, especially if recovery technologies are a focus. Reservoir characterization in particular may need to be done in great detail to allow development of models to predict recovery and economic results with a sufficiently low degree of uncertainty. Well placement and completion configurations will be strongly dependent on the results of this

modeling optimization.

### ***Operational Optimization***

Implementation of new technologies in a reservoir is likely to mean that operational procedures and associated technologies will need to be adjusted for best reservoir performance.

## **SCALING THE RESERVOIR CHARACTERIZATION EFFORT**

If additional recovery is an objective, reservoir characterization plays a major role in four of the five major steps in plan development. In the development of any given reservoir management plan, four separate reservoir characterizations may not have to be performed, however. If estimates of the size of the recovery target are highly uncertain (i.e., are uncertain to the point of being unable to define whether an economic target is present), basic reservoir characterization data should be collected to reduce that uncertainty before proceeding. This approach avoids the expenditure of large amounts of effort and money to build a highly detailed reservoir characterization model for a reservoir that turns out to have an unjustifiably small target.

Initial estimation of the location of a recovery target and post-screening selection of appropriate recovery method or process may require more accurate and more detailed information about the reservoir than that needed for rough target size estimation. Optimizing the implementation of a selected methodology, however, will require a degree of detail and uncertainty dictated by the method selected. In many instances, especially when recovery processes involving large investments in chemicals are involved, this will require a level of detail much greater and uncertainty much lower than that for initial process selection. This step might be thought of as an extremely detailed refinement of the initial target location step.

### **Steps in Constructing an Appropriate Reservoir Characterization Model**

The general methodology involved in constructing a reservoir characterization model to fit any stage of reservoir management plan preparation may be summarized in a small number of sequential steps. In practical application, the steps may need to be followed through several iterations to achieve an acceptable product. A flowchart summarizing typical activities in these steps is presented in Figure 2.

### ***Specify Appropriate Resolution and Uncertainty Characteristics***

This step consists of making an initial estimate of the of detail and degree of uncertainty necessary to perform the evaluation. This will be a function of the stage of reservoir management plan development under which the reservoir characterization is being performed. The required level of model detail may vary from place to place within the reservoir or the model may be entirely focused on a segment of the reservoir.

### ***Incorporate Existing (or New) Information***

Information that goes into the building of a reservoir characterization model originates in: (1) data collected from different sources (e.g., rock and fluid samples, wireline logs, seismic, well tests, production data, etc.), (2) data collected at different resolution, and (3) data collected with inherently different degrees of uncertainty (including both deterministic and conceptual or analog information). A reservoir characterization model must provide information throughout the 3-D volume of that portion of the reservoir that is of interest, but this does not mean that each deterministic data type needs to be collected throughout the entire volume of interest. Instead, information derived from various data sources is incorporated by interpolation, extrapolation, or correlation with other data of deterministic or conceptual/analog origin. This diverse information is incorporated in mutual support of a single reservoir characterization model or a small number of models that express the probable range of variation. Information derived from geoscience, reservoir engineering, and other data is continually compared and contrasted to test various details of the emerging reservoir characterization model(s) until indications from all existing sources are in agreement. Inconsistent information or conflicting information derived from different sources, scales, or uncertainty models may have to be addressed with additional data collection before full confidence is achieved.

### ***Test the Model Against Known Reservoir Performance***

Models from the previous step are tested either qualitatively or quantitatively using simulation or simpler approaches to measure their ability to serve as a basis for predictions of reservoir pressure and production. Failure of the reservoir characterization models to support a reasonable match with actual reservoir past performance indicates that the models need correction through incorporation of new information. If models perform well, they are ready for use in predicting future performance of the reservoir under the plan being formulated.

### ***Identify, Collect, and Incorporate New Information***

Our knowledge of the reservoir will never be perfect, but collection of additional information can be viewed as an attempt to reduce model uncertainty and, ultimately, risk when the reservoir management plan is implemented. Several guidelines govern judicious collection of information. The primary objective is to obtain the maximum information affordable, in terms of proposed reservoir management project economics, to reduce uncertainty in prediction of project outcome. If the cost of reducing uncertainty to an acceptable level is found to be too high, the reservoir management plan may have to be redesigned. Information from all potential sources should be evaluated in terms of possible contribution to reducing model uncertainty. Potential contributors of low-cost information such as conceptual models from the published literature should not be overlooked. After a reservoir characterization model has been revised or refined by incorporation of new information, it should be retested.

### ***Use the Model to Predict Future Reservoir Performance***

Production performance predictions obtained by simulation or other means from reservoir characterization models will form the basis for economic analysis of various possible scenarios for inclusion in the reservoir management plan. This step enables plan optimization through selection of the best economically performing activities, processes, process implementation strategies, operational strategies, etc. If economic analysis indicates that results will be unacceptable or if the range of probable outcomes includes unacceptable economic performance, the plan may need to be redesigned.

## **THE RESERVOIR MANAGEMENT PROCESS**

The world of reservoir management is dynamic rather than stable. Technologies are evolving rapidly on numerous fronts, and the petroleum business environment is ever changing. Changing business and technological contexts de-optimize previously existing reservoir management plans. The formulation, implementation, and revision of reservoir management plans can therefore be considered to be a fundamental reservoir management process. It is by necessity an iterative process (see Figure 3) requiring regular if not continuous attention or monitoring for every reservoir being managed.

The reservoir management process consists of first formulating an appropriate reservoir management plan in the context of reservoir knowledge, knowledge of technologies, and a knowledge of the business environment as has been discussed in previous sections of this

paper. The plan is then implemented as specified. Once the plan has been implemented, monitoring of both the performance of the reservoir and of the current status of knowledge of the reservoir, technologies and the business environment should begin immediately.

### **Events Triggering Reservoir Management Plan Revision**

The reservoir management plan itself may specify a condition or set of conditions that, when met, indicate the plan should be reevaluated. These criteria may include such items as cumulative volume, relative volume, or rate of production or injection of a specified fluid, passage of a specific period of time, or attaining a particular stage of reservoir development.

At any time, however, reservoir performance anomalies of any kind (e.g., production or injection volumes, facilities usage, or regulatory compliance) with respect to plan expectations or predictions may indicate immediate need for plan revision. Ideally, the plan should specify guidelines for tolerance in variation from plan prediction in all critical performance areas. When these tolerances are exceeded, the plan should be reviewed and revised.

New information may also be just cause for plan revision at any time. New information may take various forms. It may be new reservoir information, perhaps extracted from data collected under specifications of the current plan, that indicates a conflict with the assumptions that went into formulating the plan. It may be in the form of the introduction of new technologies, ideas, or procedures not available or known at the time the plan was formulated. The critical new information may even be in the form of performance anomalies arising in analogous reservoirs.

Unexpected or unpredicted changes in circumstances or opportunities related to the general or operator-specific business environment may also present cause to reevaluate the reservoir management plan. Examples of factors that may be significant include market economics, new laws and regulations, changes in key personnel, and decisions to buy, sell, or trade reservoirs.

### **Influence of the Reservoir Management Process on Reservoir Characterization**

From the preceding discussion we have seen that reservoir characterization is a multidisciplinary endeavor that plays an important role in developing a knowledge of the reservoir system and it is, in turn, critical to development of a reservoir management plan. We have also seen that implemented reservoir management plans are likely to become less than optimum as changes in technology and the business environment take place or as reservoir performance anomalies are recognized. The resulting periodic requirement for development of revised reservoir management plans means that revised reservoir characterization models may need to be

built to properly fit new plans to the revised reservoir management contexts. Reservoir characterization, therefore, becomes a consideration that must be addressed numerous times throughout the life of a reservoir.

## **CASE STUDY EXAMPLES FROM THE DEPARTMENT OF ENERGY'S RESERVOIR MANAGEMENT DEMONSTRATION PROGRAM**

Projects supported by the Department of Energy under the Reservoir Management Demonstration Program are limited to oil reservoirs operated by small business organizations. Multiple operators must be involved in proposed projects, although participation by research organizations, state government agencies, service companies, consultants, etc. is encouraged. Projects must address resources significant to the region in which they occur and/or must address a major technological need. Projects are performed under a Cooperative Research and Development Agreement (CRADA) at a total level of funding up to about \$500,000, at least 50% of which must be cost-shared by industry partners. DOE's contribution is mainly in the form of professional labor supplied through BDM-Oklahoma, but data acquisition and analysis, additional consulting expertise etc. may also be included in DOE's contribution. Projects are intended to be short, of 12 to 18 months maximum duration, and technology transfer is a major focus of each. All projects have a common goal to develop a comprehensive reservoir management strategy to improve the operational economics and optimize the oil recovery from the target field.

As initially conceived, the Reservoir Management Demonstration Program will include 15 projects, one in each of the ten Petroleum Technology Transfer Council (PTTC) Regions (see Figure 4), three projects involving Native American reservoirs, and two offshore projects. At the present time, three projects have been initiated under the program. One project, begun in early 1995 in the East Randolph field in Ohio, is nearing completion. This project in the Appalachian PTTC Region deals with a small recently discovered oil reservoir in a newly developing play in an area of mostly mature production. A second project, begun in late 1995 in the Citronelle field in Alabama, is a little more than half completed. This project, being performed in the Eastern Gulf PTTC Region, involves developing a strategy for a mature domestic giant reservoir (160 MMBO cumulative production). A third project has just been launched in late 1996 in the Bainville North field in Montana. This project in the Rocky Mountain PTTC Region will deal with the unique problems and opportunities related to optimizing a strategy for and optimization of multiple producing horizons within a field.

## **Summary of the Plan-Building Process for the East Randolph Field**

Since 1992, PEP Drilling Company and Belden & Blake Corporation have developed this unique but significant oil reservoir in the Cambrian Rose Run Formation in Portage County, Ohio (see Figure 5). One of only a few fields to produce oil from the Rose Run, the East Randolph field covers about 1,500 acres, lies at a depth of about 7,200 ft, and contains an average of about 15 ft of pay in the upper three of five marginal marine sand zones typically present. The field contains just over 30 wells and had produced about 450,000 bbl of 42° API oil and 1.2 BCFG as of June 1996. Two items of context associated with the East Randolph field had an especially important bearing on the development of the reservoir management plan for the reservoir. First, the field has been and continues to be developed by small independent operators. Second, the field has been entirely developed in the 1990s. In fact, rapid development is still going on as efforts continue to define the limits of the field.

In the proposal submitted by the operators, they outlined a list of potential targets or opportunities to pursue as reservoir management goals for the plan to address. The list included:

- Optimum development and infill well locations
- Optimum selection and implementation of secondary recovery method
- Optimum hydraulic fracturing techniques
- Address paraffin buildup problem in producing wells

In the proposal, the operators also suggested a list of project tasks and teaming arrangements that might be used to best address those tasks.

A kickoff meeting of all project participants was held at the project outset to further prioritize targets and to assign specific plan development tasks to teams and subteams. It was expected that the plan development process would be flexible and capable of changing to accommodate the course suggested by new information obtained.

### ***Role of Reservoir Characterization***

Reservoir characterization played a major role in arriving at the reservoir management plan for this project, particularly in pursuit of the targets selected as highest priority, i.e., defining development and infill well locations and selecting an optimum secondary recovery method. A series of incremental and sometimes iterative steps was performed in arriving at the final reservoir characterization model employed (Salamy et al., 1996). The steps involved analysis of existing data, identifying data insufficiencies, obtaining and incorporating new information into the emerging model, and testing the predictive limits of the model.

At the project outset, field limits were not yet accurately defined; pre-project estimates of OOIP were in the neighborhood of 4.4 MMBO. Although the three productive sand intervals in the Rose Run were recognized as such, the high GOR observed for most wells (1,500 to 2,000 SCF/STB) was attributed to conditions in all three sand zones.

Initial geologic work with neutron and density logs digitized in the project suggested that the uppermost sand zone had a much higher gas saturation. Analysis of production data showed a correlation between high initial GORs and occurrence of a well-developed upper sand zone, further suggesting a possible gas cap. Field-wide work based on digital logs and previously existing sidewall core analysis data determined structural heterogeneities (faults), vertical layering of rock properties, and horizontal variations in rock properties (Thomas and Safley, 1996). Zone mapping and volumetric analysis based on this geologic model yielded an OOIP figure of approximately 11 MMBO. This discrepancy in OOIP estimates was considered to be important to resolve considering its potential impact on continued development and future recovery.

In parallel with the initial geological work, and as an initial and potentially cost effective check on reservoir parameters, a single-well reservoir model was developed on one of the highest GOR wells in the field. PVT parameters input to this model were derived using published correlation techniques from initial reservoir parameters. Relative permeability and capillary pressure data input to the model were taken from analogous fields nearby. Model results were unstable in predicting production and indicated the need for more representative values for PVT and relative permeability parameters, additional field pressure data, and field volumetric information. As a result, a pressure buildup was run and surface-recombined fluid samples were obtained from an existing field well.

The new PVT data (which indicated only 485 SCF/STB), new pressure data, and production data were then used in a material balance calculation. A sensitivity analysis done on gas/oil volume ratios indicated that gas/oil volume ratios in the range of .16 to .2 would yield OOIP in the observed range 13 to 11 MMBO, respectively). Using a gas/oil volume ratio of .17 and OOIP of 12 MMBO yielded a reasonable match with observed field pressure history. This analysis confirmed that the field's high GOR was not a result of gas coming out of solution.

A second single-well simulation was run using a 3-layer (1 gas layer, 2 oil layers) model, the new PVT data, and, again, relative permeability data from analogous fields. This modeling confirmed the upper zone as predominantly a gas zone and accurately predicted reservoir pressure encountered by a subsequently drilled well at the edge of the modeling area. Predictions, however, were still found to be sensitive to relative permeability data and the recommendation was made that this new information be obtained.

An infill well was drilled and cored, and relative permeability and capillary pressure data were obtained on samples from the core. A CMR log was run to better define water saturation



distribution, and an FMI log was run to investigate distribution and orientation of natural fractures. Cleaning the samples for special core analysis also gave insight into the nature of the paraffin deposition problem and anomalously low measured permeabilities from routine core analysis samples.

As a final step, a full-field simulation was undertaken using all the newly collected information. The simulation study was completed in two steps. The first step, history matching of field production and pressure data, was done holding constant all known field and experimental data. Results of this first step showed a good match with oil and gas production and field pressure data, thus validating the basic model. The second step used the model to predict waterflood and gas injection results as potential secondary recovery methods for the field. Simulation results indicated that a high producing water/oil ratio coupled with low oil recovery makes waterflooding a less favorable option than gas injection for secondary recovery. The base case simulation indicates that ultimate primary recovery is 8% of OOIP. Waterflooding only adds an additional 0.5% recovery, while gas injection results in an additional 7.8% recovery of OOIP.

## ***Discussion***

The fact that the field is operated by small independents governed not only the nature of the implementations recommended by the plan, but the expenditure of effort and capital in collecting and analyzing data to arrive at the plan. Collection of new information had to be adequately justified. Although mutually supportive evidence from different reliable and cost-effective sources was sought, highly redundant confirmations were avoided as unnecessary and unjustifiable. Continued rapid development of the field while the plan was being formulated meant that new information had to be considered and incorporated on a continual basis and that rapid development of a plan was necessary to optimize field development and definition activities.

The incremental approach to reservoir description for plan development employed in this project results in an efficiency in data collection. Existing data were analyzed at each step with the objective of determining whether the uncertainty associated with the predictive power of the models based on those data was acceptable. If not, the type and quantity of new data needed to constrain the modeling efforts were identified and obtained after first considering the potential cost-effectiveness of the new information. This approach avoids the collection of unnecessary data and fits very well with the typical independent operator's economic constraints in reservoir characterization

## Summary of the Plan-Building Process for the Citronelle Field

Citronelle field, in Mobile County, Alabama (see Figure 6), has been producing since its discovery in 1955 from fluvial sandstones of the Cretaceous Rodessa Formation at a depth of greater than 10,000 ft. The field, located over a deep-seated salt intrusion, was developed and essentially remains today on 40-acre spacing, covering a surface area of 16,400 acres with 468 wells. An 800-ft-thick gross pay interval contains at least 42 productive sand zones that form over 300 separate reservoirs, each with highly variable permeability characteristic of fluvial deposition. Field pressure declined relatively rapidly, leading to the inception of waterflooding in 1961. By early 1995, approximately 15,000 bbl of water were being injected each day into 50 injection wells to produce about 3,600 bbl of oil from about 175 producers. Cumulative recovery is about 160 MMBO, 120 MMBW, and 1.2 BCFG. Items of context associated with this field that had important influence on plan construction include the fact that both major and independent companies have conducted studies and collected voluminous data (several versions of some parameters) from the field over the course of its 40-year history and the fact that the field is currently being managed in its mature waterflood stage by small operators for the most part.

In the proposal submitted, the operators identified several possible targets for improving the economic performance of the field. These included:

- Create a computerized field database for future analyses
- Identify untapped, incompletely drained, and new pool targets
- Optimize the waterflood strategy
- Investigate alternate recovery methods
- Evaluate drilling and completion techniques
- Investigate casing leak prevention and repair
- Investigate production problems related to paraffin, chlorite, scaling, etc.
- Investigate improvement of downhole hydraulic pump life

The operators also suggested a list of tasks to address the targets listed above and made tentative assignment of team members to the tasks. In addition to appropriate personnel from BDM-Oklahoma, the reservoir management team for this project included geoscience, engineering, management, and other professionals representing operators of the 341 Tract, East, Southeast, and Northwest Units of the Citronelle field; operators of geologically analogous reservoirs in the area; the Alabama Geological Survey; the State Oil and Gas Board of Alabama; and the University of Alabama. The team also included a private engineering consultant with a long history of association with the Citronelle field.

Several major reservoir management decisions were made by the team very early in the project, even before a detailed blueprint was arrived at for constructing the reservoir management

strategy. All recognized that, under current operations, the economic limit for the field was approaching within a few years. There was also a general agreement that, based on the what was already known about the field and its performance, a substantial oil target remains in the Citronelle field that justifies a reservoir management effort for its recovery. Discussions focused on the necessity of achieving a cost-effective approach through careful matching of the limited resources available for investment by the operators to the probability of improving production and or profitability. The resulting circumscribing of reservoir management activities was, in reality, the beginning of reservoir management plan development.

It was further agreed that, rather than considering the entire field, the most economically reasonable approach would be to concentrate, initially at least, on geographic areas where certain significant problems or opportunities were prevalent. Solutions developed in these areas should have the most significant impact on profitability per dollar expended.

Although the operators had done a considerable amount of work in identifying potential opportunities for improving profitability, a kickoff workshop with the full reservoir management team in attendance was held at project inception to further identify and delineate problems and opportunities to be addressed. Specifically the kickoff workshop addressed:

#### **Identifying and prioritizing opportunities to be pursued**

Identifying and prioritizing geographic areas in the field where opportunities are best developed or most prominent

Reviewing the data available to address opportunities in the areas identified

Identifying additional data requirements

Developing a detailed procedure and schedule to govern plan building activities based on the results of the steps above

Assigning team personnel responsible for execution of the tasks delineated in the previous step

Identifying possible opportunities for technology transfer

The highest priority opportunity identified at the kickoff workshop was that of waterflood optimization. Boundary areas (see Figure 7) between the Citronelle 341 Tract Unit and the East and Southeast Units were identified as areas where the current waterflood has been least efficient in recovering oil reserves because no unified effort has been made in those areas in the past to optimize injection or production strategies.

## ***Role of Reservoir Characterization***

The long history of the Citronelle field has included numerous field-wide geological and engineering studies performed at various times. These studies, which were based on a strong foundation of core and wireline log data, include most of the current wells in the field. Computerized databases were originally associated with some of these studies, while others were based on work done strictly by hand. Remaining data from all these earlier studies was available only in hardcopy form at project inception, however. The quality of much of the work done in the past was judged to be sufficient to justify using it as a basis for the reservoir characterization needs of the current study.

A decision was made early in the project to pursue two parallel approaches to reservoir characterization for the Citronelle project. The first approach would involve using interpreted sand geometries and associated volumetric parameters derived from past studies along with past pay determinations and preliminary estimates of permeabilities, porosities, and water saturations from past engineering studies to perform preliminary characterization of the reservoir in the areas of interest along the Unit boundaries. A second and simultaneous approach involved entering gross and net pay data along with gradually refined estimates of permeabilities, porosities, and water saturations into a field-wide database that could be used with modern mapping tools to create minimally biased volumetric and other estimates in the late stages of the current study and in future studies beyond the scope of the current work. Production data were obtained from the state of Alabama and cumulative values at various points in time were entered into this database also.

As a first step in determining the best areas and approaches for obtaining additional waterflood recovery, cross sections in the areas of interest defined along the unit boundaries were used to define potential flow units as isolatable targets for improved recovery. These flow units were defined by combining into one package sands that are likely to be in vertical and horizontal communication with each other across the area of interest, but at the same time separated from adjoining sands or packages by substantial shale barriers. Due to past hydraulic fracturing practices in the field, a 30-ft minimum thickness was used to define effective shale barriers separating sand packages. As a next step toward identifying potential recovery targets, floodable OOIP volumetrics were calculated for each of the approximately 20 sand packages or flow units identified.

Flow units do not occur in isolation, however. Several flow units are commonly present in a single well, as well as numerous sands not identified as belonging to discrete flow units. The next step involved looking at groups of wells characterized by presence of multiple flow units in common. These wells form logical groups to consider for production optimization through

alteration of injection/production strategies. Identifying these groups of wells and prioritizing them on the basis of their OOIP volumetrics is now nearing completion.

The anticipated next step is to review the completion, production, and injection histories of the associated wells for the top priority groups to determine the size of the remaining potential recovery target. The final step will be to evaluate and strategize recompletions and injection/production geometries to maximize recovery for all sand packages and flow units involved in the groups.

## ***Discussion***

The series of steps involving progressive prioritization first on the basis of OOIP and then on the basis of remaining or recovery potential is meant to assist in assuring that areas with the best recovery economics can be addressed first. In its refined form, this general methodology can then be applied throughout the field to maximize economic recovery from other sand packages. Such an approach would allow the untapped profitability potential of the field to be developed in small incremental steps that are more financially feasible for small operators than if the entire field were examined in detail at once.

## **Summary of the Plan Building Process for the Bainville North Field**

The Bainville North field was discovered in 1979 in the Williston Basin in Roosevelt County, Montana (see Figure 8), with establishment of production from the Devonian Winnipegosis Formation at a depth of 11,500 ft. Production has since been added from four additional zones between the Mississippian Ratcliffe Formation at 8,500 ft and the Ordovician Red River Formation at 12,500 ft. Fifteen wells currently produce in the field whose cumulative production is 2.8 MMBO, 2.8 BCFG, and 1.4 MMBW through early 1996.

In the 1990s, Nance Petroleum Corporation has substantially increased production from the Red River Formation through use of 3-D seismic and other advanced rock, fluid, and high-resolution wireline log data to locate infill wells. Although only seven wells are currently producing from the Red River interval, through early 1996 cumulative production from the interval was 1.0 MMBO and 762 MMCFG.

In the operators' proposal, reservoir characterization of the highly heterogeneous dolomitic Red River reservoir for purposes of improved recovery implementation was presented as a top priority. The reservoir management strategy developed in the project will also address the design and implementation of improved recovery processes within the context of the field's multiple productive horizons. This will include considerations of well spacing and utilization,

artificial lift optimization, and facilities requirements. Additional problems to be addressed may include paraffin deposition, scaling, corrosion, and casing collapse.

### ***Role of Reservoir Characterization***

Reservoir characterization is expected to proceed by integration of existing core data, fluid data, wireline log data, pressure data, 3-D seismic data, and any additional data deemed necessary into reservoir models for use in simulation. Historical performance of the field will be simulated and predictions made for the implementation of improved recovery techniques. From these results, a reservoir management strategy will be formulated.

### ***Discussion***

This project is just beginning, but it has potential for significant impact on Williston Basin petroleum development. Because of the geologic similarities between the various producing horizons in the basin, and because very few advanced recovery projects have been implemented in the basin, the reservoir management strategies developed to address the opportunities at Bainville North will be applicable to most reservoirs in the region.

### **CONCLUSIONS**

Reservoir management is not optional; anyone who is responsible for a reservoir is managing it. Reservoir management is not a luxury reserved for large recently discovered reservoirs or for major oil companies. Reservoir management does not necessarily imply a "high-tech" approach.

A plan or strategy that guides the operator's interaction with the reservoir is the heart of reservoir management. Efficient reservoir management is the creation of a plan that maximizes the profitability of a reservoir to a specific operator. An appropriate reservoir management plan can not be "bought off-the-shelf" or transported from one reservoir to another or from operator to operator; it must be custom built. To accomplish this requires a knowledge of the business environment, a knowledge of technologies available to describe, analyze, and exploit the reservoir, and a knowledge of the reservoir system including its rocks, fluids, wellbores, and surface facilities.

Reservoir characterization is an important technique to gain needed knowledge of the reservoir for reservoir management plan building. Reservoir characterization approaches can be appropriately scaled by considering the reservoir management context, both the context within

the reservoir management plan-building process and the context of the business environment and the status of technology.

Reservoir management is a dynamic process. Reservoir management plans de-optimize as technology and business environment change or as new reservoir information indicates the reservoir characterization models on which the current plan is based are inadequate. Continual monitoring will allow identification of reservoir management plans that are no longer optimum. De-optimized plans should be revised to maintain maximum profitability and recovery. Revision of plans commonly calls for a revised reservoir characterization model or models as well.

The generally risk-averse approach to reservoir management, especially of domestic reservoirs, taken by industry means that many reservoirs are operated under less-than-optimum reservoir management plans. The potential to increase profitability and recovery from domestic reservoirs is therefore great. The Department of Energy's Reservoir Management Demonstration Program focuses on this concept. The program is seeking to improve domestic reservoir recovery and profitability and delay abandonment through encouraging operators to develop, apply, and disseminate efficient reservoir management techniques.

Work accomplished in two program projects demonstrates the scaling of reservoir characterization efforts in developing reservoir management plans for reservoirs under widely contrasting contexts. Both projects were cognizant that small operators have limited capital resources to invest in extensive reservoir characterization efforts. Reservoir characterization in the East Randolph field project took an incremental approach to defining critical reservoir parameters while this small newly discovered field was still under active development and definition. In the Citronelle project, the focus is on developing an improved recovery approach or methodology for small areas of high potential in this already mature waterflood. The methodology developed can then be repeated by the operators for remaining improved recovery targets in this large field.

## **ACKNOWLEDGMENTS**

The authors and other researchers participating in the Department of Energy's program of reservoir management demonstrations are appreciative of the Department's foresight in supporting methodological research and demonstration in the critical areas of reservoir management and reservoir characterization. Neither would this product have been possible without the dedication and support received from all members of the East Randolph, Citronelle, and Bainville North field reservoir management teams. We are also grateful to the BDM-Oklahoma Information Services Department for their support.

## REFERENCES

- Cole, E.L., R.S. Sawin, and W.J. Weatherbie, 1993, Reservoir Management Demonstration Project, The University of Kansas, Energy research Center, Technology Transfer Series 93-5.
- Cole, E.L., M.L. Fowler, S.P. Salamy, P.S. Sarathi, and M.A. Young, 1994, Research Needs for Strandplain/Barrier Island Reservoirs in the United States, report DE95000118, United States Department of Energy, Bartlesville, Oklahoma, 186p.
- Fowler, M.L., M.A. Young, E.L. Cole, and M.P. Madden, 1996, Some practical aspects of reservoir management, SPE Paper 37333 presented at the Eastern Regional Meeting in Columbus, Ohio, October 23-25.
- Jackson, S.R., and L. Tomutsa, 1991, Reservoir characterization---state-of-the-art review: in Research Needs to Maximize Economic Producibility of the Domestic Oil Resource, Part I - literature review and areas of recommended research, Department of Energy Report NIPER-527, p. 143-172.
- Lake, L.W., and H.B. Carroll, Jr., 1986, Preface, in L.W. Lake and H.B. Carroll, Jr., eds., Reservoir Characterization, Academic Press, Orlando, Florida, 659pp.
- Riley, R.A., and M.T. Baranoski, 1992, Reservoir heterogeneity of the Rose Run Sandstone and adjacent units in Ohio and Pennsylvania, presented at the Ohio Oil and Gas Association Winter Meeting, Canton, Ohio, October 20.
- Salamy, S.P., M.A. Young, L.E. Safley, J.L. Wing, and J.B. Thomas, 1996, Application of reservoir management techniques to the East Randolph field, Portage County, Ohio: Reservoir engineering study, SPE Paper 37334 presented at the Eastern Regional Meeting in Columbus, Ohio, October 23-25.
- Satter, A., and G.C. Thakur, 1994, Integrated Petroleum Reservoir Management - A Team Approach, Pennwell Publishing Co., Tulsa, OK, 335p.
- Satter, A., J.E. Varnon, and M.T. Hoang, 1992, Reservoir management: technical perspective, SPE Paper 22350, presented at the International Meeting on Petroleum Engineering in Beijing, China, March 24-27.
- Thakur, G.C., 1991, Waterflood surveillance techniques - a reservoir management approach, Journal of Petroleum Technology, v. 43, no. 10, p. 1180-1188.
- Thomas, J.B., and L.E. Safley, 1996, Improved reservoir characterization of the Rose Run Sandstone in East Randolph field, Portage County, Ohio, presented at the Fourth Annual Technical Canton Symposium, Canton, Ohio, October 8-9.
- Wiggins, M.L., and R.A. Startzman, 1990, An approach to reservoir management, SPE Paper 20747, reservoir management panel discussion, 65th Annual Technical Conference and Exhibition, New Orleans, Louisiana, September 23-26.



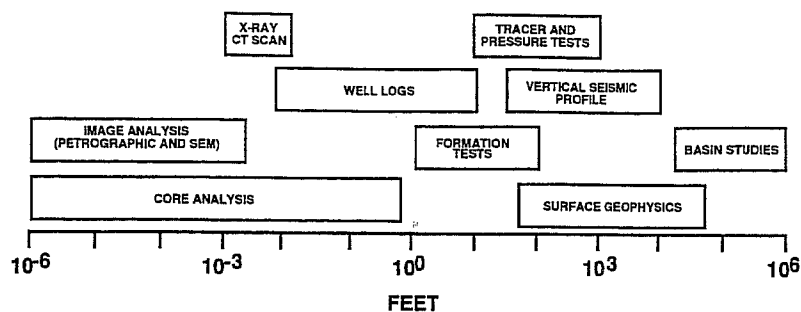


Figure 1—Scales of measurement and relative resolution of some common deterministic reservoir characterization tools (modified from: Jackson and Tomutsa, 1991).

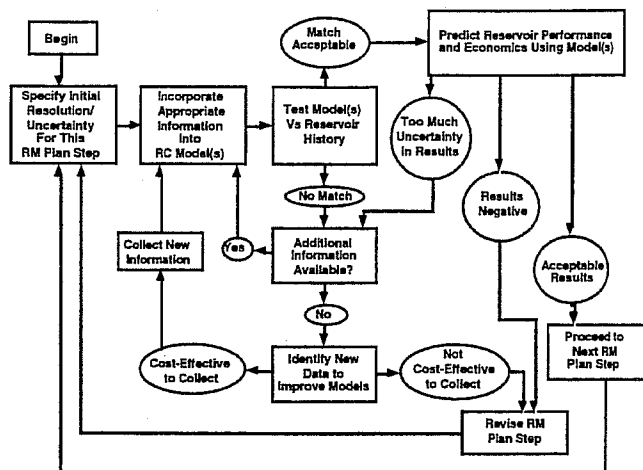


Figure 2—Construction of appropriate reservoir characterization (RC) models is an interactive procedure strongly controlled by reservoir management (RM) context and the cost-effective availability of information.

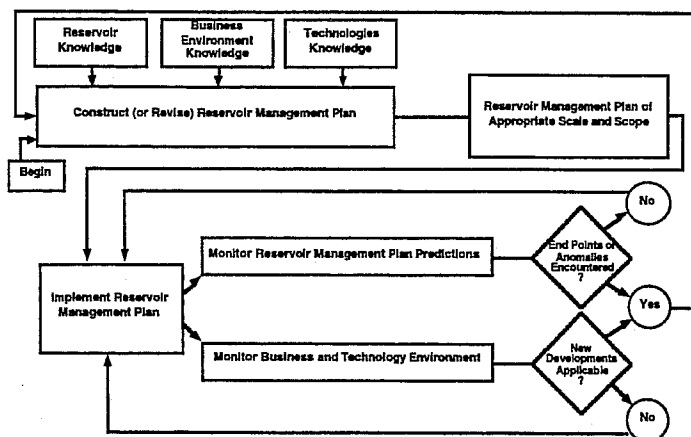


Figure 3—The reservoir management process is an interactive procedure involving plan construction (or revision), plan implementation, and monitoring of reservoir performance, technological advancements, and the reservoir management business environment (from Fowler et al., 1996).

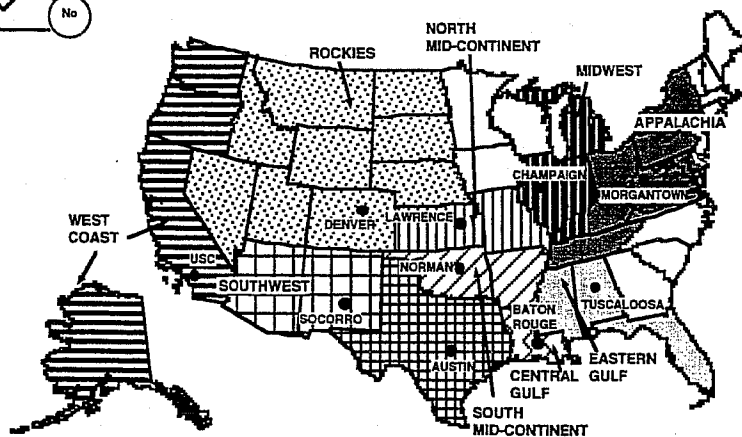


Figure 4—The ten Petroleum Technology Transfer Council regions and the cities in which their Regional Lead Organizations are located.

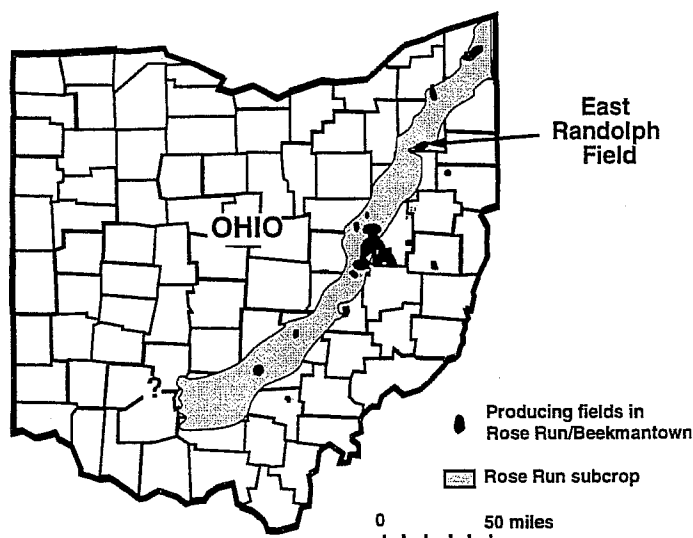


Figure 5—The East Randolph field is located in eastern Ohio in a northeast-southwest trend of reservoirs producing mostly gas from the Rose Run (from Fowler et al., 1996; Riley and Baranoski, 1992).

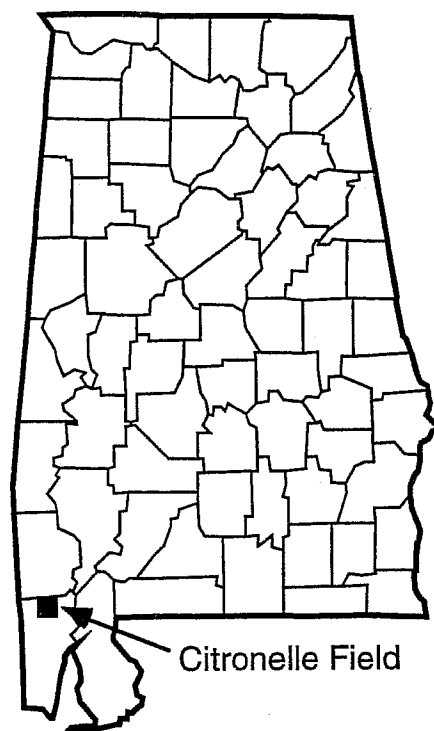


Figure 6—The Citronelle field is located on the eastern edge of the Mississippi Interior Salt Basin in Mobile County, Alabama (from Fowler et al., 1996).

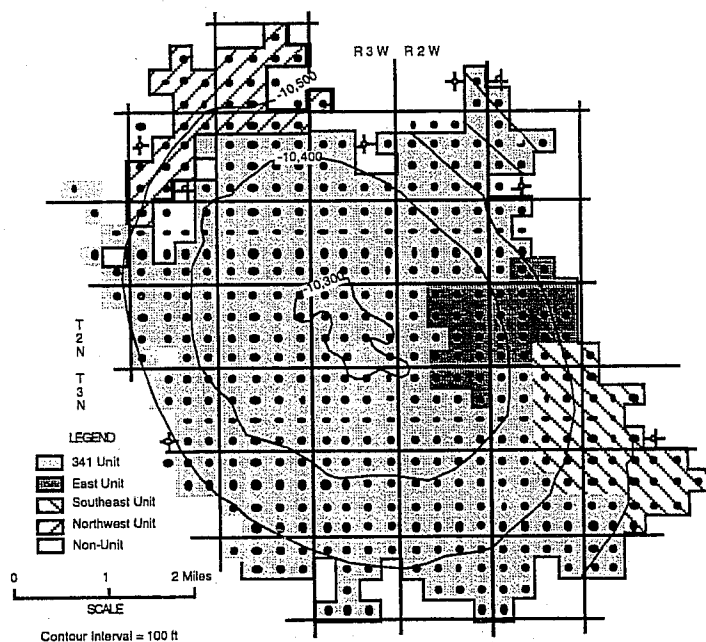


Figure 7—The boundary areas between the units in the Citronelle field are the primary focus of the current reservoir management study. Structural contours are on the base of the Ferry Lake Anhydrite immediately overlying the Citronelle reservoir (from Fowler et al., 1996).

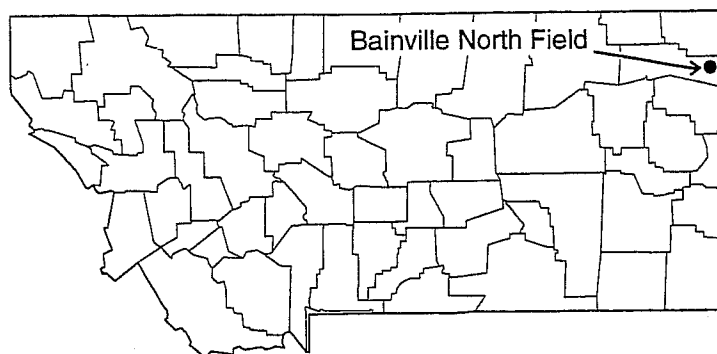


Figure 8—The Bainville North field is located in Roosevelt County, Montana in the Williston Basin.

**ADVANCED RESERVOIR CHARACTERIZATION  
FOR IMPROVED OIL RECOVERY IN A  
NEW MEXICO DELAWARE BASIN PROJECT**

**Authors:**

**F. David Martin  
Richard P. Kendall  
Earl M. Whitney  
Dave Martin and Associates, Inc.  
917 Belmont Drive  
Socorro, New Mexico 87801**

**Dr. Bob A. Hardage  
The University of Texas at Austin  
Bureau of Economic Geology  
University Station, Box X  
Austin, Texas 78713-7508**

**Bruce A. Stubbs  
Pecos Petroleum Engineering, Inc.  
P.O. Box 2885  
Roswell, New Mexico 88202**

**Bruce Uszynski  
Territorial Resources, Inc.  
P.O. Box 1521  
Roswell, New Mexico 88202**

**William W. Weiss  
New Mexico Petroleum Recovery Research Center  
801 Leroy Place  
Socorro, New Mexico 87801**

**Acknowledgment:**

**Mr. Mark B. Murphy  
Strata Production Company  
P.O. Box 1030  
Roswell, New Mexico 88202**

## ABSTRACT

The Nash Draw Brushy Canyon Pool in Eddy County, New Mexico is a field demonstration site in the Department of Energy Class III program. The basic problem at the Nash Draw Pool is the low recovery typically observed in similar Delaware fields. By comparing a control area using standard infill drilling techniques to a pilot area developed using advanced reservoir characterization methods, the goal of the project is to demonstrate that advanced technology can significantly improve oil recovery.

During the first year of the project, four new producing wells were drilled, serving as data acquisition wells. Vertical seismic profiles and a 3-D seismic survey were acquired to assist in interwell correlations and facies prediction.

Limited surface access at the Nash Draw Pool, caused by proximity of underground potash mining and surface playa lakes, limits development with conventional drilling. Combinations of vertical and horizontal wells combined with selective completions are being evaluated to optimize production performance.

Based on the production response of similar Delaware fields, pressure maintenance is a likely requirement at the Nash Draw Pool. A detailed reservoir model of pilot area was developed, and enhanced recovery options, including waterflooding, lean gas, and carbon dioxide injection, are being evaluated.

## INTRODUCTION

The Nash Draw Brushy Canyon Pool, operated by Strata Production Company (Strata), is located in Sections 12-, 13-, and 14-T23S-R29E, and Section 18-T23S-R30E, in Eddy County, NM. General characteristics of this Slope Basin Clastic reservoir are listed in Table 1. Production at Nash Draw Pool (NDP) is from the basal Brushy Canyon zones of the Delaware Mountain Group of Permian, Guadalupian age.

The primary concerns at the NDP are: (1) the low primary oil recovery of approximately 10%, (2)

a steep oil production decline rate, and (3) rapidly increasing gas-oil ratios. This low recovery is caused by low reservoir energy, and less than optimum permeabilities and porosities. Initial reservoir pressure is just above the bubble-point pressure and declines to below the bubble point after a few months of production. With the solution gas drive reservoir, oil production declines approximately 50% in the first year, and gas/oil ratios increase dramatically. These concerns point out the importance of considering various reservoir management strategies to maximize the economic recovery of oil at the NDP. Based on the production characteristics that have been observed in similar Delaware fields, pressure maintenance is a likely requirement at the NDP.

Early in the NDP development, Strata identified three basic constraints: (1) limited areal and interwell geologic knowledge, (2) lack of an engineering tool to evaluate the various producing strategies, and (3) limited surface access that will prohibit development with conventional drilling. The limited surface access at the NDP is caused by the proximity of underground potash mining and surface playa lakes (see Fig. 1). Based on the risk involved in developing advanced technologies to address these constraints, Strata submitted a proposal under the DOE Class III solicitation. The project was approved by the DOE and began in September 1995. The objectives of the project are: (1) to demonstrate that a development drilling program and pressure maintenance program, based on advanced reservoir management methods, can significantly improve oil recovery compared with existing technology applications, and (2) to transfer the advanced methodologies to oil and gas producers, especially in the Permian Basin.

Typical of small independent producers, Strata lacked the in-house expertise to address all of the needs of the Class III project, and, therefore assembled a diverse team of experts to manage and analyze the NDP. Strata is responsible for the management and day-to-day operations of the NDP; the Petroleum Recovery Research Center (PRRC) provides technical support and technology transfer functions; Dave Martin and Associates, Inc., with Drs. Richard Kendall, Earl Whitney, and John Killough, provides reservoir characterization and simulation services; Dr. Bob Hardage of the Bureau of Economic Geology (BEG) at

the University of Texas at Austin provides seismic and geophysical expertise; Territorial Resources, Inc. provides geological expertise; and Pecos Petroleum Engineering, Inc. provides reservoir, production, and drilling engineering services. One challenge to this type of organization is providing communication and coordination between the team members located in a diverse geographic area. Reporting and coordinating of five subcontractors uses advanced technologies to communicate and coordinate efforts. The use of E-mail, the Internet, and high capacity data transfer are used successfully to exchange data and conclusions between each group.

## **RESULTS AND DISCUSSION**

A number of planning sessions of the "virtual project team" were held during the early stages of the NDP project. As a result of these meetings, a project plan was developed for the first phase of the project. This paper will highlight results of the first year of the NDP project; detailed results are contained in the first annual report (**Murphy 1996**) submitted to the DOE.

### **Data Acquisition**

The data acquisition portion of the project included compiling existing reservoir and engineering data as well as acquiring new data. As part of the project, four new wells have been drilled to date for data acquisition, and the NDP now consists of 15 producing wells and one salt water disposal well (see **Fig. 1**). Multiple sidewall cores were obtained for analysis when each new well was drilled, and, when Well No. 23 was drilled, 66.6 m (203 ft) of full core was cut for laboratory analysis. Normal suites of logs were obtained in all of the wells, and a magnetic resonance tool was run in Well No. 23 for comparison to the core analysis. Two vertical seismic profiles (VSPs) and a 3-D seismic survey were recorded in Well No. 25 to aid the characterization of the NDP reservoir.

Production, transmissibility, capillary pressure data, and geological interpretations were combined to arrive at reservoir maps which honor the available data. It was necessary to perform a detailed correlation of the sands in the basal Brushy Canyon sands in order to better understand the lateral and vertical

distribution of the reservoirs. Detailed correlations also facilitate a more accurate geological model for use in the reservoir simulation phase of the study. The data were compiled into a spreadsheet for ease of use between all members for the project team. Well data were compiled for each of the wells within and directly adjacent to the Nash Draw Pool for the purposes of constructing the maps for the initial structural and stratigraphic model.

### **Geology of the NDP**

The structure trend at the NDP is N-S to NE-SW, and there were at least three depositional events. The sandstone reservoirs of the basal Brushy Canyon sequence lie above the Bone Spring Formation (**Fig. 2**). The top of the Bone Spring is marked by a regionally persistent limestone varying from 16.4 to 32.8 m (50 to 100 ft) in thickness that provides an excellent regional mapping horizon. Regional dip is to the east-southeast in the area of the NDP. The structural dip resulted from an overprint of post-depositional tilting that is reflected in reservoir rocks of the Delaware Formation and impacts the trapping mechanism in the sands.

The reservoir consists of complex sands - a series of stacked micro-sands, vertical permeability is extremely low, and horizontal permeability is poor to good. The main producing intervals of the Brushy Canyon formation, the "K" and "L" sands, have multiple lobes, and both sands can be divided in four sub-units. Mineralogy of the "K" and "L" sands are similar. Both zones contain some clays - illite and chlorite. The "K" sand has up to 2% more chlorite that occludes permeabilities and may have influenced higher initial water saturation in the "K" sand. Overall, the "K" sand has a higher water saturation than the "L" sand.

### **Comparison of NDP Data to Other Nearby Delaware Fields**

Log and core data were obtained from wells in the E. Loving Delaware Pool and the Texaco wells southeast of the NDP. These data were analyzed to determine if the zone characteristics were uniform over this general area. Results indicate that the core data are in good agreement, especially in the "L" Zone. Data from wells in these fields and from Maralo wells offsetting the NDP were obtained and analyzed. Structure

maps and cumulative oil, gas, and water production for the E. Loving Pool, and data from all three fields were analyzed and compared to data from the NDP. Core data correlate very well in the "L" zone, but there is less agreement in the data from the "K" and "K-2" zones.

Sixteen wells in the E. Loving Pool in Section 14, T23S-R28E were selected as an analogy to the NDP. These wells represent varying structural positions and corresponding production characteristics. Logs have been obtained from each well, structure maps have been constructed, and available core data have been obtained for the wells in the study area. A series of preliminary structure and isopach maps have been developed in the analog area using the same criteria that were used in the NDP area. It appears that the rock characteristics in the analog area are similar enough to those in the NDP to allow accurate comparisons of the production data and characteristics of the two areas.

### **Petrophysical Data**

Sidewall core data from each well in the NDP were compiled, and porosity/permeability ( $\phi/k$ ) relationships were determined. These relationships were compared to the whole core data and found to be in good correlation.

The whole core obtained from Well No. 23 was cut from the "J" zone through the "L" zone. Basic core data including porosity, permeability, oil and water saturations, grain density, show description, and lithology description, were measured for each foot of core. The core data were used to prepare a transform to correct the log cross-plot porosity to yield a true porosity based on the whole core porosity. The relationship between cross-plot log porosity (logs run on a limestone matrix) and core porosity was determined to be:

$$\phi_{\text{CORR}} = (\phi_{\text{x-plot}} - 3.7685) / .848294 \quad (1)$$

Permeability was plotted against porosity, and a regression analysis was performed to generate equations to fit the data. These relationships were used to predict the permeability of each zone based on corrected log



porosities. Permeability/porosity distributions were prepared for each zone as presented in Fig. 3.

Generally, the rock is fine to very fine-grained, massive to very thinly laminated. There is some evidence of turbulence as exhibited by sets of low to medium angle cross bedding within some of the sand units. Evidence of bioturbation occurs in some of the shaley and silty zones. There is also carbonate clastic debris present in some intervals within the core. Examination of the core under ultraviolet light shows the discontinuous character of the hydrocarbon distribution throughout the reservoir. This correlates with the erratic vertical distribution of calculated oil and water saturations seen in the log analysis.

These data were used to calibrate the logs and determine pay distribution in each zone. By performing a detailed core calibrated log analysis of  $S_{xo}$ ,  $S_w$  and porosity, a detailed analysis was applied to the digitized logs to determine the productive and water zones in each interval. The application of porosity/permeability transforms and relative permeability data to each zone yielded flow capacity data for each interval. These data were summed for each layer to be input into the reservoir simulator.

#### **Permeability ( $k_a$ )/ Porosity Relationships for Each Interval**

Porosity/permeability relationships were developed from the sidewall cores and full core analyses. The flow unit variables  $a$  and  $b$  are given in Table 2 for the power function:

$$k = 10^{a\phi - b} \quad (2)$$

A data file was prepared for each well that included digitized log files, perforations, cement programs, tracer logs, completion information, and frac treatments. These data were used to allocate production, estimate drainage areas, determine productivity, estimate saturations for each interval, and prepare data files for reservoir simulation.

Using core and log data, each well was calibrated to match production, net pay, and transmissibility. By calculating a  $kh/\mu$  value for each interval, production rates and cumulative production was allocated to each interval. The transmissibility for each layer will be used as input into reservoir simulation model along

with saturation data to determine the producing characteristics of each layer. **Figure 4** shows the transmissibility values used to establish production from the various zones for 14 of the 15 wells in the NDP.

### **Reservoir Model of the NDP**

The structure and isopach maps were loaded into Landmark's Stratamodel® program, and a preliminary 3-D geological layer model was developed. Surface intersections in the multi-layered model were eliminated by fine tuning the relationships of the structural surfaces using isopach maps. The model was constructed from the bottom up using the Bone Spring surface as the basal surface (see **Fig. 5**).

An initial ten-layer geological model has been developed for the basal Brushy Canyon sands in order to develop a more detailed reservoir model for simulation. The "K" and "L" sands were divided into four sub-units. The sands were correlated laterally from well to well in the NDP. Gross isopach, net porosity isopach and log-derived net pay maps were constructed for each of the sub-units of the "K" and "L" sands as well as the "K-2" and "J" sands. The maps were contoured to conform to the overall gross interval isopach maps for the respective pay zones that were used to construct the geological model. Reservoir attributes such as porosity, relative permeability, and oil and water saturations will be distributed vertically and laterally throughout the layers in the simulation model.

To date, two "generations" of models have been developed. Both of these are based solely on petrophysical measurements, that is, they exclude any geophysical input. In the first instance, a full NDP model was developed from the initially-available geological interpretation based on logs and cores. The second generation model was based on this data plus newly-interpreted pressure transient data. The integration of the log, core and pressure transient data led to an interpretation of the NDP with three non-communicating lobes of oil. The pilot area is confined to one of these lobes. It is anticipated that the inclusion of geophysical data like seismic amplitude will lead to further refinement of the present model--a third generation model.

Digitized maps of the interpreted horizons ("J", "K" with four subzones, "K-2," "L" with four subzones,

and the top of the Bone Spring formation) were imported into SGM® to create a stratigraphic framework model of the eastern half of the NDP (which contains the oil lobe supporting the pilot). Since the producing zones and subzones are relatively thin, great care had to be exercised to prevent intersections of the horizons. It is also critical that the surfaces tie to the well picks of the lithological markers in the well traces. In general, the most successful approach to this problem was based on the use of gross isopach thickness interpretations building from the structural top of the Bone Springs formation to the structural top of the "J" sand.

The next major step was the development of a well attribute model. This activity was supported by the Lotus engineering database. For each of the 15 NDP wells, the following attributes were imported into the well model: neutron porosity and gamma ray, interpreted porosity and permeability, perforated interval and fractured interval, net pay, and water saturation. In some instances, these attributes were available on a foot-by-foot basis for one or more of the producing zones. Not all of the attributes were available for each well. For reservoir simulation, the most important reservoir attributes are fluid conductivity and rock matrix storage capacity. The distribution of these properties throughout the NDP have been based on the well attribute model. Within SGM, these distributions are interpolated deterministically, that is, weighted by the reciprocal of the square of the distance between the location of interest and nearby wells in the reservoir model. The distribution of net pay, porosity, and water saturation are shown in **Figs. 7, 8, and 9**, respectively. Techniques like kriging (and co-kriging) may be used to distribute these attributes in the third generation model.

### **Reservoir Simulation**

Having completed the supporting geological model, attention focused on the generation of a reservoir simulation model for the pilot area. It is envisioned that a single well in the pilot area will be converted to injector status to test the efficacy of injecting water, lean gas (immiscible), and/or CO<sub>2</sub> (immiscible or miscible) to improve oil recovery at the NDP. The following tasks are required to complete the pilot simulation phase: possible scale-up of lithological units, interpolation of geological attributes on the

simulation grid, validation of pilot simulation model, and design and execution of prediction cases.

### **3-D Seismic**

The VSP calibration data acquired in Well No. 25 established the top of the Bone Spring as a robust reflection peak, the "L" sequence was associated with the first reflection trough immediately above the Bone Spring and the "K" sequence began just above the first reflection peak above the Bone Spring. The 3-D seismic survey generated amplitude maps that show the producing trends and high amplitude areas. Well productivity appears to be directly correlatable to the amplitude of the dominant "K" reflection peak and "L" reflection trough. Future wells will be drilled to confirm this analogy and evaluate targeted drilling of the seismic anomalies.

### **Conclusion**

The reservoir characterization, geological modeling, seismic interpretation, and simulation studies should yield a detailed model of the Brushy Canyon zones. This model will be used to predict the success of different reservoir management scenarios and to aid in determining the most favorable combination of targeted drilling, pressure maintenance, stimulation, and well spacing to optimize recovery from the Nash Draw Pool.

### **REFERENCE CITED**

Murphy, M.B., B.A. Stubbs, B.J. Uszynski, F.D. Martin, R.P. Kendall, E.M. Whitney, B.A. Hardage, and W.W. Weiss: "Advanced Oil Recovery Technologies for Improved Recovery from Slope Basin Clastic Reservoirs, Nash Draw Brushy Canyon Pool, Eddy County, N.M.," First Annual Report to the U.S. Department of Energy, DOE Cooperative Agreement No. DE-FC-95BC14941 (October 1996).

## Figures

1. Map of the Nash Draw Unit area.
2. Type log.
3. Permeability versus porosity.
4. Productivity values used for production allocations.
5. Stratigraphic framework model.
6. Net pay distribution.
7. Porosity distribution.
8. Water saturation distribution.
9. VSP image.
10. Seismic grid.
11. "K" zone amplitude map.
12. "L" zone amplitude map.

## Figures

1. Map of the Nash Draw Unit area.
2. Type log.
3. Permeability versus porosity.
4. Productivity values used for production allocations.
5. Stratigraphic framework model.
6. Net pay distribution.
7. Porosity distribution.
8. Water saturation distribution.
9. VSP image.
10. Seismic grid.
11. "K" zone amplitude map.
12. "L" zone amplitude map.

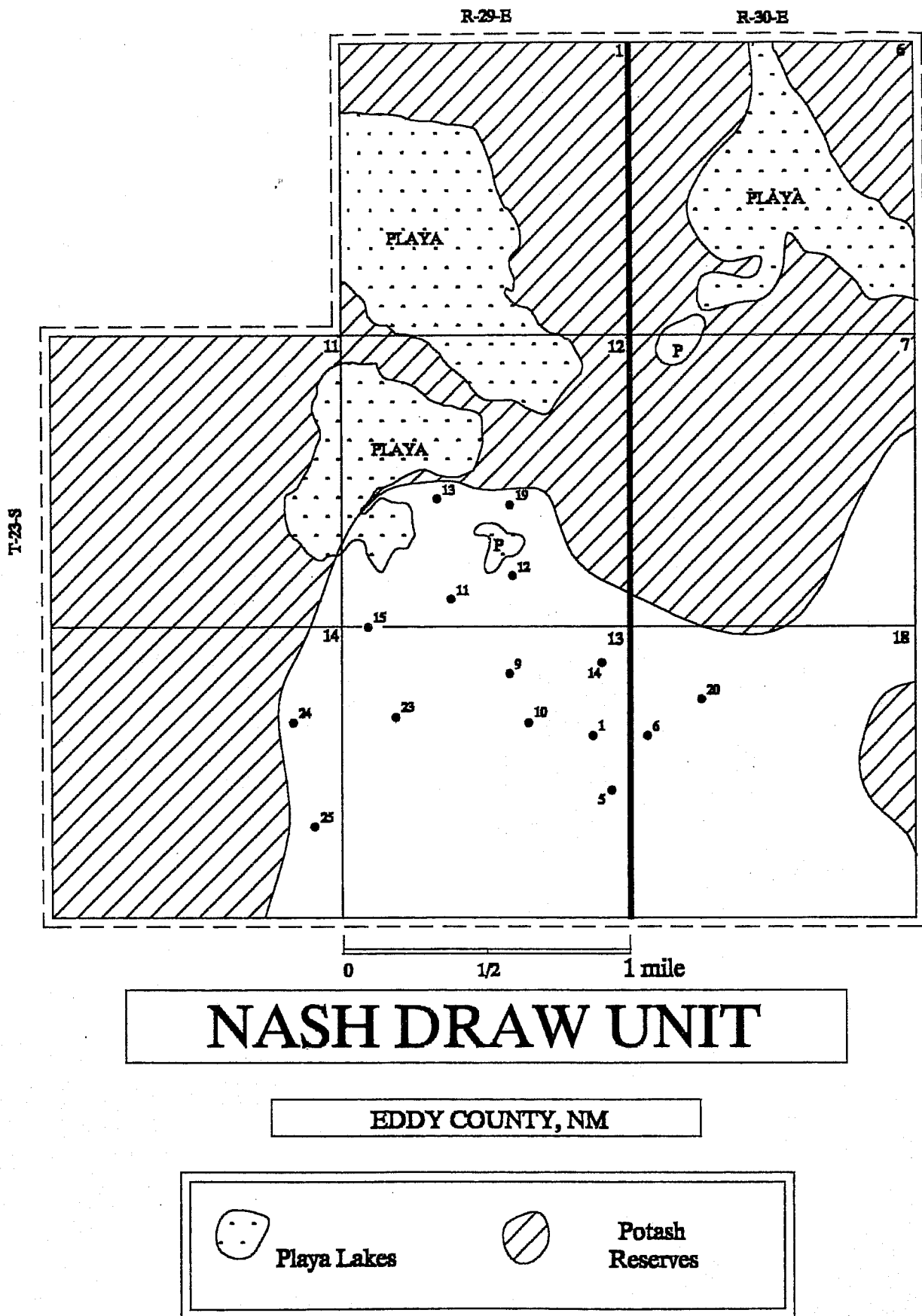
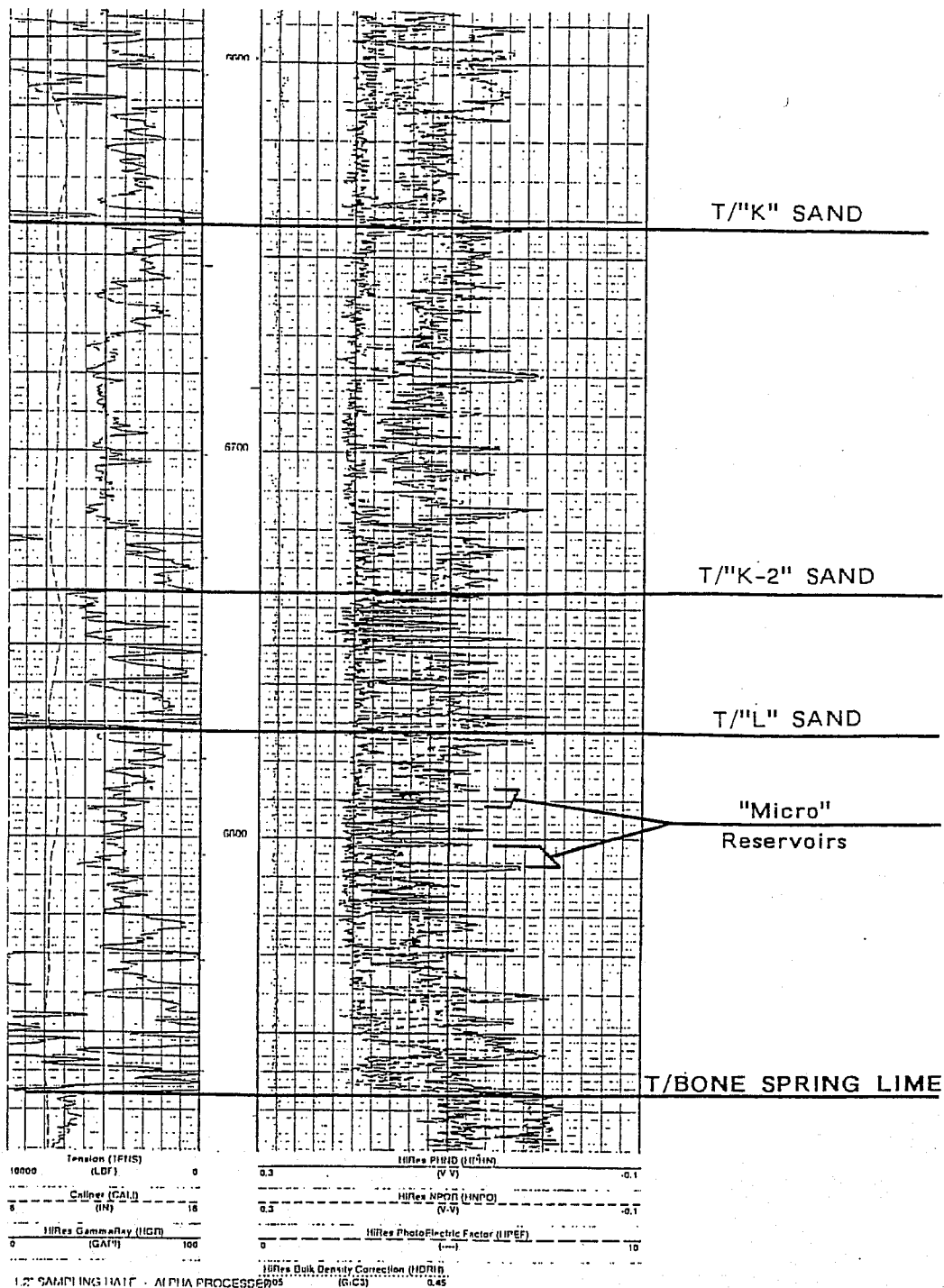


Fig. 1 Map of the Nash Draw Unit area.

# TYPE LOG

STRATA PRODUCTION COMPANY

NASH UNIT #15



Basal Brushy Canyon Sands Showing Stacking of Thin, Multiple Reservoir Packages. Each Sand is Composed of Stacked "Micro" Reservoirs with Vertical Permeability Barriers.

Fig. 2 Type log.



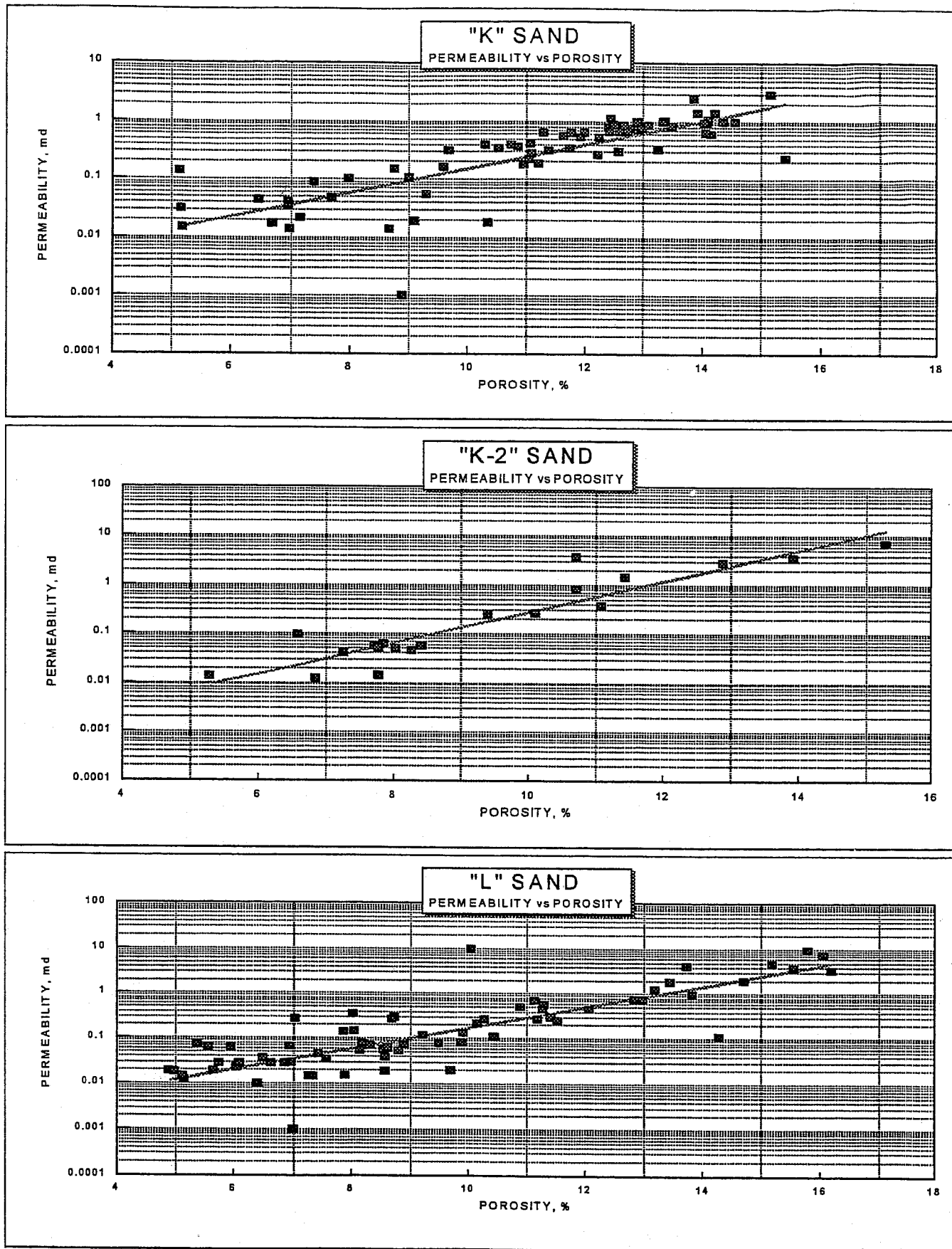
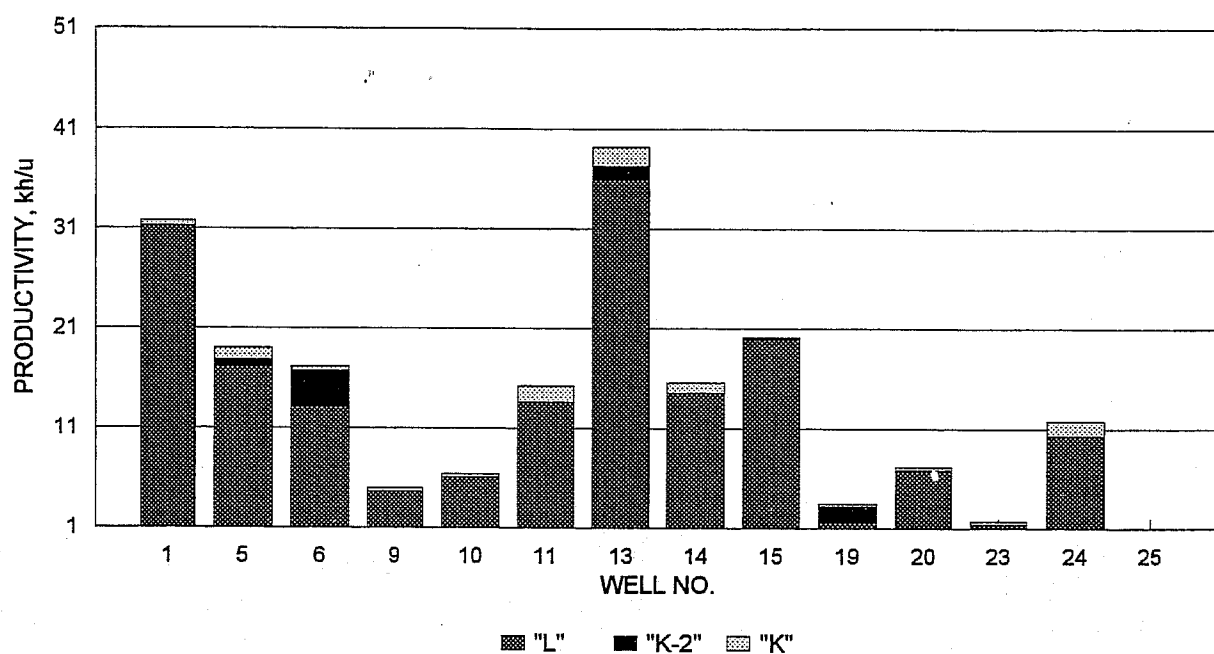
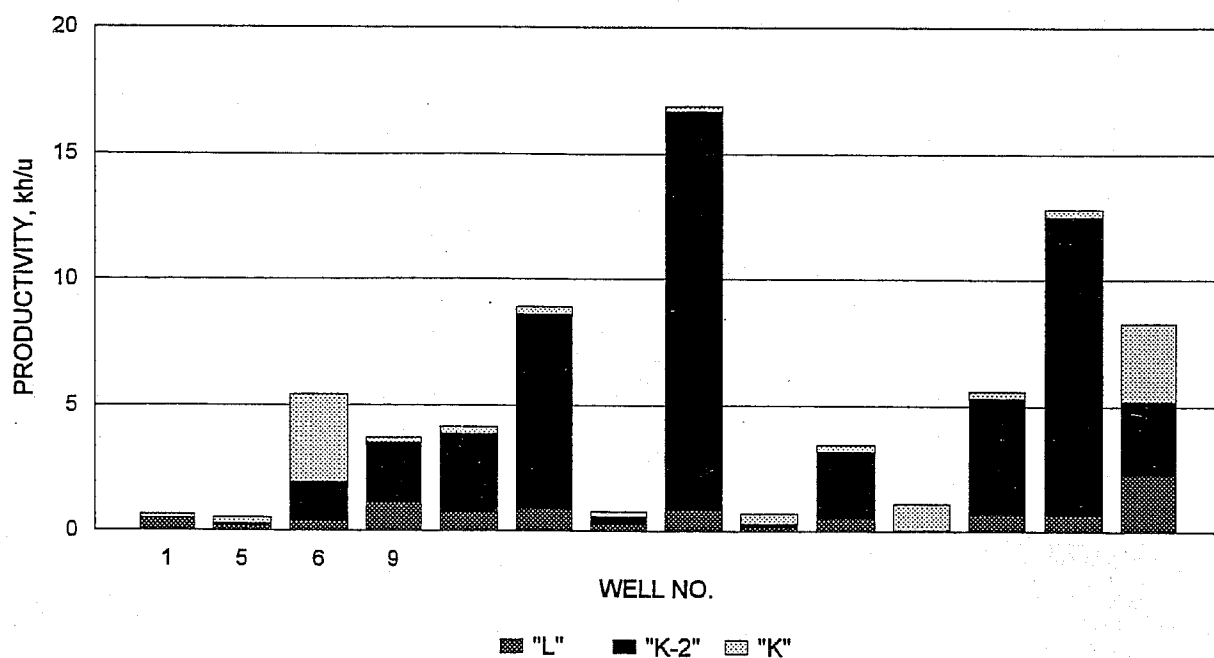


Fig. 3. Permeability versus porosity.

## OIL PRODUCTIVITY



## WATER PRODUCTIVITY



**Fig. 4 Productivity values used for production allocations.**

# Nash Draw Project Stratigraphic Framework Model

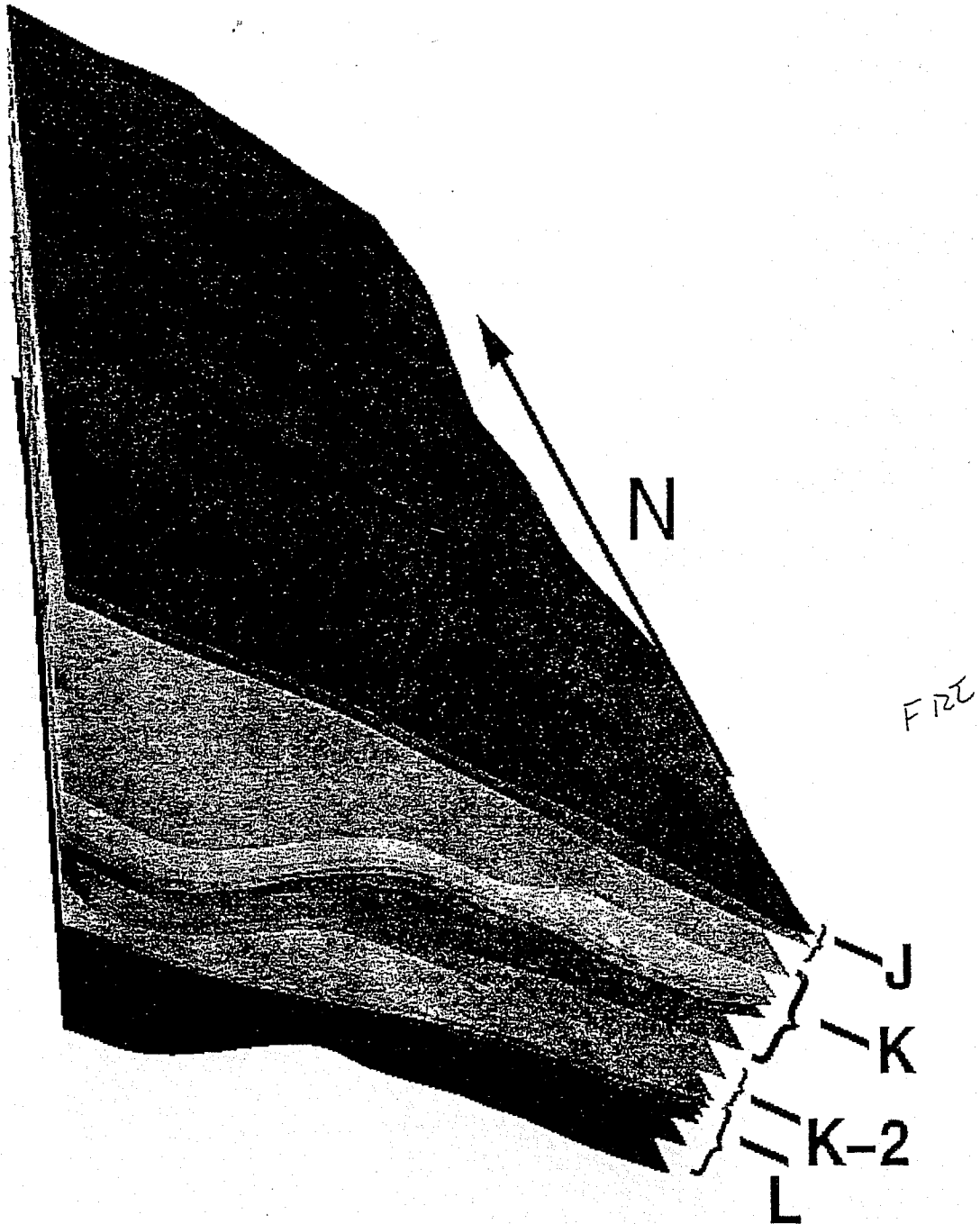
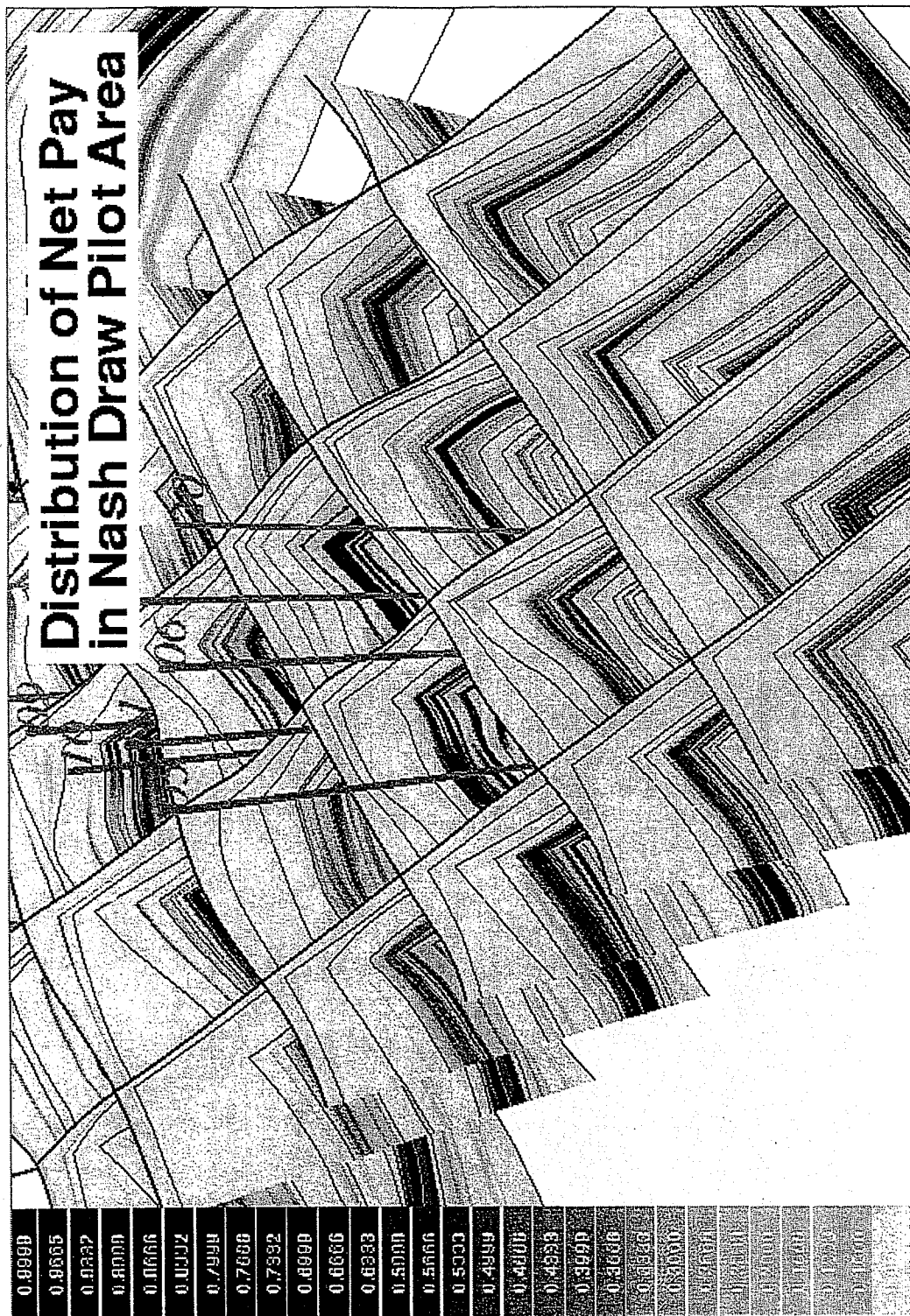
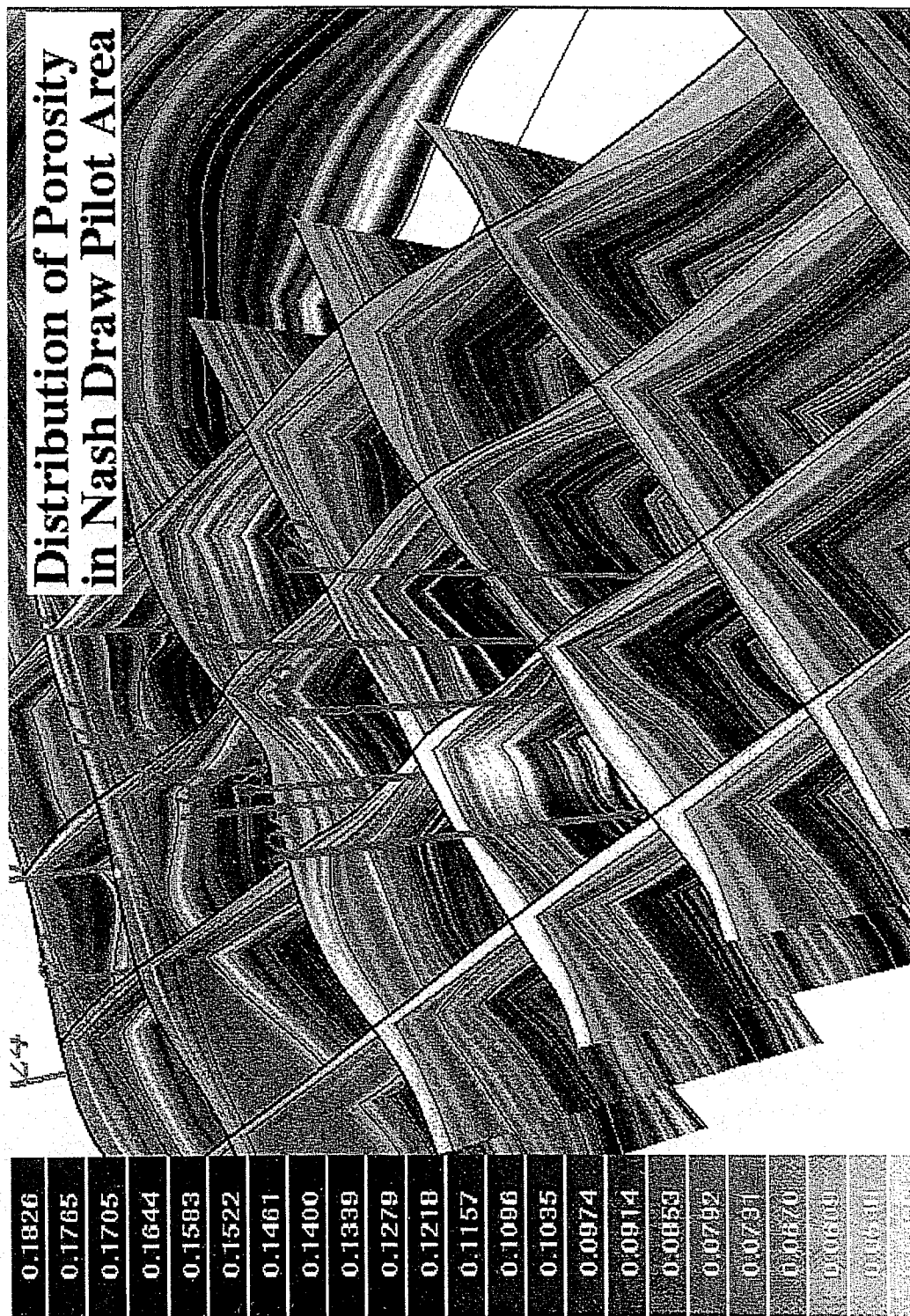


Fig. 5 Stratigraphic framework model.



**Fig. 6 Net pay distribution.**



**Fig. 7 Porosity distribution.**

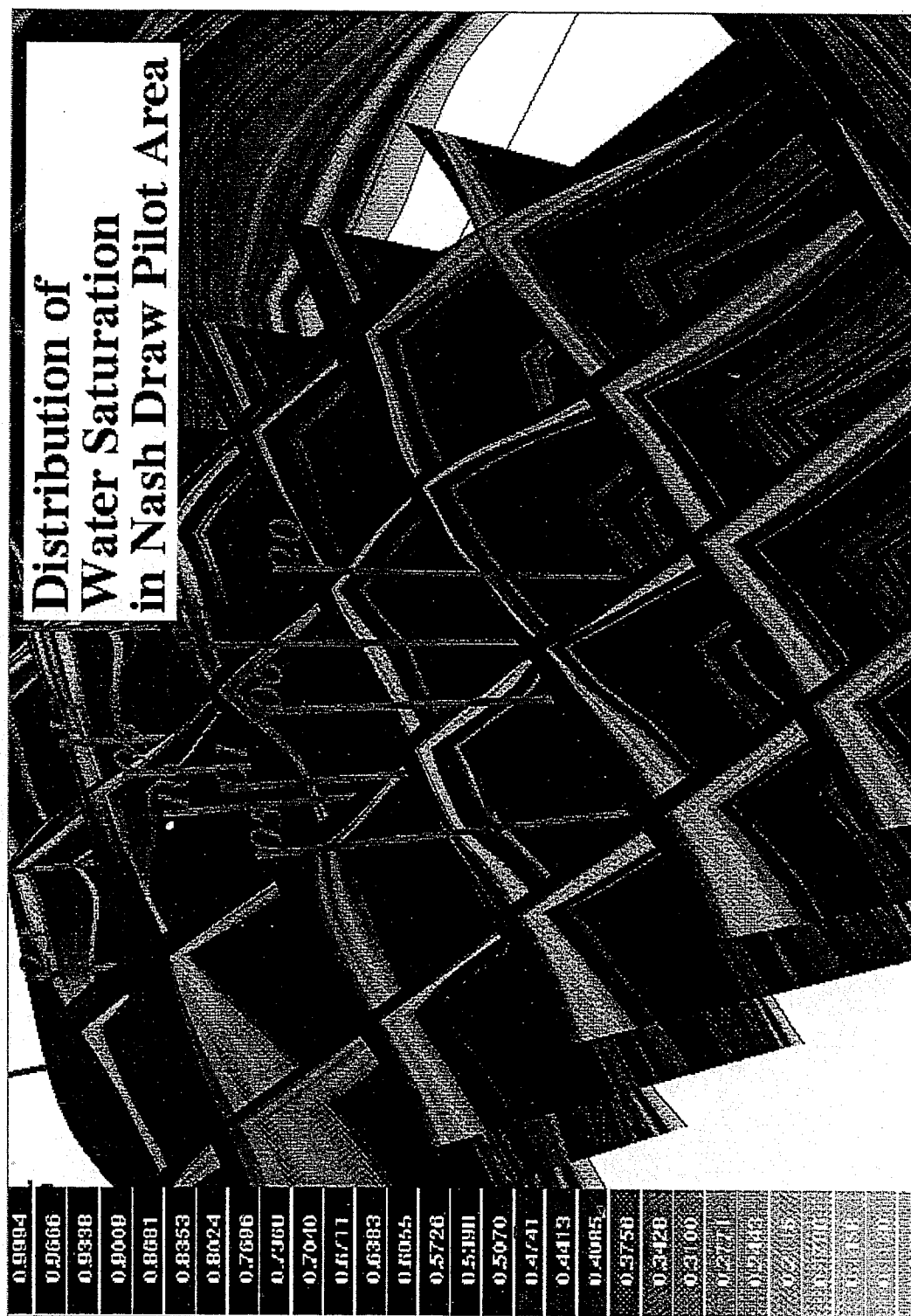


Fig. 8 Water saturation distribution.

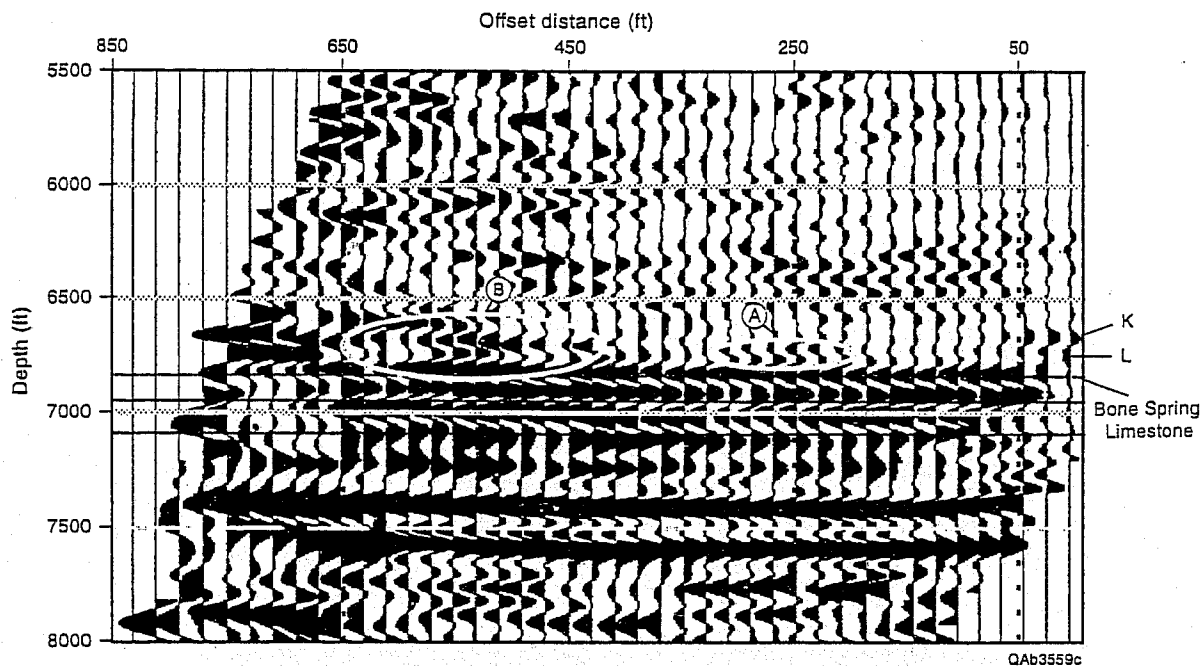


Fig. 9 VSP image.

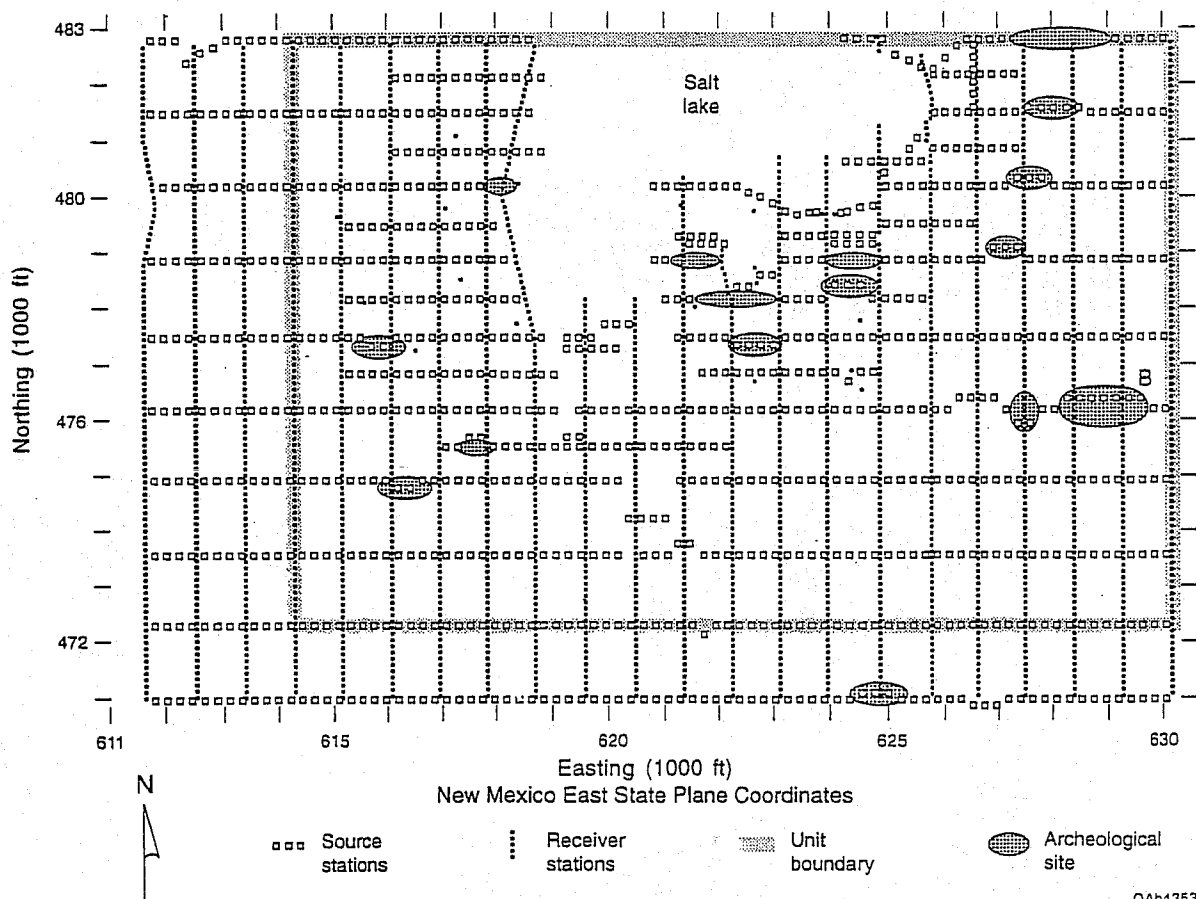


Fig. 10 Seismic grid.



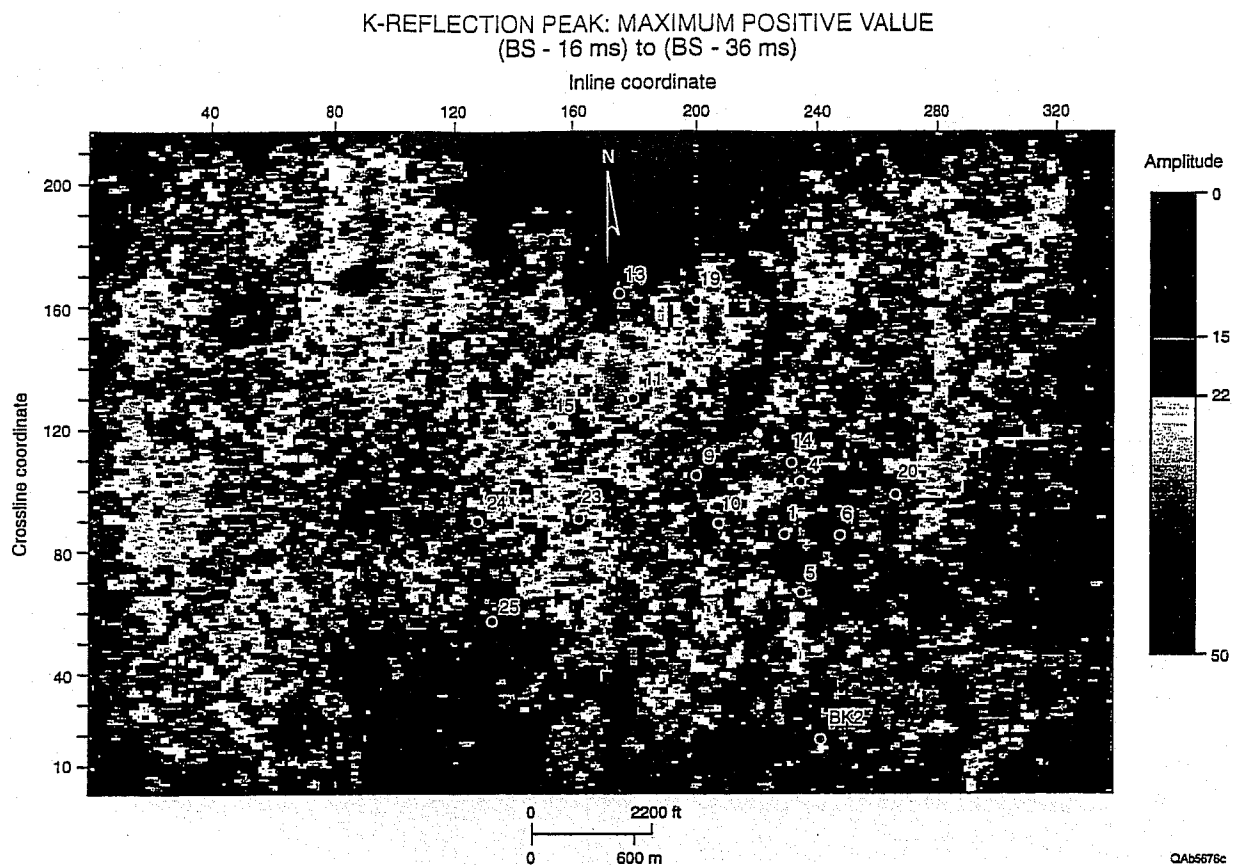


Fig. 11 "K" zone amplitude map.

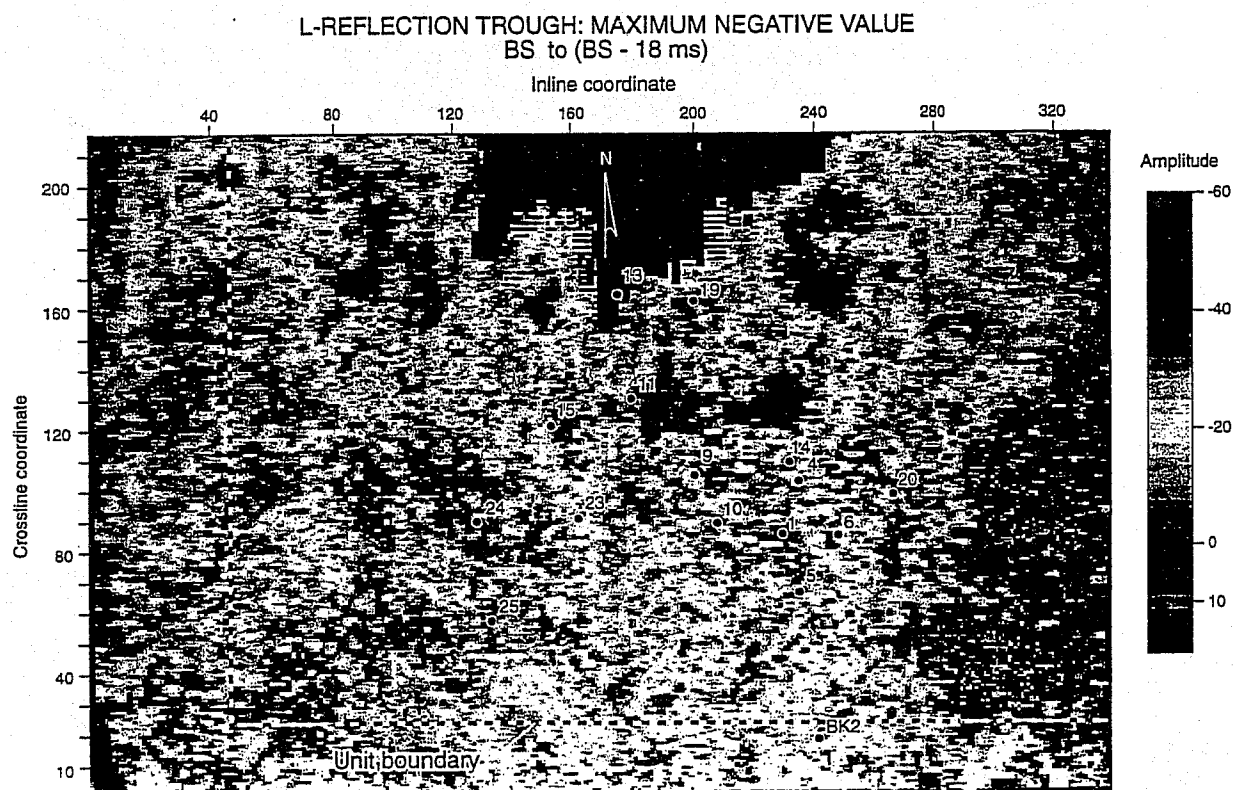


Fig. 12 "L" zone amplitude map.



Table 1. General Characteristics of the Nash Draw Delaware Field, Eddy County, New Mexico.

Discovery Date	1992
Trapping Mechanism	Stratigraphic Trap
Current Number of Wells	15
Current Production	490 BOPD + 2.4 MMCFGPD + 500 BWPD
Reservoir Depth	6600 to 7000 ft
Pay Thickness—K & L Sandstones	20 to 50 ft
Reservoir Porosity	12 to 20%
Reservoir Permeability	0.2 to 6 md
Initial Reservoir Pressure	2963 psi
Bubble Point Pressure	2677 psi
Drive Mechanism	Solution Gas Drive
Oil Gravity	42.4° API
Primary Recovery Factor	10 to 15% oil in place
Estimated Oil in Place	25 to 50 MMbbl
Reserves, Primary Recovery	2.5 to 5 MMbbl

Table 2. Permeability/Porosity Correlations.

Flow Unit	Sidewall	Core	Full	Core
Variable	a	b	a	b
"K"	0.164915	2.25338	0.207675	2.8858
"K-2"	0.186535	2.06872	0.315038	3.69966
"L"	0.179787	2.45666	0.231250	3.06330

Table 1. General Characteristics of the Nash Draw Delaware Field, Eddy County, New Mexico.

Discovery Date	1992
Trapping Mechanism <sup>a</sup>	Stratigraphic Trap
Current Number of Wells	15
Current Production	490 BOPD + 2.4 MMCFGPD + 500 BWPD
Reservoir Depth	6600 to 7000 ft
Pay Thickness—K & L Sandstones	20 to 50 ft
Reservoir Porosity	12 to 20%
Reservoir Permeability	0.2 to 6 md
Initial Reservoir Pressure	2963 psi
Bubble Point Pressure	2677 psi
Drive Mechanism	Solution Gas Drive
Oil Gravity	42.4° API
Primary Recovery Factor	10 to 15% oil in place
Estimated Oil in Place	25 to 50 MMbbl
Reserves, Primary Recovery	2.5 to 5 MMbbl

Table 2. Permeability/Porosity Correlations.

Flow Unit	Sidewall	Core	Full	Core
Variable	a	b	a	b
“K”	0.164915	2.25338	0.207675	2.8858
“K-2”	0.186535	2.06872	0.315038	3.69966
“L”	0.179787	2.45666	0.231250	3.06330